Single and coupled electrochemical treatment of food azo dyes

Abdoulaye Thiam

Universitat de Barcelona

Programa de Doctorado: Electroquímica. Ciencia y Tecnología

Single and coupled electrochemical treatment of food azo dyes

Tesis que presenta **Abdoulaye Thiam**

para optar al título de Doctor por la Universitat de Barcelona

Directores de tesis:

Dr. Enric Brillas Coso

Departamento de Química Física

Universitat de Barcelona

Dr. Ignacio Sirés Sadornil

Departamento de Quimica Fisica

Universitat de Barcelona

Barcelona, Mayo 2015

Universitat de Barcelona

Facultad de Química

Departamento de Química Física

Laboratori d'Electroquímica de Materials i del Medi Ambient

Single and coupled electrochemical treatment of food azo dyes

Abdoulaye Thiam

Directores de tesis:

Dr. Enric Brillas Coso

Departamento de Química Física

Universitat de Barcelona

Dr. Ignacio Sirés Sadornil

Departamento de Quimica Fisica

Universitat de Barcelona

Agradecimientos

La presente Tesis Doctoral es el resultado de cuatro años de trabajo durante los que he contado con el apoyo de una gran cantidad de personas e instituciones sin los cuales, en el mejor de los casos, me hubiera resultado muy difícil llegar hasta este punto. A ellos debo mi agradecimiento.

En primer lugar, agradecer a la Agencia Española de Cooperación Internacional para el Desarrollo (AECID) del Ministerio de Asuntos Exteriores y de Cooperación por la beca que me ha permitido realizar esta Tesis Doctoral.

Quiero agradecer y expresar mi más profunda gratitud a mis directores de tesis, Profs. **Dr. Enric Brillas Coso** y **Dr. Ignacio Sirés Sadornil**, por la enorme confianza que han depositado en mí a lo largo de estos años de duro trabajo y la ayuda que en todo momento me han brindado de forma sincera. Sin su paciencia, comprensión, esfuerzo y dedicación esta Tesis Doctoral no habría sido posible. A todos los profesores del grupo LEMMA, **Dra. Conchita Arias, Dr. José Antonio Garrido, Dra. Rosa María Rodríguez, Dr. Francesc Centellas** y **Dr. Pere Lluís Cabot**, siempre preocupados resolviendo todos los problemas del laboratorio y pendientes de que no faltase material o de dar apoyo emocional. Agradezco también a la **Dra. Elvira Gómez** su ayuda en muchas gestiones.

A los compañeros de laboratorio: **Amado**, **Sergi**, **Abdellatif**, **Isaraín**, **Griselda** y **Nelly** cuya inestimable ayuda y acompañamiento en buenos y malos momentos ha sido fundamental. No puedo dejar de mencionar a aquellos que por periodos cortos estuvieron haciendo estancia en este laboratorio, en particular a **Alejandro** y **Fabio** con quienes tuve la oportunidad de trabajar en colaboración. A **Ramón** y **Lidia** por su buena disposición en todo momento.

A los profesores del programa de Doctorado "Electroquímica. Ciencia y Tecnología" y los compañeros con los que hice los cursos en Cartagena (2011).

Quiero dejar constancia de mi más sincero agradecimiento al **Dr. Birame Boye** por el apoyo incondicional que me ha brindado durante todo este tiempo y por transmitirme sus amplios conocimientos en la materia y la pasión por la investigación.

En 2013 efectué una estancia de 5 meses en el College of Environmental Science and Engineering de la Nankai University (Tianjin, China). Se inició un proyecto que permitió la publicación de dos artículos que forman parte de esta Tesis. Este periodo fue toda una experiencia vital para mí. Durante ese tiempo pude aprender una gran cantidad de técnicas nuevas y adquirir numerosas habilidades que me serán muy útiles profesionalmente. I am very grateful to **Dr. Minghua Zhou** and the rest of researchers of the *College of Environmental Science and Engineering*, for giving me the opportunity to complete a short research stay under their supervision. My gratitude is for all of them due to their sincere help at every time I needed. I sincerely thank all the colleagues with whom I had the opportunity to work in Tianjin for their kindness and lovely daily discussions and for making me feel one more within the research group since the first minute I was there.

Por último, en el apartado más personal, deseo mostrar mi agradecimiento más emotivo a mis padres, **El Hadji Cheikhou Thiam** (RIP) y **Fama Sall**, que han sabido inculcarme el valor del trabajo bien hecho, de la responsabilidad y de la recompensa moral que ello conlleva. Ellos son mi guía, mi referente y el motivo por el cual hoy estoy escribiendo estas líneas que simbolizan el final de una Tesis Doctoral que ahora les dedico. Sirva esta mención como sentido reconocimiento por estar siempre a mi lado y ser un ejemplo de lucha, fuerza y valentía. Gracias, una y otra vez, por todo lo que habéis dado, habéis hecho y habéis arriesgado por y para vuestros hijos. Quiero extender dicha gratitud a mis hermanos, por sus grandes apoyos y consejos durante toda la Tesis.

Mi gratitud a todas las personas especiales que me han acompañado, de una forma u otra, durante estos años.

ÍNDICE

Acrónimos

ADE	Electrodo de difusión de aire (*air-diffusion electrode*)
AOPs	Procesos de oxidación avanzada (*advanced oxidation processes*)
AR 14	Rojo Ácido 14 (*Acid Red 14*)
AR 18	Rojo Ácido 18 (*Acid Red 18*)
AR AC	Rojo Allura AC (*Allura Red AC*)
AY 23	Amarillo Ácido 23 (*Acid Yellow 23*)
BDD	Diamante dopado con boro (*boron-doped diamond*)
BP-S	Bipolar en serie
CE	Comunidad Europea
CEE	Comunidad Económica Europea
CI	Índice Internacional del Color (*Color Index International*)
CR	Eliminación del color (*color removal*)
DBO_5	Demanda bioquímica de oxígeno a los cinco días
DPD	*N*-*N*-dietil-parafenilendiamina
DSA	Ánodo dimensionalmente estable (*dimensionally stable anode*)
DQO	Demanda química de oxígeno
EAOPs	Procesos electroquímicos de oxidación avanzada (*electrochemical advanced oxidation processes*)
EC	Electrocoagulación
EC_{TOC}	Consumo energético por unidad de masa de TOC (*energy consumption per unit TOC mass*)
EC_V	Consumo energético por unidad de volumen (*energy consumption per unit volume*)

EC-SCF	Comité Científico sobre Alimentos de la UE (*European Commission Scientific Committee on Food*)
EDTA	Ácido etilendiaminotetraacético
EEUU	Estados Unidos
EF	Electro-Fenton
EFSA	Autoridad Europea de Seguridad Alimentaria (*European Food Safety Authority*)
EO	Electrooxidación
FAO	Organización de las Naciones Unidas para la Alimentación y la Agricultura (*Food and Agriculture Organization of the United Nations*)
FDA	Administración de Medicamentos y Alimentos de EEUU (*US Food and Drug Administration*)
FSA	Agencia Británica de Seguridad Alimentaria (*Food Standards Agency*)
GC-MS	Cromatografía de gases acoplada a espectrometría de masas (*gas chromatography-mass spectrometry*)
HFCVD	Deposición química de vapor por filamento caliente (*hot filament chemical vapour deposition*)
HPLC	Cromatografía líquida de alta presión (*high pressure liquid chromatography*)
IC	Cromatografía iónica (*ion chromatograhpy*)
IDA	Ingesta diaria admisible (*acceptable daily intake*)
JECFA	Comité Mixto FAO/OMS de Expertos en Aditivos Alimentarios (*Joint FAO/WHO Expert Committee on Food Additives*)

LEMMA	Laboratori d'Electroquímica de Materials i del Medi Ambient
LSV	Voltamperometría de barrido lineal (*linear sweep voltammetry*)
MCE	Eficiencia de corriente de mineralización (*mineralization current efficiency*)
MP-P	Monopolar en paralelo
MP-S	Monopolar en serie
NDIR	Detector de infrarrojos no dispersivo (*non-dispersive infrared detector*)
NPOC	Carbono orgánico no purgable (*non-purgeable organic carbon*)
OMS	Organización Mundial de la Salud (*World Health Organization*)
PEF	Fotoelectro-Fenton con luz UVA (*UVA photoelectro-Fenton*)
PNUMA	Programas de las Naciones Unidas para el Medio Ambiente
POPs	Contaminantes orgánicos persistentes (*persistent organic pollutants*)
PTFE	Politetrafluoroetileno
ROS	Especies de "oxígeno activo" (*reactive oxygen species*)
SHE	Electrodo estándar de hidrógeno (*standard hydrogen electrode*)
SPEF	Fotoelectro-Fenton solar (*solar photoelectro-Fenton*)
SS	Acero inoxidable (*steel stainless*)
TC	Carbono total (*total carbon*)
TN	Nitrógeno total (*total nitrogen*)
TOC	Carbono orgánico total (*total organic carbon*)
UB	Universitat de Barcelona
UE	Unión Europea

UNCCD	Convención de las Naciones Unidas para la Lucha contra la Desertificación (*United Nations Convention to Combat Desertification*)
US	Ultrasonidos
UVA	Ultravioleta de onda larga (*ultraviolet A*)
WWAP	Programa Mundial de Evaluación de los Recursos Hídricos (*World Water Assessment Programme*)

1. Introducción

1.1 El agua: recursos y necesidades

El agua es un recurso natural de inestimable valor, imprescindible para la subsistencia de todos los seres vivos, tratándose por tanto de un factor esencial para satisfacer las necesidades básicas. La búsqueda colectiva para alcanzar un mayor nivel de vida, unida a su importancia para los frágiles ecosistemas de nuestro planeta, hacen de este elemento un recurso natural único. El agua es sin duda un elemento con gran presencia en nuestro planeta, ya que ocupa aproximadamente el 71% de la superficie de la corteza terrestre. Sin embargo, únicamente el 2,5% corresponde a agua dulce, siendo el resto agua salada. Además, sobre las dos terceras partes del agua dulce se encuentran inmovilizadas en glaciares o al abrigo de nieves perpetuas. A nivel mundial, se estima que el 70% del agua dulce disponible es empleada para fines agrícolas, la industria absorbe una media del 22%, empleándola en tareas de refrigeración, transporte y como disolvente de una gran variedad de sustancias químicas, mientras que el consumo doméstico sólo usa el 8% restante.

La distribución de los usos del agua dulce disponible en el planeta depende de los ingresos de cada país (**Figura 1**). El uso industrial del agua es mayor cuanto más elevado es el nivel de ingresos del país, variando desde el 10% en países con ingresos medios y bajos hasta el 59% en países con mayores ingresos. En cuanto al uso en el sector agrícola, según la UNESCO-WWAP, se observa un gran consumo de hasta el 82% en países con ingresos medios y bajos, siendo sólo el 30% en países con ingresos elevados. Conviene tener en cuenta que la capacidad de aprovechamiento del escaso porcentaje de agua dulce disponible disminuye notablemente debido a los cambios de hábitos de la población, conduciendo inexorablemente a su deterioro y escasez.

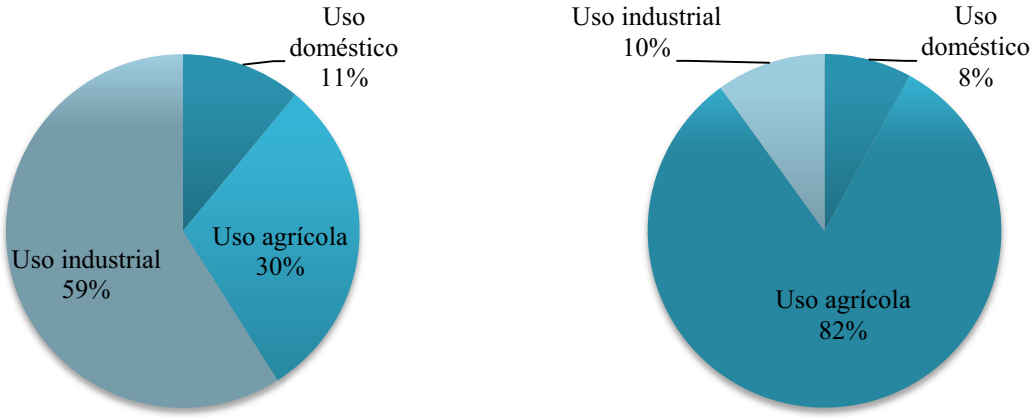

(a) Países con ingresos elevados (b) Países con ingresos medios/bajos

Figura 1. Usos alternativos del agua según el nivel de ingresos de los países.

1. Introducción

El agua dulce es un recurso finito y vulnerable, esencial para sostener la vida, el desarrollo de la sociedad y el medio ambiente. Las principales fuentes inmediatas de agua dulce renovable para consumo humano son las aguas superficiales (lagos, ríos, mares, etc.) y los acuíferos de aguas subterráneas de poca profundidad. A priori, esta cantidad de agua dulce es suficiente para satisfacer las necesidades de toda la población mundial, pero se plantean algunos problemas. Por un lado, esta cantidad de agua se distribuye de forma irregular en las distintas regiones del mundo, no siendo de la misma calidad en todas ellas. Además, la accesibilidad es muy diferente en función de la zona geográfica en la que nos encontramos y el grado de desarrollo de los distintos países. Así, en países con mayores recursos es más fácil la explotación y la distribución del agua, lo que permite abastecer a todas las personas y sectores. Por otro lado, esta pequeña proporción de agua aprovechable para el uso humano viene sufriendo una acelerada pérdida de calidad y cantidad. Por ejemplo, más de la mitad de los principales ríos del planeta se encuentran gravemente agotados o contaminados, por lo que degradan y contaminan los ecosistemas y amenazan la salud de los seres vivos. Según datos de la OMS y de UNICEF, 780 millones de personas no tienen acceso al agua potable, de las cuales 185 millones recurren a agua superficiales para satisfacer sus necesidades diarias (OMS y UNICEF, 2012). Una proporción importante de estos habitantes se concentra en Oceanía y África. De hecho, actualmente, prácticamente todos los países que aún tienen menos del 50% de cobertura en el abastecimiento de agua potable se ubican en la región del África subsahariana (**Figura 2**) (OMS y UNICEF, 2012). A esta falta de abastecimiento de agua de consumo en esta zona del planeta se añade un proceso acusado de desertificación, la degradación del suelo y la sequía, factores que pueden provocar impactos negativos en la disponibilidad, calidad y cantidad de los recursos hídricos, lo que se traduce finalmente en escasez de agua.

Estos datos tienen un impacto antropológico y sociológico dramático ya que se prevé que la escasez de agua en algunas tierras áridas y semiáridas forzará el desplazamiento de entre 75 y 250 millones de personas en África (UNCCD, 2009). Además, ante el escenario actual de cambio climático, casi la mitad de la población mundial habitará áreas con grandes problemas de disponibilidad de agua antes de 2030. En 2025, India, China y algunos países de Europa y África se enfrentarán a la escasez de agua si no se implementan iniciativas efectivas y sostenibles de gestión del agua (Vasudevan y Oturan, 2014).

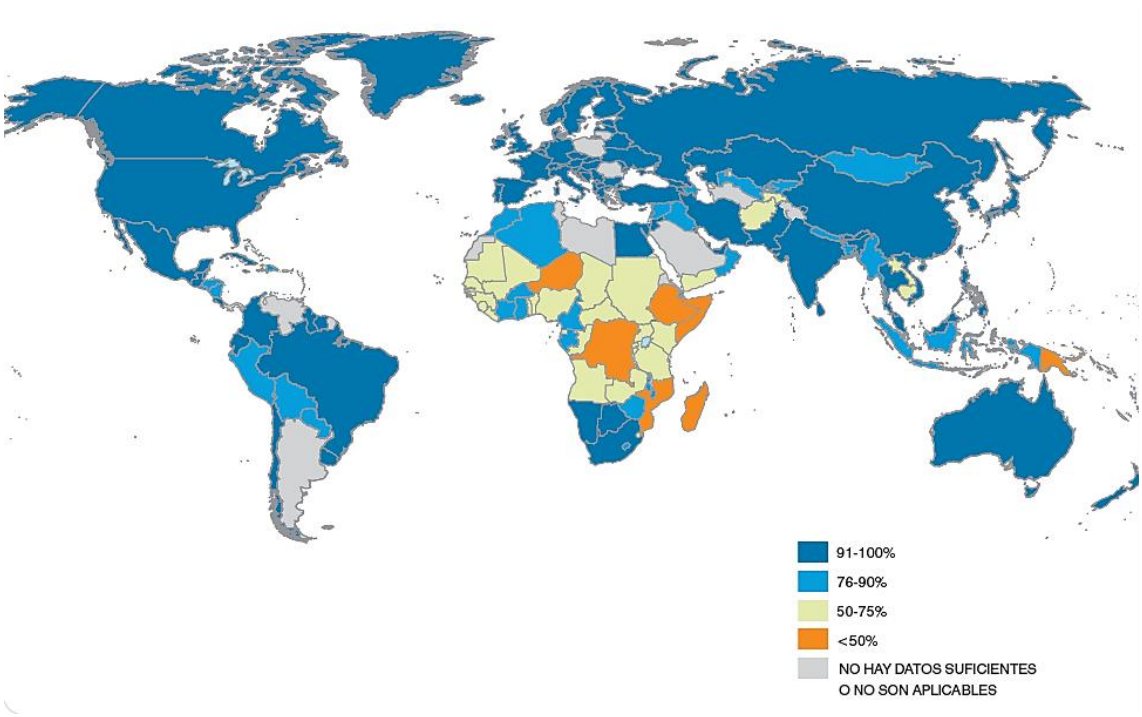

Figura 2. Proporción de la población mundial que consume agua de fuentes mejoradas.

La forma en que se utilizan los recursos hídricos es fundamental para hacer frente al reto de mejorar la salud y la seguridad alimentaria y conservarlas en todo el mundo. Sin embargo, como se ha mencionado, la escasez de agua es cada vez más acusada. Está aumentando la salinización, la contaminación de los cursos y las masas de aguas, y la degradación de los ecosistemas acuáticos. Muchos grandes ríos sólo conservan un pequeño porcentaje de los antiguos volúmenes de agua en sus caudales y algunos ya no llegan al mar durante todo el año. Los grandes lagos y mares interiores se han reducido, y muchos de los humedales en el mundo ya no existen. La extracción de agua a nivel mundial se ha triplicado durante los últimos cinco años con el fin de satisfacer las demandas de una población cada vez mayor y con niveles crecientes de bienestar, lo que implica una sobreexplotación de los acuíferos y otras fuentes naturales de agua dulce. Como se ha expuesto anteriormente, la agricultura es, globalmente, el sector con mayor demanda de recursos hídricos a nivel mundial, siendo las extracciones para este fin insostenibles en muchas áreas debido a un balance hídrico con riesgo de desequilibrio a largo plazo, como lo demuestra la sobreexplotación de acuíferos y la dependencia de grandes proyectos de trasvase de agua. Según los PNUMA, muchos centros agrícolas importantes dependen en gran medida del agua subterránea, incluyendo regiones del noreste de la India, China y Pakistán, el valle central de California y la región occidental de los EEUU (**Figura 3**).

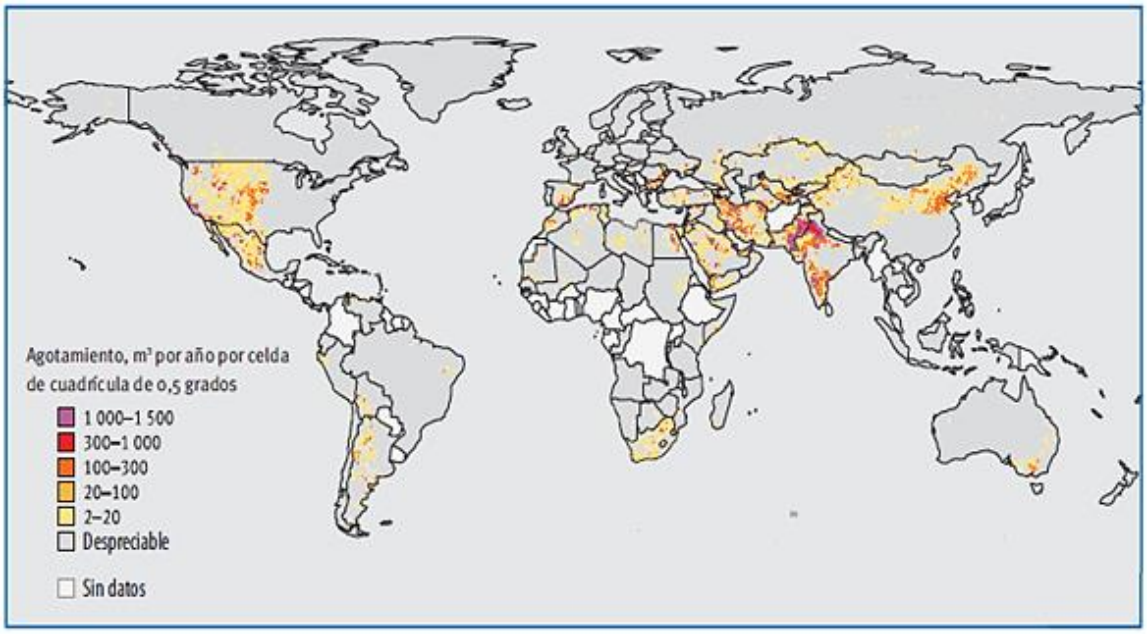

Figura 3. Agotamiento anual de los acuíferos a nivel mundial, 2000.

La tendencia hacia un claro deterioro de la capacidad de los ecosistemas para proporcionar bienes y servicios esenciales afecta actualmente a la salud humana y al potencial de abastecimiento de zonas productoras de alimentos básicos. Si esta situación continúa, las repercusiones para la salud y la seguridad alimentaria serán mayores en los países en desarrollo, donde los nutrientes del suelo y el agua son menos abundantes. Muchos gobiernos afrontarán retos para satisfacer incluso las necesidades fundamentales de su población, ya que deberán hacer frente a los cambios demográficos, las limitaciones de los recursos, los efectos del cambio climático y los riesgos que representarán los brotes de enfermedades infecciosas a nivel mundial.

1.2. La contaminación del agua

Las aguas superficiales, las cuales constituyen las principales fuentes inmediatas de agua dulce para el consumo humano, son objeto día a día de una severa contaminación. Los causantes de la contaminación del agua son muy diversos, pudiéndose identificar los de tipo antropogénico de los de origen natural. Por ejemplo, los metales pesados que se encuentran de forma consustancial en la corteza terrestre y en los océanos generan contaminación natural. De manera similar ocurre con los hidrocarburos y con muchos otros productos. Normalmente, las fuentes de contaminación natural están muy dispersas y no provocan altas tasas de polución, excepto en algunos lugares muy concretos en los cuales se puede dar una exposición magnificada.

A dichos eventos contaminantes propios de la naturaleza se han añadido nuevas y continuadas actividades humanas que han acabado convirtiéndose en los principales "motores" de presión sobre los sistemas hídricos de nuestro planeta. Estos fenómenos suelen ir ligados al desarrollo humano y al crecimiento económico. El desarrollo de la sociedad de consumo conlleva al aumento de la actividad industrial y, por consiguiente, propicia la creación de una enorme cantidad de sustancias químicas que en algún momento acaban entrando en el ciclo del agua a través de diferentes vías. Este hecho pone en peligro el frágil equilibrio natural del cual depende la vida en la Tierra, ya que millones de seres humanos y animales mueren cada año a causa de enfermedades relacionadas con la escasez de agua. Al mismo tiempo, la contaminación de los recursos hídricos y la destrucción de los ecosistemas aumentan incesantemente.

Hoy en día, el planeta está sufriendo muchos cambios debido al incremento de la población, el alto nivel de vida y la industrialización que ha dado paso a una mayor generación de residuos y un mayor nivel de contaminación de las aguas. La generación de residuos, con una contribución cada vez mayor de compuestos altamente tóxicos, crece de forma espectacular. El aumento de la peligrosidad de los residuos proviene de la diversificación e intensificación de la actividad industrial. Por ejemplo, a menudo las aguas residuales industriales contienen sólidos en suspensión que sedimentan en los ríos e impiden la vida de los organismos que viven en sus lechos y el desove de los peces. Otro ejemplo son los residuos orgánicos que consumen oxígeno disuelto, limitando así su disponibilidad para otros organismos acuáticos, mientras que otros constituyen una amenaza directa para la salud humana.

Entre los residuos industriales, los metales pesados se han convertido desde hace años en un tema relevante tanto en el campo ambiental como en el de la medicina y veterinaria. Los daños que causan estos contaminantes inorgánicos son tan severos y, en ocasiones ausentes de síntomas a corto y medio plazo, que las autoridades ambientales y sanitarias de todo el mundo ponen mucha atención en minimizar la exposición de la población a estos elementos tóxicos. El plomo es uno de los metales nocivos que se encuentra de forma natural en la corteza terrestre. Su uso generalizado ha dado lugar en muchas partes del planeta a una importante contaminación del medio ambiente, un nivel considerable de exposición humana y graves problemas de salud pública. Según la OMS, el plomo es una sustancia tóxica que se va acumulando en el organismo, afectando el funcionamiento de diversos órganos, con efectos especialmente dañosos en

los niños de corta edad. La intoxicación por plomo, en gran parte debida a su uso en pinturas, sigue siendo uno de los principales problemas de salud para los niños. En 2013, los PNUMA informaron de que la exposición al plomo se cobra cada año un total de 143.000 vidas, registrándose las tasas más altas de mortalidad en las regiones en desarrollo, y 600.000 nuevos casos de discapacidad intelectual en niños. El plomo no es biodegradable y persiste en el suelo, en el aire, en el agua y en el ámbito doméstico. Entre las principales fuentes de contaminación ambiental destacan la explotación minera, la metalurgia, las actividades de fabricación y reciclaje, y el uso persistente de pinturas y gasolinas con plomo. El arsénico es otro elemento que se encuentra en la corteza terrestre, y que en su forma inorgánica resulta ser muy tóxico. Su mayor amenaza para la salud pública reside en la utilización de agua contaminada para beber, preparar alimentos y regar cultivos alimentarios. La exposición prolongada a arsénico a través del consumo de agua y alimentos contaminados puede causar cáncer y lesiones cutáneas. También se ha asociado a problemas de desarrollo, enfermedades cardiovasculares, neurotoxicidad y diabetes. El mercurio es también una poderosa neurotoxina que, una vez introducida en un ecosistema, contamina la flora, la fauna y la cadena alimentaria humana a nivel mundial. Además, cabe destacar que elementos como el cadmio, el plomo y el mercurio son especialmente peligrosos porque pueden interferir con las hormonas, convirtiéndose en disruptores endocrinos, y en la reproducción. El cobre y el cinc son menos peligrosos para los seres humanos, pero son tóxicos para la vida acuática (WWAP, 2003).

Respecto a los microorganismos, en condiciones normales, muy pocos de ellos se encuentran en aguas subterráneas debido a la escasez de nutrientes, al escaso o nulo aporte energético y al filtrado que sufre el agua al atravesar los materiales del acuífero. La mayoría de las bacterias presentes no son patógenas, pero la acción del hombre ha modificado el funcionamiento normal de los acuíferos, especialmente cuando se introducen sustancias y formas de energía que son extrañas a ellos, ya que pueden provocar una proliferación anormal de microorganismos o bien la presencia de especies patógenas provenientes del exterior. En consecuencia, varios microorganismos de transmisión fecal-oral pueden estar presentes en el agua no tratada; por ejemplo, bacterias tales como *Salmonella, Shigella* y *Vibrio cholerae* son clásicos patógenos que suscitan gran preocupación (Arias, 2004). Estas bacterias, así como varios agentes virales, se han encontrado en abastecimientos de agua desde hace mucho tiempo. Sin

embargo, hoy en día se han identificado otros patógenos importantes en el agua, como algunos protozoos, cuya presencia podría conllevar graves problemas.

En las últimas décadas, una de las mayores preocupaciones en el ámbito ambiental es el riesgo asociado a la polución derivada de los contaminantes orgánicos persistentes (POPs). Los POPs son un conjunto de compuestos químicos que son muy estables y resisten en grado variable a distintos tipos de degradaciones como las fotoquímicas, químicas, bioquímicas, etc., lo que causa que su vida media en el ambiente sea elevada. Como consecuencia, muchos POPs han sido detectados en bajas cantidades (mg L^{-1}) en ríos, lagos y océanos de todo el mundo, e incluso en el agua potable (Brillas y col., 2009). Aunque las propiedades carcinogénicas, mutagénicas y bactericidas de la mayoría de los POPs siguen siendo desconocidas, existe un gran interés por su eliminación de las aguas para evitar sus potenciales consecuencias tóxicas y los posibles efectos peligrosos en la salud de los organismos vivos, incluidos los seres humanos. La pronta identificación e investigación de los riesgos asociados a los POPs es fundamental para la protección de la vida. Estos contaminantes tienen diferentes orígenes, siendo algunos fácilmente degradables biológicamente o químicamente mientras que otros son recalcitrantes a los métodos convencionales de tratamiento. En su mayoría, los contaminantes orgánicos, no sólo los POPs, son responsables de una gran cantidad de daños cuando son acumulados en el medio ambiente (Relyea, 2012). La contaminación del entorno natural por compuestos orgánicos constituye un tema crítico a nivel global, de manera que el estudio de nuevos procesos que utilicen tecnologías simples, seguras, eficaces, eficientes y viables económicamente para solucionar los problemas de contaminación de las aguas ha adquirido gran relevancia. En conclusión, es necesario investigar nuevas tecnologías que permitan optimizar los procesos industriales de descontaminación de agua.

Cabe mencionar que los destacados avances en las metodologías e instrumentación analítica en los últimos años han permitido la detección de concentraciones muy bajas de diversos compuestos en aguas, cuando hasta hace poco tiempo no se sabía ni siquiera de su presencia en las mismas. De entre todos los tipos de contaminantes citados, un grupo de compuestos recalcitrantes está formado por los colorantes sintéticos, los cuales se descargan en el medio acuático en gran cantidad a partir de actividades industriales de manufactura y teñido, primordialmente. Su acumulación en el medio ambiente constituye un riesgo para la flora y la fauna acuática. Estos compuestos son muy

difíciles de degradar, principalmente porque suelen presentar una estructura muy compleja que los hace bastante estables y, en consecuencia, poco biodegradables (Fewson, 1998; Seshadri y col., 1994; Gupta y Suhas, 2009; Srinivasan y Viraraghavan, 2010). En consecuencia, el tratamiento de colorantes sintéticos en medio acuoso constituye uno de los mayores desafíos en el campo del tratamiento de aguas debido a su impacto visual, aumento notable de la carga orgánica y toxicidad asociada a ellos mismos y sus intermedios.

1.2.1. Los colorantes

Definición

A lo largo de la historia, el color ha desempeñado un papel importante en la vida del hombre como medio de identificación y por su valor estético. En los productos textiles, alimenticios, farmacéuticos y cosméticos resulta fundamental porque les proporciona la apariencia física más apropiada. Los colorantes son sustancias capaces de absorber determinadas longitudes de onda del espectro visible gracias a sus grupos cromóforos. Así, tras su fijación sobre materiales base, son capaces de conferirles color de manera estable frente factores fisicoquímicos como por ejemplo la luz, los lavados, los agentes oxidantes, etc. Para que un colorante sea útil, debe ser capaz de unirse fuertemente al material base, y que éste no se decolore con el tiempo. Los colorantes pueden ser empleados con diferentes fines, por ejemplo, como indicadores de mezcla o con el único propósito de impartir color. En la actualidad no sólo es importante determinar que el colorante cumple con las propiedades antes mencionadas, sino que también se ha de establecer si éste se encuentra aprobado por las autoridades reguladoras del país donde va a ser comercializado; puesto que no todos los colorantes que están permitidos en un país lo están a su vez en otros, lo que es debido en parte a la diferencia de interpretación de los estudios toxicológicos disponibles. Actualmente existen diferentes tipos de colorantes que se pueden clasificar en diferentes grupos.

Clasificación

El color generado por la presencia de un colorante depende de sus grupos cromóforos, que constituyen la parte estructural responsable de la absorción de la luz en un determinado rango de longitud de onda. Además, pueden estar presentes en la

estructura también uno o más grupos auxocrómicos, conformados por un grupo de átomos ligados al grupo cromóforo y con capacidad para modificar la afinidad de éste para absorber la luz. Los colorantes pueden ser clasificados, de acuerdo a su origen, como orgánicos e inorgánicos, o como naturales o sintéticos, o bien en base a su estructura química como azoicos, xanténicos, quinoleínicos, trifenilmetanos, indigoides, ftalocianínicos, etc. (**Figura 4**). Asimismo, pueden ser clasificados según su uso o modo de aplicación. Los colorantes naturales se obtienen de fuentes minerales, animales o vegetales. Generalmente se consideran como inocuos y consecuentemente las limitaciones específicas en relación a su utilización son menores que las que afectan a los colorantes artificiales. Su principal desventaja es la complejidad con la que se encuentran en la naturaleza. Además, suelen tener un poder de tinción menor que los colorantes sintéticos, hecho que conlleva el uso de una mayor dosis, aumentando así el coste, y son más inestables ante las diferentes condiciones externas (pH, temperatura, humedad, irradiación, etc.). Con todo, su utilización comporta un mayor valor añadido debido al interés que muestran los consumidores por los productos naturales.

En 1856, William Henry Perkin preparó el primer colorante sintético (Saratale y col., 2011) mientras intentaba sintetizar la quinina, una sustancia utilizada para tratar la malaria. Este descubrimiento marcó el inicio de la industria de los colorantes sintéticos. En la actualidad, la mayor parte de los colorantes empleados son sintéticos orgánicos y, si bien se desconoce la cantidad exacta de colorantes sintetizados en el mundo, varios informes financieros estiman su aumento continuo en el mercado, llegándose a alcanzar ventas de hasta aproximadamente 11.000 millones de dólares estadounidenses. En 2008, la producción mundial de colorantes sobrepasó las 700.000 toneladas, correspondiendo entorno al 60-70% a los colorantes azoicos (Martínez-Huitle y Brillas, 2009). Los principales centros geográficos de producción se encuentran en Europa y Asia. Países como Alemania, Inglaterra, Suiza, Japón, Korea, Taiwán, China, India, Brasil y México son destacados productores de colorantes, especialmente para su uso en la industria textil. En comparación con los colorantes naturales, los colorantes sintéticos presentan algunas ventajas importantes, tales como una mayor estabilidad conferida por las estructuras más complejas, una gama más extensa de colores y precios más competitivos. Sin embargo, esta alta estabilidad tiene su parte negativa, puesto que convierte a los colorantes sintéticos en compuestos más resistentes a la biodegradación y a los tratamientos convencionales para su eliminación de los efluentes acuosos.

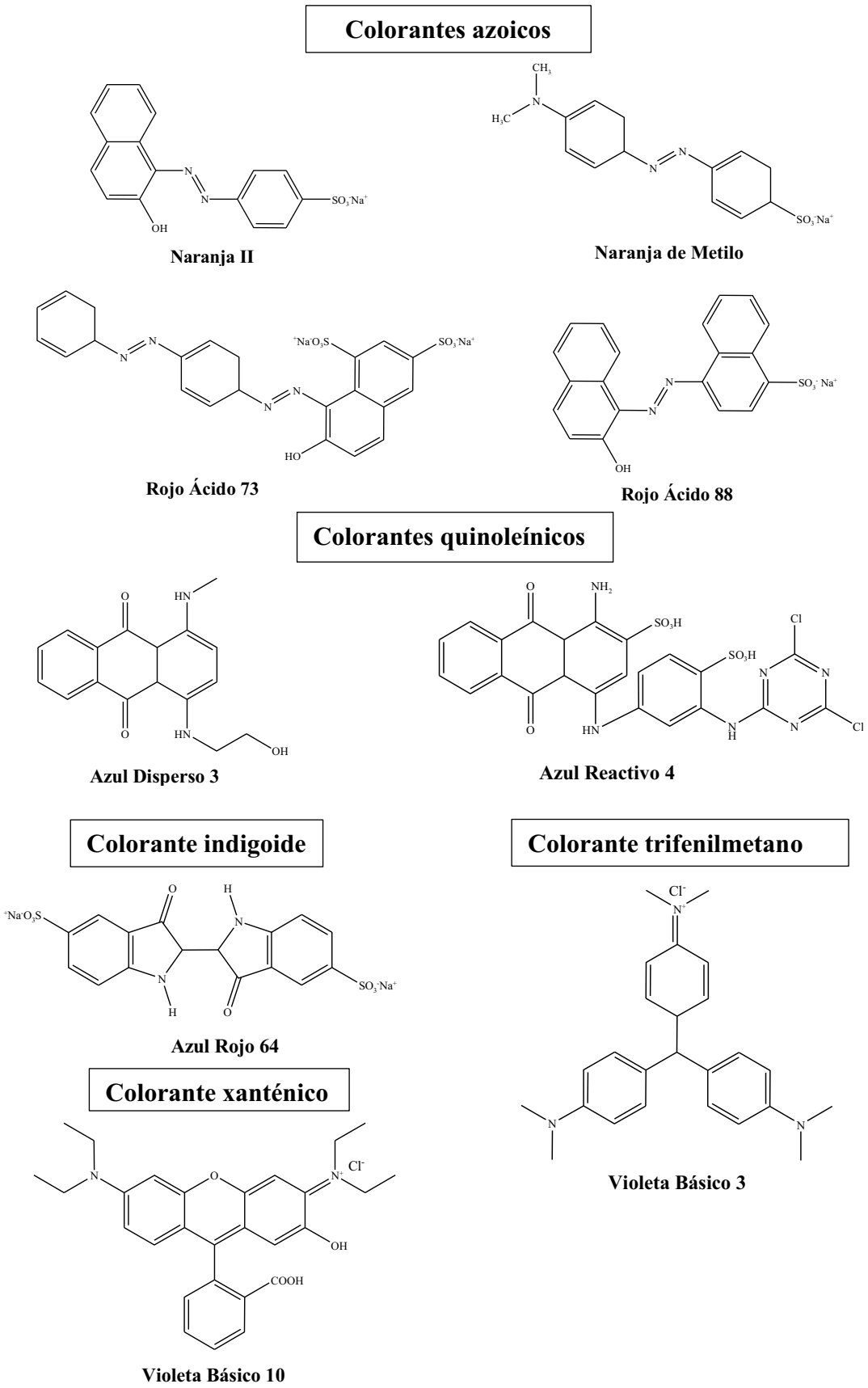

Figura 4. Estructura química de algunos colorantes orgánicos sintéticos típicos clasificados según su grupo cromóforo.

Los colorantes azoicos

Los colorantes azo o azoicos forman el grupo más extenso dentro de los colorantes sintéticos (Martínez-Huitle y Brillas, 2009; Fernandes y col., 2004). Su producción resulta relativamente económica y se pueden utilizar en una gran variedad de sectores, incluyendo la industria textil, alimentaria, papelera y farmacéutica, entre otras. Se caracterizan por la presencia de uno o varios grupos cromóforos azo (-N=N-) que pueden estar unidos a grupos benceno o naftaleno y contener iones cloruro ($-Cl^-$) y grupos nitro ($-NO_2$), metilo ($-CH_3$), amino ($-NH_2$), hidroxilo (-OH) y carboxilo (-COOH). Con frecuencia, se encuentra también algún grupo sulfónico ($-SO_3H$), en cuyo caso los colorantes son llamados azo sulfonados. Los colorantes azoicos se clasifican principalmente en 7 grupos, ácidos, básicos, directos, reactivos, dispersos, mordantes y solventes, según su naturaleza y la manera en que se fijan al material base. Los ácidos, directos y reactivos son aniónicos, los básicos son catiónicos, y los dispersos, mordantes y solventes son neutros, es decir, no iónicos. Para una mejor aplicación sobre el material, generalmente se utilizan mezclas de diferentes colorantes del mismo grupo, obteniéndose así la tonalidad, intensidad y fijación deseadas. Todos los colorantes azoicos se obtienen por síntesis química, no existiendo ninguno de ellos en la naturaleza. La síntesis tiene lugar mediante la diazoación o diazotación de una arilamina primaria en presencia de nitrito sódico en medio ácido clorhídrico, obteniéndose una sal de diazonio (Umape y col., 2013; Valizadeh y col., 2015). Posteriormente, se hace reaccionar con una amina aromática o un compuesto alcohólico, con objeto de formar el colorante. Esta última reacción, denominada de “acoplamiento” o “copulación”, se suele realizar en medio ácido en el caso de las aminas y en medio básico en el caso de los alcoholes.

Si bien los colorantes azoicos encuentran su mayor mercado en el teñido de fibras textiles, algunos de ellos se usan en la industria alimentaria para proporcionar o potenciar el color de los alimentos, ya sea porque el alimento ha perdido color en su tratamiento industrial o bien para hacerlo más agradable a la vista y más apetecible al consumidor.

Los colorantes alimentarios

En la actualidad, la industria alimentaria emplea colorantes como uno más de los muchos aditivos que tienen por objetivo la modificación de las preferencias del

consumidor. El color es uno de los principales atributos para la elección de un alimento, como sucede con cualquier objeto. Los colorantes alimentarios se consideran en ocasiones un aditivo inútil o engañoso, ya que con frecuencia sólo pretenden hacer creer que el alimento es mejor de lo que realmente es. Los colorantes alimentarios se utilizan para embellecer el aspecto de alimentos sólidos y bebidas. En el caso de determinados colorantes sintéticos, y en concreto los de tipo azoico, la Autoridad Europea de Seguridad Alimentaria (EFSA) ha avisado en diversas ocasiones acerca del riesgo de reacciones adversas relacionadas con estos aditivos. Un estudio encargado por la Agencia Británica de Seguridad Alimentaria (FSA) a la Universidad de Southampton en Inglaterra sobre colorantes alimentarios ha encontrado una relación estadística entre ciertas combinaciones de estas sustancias, utilizadas frecuentemente en bebidas refrescantes y en otros productos consumidos por niños, y un incremento de la hiperactividad infantil.

En cuanto a los riesgos que suponen estos colorantes para la salud del consumidor medio, cabe decir que es cierto que no causan reacción alérgica directa, pero pueden potenciar las reacciones alérgicas a otras sustancias, incluidos los fármacos. Además, pueden no ser tolerados por quienes no toleran los salicilatos y la mayoría son productores de histamina y pueden intensificar los síntomas del asma (Oliveira y col, 2011). Durante los últimos años, los colorantes azoicos han sido cuestionados reiteradamente, debido a que muchos compuestos de esta familia han demostrado ser cancerígenos en experimentos con animales, si bien este hecho no ha sido demostrado para los colorantes azoicos autorizados para uso alimentario. Una diferencia fundamental es que los colorantes cancerígenos presentan una baja polaridad, son solubles en grasas y atraviesan con cierta facilidad la barrera intestinal, incorporándose al organismo. En cambio, los colorantes autorizados son muy polares y por tanto solubles en agua, de manera que su absorción en el organismo es menos probable. El número de colorantes alimentarios autorizados actualmente es pequeño en comparación con el total de colorantes azo existentes. De hecho, varios colorantes azo han sido prohibidos debido a su efecto potencialmente perjudicial para la salud. Esto se ha evidenciado en especial en colorantes para grasas, siendo un ejemplo típico el denominado "*amarillo mantequilla*", utilizado hace tiempo para colorear este alimento. En 1918 se introdujo en EEUU, pero se prohibió el mismo año al afectar a los obreros que lo manejaban (Maga y Tu, 1994). En otros países, especialmente en Japón, se

utilizó hasta los años 40, cuando se demostraron incuestionablemente sus efectos carcinógenos, puesto que se absorbe en gran proporción y se metaboliza en el hígado. No existen datos que permitan sospechar que sucede lo mismo en el caso de los colorantes que se utilizan actualmente, que tienen como característica general la de absorberse muy poco en el intestino, siendo destruidos en su mayoría por la flora bacteriana intestinal. Los fragmentos de colorantes que sí son asimilados se eliminan por vía urinaria y/o biliar. Con todo, no existen certezas sobre el potencial tóxico de los colorantes alimentarios y sus intermedios de degradación o metabolización, en especial sobre seres vivos sobreexpuestos o altamente sensibles, así que no pueden dejar de ser considerados como contaminantes de las aguas.

Además de las consideraciones relacionadas con la salud humana y la vida de otros seres, se debe tener en cuenta que durante los procesos de teñido los colorantes no se fijan completamente a los alimentos, por lo cual un gran porcentaje se pierde durante el proceso de lavado y en el vaciado de los baños. En conclusión, las aguas residuales procedentes de la producción y otras actividades industriales pueden constituir una grave amenaza para los ecosistemas circundantes y la salud de los seres vivos (Ghoneim y col., 2011).

Impacto ambiental de los colorantes

El incremento en la producción y uso de los colorantes en varios sectores industriales ha dado origen a una preocupación creciente sobre el efecto que dichos compuestos tienen sobre los ecosistemas terrestres y acuáticos. El problema ambiental más fácilmente identificable es estético y está relacionado con la coloración de las aguas, incluso a muy bajas concentraciones de colorante (Garcia-Segura y col., 2011). Un gran porcentaje de los colorantes no son directamente tóxicos para los organismos vivos, aunque la fuerte coloración que confieren a los medios de descarga puede tener efectos nocivos para el medio ambiente, en particular para la flora y la fauna acuática, por lo que su manejo debe ser controlado. Entre los efectos más importantes de la coloración de las aguas por parte de los colorantes se encuentra la obstaculización del paso de la luz solar a través del agua, hecho que puede llegar a eliminar los procesos fotosintéticos y disminuir el oxígeno disuelto, lo que limita el crecimiento de las plantas acuáticas y los procesos de autodepuración (Akbari y col., 2002). Además, los colorantes disueltos en las aguas residuales representan un serio problema de

contaminación no sólo por el efecto directo sobre el volumen acuoso considerado y sus constituyentes, sino también porque afecta muy negativamente al correcto funcionamiento de los procesos biológicos en las plantas de tratamiento de aguas residuales, dado que son compuestos difícilmente biodegradables por su compleja estructura (Flox y col., 2006a; Shi y col., 2007; El Qada y col., 2008). Para agravar más la situación, los productos de (bio)degradación de muchos colorantes azoicos, principalmente sulfonados y aminas aromáticas no sulfonadas, son tóxicos para los organismos acuáticos y sospechosos de ser carcinogénicos y mutagénicos para los seres humanos, o teratogénicos para varias especies microbiológicos y peces (Daneshvar y col., 2003a; El-Desoky y col., 2010).

Debido a los importantes efectos adversos de los colorantes sobre los seres vivos y el entorno, resulta prioritario establecer normas y reglamentos con el fin de regular el uso de tales compuestos orgánicos persistentes y la búsqueda de métodos eficaces para la eliminación de éstos y de sus intermedios de degradación.

1.2.2. Legislación

Con el fin de evitar el uso indiscriminado de los colorantes como aditivos alimentarios, se han sido desarrollados leyes y reglamentos por parte de muchos países y organismos internacionales como la Unión Europea (UE), EEUU o la Organización Mundial de la Salud (OMS), los cuales limitan las cantidades de colorantes alimentarios autorizados. Las autoridades sanitarias que marcan la pauta en normativas de uso de aditivos alimentarios son la EFSA en la UE y la Food and Drug Administration (FDA) en EEUU. Las autoridades sanitarias y expertos, antes de aprobar un aditivo, analizan los datos de estudios previos efectuados sobre los efectos de consumo agudo y crónico del ingrediente, definiendo una Ingesta Diaria Admisible (IDA) con un amplio margen de seguridad. Sin embargo, hay países que difieren respecto a las propuestas de los organismos antes mencionados, por lo que es importante, antes de emprender en este nicho de negocio, conocer las normas específicas de cada país (por ejemplo, el Rojo Allura AC, cuyo Índice Internacional del Color (CI) es el 16035, es comúnmente utilizado en EEUU, pero está prohibido en muchos países europeos.

En la UE, todos los aditivos, incluidos los colorantes alimentarios, deben contar con una autorización y cumplir con el reglamento *CE 1333/2008* para ser utilizados. Son identificados con la letra E seguida de un número, que en el caso de los colorantes

corresponde a valores entre 100 y 199. La lista de los colorantes alimentarios autorizados en la UE y los niveles máximos permitidos en los productos alimenticios se establecen en los anexos de la Directiva del Consejo *94/36/CE*. La Comisión Europea ha aprobado recientemente un paquete de leyes según las cuales los alimentos y bebidas que circulen en la UE y que contengan colorantes azoicos deben ser etiquetados no sólo con el número E sino también con la advertencia de que su consumo puede provocar un efecto adverso en la atención y actividad de los niños. Los colorantes afectados son: Tartrazina (E 102), Amarillo Ocaso FCF (E 110), Azorrubina o Carmoisina (E 122), Amaranto (E 123), Ponceau 4R (E 124), Rojo Allura (E 129), Negro Brillante (E 151), Pardo FK (E 154), Pardo HT (E 155) y Litolrubina BK (E 180).

En EEUU, la regulación federal contempla dos tipos de aditivos, los llamados aditivos directos (añadidos a los alimentos) y los aditivos indirectos (materiales de envases y embalajes susceptibles de liberar sustancias hacia los alimentos con los que están en contacto). El concepto de aditivo difiere en cierto modo del concepto que se emplea en la UE. Además, se encuentran otras diferencias entre la legislación de EEUU y la que se rige en la UE sobre aditivos. De entre éstas, podemos destacar la forma de nombrar los aditivos, puesto que la nomenclatura seguida en la UE (E xxx) no resulta válida en EEUU. Algunos aditivos no autorizados en la UE si lo están en EEUU, y viceversa. La FDA clasifica los colorantes permitidos en dos categorías:

(i) Colorantes certificados, los cuales son producidos sintéticamente y cada lote debe ser comprobado por el fabricante y la FDA para asegurar que cumple con las especificaciones de pureza necesarias. Los colorantes se identifican con el prefijo FD&C o D&C, seguido del color y un número. Por ejemplo: FD&C Yellow No. 6 es la Tartrazina. Éste es uno de los nueve autorizados en alimentos actualmente, junto con FD&C Blue No. 1, FD&C Blue No. 2, FD&C Green No. 3, Orange B, FD&C Citrus Red No. 2, FD&C Red No. 3, FD&C Red No. 40, FD&C Yellow No. 5 y FD&C Yellow No. 6.

(ii) Colorantes libres de certificación, que son los que incluyen pigmentos derivados de fuentes naturales como frutas, hortalizas, minerales o animales. Algunos ejemplos son el extracto de annatto (amarillo), betarragas deshidratadas, caramelo, beta-caroteno y extracto de piel de uva.

El problema de los colorantes azoicos es más complejo en el caso de la contaminación ambiental asociada y el establecimiento de normativas al respecto. Hoy

en día está universalmente aceptado que los problemas ambientales no respetan fronteras. Por su parte, los estados se han visto en la necesidad de introducir la variable ambiental en sus políticas sectoriales, así como a establecer normas específicas en materia de protección del medio ambiente en los campos más variados. En EEUU, el control de la contaminación del agua producida por las actividades industriales comenzó con la aprobación por el Congreso de la enmienda de 1972 a la *Federal Water Pollution Control Act*, que estableció un sistema nacional de descarga y eliminación de contaminantes. Las enmiendas de 1977 y 1987, conocidas como *Clean Water Act* y *Water Qualty Act*, completan la regulación legal norteamericana.

Por su parte, la UE establece un marco comunitario para la protección y la gestión del agua y la limitación de la cantidad de determinadas sustancias químicas en las aguas superficiales que presentan un riesgo significativo para el medio ambiente y la salud. En este sentido, existen diferentes directrices que hacen referencia a la calidad y la importancia del agua potable. Entre ellas, se encuentra la Directiva *2000/60/CE* (o Directiva Marco de aguas) donde se incluyen 33 sustancias prioritarias. La Directiva *76/464/CEE* trata sobre la contaminación causada por determinadas sustancias peligrosas vertidas al medio acuático de la Comunidad. Esta Directiva recoge las denominadas Listas Negras y Gris de sustancias especialmente nocivas para el medio ambiente. En la Directiva *91/271/CEE* relativa al tratamiento de aguas residuales urbanas se recoge la definición de las diferentes aguas residuales así como la regulación de vertidos de aguas residuales industriales biodegradables. La Directiva *91/689/CEE* trata sobre los residuos peligrosos, y por medio de esta Directiva se establece el uso de tecnologías limpias y de productos menos contaminantes así como la reutilización de los residuos. La Directiva *2008/105/CE* (por la que se deroga la Directiva *86/280/CEE* y se modifica la Directiva *2000/60/CE*) hace referencia a los valores límite y objetivos de calidad ambiental en el ámbito de la política de aguas para los vertidos de determinadas sustancias peligrosas comprendidas en la Lista I (Lista Negra) de la Directiva *76/464/CEE.*

A pesar de este control cada vez más exhaustivo por parte de los diferentes organismos, varios estudios sobre la contaminación del medio acuático demuestran que un gran número de contaminantes orgánicos tóxicos, entre ellos algunos colorantes y sus intermedios de degradación, persisten en las aguas. Si bien su concentración en aguas naturales y de consumo es baja, es necesario hacer un seguimiento de su

evolución y un profundo estudio de sus posibles efectos nocivos para los seres vivos, y a su vez encontrar métodos eficaces para su eliminación total de las aguas.

1.3. Tratamiento de aguas residuales

Las aguas contaminadas provienen de diferentes fuentes, como pueden ser las industrias o las zonas habitadas, por lo que están compuestas por elementos muy variados, tanto en tamaño como en composición. El tipo de contaminación y el destino de las aguas residuales condicionan el proceso a emplear para su tratamiento. En su día, el uso cotidiano de productos de limpieza dio lugar a episodios de contaminación orgánica que se solventaron con tratamientos de cultivos de bacterias (depuradoras biológicas), pero la aparición de compuestos orgánicos resistentes a estos tratamientos no se hizo esperar. Así, disolventes orgánicos, colorantes, pesticidas, desinfectantes, etc., no sólo no eran degradados (compuestos biorefractarios) sino que además podían inhabilitar los métodos de descontaminación biológica al destruir los cultivos. En general, la eficacia del tratamiento varía en función del tipo y de la concentración del contaminante, de la concentración de otras sustancias presentes y de la forma en que se presentan en las aguas contaminadas. Por esta razón es conveniente conocer todos los detalles sobre las fases de generación de los efluentes para determinar su composición exacta. Los estudios de toxicidad y biodegradabilidad de los productos puros o mixtos son también una parte importante en el análisis del problema. En último término, la elección del tipo de tratamiento de agua requiere una investigación específica tanto del efluente en particular como de los factores externos tales como los aspectos económicos, el marco legal, etc.

1.3.1. Tratamientos convencionales

Las tecnologías disponibles en la actualidad para el tratamiento de aguas contaminadas con compuestos orgánicos son muy diversas. De manera general, los tratamientos convencionales de residuos en agua que se usan con más frecuencia se pueden clasificar en tres grandes grupos, tratamientos físicos, químicos y biológicos.

Los *métodos físicos* no generan sustancias nuevas, sino que concentran los contaminantes al evaporar el agua o separar los sólidos de tamaño considerable, como sucede en la coagulación/floculación (Di Bella y col., 2014; Lau y col., 2014), la sedimentación o decantación (Allegre y col., 2004), los procesos de membrana (Mo y

col., 2008) o la adsorción sobre carbón activo (Amin, 2008; Ghaedi y col., 2012). Estos métodos consiguen separar los contaminantes del agua, transfiriendo el problema sin promover su degradación. Los métodos más utilizados son:

(i) los procesos de adsorción, que consisten en la captación de sustancias solubles sobre la superficie de un sólido como por ejemplo carbón activo (Amin, 2008; Ghaedi y col., 2012), zeolitas (Liu y col., 2014) o resinas (Huang y col., 2013). El área superficial del sólido es un parámetro fundamental en este tratamiento, dado que el compuesto soluble a eliminar se ha de concentrar en la superficie del mismo,

(ii) la coagulación/flotación. La coagulación consiste en la desestabilización química de las partículas coloidales que se produce al neutralizar las fuerzas que las mantienen separadas por medio de la adición de los coagulantes químicos. Los coagulantes comúnmente utilizados son los inorgánicos (sulfato de aluminio o hierro, cloruro férrico, aluminato de sodio), polímeros catiónicos o polielectrolitos. La floculación consiste básicamente en la aglomeración de los coloides mediante la atracción o aglutinamiento de las partículas que se logra por la presencia de sustancias conocidas como floculantes. Los procesos de coagulación/floculación han sido ampliamente utilizados para decolorar aguas residuales (Moghaddam y col., 2010; Verma y col., 2012), y

(iii) la sedimentación, que consiste en aprovechar la fuerza de la gravedad que hace que una partícula más densa que el agua tenga una trayectoria descendente, depositándose en el fondo del sedimentador. Esta operación es más eficaz cuanto mayor sea el tamaño y la densidad de las partículas a separar del agua, es decir, cuanto mayor sea su velocidad de sedimentación, siendo el principal parámetro de diseño para estos equipos. A esta operación de sedimentación se le suele denominar también decantación.

Los *métodos químicos* se aplican generalmente para el tratamiento de compuestos orgánicos peligrosos presentes en bajas concentraciones, y en muchas ocasiones sirven como pretratamiento antes de los procesos biológicos, con el objetivo de reducir la carga de contaminantes. Se basan en la oxidación de los compuestos orgánicos mediante oxidantes químicos como cloro (Osugi y col., 2009), permanganato de potasio (Sorlini y Gialdini, 2010), peróxido de hidrógeno (Ksibi, 2006) y ozono (Szpyrkowicz y col., 2001; Skoumal y col., 2006), entre otros. Los reactivos más utilizados para este tipo de tratamiento son el peróxido de hidrogeno y el cloro. En los procesos químicos hay que considerar que el uso de oxidantes puede derivar en una contaminación secundaria, ya

que durante el proceso se pueden obtener productos de oxidación de elevada toxicidad como en el caso de organoclorados (Zhang y col., 2013), o subproductos de la reacción que deben ser eliminados de las aguas antes de poder verterlas al medio, como por ejemplo MnO_2 (Crimi y Ko, 2009), lo que encarece el tratamiento sobre todo si lo comparamos con los procesos biológicos.

Los *métodos biológicos* consisten en la degradación de los compuestos orgánicos presentes en el efluente por parte de microorganismos que se alimentan de la materia orgánica disuelta. En el caso de los colorantes, la decoloración puede darse a través de biosorción, degradación enzimática o una combinación de ambos (Solís y col., 2012). La mayoría de los colorantes son muy estables y, por tanto, poco biodegradables (Sobana y Swaminathan, 2007; Daneshvar y col., 2008; Martínez-Huitle y Brillas, 2009). Sin embargo, varios estudios han demostrado la biodegradación parcial o total de algunos colorantes por vía biológica (Martins y col., 2003; Yasar y col., 2012). Si bien los métodos biológicos son adecuados para tratar un gran número de contaminantes orgánicos, no son siempre aplicables a los efluentes industriales, debido a la alta variedad y/o concentración de contaminantes presentes y la excesiva toxicidad de algunos compuestos que pueden matar a los microorganismos, lo que comporta una baja biodegradabilidad del volumen a tratar. En los efluentes residuales, la biodegradación es favorable cuando la relación entre la demanda química de oxígeno (DQO) y la demanda bioquímica de oxígeno a los cinco días (DBO_5), es decir el factor DQO/DBO_5, es menor que 0,5, mientras que es muy limitada cuando la relación excede 0,5 (Fernandes y col., 2014; Renou y col., 2008). Cabe destacar que estos métodos generan grandes cantidades de lodos orgánicos, los cuales deben ser reciclados. Los métodos biológicos más utilizados pueden agruparse en dos grandes grupos, los procesos aerobios y anaerobios. En el primer caso, los dispositivos de aireación permiten a las bacterias incrementar su metabolismo y, en consecuencia, su acción, puesto que la digestión aerobia es un proceso que ocurre en presencia del oxígeno. Bajo condiciones aeróbicas, las bacterias consumen rápidamente la materia orgánica y la convierten en dióxido de carbono. Por su parte, la digestión anaerobia es el proceso en que los microorganismos descomponen material biodegradable en ausencia de oxígeno, generando diversos gases entre los cuales se encuentran principalmente el dióxido de carbono y el metano dependiendo del material degradado. En biodigestores se aprovecha esta liberación de gases para luego ser usados como combustible.

Sin embargo, el uso de los métodos convencionales no está completamente aceptado en la actualidad debido a que suelen resultar bastante caros y conllevan problemas operacionales (Robinson y col., 2001; Forgacs y col., 2004). Además, no son muy eficientes para el tratamiento de contaminantes persistente en agua, como en el caso de los colorantes, ya que muchos de estos compuestos tienen estructuras complejas y, por tanto, se caracterizan por una alta estabilidad que dificulta su degradación completa o al menos profunda. El problema de la contaminación resultante de varios de los métodos es también una desventaja importante. Por ello, es necesario adoptar sistemas más modernos como por ejemplo los procesos de oxidación avanzada (AOPs).

1.3.2. Procesos de oxidación avanzada (AOPs)

Los AOPs constituyen una alternativa muy interesante a los tratamientos convencionales. Se definen como aquellos procesos de oxidación que implican la generación de especies de "oxígeno activo" (ROS), principalmente el radical hidroxilo ($^{\bullet}$OH), en cantidad suficiente como para interactuar con los compuestos orgánicos (Garrido y col., 2007; Brillas y col., 2009; Rivera-Utrilla y col., 2013). Se trata de una familia de métodos que utilizan la extraordinaria capacidad oxidante de los radicales $^{\bullet}$OH, y que se diferencian entre sí en la forma en la que éstos se generan. En este sentido, los AOPs pueden clasificarse en dos grandes bloques, los procesos homogéneos y los procesos heterogéneos, distinguiéndose a su vez entre los que operan con un aporte externo de energía (energía radiante, energía ultrasónica (US), energía eléctrica) y los que no lo emplean.

Los radicales hidroxilo resultan óptimos dentro del grupo de oxidantes potentes porque satisfacen una serie de exigencias:

- No generan residuos adicionales.
- No son tóxicos y tienen un tiempo de vida muy corto.
- No son corrosivos para los equipos.
- Generalmente se producen mediante montajes que son simples de manipular.

Según estas consideraciones, los AOPs son tecnologías compatibles con el medio ambiente, y en base a ellos se vienen desarrollando procesos competitivos desde un punto de vista económico. La viabilidad de los AOPs depende de la eficacia del radical $^{\bullet}$OH, que es la segunda especie conocida con mayor poder oxidante (E^{o} = 2,80 V vs. SHE), después del flúor (Guinea y col., 2008; Brillas y col., 2009) (**Tabla 1)**.

Tabla 1. Potenciales de reducción estándar en medio acuoso de los agentes oxidantes más utilizados para la destrucción de contaminantes orgánicos (Brillas y col., 2009).

Oxidante	Reacción de reducción	$E°$ / V vs SHE
Flúor	$F_{2(g)} + 2H^+ + 2e^- \rightarrow 2HF$	3,05
	$F_{2(g)} + 2e^- \rightarrow 2F$	2,87
Radical hidroxilo	$^{\bullet}OH + H^+ + e^- \rightarrow H_2O$	2,80
Anión radical sulfato	$SO_4^{\bullet -} + e^- \rightarrow SO_4^{2-}$	2,60
Ion ferrato	$FeO_4^{2-} + 8H^+ + 3e^- \rightarrow Fe^{3+} + 4H_2O$	2,20
Ozono	$O_{3(g)} + 2H^+ + 2e^- \rightarrow O_{2(g)} + H_2O$	2,08
Ion peroxodisulfato	$S_2O_8^{2-} + 2e^- \rightarrow 2SO_4^{2-}$	2,01
Peróxido de hidrógeno	$H_2O_2 + 2H^+ + 2e^- \rightarrow 2H_2O$	1,76
Ion permanganato (a)	$MnO_4^- + 4H^+ + 3e^- \rightarrow MnO_{2(s)} + 2H_2O$	1,67
Ion hidroperoxilo (a)	$HO_2^{\bullet} + 3H^+ + 3e^- \rightarrow 2H_2O$	1,65
Ion permanganato (b)	$MnO_4^- + 8H^+ + 5e^- \rightarrow Mn^{2+} + 4H_2O$	1,51
Ion hidroperoxilo (b)	$HO_2^{\bullet} + H^+ + e^- \rightarrow H_2O_2$	1,44
Ion dicromato	$Cr_2O_7^{2-} + 14H^+ + 6e^- \rightarrow 2Cr^{3+} + 7H_2O$	1,36
Cloro	$Cl_2(g) + 2e^- \rightarrow 2Cl^-$	1,36
Dióxido de manganeso	$MnO_2 + 4H^+ + 2e^- \rightarrow Mn^{2+} + 2H_2O$	1,23
Oxígeno	$O_{2(g)} + 4H^+ + 4e^- \rightarrow 2H_2O$	1,23
Bromo	$Br_{2(l)} + 2e^- \rightarrow 2Br^-$	1,07

El radical $^{\bullet}OH$ actúa de manera no selectiva sobre los contaminantes orgánicos y organometálicos en medio acuoso, resultando muy efectivo para transformarlos y conducir en muchos casos a su mineralización completa a CO_2, agua e iones inorgánicos (Pera-Titus y col., 2004; Martínez-Huitle y Ferro, 2006; Serra y col., 2009, Feng y col.,

2013; Sirés y col., 2014). El radical $^{\bullet}OH$ es una especie altamente reactiva, y por tanto no se acumula en el medio, pero es capaz de reaccionar eficientemente con contaminantes orgánicos que resultan refractarios ante la acción de otros oxidantes, dando lugar a constantes de velocidad del orden de 10^6-10^{10} M^{-1} s^{-1} (Andreozzi y col., 1999; Bokare y Choi, 2014).

Los radicales hidroxilo pueden degradar los compuestos orgánicos u organometálicos mediante tres mecanismos de degradación, dependiendo de la naturaleza del compuesto:

(i) Deshidrogenación o abstracción de un átomo de hidrógeno para formar agua, si el substrato posee enlaces C-H (alcanos), y radical $R^{\bullet}$ que en presencia de oxígeno molecular puede dar el radical peroxilo $ROO^{\bullet}$ e iniciar así una secuencia oxidativa que puede conducir a la mineralización (reacciones (1)-(3)),

(ii) Hidroxilación del compuesto orgánico por ataque del $^{\bullet}OH$ en los sitios de alta densidad electrónica, adicionándose a los enlaces insaturados de compuestos aromáticos o alifáticos e iniciando una cadena de reacciones de oxidación (reacciones (4)-(6)), y

(iii) Transferencia de carga por oxidación-reducción, causando la ionización de la molécula (reacción 7).

$$RH + {}^{\bullet}OH \rightarrow H_2O + R^{\bullet} \quad (1)$$

$$R^{\bullet} + O_2 \rightarrow ROO^{\bullet} \quad (2)$$

$$ROO^{\bullet} + n({}^{\bullet}OH/O_2) \rightarrow xCO_2 + yH_2O \quad (3)$$

$$ArH + {}^{\bullet}OH \rightarrow ArH(OH)^{\bullet} \quad (4)$$

$$ArH(OH)^{\bullet} + O_2 \rightarrow [ArH(OH)OO]^{\bullet} \quad (5)$$

$$[ArH(OH)OO]^{\bullet} \rightarrow ArH(OH) + HO_2^{\bullet} \quad (6)$$

$$^{\bullet}OH + RX \rightarrow RX^{\bullet+} + OH^{-} \quad (7)$$

Los mecanismos radicalarios son complejos, de manera que la oxidación de la materia orgánica por los radicales $^{\bullet}OH$ implica varios tipos de especies y reacciones:

- Reacciones de iniciación durante las cuales se forman especies radicalarias $R^{\bullet}$ (reacción (1)).
- Reacciones de propagación que implican especies radicalarias $R^{\bullet}$ que reaccionan con otras moléculas orgánicas neutras (reacción (8)) o con el oxígeno disuelto en la solución (reacción (2)).

$$R^{\bullet} + R'H \rightarrow RH + R'^{\bullet} \quad (8)$$

- Reacciones de terminación donde los radicales se combinan entre ellos (reacciones (9)-(11)).

$$R^{\bullet} + R^{\bullet} \rightarrow R\text{-}R \quad (9)$$

$$R^{\bullet} + {}^{\bullet}OH \rightarrow R\text{-}OH \quad (10)$$

$${}^{\bullet}OH + {}^{\bullet}OH \rightarrow H_2O_2 \quad (11)$$

La mayoría de las reacciones y de las variables que gobiernan la reactividad en los AOPs son similares, aunque es importante comprender las diferencias fundamentales que existen entre los principales métodos, puesto que éstas afectan a la eficacia del tratamiento y los costes económicos. Por su sencillez, alta efectividad y bajo coste, los procesos Fenton y foto-Fenton son considerados como unos de los más prometedores en la remediación de aguas contaminadas con compuestos tóxicos y/o no biodegradables, especialmente en el caso de efluentes ácidos (Poyatos y col., 2010).

El proceso Fenton y foto-Fenton

En el proceso Fenton, los radicales hidroxilo se forman al combinar el peróxido de hidrógeno con un sal metálica, normalmente de hierro Fe^{2+}, que actúa como catalizador en medio ácido para evitar la precipitación del hierro. Dicha reacción se conoce como reacción de Fenton (reacción (12)) (Sun y Pignatello, 1993; Boye y col., 2002, Guinea y col., 2008). Alternativamente pueden utilizarse otros catalizadores como Cu^{2+}, Mn^{2+}, Ti^{3+} o Sn^{2+}.

$$Fe^{2+} + H_2O_2 + H^{+} \rightarrow Fe^{3+} + {}^{\bullet}OH + H_2O \quad (12)$$

La eficiencia de la reacción de Fenton depende en gran medida de la capacidad para regenerar el Fe^{2+} a partir de las especies de Fe^{3+}. La reacción más importante en este sentido es la del Fe^{3+} con el H_2O_2 para dar Fe^{2+} (reacción (13)), llamada reacción *Fenton-like*, y con el radical hidroperoxilo, de menor poder oxidante que el radical hidroxilo (reacción (14)). También puede ser regenerado por la reacción entre el Fe^{3+} y el ion superóxido (reacción (15)). Cabe señalar que mientras que la constante de velocidad de la reacción (12) varía entre 63 y 76 M^{-1} s^{-1}, la constante de la reacción (13) es del orden de 0,01-0,02 M^{-1} s^{-1} (Basturk y Karatas, 2014). Esto indica que el consumo

de iones ferroso es más rápido que su regeneración, con lo cual el poder oxidante del método se ve afectado a lo largo del tratamiento.

$$H_2O_2 + Fe^{3+} \rightarrow Fe^{2+} + HO_2^{\bullet} + H^+ \quad (13)$$

$$Fe^{3+} + HO_2^{\bullet} \rightarrow Fe^{2+} + O_2 + H^+ \quad (14)$$

$$Fe^{3+} + O_2^{\bullet -} \rightarrow Fe^{2+} + O_2 \quad (15)$$

En ausencia de un substrato orgánico, el radical hidroxilo oxida los reactantes de la reacción de Fenton (reacciones (16) y (17)). Éstas son las principales reacciones parásitas causantes de la destrucción de $^{\bullet}OH$ en eventos no deseados. Este radical puede ser regenerado lentamente por algunas reacciones simultáneas (reacciones (18) y (19)).

$$^{\bullet}OH + Fe^{2+} \rightarrow Fe^{3+} + OH^- \quad (16)$$

$$^{\bullet}OH + H_2O_2 \rightarrow H_2O + HO_2^{\bullet} \quad (17)$$

$$HO_2^{\bullet} + H_2O_2 \rightarrow {}^{\bullet}OH + H_2O + O_2 \quad (18)$$

$$HO_2^{\bullet} + HO_2^- \rightarrow {}^{\bullet}OH + OH^- + O_2 \quad (19)$$

En presencia de materia orgánica (RH), el radical hidroxilo la oxida, por ejemplo deshidrogenándola para dar $R^{\bullet}$ (reacción (1)). A su vez, el radical $R^{\bullet}$ puede regenerar el Fe^{2+} a partir del Fe^{3+} produciendo el catión R^+ (reacción (20)), el cual puede dar lugar a un derivado hidroxilado (reacción (21)). Alternativamente, el radical $R^{\bullet}$ puede promover una reacción parásita de oxidación del Fe^{2+} (reacción (22)).

$$R^{\bullet} + Fe^{3+} \rightarrow R^+ + Fe^{2+} \quad (20)$$

$$R^+ + H_2O \rightarrow ROH + H^+ \quad (21)$$

$$R^{\bullet} + Fe^{2+} \rightarrow R^- + Fe^{3+} \quad (22)$$

La efectividad y eficiencia del proceso Fenton dependen de muchos factores, incluyendo el pH, la temperatura y las concentraciones de H_2O_2 y de catalizador. La capacidad catalítica de la especies de hierro queda fundamentalmente determinada por el pH. Así, a pH 2,8-3,0, la concentración de Fe^{2+} libre en el medio de reacción es máxima, lo que da lugar a la mayor velocidad de la reacción de Fenton. Por el contrario, a pH > 5, el hierro se encuentra en gran parte en forma de hidróxidos y oxihidróxidos, disminuyendo de este modo la concentración de catalizador disuelto en la solución. En tales condiciones tiene lugar un proceso de Fenton heterogéneo, menos efectivo que el

homogéneo, implicando la reacción superficial del H_2O_2 sobre las partículas de hierro. Por lo tanto, se requiere un control estricto del pH para operar siempre en un medio de acidez óptima. Por otra parte, un aumento de la temperatura mejora la cinética de reacción, si bien también favorece la descomposición del H_2O_2 a O_2 y H_2O, así que es conveniente trabajar a temperatura controlada. En cuanto a la concentración de los dos componentes del reactivo de Fenton, su efecto está estrechamente vinculado, siendo negativo el exceso de ellos porque pueden convertirse en trampas para los radicales $^{\bullet}OH$ (reacciones (16) y (17)). En general, los experimentos se realizan sobre la base de la optimización de la relación $[Fe^{2+}]/[H_2O_2]$, que es un factor clave por lo que se refiere a la eficiencia del proceso.

La gran capacidad oxidativa del reactivo de Fenton se ha confirmado con muchos compuestos orgánicos, como el fenol (Shimizu y col., 2012), varios clorofenoles (Vallejo y col., 2014), colorantes azoicos (Ramirez y col., 2007; Sun y col., 2009) o herbicidas (Oturan y col., 2011a). Los procesos de deshidrogenación, hidroxilación y transferencia electrónica, como se ha indicado anteriormente, prosiguen hasta transformar los contaminantes orgánicos en compuestos más pequeños. Algunos de estos intermedios pueden convertirse en CO_2, H_2O e iones inorgánicos. Sin embargo, pueden formarse también complejos con el Fe(III), como ocurre en el caso de los ácidos carboxílicos lineales de cadena corta (Nakagawa y Yamaguchi, 2012). Algunos de estos complejos son muy estables frente al radical hidroxilo, lo que disminuye la eficiencia del proceso Fenton (Oturan y col., 2008).

Según algunos estudios (Sirés y col., 2006; Iurascu y col., 2009; Minella y col., 2014), la irradiación con luz de longitud de onda entre 320 y 480 nm permite mejorar considerablemente el porcentaje de mineralización. La combinación entre la luz y el reactivo de Fenton se define como proceso foto-Fenton. En condiciones óptimas de pH (2,8-3,0), los iones Fe^{3+} se encuentran en forma de $[Fe(OH)]^{2+}$. Por tanto, la mejoría resulta de la fotorreducción del ion $Fe(OH)^{2+}$ por la reacción (23), lo que induce la regeneración del ion Fe^{2+} junto con la producción de más radical hidroxilo (Hernández-Rodríguez y col., 2014).

$$[Fe(OH)]^{2+} + h\nu \rightarrow Fe^{2+} + {}^{\bullet}OH \qquad (23)$$

La luz UVA de λ_{max} = 360 nm también puede inducir la fotodegradación de algunos subproductos de oxidación y/o de sus complejos de Fe(III). Este es el caso de la

fotodescarboxilación de especies de Fe(III)-carboxilato mediante la reacción (24) tales como los complejos de Fe(III)-oxalato, que promueven la regeneración de Fe^{2+} (Brillas y col., 2003b; Flox y col., 2007).

$$Fe(OOCR)^{2+} + h\nu \rightarrow Fe^{2+} + CO_2 + R^{\bullet} \quad (24)$$

Alternativamente, cuando se irradia con luz a 254 nm (luz UVC), se produce la fotólisis directa de disoluciones ácidas que contienen peróxido de hidrógeno para generar el radical $^{\bullet}OH$ a través de su ruptura homolítica:

$$H_2O_2 + h\nu \rightarrow 2^{\bullet}OH \quad (25)$$

Estos AOPs se han aplicado en el tratamiento de aguas con contaminantes orgánicos, incluyendo colorantes azoicos, si bien presentan algunas limitaciones, pues es difícil conseguir la mineralización completa de las disoluciones, existen riesgos relacionados con el suministro, almacenamiento y transporte de H_2O_2, se requieren dosis elevadas de Fe^{2+} y H_2O_2, surge una acumulación significativa de lodos que deben gestionarse al final de tratamiento y, en general, presentan un elevado coste debido a los reactantes. Estos métodos resultan muy eficientes para tratar disoluciones con DQO < 1000 mg L^{-1}, aunque muy a menudo se utilizan como tratamientos terciarios para ajustar los límites de vertido de ciertos compuestos orgánicos no biodegradables a los marcados por la legislación.

La generación de radicales hidroxilo puede regularse de un modo más controlado, efectivo y eficiente por medio de los métodos electroquímicos, que son métodos emergentes de gran alcance para el tratamiento de aguas residuales. El presente trabajo se centra en la aplicación de tecnologías electroquímicas, tanto convencionales como avanzadas, para degradar más eficazmente varios colorantes alimentarios azoicos.

1.4. Los procesos electroquímicos

Muchos grupos de investigación de todo el mundo han estado y siguen involucrados en el estudio del potencial de la electroquímica ambiental como generadora de nuevas herramientas para la preservación de los recursos hídricos y el medio ambiente. De estos grupos de investigación, los principales contribuyentes en la parte teórica y práctica son los grupos de E. Brillas (Brillas y col., 2004, 2009; Martínez-Huitle y Brillas 2009; Sirés y Brillas, 2012), M.A. Oturan, (Oturan y Pinson, 1995; Oturan, 2000; Oturan y col., 2000, 2008), Ch. Comninellis (Pulgarin y col., 1994;

Comninellis y De Battisti, 1996; Perret y col., 1999), M. Panizza (Panizza y col., 2000, 2001; Panizza y Cerisola, 2009a, 2010a, 2010b), M.A. Rodrigo (Cañizares y col., 2002, 2004, 2005; Rodrigo y col., 2010), A.M. Polcaro (Polcaro y col., 2000, 2005), A. De Battisti (Bonfatti y col., 2000; De Battisti y col., 2001; Ferro y De Battisti, 2002; Martínez-Huitle y col., 2004), O. Scialdone (Scialdone y col., 2008, 2009; Randazzo y col., 2011) y C.A. Martínez-Huitle (Martínez-Huitle y col., 2004; Martínez-Huitle y Ferro, 2006). En los últimos años, estos grupos han propuesto y desarrollado una gran variedad de métodos electroquímicos para la eliminación de contaminantes orgánicos tóxicos y no biodegradables de diversas matrices acuosas. De entre estas tecnologías electroquímicas se pueden destacar dos tipos:

(i) las clásicas, de mayor aplicación industrial, como son las de separación de fase (electrocoagulación, electrofloculación y electroflotación) utilizadas para depurar efluentes que contienen partículas coloidales orgánicas procedentes de refinerías e industrias de tintes, pinturas, textil, alimentación, etc., y

(ii) los procesos electroquímicos de oxidación avanzada (EAOPs), que ofrecen una serie de ventajas como son una alta eficiencia energética y seguridad de manejo, ya que se trabaja a temperatura y presión ambiental, una gran versatilidad, debido a que pueden aplicarse a sólidos, líquidos o gases con una DQO entre 0,1 a 100 g L^{-1} (Sirés y col., 2014), y una interesante adaptabilidad que deriva del diseño modular de los reactores electroquímicos. Los EAOPs son compatibles con el medio ambiente, evitándose normalmente tanto la adición de productos químicos nocivos, hecho que elimina los riegos asociados a su manipulación, transporte y almacenamiento, como la extracción de residuos secundarios al final del tratamiento. En estas técnicas el reactivo principal es el electrón, que es barato y limpio siempre y cuando la corriente eléctrica provenga de una fuente de energía renovable, por lo que su potencial interés industrial es enorme.

Con el objetivo de incrementar la viabilidad de las tecnologías electroquímicas de tratamiento de aguas, promoviendo una mayor aceptación por parte de la industria, en esta Tesis Doctoral se han desarrollado *nuevos sistemas electroquímicos integrados* donde se aprovechan las mejoras capacidades de cada técnica acoplada. En concreto, se ha estudiado la degradación de colorantes utilizando la electrocoagulación (uno de las pocos métodos electroquímicos de aplicación en la industria) como pretratamiento y los EAOPs como post-tratamiento, aprovechando el máximo rendimiento de cada uno, minimizando así el tiempo de tratamiento y el consumo eléctrico, lo que revierte en un

menor coste. La eficiencia de las tecnologías acopladas es susceptible de ser superior a la de los métodos individuales debido a su acción sinérgica.

1.4.1. Procesos electroquímicos de oxidación avanzada (EAOPs)

Como se ha expuesto anteriormente, los EAOPs proporcionan varias ventajas para la prevención y resolución de los problemas de contaminación de las aguas. En comparación con otros AOPs como por ejemplo la fotocatálisis heterogénea, el Fenton químico, los métodos basados en O_3 o H_2O_2 o los procesos a alta presión y temperatura, estos procesos constituyen una de las formas más limpias, eficaces y baratas para producir in situ el radical $^{\bullet}OH$, dado que no requieren la adición de productos químicos caros y/o peligrosos y no suelen generar residuos secundarios. Los EAOPs estudiados en este trabajo pueden ser clasificado en directos (electrooxidación (EO)) e indirectos (electro-Fenton (EF), fotoelectro-Fenton UV (PEF) y fotoelectro-Fenton solar (SPEF)).

1.4.1.1. Electrooxidación

La EO, también llamada oxidación anódica o incineración electroquímica, es sin duda el EAOP más popular para la eliminación de contaminantes orgánicos contenidos en aguas residuales (Martínez-Huitle y Ferro, 2006; Vahid y Khataee, 2013). Se basa en el uso de ánodos de elevado sobrepotencial de evolución de oxígeno, los cuales favorecen la electrogeneración de radical hidroxilo adsorbido en su superficie ($^{\bullet}OH_{(ads)}$) a partir de la oxidación de agua. Como es bien sabido, a potenciales suficientemente anódicos tiene lugar la oxidación del agua según la siguiente reacción:

$$2H_2O \rightarrow O_2 + 4H^+ + 4e^- \quad (26)$$

Se han propuesto diferentes mecanismos para explicar la producción electroquímica de oxígeno. En todos ellos, la primera etapa implica una transferencia monoelectrónica y la adsorción de un radical $^{\bullet}OH$ en un sitio activo del ánodo (M). Si la reacción se lleva a cabo en medio ácido se puede escribir como:

$$M + H_2O \rightarrow M(^{\bullet}OH)_{ads} + H^+ + e^- \quad (27)$$

Las siguientes etapas del mecanismo dependen de la naturaleza del ánodo utilizado y de su afinidad por el especie adsorbida ($M(^{\bullet}OH)_{ads}$). Se pueden distinguir dos tipos de mecanismos, los cuales están asociados a dos tipos de ROS:

(i) En los ánodos "activos", el radical se encuentra quimisorbido, es decir, fuertemente adsorbido sobre la superficie de M, llegándose a producir la oxidación de éste para dar un óxido metálico MO:

$$M(^{\bullet}OH)_{ads} \rightarrow MO + H^{+} + e^{-} \quad (28)$$

La evolución del oxígeno se produce por la reducción del sitio electroactivo oxidado al estado inicial:

$$MO \rightarrow M + \tfrac{1}{2}O_2 \quad (29)$$

(ii) En los ánodos "no activos", el radical se encuentra fisisorbido, es decir, débilmente adsorbido en un sitio electroactivo de M, con lo cual a continuación se da la oxidación electroquímica del mismo para dar oxígeno:

$$M(^{\bullet}OH)_{ads} \rightarrow M + \tfrac{1}{2}O_2 + H^{+} + e^{-} \quad (30)$$

En referencia a la degradación de los contaminantes orgánicos en medio acuoso se han planteado dos estrategias, dependiendo del tipo de ánodo empleado (Marselli y col., 2003; Panizza y Cerisola, 2009b):

- La conversión electroquímica, donde los compuestos orgánicos son transformados selectivamente en compuestos más sencillos y más biodegradables, generalmente ácidos carboxílicos.
- La combustión electroquímica, en que los compuestos orgánicos son totalmente mineralizados, es decir, transformados en CO_2, H_2O e iones inorgánicos.

Estas dos estrategias se basan en los dos mecanismos anteriormente citados. En concreto, Comninellis (1994) propuso un modelo integral para la destrucción de compuestos orgánicos en medio ácido. Según este modelo, los ánodos "activos", que promueven la reacción electroquímica de evolución de oxígeno, favorecen la conversión electroquímica de la materia orgánica, mientras que los "no activos", que son menos electrocatalíticos para la evolución de oxígeno, requiriendo mayores sobrepotenciales anódicos, favorecen la combustión electroquímica de la materia orgánica. En ambos casos, la primera etapa del proceso corresponde a la formación de radical hidroxilo adsorbido (reacción (27)), el cual puede existir como tal sobre ánodos "no activos" pero es transformado fácilmente a MO (reacción (28)) en ánodos "activos". Esto supone la existencia de dos tipos de ROS en la superficie del ánodo, $M(^{\bullet}OH)_{ads}$ y MO, que pueden transformar la materia orgánica de diferente manera.

En ausencia de contaminantes orgánicos, ambas especies producen oxígeno por las reacciones (29) y (30). En cambio, en presencia de un contaminante orgánico (R), el radical fisisorbido provoca su combustión completa mediante la reacción (31), mientras que el oxígeno quimisorbido participa a la formación de compuestos parcialmente oxidados RO por la reacción (32):

$$R + M(^{\bullet}OH)_{ads} \rightarrow M + mCO_2 + nH_2O + H^+ + e^- \quad (31)$$

$$R + MO \rightarrow M + RO \quad (32)$$

Los ánodos que favorecen la conversión electroquímica presentan una concentración de $M(^{\bullet}OH)_{ads}$ próxima a cero, lo cual ocurre cuando la reacción (28) es mucho más rápida que la reacción (27). La combustión electroquímica, por el contrario, tiene lugar en ánodos con una elevada concentración superficial de radicales hidroxilo al ser insignificante la velocidad de la reacción (28). En estos materiales, de manera similar a lo explicado para los AOPs a través de las reacciones (1)-(6), la acción de $M(^{\bullet}OH)_{ads}$ comporta la hidroxilación (reacción (33)) o la deshidrogenación (reacción (34)) de los compuestos orgánicos R o R'H, respectivamente. En este último caso, el O_2 puede reaccionar con el radical orgánico $R'^{\bullet}$ resultante dando lugar al radical peroxilo $R'OO^{\bullet}$ por la reacción (35), el cual es suficientemente activo como para abstraer un átomo de hidrógeno de otro contaminante R"H por la reacción (36). Los hidroperóxidos R'OOH obtenidos son inestables y se fragmentan gradualmente para dar otros intermedios.

$$R + M(^{\bullet}OH) \rightarrow ROH^{\bullet} + M \quad (33)$$

$$R'H + M(^{\bullet}OH) \rightarrow R'^{\bullet} + M + H_2O \quad (34)$$

$$R'^{\bullet} + O_2 \rightarrow R'OO^{\bullet} \quad (35)$$

$$R'OO^{\bullet} + R"H \rightarrow R'OOH + R"^{\bullet} \quad (36)$$

Las reacciones de escisión continúan hasta producir la combustión total. La relativamente elevada concentración de radicales $^{\bullet}OH$ en las inmediaciones de un ánodo "no activo" en condición de polarización es la principal razón por la que los electrodos de diamante dopado con boro (BDD), PbO_2 y SnO_2 son más adecuados para la mineralización de compuestos orgánicos mediante EO (Flox y col., 2005; Sirés y col., 2008, 2010; Hmani y col., 2012). Estos electrodos presentan una capacidad muy superior para lograr la oxidación total de compuestos orgánicos en comparación con los

ánodos carbonosos, ánodos de patino (Pt) o ánodos dimensionalmente estables (DSA) de RuO_2 o IrO_2 (Sirés y col., 2008; Hamza y col., 2009). Dado que el agua no se oxida sobre los ánodos "no activos" hasta llegar a un potencial de ~ 2 V vs. SHE, existe una amplia ventana de potenciales de electrodo disponible para las reacciones de transferencia directa de electrones. Se ha demostrado que estas reacciones constituyen un mecanismo adicional para la oxidación de los compuestos orgánicos, donde un electrón es transferido directamente desde el contaminante (R) hacia el ánodo:

$$R \rightarrow (R^{\bullet})^{+} + e^{-} \quad (37)$$

En la práctica, todos los ánodos exhiben un comportamiento mixto, ya que ambos mecanismos tienen lugar simultáneamente. Los ánodos "no activos" pueden presentar defectos en su superficie o sitios parcialmente oxidados, mientras que en el caso de los electrodos "activos" no se puede excluir la formación de radicales fisisorbidos a potenciales muy positivos, aunque la superficie sea altamente reactiva. Cabe mencionar que, como regla general, cuanto menos positivo es el potencial al que se produce la evolución de oxígeno, mayor es la participación de la superficie del ánodo en la reacción.

Cabe señalar que los electrodos "no activos" resultan muy adecuados para la producción electroquímica de otras especies oxidantes menos potentes que los radicales $^{\bullet}OH$, como el ozono y el peróxido de hidrógeno mediante las reacciones (38) y (39), respectivamente, gracias al elevado sobrepotencial de evolución de oxígeno de estos materiales, o a la recombinación de los radicales hidroxilo por la reacción (40) (Panizza y Cerisola, 2005; Flox y col., 2006b; Kapalka y col., 2009; Borràs y col., 2010; Sirés y Brillas, 2012):

$$3H_2O \rightarrow O_3 + 6H^{+} + 6e^{-} \quad (38)$$

$$2H_2O \rightarrow H_2O_2 + 2H^{+} + 2e^{-} \quad (39)$$

$$2^{\bullet}OH \rightarrow H_2O_2 \quad (40)$$

En la **Figura 5** se muestra el esquema de reacción generalizado para la oxidación de un compuesto orgánico R y la formación electroquímica de oxígeno simultánea, para los dos tipos de ánodos propuestos.

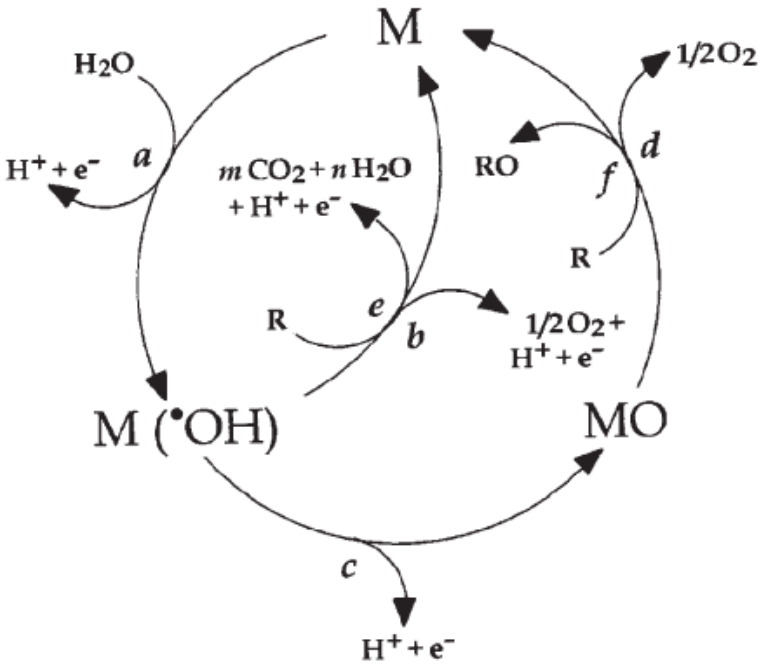

Figura 5. Esquema de oxidación de un compuesto orgánico R simultánea a la producción electroquímica de oxígeno sobre un ánodo (M): (a) formación de radicales •OH adsorbidos, (b) producción de oxígeno por oxidación electroquímica de especies •OH, (c) formación de un sitio con estado de oxidación superior por oxidación electroquímica del radical •OH, (d) producción de oxígeno por descomposición química del sitio con estado de oxidación superior, (e) combustión del compuesto orgánico R por radicales •OH fisisorbidos y (f) oxidación química del compuesto orgánico en un sitio con estado de oxidación superior (Marselli y col., 2003).

El uso reciente del BDD en la EO ha aumentado considerablemente el interés por la aplicación de este método en el tratamiento de aguas, pues los compuestos orgánicos son mineralizados completamente por los radicales BDD($^{\bullet}OH)_{ads}$. Hay que destacar que este ánodo exhibe buena estabilidad química y electroquímica, una superficie inerte con propiedades de baja adsorción, larga vida y una amplia ventana de potencial para la descarga del agua (Iniesta y col., 2001; Hupert y col., 2003), y por lo tanto, resulta ser un electrodo prometedor para el tratamiento de descontaminación, si bien su elevado precio resulta algo prohibitivo actualmente para su escalado industrial. Se ha demostrado que muchos compuestos biorecalcitrantes incluidos fenoles, clorofenoles, nitrofenoles, pesticidas, colorantes sintéticos, fármacos y lixiviados industriales pueden ser mineralizados completamente con alta eficiencia de corriente, incluso cercana al 100%, utilizando ánodo de BDD (Boye y col., 2006; Cañizares y col., 2006; Oturan y col., 2011b; El-Ghenymy y col., 2012, Cavalcanti y col., 2013; Rabaaoui y col., 2013a, 2013b; Sales Solano y col., 2013).

La composición del electrolito soporte o los diferentes iones presentes en las aguas reales industriales pueden variar la efectividad del proceso EO. Durante las electrolisis con ánodos de BDD, de manera simultánea a la generación de radicales hidroxilo (reacción (27)), así como de O_3 y H_2O_2 (reacciones (38)-(40)), tienen lugar numerosas reacciones que pueden dar lugar a otros oxidantes en función de los iones presentes en el volumen tratado. En medio sulfato se puede producir la oxidación de los iones sulfato a peroxodisulfato (Flox y col., 2006b; Oturan y col., 2011b):

$$2SO_4^{2-} \rightarrow S_2O_8^{2-} + 2e^- \quad (41)$$

Se encuentra un comportamiento muy particular cuando la disolución contiene iones cloruro, ya que se produce la electrogeneración de cloro activo en forma de cloro gas, ácido hipocloroso o ion hipoclorito mediante los reacciones (42)-(44). En estas condiciones, la materia orgánica puede ser atacada competitivamente por los radicales $^{\bullet}OH$ producidos en la superficie del ánodo y el cloro activo producido y difundido hacia el seno de la disolución. Como contrapunto, puede darse la formación de intermedios organoclorados, los cuales pueden ser incluso más recalcitrantes y más tóxicos que los contaminantes iniciales.

$$2Cl^- \rightarrow Cl_2 + 2e^- \quad (42)$$

$$Cl_2 + H_2O \rightarrow HClO + Cl^- + H^+ \quad (43)$$

$$HClO \leftrightarrows ClO^- + H^+ \quad (44)$$

Cuando se usa un ánodo “no activo” como el BDD, los iones hipoclorito se generan también a partir de la oxidación de los iones cloruro por parte de los radicales $^{\bullet}OH$ adsorbidos sobre el BDD por la reacción (45). El ion resultante se puede oxidar consecutivamente a clorito, clorato y perclorato según la reacciones (46)-(48) (Bergmann et al., 2009; Sánchez-Carretero et al., 2011).

$$Cl^- + {}^{\bullet}OH \rightarrow ClO^- + H^+ + e^- \quad (45)$$

$$ClO^- + {}^{\bullet}OH \rightarrow ClO_2^- + H^+ + e^- \quad (46)$$

$$ClO_2^- + {}^{\bullet}OH \rightarrow ClO_3^- + H^+ + e^- \quad (47)$$

$$ClO_3 + {}^{\bullet}OH \rightarrow ClO_4^- + H^+ + e^- \quad (48)$$

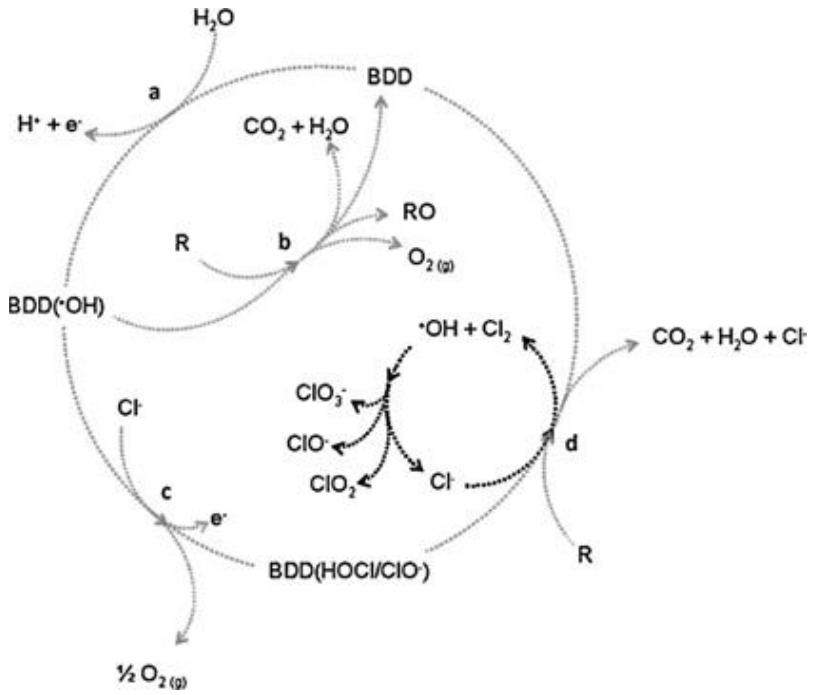

Figura 6. Esquema simplificado para el mecanismo de oxidación de los compuestos orgánicos por los radicales •OH y los oxidantes formados en medio cloruro. (a) Formación de radicales •OH fisisorbidos, (b) combustión del compuesto orgánico R por radicales •OH fisisorbidos con producción simultánea de oxígeno, (c) oxidación de los iones cloruro a cloro activo, (d) producción de cloro activo por reacción entre los iones cloruro y los radicales •OH y oxidación de los compuestos orgánicos por el cloro activo (Sales Solano y col., 2013).

En la **Figura 6** se muestra un esquema de reacción generalizado para la formación de radical •OH adsorbido y la oxidación de los iones cloruro por parte de estos radicales utilizando un ánodo de BDD.

Es interesante mencionar que una de las aplicaciones a gran escala más desarrolladas en el ámbito de los EAOPs es la desinfección electroquímica de agua de piscina y spa utilizando equipos automatizados con ánodos de BDD. En este campo, se han desarrollado productos especializados como Oxineo® y Sysneo® para instalaciones privadas y públicas. En comparación con otros métodos de desinfección, estos sistemas tienen varias ventajas, pues desaparece el olor a cloro típico de la cloración salina, no hay acumulación de productos químicos en el agua de la piscina con la consecuente reducción de las reacciones alérgicas, y no hay necesidad de agentes para combatir el crecimiento de algas. Muchos de estos sistemas se encuentran ya instalados en piscinas privadas de todo el mundo y varias piscinas y spas públicos en Europa.

1.4.1.2. Electro-Fenton

El proceso EF es sin duda el más empleado entre los métodos electroquímicos basados en el reactivo de Fenton. Se puede considerar como una modificación del proceso de Fenton químico explicado anteriormente, constituyendo una alternativa electroquímica para la producción de radicales hidroxilo en solución acuosa (Guivarch y col., 2003; Flox y col., 2006a; Zhou y col., 2008, 2012; Isarain-Chávez y col., 2011). Al contrario que en la EO, en este proceso el radical $^{\bullet}OH$ se genera de manera indirecta en el seno de la disolución, a través de la reacción de Fenton en medio ácido (reacción (12)) para evitar la precipitación del catión metálico. La principal diferencia con su alternativa no electroquímica es la generación del peróxido de hidrógeno in situ en la disolución contaminada a partir de la reducción bielectrónica de oxígeno en el cátodo (Pletcher; 1999; Boye y col., 2002; Panizza y Cerisola, 2009a).

$$O_2 + 2H^+ + 2e^- \rightarrow H_2O_2 \qquad (49)$$

La producción de H_2O_2 tiene lugar de forma eficiente al emplear cátodos carbonosos como el grafito (Rosales y col., 2009), nanotubos de carbono (Khataee y col., 2013), fibra de carbón activada (Wang y col., 2005, 2008), esponja de carbón (Özcan y col., 2008), fieltro de carbón (Daneshvar y col., 2008; Panizza y Oturan, 2011), fieltro de grafito (Özcan y col., 2009; Dirany y col., 2010, 2012; Oturan y col., 2012) y electrodos de difusión de gas (O_2 o aire) de carbón-politetrafluoroetileno (PTFE) (Guinea y col., 2010; Ruiz y col., 2011a; Salazar y col., 2012).

En esta Tesis se ha empleado siempre una celda no divida para los procesos basados en la reacción de Fenton. En estas condiciones, los compuestos orgánicos son oxidados simultáneamente por los radicales M($^{\bullet}OH$) producidos en la superficie del ánodo y los formados en el seno de la disolución mediante la reacción de Fenton. Aparte de la producción in situ del H_2O_2, lo cual evita los problemas y costes relacionados con su compra, transporte, manejo y almacenamiento, una extraordinaria ventaja del proceso EF es que la reacción de Fenton puede propagarse gracias al ciclo catalítico sostenido del par redox Fe^{3+}/Fe^{2+}. Así, el Fe^{2+} se regenera continuamente a partir de reducción del Fe^{3+} en el cátodo mediante la reacción (50)) (Sirés y Brillas, 2012; Sirés y col., 2014), la cual suele ser mucho más efectiva que las reacciones (13)-(15) y (20). Este hecho, a su vez, minimiza de manera significativa la producción de lodos.

$$Fe^{3+} + e^{-} \rightarrow Fe^{2+} \quad (50)$$

De manera análoga a lo que ocurre en el proceso Fenton químico, el pH óptimo para la aplicación del proceso EF es 2,8-3,0 (Brillas col., 2009). A pH inferior el protón actúa como secuestrador (*radical scavenger*) del $^{\bullet}OH$, disminuyendo su disponibilidad para las reacciones con las moléculas orgánicas, mientras que a pH superior la precipitación de hidróxidos de hierro afecta considerablemente la concentración del Fe^{2+} libre en la disolución. La eficiencia del proceso es función de los parámetros de operación tales como la temperatura, el pH de la disolución, el flujo de aire suministrado a la disolución o inyectado al cátodo de difusión de gas, las condiciones hidrodinámicas, la naturaleza de los iones inorgánicos presentes, la intensidad o voltaje aplicados y las concentraciones del catalizador y del contaminante. La principal limitación del proceso EF, al igual que ocurre en el Fenton químico, es la generación de intermedios recalcitrantes como por ejemplo los ácidos carboxílicos de cadena corta. Ácidos como el oxálico, oxámico o fórmico forman complejos con los iones Fe^{3+}, los cuales son muy recalcitrantes frente a los radicales hidroxilo e impiden la mineralización completa de la disolución tratada.

1.4.1.3. Fotoelectro-Fenton UV y fotoelectro-Fenton solar

El proceso PEF fue ideado en los años 90 por el grupo LEMMA encabezado por el Dr. Brillas, y ha sido estudiado ampliamente utilizando una celda no dividida equipada con un cátodo de difusión de aire (ADE) y un ánodo, dando lugar a celdas Pt/ADE o BDD/ADE (Brillas y col., 2009). En este proceso, la disolución tratada bajo condiciones de EF se irradia simultáneamente con luz UVA para favorecer la reducción fotoinducida de los hidroxocomplejos de Fe(III) por la reacción (23). Esto da lugar a la producción de más radicales hidroxilo y a la regeneración del catalizador Fe^{2+}, lo cual propaga la reacción de Fenton (12). No obstante, el efecto más relevante de la luz está relacionado con la destrucción de los complejos Fe(III)-carboxilato. La radiación permite la fotodescarboxilación, favoreciendo la mineralización completa de la materia orgánica y la liberación del ion hierro complejado mediante la reacción (24).

El principal inconveniente que tiene este proceso, al igual que otros AOPs fotoquímicos, es el coste adicional de las lámparas UVA. Afortunadamente, en los últimos años el grupo LEMMA ha desarrollado la tecnología SPEF, en la cual las lámparas UVA se substituyen por la irradiación con luz solar (Ruiz y col., 2011b;

Salazar y col., 2011). La luz solar es una fuente inagotable, gratuita y de mayor intensidad de radiación que las lámparas comerciales, y por tanto, permite una degradación más eficaz con una reducción drástica del consumo energético.

En definitiva, los EAOPs son tecnologías muy prometedoras que permiten en muchos casos la mineralización completa de las disoluciones contaminadas con compuestos orgánicos, pero su explotación es aún limitada debido a los costes de operación relativamente altos que son inherentes al largo tiempo de tratamiento requerido.

1.4.2. Electrocoagulación (EC)

Tradicionalmente, los contaminantes presentes en las aguas residuales son eliminados antes de su vertido mediante tecnologías secuenciales que incluyen algunos métodos de tratamiento fisicoquímico, entre ellos la coagulación química. Este tratamiento consiste en la adición de agentes coagulantes que involucran iones Fe^{3+} o Al^{3+}, generalmente en forma de cloruros, para la separación de los contaminantes. Hace ya varios años, se desarrolló la EC como alternativa a la coagulación química. Varios efluentes líquidos de industrias de sectores muy dispares se han tratado por EC (Kobya y col., 2003; Mollah y col., 2004), obteniéndose resultados muy alentadores en cuanto a la eliminación de contaminantes orgánicos e inorgánicos, hecho que ha despertado el interés de algunos grupos de investigación e incluso de la industria por invertir e implantar esta tecnología en el tratamiento de aguas residuales. Al igual que la coagulación convencional, la EC se basa en la adición de iones metálicos a la disolución contaminada. Sin embargo, este proceso utiliza la corriente para disolver ánodos de sacrificio de Fe (o acero) o Al sumergidos en la disolución, dando así lugar a iones metálicos en diferentes estados de oxidación (Fe^{2+}, Fe^{3+} o Al^{3+}). Simultáneamente, se originan iones hidróxido a partir de la reducción catódica del agua, con lo cual los iones metálicos se transforman inmediatamente en hidróxidos metálicos tales como $Al(OH)_3$ y $Fe(OH)_n$ que actúan como coagulantes. Estas partículas sólidas tienen grandes superficies y son capaces de eliminar grandes porcentajes de contaminantes.

Durante el tratamiento mediante EC, las partículas de contaminantes coloidales interaccionan con los complejos e hidróxidos metálicos, de manera que se desestabilizan debido a la compresión de su doble capa difusa. Los complejos metálicos favorecen también la neutralización de cargas presentes en el agua residual y la reducción de las

repulsiones entre los coloides, dando paso al proceso de coagulación. La materia coagulada puede sedimentarse en el reactor, o bien puede separarse por electroflotación cuando las partículas coaguladas se asocian a las burbujas de H_2 generadas en el cátodo y transportadas a la superficie (Kobya y col., 2006). La efectividad del proceso EC depende de diferentes factores, entre los cuales destacan la naturaleza y concentración de los contaminantes, el pH y la conductividad específica de la disolución tratada, la composición y número de electrodos utilizados, la distancia interelectródica y el modo de conexión eléctrica. Estos factores determinan y controlan las reacciones ocurridas en el sistema, sobre todo la formación del coagulante.

Cuando se utiliza un ánodo de hierro o acero, se producen iones Fe^{2+} en la disolución contaminada a partir de la oxidación del Fe según la reacción (51), mientras que en el cátodo se genera H_2 gas por la reducción del agua mediante la reacción (52).

$$Fe \rightarrow Fe^{2+} + 2e^- \quad (51)$$

$$2H_2O + 2e^- \rightarrow 2OH^- + H_2 \quad (52)$$

La producción de OH^- según la reacción (52) provoca un aumento del pH durante las electrolisis. A pH ≥ 5.5, el Fe^{2+} precipita en forma de $Fe(OH)_2$ insoluble:

$$Fe^{2+} + 2OH^- \rightarrow Fe(OH)_2 \quad (53)$$

La reacción global para el proceso electrolítico a partir de la secuencia de reacciones (51)-(53) es:

$$Fe + 2H_2O \rightarrow Fe(OH)_2 + H_2 \quad (54)$$

En disoluciones aireadas, que son las más típicas, la presencia de oxígeno lleva a la oxidación del Fe^{2+} disuelto a $Fe(OH)_3$:

$$4Fe^{2+} + 10H_2O + O_2 \rightarrow 4Fe(OH)_3 + 8H^+ \quad (55)$$

A su vez, los protones pueden ser reducidos directamente a H_2 gas en el cátodo

$$8H^+ + 8e^- \rightarrow 4H_2 \quad (56)$$

La reacción global obtenida combinando las reacciones (51), (55) y (56) es:

$$4Fe + 10H_2O + O_2 \rightarrow 4Fe(OH)_3 + 4H_2 \quad (57)$$

Además, dependiendo del pH, los iones Fe^{2+} y Fe^{3+} pueden formar varias especies monoméricas solubles como Fe^{3+}, $Fe(OH)_2^+$, $Fe(OH)_4^-$ y/o complejos poliméricos de

hidróxidos de metales (Golder y col., 2007). De todas maneras, tanto el $Fe(OH)_2$ y como el $Fe(OH)_3$ tienen una mayor capacidad de retención de las especies coloidales e iónicas, dando lugar a una coagulación más efectiva.

En el caso de la EC con un ánodo de aluminio, el Al^{3+} se genera en la disolución contaminada a partir de la oxidación del Al:

$$Al \rightarrow Al^{3+} + 3e^- \quad (58)$$

y a su vez, en el cátodo se genera ion hidróxido y H_2 gas por la reducción del agua:

$$3H_2O + 3e^- \rightarrow 3OH^- + (3/2)H_2 \quad (59)$$

Por otro lado, a valores de pH muy alcalinos, tanto el cátodo como el ánodo pueden ser atacados químicamente por los iones OH^- (Cañizares y col., 2007):

$$2Al + 6H_2O + 2OH^- \rightarrow 2Al(OH)_4^- + 3H_2 \quad (60)$$

Los iones Al^{3+} y OH^- generados por las reacciones (58) y (59) en los electrodos reaccionan para formar varias especies monoméricas como $Al(OH)^{2+}$, $Al(OH)_2^+$, $Al(OH)_3$, $Al(OH)_4^-$ y especies poliméricas tales como $Al_6(OH)_{15}^{3+}$, $Al_7(OH)_{17}^{4+}$, $Al_8(OH)_{20}^{4+}$, $Al_{13}O_4(OH)_{24}^{7+}$, $Al_{13}(OH)_{34}^{5+}$, los cuales se transforman finalmente en $Al(OH)_3$ (Mollah y col., 2001; Gürses y col., 2002; Bayramoglu y col., 2004; Kobya y col., 2006). En definitiva, se puede escribir de manera global la transformación de los iones Al^{3+} como:

$$Al^{3+} + 3H_2O \rightarrow Al(OH)_3 + 3H^+ \quad (61)$$

El $Al(OH)_3$ es una sustancia amorfa de consistencia gelatinosa que exhibe una gran área superficial, la cual es muy beneficiosa para la adsorción de los compuestos iónicos solubles y partículas coloidales, que se acaban separando del agua por sedimentación o electroflotación (Can y col., 2003; Kobya y col., 2003).

La aplicación de la EC en el tratamiento de aguas residuales ha adquirido un interés considerable en la última década. Se trata, por tanto, de una tecnología conocida desde hace tiempo, pero emergente en el sector, una vez se han comprobado los resultados tan positivos en cuanto a la eliminación de grandes cantidades de materia orgánica con dispositivos sencillos, seguros y económicos. Una de las aplicaciones más conocidas y populares de la EC ha sido el tratamiento de agua contaminada con colorantes (Mollah y col., 2004; Danhesvar y col., 2006; Modirshahla y col., 2007; Aleboyeh y col., 2008; Ayhan Sengil y Özacar, 2009). También se ha estudiado la aplicabilidad de este proceso

sobre aguas residuales de lavandería (Wang y col., 2009) e industrias textiles (Can y col., 2006; Bayramoglu y col., 2007), así como para la eliminación de iones arsénico (Balasubramanian y Madhavan, 2001; Gomes y col., 2007; Kobya y col., 2011) y la potabilización de agua (Holt y col., 2005; Parga y col., 2005). La EC presenta muchas ventajas en comparación con otros métodos alternativos, tales como una alta eficiencia con bajo coste de operación, utilización de equipos sencillos con facilidad de manejo y capacidad de controlar el proceso con precisión. En particular, las ventajas respecto a la coagulación química incluyen la ausencia de la adición de productos químicos, eliminando así los costes asociados y los riesgos de transporte y almacenamiento, y la generación de lodos más secos y compactos y en menor cantidad, lo que conlleva una menor problemática de gestión de los mismos.

Sin embargo, la EC presenta algunos inconvenientes respecto a algunos procesos comentados anteriormente. En primer lugar, es necesario reponer los ánodos de sacrificio periódicamente, lo que implica en algunos casos la realización de paradas técnicas y, sobre todo, un consumo programado de electrodos. Además, los lodos contienen hierro y aluminio, dependiendo del material del electrodo de sacrificio utilizado, de manera que su gestión debe ser cuidadosa. En algunos casos, el óxido formado sobre el ánodo puede formar una capa que dificulta el paso de la corriente eléctrica, disminuyendo de esta forma la eficiencia del proceso. Pero, ante todo, la EC no permite la eliminación completa de los compuestos orgánicos, llegándose a porcentajes del 60-80% en los mejores casos, la materia es simplemente separada y no mineralizada, y pueden persistir en disolución algunos productos tóxicos no coagulables.

1.4.3. Combinación secuencial EC/EAOPs

Como se acaba de indicar, la EC, proceso de gran interés industrial, presenta algunas limitaciones importantes como su insignificante capacidad para destruir la materia orgánica, permitiendo sólo la transferencia de compuestos coagulables desde la fase líquida hacia la fase sólida. En cuanto a los EAOPs, aunque son procesos prometedores, su potencial explotación se ve todavía limitada debido a los costes relativamente elevados de operación por el largo tiempo de tratamiento que requieren. Con el doble objetivo de lograr una descontaminación más efectiva de las disoluciones acuosas y acortar el tiempo de tratamiento, se desarrollaron por parte del LEMMA los

procesos de peroxi-coagulación y fotoperoxi-coagulación. Estos procesos utilizan un ánodo de sacrificio generalmente de hierro para suministrar Fe^{2+} a la disolución, buena parte del cual es transformado en $Fe(OH)_3$, y un cátodo que genera H_2O_2 (Brillas y col., 2003a). En estas condiciones, los contaminantes son eliminados por los radicales $^{\bullet}OH$ generados a partir de la reacción de Fenton (12) y mediante coagulación con el $Fe(OH)_3$ formado. Mientras que en los tratamientos de EF, PEF y SPEF el H_2O_2 se acumula en el medio, en la (foto)peroxi-coagulación se consume completamente, probablemente debido a su rápida reacción con la alta concentración de Fe^{2+} presente en el seno de la disolución, dando lugar a una alta concentración de radicales $^{\bullet}OH$ que pueden conducir a un gran porcentaje de mineralización de los contaminantes.

Sin embargo, estos procesos en presencia de Fe^{2+} y H_2O_2 presentan algunos inconvenientes importantes:

- El exceso de Fe^{2+} derivado de la disolución del ánodo promueve la destrucción de los radicales $^{\bullet}OH$ mediante la reacción (16).
- El tiempo de vida del cátodo y su capacidad para producir H_2O_2 se reduce drásticamente debido a: (i) la adsorción de las partículas coaguladas, que bloquean los poros de difusión y los sitios activos y (ii) la abrasión de su superficie, causada por hidróxidos precipitados y la materia coagulada.
- El efecto de la luz irradiada en fotoperoxi-coagulación es insignificante debido al efecto barrera del precipitado de hierro.

En este contexto, la combinación secuencial de la EC y los EAOPs se perfila como una buena alternativa para reducir al mínimo los costes relacionados con el consumo energético y permitir una descontaminación más profunda de las disoluciones. La combinación EC/EAOPs se realiza en dos pasos sucesivos, en lugar de utilizar un único montaje experimental como el proceso de peroxi-coagulación. La combinación de procesos permite explotar las características positivas de cada proceso, minimizando las reacciones parásitas. Dadas estas ventajas, en los últimos años han aparecido algunos estudios sobre la combinación de procesos con el fin de mejorar la tecnología global de tratamiento de efluentes acuosos y minimizar los costes de operación. En este sentido, Raju y col. (2008) y Panizza y Cerisola (2010b) han descrito la combinación EC/EO, mientras que Durante y col. (2010) han investigado una combinación EC/AOPs.

Por lo que conocemos, en esta Tesis Doctoral se investiga por primera vez la combinación secuencial de la EC y de EAOPs basados en la reacción de Fenton. Esta combinación tiene como objetivo:

- Aplicar la EC como pretratamiento para eliminar una gran cantidad de materia orgánica por coagulación, actuando a su vez como fuente de catalizador metálico (Fe^{2+}).
- Electrogenerar un agente oxidante muy fuerte como el radical $^{\bullet}OH$, e incluso cloro activo en presencia de cloruro, para propiciar la mineralización completa de la disolución pretratada durante el post-tratamiento llevado a cabo con EAOPs.

1.5. Colorantes estudiados en el presente trabajo

Ponceau 4R

El Ponceau 4R (2-hidroxi-1-(4-sulfonato-1-naftilazo)-naftaleno-6,8-disulfonato trisódico, N^{o} CAS: 2611-82-7), también conocido como Rojo Ácido 18 (AR 18), CI 16255 o aditivo E124 (ver su estructura en la **Figura 7**), es un colorante sintético azo sulfonado empleado en la industria alimentaria para dar color rojo a los productos alimenticios. Este colorante ha sido evaluado por el Comité Mixto FAO/OMS de Expertos en Aditivos Alimentarios (JECFA) en 1983 y por el Comité Científico sobre Alimentos de la UE (UE-SCF) en 1984. Ambos comités establecieron una IDA de 0-4 mg/kg de peso corporal por día. En los últimos años se han realizado nuevos estudios, incluido el de Tsuda y col. (2001) informando sobre los efectos de la migración del ADN nuclear en ratones, así como el realizado por McCann y col. (2007) y el financiado por la Agencia Británica de Seguridad Alimentaria, los cuales han revelado que cuando el AR 18 se ingiere junto con otros colorantes y conservantes de alimentos induce un aumento de la hiperactividad en niños (EFSA, 2008; Oliveira y col., 2011). En vista de los riesgos para la salud ocasionados por su consumo indiscriminado, recientemente la EFSA ha decidido reducir la IDA para el AR 18 de 4 mg/kg a 0.7 mg/kg en peso corporal (EFSA, 2009b). En algunos países como EEUU, Noruega y Finlandia, este colorante se clasifica como carcinógeno, y actualmente está catalogado como sustancia prohibida por la FDA (Oliveira y col., 2011).

Aparte de los riegos relacionados con la salud, la presencia del colorante AR 18 en el medio ambiente también puede resultar problemático. Para solucionar este problema

ambiental, se han aplicado diferentes tecnologías basadas en procesos biológicos, AOPs y EAOPs. Los primeros han demostrado ser efectivos en cuanto a la decoloración, pero son insuficientes para la mineralización de sus disoluciones (Koupaie y col., 2011, 2012) debido al carácter biorefractario de los colorantes azoicos, los cuales ya se ha comentado que suelen ser altamente resistentes a los tratamientos convencionales. Algunos AOPs, como la fotocatálisis heterogénea con TiO_2 (Mozia y col., 2005, 2006, 2007; Sadik y col., 2007; Sobana y Swaminathan, 2007; Oliveira y col., 2011) y el proceso de Fenton químico (Barbusiński y Majewski, 2003), también han demostrado ser eficaces para la decoloración, pero tampoco consiguen la mineralización completa que asegure reducir la toxicidad del efluente. En el presente trabajo se ha tratado el colorante AR 18 mediante tecnologías electroquímicas (EAOPs), incluyendo EO, EF y PEF, en diferentes electrolitos soportes y utilizando diferentes reactores a escala de laboratorio.

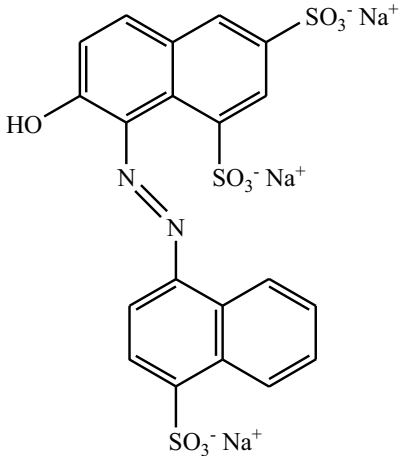

Figura 7. Estructura molecular del colorante Ponceau 4R (E124), $C_{20}H_{11}N_2O_{10}S_3Na_3$, 604.47 g mol^{-1}, λ_{max} = 508 nm.

Rojo Allura AC

El Rojo Allura AC (2-hidroxi-1-(2-metoxi-5-metil-4-sulfonatofenilazo)-naftaleno-6-sulfonato disódico, N^o CAS: 25956-172-6), también conocido como AR AC, CI 16035 o aditivo E129 (ver su estructura en la **Figura 8**) es un colorante sintético azo sulfonado empleado en la industria alimentaria para dar color rojo a los productos alimenticios. El AR AC está permitido como aditivo alimentario en la UE en virtud de la Directiva 94/36/CE. Este colorante ha sido evaluado por el JECFA en 1974, 1980 y 1981, y por el UE-SCF en 1975, 1984 y 1989. Ambos comités establecieron una IDA de

0-7 mg/kg de peso corporal por día (EFSA, 2009a). Como todos los colorantes azoicos, el colorante AR AC ha sido sometido a muchas pruebas, las cuales revelaron que cuando se utiliza con otros colorantes y conservantes de alimentos induce un aumento de la hiperactividad en niños (EFSA, 2009a). Se han realizado experimentos toxicológicos en animales y se ha comprobado que al ser empleado en grandes dosis puede causar cáncer de vejiga. Después de todos los estudios realizados, la EFSA concluyó que la base de datos actual no justifica una disminución de la IDA. En algunos países de Europa como Dinamarca, Bélgica, Francia, Alemania, Suiza, Suecia, Austria y Noruega se ha retirado como colorante de alimentos infantiles. En EEUU se introdujo a principio de los años ochenta para reemplazar el colorante Amaranto (E 123).

Como todos los colorantes azoicos, el colorante AR AC puede generar problemas ambientales, pero hasta la fecha no existen trabajos sobre el tratamiento de agua contaminada por él. En esta Tesis se ha estudiado la degradación de disoluciones de AR AC mediante diferentes EAOPs a escala laboratorio y en planta pre-piloto.

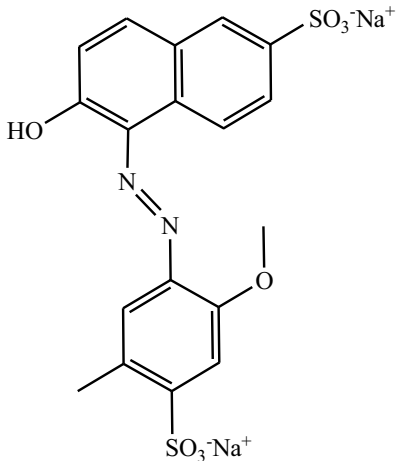

Figura 8. Estructura molecular del colorante Rojo Allura AC (E129), $C_{18}H_{14}N_2O_8S_2Na_2$, 496,42 g mol^{-1}, λ_{max} = 500 nm.

Carmoisina

La Carmoisina (sal disódica del ácido 2-(4-sulfo-naftilazo)-1-naftol-4-sulfónico, N^o CAS: 3567-69-9), también conocida como Rojo Ácido 14 (AR 14), CI 14720 o aditivo E122 (ver su estructura en la **Figura 9**) es un colorante sulfónico monoazo empleado en la industria alimentaria y textil para dar color rojo a los productos. El AR 14 está permitido como aditivo alimentario en la UE y ha sido evaluado por el JECFA en 1983 y por el UE-SCF en 1984. Ambos comités establecieron una IDA de 0-4 mg/kg de peso

corporal por día (EFSA, 2009d). Adicionalmente, algunos estudios han informado de que dicho colorante puede provocar alteraciones en la morfología de los cromosomas somáticos del *Secale cereale* (centeno), mientras que un estudio realizado por McCann y col. (2007) ha revelado que cuando se utiliza con otros colorantes y conservantes de alimentos induce un aumento de la hiperactividad en niños, al igual que en el caso del AR 18 y AR AC (EFSA, 2009d), si bien los efectos encontrados no se consideraron estadísticamente significativos. En el contexto del conjunto de las pruebas realizadas y en vista de las considerables incertidumbres que surgieron, tales como la falta de coherencia, la debilidad relativa del efecto y la ausencia de información sobre la relevancia clínica de los cambios observados en el comportamiento, la EFSA concluyó que los resultados de los estudios llevados a cabo no se pueden utilizar como base para reducir el IDA establecido de 4 mg/kg de peso corporal/día.

En los últimos años, la Carmoisina ha sido elegida por muchos autores como molécula modelo para comprobar la efectividad de varios tratamientos para la eliminación de colorantes, incluyendo la ozonización (Gao y col., 2012), la electrocoagulación (Aleboyeh y col., 2008), la fotocatálisis heterogénea (Daneshvar y col., 2003b, 2004; Mahmoodi y Arami, 2006; Xia y col., 2014), la sonoquímica (Lin y col., 2008) y el Fenton químico (Idel-Aouad y col., 2011). Por su parte, se ha investigado la degradación mediante diferentes EAOPs como la EO (Wang y col., 2004), el EF (Wang y col., 2005) y el PEF (Wang y col., 2008) utilizando un ánodo de Ti/SnO_2 o Ti/RuO_2 y un cátodo de fibras de carbón activadas para electrogenerar H_2O_2.

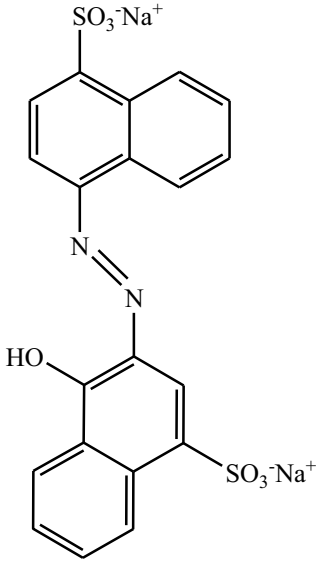

Figura 9. Estructura molecular del colorante Carmoisina (E122), $C_{20}H_{12}N_2O_7S_2Na_2$, 502,43 g mol^{-1}, λ_{max} = 514 nm.

En la presente Tesis se ha tratado el colorante AR 14 mediante los procesos EO y EF utilizando un ánodo de BDD, siendo muy interesante la ausencia de estudios que evalúen el comportamiento de este ánodo para su degradación.

Tartrazina

La Tartrazina ((4E)-5-oxo-1-(4-sulfonatofenil)-4-[(4-sulfonatofenil)hidrazono]-3-pirazolcarboxilato trisódico, N^{o} CAS: 1934-21-0), también conocida como Amarillo Ácido 23 (AY 23), CI 19140 o aditivo E102 (ver su estructura en la **Figura 10**) es un colorante azo sulfonado empleado en la industria alimentaria para dar color entre amarillo y naranja brillante a los productos alimenticios. También se emplea en productos cosméticos y en medicamentos. Su potencial comercial ha aumentado considerablemente en los últimos años porque además de los tonos amarillos-anaranjados, al mezclarse con otros colorantes como el azul brillante (E133) o el verde S (E142) se obtienen diversas tonalidades verdosas. La Tartrazina ha sido evaluada por la JECFA en 1966 y por el UE-SCF en 1975 y 1984. Ambos comités establecieron una IDA de 0-7,5 mg/kg de peso corporal por día (EFSA, 2009c). Se han realizado muchos estudios para reevaluar la Tartrazina, incluido el llevado a cabo por Sasaki y col. (2002) que informó sobre los efectos sobre la migración del ADN nuclear en ratones, y un estudio de McCann y col. (2007) que reveló que las mezclas de colorantes y/o conservantes que incluyen el AY 23 inducen un aumento de la hiperactividad en niños (ESFA, 2008). Los estudios científicos realizados hasta la fecha no han demostrado ningún efecto carcinogénico. Teniendo en cuenta todo los estudios publicados y los efectos documentados sobre la salud, la EFSA concluyó que la IDA de 7,5 mg/kg de peso corporal/día no debe ser reconsiderada por el momento. El uso de este colorante está prohibido en algunos países como Alemania, Austria, Finlandia y Noruega, y recientemente ha sido propuesta su prohibición en Reino Unido.

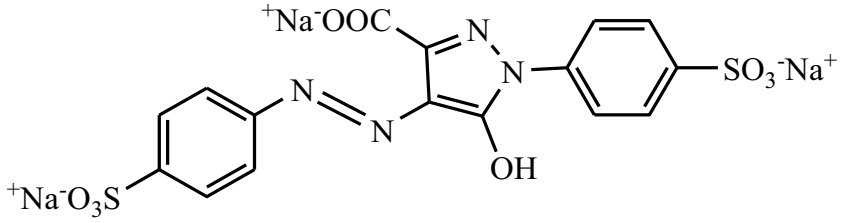

Figura 10. Estructura molecular del colorante Tartrazina (E102), $C_{16}H_9N_4O_9S_2Na_3$, 534,36 g mol^{-1}, λ_{max} = 428 nm.

2. Objetivos

2. Objetivos

El *objetivo general* del trabajo de investigación realizado en esta Tesis Doctoral ha sido el estudio exhaustivo de la eliminación de colorantes alimentarios azoicos contenidos en matrices acuosas mediante tecnologías electroquímicas de separación y destrucción usadas individualmente o acopladas. Como se ha descrito en la introducción, existen varias tecnologías electroquímicas efectivas para el tratamiento de contaminantes orgánicos, si bien su uso para el eliminación de colorantes empleados en la alimentación no se había desarrollado en detalle.

La mayor parte del trabajo ha sido realizado en el LEMMA de la Universitat de Barcelona (UB) bajo la dirección del **Dr. Enrique Brillas Coso** y el **Dr. Ignacio Sirés Sadornil**. En esta parte se ha estudiado la capacidad de varios EAOPs para decolorar y mineralizar disoluciones sintéticas ácidas de los colorantes AR 14, AR 18 y AR AC, tratados de manera individual o bien en mezclas de todos ellos. En particular, se han aplicado los procesos de EO, EF, PEF y SPEF. En EO se ha usado un ánodo de BDD o Pt y un cátodo de acero inoxidable o de difusión de aire (ADE). Por su parte, en los EAOPs basados en la reacción de Fenton se ha usado un ánodo de BDD o Pt y un cátodo de difusión de aire (ADE), en presencia de catalizador Fe^{2+} añadido a la disolución. El trabajo se ha centrado en la elección de la tecnología apropiada y la optimización progresiva de las condiciones de operación para una eliminación eficaz y eficiente de los colorantes. Para cumplir con el objetivo principal antes descrito, se plantearon los siguientes *objetivos específicos*:

- Investigar la decoloración y mineralización de disoluciones de los tres colorantes alimentarios en matrices de agua ultrapura y agua real, utilizando una celda monocompartimental o dividida a escala de laboratorio de 130 mL con electrodos de 3 cm^2 de área mediante diferentes EAOPs. En primer lugar se estudió el comportamiento de los colorantes de forma individual, y en último término se realizaron mezclas de los tres compuestos para confirmar la capacidad de los métodos para tratar disoluciones multicomponente.
- Determinar el porcentaje de decoloración durante las electrolisis y la velocidad de mineralización correspondiente para cada colorante al aplicar EO, EF y PEF. Para ello, se utilizaron los descensos de la absorbancia UV-vis y medidas del carbono orgánico total (TOC).
- Escalar los procesos en una planta pre-piloto de 2,5 L con recirculación. El sistema se compone de una celda filtro-prensa de Pt/ADE o BDD/ADE, con

electrodos de 20 cm^2 de área electródica, acoplada a un fotorreactor solar en el caso del método SPEF. Esta planta pre-piloto permite desarrollar la experimentación en las condiciones más reales posibles, ajustando todos los parámetros de control con el objetivo de obtener resultados más útiles desde el punto de vista aplicativo.

- Calcular la eficiencia de corriente de mineralización (MCE) y el consumo energético requerido para el tratamiento de cada colorante mediante cada uno de los procesos utilizados, tanto como en celda a escala de laboratorio como en planta pre-piloto.
- Estudiar diferentes aspectos relacionados con la decoloración y la mineralización de las disoluciones de los colorantes, así como determinar las condiciones de operación adecuadas para alcanzar la máxima eficacia y eficiencia en su oxidación y la de sus productos de degradación. Tales resultados pueden servir para la elección de una tecnología en base a diferentes criterios (ambiental, económico, etc.). Con este fin, se ha evaluado el efecto de los parámetros operativos principales que intervienen en este tipos de tratamiento, como son la intensidad de corriente aplicada al sistema (se ha trabajado en modo galvanostático), la naturaleza y concentración del electrolito soporte, la concentración inicial de cada colorante y del catalizador, la naturaleza y configuración de los electrodos y la presencia de luz UVA o solar.
- Determinar la cinética de degradación de colorantes mediante cromatografía líquida de alta presión (HPLC) de fase inversa.
- Identificar los intermedios aromáticos y los ácidos carboxílicos producidos durante la degradación de cada colorante mediante cromatografía de gases acoplada a espectrometría de masas (GC-MS) y/o HPLC. Se ha seguido además la generación y destrucción de los ácidos carboxílicos en cada método mediante HPLC de exclusión iónica.
- Seguir la evolución de los iones SO_4^{2-}, NH_4^+ y/o NO_3^- generados a partir de los heteroátomos de los colorantes mediante cromatografía iónica (IC). Asimismo, seguir la evolución de los aniones clorados formados al trabajar en medio Cl^-.
- Proponer un camino de reacción para cada colorante estudiado al aplicar los EAOPs.

2. Objetivos

Con la finalidad de ampliar los estudios de degradación de los colorantes azoicos iniciados en el LEMMA (UB), en 2013 se efectuó una estancia pre-doctoral de 5 meses (subdividida en dos periodos de 2 meses y medio) en el *College of Environmental Science and Engineering* de la *Nankai University* (Tianjin, China) bajo la supervisión del **Dr. Minghua Zhou**. El *objetivo principal* de la estancia fue idear un sistema para lograr una mineralización más eficiente de los colorantes azoicos y acortar el tiempo de tratamiento, de cara a reducir los costes relativamente elevados de operación debidos al largo tiempo de tratamiento que requieren los EAOPs. Para ello, se estableció un estudio comparativo entre diferentes tecnologías electroquímicas para el tratamiento de aguas. En primer lugar se aplicaron individualmente y, una vez seleccionadas las mejores condiciones, se diseñó un sistema acoplado para buscar la sinergia de varios fenómenos. En particular, durante este periodo se estudió la degradación del colorante Tartrazina presente en una disolución de agua sintética mediante EC, que es un proceso de alto interés industrial, varios EAOPs y la combinación secuencial EC/EAOPs. Para ello se plantearon los siguientes *objetivos específicos*:

- Degradar el colorante Tartrazina en matrices de agua ultrapura, utilizando una celda monocompartimental a escala de laboratorio (130 mL), mediante varias configuraciones de EC y EAPOs aplicados individualmente.
- Estudiar el efecto de los parámetros operativos principales que intervienen en los procesos EC y EAOPs, tales como: la intensidad de corriente aplicada al sistema, la naturaleza y concentración del electrolito soporte, la concentración inicial del colorante y el catalizador metálico, la naturaleza y configuración de los electrodos, el modo de conexión eléctrica en EC y la presencia de luz UVA en los EAOPs.
- Estudiar la degradación del colorante mediante procesos electroquímicos integrados EC/EAOPs, con EAOPs como la EO con BDD/acero, BDD/ADE, Pt/acero y Pt/ADE; el EF con BDD/ADE y Pt/ADE y el PEF con BDD/ADE y Pt/ADE, bajo las condiciones óptimas de cada proceso para tratar de conseguir mayor eficiencia que los procesos individuales.
- Identificar los intermedios aromáticos formados durante la degradación mediante los procesos electroquímicos integrados y proponer un camino de reacción para la Tartrazina.

- Escalar los procesos electroquímicos integrados en una planta pre-piloto de 2 L de capacidad para evaluar la viabilidad de la degradación de colorantes alimentarios azoicos.
- Evaluar el consumo energético requerido en la degradación del colorante para cada uno de los procesos utilizados tanto en celda de laboratorio como, sobre todo, en planta pre-piloto.

3. Parte experimental

3.1. Reactivos químicos

Todas las disoluciones sintéticas electrolizadas en la celda a escala de laboratorio, así como las fases móviles empleadas en los análisis cromatográficos (HPLC e IC), se prepararon con agua ultrapura obtenida con un sistema Millipore Milli-Q, con una resistividad inferior a 18 MΩ cm a 25 °C. En los ensayos realizados con agua real, la matriz acuosa se recogió a partir del efluente de la primera decantación de una estación municipal de depuración de aguas residuales situada en Gavà-Viladecans (Barcelona, España) y se conservó en un refrigerador a 4 °C hasta ser utilizada para los ensayos. Esta planta se ocupa del tratamiento de 25.000-50.000 m^3/día de aguas urbanas y algunas aguas industriales seleccionadas. Las características de esta agua real se resumen en la **Tabla 2**.

Tabla 2. Características principales del agua real utilizada.

Parámetros	Valores
Carbono total (mg L^{-1})	103,1
TOC (mg L^{-1})	15,0
Nitrógeno total (mg L^{-1})	66,0
Conductancia (mS)	2,6 (equivale a Na_2SO_4 12 mM)
pH	7,5
Na^+ (mM)	11,6
Ca^{2+} (mg L^{-1})	1,5
K^+ (mM)	1,0
N-NH_4^+ (mM)	1,5
N-NO_3^- (mM)	0,02
SO_4^{2-} (mM)	1,3
Cl^- (mM)	11,4

Como se puede ver, esta agua tiene el carbono total muy alto en comparación con el TOC, lo que sugiere la presencia de grandes cantidades de iones HCO_3^- o CO_3^{2-} debido al pH alcalino. La pequeña cantidad de TOC en el agua indica la presencia de compuestos orgánicos, algunos de los cuales pueden ser contaminantes orgánicos como los POPs y otros forman parte de la llamada materia orgánica natural (ácidos húmicos y fúlvicos). Su conductancia es muy baja en comparación con la de una disolución de Na_2SO_4 0,05 M (10,5 mS), debido al reducido contenido en sales inorgánicas. No se detectaron iones de hierro, mientras que se encontraron concentraciones muy altas de ion cloruro, lo que puede afectar a capacidad de oxidación de los EAOPs estudiados en la presente Tesis.

Por otra parte, las disoluciones tratadas en la planta pre-piloto se prepararon con agua desionizada obtenida del sistema de producción propio de la Facultad de Química (UB).

El Ponceau 4R (contenido de colorante 100%) utilizado era de la casa Acros Organics. El Rojo Allura AC (contenido de colorante ≥ 80%), la Carmoisina (contenido de colorante ≥ 60%) y la Tartrazina (contenido de colorante ≥ 85%) fueron suministrados por Sigma-Aldrich. Los cuatro colorantes se usaron tal y como se recibieron. El sulfato de sodio anhidro, el cloruro de sodio, el nitrato de sodio y el perclorato de litio, usados como electrolito de fondo, eran de Fluka y Sigma-Aldrich. En los EAOPs basados en la reacción de Fenton se empleó como fuente de catalizador el sulfato de hierro (II) heptahidratado de la casa Sigma-Aldrich. El pH se ajustó mediante la adición de ácido sulfúrico, clorhídrico, nítrico o perclórico de grado analítico suministrados por Merck, Acros Organics y Panreac. El H_2O_2 (33% v/v) utilizado para realizar la recta de calibración para determinar el H_2O_2 electrogenerado fue suministrado por Panreac. La concentración de H_2O_2 electrogenerado se determinó empleando oxisulfato de titanio (IV) hidratado ($TiOSO_4 \cdot H_2O$) de Riedel-de-Haën. Los disolventes orgánicos para la preparación de la fase móvil en HPLC y otros productos cromatográficos fueron de grado HPLC o analítico de Aldrich, Lancaster, Merck o Panreac. La **Tabla 3** presenta los ácidos carboxílicos alifáticos de cadena corta, de grado analítico, utilizados como patrones para la identificación y cuantificación de los ácidos generados durante la degradación de los colorantes; dicho análisis se realizó mediante HPLC de exclusión iónica.

Tabla 3. Ácidos carboxílicos de cadena corta identificados como productos de degradación de los colorantes estudiados.

Ácido	Estructura	Proveedor	Pureza
Fórmico	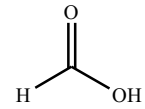	Panreac	98%
Oxálico	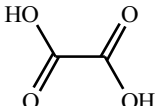	Panreac	99%
Oxámico	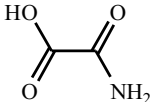	Avocado	98%
Tartrónico	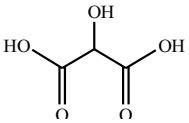	Alfa Aesar	98%
Maleico	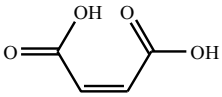	Panreac	99%
Fumárico	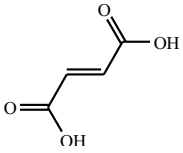	Panreac	99%
Tartárico	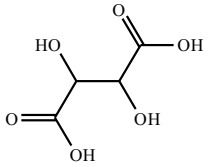	Aldrich	99%

3.2. Sistema experimental

3.2.1. Experimentos a escala de laboratorio

Los experimentos a escala de laboratorio se llevaron a cabo en condiciones galvanostáticas, suministrando una intensidad de corriente constante mediante un potenciostato-galvanostato EG&G modelo 273A. El voltaje se determinó en continuo mediante un multímetro 601 BR de la casa Demestres. Los ensayos se efectuaron en una celda cilíndrica monocompartimental o dividida de vidrio con capacidad para unos 150 mL, dotada de una camisa por la que circulaba agua a temperatura contante regulada por un baño termostático. En todos los experimentos se introdujo en la celda 130 mL de la disolución a tratar, manteniendo su temperatura a 25 °C bajo agitación vigorosa con un

núcleo magnético a 800 rpm para favorecer el transporte de materia de las especies hacia los electrodos y viceversa.

Los experimentos de EO se llevaron a cabo tanto en celda dividida como no dividida. Para operar en celda divida se utilizó un tubo de vidrio con una placa fritada en su parte inferior para separar el catolito del anolito (**Figura 11**). En el tubo se introdujo un hilo de acero inoxidable o Pt como cátodo o ánodo, respectivamente, y 5 mL de la misma disolución soporte que se añadió al compartimento principal pero sin colorante. En el compartimento principal se introducía una placa de Pt, BDD o acero inoxidable de 3 cm^2. Se estudiaron distintas combinaciones de electrodos (BDD ‖ hilo de acero, Pt ‖ hilo de acero, hilo de Pt ‖ acero e hilo de Pt ‖ADE) para evaluar la contribución de ánodo y del cátodo durante la degradación de los colorantes. Por su parte, la EO en celda no dividida se realizó en la misma celda cilíndrica que los procesos EF y PEF (**Figura 12)**, dentro de la cual se colocaron directamente las placas usadas como ánodo y cátodo o bien el cátodo de ADE.

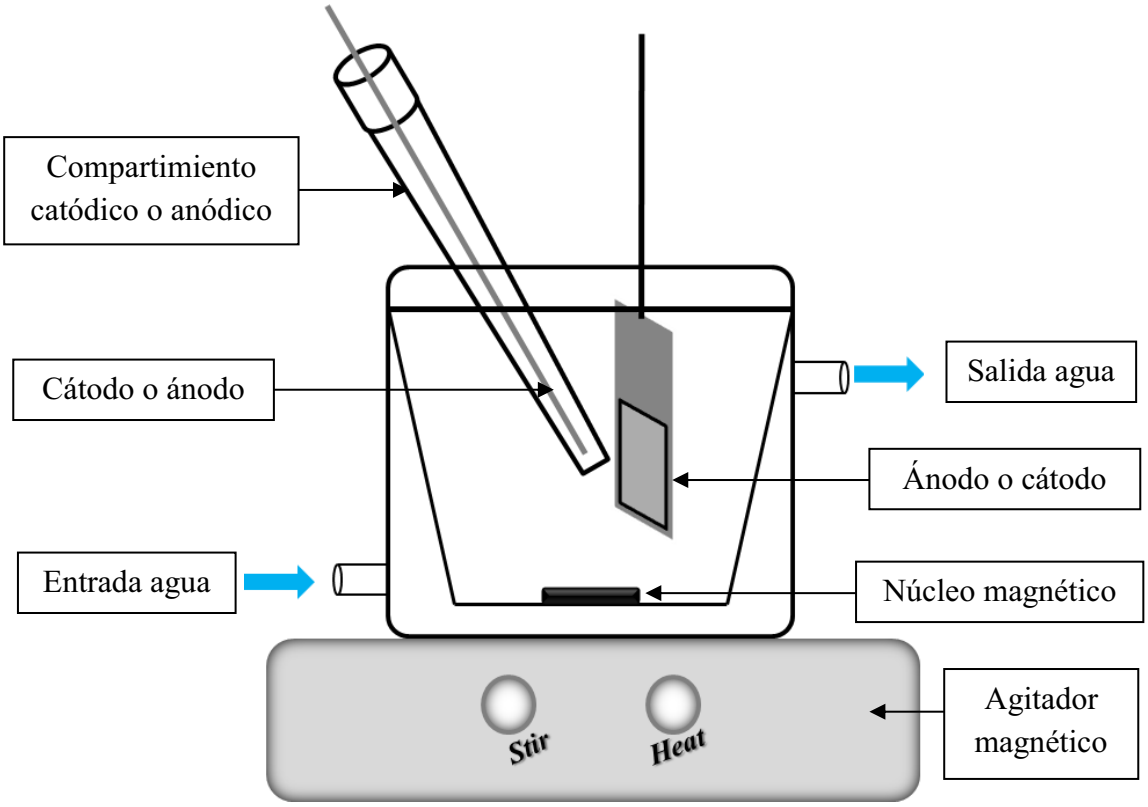

Figura 11. Sistema experimental utilizado para la EO en celda dividida.

En todos los experimentos realizados en el LEMMA (UB) se usó un ánodo de BDD suministrado por NeoCoat (La-Chaux-de-Fonds, Suiza) o Pt (pureza > 99.99%) suministrado por SEMPSA (Barcelona, España), y un cátodo de acero inoxidable (AISI 304) para la EO sin electrogeneración de H_2O_2 o de difusión de aire proporcionado por E-TEK (Somerset, NJ, USA) para la EO con electrogeneración de H_2O_2 (EO-H_2O_2), EF y PEF. El área electroactiva fue de 3 cm^2 en todos los casos y la distancia entre electrodos se mantuvo aproximadamente en 1 cm con el objetivo de obtener una buena reproducibilidad, minimizar la caída óhmica y aplicar el menor voltaje de celda posible. Sólo en los experimentos en celda dividida algunas de estas placas electródicas se substituyeron por hilos apropiados. Los electrodos de BDD y ADE han sido los más utilizados en la Tesis, motivo por el cual se describen sus preparaciones a continuación.

El ánodo más prometedor y ampliamente estudiado en los EAOPs en esta Tesis es el de BDD. Los electrodos de BDD son comúnmente preparados mediante la técnica de deposición química de vapor por filamento caliente (HFCVD) sobre una lámina conduc-

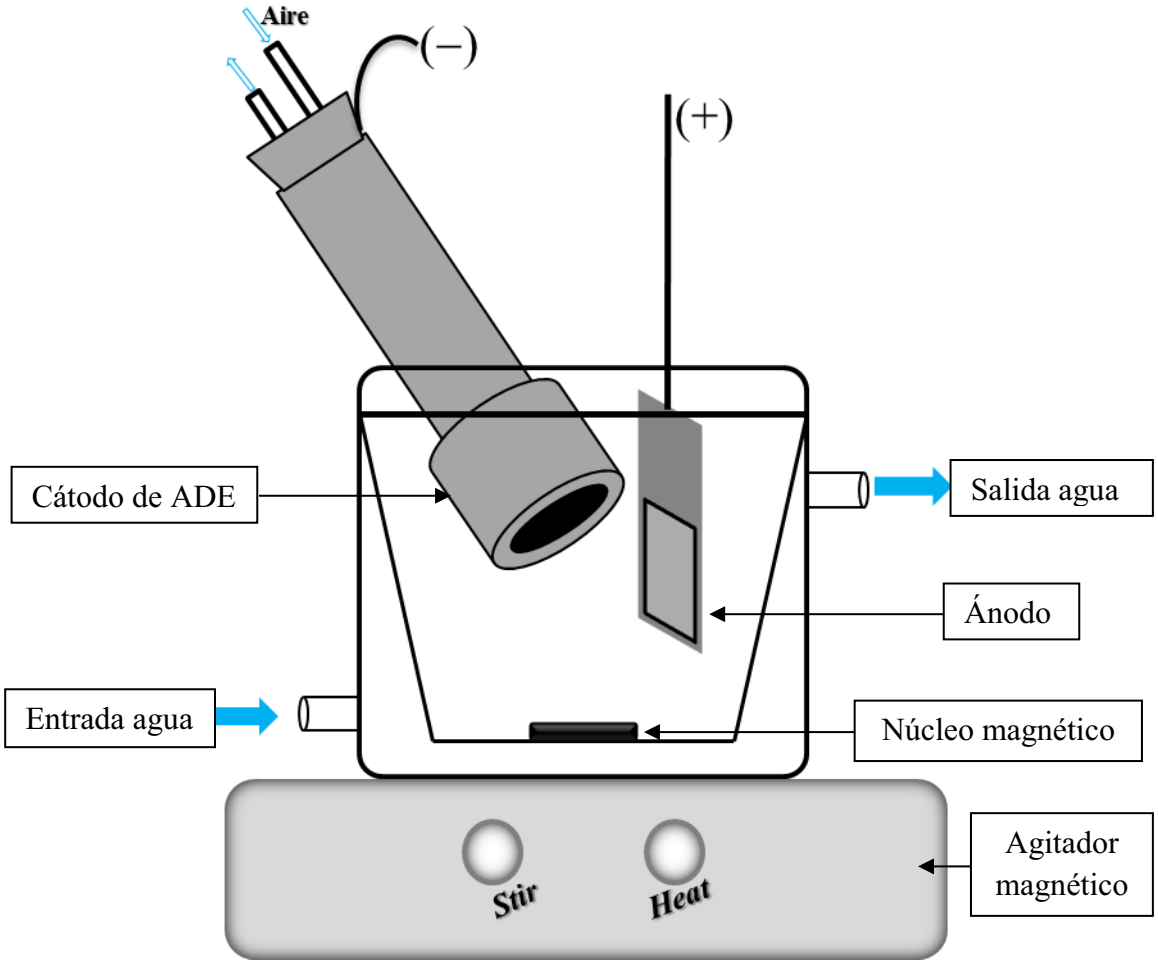

Figura 12. Sistema experimental utilizado para los experimentos en celda no dividida.

tora de *p*-silicio policristalino con resistividad = 1 Ω cm^{-2}. También se han utilizado otros soportes mecánicamente más resistentes como titanio, molibdeno y niobio. Básicamente, el procedimiento de deposición implica una reacción en fase gaseosa, utilizando un exceso de hidrógeno mezclado con un precursor de hidrocarburo (normalmente metano) para depositar diamante sobre el sustrato. El diamante es un aislante eléctrico, pero la introducción de algún átomo dopante en su estructura le confiere propiedades de semiconductor e incluso de material electrónico. El dopante más utilizado es el boro, el cual da lugar a un diamante semiconductor tipo *p*. La fuente de boro puede ser un compuesto volátil que se introduce en los gases reactivos, como el trimetilborato. La mezcla gaseosa pasa a través de un filamento caliente de W o Ta (2200-2600 °C), que juega el papel de proveedor de energía y catalizador en la disociación de H_2 y la formación de radical metilo. Esta mezcla activa se dirige hacia la superficie del sustrato donde se forma una película de carbón por adsorción o fusión, como se puede observar en la **Figura 13**. El sustrato se mantiene a 830 °C y a 20-25 bares de presión durante todo el proceso. Mediante esta técnica se obtienen depósitos delgados de BDD de diferentes espesores. Los electrodos utilizados en el presente trabajo tenían un espesor entre 2,5 y 3,5 µm con un dopaje de 700 ppm de boro.

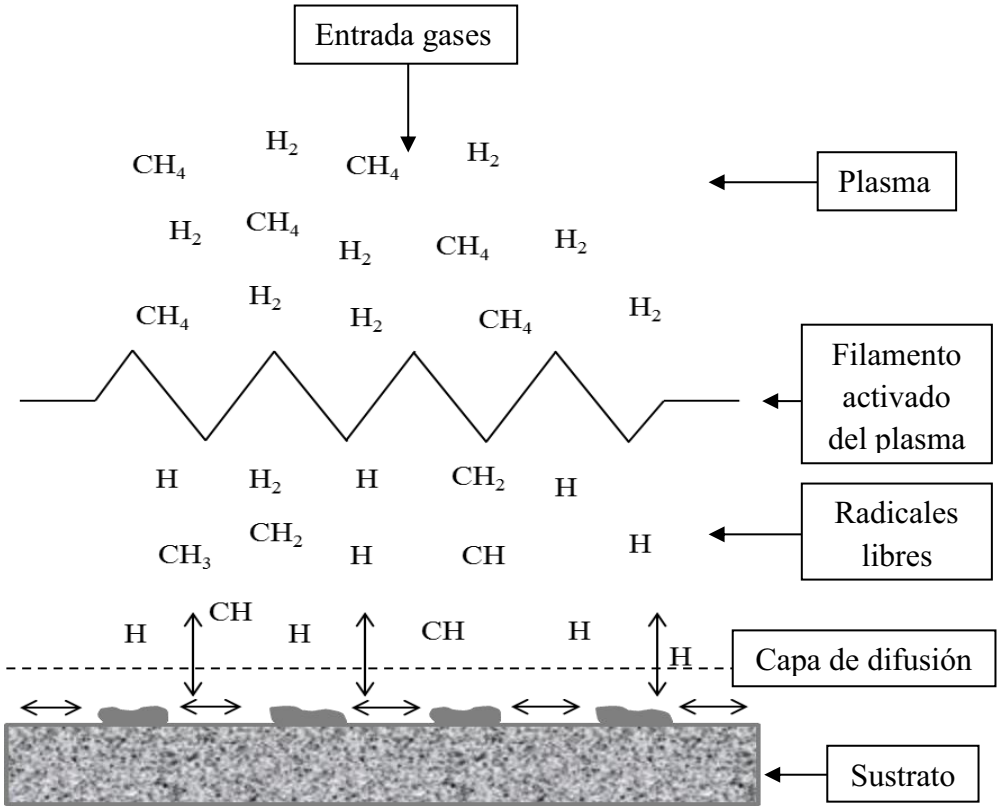

Figura 13. Esquema de la síntesis del BDD en un reactor HFCVD.

En la **Figura 14** se muestran los diferentes componentes del ADE utilizado para realizar los tratamientos de EO-H_2O_2, EF y PEF. El ADE consta de una tela comercial de carbón-politetrafluoroetileno (C-PTFE) que se corta en secciones circulares de 2 cm de diámetro para ser utilizado como cátodos, colocándose en la parte inferior de un tapón de rosca de polipropileno. El lado exterrno, es decir, la cara en contacto con la disolución, es la parte electroactiva de la tela. Para mejorar y distribuir adecuadamente la carga eléctrica aplicada en toda la superficie del tejido, así como su resistencia mecánica, se coloca sobre el lado interno una malla de Ni con las mismas dimensiones que la tela. La malla de Ni actúa de colector eléctrico y está en contacto con un hilo de Ni-Cr cuya función es de conector o contacto eléctrico. El aire se introduce a través de un tubo de vidrio, colocado en la parte interna del soporte de polipropileno, con un flujo de 1 L min^{-1}. El exceso de aire se expulsa gracias a un tubo de salida con el fin de evitar un exceso de sobrepresión. El ADE presenta una eficiencia muy alta para la generación de H_2O_2 mediante la reacción (49) (Garcia-Segura y col., 2011).

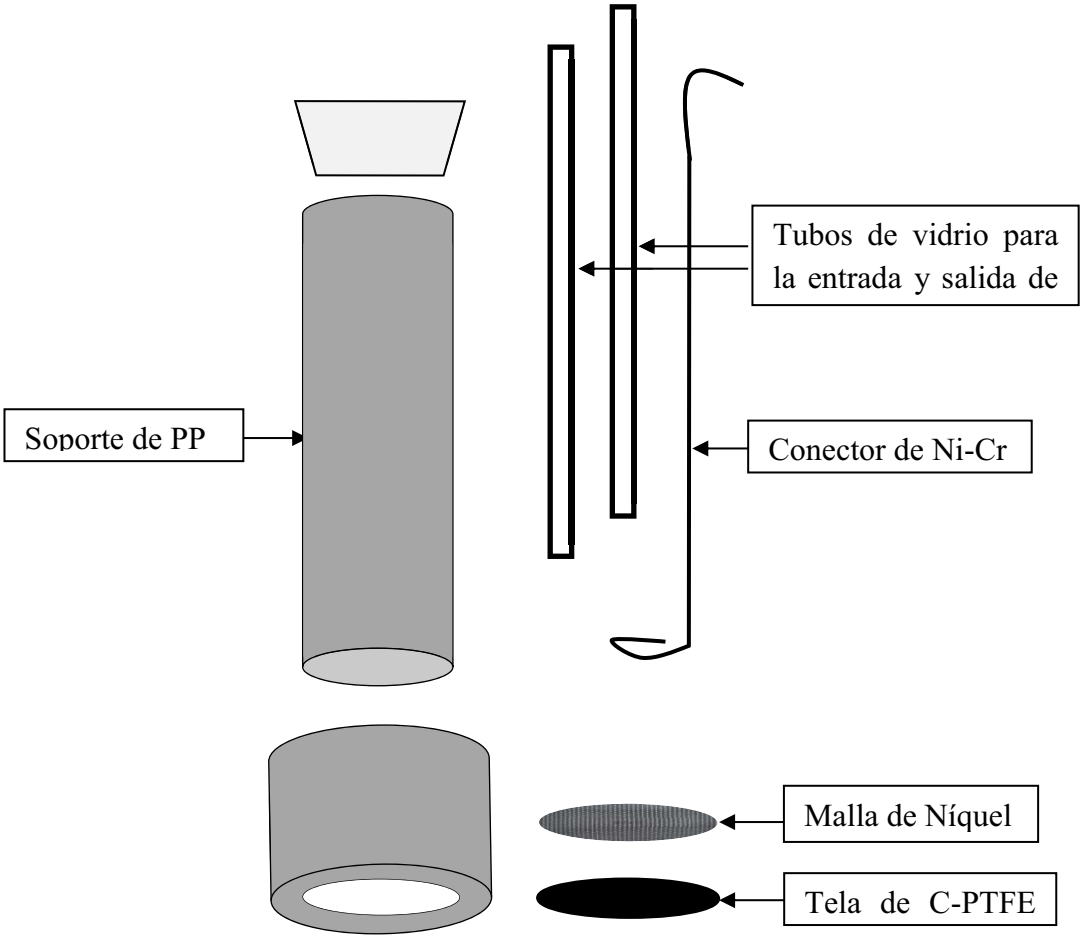

Figura 14. Esquema del electrodo de difusión de aire (ADE).

Durante la estancia realizada en la Nankai University (Tianjin, China) se realizó un estudio comparativo de la degradación del colorante Tartrazina mediante los procesos individuales de EC y EAOPs y la combinación secuencial de los dos (EC/EAOPs). Los EAOPs se llevaron a cabo en las mismas condiciones descritas anteriormente utilizando los mismos electrodos. En cuanto al proceso de EC, los experimentos se llevaron a cabo en la misma celda no dividida descrita para los EAOPs, utilizando como ánodo una placa de hierro o aluminio con un área electroactiva de 10 cm^2 (3 cm × 1.5 cm, con 0.25 cm de grosor), siendo el cátodo de acero inoxidable (AISI 304). La distancia entre los electrodos se mantuvo en 1 cm. Se determinó el peso de los electrodos antes y después de cada experimento para saber la pérdida de peso de cada ánodo con el fin de calcular la eficiente de corriente del proceso. De cara a realizar los procesos integrados de EC/EAOPs, se filtraron las disoluciones tratadas por EC con el fin de eliminar el precipitado y recuperar la parte líquida, la cual se trató mediante los EAOPs deseados.

El acondicionamiento de los electrodos previamente a su utilización es muy importante para conseguir unas condiciones reproducibles. Se encontró que una polarización preliminar en 130 mL de una disolución de Na_2SO_4 0,05 M a 300 mA durante 180 min permitía la eliminación de las impurezas del ánodo de BDD y la activación del ADE. Por otra parte, el ADE se lava con HCl (25% en volumen) y agua milli-Q después de cada experimento de EF y PEF para eliminar el hierro que se deposita sobre la tela. Los electrodos de hierro y aluminio utilizados en EC fueron pulidos mecánicamente con papel de SiC para eliminar incrustaciones, seguido de una limpieza con NaOH 0,1 M o una disolución de H_2SO_4 (20% en volumen) y una limpieza final con ultrasonidos en agua milli-Q.

En los experimentos de PEF, las disoluciones se irradiaron simultáneamente con luz UVA, utilizando para ello un fluorescente Philips de 6W, cuya espectro de emisión se sitúa entre 300 y 420 nm con una longitud de onda máxima a 360 nm. La lámpara se colocó 7 cm por encima de la superficie de la disolución, emitiendo una energía de fotoionización en la disolución de 5 W m^{-2}, la cual se determinó con un radiómetro de la casa Kipp & Zonen modelo CUV 5.

3.2.2. Experimentos en planta pre-piloto

Los resultados obtenidos en la celda pequeña mediante los procesos de EC y EAOPs y la combinación de EC/EAOPs constituyen un buen punto de partida para el

escalado. Así, se ha utilizado una planta pre-piloto con recirculación para demostrar la viabilidad de los métodos durante el tratamiento de mayores volúmenes. Para los EAOPs, las electrolisis se realizaron en una planta pre-piloto de 2,5 L de capacidad, cuyo esquema se presenta en la **Figura 15**. La disolución contaminada por los colorantes a tratar se introduce en el depósito y es impulsada a lo largo del circuito mediante una bomba centrífuga. La velocidad de flujo se mantuvo constante a 200 L h^{-1} utilizando un rotámetro, y la temperatura de la disolución se reguló siempre a 35 ºC utilizando un baño termostático y dos intercambiadores de calor. Se utilizó una celda electroquímica tipo filtro-prensa de un compartimento. El esquema detallado del reactor electroquímico se presenta en la **Figura 16**. La celda contenía componentes de 8 cm × 12 cm de dimensiones, separados por juntas de vitón para evitar fugas, y estaban empaquetados entre dos grandes placas terminales de acero inoxidable.

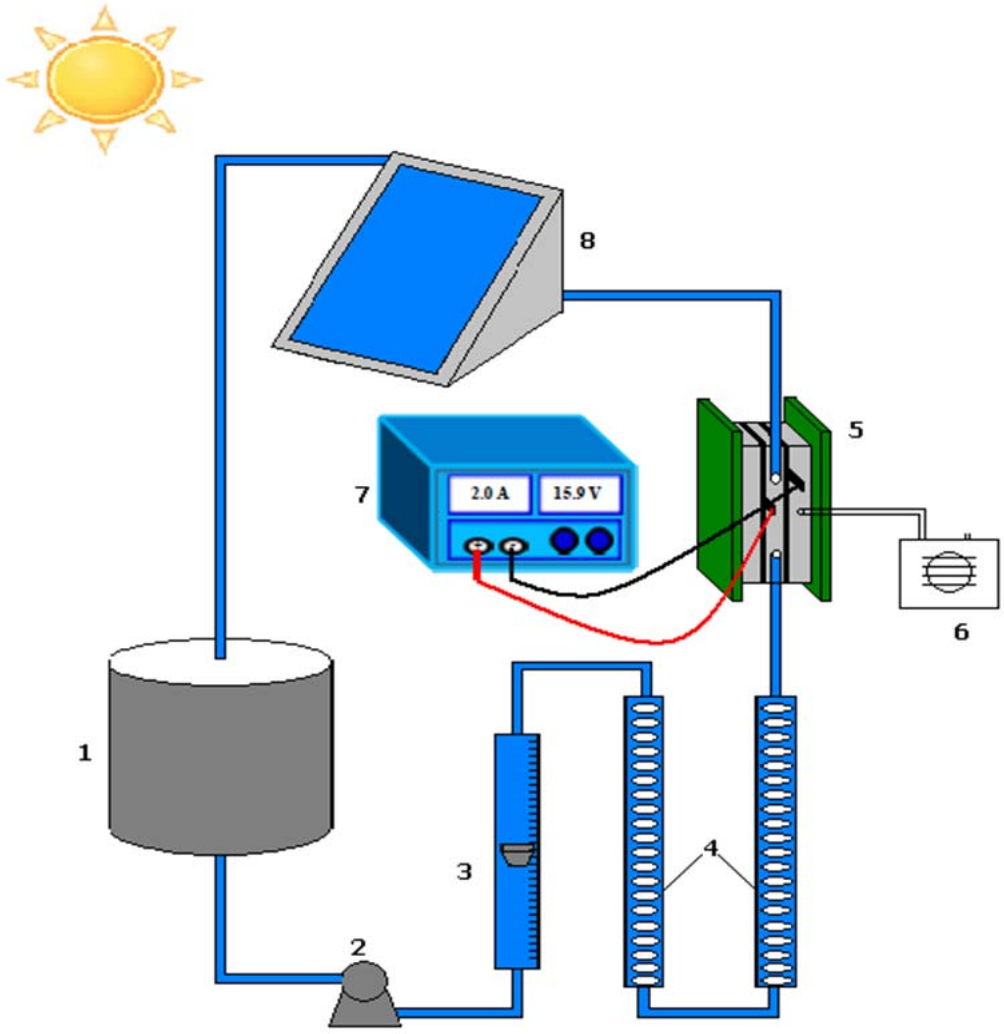

Figura 15. Planta pre-piloto de 2,5 L de capacidad para el tratamiento electroquímico de aguas mediante EAOPs usada en el LEMMA: (1) Depósito, (2) bomba centrífuga, (3) rotámetro, (4) intercambiadores de calor, (5) celda electroquímica, (6) bomba de aire, (7) fuente de alimentación y (8) fotorreactor.

En los trabajos realizados en el LEMMA, se utilizó como ánodo una placa de Pt (pureza del 99,99%) de SEMPSA (Barcelona, España) o BDD de Adamant Technologies, y como cátodo un ADE de C-PTFE de E-TEK (Somerset, NJ, USA). Entre los dos electrodos se coloca un compartimento de PVC (volumen de 24 mL) con una ventana central de 4 cm × 5 cm (área expuesta de 20 cm^2) para contactar la disolución a tratar con sus caras exteriores, con 1,2 cm de separación entre ambas. La cara interna del cátodo es presionada contra una malla de Ni empleada como colector, como en el caso del ADE a escala de laboratorio, y está en contacto con una cámara de PVC alimentada con aire atmosférico a un sobrepresión de 8,6 kPa para producir continuamente H_2O_2. Tras su salida de la celda filtro-prensa, la disolución pasa a través de un fotorreactor solar. Éste consiste en un recipiente rectangular de policarbonato de dimensiones 24 cm × 24 cm × 2,5 cm (600 mL de volumen de disolución, colocado con una inclinación de 41^o y que posee un espejo en el fondo para reflejar la radiación solar. Los experimentos de SPEF se llevaron a cabo durante los veranos de 2013 y 2014 en el LEMMA, Barcelona (latitud: 41º 21'N, longitud: 2º 10'E), con una radiación solar incidente promedio de alrededor de 30 W m^{-2}.

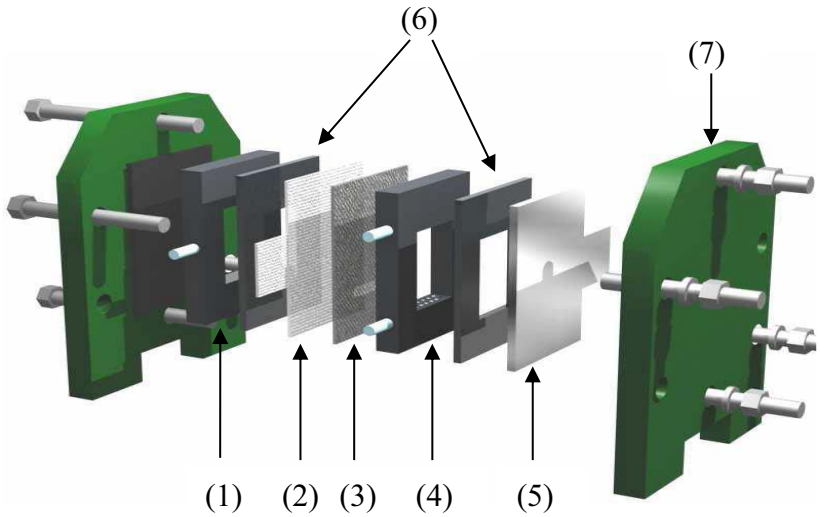

Figura 16. Esquema del reactor electroquímico tipo filtro-prensa: (1) Compartimento de aire, (2) malla de níquel, (3) tela de C-PTFE, (4) compartimento del líquido, (5) ánodo de BDD o Pt, (6) juntas de vitón y (7) placas terminales de acero inoxidable.

Durante el segundo periodo en la Nankai University se escalaron en una planta pre-piloto de 2 L de capacidad los sistemas de EC y EC/EAOPs estudiados a escala pequeña durante la primera estancia. Los EAOPs se llevaron a cabo en un sistema similar al

presentado en el apartado anterior. Se utilizó como ánodo un DSA (ánodo de Ti/IrO_2-RuO_2 preparado por descomposición térmica) suministrado por Baoji Zhiming Special Metals Co. Ltd, (China), y como cátodo un ADE de C-PTFE de E-TEK (Somerset, NJ, USA). En los experimentos de PEF, las disoluciones se irradiaron directamente en el depósito con luz UVA por medio de una lámpara de 125 W de Philips, con una longitud de onda máxima de 360 nm (**Figura 17)**. Por su parte, el sistema para los ensayos de EC consistió en un reactor de tanque abierto paralelepípedo con una base trapezoidal, de material acrílico y con una capacidad de 2 L (**Figura 18**). La disolución se mantenía bajo agitación vigorosa mediante un agitador a 800 rpm para favorecer el transporte de materia de las especies hacia los electrodos y viceversa. Se utilizaron cuatro placas de hierro con dimensiones 11 cm × 10 cm (0,1 cm de espesor) como electrodos, con una superficie sumergida de 7.5 cm × 10 cm. Como la parte anterior y posterior de cada pieza, así como sus lados, están en contacto con la disolución, su área sumergida resultaba ser de 150 cm^2. Los electrodos se conectaron a una fuente de alimentación en tres modos de conexión eléctrica (**Figura 19**).

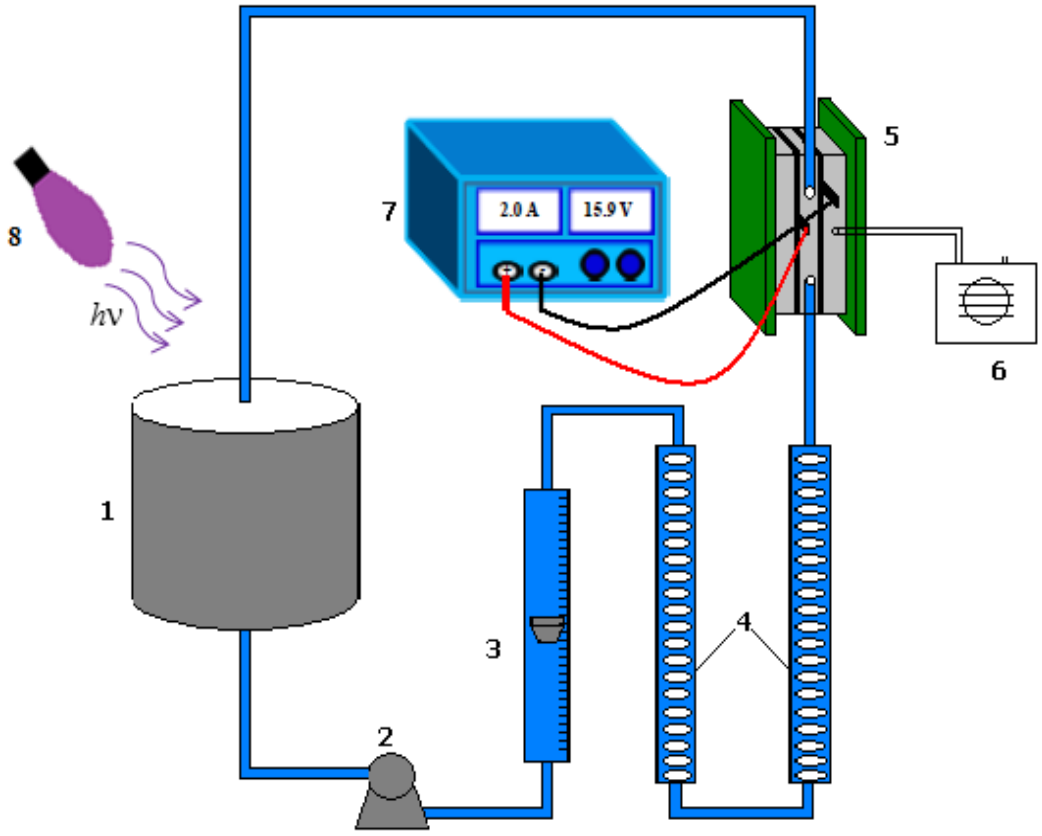

Figura 17. Planta pre-piloto de 2 L de capacidad para el tratamiento electroquímico de aguas mediante EAOPs en Nankai: (1) Depósito, (2) bomba centrífuga, (3) rotámetro, (4) intercambiadores de calor, (5) celda electroquímica, (6) bomba de aire, (7) fuente de alimentación y (8) lámpara UVA.

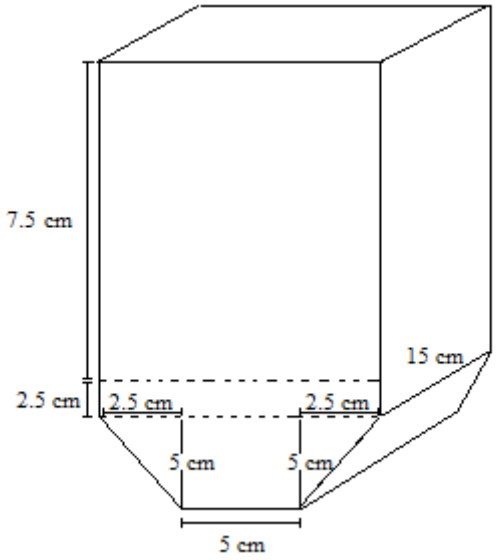

Figura 18. Esquema del reactor de tanque abierto paralelepípedo con una base trapezoidal utilizado para los experimentos de EC en Nankai.

✓ Monopolar en paralelo (MP-P):

Cada uno de los cuatro electrodos se conectan individualmente a la fuente de alimentación; dos ánodos y dos cátodos se colocan alternados en el paquete de electrodos (**Figura 19a**). Los dos electrodos con polaridad positiva se consumen durante los experimentos, mientras que los otros dos con polaridad negativa son insolubles.

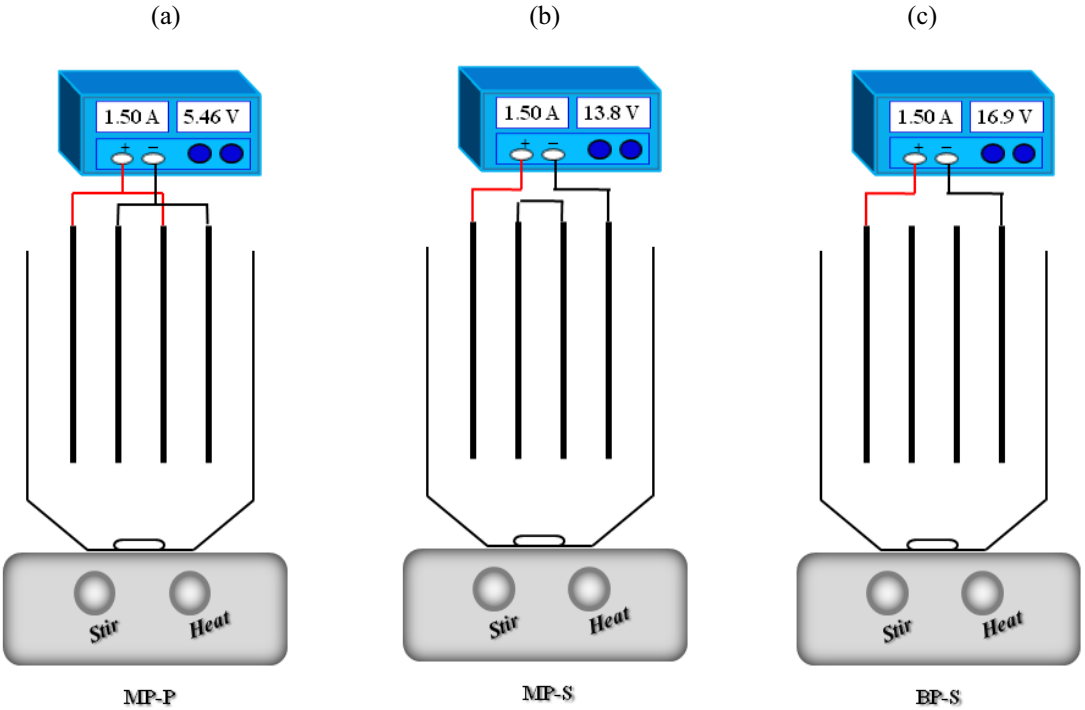

Figura 19. Diferentes modos de conexión eléctrica para llevar a cabo la EC a escala de planta pre-piloto: (a) monopolar en paralelo, (b) monopolar en serie y (c) bipolar en serie.

- ✓ Monopolar en serie (MP-S):

Los dos electrodos extremos se conectan a la fuente de alimentación como ánodo y cátodo, respectivamente, mientras que los dos internos se conectan entre ellos (**Figura 19b**).

- ✓ Bipolar en serie (BP-S):

En esta configuración, se conectan solamente los dos electrodos extremos, como en la configuración MP-S, pero los dos electrodos internos no están conectados entre ellos operando como placas bipolares (**Figura 19c**). Los dos electrodos internos funcionan como electrodos gracias a la polarización inducida por los electrodos externos.

3.3. Métodos de análisis

3.3.1. Cuantificación del H_2O_2 y del Fe^{2+}

Una de las formas de detectar el H_2O_2 es mediante análisis espectrofotométrico del peroxocomplejo que forma con la especie Ti(IV) en medio ácido y en presencia de ion sulfato según la reacción (62):

$$Ti^{4+} + H_2O_2 + 2SO_4^{2-} \leftrightarrows [TiO_2(SO_4)_2]^{2-} + 2H^+ \qquad (62)$$

Este complejo, cuya absorción máxima se da a 408 nm, tiene un color amarillo-naranja y su intensidad es directamente proporcional a la concentración de H_2O_2. La medida puede verse distorsionada por la presencia de hidroxocomplejos de Fe(III) de color amarillo que absorben también a la longitud de onda de medida. Esta interferencia puede eliminarse en medio acido. La técnica espectrofotométrica es más rápida y sensible que la valoración permanganométrica, que se ha utilizado en ocasiones para determinar la concentración de H_2O_2, debido a la existencia de reductores (Fe^{2+}, materia orgánica, etc.) que interfieren en este último método.

El procedimiento para el seguimiento de la evolución de H_2O_2 consta de dos pasos fundamentales, la preparación del reactivo de titanio y la obtención de la recta de calibración que relaciona la absorbancia de las muestras con la concentración del H_2O_2:

(a) Para obtener el reactivo de titanio, se prepara una disolución de concentración 20 mM a partir de $TiO(SO_4)$, sólido blanco, pesando 3,20 g que se disuelven en un 1 L de una mezcla de agua milli-Q con ácido sulfúrico concentrado.

(b) Para obtener la recta de calibración, se utilizó una disolución comercial de H_2O_2 (33%), y se valora con permanganato de potasio previamente estandarizado con

H_2O_2 al 33% v/v. A partir de ella se prepararon 5 disoluciones diluidas, la cuales se valoraron permanganométricamente para determinar su concentración exacta. La curva de calibración espectrofotométrica para el complejo peroxo-titanato se determinó midiendo la absorbancia para cada disolución diluida, utilizando un espectrofotómetro UV/vis de doble haz Unicam UV4 Prisma, termostatizado a 25 °C, con cubetas de 1 cm de camino óptico.

Las medidas, tanto de las disoluciones patrón como de las muestras electrolizadas, se realizaron tomando 0,5 mL de las disoluciones y añadiendo 4 mL del reactivo de Ti(IV) y 1,5 mL de disolución de Na_2SO_4 0,05 M, enrasándose finalmente a 10 mL con agua milli-Q. La absorbancia de las muestras se determinó frente a un blanco que contenía la misma disolución excepto el peróxido de hidrógeno.

En cuanto a la concentración de las especie Fe^{2+}, ésta se ha determinado también mediante el método espectrofotométrico UV-vis, el cual detecta el complejo rojo que forma el Fe^{2+} con la *o*-fenantrolina a λ = 508 nm. El procedimiento consistió en añadir 1 mL de *o*-fenantrolina y 1 mL de tampón de acetato a 4 mL de muestra. Para conocer la concentración de hierro total se añadió a la mezcla anterior una cantidad sólida de ácido ascórbico, la cual reduce el posible Fe^{3+} a Fe^{2+}.

3.3.2. Cuantificación del cloro activo

El cloro activo se determinó mediante espectrofotometría UV-vis con *N*-*N*-dietilparafenilendiamina (DPD). El fundamento de este método consiste en que el cloro

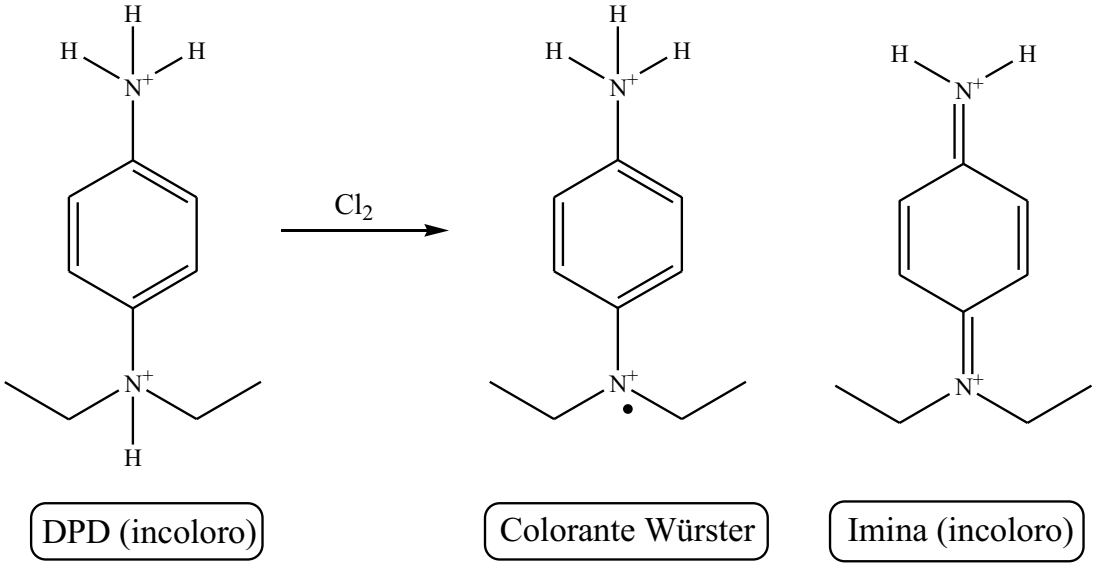

Figura 20. Mecanismo de oxidación del DPD por parte del cloro activo.

activo, al reaccionar con la DPD, genera un color rosa proporcional a su concentración en la muestra, cuyo máximo de absorción se produce a 515 nm (APWA, AWWA,WEF, 2005). Cuando la DPD reacciona con pequeñas cantidades de cloro activo a un pH casi neutro, el colorante llamado Würster es el producto de oxidación principal. A cantidades muy elevadas del oxidante, la formación de la imina incolora se favorece. El mecanismo de oxidación del DPD por el cloro activo se muestra en la **Figura 20**.

Las principales interferencias que pueden aparecer en esta técnica se deben a la presencia de oxidantes, como el manganeso o el cobre. Estas interferencias pueden ser controladas por el EDTA hasta una concentración de 10 mg L^{-1} (Navajas y col., 2001). Los principales reactivos utilizados en esta técnica son una disolución indicadora de DPD y una disolución de tampón de fosfato. Para preparar 1 L de la primera, se disuelven 1,1 g de sulfato de DPD en agua Milli-Q acidificada previamente con 20 mL de ácido sulfúrico al 10% v/v, conteniendo además 25 mL de disolución de EDTA disódico al 0,8%. Para preparar 1 L de tampón, se disuelven 24 g de Na_2HPO_4 anhidro y 46 g de KH_2PO_4 anhidro en agua milli-Q y se mezclan con 100 mL de disolución de EDTA disódico al 0,8%. La recta de calibración se obtiene disolviendo 0,891 g de $KMnO_4$ en 1 L de agua milli-Q, lo que equivale a 1000 mg L^{-1} de cloro activo. Esta disolución se estandariza con oxalato de sodio. Las medidas se llevaron a cabo tomando 10 mL de muestra, a las que se añadieron 0,5 mL de disolución indicadora de DPD y 0,5 mL de disolución tampón. La absorbancia se determinó tras 2 min, utilizando un espectrofotómetro UV-Vis de la casa Shimadzu modelo 1800 (**Figura 21**).

Adicionalmente, la concentración de hipoclorito se determinó midiendo la absorbancia de la muestra electrolizada a λ = 292 nm con el mismo instrumento.

3.3.3. Estudio de la decoloración mediante espectrofotometría UV-visible

La decoloración de las disoluciones acuosas de los diferentes colorantes azoicos se siguió a través del descenso de la absorbancia (A) a la longitud de onda máxima característica de cada colorante, haciendo uso del espectrofotómetro UV-vis de doble haz Shimadzu 1800, termostatizado a 35 ºC. El porcentaje de eliminación de color (% CR) o eficiencia de decoloración se calcula como sigue:

$$\text{CR (\%)} = \frac{A_0 - A_t}{A_0} \times 100 \qquad (63)$$

donde A_0 y A_t son la absorbancia al tiempo inicial y a tiempo t, respectivamente.

Figura 21. Espectrofotómetro UV-vis Shimadzu modelo 1800.

3.3.4. Determinación del carbono orgánico total

La medida del TOC de las disoluciones iniciales y tratadas se efectuó utilizando un equipo TOC-VCSN de Shimadzu (**Figura 22**). El equipo era previamente calibrado con patrones de hidrogenoftalato de potasio, alcanzándose una reproducibilidad del ±1%. Para la medida del TOC, el equipo inyecta un pequeño volumen de muestra en un horno catalítico a 680 ºC, de manera que todo el carbono contenido en la disolución se incinera a CO_2. Éste es arrastrado por una corriente de aire sintético hacia un detector de infrarrojos no dispersivo que proporciona una señal que es directamente proporcional a su concentración. Esta medida corresponde al carbono total (TC), que es la suma del carbono orgánico e inorgánico. El TOC de las disoluciones se puede determinar midiendo el carbono inorgánico. Sin embargo, en esta Tesis se ha utilizado el método de

Figura 22. TOC-VCSN acoplado a un módulo TNM-1.

Figura 23. Multi N/C®3100 Analyzer de Analytik Jena.

la medida del carbono orgánico no purgable (NPOC), que consiste en acidificar las muestras y gasificar para purgar el CO_2 generado a partir del carbono inorgánico antes de que la muestra se inyecte en el horno.

El TOC-VCSN de Shimadzu utilizado en este trabajo está acoplado a un módulo TNM-1 (*total nitrogen measurement*) para medir el nitrógeno total en algunas muestras estudiadas. La medida del nitrógeno total se basa en la combustión de todas las especies de nitrógeno a monóxido de nitrógeno en el horno a 680 ºC.

Durante mi estancia en China, las medidas del TOC y TN se efectuaron utilizando un equipo Multi N/C®3100 Analyzer de Analytik Jena (**Figura 23**).

3.3.5. Identificación de los intermedios de degradación

Los intermedios de degradación se identificaron por cromatografía, un método que permite la separación de los compuestos de una mezcla. Una de las características principales de la cromatografía es la presencia de dos fases, una estacionaria y otra móvil. La clave de la separación es que la velocidad con la que se mueve cada sustancia depende de su afinidad relativa por ambas fases. En general, los componentes más afines a la fase estacionaria avanzan lentamente (más retenidos), mientras que los más afines a la fase móvil (menos retenidos) se mueven con mayor rapidez. En consecuencia, la fase estacionaria funciona como un controlador de la velocidad de cada sustancia que constituye la mezcla, logrando así su separación y, mediante el uso de un detector, su análisis cualitativo y/o cuantitativo.

Figura 24. Cromatógrafo líquido HPLC Waters 600 acoplado a un detector de fotodiodos Waters 996.

3.3.5.1. Identificación y cuantificación de los colorantes y ácidos carboxílicos mediante HPLC

La identificación y cuantificación de los ácidos carboxílicos de cadena corta generados durante la degradación de los colorantes se realizaron por cromatografía HPLC de exclusión iónica utilizando un equipo Waters 600 acoplado a un detector de fotodiodos Waters 996 (**Figura 24**). La detección se realizó a λ = 210 nm. Se empleó una columna Aminex modelo HPX 87H (Bio-Rad) de 300 mm × 7,8 mm a 35 ºC por la que circuló una fase móvil de H_2SO_4 0,4 mM a 0,6 mL min^{-1}, inyectando 20 µL de muestra previamente filtrada con filtros Whatman de 0,45 µm. Los tiempos de retención obtenidos en estas condiciones para los ácidos identificados se recogen en la **Tabla 4**.

Tabla 4. Ácidos carboxílicos identificados por HPLC junto a su tiempo de retención.

Compuesto	t_r (min)	Compuesto	t_r (min)
Ácido oxálico	6,9	Ácido oxámico	9,4
Ácido tartrónico	7,9	Ácido fórmico	13,7
Ácido maleico	8,2	Ácido acético	14,8
Ácido tartárico	8,4	Ácido fumárico	14,9

En el caso de los colorantes, se determinó la cinética de degradación del AR 18 por cromatografía de fase inversa utilizando el mismo HPLC de Waters, a λ = 508 nm. Se empleó una columna ODS Hypersil de 5 μm, de 150 mm × 3 mm, de Thermo Electron Corporation utilizando una fase móvil de acetonitrilo/agua 80:20 (v/v) con adición de 2,4 mM butilamina a 0,2 mL min^{-1}.

3.3.5.2. Identificación de los intermedios aromáticos mediante GC-MS

Los intermedios aromáticos se detectaron mediante GC-MS. Esta técnica se basa en la diferencia de volatilidad de los compuestos químicos al aplicar una rampa de temperatura en el cromatógrafo de gases. Al salir del cromatógrafo, los compuestos son analizados en un espectrómetro de masas donde las moléculas sufren el impacto de un haz de electrones (método de impacto electrónico), produciéndose diferentes cationes y cationes-radicales que son separados por un campo eléctrico según la relación masa/carga (*m/z*). Los fragmentos producidos y su abundancia relativa (llamada huella o patrón de fragmentación) son característicos de cada sustancia química, lo que permite su identificación al compararlos con los obtenidos para productos puros, normalmente recogidos en una librería asociada al instrumento de medida.

El análisis por GC-MS requiere de un pretratamiento que permita eliminar el agua de las muestras a analizar. En este trabajo se han utilizado dos métodos, la extracción líquido-líquido con diclorometano (CH_2Cl_2) y la liofilización, después de electrolizar las disoluciones de 130 mL de los colorantes en unas condiciones determinadas durante tiempos cortos o largos. En el primer caso, se extrajeron las especies orgánicas obtenidas varias veces con volúmenes iguales de unos 25 mL de CH_2Cl_2. La disolución orgánica final se seca con Na_2SO_4 anhidro, se filtra y se rotavapora (o bien se utiliza una corriente suave de N_2 gas) a 40 °C con un rotavapor BUCHI modelo R-210 hasta sequedad. En ciertas ocasiones, después de su extracción los intermedios formados se derivatizaron añadiendo 2 mL de anhídrido acético o etanol antes de evaporar. Finalmente, la fase líquida se inyecta en el GC.

En cuanto a la liofilización, se transfirió el volumen de la disolución electrolizada a un tubo cónico de plástico y se congela con N_2 líquido. A continuación, se introduce el tubo en un liofilizador VirTis modelo BenchTop 6K (P < 5 mTorr a -55 °C), con lo que se elimina el agua de la muestra por sublimación. El proceso de liofilización duraba

varios días y, una vez finalizado, el residuo sólido en el que se encuentran tanto los intermedios orgánicos de degradación como las sales inorgánicas se trataba con un pequeño volumen de CH_2Cl_2 o etanol agitándose durante unos minutos. Se deja decantar hasta el día siguiente y se filtra la fase liquida para eliminar los compuestos insolubles. Como en el caso anterior, la fase líquida se inyecta en el cromatógrafo de gases. Los análisis de estas muestras se llevaron a cabo utilizando un sistema Agilent Technologies compuesto por un cromatógrafo de gases 6890N acoplado a un espectrómetro de masas 5975 operando en modo de impacto electrónico (EI) a 70 eV. Se han utilizado dos columnas diferentes, una apolar Agilent J&W HP-5ms y una polar HP INNOWax, ambas de 0,25 m × 30 m × 0,25 mm. Se aplicó la siguiente rampa de temperatura: 36 °C durante 1 min, con un incremento de 5 °C hasta alcanzar 300 °C y 250 °C para las columnas apolar y polar respectivamente, tras lo cual se mantiene el sistema a esta temperatura durante 10 min. La temperatura de la línea de entrada, la fuente y la línea de transferencia es de 250, 230 y 280 °C, respectivamente, para la columna apolar, y 250, 230 y 250 °C para la columna polar. Los espectros de masas obtenidos fueron comparados con los proporcionados por la librería NIST05.

3.3.5.3. Identificación y cuantificación de los iones inorgánicos mediante cromatografía iónica

Los iones inorgánicos fueron identificados y cuantificados mediante cromatografía iónica utilizando un HPLC Shimadzu modelo LC-10 ADvp equipado con un detector de conductividad Shimadzu CDD 10 Avp y un horno CTO-10 ACvp, estando todos ellos interconectados con el módulo de control SCL-10Asp (**Figura 25**). Se emplearon dos columnas diferentes, una para cationes Shodex IC YK-421, 125 mm × 4,6 mm, y otra para aniones Shim-Pack IC-A1S, 100 mm × 4,6 mm, conectadas a una precolumna Shodex-IA-G. La fase móvil para determinar cationes fue una disolución con ácido tartárico 5 mM, ácido dipicolinico 2 mM, ácido bórico 24 mM y éter corona 1,5 mM a un flujo de 1 mL min^{-1}. Para los aniones, la fase móvil fue una disolución de ácido ftálico 2,6 mM y tris(hidroximetil)aminometano 2,4 mM a un flujo de 1,5 mL min^{-1}. Los tiempos de retención de los iones identificados en este trabajo se recogen en la **Tabla 5**.

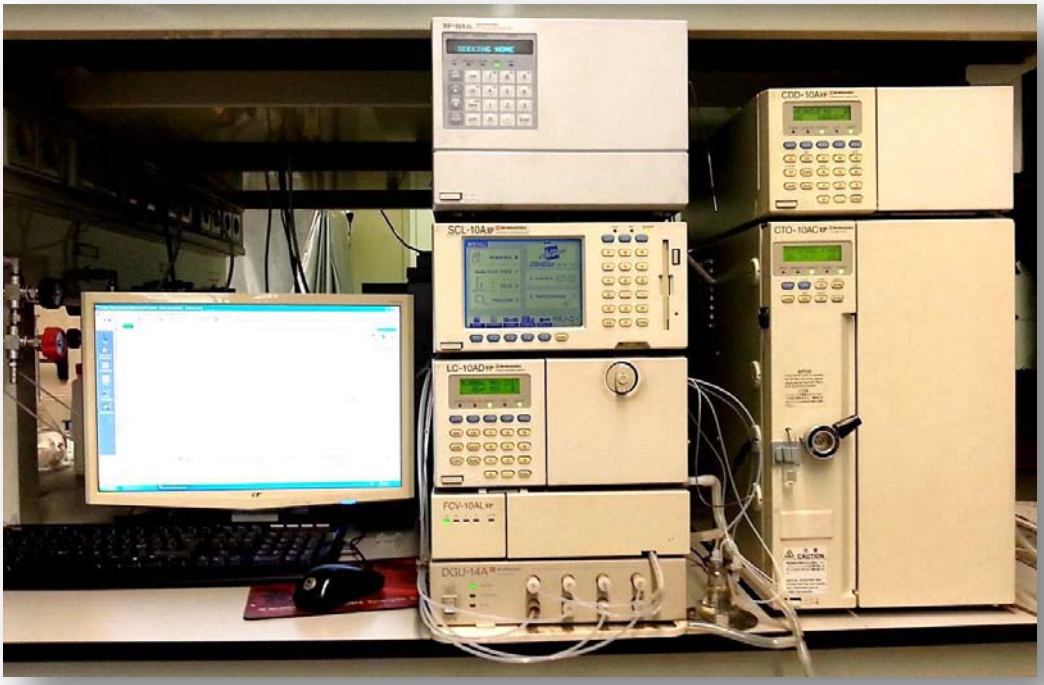

Figura 25. Cromatógrafo de líquidos Shimadzu LC-10 ADvp equipado con un detector de conductividad Shimadzu CDD 10 Avp y un horno CTO-10 ACvp.

3.3.6. Análisis mediante voltamperometría

Para la caracterización electroquímica de los ánodos, se estudiaron los procesos de oxidación que tiene lugar sobre su superficie en todos los electrolitos soporte empleados, en presencia y ausencia de colorante, utilizando un potenciostato-galvanostato Ecochemie modelo Autolab PGSTAT100 controlado mediante el software

Tabla 5. Iones inorgánicos identificados por IC junto su tiempo de retención.

Iones	Flujo (L min^{-1})	t_r (min)
NH_4^+	1,0	4,3
NO_3^-	1,5	3,8
SO_4^{2-}	1,5	5,2
Cl^-	1,5	2,5
ClO_3^-	1,5	3,4
ClO_4^-	1,5	15,2

Figura 26: Potenciostato-galvanostato Ecochemie Autolab PGSTAT100.

Autolab Nova 1.5 (**Figura 26**). Se utilizó una celda no dividida de 3 electrodos conteniendo 130 mL de disolución. Como electrodo de trabajo se utilizó un ánodo de BDD o Pt de 3 cm^2, siendo el contraelectrodo una espiral de Pt y el electrodo de referencia un electrodo de Ag|AgCl (KCl 3M, $E°$ = 0,197 V vs SHE). Todos los voltamperogramas se registraron a velocidades de barrido de 1-10 mV s^{-1} y a temperatura ambiente (25 ºC).

3.4. Análisis de datos

3.4.1. Eficiencia de corriente de mineralización

La eficiencia de la corriente aplicada en los EAOPs para mineralizar los compuestos orgánicos se evaluó a través de la eficiencia de corriente de mineralización (MCE), que se define como la relación entre la cantidad experimental de compuesto mineralizado mediante un proceso electroquímico avanzado y la esperada teóricamente si toda la carga eléctrica suministrada se emplease en la transformación del compuesto orgánico hasta CO_2, H_2O e iones inorgánicos. La MCE se calcula a partir de la siguiente expresión:

$$\text{MCE}\ (\%) = \frac{(\Delta \text{TOC})_{\text{exp}}\, n\, F\, V_s}{4{,}32 \times 10^7\, m\, I\, t} \times 100 \qquad (64)$$

donde n es el número de electrones consumido para mineralizar completamente el contaminante, determinado a partir de la reacción (65) para el Rojo Ácido 18, la reacción (66) para Rojo Ácido 14, la reacción (67) para el Rojo Allura AC y la reacción (68) para la Tartrazina, F es la constante de Faraday (96.487 C mol^{-1}), V_s es el volumen de disolución tratada (L), $\Delta(TOC)_{exp}$ es el descenso experimental del TOC (mg L^{-1}),

$4{,}32 \times 10^7$ es un factor de homogeneización de unidades (3.600 s h^{-1} × 12.000 mg mol^{-1}), *m* es el número de átomos de carbono por molécula de contaminante, *I* es la corriente aplicada (A) y *t* es el tiempo de electrolisis (h).

$$C_{20}H_{11}N_2O_{10}S_3^{3-} + 48H_2O \rightarrow 20CO_2 + 2NO_3^- + 3SO_4^{2-} + 107H^+ + 102e^- \quad (65)$$

$$C_{20}H_{12}N_2O_7S_2^{2-} + 47H_2O \rightarrow 20CO_2 + 2NO_3^- + 2SO_4^{2-} + 106H^+ + 102e^- \quad (66)$$

$$C_{18}H_{14}N_2O_8S_2^{2-} + 42H_2O \rightarrow 18CO_2 + 2NO_3^- + 2SO_4^{2-} + 98H^+ + 94e^- \quad (67)$$

$$C_{16}H_9N_4O_9S_2^{3-} + 43H_2O \rightarrow 16CO_2 + 4NO_3^- + 2SO_4^{2-} + 95H^+ + 90e^- \quad (68)$$

3.4.2. Consumo energético

La cantidad de energía total consumida durante el proceso de eliminación de los compuestos orgánicos por unidad de volumen tratado, es decir, el consumo energético por m^3 a un tiempo *t*, se ha determinado a partir de la siguiente expresión:

$$EC_V\ (kWh\ m^{-3}) = \frac{VIt}{V_s} \quad (69)$$

donde *V* es la diferencia de potencial media entre ánodo y cátodo.

Alternativamente, se puede determinar el consumo energético por unidad de masa de TOC a un tiempo *t* según:

$$EC_{TOC}\ (kWh\ (g\ TOC)^{-1}) = \frac{VIt}{(\Delta TOC)_{exp} V_s} \quad (70)$$

4. Results and discussion

4.1. In-situ hydrogen peroxide electrogeneration at lab-scale and in pre-pilot plant

The performance of the EAOPs based on Fenton's reaction for the degradation of organic pollutants is related to the amount of hydroxyl radical produced in the bulk. This is affected by the production rate of H_2O_2, which is obtained via the two electron reduction of O_2 at the cathode (reaction (49)). Therefore, the assessment of the production rate of H_2O_2 at the carbon-PTFE cathode is very important. In order to quantify the amount of accumulated H_2O_2, several trials were carried out in acidic medium under different experimental conditions.

The ability of the electrolytic system to accumulate H_2O_2 supplied by the air-diffusion cathode was tested by electrolyzing 130 mL of a 0.05 M Na_2SO_4 solution of pH 3.0 at different current values, at 25 ºC. **Figure 27** shows the effect of applied current (10, 50, 100, 300 and 450 mA) on the electrogeneration of H_2O_2. By increasing current, H_2O_2 electrogeneration rate increased mainly due to a greater electric charge passage. Moreover, under all conditions, H_2O_2 concentration did not increase linearly during all the electrolysis, but two different regions appear in the figure. The first one demonstrates linearity between the amount of produced H_2O_2 and time up to 180 min. Afterwards, the accumulation rate of H_2O_2 gradually decreases and tends to a plateau that can be related to a steady-state concentration. This behavior is characteristic of undivided electrolytic cells with an air-diffusion cathode. The steady-state concentration can be due to the simultaneous destruction of H_2O_2 via anodic reactions ((71) and (72)) and decomposition in the bulk solution (reaction (73)). The plateau is then reached once the H_2O_2 electrogeneration rate becomes equal to its destruction rate.

$$H_2O_2 \rightarrow HO_2^{\bullet} + H^+ + e^- \quad (71)$$

$$HO_2^{\bullet} \rightarrow O_2 + H^+ + e^- \quad (72)$$

$$H_2O_2 \rightarrow H_2O + \tfrac{1}{2}O_2 \quad (73)$$

To operate in electro-Fenton conditions, experiments at 50 and 300 mA were carried out by adding 0.5 mM Fe^{2+}. **Figure 28** depicts the amount of H_2O_2 produced as a function of the electrolysis time at 50 and 300 mA in the presence and absence of Fe^{2+}. The accumulation rate of H_2O_2 was found to decrease upon addition of Fe^{2+}. The results can be explained by the more rapid destruction of H_2O_2 due to the additional consumption via Fenton's reaction (12), which can be further accelerated by other homogeneous destruction reactions, for example, with Fe^{3+} and $^{\bullet}OH$ (reaction (13) and (17)). However, H_2O_2 is always present in excess in the medium as can be seen in

Figure 28, indicating that the system maintains an optimal production of $^{\bullet}OH$, thus allowing the fastest destruction of organic pollutants with this oxidant.

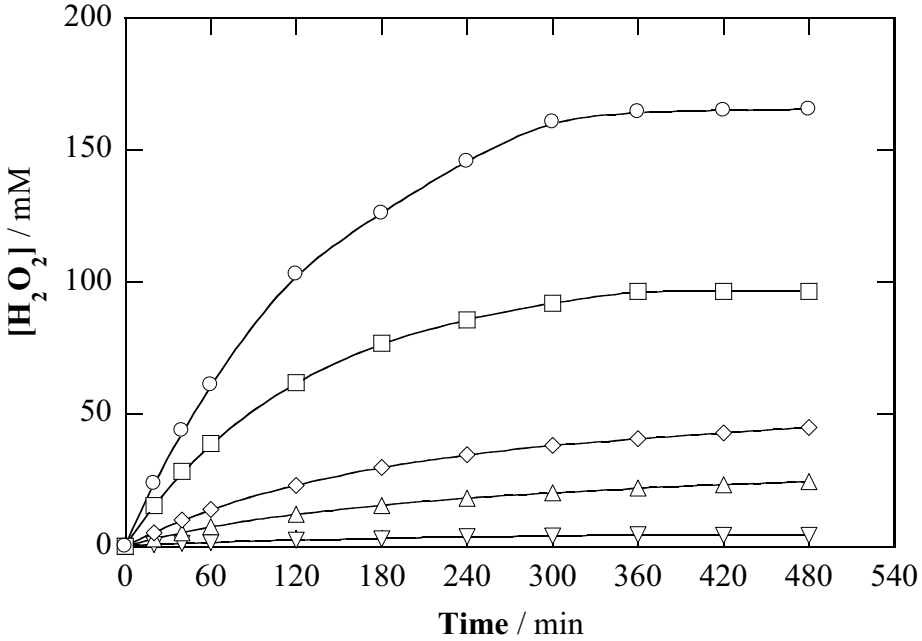

Figure 27. Effect of applied current on the change of H_2O_2 concentration with time during the electrolysis of 130 mL of solutions containing 0.05 M Na_2SO_4 at pH 3.0 and 25 ºC using Pt as the anode and an air-diffusion electrode as the cathode: Current: (▽) 10 mA, (△) 50 mA, (◇) 100 mA, (□) 300 mA, and (○) 450 mA.

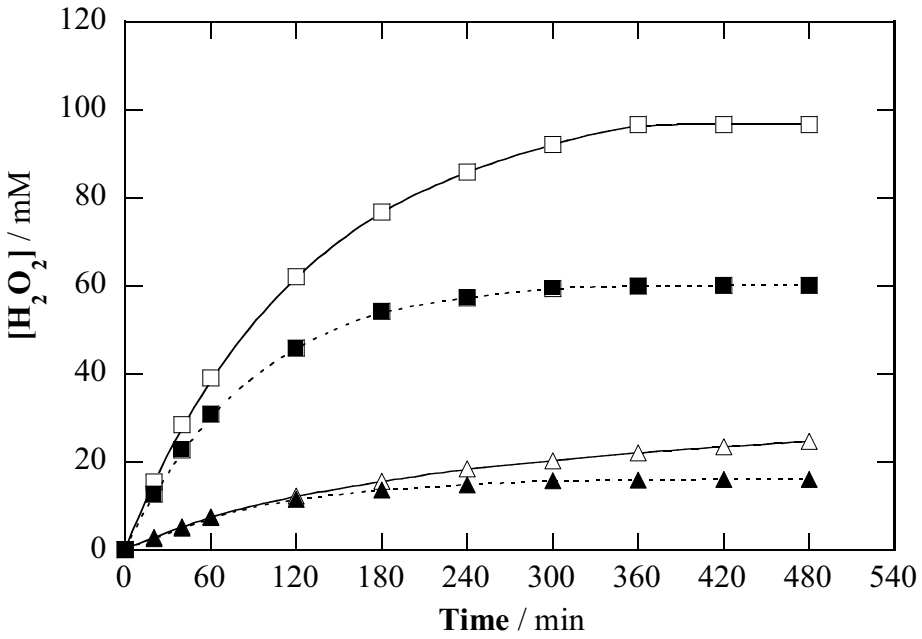

Figure 28. Variation of accumulated H_2O_2 concentration with time during the electrolysis of 130 mL of solutions containing 0.05 M Na_2SO_4 at pH 3.0 and 25 ºC using Pt as the anode and ADE as the cathode. Conditions: (△) 50 mA, (▲) 50 mA with 0.5 mM Fe^{2+}, (□) 300 mA and (■) 300 mA with 0.5 mM Fe^{2+}.

The electrogeneration of H_2O_2 was also tested when scaling up to the pre-pilot plant. **Figure 29** shows the evolution of the accumulated H_2O_2 concentration during the electrolysis of 2.5 L of solutions containing 0.05 M Na_2SO_4 at pH 3.0 and 35 ºC in the pre-pilot plant equipped with a Pt/air-diffusion cell for 480 min. At different current values, **Figure 29** reports the same behavior for the H_2O_2 production compared to that found at laboratory scale. The production of H_2O_2 was found to increase with increasing applied current, whereas the presence of Fe^{2+} caused a decrease in the concentration of H_2O_2. Similar curves were obtained with a BDD/air-diffusion cell (not shown).

In order to gain a better knowledge of H_2O_2 electrogeneration for application in wastewater treatment, various experiments were performed in the pre-pilot plant with a BDD/air-diffusion cell using sodium sulfate, sodium chloride and lithium perchlorate as supporting electrolyte. The most relevant results are depicted in **Figure 30**. A similar H_2O_2 evolution was found in both, SO_4^{2-} and ClO_4^- media, indicating that the main route for H_2O_2 decay was the same and anions do not participate in the destruction reactions. In contrast, the H_2O_2 production rate decreased in chloride medium. The destruction of H_2O_2 in this electrolyte can be accounted for by its reaction with HClO, formed via reactions (42)-(44), to form Cl^- ion and O_2 gas as follows:

$$HClO + H_2O_2 \rightarrow Cl^- + O_{2(g)} + H_2O + H^+ \quad (74)$$

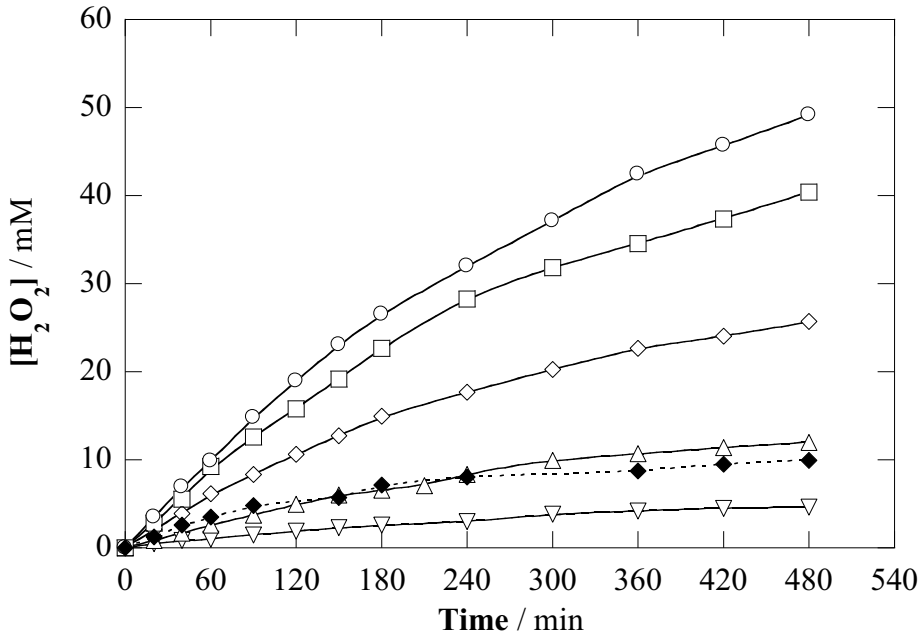

Figure 29. Variation of accumulated H_2O_2 concentration with time during the electrolysis of 2.5 L of solutions containing 0.05 M Na_2SO_4 at pH 3.0 and 35 ºC using a Pt/air-diffusion cell. Conditions: (▽) 10 mA cm^{-2}, (△) 25 mA cm^{-2}, (◇) 50 mA cm^{-2}, (◆)50 mA cm^{-2} with 0.5 mM Fe^{2+}, (□) 75 mA cm^{-2}, and (○) 100 mA cm^{-2}.

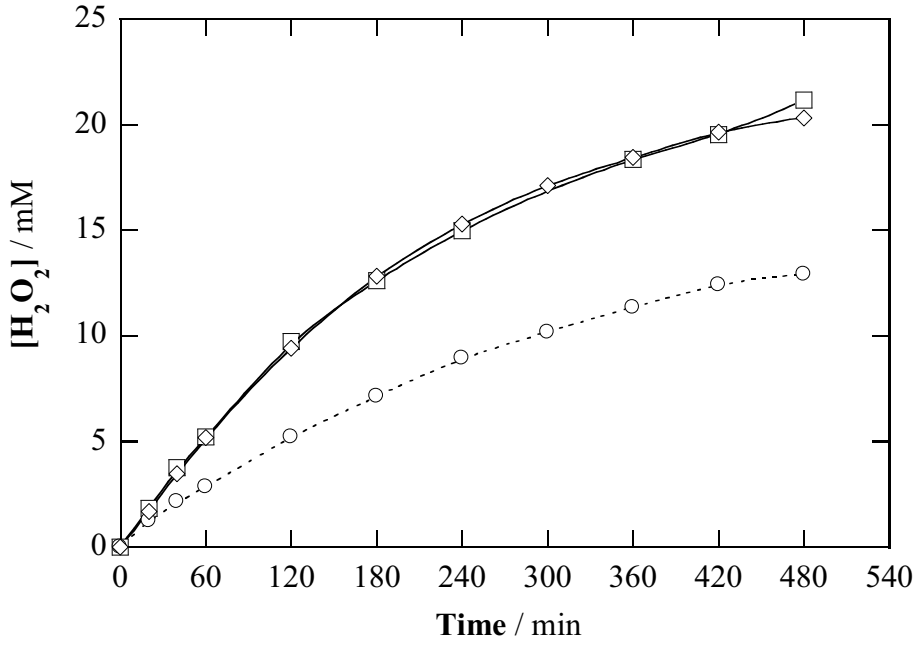

Figure 30. Effect of supporting electrolyte on the change of H_2O_2 concentration with time during the electrolysis of 2.5 L of solutions containing 0.05 M of supporting electrolyte at pH 3.0, 100 mA cm^{-2} and 35 ºC using a BDD/air-diffusion cell. Supporting electrolyte: (□) Na_2SO_4, (◇) $LiClO_4$ and (○) NaCl.

4.2. Electrochemical advanced oxidation processes applied to the treatment of aqueous solutions contaminated by Ponceau 4R at lab-scale (130 mL)

In recent years, several EAOPs have been devised and applied in the research group LEMMA for the elimination of a broad-range of organic contaminants from water, such as pesticides, herbicides and pharmaceuticals. However, the treatment of wastewater contaminated by azo dyes has not been thoroughly tested yet. As mentioned in section 1, azo dyes have complex structures, which confer them large stability against physicochemical attack and bio/photodegradation, as in the case of sulphonated azo dyes. Therefore, it is necessary to shed some light on the degradation of water polluted by azo dyes upon application of EAOPs.

This section is focused on the study of the feasibility of EAOPs to degrade the food azo dye Ponceau 4R. The electrochemical treatment of Ponceau 4R solutions by EO with or without H_2O_2 production, EF and PEF using small undivided and divided batch cells with either Pt or BDD as the anode was thoroughly studied in **Paper 1**. First, in order to elucidate the change in reactivity, the electrolyses were performed in different electrolytes (Na_2SO_4, NaCl, $NaNO_3$ and $LiClO_4$). Complete color removal was achieved regardless of the anode, cathode, process and medium, thus confirming the extraordinary ability of EAOPs to ensure the effective removal of aesthetic contamination caused by azo dyes. However, a large range of decolorization rates was observed. In EO, the use of BDD instead of Pt in SO_4^{2-} and ClO_4^- media accelerated the decolorization rate, needing 450 min for 100% color removal, owing to the superiority of BDD($^\bullet$OH) over Pt($^\bullet$OH). In contrast, EF and PEF with either Pt or BDD allowed the almost complete color removal in only ca. 60 min. The superior performance of EAOPs based on Fenton's reaction can be explained by: (i) the much higher concentration of $^\bullet$OH thanks to the simultaneity of two generation ways, and (ii) the minimization of the diffusional limitations which are inherent to the electrode processes such as the anodic oxidation. Indeed, in EO, the action is confined to the electrode surface and so, the dye molecules have to reach the surface to be oxidized. In contrast, in EF, the organic molecules are destroyed by $^\bullet$OH both at the anode and in the bulk solution and thus, the interactions between Ponceau 4R and the radicals are less restricted.

The superiority of EAOPs based on Fenton's reaction was confirmed by the kinetic decays of the dye. The mean values of k_{app} (10^{-2} min^{-1}) with their 95% confidence intervals were 0.96 ± 0.78, 10.56 ± 1.47 and 16.76 ± 0.96 for EO, EF and PEF with BDD, respectively (**Figure 31**).

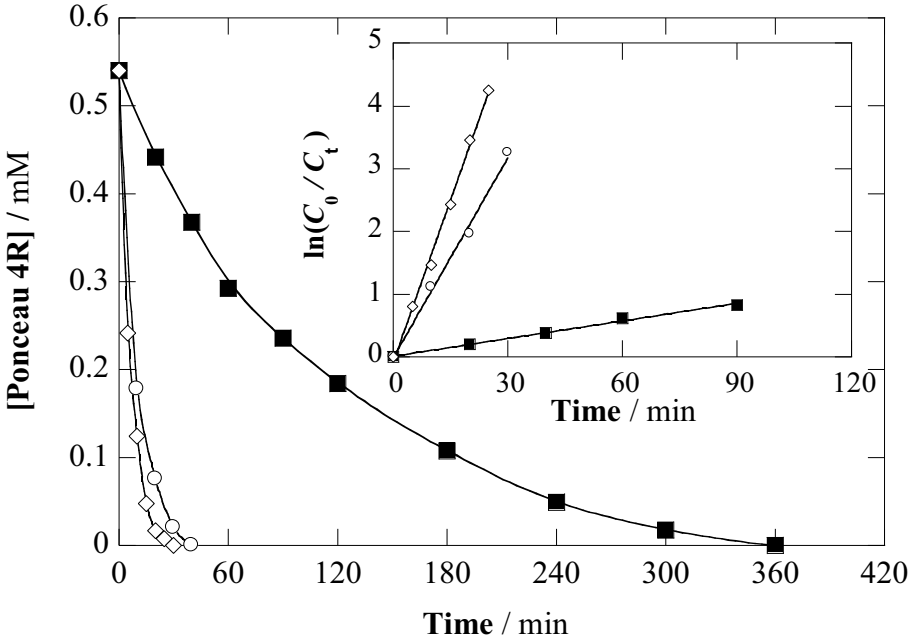

Figure 31. Decay of the dye concentration during the degradation of 130 mL of 254 mg L^{-1} of Ponceau 4R in 0.05 M Na_2SO_4 at pH 3.0 and 300 mA. Treatment: (■) EO with BDD, (○) EF with BDD and (◇) PEF with BDD. In EF and PEF, 0.50 mM Fe^{2+} was added to the solution.

Surprisingly, in NO_3^- medium, which was expected to behave as an inert electrolyte, only 180 and 120 min were required in EO and EO-H_2O_2 with BDD, respectively, which turned out to be a very significant enhancement compared to their trends in the two previous media. In my Thesis, we have concluded that such an unexpected behavior in this medium might be explained by the adsorption of NO_3^- on the anode and/or the steel cathode surface, thus causing the partial blockage of some active sites. This, in turn, increases the corresponding current densities, which leads to the enhanced degradation of the dye. A very different behavior was found in Cl^- medium, since the eight tested processes led to the overall decolorization in only 15-25 min because of the prevailing oxidizing role of active chlorine.

Regarding the TOC, the mineralization rate and/or degree increased in the order: EO ~ EO-H_2O_2 with Pt << EF with Pt < EO with BDD < EO-H_2O_2 with BDD < EF with BDD < PEF with Pt ~ PEF with BDD. Much quicker mineralization rate was obtained in PEF systems in all media, with 100% TOC removal in less than 240 min except in Cl^- medium where longer time was needed to achieve complete mineralization. This behavior can be accounted for by the action of $^{\bullet}OH$ formed from Fenton's reaction (12) and, even more relevant, the photodegradation of Fe(III)-carboxylate complexes by UV photons according to reaction (24). Furthermore, in PEF,

free Fe^{3+} was simultaneously photoreduced to Fe^{2+} via reaction (23) to yield more $^{\bullet}OH$. The slightly slower mineralization in Cl^- medium compared to that obtained in other media has been related to: (i) the partial consumption of $^{\bullet}OH$ by Cl^- to form less oxidizing species and (ii) the formation of refractory chloroderivatives.

In order to study the possible influence of cathodic reduction on decolorization and mineralization rates, comparative electrolyses of 130 mL of 254 mg L^{-1} Ponceau 4R solutions in different divided and undivided BDD/SS and Pt/SS batch cells were carried out. Results showed analogous trends for undivided and divided (with dye contained in the anolyte) cells in both cases, therefore revealing the insignificant contribution of cathodic reduction of Ponceau 4R and/or its colored by-products. However, almost 40% color removal was attained at 480 min when the dye solution was placed in the catholyte, which actually confirmed the existence of such cathodic reduction.

From the aforementioned findings, it is clear that the type of electrode materials can greatly influence the electrochemical oxidation processes, which can be attributed to their different electrocatalytic properties. Linear sweep voltammetries (LSV) were recorded to find out the oxidation behavior of Ponceau 4R on BDD and Pt anode electrodes. According to LSV curves, in the presence of Na_2SO_4 alone, no current flow was detected until O_2 evolution occurred from H_2O oxidation on Pt at ca. 1.2 V. In the presence of Ponceau 4R, an oxidation peak appeared at 1.0 V, its current peak being proportional to the dye concentration. This finding reveals that Ponceau 4R is electroactive and may undergo direct oxidation as well. LSV was also carried out using BDD instead of Pt. In the presence of dye, a wave appeared at about 2 V in all media.

The composition of dye wastewater usually includes large amounts of both, Cl^- and SO_4^{2-} ions, thus being necessary from an applicative standpoint to investigate the performance of EAOPs (for example, PEF-BDD) in sulphate/chloride mixtures. In solutions with 100% SO_4^{2-}, solutions became completely colorless in 50 min, whereas the gradual increase of Cl^- concentration progressively accelerated the degradation thanks to the participation of active chlorine, up to attaining total color removal in 15-25 min when > 60% Cl^- was used. However, for the mineralization, progressively greater Cl^- contents were clearly detrimental, causing slower TOC decays. The drop in mineralization rate upon increase of Cl^- content affected the MCE trends, where maximum efficiency values were attained during the first stages.

Finally, the fate of Cl^- ions during the application of EAOPs in this medium was thoroughly assessed. During the electrolyses, Cl^- totally disappeared after 360 min due to its destruction by M($^\bullet$OH) or by direct electron transfer via reaction (42), giving rise to ClO_3^- and ClO_4^- ions and to active chlorine. The contribution of M($^\bullet$OH) to Cl^- oxidation was ascertained by carrying out similar electrolyses, but in the presence of 20 mM *t*-BuOH, which acted as a radical scavenger. Much slower disappearance of Cl^- and very low accumulation of ClO_3^- and ClO_4^- ions and active chlorine were observed.

Aiming to gain more thorough knowledge about the fate of food azo-colors upon application of EAOPs, **Paper 2** compares the performance of EO-H_2O_2, EF and PEF for the treatment of aqueous solutions of Ponceau 4R in Na_2SO_4 using an undivided cell with a BDD anode and air-diffusion cathode in terms of color, dye concentration and TOC removal. First, PEF treatments of acidic solutions of 254 mg L^{-1} of Ponceau 4R in ultrapure water with Na_2SO_4 were performed to assess the effect of applied current as well as Na_2SO_4 and dye concentrations. Regarding the effect of applied current, total decolorization was reached after 70, 60, 50 and 40 min at 33.3, 66.7, 100 and 150 mA cm^{-2}, respectively. This behavior can be related to the concomitant increase in rate of electrode reactions, allowing the production of larger amounts of BDD($^\bullet$OH) as well as H_2O_2, which leads to a larger accumulation of $^\bullet$OH in the bulk at a given time from Fenton's reaction. The positive effect on degradation as current rises can be better observed on the decays kinetics of the dye. Ponceau 4R disappeared in 40, 35, 30 y 25 min when increasing from 33.3 to 150 mA cm^{-2}. This confirms the great oxidizing ability of PEF system, but it also reveals the formation of colored by-products along the treatment because, in all cases, Ponceau 4R disappeared somewhat earlier than color. Good linear correlations were obtained assuming a pseudo-first-order reaction for the kinetic analysis of concentration decays, with R^2 = 0.997 and apparent rate constants (k_{app}, 10^{-2} min^{-1}) of 11.39 ± 1.74, 13.28 ± 1.26, 16.76 ± 0.96 and 18.60 ± 2.56 as current was raised (mean values along with their computed 95% confidence intervals are provided). A faster mineralization was also observed as the current rises from 33.3 to 150 mA cm^{-2}. The degradation by PEF at 150 mA cm^{-2} was remarkably faster and, in fact, total mineralization was reached after only 180 min, whereas the electrolyses at 33.3-100 mA cm^{-2} had to be prolonged for 240 min to completely remove the organic matter. However, the MCE was simultaneously reduced because the increase in current

enhanced the parasitic reactions and thus, maximum MCE values of 55%, 29%, 21% and 18% were obtained after 90-120 min as current increased.

The effect of Na_2SO_4 concentration from 0.010 to 0.30 M on PEF treatment was investigated. Total color removal was always attained at 70 min. However, the extreme Na_2SO_4 concentration values yielded the quickest absorbance decays. Low Na_2SO_4 concentration yielded the quickest absorbance decays due to the minimization of the parasitic anodic generation of the weaker oxidant $S_2O_8^{2-}$. Following this reasoning, a content as high as 0.30 M Na_2SO_4 could seem largely detrimental, since part of BDD($^{\bullet}$OH) is expected to be wasted by the large formation of $S_2O_8^{2-}$ ion. Conversely, it has been concluded that the presence of large amounts of SO_4^{2-} ions favours the transport of the negatively charged (sulphonated) Ponceau 4R molecules towards the anode surface, eventually accelerating their oxidation. On the other hand, the effect of the Na_2SO_4 concentration on TOC removal was negligible, leading to overlapped curves for 240 min. In conclusion, BDD anode plays an important role during the initial decolorization steps, whereas Fenton's reaction and photolytic reactions ensure the progressive TOC abatement.

The effect of initial dye concentration on its decolorization and mineralization trends by PEF was also examined for 127-1270 mg L^{-1} of Ponceau 4R (50-500 mg L^{-1} TOC) in 0.05 M Na_2SO_4 with 0.50 mM Fe^{2+} at 100 mA cm^{-2}. Complete color removal and mineralization was observed regardless of the dye content, needing longer times from 20 to 240 min and 135 to 480 min, respectively. Worth noting, the PEF treatment became more efficient as the organic matter content was raised. This behavior arises from the greater probability for favourable events in the presence of more organic molecules, thus minimizing the parasitic reactions that involve BDD($^{\bullet}$OH) and $^{\bullet}$OH.

The mineralization of Ponceau 4R leads to the conversion of nitrogen and sulphur atoms present in the molecule to inorganic ions, such as nitrate, ammonium and sulfate. Therefore, the release and evolution of their concentration was monitored by IC analyses. The N atoms forming the -N=N- bond were preferentially transformed into NO_3^- ion (50% of initial N) and, to a smaller extent, into NH_4^+ ions (25%). A significant proportion of the initial N was then lost as volatile nitrogenated products, like N_2 and N_xO_y. Regarding the sulfur content, in all these treatments, a final SO_4^{2-} content of 1.25 mM corresponding to 100% of initial S was obtained, thereby corroborating that the three sulfonic groups of Ponceau 4R are completely released as SO_4^{2-} ion.

4. Results and discussion

GC-MS analyses with polar and nonpolar columns allowed the identification of 22 aromatic by-products with 1 or 2 aromatics rings. Based on these findings, a general reaction scheme including different pathways for the formation of all the aromatic by-products has been proposed. The electrochemical degradation of Ponceau 4R involves simultaneous routes that yield *N*-containing and non-*N*-containing derivatives. The cleavage of any of the 22 aromatic structures caused the formation of aliphatic compounds, which were finally mineralized to CO_2.

The electrochemical oxidation of Ponceau 4R was also studied in a real water matrix in order to investigate the viability of EAOPs to treat dye wastewater. The performance of EO-H_2O_2, EF and PEF during the degradation of 254 mg L^{-1} of Ponceau 4R in a real water matrix (i.e., water sample from a wastewater treatment facility) at pH 3.0 and 33.3 mA cm^{-2} was assessed. Total color removal was attained after 180, 100, and ca. 70 min, respectively, in agreement with the oxidizing ability of the methods in the order EO-H_2O_2 < EF < PEF. Note that the time needed in PEF is similar to that found for the treatment under analogous conditions but using ultrapure water, which means that the water matrix does not impede the fast decolorization of the dye solutions. The decay of dye concentration confirms the formation of colored by-products, since Ponceau 4R disappeared after 150 min in EO-H_2O_2, only requiring 40 min in EF and PEF. The mean values of k_{app} (10^{-2} min^{-1}) with their 95% confidence intervals were 2.72 ± 0.41, 12.31 ± 0.53 and 13.35 ± 0.66 for EO-H_2O_2, EF and PEF. Regarding the mineralization, at 360 min, 57%, 74% and ~ 100% TOC removal was attained by the three methods, respectively. This result, along with the fast color and Ponceau 4R removals, verifies the viability of PEF process for the treatment of real dye wastewater.

.

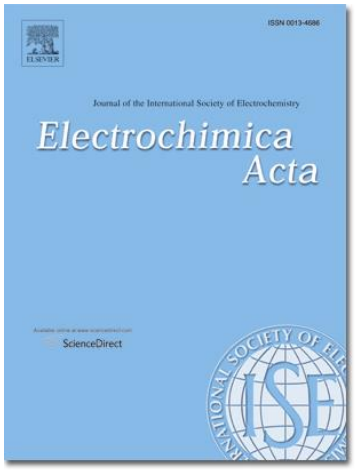

Paper 1

Electrochemical reactivity of Ponceau 4R (food additive E124) in different electrolytes and batch cells

---

Electrochimica Acta

Submitted (Manuscript No: TM15-100)

Electrochemical reactivity of Ponceau 4R (food additive E124) in different electrolytes and batch cells

Abdoulaye Thiam, Enric Brillas[1], Francesc Centellas, Pere L. Cabot[1], Ignasi Sirés[1,*]

Laboratori d'Electroquímica dels Materials i del Medi Ambient, Departament de Química Física, Facultat de Química, Universitat de Barcelona, Martí i Franquès 1-11, 08028 Barcelona, Spain

Paper submitted to be published in Electrochimica Acta

* Corresponding author: Tel.: +34 934021223; fax: +34 934021231.

E-mail address: i.sires@ub.edu (I. Sirés)

[1] ISE Member

4. Results and discussion

Abstract

The occurrence of food color additives in waters is becoming a hot topic due to their potential health effects, especially on children. The treatment of Ponceau 4R solutions by electro-oxidation (EO) with or without H_2O_2 production, electro-Fenton (EF) and photoelectro-Fenton (PEF) using small undivided and divided batch cells with either Pt or BDD as the anode has been thoroughly studied. The electrolyses were performed in different electrolytes like Na_2SO_4, NaCl, $NaNO_3$ and $LiClO_4$ in order to elucidate the changes in reactivity. Depending on the anode, cathode, process and electrolyte, the azo dye could be degraded due to the single or combined action of: (i) direct cathodic reduction and/or anodic oxidation, (ii) $^{\bullet}OH$-mediated oxidation at the anode vicinity or in the solution bulk, and (iii) active chlorine-mediated oxidation. The presence of Cl^- led to the fastest decolorization, whereas it became detrimental for total organic carbon abatement. The oxidation of Cl^- to active chlorine (Cl_2 and HClO) and oxychlorine anions (ClO_3^- and ClO_4^-) by direct charge transfer or by M($^{\bullet}OH$) and $^{\bullet}OH$ was investigated. Color removal was much slower in SO_4^{2-}, ClO_4^- and NO_3^- media, although the latter was particularly beneficial in PEF and/or using BDD. Regarding the mineralization, PEF outperformed the other technologies. Similar trends were observed in SO_4^{2-} and ClO_4^- media, being slightly favored in NO_3^-. In contrast, Cl^- medium tended to be detrimental due to the formation of refractory chloroderivatives, the destruction of M($^{\bullet}OH$) to form less oxidizing (oxy)chloro radicals, oxychlorine anions and active chlorine, and the reaction between HClO and H_2O_2. Experiments in divided cells demonstrated the very small contribution of cathodic reduction of the dye and its by-products. Linear sweep voltammetry revealed the direct oxidation of both, Ponceau 4R and Cl^- on the anode surface.

Keywords: Acid Red 18; Active chlorine; BDD anode; Food color; Photoelectro-Fenton.

1. Introduction

The worldwide occurrence of large volumes of wastewater containing synthetic dyestuffs has become one of the biggest threats to biodiversity on Earth due to the potentially toxic, teratogenic, mutagenic and carcinogenic effects of both, parent molecules and their degradation by-products like aromatic amines [1,2]. In particular, azo dyes are the ubiquitous in industry and account for over 70% of total dye production. They present one or various azo (-N=N-) groups and usually exhibit complex structures that confer them large stability against physicochemical attack and bio/photodegradation, as in the case of sulfonated azo dyes, thus becoming persistent in water streams [3,4]. While major attention has been paid to textile azo dyes, synthetic azo-colors used as food additives have been much less investigated so far. Among them, Ponceau 4R (Acid Red 18, New Coccine or additive E124) is a sulfonated azo dye extensively employed in the food industry to give red coloring to various foodstuffs such as alcoholic beverages and soft drinks, candies, syrups, bakery products, tomato sauce, cherry marmalade and yogurts. Lately, serious concerns have arisen since the intake of Ponceau 4R affects children's behavior, resulting in increased hyperactivity and intolerance [5]. As a result, in 2009, the European Food Safety Authority (EFSA) provided a scientific opinion re-evaluating the safety of this dye as a food additive, eventually reducing the Acceptable Daily Intake (ADI) from 0-4 to 0.7 mg (kg body weight)$^{-1}$ [6]. Despite being negative in *in vitro* genotoxicity as well as in long-term carcinogenicity studies conducted by the EFSA, the topic is still controversial [7]. For instance, Ponceau 4R is currently listed as a banned substance by US Food and Drug Administration [8], not being approved in some countries including the United States, Canada, Norway and Finland. Therefore, wastewater resulting from its manufacture and usage becomes a threat for living beings [9].

The advanced oxidation processes (AOPs) are very effective technologies for the treatment of wastewater containing organic pollutants since they allow the generation of a very powerful oxidizing agent like hydroxyl radical ($^{\bullet}$OH, E^{o} = 2.80 V/SHE), which may promote the quick and nonselective transformation of contaminants into biodegradable by-products or even their complete conversion to CO_2. The great ability of heterogeneous photocatalysis using TiO_2 [10] and ZnO [11], ozone-electrolysis with Pt anode [12] and chemical Fenton's reagent [13] to degrade Ponceau 4R has been demonstrated. Conversely, as far as we know, the electrochemical AOPs (EAOPs) have not been thoroughly tested yet.

In recent years, the feasibility of several EAOPs to decontaminate waters based on the preponderant action of $^{\bullet}$OH on the organic matter content has been largely ascertained [14-16]. There exist three main routes to generate this radical in electrolytic cells: (i) direct electrochemical

production via water electro-oxidation (EO), (ii) indirect electrochemical production by Fenton-based EAOPs, and (iii) photochemical activation of semiconductor anodes like TiO_2. The former two methods are the most employed ones because of their much greater oxidation power and thus, they will be the scope of the present work.

The greatest advances have been achieved in EO because it combines two fundamental technological characteristics such as simplicity and adaptability. In this process, organic pollutants can be directly oxidized at the anode surface (M) and/or much more rapidly destroyed by adsorbed hydroxyl radical M($^{\bullet}$OH) produced via reaction (1) at high applied current [15]. While active anodes like Pt, IrO_2 and RuO_2 foster the conversion to a less oxidizing species such as chemisorbed MO, high oxidation power materials like PbO_2 and boron-doped diamond (BDD) favor the electrochemical incineration of organics in the anode vicinity. Modular setups can then be used to treat raw wastewater regardless of its physicochemical characteristics [16].

$$M + H_2O \rightarrow M(^{\bullet}OH) + H^+ + e^- \quad (1)$$

Electro-Fenton (EF) is the simplest method among Fenton-based EAOPs. It consists in the in situ electrogeneration of H_2O_2 from the two-electron reduction of O_2 gas at a carbonaceous cathode [16]. H_2O_2 is not a powerful oxidant but it can be oxidized to another weak reactive oxygen species (ROS) such as hydroperoxxyl radical ($HO_2^{\bullet}$) at the anode. In the absence of a metal catalyst, the process is called EO-H_2O_2. In contrast, the presence of Fe^{2+} leads to the production of $^{\bullet}$OH in the bulk via Fenton's reaction (2) at optimum pH ~ 3 [16], which then acts in concomitance with M($^{\bullet}$OH) to destroy organics. If UVA lamps are used, the process is called photoelectro-Fenton (PEF), which enhances the mineralization by promoting the photoreduction of $Fe(OH)^{2+}$ via reaction (3) and the photolysis of Fe(III)-carboxylate products via reaction (4).

$$H_2O_2 + Fe^{2+} \rightarrow Fe^{3+} + {}^{\bullet}OH + OH^- \quad (2)$$

$$Fe(OH)^{2+} + h\nu \rightarrow Fe^{2+} + {}^{\bullet}OH \quad (3)$$

$$Fe(OOCR)^{2+} + h\nu \rightarrow Fe^{2+} + CO_2 + R^{\bullet} \quad (4)$$

When the treated solution contains Cl^- ions, M($^{\bullet}$OH) and/or $^{\bullet}$OH oxidize in parallel to active chlorine species (Cl_2, HClO and/or ClO^-, which predominate at pH < 3.0, 3.0-8.0, and > 8.0, respectively) produced in the bulk via reactions (5)-(7) [4,16]. Furthermore, oxychlorine anions [17-19], (oxy)chlorine radicals [21], chloramines [21], trihalomethanes and haloacetic acids [22], as well as refractory organochlorinated by-products, may appear during the electrolyses:

$$2\,Cl^- \rightarrow Cl_{2(aq)} + 2\,e^- \quad (5)$$

$$Cl_{2(aq)} + H_2O \rightarrow HClO + Cl^- + H^+ \quad (6)$$

$$HClO \leftrightarrows ClO^- + H^+ \quad (7)$$

The large ability of both kinds of EAOPs to quickly decolorize and even completely mineralize azo dye solutions has been confirmed [9,23-34]. Among the operating parameters that determine their performance, the supporting electrolyte is critical because different inorganic salts are present in real wastewater. This is often disregarded, but some studies are available for the treatment of organic pollutants [33-46]. Regarding the azo dyes, much is known about EO [35,36,44,46], whereas scarce information is available on EF and PEF [33,34,38,42]. The performance of EO in terms of color removal is higher in Cl^- medium due to active chlorine production. In contrast, the effect of electrolyte is much more controversial in Fenton-based EAOPs. For example, the use of Cl^- was found to accelerate the decolorization of Acid Red 14 [33] and Methyl Red [42], but no significant enhancement [34] or even a detrimental effect [38] was reported for Allura Red AC and Orange II, respectively. More detailed studies are then needed to clarify this behavior.

In this work, the electrochemical treatment of Ponceau 4R by EO, EO-H_2O_2, EF and PEF with a Pt or BDD anode has been performed in divided and undivided cells. The electrolyses were made with either, an air-diffusion cathode for H_2O_2 electrogeneration or a stainless steel (SS) one, which could contribute to the azo dye reduction. The effect of the supporting electrolyte involving SO_4^{2-}, Cl^-, NO_3^- or ClO_4^- ions on color and total organic carbon (TOC) decay was assessed along the experiments. Oxychlorine anions and active chlorine produced in Cl^- medium were analyzed. The electroactivity of Ponceau 4R was studied by linear sweep voltammetry (LSV).

2. Experimental

2.1. Chemicals

Ponceau 4R (trisodium 2-hydroxy-1-(4-sulphonato-1-naphthylazo)-naphthalene-6,8-disulphonate, $C_{20}H_{11}N_2O_{10}S_3Na_3$, CI 16255, see chemical structure in Fig. 1) was purchased from Acros Organics (100% content, λ_{max} = 508 nm). Anhydrous sodium sulfate, sodium chloride, lithium perchlorate and sodium nitrate used as supporting electrolytes, as well as iron(II) sulfate heptahydrate used as catalyst in EF and PEF, were of analytical grade from Merck and Fluka. Sulfuric, hydrochloric, perchloric and nitric acids and sodium hydroxide used to regulate the pH were of analytic grade from Merck, Acros Organics and Panreac. Organic solvents and other chemicals used were of high-performance liquid chromatography (HPLC) or analytical grade from Sigma-Aldrich, Lancaster, Merck and Panreac. Solutions were prepared with ultrapure water from a Millipore Milli-Q system with resistivity >18 MΩ cm at 25 ˚C.

2.2. Electrolytic cells

Most experiments were conducted in an open, undivided, cylindrical glass tank reactor of 150 cm^3 capacity equipped with a double jacket for recirculation of thermostated water at 25 °C. The anode was a Pt sheet from SEMPSA (Barcelona, Spain) or a BDD thin-film electrode from NeoCoat (La-Chaux-de-Fonds, Switzerland), whereas the cathode was a carbon-PTFE air-diffusion electrode from E-TEK (Somerset, NJ, USA), which was fed with air pumped at 1 dm^3 min^{-1} for continuous H_2O_2 generation, or a SS sheet (AISI 304). The geometric area of each electrode was 3 cm^2 and the interelectrode gap was 1 cm. All these experiments were carried out using 130 cm^3 of solutions at pH 3.0 under vigorous stirring with a magnetic bar to ensure homogenization and the transport of reactants towards/from the electrodes. In EF and PEF, 0.50 mmol dm^{-3} Fe^{2+} was employed as catalyst because this content was found optimal for analogous treatments of aromatic pollutants [16]. In PEF assays, the solution was irradiated with a Philips TL/6W/08 fluorescent black light blue tube (λ_{max} = 360 nm, photoionization energy of 5 W m^{-2}) placed 7 cm above the solution. Cleaning of the anode and activation of the air-diffusion cathode were achieved under polarization in 0.05 mol dm^{-3} Na_2SO_4 at 100 mA cm^{-2} for 180 min.

Some experiments were carried out in an analogous divided tank reactor. In general, the anodic compartment contained the Pt or BDD anode immersed into 130 cm^3 of solution, whereas the cathodic one was a glass tube with its bottom sealed with a glass filter separator (porosity number 2) in contact with the solution, containing a SS wire immersed into 5 cm^3 of solution. In some assays, the catholyte contained 130 cm^3 of solution and a SS sheet as cathode, whereas a Pt wire was immersed as the anode inside the separator. Depending on the trial, the anolyte or catholyte then contained 130 cm^3 of Ponceau 4R in 0.50 mol dm^{-3} Na_2SO_4 to reduce the ohmic drop, whereas the other half cell only contained the same electrolyte.

2.3. Instruments and analytical procedures

The solution pH and the electrical conductance were measured with a Crison 2000 pH-meter and a Metrohm 644 conductometer, respectively. Constant current electrolyses were performed with an EG&G PAR 273A potentiostat-galvanostat and the potential difference between the anode and cathode (E_{cell}) was provided by a Demestres 601BR digital multimeter. Samples withdrawn from electrolyzed solutions were microfiltered with 0.45 μm PTFE filters from Whatman prior to immediate analysis. The decolorization of Ponceau 4R solutions was monitored by measuring their absorbance decay at λ_{max} = 508 nm on a Shimadzu 1800 UV-Vis spectrophotometer at 25 ºC. The mineralization of solutions was assessed from their TOC abatement, determined on a Shimadzu

TOC-VCNS analyzer. Reproducible TOC values with an accuracy of ±1% were found by injecting 50 μL aliquots into the analyzer.

Generated carboxylic acids were detected by ion-exclusion HPLC as described elsewhere [34]. The time course of the concentration of NO_3^-, Cl^-, ClO_3^- and ClO_4^- ions was assessed by ion chromatography (IC) as previously reported [47]. Since overlapping peaks were obtained for Cl^- and ClO^- [48], the signals for the former ion were corrected by taking into account the ClO^- concentrations found upon spectrophotometric determination of its peak at 292 nm on the above UV/Vis spectrophotometer [49]. The NH_4^+ content was determined with a flow injection system [47]. Since no traces of this ion were found in any of the experiments, the number of electrons (n) exchanged per each substrate molecule was taken as 102, assuming that Ponceau 4R is completely mineralized as follows:

$$C_{20}H_{11}N_2O_{10}S_3^{3-} + 48\ H_2O \rightarrow 20\ CO_2 + 2\ NO_3^- + 3\ SO_4^{2-} + 107\ H^+ + 102\ e^- \quad (8)$$

The mineralization current efficiency (MCE) values for each trial at current I (in A) and time t (in h) was then estimated as follows:

$$\text{MCE}\ (\%) = \frac{(\Delta \text{TOC})_{\text{exp}}\ n\ F\ V_s}{4.32 \times 10^7\ m\ I\ t} \times 100 \quad (9)$$

where F is the Faraday constant (96,487 C mol^{-1}), V_s is the solution volume (in dm^3), $\Delta(TOC)_{exp}$ is the experimental TOC abatement (in mg dm^{-3}), 4.32×10^7 is a conversion factor to homogenize units (= 3600 s h^{-1} × 12000 mg carbon mol^{-1}) and m is the number of carbon atoms of Ponceau 4R.

Active chlorine (i.e., available hlorine) produced in experiments carried out in Cl^- medium was determined by the *N,N*-diethyl-*p*-phenylenediamine (DPD) colorimetric method [50]. To do this, aliquots of the electrolyzed solution were collected in a tube containing DPD in phosphate buffer. DPD was oxidized by active chlorine to generate a pink product, whose color intensity at λ =515 nm was proportional to the active chlorine concentration. A calibration curve was previously prepared with potassium permanganate.

For the electrochemical characterization, LSV was performed with an Autolab PGSTAT30 instrument, using a three-electrode, undivided glass cell containing 130 cm^3 of solution at 25 ^oC, with a large area Pt gauze and Ag|AgCl (3 mol dm^{-3} KCl) as the counter and reference electrodes, respectively. The exposed area of Pt or BDD used as the working electrode was 3 cm^2. All potentials are referred to the reference electrode. The solutions were deaerated with N_2 for 20 min prior to measurements.

3. Results and discussion

3.1. Decolorization of Ponceau 4R solutions

Solutions of 130 cm^3 containing 254 mg dm^{-3} (0.42 mmol dm^{-3}) Ponceau 4R in 0.05 mol dm^{-3} of either Na_2SO_4, NaCl, $NaNO_3$ or $LiClO_4$ as supporting electrolyte at pH 3.0 were comparatively treated at 300 mA by eight different EAOPs, including EO with Pt, EO-H_2O_2 with Pt, EO with BDD, EO-H_2O_2 with BDD, EF with Pt, EF with BDD, PEF with Pt and PEF with BDD. EO and EO-H_2O_2 treatments were made with a SS and air-diffusion cathode, respectively. First, the decolorization efficiency or percentage of color removal over electrolysis time was calculated from the absorbance at initial time (A_0) and after an electrolysis time t (A_t), as follows:

$$\text{Color removal (\%)} = \frac{A_0 - A_t}{A_0} \times 100 \quad (10)$$

Fig. 2 exemplifies the two kinds of UV-Vis spectra obtained from Ponceau 4R solutions in different media. The initial spectrum in SO_4^{2-}, NO_3^- and ClO_4^- medium and its time course upon application of EAOPs typically looked like those shown in Fig. 2a. At time zero, the spectrum exhibited a main band in the visible region at λ_{max} = 508 nm, which agrees with the bright red color of the solutions, as also reported for other red azo dyes like Acid Red 88 that presents a very similar structure with only one sulfonate group [29]. Apart from this band, which was due to the absorption of the chromophore –N=N- group, other two bands appeared in the UV region, at 240-250 and 330-340 nm, which can be ascribed to the $\Pi \rightarrow \Pi^*$ transition in the naphthalene rings linked to the azo bond [12]. The intensity of all the peaks in the UV and visible regions progressively decreased to zero upon protracted electrolyses for 360 min, thus confirming the effectiveness of oxidants generated in all the EAOPs under study for degrading the aromatic rings and decolorizing. Note also that the maximal at 508 nm was slightly shifted to shorter wavelengths as the electrolysis proceeded. Such hypsochromic shift suggests the structural modification of the parent molecule upon electrochemical treatment, which can be related to the formation of colored by-products. On the other hand, Fig. 2b shows the UV/Vis spectra obtained in Cl^- medium, which were very similar to those commented above, although the absorbance disappeared in only 12 min. This suggests the generation of additional oxidizing species like active chlorine, as explained below, being much more efficient for decolorization than oxidants formed in the other media. Note that some authors have reported the appearance of an additional shoulder at 292 nm owing to the formation of ClO^- ion at higher pH [49], as also demonstrated during the electrolysis of KCl with BDD anode [35].

However, in Fig. 2b, that shoulder is almost inexistent, since pH 3.0 favors the formation of HClO instead of ClO^- ion.

Fig. 3 shows the percentage of color removal at 508 nm vs electrolysis time for the eight EAOPs performed in the four electrolytes. As summarized in Table 1, the specific conductivity in 0.05 mol dm^{-3} electrolyte was high enough in all cases, thus minimizing ohmic drops that could otherwise hamper the production of species like H_2O_2, M($^{\bullet}$OH) and active chlorine, among others, on the electrode surface. As expected, BDD anode and air-diffusion cathode led to the largest E_{cell} values. The first important result upon comparison of Fig. 3a-d is the complete color removal achieved regardless of the anode, cathode, process and medium, thus confirming the extraordinary ability of EAOPs to ensure the effective removal of aesthetic contamination caused by azo dyes. However, a large range of decolorization rates can be observed.

As shown in Fig. 3a, the dye solutions prepared in SO_4^{2-} medium became colorless earlier in the Fenton-based EAOPs. The slowest decolorization among all methods occurred in EO with Pt, being still incomplete at 480 min. This can be explained by the low oxidation power of Pt($^{\bullet}$OH) and the slow or unfavorable direct oxidation and/or reduction at Pt and SS, respectively. The use of an air-diffusion cathode instead of SS in EO-H_2O_2 with Pt allowed a slightly faster color removal. This can be related to the simultaneous action of $HO_2^{\bullet}$ formed from H_2O_2 oxidation at the Pt anode, since in a parallel experiment it was shown that Ponceau 4R was not attacked upon addition of 50 mmol dm^{-3} H_2O_2. The use of BDD instead of Pt in EO and EO-H_2O_2 accelerated the degradation, yielding similar trends in both cases with solutions becoming colorless at 450 min owing to the superiority of BDD($^{\bullet}$OH) over Pt($^{\bullet}$OH). The BDD anode is then preferred for such processes since it generates large quantities of physisorbed BDD($^{\bullet}$OH) owing to the very weak BDD-$^{\bullet}$OH interaction that results in a greater O_2-overpotential and a quicker destruction of colored organics [15]. This anode is also able to produce other weaker oxidants like H_2O_2, O_3 and $S_2O_8^{2-}$ in this medium [15,16]. In contrast, EF and PEF with either Pt or BDD allowed the almost complete color removal in only ca. 60 min. The four systems yielded similar trends, which is an evidence of the pre-eminent role of $^{\bullet}$OH formed in the bulk from Fenton's reaction (2). This species was much more effective than (i) BDD($^{\bullet}$OH), because this one presents mass transport limitations that are inherent to near-surface reactions, and (ii) photoregenerative reactions, especially reaction (3) in PEF caused by UVA photons that is expected to produce more $^{\bullet}$OH and feed Fe^{2+} back into Fenton's reaction as electrolysis progresses. Note that UVA irradiation alone caused no decolorization, being Ponceau 4R quite photostable.

4. Results and discussion

Results obtained in the presence of a typically inert anion such as ClO_4^- were practically analogous to those found in SO_4^{2-}, as depicted in Fig. 3d. This confirms the extremely low oxidation power of peroxosulfate ions formed under the conditions of Fig. 3a, along with the preponderant role of M(•OH) and •OH in non-Fenton and Fenton-based processes, respectively. Supposedly, NO_3^- was expected to be an inert electrolyte as well, therefore allowing an evident acceleration of color removal in Fenton-based EAOPs, as discussed for SO_4^{2-} and ClO_4^- media. According to Fig. 3c, this was found again, but several differences are worth commenting. The use of Pt in EO and EO-H_2O_2 led to the slowest decolorization, being needed 450-480 min, but the latter method was the least efficient despite the production of H_2O_2. In contrast, only 180 and 120 min were required in EO and EO-H_2O_2 with BDD, respectively, representing a very significant enhancement compared to their trends in the two previous media. The stability of NO_3^- ions against oxidation in EO with either Pt or BDD was verified, thus arising a hypothesis to explain the unexpected behavior in this medium: NO_3^- adsorption on the anode and/or the SS cathode surface could partially block some active sites, thus increasing the corresponding current densities, which leads to the enhanced degradation in EO with Pt as well as in systems with BDD. The very positive results in the latter case could then be explained by the larger BDD(•OH) production. In the presence of H_2O_2, self-destruction of BDD(•OH) could be partly avoided, producing more radicals like $HO_2^•$ that led to the great performance of EO-H_2O_2 with BDD. This possibility was further confirmed by carrying out two experiments (not shown): (i) the EO treatment with BDD in the presence of 100 mmol dm^{-3} of added H_2O_2, which outperformed the EO process, and (ii) the EO-H_2O_2 treatment with N_2 supply instead of air supply, which yielded a much slower decolorization. On the other hand, Fenton-based EAOPs were superior because of the main oxidizing role of •OH in the bulk, but they did not present an identical behavior, in contrast to that observed in SO_4^{2-} and ClO_4^-. The use of a BDD anode and/or UVA irradiation slightly accelerated color removal, indicating again the contribution from NO_3^- adsorption on the anode surface. Furthermore, in PEF with either Pt or BDD, a progressive decay of the NO_3^- concentration (not shown) suggested its reaction with photolyzed organic species, possibly inducing the appearance of a more oxidizing environment. As a result, total color removal was achieved in short times of 30-40 min in PEF systems.

Results in Cl^- medium depicted in Fig. 3d showed a very different behavior since the eight EAOPs led to complete decolorization in only 15-25 min because of the prevailing oxidizing role of active chlorine produced from reactions (5)-(7). Note that the four systems with BDD allowed a

slightly faster color removal that cannot be justified by a greater active chlorine concentration, as will be explained below, but should be related to the simultaneous action of BDD($^{\bullet}$OH). The benefits of Cl^- over SO_4^{2-} were also reported for the EO treatment of azo dyes Reactive Red 141, Direct Black 22 and Disperse Orange 29 with BDD anode [46]. However, Daneshvar et al. [38] showed that the decolorization efficiency for the EF treatment of Orange II with a graphite-felt cathode followed the order $ClO_4^- > Cl^- > SO_4^{2-}$. This difference was assigned to the formation of chloro or sulfato-complexes, which decreased the free Fe^{2+} concentration and consequently affected the Fenton's reaction. This fact is not observed when comparing EF or PEF treatments of Fig. 3a and 3d. Conversely, no iron complexes are expected in ClO_4^- and NO_3^- media [51]. Moreover, Cl^- and SO_4^{2-} are considered as radical scavengers that might retard the oxidation reaction. The better performance observed for our EF and PEF systems in Cl^- compared to the other media can then be mainly ascribed to the use of an air-diffusion instead of the graphite-felt cathode, since it allows the production of larger amounts of H_2O_2 to produce more $^{\bullet}$OH from Fenton's reaction.

3.2. Mineralization of Ponceau 4R solutions

Fig. 4 shows the TOC decay with electrolysis time for all the trials shown in Fig. 3. While all the systems allowed total decolorization, some of them were unable to yield complete mineralization of solutions. A first look to Fig. 4a, which corresponds to electrolyses in SO_4^{2-} medium, highlights some features that are common to the four electrolytes: (i) the use of BDD instead of Pt was beneficial in EO, EO-H_2O_2 and EF, leading to larger and/or quicker mineralization, whereas undistinguishable trends were obtained in PEF, (ii) considering each anode, the PEF treatment led to faster and larger TOC removals than EF, which in turn performed better than EO and EO-H_2O_2. As a result, in all the electrolytes the mineralization rate and/or degree increased in the order: EO ~ EO-H_2O_2 with Pt << EF with Pt < EO with BDD < EO-H_2O_2 with BDD < EF with BDD < PEF with Pt ~ PEF with BDD.

Except the trials made in Cl^-, total mineralization at times ≤ 480 min was only reached in EF with BDD and, even earlier, in the PEF systems. The very poor TOC decay (< 10%) achieved in EO and EO-H_2O_2 with Pt was due to its extremely low oxidation power, since Pt($^{\bullet}$OH) is readily converted to a much less active chemisorbed species (PtO_x) that can degrade the parent molecule (see Fig. 3a) but is unable to destroy its by-products. When Pt was replaced by BDD, 90% mineralization was reached in EO owing to the powerful BDD($^{\bullet}$OH), which progressively oxidized Ponceau 4R and all its oxidation and reduction by-products. Faster TOC abatement with total mineralization at 480 min was achieved in EO-H_2O_2 with BDD, which could be explained by: (i)

the concomitant action of $HO_2^{\bullet}$ formed from H_2O_2 oxidation and/or (ii) the lower accumulation of by-products from cathodic reduction, which can be less prone to oxidation. Alternatively, using Pt, EF was also much more effective than EO and EO-H_2O_2, thanks to the large production of $^{\bullet}OH$ in the bulk. This radical efficiently oxidized the parent molecule (see Fig. 3a) and its primary intermediates, but it was unable to remove very refractory final by-products, which were then accumulated in solution mainly as Fe(III) complexes and were responsible for the residual TOC content (~ 35%) at 480 min. Four short-chain aliphatic carboxylic acids, namely tartronic, oxalic, oxamic and formic acids, were identified as the main organic by-products that accounted for a large percentage of the residual TOC. Note that the same acids were found during the treatment of Acid Red 88 by Fenton-based EAOPs [29]. Again, the use of BDD instead of Pt was beneficial, yielding 100% mineralization due to the gradual destruction of all the refractory complexed and uncomplexed molecules by BDD($^{\bullet}OH$). The electrocatalytic effect of BDD anode is thus demonstrated and hence, physisorbed hydroxyl radicals were more effective than free $^{\bullet}OH$ in the bulk to break certain bonds. Much quicker mineralization was obtained in the PEF systems, with 100% TOC removal in less than 480 min. This behavior can be accounted for by the action of $^{\bullet}OH$ formed from Fenton's reaction (2) in conjunction with the photodegradation of Fe(III)-carboxylate complexes by UV photons according to reaction (4). Furthermore, free Fe^{3+} ions were simultaneously photoreduced to Fe^{2+} ions via reaction (3) to yield more $^{\bullet}OH$ from Fenton's reaction (2). All these reactions occur in the bulk and are prevalent over the oxidation of organic matter by M($^{\bullet}OH$), as demonstrated by the insignificant influence of the anode material.

The supporting electrolyte had marked impact on mineralization trends in some cases. Results obtained in ClO_4^- were analogous to those just discussed for SO_4^{2-}, as shown in Fig. 4d. Therefore, both media behave similarly, as occurred for decolorization in Fig. 3, thus confirming the negligible contribution of $S_2O_8^{2-}$ and sulfate radicals formed in SO_4^{2-}. In contrast, noticeable differences appeared in NO_3^- medium (see Fig. 4c), in agreement with findings commented from Fig. 3. In comparison with SO_4^{2-} and ClO_4^-, the treatment of dye solutions in NO_3^- by EO and EO-H_2O_2 with BDD or by PEF accelerated the degradation. For example, TOC was reduced by 82% in NO_3^- vs 60-65% in SO_4^{2-} and ClO_4^- after 240 min of EO-H_2O_2. This confirms the hypothesized contribution of BDD-NO_3^- interaction, as well as the effect of photolyzed organic species, to enhance the oxidizing ability of EAOPs in this medium. Fig. 4b presents various particular features in Cl^- medium. Overall, in contrast to findings for decolorization, this electrolyte resulted detrimental for mineralization compared to the other media [34], with some exception. Indeed, the presence of Cl^-

ions was beneficial in EO and EO-H_2O_2 with Pt, which was the least efficient EAOP in the other media, thus suggesting the ability of Pt anode to generate active chlorine species that led to 42% mineralization at 480 min. The use of BDD in the same processes allowed a more rapid TOC decay, being slightly slower compared to that found in the other media due to the partial consumption of BDD($^{\bullet}$OH) by Cl^- to form less oxidizing species such as (oxy)chloro radicals, oxychlorine anions and active chlorine (see below). Note also the almost total coincidence of curves in the presence and absence of H_2O_2, which may be explained by the destruction of this oxidant as follows [51]:

$$HClO + H_2O_2 \rightarrow Cl^- + O_{2(g)} + H_2O + H^+ \quad (11)$$

On the other hand, all the EF and PEF systems were decelerated in the presence of Cl^-. At 240 min, for instance, 32% and 89% TOC removals were attained in EF with Pt and PEF with BDD in Cl^-, respectively, whereas 55-60% and ~ 100% were reached in the other media. There exist three main causes to explain this behavior: (i) the poorer accumulation of H_2O_2 due to reaction (11) yielding lower amounts of $^{\bullet}$OH from Fenton's reaction (2), (ii) the appearance of refractory chloroderivatives and (iii) the formation of chloro-complexes, which decreased the free Fe^{2+} concentration [38,51].

The possible influence of cathodic reduction on decolorization and mineralization has been mentioned above, being reported as a typical mechanism for the partial degradation of azo dyes [52]. This aspect was then assessed by carrying out comparative electrolyses of 130 cm^3 of 254 mg dm^{-3} Ponceau 4R solutions at pH 3.0 and 100 mA in different divided and undivided BDD/SS and Pt/SS batch cells. All the experiments were made in 0.50 mol dm^{-3} Na_2SO_4 (specific conductivity of 37.4 mS cm^{-1}) in order to compensate the ohmic drop caused by the separator in divided systems and the E_{cell} values were 3.5 V with Pt and 5.5 V with BDD in the undivided cells, and from 13.0 to 14.5 V in the divided ones. Fig. 5a shows the time course of the decolorization efficiency, which was faster when using BDD instead of Pt as discussed from Fig. 3a. However, analogous trends were obtained for undivided and divided (with dye contained in the anolyte) cells in both cases, therefore revealing the insignificant contribution of cathodic reduction of Ponceau 4R and/or its colored by-products. But, an additional experiment using the Pt (wire) /SS divided cell, where the dye solution was placed in the catholyte, confirmed the existence of such cathodic reduction. As can be seen in Fig. 5a, almost 40% color removal was attained at 480 min in that system. Note that, although this degradation percentage seems remarkable, the colored molecules tended to be destroyed much more rapidly under the action of the anode, as verified in the undivided cells. The TOC abatement for all these electrolyses is shown in Fig. 5b. In agreement with Fig. 4a, a very poor mineralization was reached with Pt after 480 min, whereas much better performance was observed

with BDD due to the action of BDD($^{\bullet}$OH). Moreover, in EO with BDD, TOC removal was slightly faster using the undivided cell. This means that the superiority of EO-H_2O_2 over EO in cells with BDD (see Fig. 4a) was basically due to the beneficial formation of $HO_2^{\bullet}$ from H_2O_2 oxidation in the former process, rather than to the detrimental influence of cathodic by-products in EO. In conclusion, the small contribution of the cathodic reduction of Ponceau 4R and/or its by-products can be considered as irrelevant or slightly positive.

3.3. Voltammetric study in different electrolytes

Linear sweep voltammograms recorded from 0 to 1.6 V vs Ag|AgCl for different solutions of pH 3.0 at 25 ºC using Pt as the working electrode are shown in Fig. 6. In the presence of 0.05 mol dm^{-3} Na_2SO_4 alone, no current flow was detected until O_2 evolution occurred from H_2O oxidation on Pt at ca. 1.2 V, as observed in Fig. 6a. This confirms that Pt can be considered a low O_2-overpotential anode [15], thus leading to Pt($^{\bullet}$OH) with low oxidation power. Interestingly, an oxidation peak appeared at ca. 1.0 V in the presence of Ponceau 4R, its current peak being proportional to the dye concentration. This finding reveals that, apart from mediated oxidation by $^{\bullet}$OH and/or M($^{\bullet}$OH) in EAOPs tested in Na_2SO_4 medium, the azo dye is electroactive and may undergo direct oxidation as well. The effect of supporting electrolyte is depicted in Fig. 6b. Blanks obtained in either 0.05 mol dm^{-3} of Na_2SO_4, $NaNO_3$ or $LiClO_4$ were identical, showing no additional relevant features before O_2 evolution, but in NaCl, the increase in current from zero occurred earlier (< 1.1 V), which can be related to the aforementioned Cl^- oxidation on Pt (see Fig. 3b and 4b). This indicates that at a low oxidation power anodes such as Pt, H_2O and Cl^- oxidation occur concomitantly [15,18]. As a result, current values in that electrolyte were much higher at all subsequent potentials. In the presence of 0.42 mmol dm^{-3} Ponceau 4R, the characteristic oxidation peak of the dye at ca. 1.0 V appeared in all the electrolytes. In NaCl, current values within the H_2O oxidation region were much closer to those obtained in the other media because of slight anode passivation due to dye adsorption [53] and the current shoulder at 1.4 V confirmed the Cl^- oxidation [45,53]. LSV was also carried out using BDD instead of Pt (not shown). Blank voltammograms in 0.05 mol dm^{-3} of electrolyte displayed no peaks, as also observed elsewhere [45]. Noticeably, current values in NaCl were lower than those obtained with Pt, which means that chlorine evolution was enhanced on this latter anode. In the presence of 0.42 and 0.84 mmol dm^{-3} Ponceau 4R, a wave appeared at about 2 V in all media, similarly to that found for other organic molecules at BDD [54].

3.4. Role of chlorine and analysis of chlorinated species

The great influence of chlorinated species formed in Cl^- medium on the decolorization and mineralization kinetics of Ponceau 4R has been demonstrated in previous sections. Since the composition of a dye wastewater usually includes large amounts of both, Cl^- and SO_4^{2-} ions, it is necessary from an applicative standpoint to investigate the performance of EAOPs in sulphate/chloride mixtures. Fig. 7a illustrates the time course of color removal during the degradation of 254 mg dm^{-3} Ponceau 4R solutions in different mixtures of both ions at pH 3.0 by PEF process with a BDD anode at 300 mA. As discussed from Fig. 3 and 4, this process was the most effective among all the EAOPs tested. Solutions with 100% SO_4^{2-} became colorless in 50 min, whereas the gradual increase of Cl^- ratio progressively accelerated the degradation thanks to the participation of active chlorine, up to attaining total color removal in 15-25 min when > 60% Cl^- was used. The fact that Cl^- contents much lower than 0.05 mol dm^{-3} allowed reaching overall decolorization within a few minutes is then very interesting. In contrast, Fig. 7b shows that progressively greater Cl^- percentage in these mixtures caused slower TOC decays, although the use of < 60% Cl^- always led to total mineralization in ca. 240 min because the H_2O_2 destruction via reaction (11) and the complexation of iron ions were minimized. It is then concluded that Ponceau 4R solutions can be treated with great efficacy within a large range of concentrations of inorganic ions. Based on those TOC values and mineralization reaction (8), the time course of MCE calculated from Eq. (9) has been plotted on Fig. 7c. Maximum current efficiencies were attained during the first stages, the highest value of 26% being found in 100% SO_4^{2-}. MCE values gradually decayed with electrolysis time due to the presence of smaller amounts of organic matter and the accumulation of largely refractory molecules like chloroderivatives and aliphatic carboxylic acids [16].

The fate of chlorinated ions during the application of EAOPs in Cl^- medium was assessed. As an example, Fig. 8 shows the concentration of various chlorinated ions accumulated upon treatment of 20 mmol dm^{-3} NaCl solutions at pH 3.0 and 300 mA using BDD. In EO-H_2O_2 (Fig. 8a), Cl^- ion totally disappeared in 360 min due to its destruction by M($^\bullet$OH) and by direct electron transfer via reaction (5), giving rise to ClO_3^- and ClO_4^- ions. Whereas an accumulation-destruction profile was found for the former one, ClO_4^- ion was gradually accumulated in solution up to accounting for almost 100% Cl concentration. Note the quite stable Cl content throughout the electrolysis, which can be explained by the insignificant loss as $Cl_{2(g)}$ and the low accumulation of active chlorine and organic chloroderivatives, which are degraded by M($^\bullet$OH). ClO^- accumulation from reaction (7)

was not even detected in assays carried out at higher pH (not shown), indicating its transformation into other oxychlorine ions and the destruction of HClO via reaction (11). In contrast, ClO^- was found at near-neutral pH when the air-diffusion cathode was replaced by a SS cathode, thus confirming the role of reaction (11) in the presence of H_2O_2 formed via cathodic O_2 reduction or anodic M($^\bullet$OH) dimerization. The contribution of M($^\bullet$OH) to Cl^- oxidation was ascertained by carrying out electrolyses in the presence of 20 mmol dm^{-3} *t*-BuOH that acted as a radical scavenger. Fig. 8a shows the much slower disappearance of Cl^-, since this ion can only undergo direct anodic oxidation, and the very low accumulation of ClO_3^- and ClO_4^- ions. As can be seen in Fig. 8b, the trends and concentrations of all the chlorinated ions in the PEF process were analogous to those found in EO-H_2O_2, only being noticeable the slight decrease of Cl content at 360 min. This might be explained by the larger loss as $Cl_{2(g)}$ upon the action of massive $^\bullet$OH formed in the bulk.

As mentioned, active chlorine was responsible for the enhanced decolorization in Cl^- medium, particularly in EO systems (see Fig. 3b). Fig. 9a depicts its evolution in EO with BDD. The treatment of 10, 20 and 50 mmol dm^{-3} NaCl solutions at pH 3.0 and 300 mA yielded maximum contents of 0.4, 2.3 and 7.2 mmol Cl_2 dm^{-3}, thereby decaying over time due to its transformation into more stable oxychlorine anions, as demonstrated in Fig. 8, and its cathodic reduction to Cl^-. The presence of *t*-BuOH led to a lower accumulation of active chlorine, thus confirming that Cl^- oxidation by M($^\bullet$OH) is a fundamental step to form $Cl_{2(aq)}$ and subsequent chlorinated species [20,55]. Nevertheless, the use of Pt allowed the accumulation of larger amounts of active chlorine. As shown in Fig. 9b, the concentration reached was almost twice (4.1 mmol Cl_2 dm^{-3}), which agrees with some results discussed above in NaCl medium: (i) the great enhancement of mineralization in EO and EO-H_2O_2 with Pt (see Fig. 4b) and (ii) the higher current values monitored by LSV (see Fig. 6b). Again, the use of *t*-BuOH caused the accumulation of lower active chlorine amounts, thus confirming the formation of Pt($^\bullet$OH) upon H_2O oxidation. Finally, a similar study by EO-H_2O_2 with either Pt or BDD (not shown) revealed the absence of active chlorine, which suggests the negligible interference of other stable oxidants ($S_2O_8^{2-}$, O_3 and H_2O_2) in these analyses.

4. Conclusions

The presence of food additives in wastewater, in particular azo dyes used for coloring foodstuffs, is becoming a matter of social concern. Such wastewater is typically characterized by the presence of several inorganic ions that could interfere during water treatment by EAOPs. In the present work, the faster decolorization of Ponceau 4R solutions in the order $SO_4^{2-} \sim ClO_4^- < NO_3^-$

<< Cl^- and mineralization in the order Cl^- << SO_4^{2-} ~ ClO_4^- < NO_3^- have been explained by the competition between several degradation routes: (i) direct electron transfer, (ii) oxidation by M($^\bullet$OH) or $^\bullet$OH, (iii) reaction with chlorinated species, particularly active chlorine, and (iv) NO_3^- adsorption and its interaction with photolyzed species. In all the electrolytes, the mineralization rate and/or degree increased in the order: EO ~ EO-H_2O_2 with Pt << EF with Pt < EO with BDD < EO-H_2O_2 with BDD < EF with BDD < PEF with Pt ~ PEF with BDD. Therefore, the PEF process with low or high oxidation power anodes is the most convenient technology to ensure the quick and total removal of Ponceau 4R and its degradation by-products from water.

Acknowledgments

The authors thank MINECO (Ministerio de Economía y Competividad, Spain) for financial support under project CTQ2013-48897-C2-1-R, co-financed with FEDER funds. The Ph.D. grant awarded to A. Thiam from MAEC-AECID (Spain) is also acknowledged.

References

[1] K.T. Chung, G.E. Fulk, A.W. Andrews, Mutagenicity testing of some commonly used dyes, Appl. Environ. Microbiol. 42 (1981) 641.

[2] K.P. Sharma, S. Sharma, S.P. Sharma, K. Singh, S. Kumar, R. Grover, P.K. Sharma, A comparative study on characterization of textile wastewaters (untreated and treated) toxicity by chemical and biological tests, Chemosphere 69 (2007) 48.

[3] I.K. Konstantinou, T.A. Albanis, TiO_2-assisted photocatalytic degradation of azo dyes in aqueous solution: kinetic and mechanistic investigations, Appl. Catal. B: Environ. 49 (2004) 1.

[4] E. Brillas, C.A. Martínez-Huitle, Decontamination of wastewaters containing synthetic organic dyes by electrochemical methods. An updated review, Appl. Catal. B: Environ. 166-167 (2015) 603.

[5] D. McCann, A. Barrett, C. Cooper, D. Crumpler, L. Dalen, K. Grimshaw, E. Kitchin, K. Lok, L. Porteous, E. Prince, E. Sonuga-Barke, J. O'Warner, J. Stevenson, Food additives and hyperactive behavior in 3-year-old and 8/9-year-old children in the community: A randomised, double-blinded, placebo-controlled trial, Lancet 370 (2007) 1560.

[6] EFSA, Scientific Opinion on the re-evaluation of Ponceau 4R (E 124) as a food additive, EFSA J. 7 (2009) 1328.

[7] L.E. Arnold, N. Lofthouse, E. Hurt, Artificial food colors and attention-deficit/hyperactivity symptoms: conclusions to dye for, Neurotherapeutics 9 (2012) 599.

[8] http://www.fda.gov/ForIndustry/ColorAdditives/ColorAdditiveInventories/ucm115641.htm

[9] M.M. Ghoneim, H.S. El-Desoky, N.M. Zidan, Electro-Fenton oxidation of Sunset Yellow FCF azo-dye in aqueous solutions, Desalination 274 (2011) 22.

[10] K. Tanaka, K. Padermpole, T. Hisanaga, Photocatalytic degradation of commercial azo dyes, Water Res. 34 (2000) 327.

[11] N. Sobana, M. Swaminathan, The effect of operational parameters on the photocatalytic degradation of acid red 18 by ZnO, Sep. Purif. Technol. 56 (2007) 101.

[12] J. Basiri Parsa, M. Golmirzaei, M. Abbasi, Degradation of azo dye C.I. Acid Red 18 in aqueous solution by ozone-electrolysis process, J. Ind. Eng. Chem. 20 (2014) 689.

[13] K. Barbusiński, J. Majewski, Discoloration of azo dye Acid Red 18 by Fenton reagent in the presence of iron powder, Pol. J. Environ. Studies 12 (2003) 151.

[14] A. Anglada, A. Urtiaga, I. Ortiz, Contributions of electrochemical oxidation to waste-water treatment: fundamentals and review of applications, J. Chem. Technol. Biotechnol. 84 (2009) 1747.

[15] M. Panizza, G. Cerisola, Electrochemical processes for the treatment of organic pollutants, Chem. Rev. 109 (2009) 6541.

[16] I. Sirés, E. Brillas, M.A. Oturan, M.A. Rodrigo, M. Panizza, Electrochemical advanced oxidation processes: today and tomorrow. A review, Environ. Sci. Pollut. Res. 21 (2014) 8336.

[17] M.E. Bergmann, J. Rollin, Product and by-product formation in laboratory studies on disinfection electrolysis of water using boron-doped diamond anodes, Catal. Today 124 (2007) 198.

[18] A.M. Polcaro, A. Vacca, M. Mascia, S. Palmas, J. Rodriguez Ruiz, Electrochemical treatment of waters with BDD anodes: kinetics of the reactions involving chlorides, J. Appl. Electrochem. 39 (2009) 2083.

[19] S. Randazzo, O. Scialdone, E. Brillas, I. Sirés, Comparative electrochemical treatments of two chlorinated aliphatic hydrocarbons. Time course of the main reaction by-products, J. Hazard. Mater. 192 (2011) 1555.

[20] F. Bonfatti, S. Ferro, F. Lavezzo, M. Malacarne, G. Lodi, A. De Battisti, Electrochemical incineration of glucose as a model organic substrate. II. Role of active chlorine mediation, J. Electrochem. Soc. 147 (2000) 592.

[21] M. Deborde, U. von Gunten, Reactions of chlorine with inorganic and organic compounds during water treatment-Kinetics and mechanisms: a critical review, Water Res. 42 (2008) 13.

[22] S.D. Richardson, New disinfection by-product issues: Emerging DBPs and alternative routes of exposure, Global NEST J. 7 (2005) 43.

[23] M. Zhou, Q. Yu, L. Lei, G. Barton, Electro-Fenton method for the removal of methyl red in an efficient electrochemical system, Sep. Purif. Technol. 57 (2007) 380.

[24] M. Panizza, G. Cerisola, Electrochemical degradation of methyl red using BDD and PbO_2 anodes, Ind. Eng. Chem. Res. 47 (2008) 6816.

[25] A. Wang, J. Qu, H. Liu, J. Ru, Mineralization of azo dye Acid Red 14 by photoelectro-Fenton process using an activated carbon fiber cathode, Appl. Catal. B: Environ. 84 (2008) 393.

[26] A. Özcan, M.A. Oturan, N. Oturan, Y. Şahin, Removal of Acid Orange 7 from water by electrochemically generated Fenton's reagent, J. Hazard. Mater. 163 (2009) 1213.

[27] E. Rosales, M. Pazos, M.A. Longo, M.A. Sanromán, Electro-Fenton decoloration of dyes in a continuous reactor: A promising technology in colored wastewater treatment, Chem. Eng. J. 155 (2009) 62.

[28] E.J. Ruiz, C. Arias, E. Brillas, A. Hernández-Ramírez, J.M. Peralta-Hernández, Mineralization of Acid Yellow 36 azo dye by electro-Fenton and solar photoelectro-Fenton processes with a boron-doped diamond anode, Chemosphere 82 (2011) 495.

[29] E.J. Ruiz, A. Hernández-Ramírez, J.M. Peralta-Hernández, C. Arias, E. Brillas, Application of solar photoelectro-Fenton technology to azo dyes mineralization: Effect of current density, Fe2+ and dye concentrations, Chem. Eng. J. 171 (2011) 385.

[30] A.R. Khataee, M. Safarpour, M. Zarei, S. Aber, Combined heterogeneous and homogeneous photodegradation of a dye using immobilized TiO_2 nanophotocatalyst and modified graphite electrode with carbon nanotubes, J. Molec. Catal. A: Chem. 363-364 (2012) 58.

[31] A. El-Ghenymy, F. Centellas, J.A. Garrido, R.M. Rodríguez, I. Sirés, P.L. Cabot, E. Brillas, Decolorization and mineralization of Orange G azo dye solutions by anodic oxidation with a boron-doped diamond anode in divided and undivided tank reactors, Electrochim. Acta 130 (2014) 568.

[32] O. Scialdone, A. Galia, S. Sabatino, Abatement of Acid Orange 7 in macro and micro reactors. Effect of the electrocatalytic route, Appl. Catal. B: Environ. 148-149 (2014) 473.

[33] A Thiam, I. Sirés, J.A. Garrido, R.M. Rodríguez, E. Brillas, Effect of anions on electrochemical degradation of azo dye Carmoisine (Acid Red 14) using a BDD anode and air-diffusion cathode, Sep. Purif. Technol. 140 (2015) 43.

[34] A Thiam, I. Sirés, J.A. Garrido, R.M. Rodríguez, E. Brillas, Decolorization and mineralization of Allura Red AC aqueous solutions by electrochemical advanced oxidation processes, J. Hazard. Mater. 290 (2015) 34.

[35] A. Fernandes, A. Morão, M. Magrinho, A. Lopes, I. Gonçalves, Electrochemical degradation of C. I. Acid Orange 7, Dyes Pigments 61 (2004) 287.

[36] H.S. Awad, N.A. Galwa, Electrochemical degradation of Acid Blue and Basic Brown dyes on Pb/PbO_2 electrode in the presence of different conductive electrolyte and effect of various operating factors, Chemosphere 61 (2005) 1327.

[37] M. Diagne, N. Oturan, M.A. Oturan, Removal of methyl parathion from water by electrochemically generated Fenton's reagent, Chemosphere 66 (2007) 841.

[38] N. Daneshvar, S. Aber, V. Vatanpour, M.H. Rasoulifard, Electro-Fenton treatment of dye solution containing Orange II: Influence of operational parameters, J. Electroanal. Chem. 615 (2008) 165.

[39] A. Özcan, Y. Şahin, A.S. Koparal, M.A. Oturan, Propham mineralization in aqueous medium by anodic oxidation using boron-doped diamond anode: Influence of experimental parameters on degradation kinetics and mineralization efficiency, Water Res. 42 (2008) 2889.

[40] S. Aquino Neto, A.R. De Andrade, Electrooxidation of glyphosate herbicide at different DSA® compositions: pH, concentration and supporting electrolyte effect, Electrochim. Acta 54 (2009) 2039.

[41] P. Cañizares, M. Hernández, M.A. Rodrigo, C. Sáez, C.E. Barrera, G. Roa, Electrooxidation of brown-colored molasses wastewater. Effect of the electrolyte salt on the process efficiency, Ind. Eng. Chem. Res. 48 (2009) 1298.

[42] X. Ma, M. Zhou, A comparative study of azo dye decolorization by electro-Fenton in two common electrolytes, J. Chem. Technol. Biotechnol. 84 (2009) 1544.

[43] T. Velegraki, G. Balayiannis, E. Diamadopoulos, A. Katsounis, D. Mantzavinos, Electrochemical oxidation of benzoic acid in water over boron-doped diamond electrodes: Statistical analysis of key operating parameters, kinetic modeling, reaction by-products and ecotoxicity, Chem Eng. J. 160 (2010) 538.

[44] P. Kariyajjanavar, N. Jogttappa, Y.A. Nayaka, Studies on degradation of reactive textile dyes solution by electrochemical method, J. Hazard. Mater. 190 (2011) 952.

[45] M. Murugananthan, S.S. Latha, G. Bhaskar Raju, S. Yoshihara, Role of electrolyte on anodic mineralization of atenolol at boron doped diamond and Pt electrodes, Sep. Purif. Technol. 79 (2011) 56.

[46] J.M. Aquino, M.A. Rodrigo, R.C. Rocha-Filho, C. Sáez, P. Cañizares, Influence of the supporting electrolyte on the electrolyses of dyes with conductive-diamond anodes, Chem. Eng. J. 184 (2012) 221.

[47] A.R.F. Pipi, A.R. De Andrade, E. Brillas, I. Sirés, Total removal of alachlor from water by electrochemical processes, Sep. Purif. Technol. 132 (2014) 674.

[48] M.E.H. Bergmann, J. Rollin, Product and by-product formation in laboratory studies on disinfection electrolysis of water using boron-doped diamond anodes, Catal. Today 124 (2007) 198.

[49] T. Chen, Spectrophotometric determination of microquantities of chlorate, chlorite, hypochlorite, and chloride in perchlorate, Anal. Chem. 39 (1967) 804.

[50] APWA, AWWA and WEF. Standard Methods for the Examination of Water and Wastewater. 21st Ed. Method number 4500-Cl Chlorine (residual) – G. DPD Colorimetric Method, American Public Health Association, Washington D.C., 2005, pp. 4-67 to 4-68.

[51] J. De Laat, G.T. Le, B. Legube, A comparative study of the effects of chloride, sulfate and nitrate ions on the rates of decomposition of H_2O_2 and organic compounds by Fe(II)/H_2O_2 and Fe(III)/H_2O_2, Chemosphere 55 (2004) 715.

[52] Y.-Z. Song, Electrochemical reduction of C.I. Acid Red 18 on multi-walled carbon nanotubes and its analytical application. Dyes Pigments 87 (2010) 39.

[53] L. Szpyrkowicz, M. Radaelli, S. Daniele, Electrocatalysis of chlorine evolution on different materials and its influence on the performance of an electrochemical reactor for indirect oxidation of pollutants, Catal. Today 100 (2005) 425.

[54] M. Panizza, G. Cerisola, Influence of anode materials on the electrochemical oxidation of 2-naphtol: Part 1. Cyclic voltammetry and potential step experiment, Electrochim. Acta 48 (2003) 3491.

[55] C. Salazar, I. Sirés, C.A. Zaror, E. Brillas, Treatment of a mixture of chloromethoxyphenols in hypochlorite medium by electrochemical AOPs as an alternative for the remediation of pulp and paper mill process waters, Electrocatalysis 4 (2013) 212.

Figure Captions

Fig. 1. Chemical structure of Ponceau 4R (C.I. Acid Red 18, additive E124).

Fig. 2. UV-Vis spectra obtained from Ponceau 4R solutions treated by EO-H_2O_2 with BDD in 0.05 mol dm^{-3} (a) Na_2SO_4 and (b) NaCl for different electrolysis times.

Fig. 3. Decolorization efficiency at 508 nm vs electrolysis time for the degradation of 130 cm^3 of 254 mg dm^{-3} (0.42 mmol dm^{-3}) Ponceau 4R solutions in 0.05 mol dm^{-3} of (a) Na_2SO_4, (b) NaCl, (c) $NaNO_3$ and (d) $LiClO_4$, at pH 3.0 and 300 mA. Treatment: (●) EO-H_2O_2 with BDD, (■) EO with BDD, (◆) EO-H_2O_2 with Pt, (▲) EO with Pt, (○) EF with BDD, (□) EF with Pt, (◇) PEF with BDD and (△) PEF with Pt. In EF and PEF, 0.50 mmol dm^{-3} Fe^{2+} was added to the solution.

Fig. 4. TOC removal with electrolysis time for the trials shown in Fig. 3.

Fig. 5. (a) Change of percentage of color removal at 508 nm and (b) TOC abatement with electrolysis time for the electrolytic degradation of 130 cm^3 of 254 mg dm^{-3} Ponceau 4R solutions in 0.50 mol dm^{-3} Na_2SO_4 at pH 3.0 and 100 mA in different undivided (U) or divided (D) tank reactors with a stainless steel (SS) cathode. Cell: (●) BDD/SS (U), (■) BDD/SS (D), (○) Pt/SS (U) and (□) Pt/SS (D), with the divided cells containing the dye in the anolyte. (△) Pt/SS (D) cell with the dye in the catholyte.

Fig. 6. Linear sweep voltammograms recorded for solutions of pH 3.0 at 25 ºC on a Pt electrode. In (a), 0.05 mol dm^{-3} Na_2SO_4 (—) alone or with (—) 0.42 mmol dm^{-3} or (—) 0.84 mmol dm^{-3} Ponceau 4R. In (b), blanks obtained for (—) 0.05 mol dm^{-3} Na_2SO_4 (identical to $NaNO_3$ and $LiClO_4$) and (—) NaCl, and in the presence of 0.42 mmol dm^{-3} of dye in 0.05 mol dm^{-3} of: (—) Na_2SO_4, (—) NaCl, (—) $NaNO_3$ and (—) $LiClO_4$. Scan rate: 10 mV s^{-1}.

Fig. 7. Variation of (a) decolorization efficiency at 508 nm, (b) TOC and (c) mineralization current efficiency with electrolysis time for the degradation of 130 cm^3 of 254 mg dm^{-3} Ponceau 4R solutions in different 0.05 mol dm^{-3} Na_2SO_4 + 0.05 mol dm^{-3} NaCl mixtures with 0.5 mmol dm^{-3} Fe^{2+} at pH 3.0 by PEF process with a BDD anode at 300 mA. [Na_2SO_4]:[NaCl] ratio: (●) 100:0, (△) 80:20, (□) 60:40, (◇) 50:50, (▽) 40:60, (○) 20:80 and (■) 0:100.

Fig. 8. Time course of the concentration of chlorinated ions accumulated during the degradation of 130 cm^3 of 20 mmol dm^{-3} NaCl solutions at pH 3.0 and 300 mA by (a) EO-H_2O_2 and (b) PEF with 0.50 mmol dm^{-3} Fe^{2+}, always using a BDD anode. Ions in the absence of *t*-BuOH: (○) Cl^-, (□)

ClO_3^-, (△) ClO_4^- and (◇) sum of chlorinated ions. Ions in the presence of 20 mmol dm^{-3} *t*-BuOH: (●) Cl^-, (■) ClO_3^- and (▲) ClO_4^-. Plot (a) also shows the formation of (▽) ClO^- when replacing the air-diffusion by a SS cathode at neutral pH.

Fig. 9. Active chlorine vs electrolysis time for the EO of 130 cm^3 of (○) 10, (□,◇,■) 20 and (△) 50 mmol dm^{-3} NaCl solutions at pH 3.0 and 300 mA. (a) BDD/SS cell: (○,□,△) in the absence of *t*-BuOH and (■) in the presence of 20 mmol dm^{-3} *t*-BuOH. (b) Pt/ SS cell: (□) without and (■) with 20 mmol dm^{-3} *t*-BuOH.

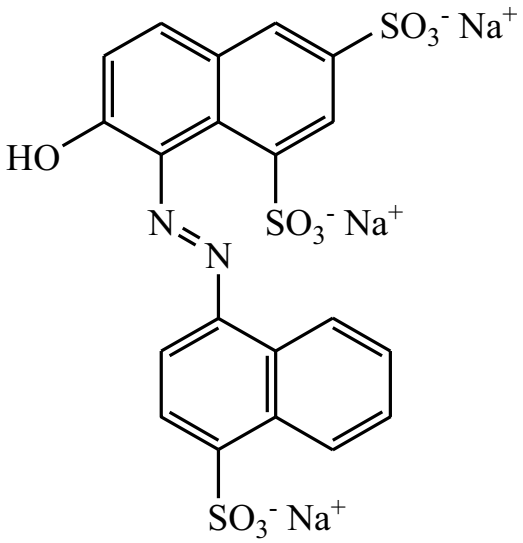

Fig. 1

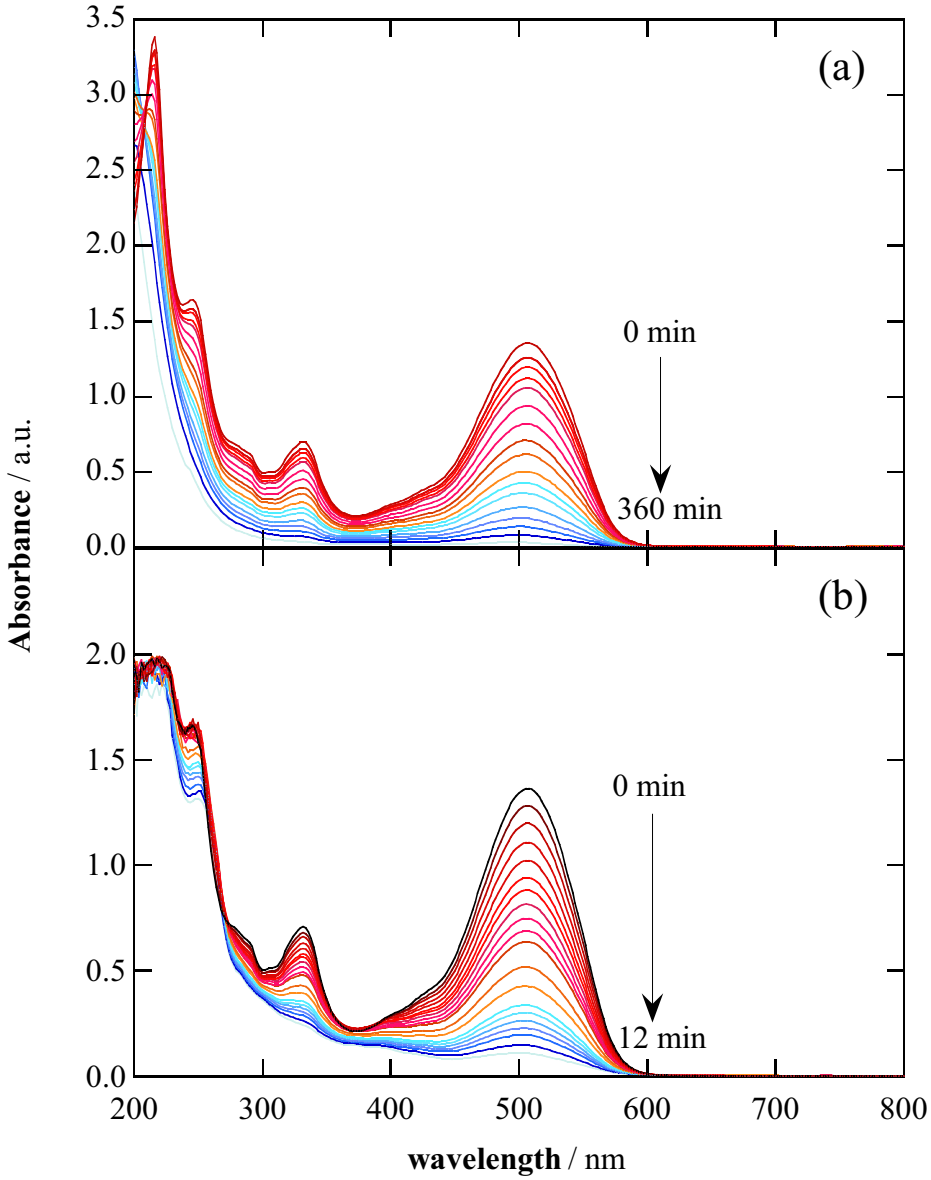
(a)
0 min
360 min
(b)
0 min
12 min
Absorbance / a.u.
wavelength / nm
3.5
3.0
2.5
2.0
1.5
1.0
0.5
0.0
200
300
400
500
600
700
800

Fig. 2

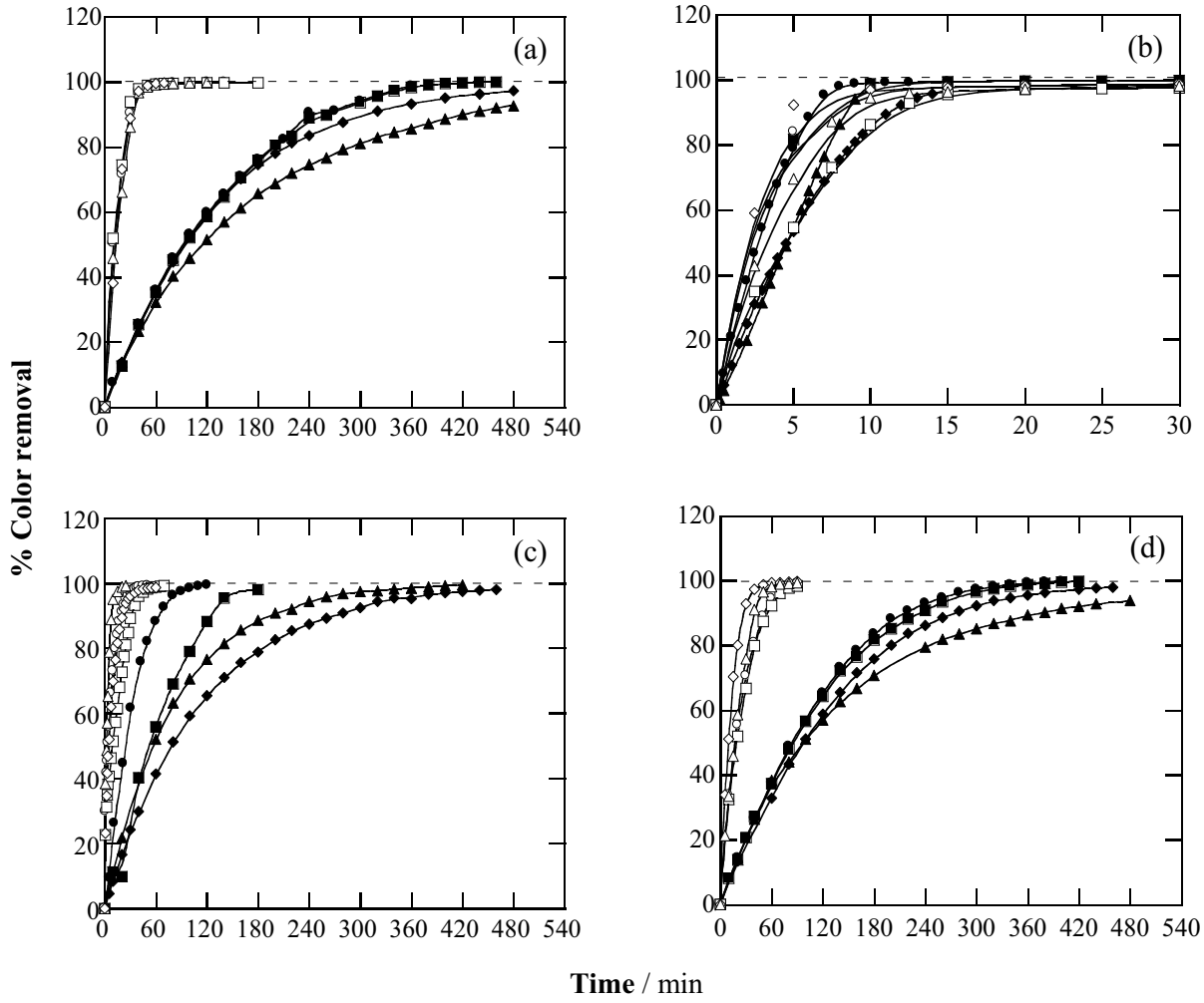

Fig. 3

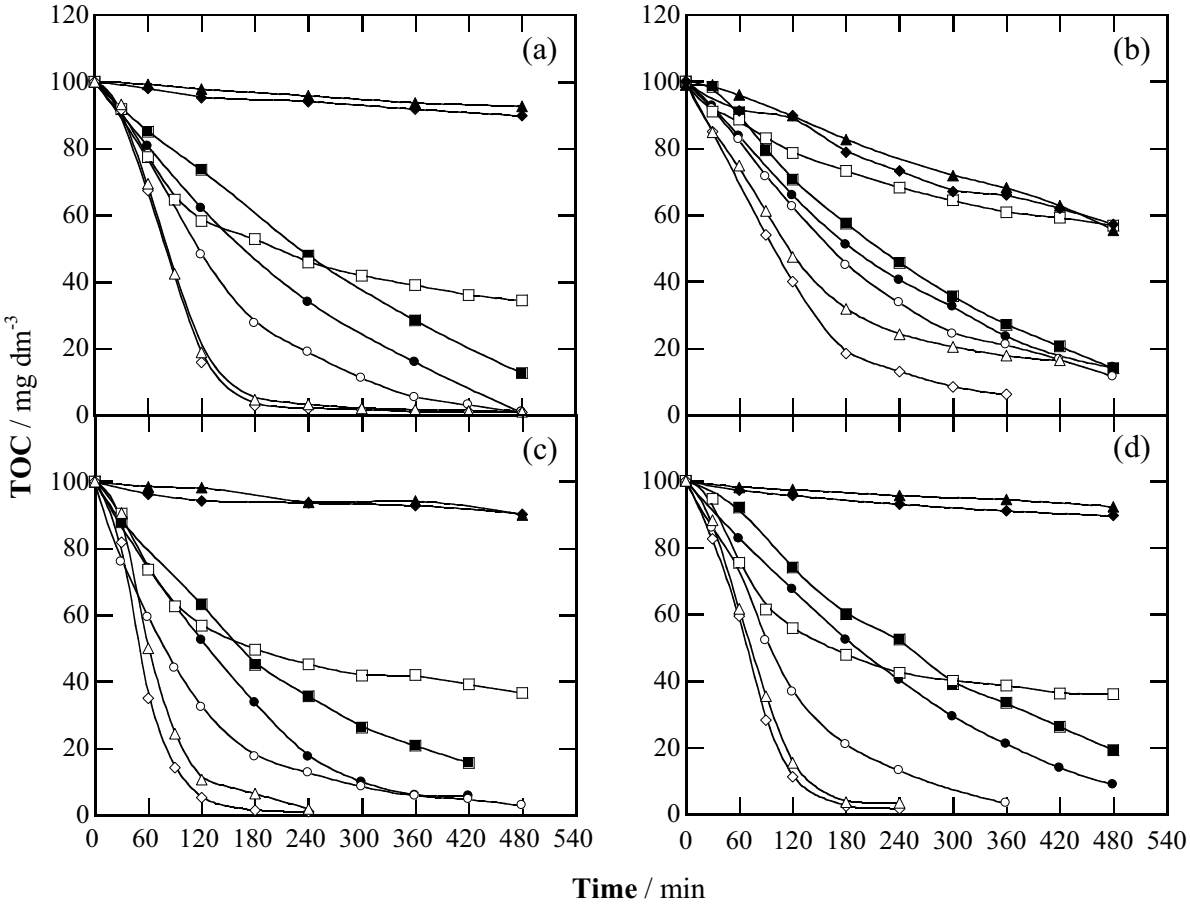
(a)
(b)
(c)
(d)
TOC / mg dm-3
Time / min
0
20
40
60
80
100
120
0
60
120
180
240
300
360
420
480
540

Fig. 4

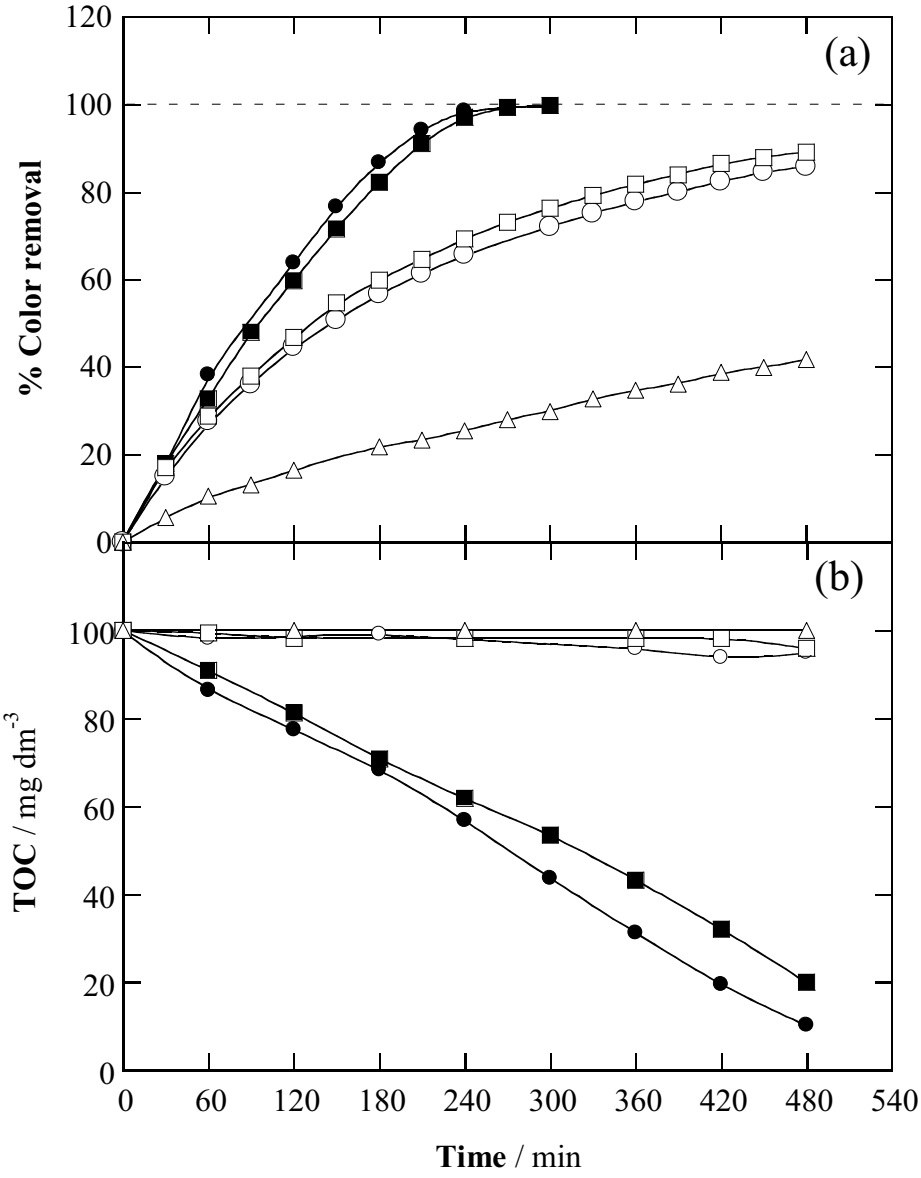
(a)
(b)
% Color removal
TOC / mg dm-3
Time / min
0
20
40
60
80
100
120
0
60
120
180
240
300
360
420
480
540

Fig. 5

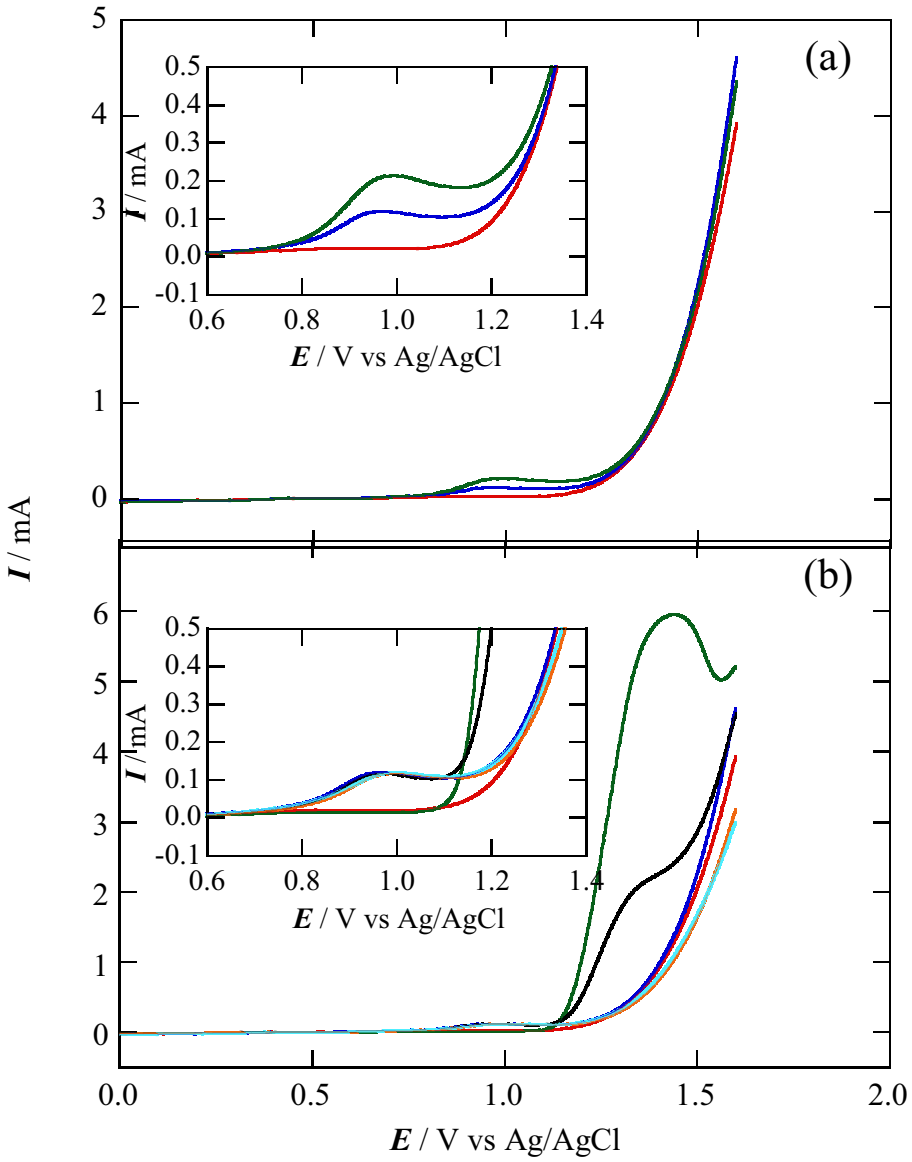

Fig. 6

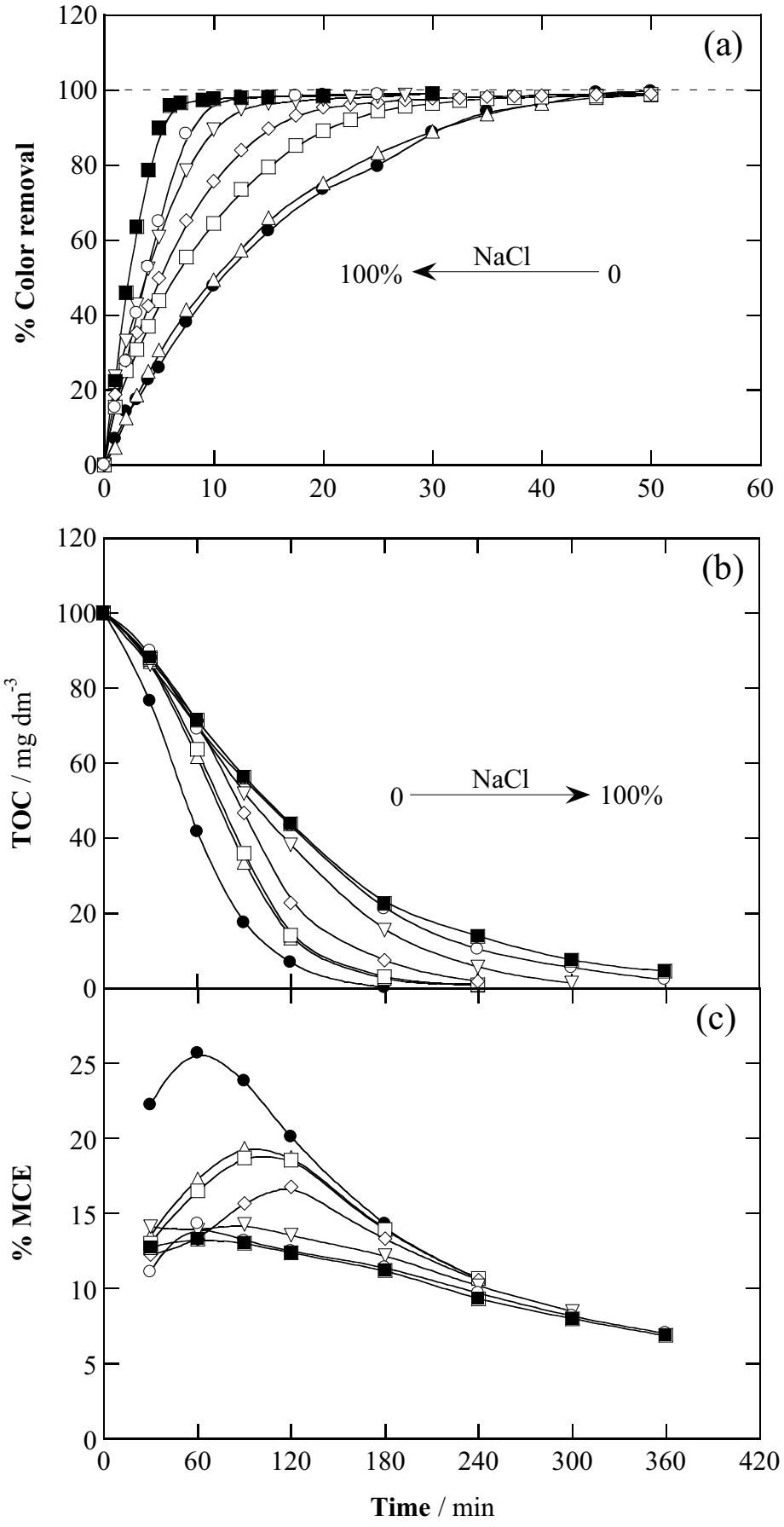

Fig. 7

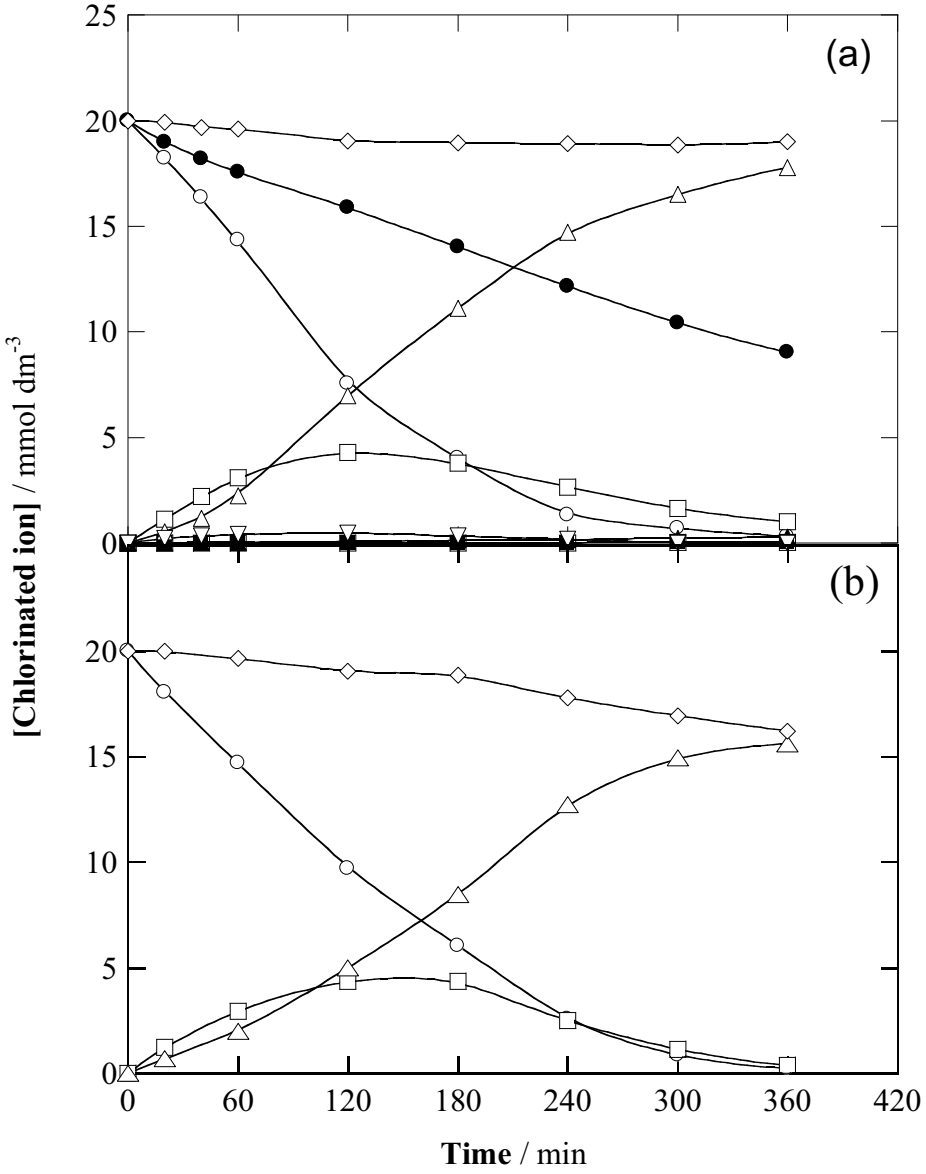
(a)
(b)
[Chlorinated ion] / mmol dm-3
Time / min
0
5
10
15
20
25
0
60
120
180
240
300
360
420

Fig. 8

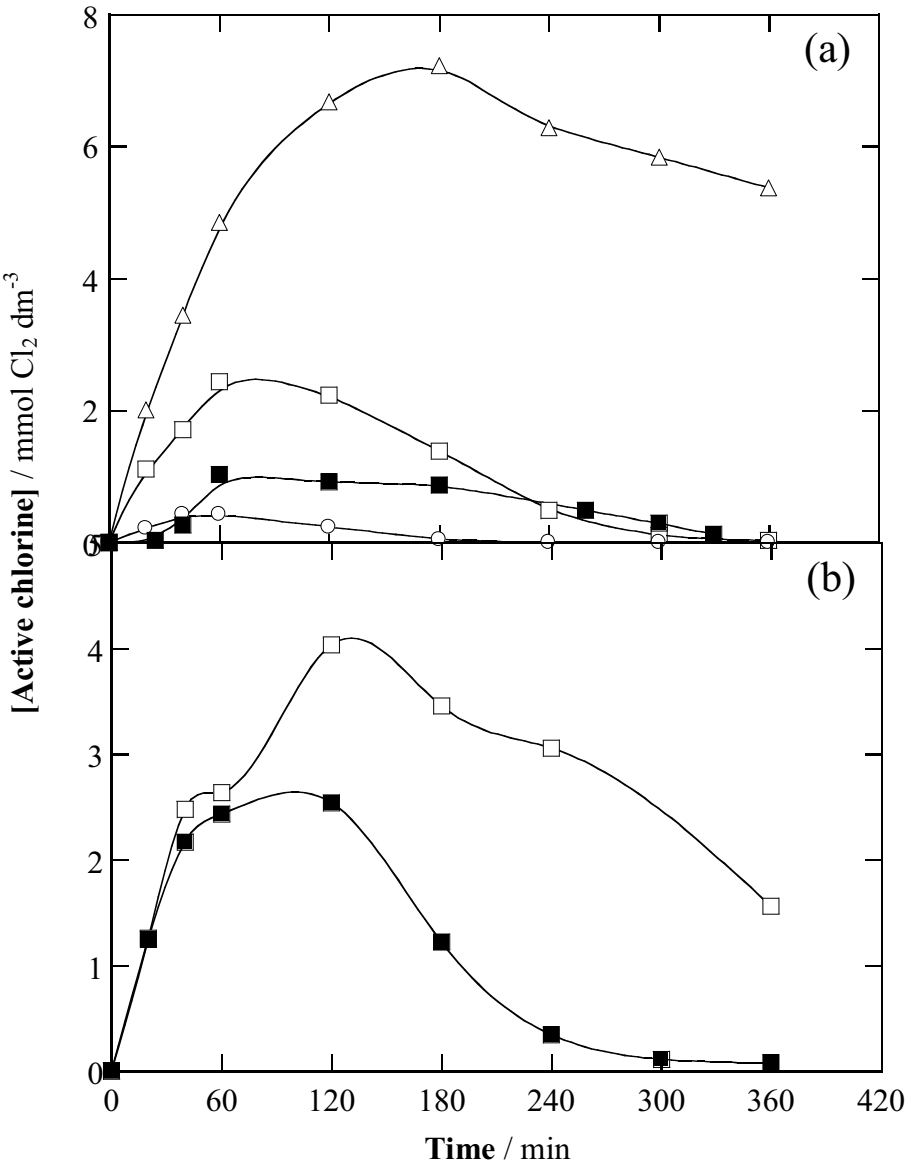
(a)
(b)
[Active chlorine] / mmol Cl2 dm-3
Time / min
0
60
120
180
240
300
360
420
1
2
3
4
6
8

Fig. 9

Table 1.

Specific conductivity of each supporting electrolyte and potential difference between the anode and cathode for each undivided tank reactor at 300 mA.

Electrolyte	κ	E_{cell} / V			
(0.05 mol dm^{-3})	/ mS cm^{-1}	Pt/SS	Pt/air-diffusion	BDD/SS	BDD/air-diffusion
Na_2SO_4	7.5	9.2	13.0	13.3	16.4
NaCl	4.9	10.6	16.4	14.0	22.0
$NaNO_3$	4.7	12.4	16.7	14.5	23.4
$LiClO_4$	4.2	13.5	19.1	17.1	24.0

.

Paper 2

Routes for the electrochemical degradation of the artificial food azo-colour Ponceau 4R by advanced oxidation processes

Applied Catalysis B: Environmental

Submitted (Manuscript No: APCATB-D-15-00906)

Routes for the electrochemical degradation of the artificial food azo-colour Ponceau 4R by advanced oxidation processes

Abdoulaye Thiam, Enric Brillas, José A. Garrido, Rosa M. Rodríguez, Ignasi Sirés*

Laboratori d'Electroquímica dels Materials i del Medi Ambient, Departament de Química Física, Facultat de Química, Universitat de Barcelona, Martí i Franquès 1-11, 08028 Barcelona, Spain

Paper submitted to be published in Applied Catalysis B: Environmental

* Corresponding author: Tel.: +34 934021223; fax: +34 934021231.

E-mail address: i.sires@ub.edu (I. Sirés)

4. Results and discussion

Abstract

The performance of three electrochemical advanced oxidation processes, namely electro-oxidation with electrogenerated H_2O_2 (EO-H_2O_2), electro-Fenton (EF) and photoelectro-Fenton (PEF) for the treatment of aqueous solutions of the food azo dye Ponceau 4R in an undivided cell with a BDD anode and an air-diffusion cathode was compared in terms of colour, dye concentration and total organic carbon (TOC) removals. PEF treatments in ultrapure water with Na_2SO_4 were performed to assess the effect of current density, as well as supporting electrolyte and dye concentrations. At 100 mA cm^{-2}, solutions of 130 mL of 254 mg L^{-1} of the dye in 0.05 M Na_2SO_4 became colourless and totally mineralized after 50 and 240 min, respectively, which can be explained by the synergistic action of BDD($^{\bullet}$OH) at the anode surface and homogeneous $^{\bullet}$OH formed in the bulk from Fenton's reaction promoted in the presence of Fe^{2+} catalyst. Furthermore, UVA photons induced the continuous Fe^{2+} regeneration and photolytic decomposition of refractory intermediate complexes. In that aqueous matrix, the cleavage of the dye molecules proceeded through several reaction routes to yield *N*-containing and non-*N*-containing derivatives with one or two aromatic rings, short-chain aliphatic carboxylic acids and inorganic ions. Oxalic and oxamic acids and sulfate ions were accumulated at different rates in EO-H_2O_2, EF and PEF. The three methods allowed the progressive decontamination of Ponceau 4R solutions in a real water matrix even without the addition of electrolyte, although complete TOC abatement after 360 min at 33.3 mA cm^{-2} was only ensured by the iron-catalyzed PEF process.

Keywords: Acid Red 18; BDD anode; Catalyzed EAOPs; Food colours; Reaction pathways.

1. Introduction

Currently, food additives such as preservatives and colouring agents are among top food safety concerns in industrialized countries, despite being carefully regulated by national and international authorities. Indeed, their effects become uncontrolled when unintended targets, particularly children or some highly sensitive person (HSP) with allergies or food intolerances, are routinely exposed to them upon drinking water consumption. According to the International Food Information Council (IFIC) and the US Food and Drug Administration (FDA), colour additives include dyes, pigments and any other substance applied to a food, drug, cosmetic or the human body to impart colour [1]. Azo compounds are the most widespread synthetic colouring substances in the food industry, as occurs in many other sectors [2,3], but the negative impact of the so-called food azo-colours has been much less investigated than that of their textile counterparts so far. These dyes present one or more azo (-N=N-) bonds and usually exhibit complex structures that confer them large stability against physicochemical attack and bio/photodegradation, thus becoming persistent in water [3].

Ponceau 4R ($C_{20}H_{11}N_2O_{10}S_3Na_3$, trisodium 2-hydroxy-1-(4-sulphonato-1-naphthylazo)-naphthalene-6,8-disulphonate, also known as Acid Red 18, New Coccine or additive E124 in the industry, CI 16255, λ_{max} = 508 nm) is a paradigmatic case of sulphonated azo dyes employed to give red colouring to foodstuffs. Lately, serious concerns have arisen since the intake of Ponceau 4R is plausibly connected to asthma and insomnia and it may increase children's hyperactivity and intolerance [4]. As a result, in 2009, the European Food Safety Authority reduced the acceptable daily intake from 4.0 to 0.7 mg (kg body weight)$^{-1}$ [5]. Despite being negative in *in vitro* genotoxicity as well as in long-term carcinogenicity studies, the topic is still controversial [6]. For instance, Ponceau 4R is currently not approved in the United States, Canada, Norway and Finland, and it is listed as a banned substance by some authorities [7]. Since information about the safety of water containing Ponceau 4R and other related azo dyes remains inconclusive [8], the best way to reduce risks is to develop much more effective water treatment technologies that ensure their complete removal before reaching end users. The great ability of advanced oxidation processes (AOPs) such as heterogeneous photocatalysis [9,10], ozone-electrolysis with Pt anode [11] and chemical Fenton's reagent [12] to degrade Ponceau 4R has been demonstrated. Conversely, to the best of the authors' knowledge, the performance of the electrochemical AOPs (EAOPs) to destroy this dye has not been reported yet.

In the last decade, considerable effort has been devoted to the study of fundamentals and scale-up of electrochemical technologies for wastewater treatment, especially focusing on the destruction of organic matter by hydroxyl radicals [13-15]. Electro-oxidation (EO) is the most popular EAOP

due to its simplicity, adaptability and outstanding performance of particular setups. This process relies on the electrocatalytic properties of the anode surface (M), since some materials like Pt only favour the partial conversion of contaminants by direct oxidation or under the action of chemisorbed oxides (MO), whereas others like boron-doped diamond (BDD) may promote the complete destruction of organic matter by physisorbed BDD($^{\bullet}$OH) formed as follows [16-22]:

$$BDD + H_2O \rightarrow BDD(^{\bullet}OH) + H^+ + e^- \quad (1)$$

The use of undivided cells with a BDD anode and an active cathode can enhance the degree and/or rate of decontamination. Thus, in EO-H_2O_2, an air- or pure O_2-fed airtight or porous carbonaceous cathode is employed to electrogenerate H_2O_2 as follows [23-27]:

$$O_{2(g)} + 2\,H^+ + 2e^- \rightarrow H_2O_2 \quad (2)$$

H_2O_2 is a weak oxidant, although it can be oxidized to $HO_2^{\bullet}$ at the anode or be further activated in metal-catalyzed EAOPs like electro-Fenton (EF) and photoelectro-Fenton (PEF) [15]. In EF, the presence of low amounts of Fe^{2+} leads to the production of $^{\bullet}$OH in the bulk through homogeneous catalysis via Fenton's reaction (3) at optimum pH ~ 3 [28]. Organics are then destroyed upon the synergistic action of heterogeneous and homogeneous catalysis (BDD($^{\bullet}$OH) and $^{\bullet}$OH, respectively).

$$H_2O_2 + Fe^{2+} \rightarrow Fe^{3+} + {}^{\bullet}OH + OH^- \quad (3)$$

If an UVA lamp is used to irradiate the solution in the EF setup, then so-called PEF process, the mineralization is enhanced because UV photons induce the photoreduction of $Fe(OH)^{2+}$ to Fe^{2+} via reaction (4) and the photolysis of refractory Fe(III)-carboxylate products by reaction (5) [15,28].

$$Fe(OH)^{2+} + h\nu \rightarrow Fe^{2+} + {}^{\bullet}OH \quad (4)$$

$$Fe(OOCR)^{2+} + h\nu \rightarrow Fe^{2+} + CO_2 + R^{\bullet} \quad (5)$$

BDD anode has an extraordinary oxidation power that favours the production of oxidants such as H_2O_2, O_3, ferrate and peroxosalts ($S_2O_8^{2-}$, $P_2O_8^{4-}$ and $C_2O_6^{2-}$) depending on the aqueous matrix composition [15]. When the treated acidic solution contains Cl^- ions, $^{\bullet}$OH and/or BDD($^{\bullet}$OH) (and UV in PEF) act in concomitance with active chlorine species (Cl_2 and HClO) produced in the bulk via reactions (6) and (7) [3,13,15]. This medium, which is typical when treating real water matrices, is quite complex since oxychlorine anions [29-31], (oxy)chlorine radicals [32], chloramines [33], trihalomethanes and haloacetic acids [34], as well as refractory chlorinated by-products, can appear:

$$2\,Cl^- \rightarrow Cl_{2(aq)} + 2\,e^- \quad (6)$$

$$Cl_{2(aq)} + H_2O \rightarrow HClO + Cl^- + H^+ \quad (7)$$

Encouraging results have been obtained for the treatment of textile azo dyes by EAOPs with a BDD anode [35-39], and very recently we have even discussed the behaviour of two food azo dyes in such systems [40,41]. In the present work, aiming to gain more thorough knowledge about the fate of food azo-colours upon application of EAOPs, Ponceau 4R has been chosen as a model pollutant. It has been comparatively degraded in EO-H_2O_2, EF and PEF systems using an undivided BDD/air-diffusion cell. Most electrolyses have been carried out in ultrapure water with added Na_2SO_4 in order to investigate the effect of parameters like current density (*j*) and electrolyte and pollutant contents on the colour, dye concentration, and total organic carbon (TOC) removals. The reaction by-products identified by chromatographic techniques have allowed the proposal of various reaction pathways. The viability of the tested EAOPs to degrade Ponceau 4R in a real water matrix in the absence and presence of supporting electrolyte has been ascertained as well.

2. Experimental

2.1. Chemicals

Ponceau 4R (100% content) was purchased from Acros Organics. Anhydrous sodium sulfate, sodium chloride and lithium perchlorate used as supporting electrolytes, as well as iron(II) sulfate heptahydrate used as catalyst in EF and PEF, were of analytical grade supplied by Merck and Fluka. Oxalic, oxamic, fumaric, tartronic, formic and maleic acids used as standards were of analytical grade purchased from Merk, Avocado and Panreac. Sulfuric, hydrochloric and perchloric acids and sodium hydroxide used to regulate the pH were of analytic grade purchased from Merck, Acros Organics and Panreac. Organic solvents and other chemicals used were of high-performance liquid chromatography (HPLC) or analytical grade supplied by Sigma-Aldrich, Lancaster, Merck and Panreac. Solutions were prepared with ultrapure water obtained from a Millipore Milli-Q system with resistivity >18 MΩ cm at 25 ˚C. Some comparative trials were also carried out with a real water matrix collected from the primary decantation effluent of a municipal wastewater treatment plant located in Manresa (Barcelona, Spain). Its main characteristics determined in the laboratory were: pH 7.3, specific conductivity = 1.9 mS cm^{-1} (equivalent to ca. 0.010 M Na_2SO_4), TOC = 25 mg L^{-1}, 1.99 mM SO_4^{2-} and 10.3 mM Cl^-. No iron ions were detected. This water was preserved at 4 ºC and used the day after collection.

2.2. Electrochemical cells

The experiments were conducted in an open, undivided, cylindrical glass tank reactor of 150 mL capacity equipped with a double jacket for recirculation of thermostated water at 25 °C. The anode was a BDD thin-film electrode purchased from Adamant, whereas the cathode was a carbon-

polytetrafluoroethylene air-diffusion electrode purchased from E-TEK, mounted as described elsewhere [25] and fed with compressed air pumped at 1 L min^{-1} for continuous H_2O_2 generation from reaction (2). The geometric area of each electrode was 3 cm^2 and the interelectrode gap was 1 cm. All experiments were carried out using 130 mL of solutions at pH 3.0 under vigorous stirring with a magnetic bar at 800 rpm to ensure homogenization and the transport of reactants towards/from the electrodes. In EF and PEF, 0.50 mM Fe^{2+} was employed as catalyst because this content was found optimal for analogous treatments of aromatic azo dyes [15,28]. In PEF assays, the solution was irradiated with a Philips TL/6W/08 fluorescent black light blue tube (λ_{max} = 360 nm, photoionization energy of 5 W m^{-2}) placed 7 cm above the solution. Before the assays, cleaning of the BDD anode and activation of the air-diffusion electrode were achieved under polarization in 0.050 M Na_2SO_4 at 100 mA cm^{-2} for 180 min.

2.3. Apparatus and analytical procedures

The solution pH and the electrical conductance were measured with a Crison GLP 22 pH-meter and a Metrohm 644 conductometer, respectively. Trials were carried out at constant *j* provided by an EG&G PAR 273A potentiostat-galvanostat and the cell voltage was determined with a Demestres 601BR digital multimeter. Samples withdrawn from electrolyzed solutions were microfiltered with 0.45 µm PTFE filters purchased from Whatman prior to immediate analysis. The decolourization of Ponceau 4R solutions was monitored by measuring their absorbance decay at λ_{max} = 508 nm on a Shimadzu 1800 UV-Vis spectrophotometer at 25 ºC. The mineralization of solutions was assessed from their TOC abatement, determined on a Shimadzu TOC-VCNS analyzer. Reproducible TOC values with an accuracy of ±1% were found by injecting 50 µL aliquots into the analyzer.

The time course of the concentration of SO_4^{2-} and NO_3^- ions in trials in ultrapure water, as well as Cl^-, ClO_3^- and ClO_4^- ions in trials in real water, was assessed by ion chromatography (IC) as previously reported [42]. The decay of the dye concentration was followed by reversed-phase HPLC using a Waters 600 LC fitted with a Thermo Scientific Hypersil ODS 5 µm, 150 mm × 3 mm, column from Thermo Scientific at room temperature and coupled with a Waters 996 photodiode array detector set at λ_{max} = 508 nm. A 80:20 (v/v) acetonitrile/water (2.4 mM butylamine) mixture at 0.2 mL min^{-1} was eluted as mobile phase. Generated carboxylic acids were detected by ion-exclusion HPLC as described elsewhere [39].

Well-defined peaks at characteristic retention times (t_R) were found in all cases: Cl^- (2.3 min), ClO_3^- (3.4 min), NO_3^- (3.8 min), SO_4^{2-} (5.2 min) and ClO_4^- (15.2 min) ions by IC, Ponceau 4R (4.3

min) by reversed-phase HPLC, and oxalic (6.9 min), tartronic (7.9 min), oxamic (9.4 min) and formic (13.7 min) acids by ion-exclusion HPLC.

Since only small traces of NH_4^+ ion, determined with a flow injection system [42], were found in any of the experiments, the number of electrons (n) exchanged per each substrate molecule was taken as 102, assuming that Ponceau 4R is mineralized as follows:

$$C_{20}H_{11}N_2O_{10}S_3^{3-} + 48\ H_2O \rightarrow 20\ CO_2 + 2\ NO_3^- + 3\ SO_4^{2-} + 107\ H^+ + 102\ e^- \quad (8)$$

The mineralization current efficiency (MCE) values for each trial at current I (in A) and time t (in h) was then estimated as follows [36]:

$$MCE\ (\%) = \frac{(\Delta TOC)_{exp}\ n\ F\ V_s}{4.32\times10^7\ m\ I\ t}\times 100 \quad (9)$$

where F is the Faraday constant (96,487 C mol^{-1}), V_s is the solution volume (in L), $\Delta(TOC)_{exp}$ is the experimental TOC abatement (in mg L^{-1}), 4.32×10^7 is a conversion factor to homogenize units (= 3,600 s h^{-1} × 12,000 mg carbon mol^{-1}) and m is the number of carbon atoms of Ponceau 4R.

To identify the aromatic by-products, various samples were withdrawn during the electrolyses and the organic components were extracted with CH_2Cl_2 (3 × 25 mL). In some cases, either derivatization with acetic anhydride or ethanol, or liofilization followed by overnight derivatization, were made prior to extraction. Each resulting organic solution was dried over anhydrous Na_2SO_4, filtered and concentrated up to 1 mL under reduced pressure to be analyzed by gas chromatography-mass spectrometry (GC-MS) using an Agilent Technologies system composed of a 6890N chromatograph coupled to a 5975C spectrometer operating in EI mode at 70 eV. Nonpolar Agilent J&W DB-5ms and polar HP INNOWax columns (0.25 μm, 30 m × 0.25 mm) were employed. The temperature ramp was: 36 ºC for 1 min, 5 ºC min^{-1} up to 300 ºC or 250 ºC for the nonpolar and polar columns, respectively, and hold time of 10 min. The temperature of the inlet, source and transfer line was 250, 230 and 280 ºC for the nonpolar column, and 250, 230 and 250 ºC for the polar one. The mass spectra were identified by comparison with those of a NIST05 MS library.

3. Results and discussion

3.1. Electrochemical degradation of solutions of Ponceau 4R by PEF with a BDD anode

The treatment of organic pollutants by PEF is known to yield much better results than EF and EO-H_2O_2, which is mainly due to the synergistic action of UVA photons that induce photochemical reactions (4) and (5). Therefore, acidic solutions of 254 mg L^{-1} (0.42 mM) of Ponceau 4R in ultrapure water with 0.05 M Na_2SO_4 as supporting electrolyte and 0.50 mM Fe^{2+} as catalyst were treated by PEF until reaching total decolourization using a BDD/air-diffusion cell. The initial

solutions were bright red, as reported for other sulphonated monoazo dyes with two naphthalenes like Acid Red 14 and Acid Red 88 employed to impart red colour to food and textiles, respectively [40,43]. Fig. 1a shows the effect of applied *j* on the decay of normalized absorbance with electrolysis time. Solutions became colourless after 70, 60, 50 and 40 min at 33.3, 66.7, 100 and 150 mA cm^{-2}, respectively. Higher current values are then beneficial in such system in terms of time, since they promote both, the production of BDD($^{\bullet}$OH) from reaction (1) and H_2O_2 from reaction (2) [36,40]. The quicker accumulation of the latter oxidant leads to a larger accumulation of $^{\bullet}$OH in the bulk at a given time from reaction (3). Consequently, this radical species is the main responsible for the fast colour removal in Fenton systems, thanks to the minimization of mass transport limitations as compared to BDD($^{\bullet}$OH) that can only act in the anode vicinity. Note that the enhancement obtained at 150 mA cm^{-2} was not very significant if compared to 100 mA cm^{-2}. This can be explained by the progressively lower current efficiency that results from: (i) the promoted cathodic and anodic destruction of H_2O_2 and (ii) the BDD($^{\bullet}$OH) self-destruction to yield O_2 at excessively high current values. Quite frequently in literature, colour removal trends are directly associated to dye disappearance, but this is rarely verified because not enough attention is paid to reaction intermediates. Fig. 1b depicts the decay of normalized dye concentration with time during the same experiments. As found in Fig. 1a, a larger abatement was attained when *j* increased from 33.3 to 150 mA cm^{-2}, only requiring 40, 35, 30 and 25 min for total dye removal, respectively. This confirms the great oxidizing ability of PEF system, but it also reveals the formation of coloured by-products along the treatment because in all cases Ponceau 4R disappeared somewhat earlier than colour. Such compounds were poorly concentrated and/or exhibited small molar extinction coefficients. As shown in the inset panel of Fig. 1b, the concentration decays fitted very well to a pseudo-first-order kinetics, with R^2 = 0.997 and increasing apparent rate constants (k_{app}, 10^{-2} min^{-1}) of 11.39±1.74, 13.28±1.26, 16.76±0.96 and 18.60±2.56 as *j* was raised from 33.3 to 150 mA cm^{-2} (mean values along with their computed 95% confidence intervals are provided). The good linearity can be accounted for by the accumulation of a constant concentration of hydroxyl radicals, both at the anode and in the bulk, at each applied *j*.

The time course of normalized TOC for the previous trials is presented in Fig. 2a. A sigmoid shape was observed in all cases, being the induction period more evident as *j* decreased. This is a symptom of the formation of refractory by-products since the very beginning of the electrolysis, which are slowly but progressively mineralized by BDD($^{\bullet}$OH) and $^{\bullet}$OH. At high current, greater concentrations of both oxidizing radicals are produced, thus accelerating the TOC abatement. For example, TOC removals of 16%, 23%, 33% and 50% were obtained at 33.3, 66.7, 100 and 150 mA

cm^{-2}, respectively, after 60 min of electrolysis. The degradation by PEF at 150 mA cm^{-2} was remarkably faster and, in fact, total mineralization was reached after only 180 min, whereas the electrolyses at 33.3-100 mA cm^{-2} had to be prolonged for 240 min to completely remove the organic matter (> 99% TOC reduction). Worth mentioning, the tail of the sigmoid curves that is typical of mass transport limitation phenomena appeared at about $TOC_t/TOC_0 = 0.20$, which means that gradual cleavage of Ponceau 4R (and/or its aromatic by-products) easily yielded CO_2 according to mineralization reaction (8), but an unavoidable accumulation of persistent free and iron-complexed by-products accounting for ca. 20% of TOC decelerated the degradation. Nonetheless, the use of UVA light allowed the slow destruction of such refractory compounds over time. The MCE values for the four experiments calculated from Eq. (9) are shown in Fig. 2b. As can be seen, after a poorly efficient early stage related to the aforementioned induction period, maximum MCE values of 55%, 29%, 21% and 18% were obtained after 90-120 min as current increased, whereupon the efficiency decayed due to the accumulation of by-products that were highly resistant to oxidation by BDD($^{\bullet}$OH) and $^{\bullet}$OH and/or UVA photolysis. High current values are then preferred if time is the key parameter for applying the treatment, whereas such choice is detrimental in terms of energy consumption since parasitic reactions of BDD($^{\bullet}$OH) and $^{\bullet}$OH are enhanced under such conditions, especially as the organic matter content diminishes [36-41].

Considering the usual variability of wastewater composition regarding the electrolyte content, it is interesting to investigate the effect of Na_2SO_4 concentration on PEF treatment. Fig. 3a shows the normalized absorbance decay over time at 33.3 mA cm^{-2} when using 0.010-0.30 M Na_2SO_4. As can be observed, total colour removal was always attained at 70 min. However, the extreme Na_2SO_4 concentration values yielded the quickest absorbance decays. It can then be deduced that 0.010 M Na_2SO_4 is sufficient so as to confer the threshold conductivity that allows an efficient production of BDD($^{\bullet}$OH) and H_2O_2 at the anode and cathode, respectively. At that low SO_4^{2-} content, the parasitic anodic generation of the weaker oxidant $S_2O_8^{2-}$ is considerably minimized, therefore giving preponderance to the much more powerful BDD($^{\bullet}$OH) [15]. Following this reasoning, a content as high as 0.30 M Na_2SO_4 could seem largely detrimental, since part of BDD($^{\bullet}$OH) is expected to be wasted by the large formation of $S_2O_8^{2-}$ ion from the simultaneous SO_4^{2-} oxidation at the BDD anode [13]. Conversely, the presence of large amounts of SO_4^{2-} ions entails a considerable increase of the specific conductivity, which favours the transport of the negatively charged (sulphonated) Ponceau 4R molecules towards the anode surface, eventually accelerating their oxidation. On the other hand, Fig. 3b reveals that the effect of the Na_2SO_4 concentration on TOC removal was negligible, leading to overlapped curves for 240 min. This can be justified by the conversion of

Ponceau 4R into non-ionic, more refractory compounds, whose mineralization takes place pre-eminently in the solution bulk under the action of $^{\bullet}OH$ from Fenton's reaction (3) and/or photolysis by UVA photons from reaction (5). Our results then point to consider that the BDD anode plays an important role during the initial decolourization steps, whereas Fenton's reaction and photolytic reactions ensure the progressive TOC abatement.

The effect of initial dye concentration on its decolourization and mineralization trends was examined for 127-1270 mg L^{-1} of Ponceau 4R (50-500 mg L^{-1} TOC) in 0.050 M Na_2SO_4 with 0.50 mM Fe^{2+} at 100 mA cm^{-2}. Fig. 4a depicts the complete decay of normalized absorbance with electrolysis time regardless of the dye content, which confirms the great oxidizing ability of PEF with BDD. Increasing times of 20, 50, 70 and 240 min were needed as the dye concentration rose from 127 to 1270 mg L^{-1}, which is simply due to the presence of larger amounts of coloured compounds that must react with a constant quantity of BDD($^{\bullet}OH$) and $^{\bullet}OH$. Worth noting, the PEF treatment became more efficient as the organic matter content was raised. This behaviour arises from the greater probability for favourable events in the presence of more organic molecules, thus minimizing the parasitic reactions that involve BDD($^{\bullet}OH$) and $^{\bullet}OH$. This can be more clearly seen in the trends of normalized TOC over time collected in Fig. 4b. Total abatement with > 99% TOC reduction was attained in all cases, needing longer times of 135, 240, 360 and 480 min for 127, 254, 635 and 1270 mg L^{-1} of the dye, respectively. The MCE values for these trials depicted in Fig. 4c show an increase in the efficiency for more concentrated dye solutions, especially at long electrolysis time when the initial recalcitrant products were completely removed. Note that the TOC profile obtained for the greatest dye content exhibits an evident shoulder (see Fig. 4b), which is indicative of the progressively larger difficulties to remove the organic matter. This resulted in a minimum MCE value at 120 min, although it further reached the highest efficiencies, which were close to 35% at times > 240 min (see Fig. 4c). Several phenomena can be responsible for the deceleration of degradation in Fenton systems at excessively high organic matter contents, including iron complexation upon generation of many aliphatic by-products, polymerization and partial blockage of the electrode surfaces that causes passivation [28].

3.2. Reaction by-products and proposed routes

As observed in Figs. 2a, 3b and 4b, the final stages of the PEF treatment were characterized by a lower mineralization rate. This kind of behaviour has been usually associated to the formation of polymers as well as short-chain carboxylic acids, whose absolute rate constants for their reaction with hydroxyl radicals tends to be much smaller than those exhibited by aromatic compounds [15,28]. In the present study, HPLC analyses of samples withdrawn from PEF experiments at 100

mA cm^{-2} revealed the formation of up to 0.02 and 0.28 mM of tartronic and formic acids, respectively, although they were easily mineralized under the action of BDD($^{\bullet}OH$) and $^{\bullet}OH$ regardless of the formation of iron complexes [28]. A more particular situation was found for oxalic and oxamic acids, whose concentration profiles with time are shown in Figs. 5a and 5b, respectively. Oxalic acid was accumulated up to a maximum content of 0.45 mM at 60 min, whereupon it gradually decayed up to its total disappearance at 180 min. A much smaller amount of oxamic acid was formed, only reaching up to 0.014 mM at 90 min with total degradation at 210 min. These two findings agree with the mentioned high oxidizing ability of the PEF process with a BDD anode (see the corresponding TOC evolution in Fig. 2a), which can then be justified by the effective degradation of both acids and the Fe(II)-carboxylate complexes under the action of BDD($^{\bullet}OH$) and $^{\bullet}OH$, along with the efficient photodegradation of Fe(III)-oxalate and Fe(III)-oxamate complexes by UVA photons [28]. Clearly different profiles were obtained upon comparative treatment of analogous Ponceau 4R solutions by EF and EO-H_2O_2 with a BDD anode, which allowed the complete mineralization at 480 min but only 80% and 65% TOC removal at 240 min, respectively (not shown). In the former method, the maximum concentrations of oxalic and oxamic acids were found at 90-120 min (0.88 and 0.012 mM, respectively, see Fig. 5). Due to the large persistence of oxalic/oxalates, its total abatement was only ensured after 480 min of EF, whereas oxamic acid disappeared at 270 min. This confirms the crucial role of UVA radiation, which was responsible for the lower accumulation and faster removal in PEF. As reported elsewhere, Fe(III)-oxalate complexes are quite refractory to $^{\bullet}OH$ formed in the bulk and thus, in EF, only BDD($^{\bullet}OH$) is able to slowly oxidize them. On the other hand, very small amounts of oxalic ($\leq$ 0.05 mM) and oxamic ($\leq$ 0.005 mM) were detected in EO-H_2O_2, which can be explained by the absence of iron complexes, therefore favouring the quick oxidation of all by-products by BDD($^{\bullet}OH$). In conclusion, the extraordinary ability of PEF with BDD to quickly degrade both, the parent pollutant and its coloured and colourless reaction by-products, allows explaining the superior performance of this process as compared to the other EAOPs. Note that GC-MS analyses of treated solutions allowed the identification of other aliphatic acids like maleic, fumaric, tartaric and propanoic acids, which were not detected by ion-exclusion HPLC due to their quick removal and very small accumulation.

Inorganic ions formed during the electrolyses were determined by IC. The N atoms forming the -N=N- bond were preferentially transformed into NO_3^- ion (50% of initial N) and, to a smaller extent, into NH_4^+ ions (25%), as stated in reaction (8). A significant proportion of the initial N was then lost as volatile nitrogenated products, like N_2 and N_xO_y, as reported for similar treatments of

other azo dyes [40,41,43]. Regarding the sulfur content, the initial S atoms were mainly released as SO_4^{2-} ion. Fig. 6 depicts its time course during the degradation of 254 mg L^{-1} Ponceau 4R (0.42 mM) solutions in 0.05 M $LiClO_4$. As can be seen in Fig. 6a, in PEF, almost 1 mM SO_4^{2-} was accumulated after 50 min (80% of initial S). At that time, no coloured sulphonated by-products were present in the solutions (see Fig. 1a), which means that S was contained in either sulphonated aliphatic compounds or colourless aromatics. All of them were quickly oxidized and/or photolyzed and, at the end of the treatment, ca. 100% of S (1.25 mM) was found as SO_4^{2-}. The trend of this ion was analogous in EF, which means that UVA light mainly affects the non-sulphonated carboxylic acids, as discussed above. A much slower accumulation was obtained in EO-H_2O_2, only attaining the expected SO_4^{2-} concentration after prolonged electrolysis. This confirms the great contribution of $^{\bullet}OH$ to mineralization, since its absence in the latter method yields lower degradation rates. On the other hand, an increase in *j* from 33.3 to 150 mA cm^{-2} in PEF led to a faster accumulation of SO_4^{2-} ions, as expected from the quicker generation of BDD($^{\bullet}OH$) and $^{\bullet}OH$ but, in all cases, this ion accounted for the release of ca. 100% of S at the end of all the treatments.

Apart from revealing the formation of some additional aliphatic carboxylic acids, as mentioned before, GC-MS analyses of treated solutions with polar and nonpolar columns allowed the identification of nitromethane as well as various aromatic by-products. Their structures, chemical names and characteristic *m/z* values have been gathered in Fig. 7, which constitutes a proposal of different degradation routes for the electrolytic degradation of Ponceau 4R in acidic aqueous medium by EO-H_2O_2, EF and PEF with a BDD anode. The final aliphatic intermediates formed upon successive cleavage are also included.

Ponceau 4R appears with *m/z* 535, which corresponds to its anionic form without the sodium counterions. Its degradation may proceed through the formation of up to six *N*-containing derivatives (highlighted in green) following four different routes (A-D). A, B and C inform about the appearance of four *N*-based heterocycles, which can be plausibly produced upon primary radical formation from electron transfer at the cathode (so-called electrochemically-induced radical cyclization [44]). Path A involves intramolecular cyclization, path B arises from intermolecular cyclization as suggested by the presence of an additional carbon to close the *N*-cycle and path C comes from intra or intermolecular cyclization because some of the carbon atoms of benzene might allow closing the *N*-cycle. Among all the heterocycles, phthalimide was the most ubiquitous one. Conversely, route D leads to two aromatic amines, which were typically formed when a stainless steel cathode was used instead of the air-diffusion electrode, thus confirming the purely oxidative degradation underwent by the azo dye in systems with BDD/air-diffusion cells.

Alternatively, Ponceau 4R can follow route E to yield up to twelve non-*N*-containing derivatives (highlighted in blue) with one or two cycles, starting with its conversion to α-naphthol. As observed, this compound is the source of most of these by-products, except indandione, via 1,4-naphthoquinone. Discontinuous arrows account for transformations that can take place or rather be GC-MS artifacts, being impossible to elucidate the exact by-product in each case. Ponceau 4R, as well as its eighteen aromatic by-products, can be further transformed into non-*N*-containing derivatives with one cycle, such as resorcinol, acetophenone and their hydroxylated by-products following route F (highlighted in pink). Worth mentioning, a condensation reaction involving acetophenone could potentially yield indandione, as occurs in well-known aldol condensation. The cleavage of any of the 22 aromatic structures caused the formation of aliphatic compounds, which were finally mineralized to CO_2 under optimized electrolysis conditions.

Some of the intermediates proposed in this work are consistent with those obtained during the degradation of other azo dyes. For example, the treatment of Acid Orange 7, which includes a phenylazonaphthol group, by TiO_2 photocatalysis yielded naphthol, naphthalene-1,4-diol, 1,4-naphtoquinone, hydroxynaphthoquinone, phthalic anhydride, 3*H*-isobenzofuran-1-one (phthalide) and phthalimide [45].

3.3. Treatments with a BDD anode in a real water matrix

The great performance of EAOPs with a BDD anode, particularly PEF, regarding the decontamination of acidic Ponceau 4R solutions has been demonstrated for pure water matrices. However, real dye wastewater is not so ideal because it usually contains natural organic matter and various inorganic anions, which may hamper the application of those technologies. Therefore, some experiments were carried out using a real water matrix (see section 2.1). First, the raw real water samples (TOC = 25 mg L^{-1}) were treated at 25 ºC and 33.3 mA cm^{-2} in the absence of the dye by EO-H_2O_2, EF and PEF. Prior to the electrolyses, the initially alkaline pH was adjusted to 3.0, and 0.50 mM Fe^{2+} was added to the solutions for the two latter treatments. The time course of natural TOC with time is shown in Fig. 8a. EO-H_2O_2 allowed a significant TOC abatement thanks to the action of BDD($^{\bullet}$OH) on organic matter, eventually reaching 86% mineralization at 360 min. TOC removal was accelerated in EF from the beginning of the treatment, with > 95% mineralization at 360 min. This suggests that the catalytic amount of Fe^{2+} favours the formation of $^{\bullet}$OH during all the electrolysis, notwithstanding the plausible partial complexation of iron ions by chelating species contained in the water sample. The rate and degree of mineralization was very similar in the case of PEF process, which means that photosensitive Fe(III) complexes such as Fe(III)-oxalate species were not formed to a large extent along the treatment.

4. Results and discussion

Since the water sample contained about 2.0 mM SO_4^{2-} and 10.3 mM Cl^-, some oxychlorine anions were formed under the oxidative action of BDD, BDD($^\bullet$OH) and $^\bullet$OH [29-31]. As an example, the evolution of chlorinated ions in PEF process is illustrated in Fig. 8b. The Cl^- concentration gradually decreased to 3.4 mM at 360 min, owing to its transformation into ClO_3^- (3.6 mM) and ClO_4^- (3.3 mM) ions. As can be observed, such conversion was quite quantitative because the sum of the three anions accounted for almost 100% of the initial Cl content. This suggests a very small accumulation of active chlorine from reactions (6) and (7) and therefore, the mineralization of organic matter in Fig. 8a can be essentially explained by the participation of hydroxyl radicals. Furthermore, the accumulation of Cl in the form of chlorinated anions ensures that the generation of toxic chlorinated organic by-products during the treatment can be neglected.

The performance of the three EAOPs during the degradation of 254 mg L^{-1} of Ponceau 4R in the same real water matrix of Fig. 8, at pH 3.0 and 33.3 mA cm^{-2}, was further assessed. Fig. 9a presents the decay of the normalized absorbance achieved by EO-H_2O_2, EF and PEF in the absence or presence of added electrolyte. When treating the dye in the raw water, total colour removal was attained after 180, 100 and ca. 70 min, respectively, in agreement with the higher oxidizing ability in the sequence EO-H_2O_2 < EF < PEF. Note that the time needed in PEF is similar to that found in Fig. 1a for the treatment under analogous conditions but using ultrapure water, which means that the water matrix does not impede the fast decolourization of the dye solutions. Actually, the real matrix was even beneficial, since 50% colour removal was reached after 10-15 min of PEF instead of 25 min required in ultrapure water (see Fig. 1a). This suggests the contribution of active chlorine to the oxidation of coloured compounds, despite the very small accumulation of such oxidant (see Fig. 8b). The participation of active chlorine was more evident when the PEF treatment was performed in the presence of 0.010 M NaCl, which allowed a quicker decolourization with total disappearance of coloured compounds at 60 min. In contrast, the addition of 0.010 M Na_2SO_4 did not enhance the process, but it was slightly detrimental by the formation of competitive $S_2O_8^{2-}$ ion.

The decay of the normalized dye concentration for the experiments of Fig. 9a without added electrolyte is shown in Fig. 9b, along with the corresponding kinetic analysis assuming a pseudo-first-order reaction. Ponceau 4R disappeared after 140 min in EO-H_2O_2, only requiring about 40 min in EF and PEF, thus confirming the superiority of Fenton processes due to the much faster reaction of the azo dye with $^\bullet$OH formed from Fenton's reaction (3). The mean values of k_{app} (10^{-2} min^{-1}) with their 95% confidence intervals were 2.72 ± 0.41, 12.31 ± 0.53 and 13.35 ± 0.66 for EO-H_2O_2, EF and PEF, respectively. As also observed in Fig. 1, the time needed for removing the dye was lower than that for colour removal. Note that Ponceau 4R disappeared at the same time in both,

ultrapure (see Fig. 1b) and real water matrices (see Fig. 9b), indicating a small participation of active chlorine.

Finally, Fig. 9c shows the TOC removal during all the trials of Fig. 9a. At 360 min, 57%, 74% and ~ 100% mineralization was attained by EO-H_2O_2, EF and PEF, respectively. This result, along with the fast colour and Ponceau 4R removals, verifies the viability of PEF process for the treatment of real wastewater. Comparison with the TOC abatement in ultrapure water (see Fig. 2a), where total mineralization was reached after 240 min, allowed concluding that the degradation proceeded somewhat more slowly, with 93% TOC decay at that time. This can be explained by: (i) the presence of a larger amount of organic matter due to the natural constituents, (ii) the partial consumption of BDD($^{\bullet}$OH) by Cl^- to form less oxidizing species [29-32], (iii) the partial destruction of H_2O_2 by HClO formed via reactions (6) and (7) [31] and (iv) the formation of chloro-complexes that reduce the amount of free iron ions [46]. While the presence of Cl^- resulted positive for colour removal (see Fig. 9a), it became detrimental regarding the TOC abatement. This was confirmed when treating the dye in the presence of 0.010 M NaCl, since only 82% and 92% mineralization could be attained after 240 and 360 min of PEF, respectively. In contrast, the effect of added Na_2SO_4 was insignificant, as discussed above.

4. Conclusions

Iron-catalyzed PEF treatment using a BDD/air-diffusion cell has been proven a promising technology for the degradation of food azo-colours like Ponceau 4R contained in real water matrices thanks to the synergistic action of BDD($^{\bullet}$OH), $^{\bullet}$OH and UVA photons. No significant detrimental effects of the real matrix were observed, since the time required for the complete dye and colour removals was comparable to that needed in ultrapure water, whereas only a slight deceleration of TOC decay was revealed as a result of parasitic reactions induced by the presence of Cl^-. Up to 22 aromatic by-products, 8 carboxylic acids and nitromethane were identified upon treatment of Ponceau 4R by EAOPs with BDD. The total mineralization of all these by-products to yield CO_2, NO_3^-, NH_4^+ and SO_4^{2-} proceeded via various simultaneous reaction routes.

Acknowledgments

The authors thank MINECO (Ministerio de Economía y Competividad, Spain) for financial support under project CTQ2013-48897-C2-1-R, co-financed with FEDER funds. The Ph.D. grant awarded to A. Thiam from MAEC-AECID (Spain) is also acknowledged.

References

[1] IFIC and FDA, Food ingredients and colors, pp. 1-7 (http://www.fda.gov/downloads/Food/IngredientsPackagingLabeling/ucm094249.pdf; November 2004, revised April 2010).

[2] I.K. Konstantinou, T.A. Albanis, Appl. Catal. B: Environ. 49 (2004) 1-14.

[3] E. Brillas, C.A. Martínez-Huitle, Appl. Catal. B: Environ. 166-167 (2015) 603-643.

[4] D. McCann, A. Barrett, C. Cooper, D. Crumpler, L. Dalen, K. Grimshaw, E. Kitchin, K. Lok, L. Porteous, E. Prince, E. Sonuga-Barke, J. O'Warner, J. Stevenson, Lancet 370 (2007) 1560-1567.

[5] EFSA, EFSA J. 7 (2009) 1328-1366.

[6] L.E. Arnold, N. Lofthouse, E. Hurt, Neurotherapeutics 9 (2012) 599-609.

[7] http://www.fda.gov/ForIndustry/ColorAdditives/ColorAdditiveInventories/ucm115641.htm

[8] M.M. Ghoneim, H.S. El-Desoky, N.M. Zidan, Desalination 274 (2011) 22-30.

[9] K. Tanaka, K. Padermpole, T. Hisanaga, Water Res. 34 (2000) 327-333.

[10] N. Sobana, M. Swaminathan, Sep. Purif. Technol. 56 (2007) 101-107.

[11] J. Basiri Parsa, M. Golmirzaei, M. Abbasi, J. Ind. Eng. Chem. 20 (2014) 689-694.

[12] K. Barbusiński, J. Majewski, Pol. J. Environ. Studies 12 (2003) 151-155.

[13] M. Panizza, G. Cerisola, Chem. Rev. 109 (2009) 6541-6569.

[14] B.P. Chaplin, Environ. Sci. Process. Impacts 16 (2014) 1182-1203.

[15] I. Sirés, E. Brillas, M.A. Oturan, M.A. Rodrigo, M. Panizza, Environ. Sci. Pollut. Res. 21 (2014) 8336-8367.

[16] L. Ciríaco, C. Anjo, J. Correia, M.J. Pacheco, A. Lopes, Electrochim. Acta 54 (2009) 1464-1472.

[17] M.A. Rodrigo, P. Cañizares, A. Sánchez-Carretero, C. Sáez, Catal. Today 151 (2010) 173-177.

[18] A. El-Ghenymy, F. Centellas, J.A. Garrido, R.M. Rodríguez, I. Sirés, P.L. Cabot, E. Brillas, Electrochim. Acta 130 (2014) 568-576.

[19] M. Panizza, Environ. Sci. Pollut. Res. 21 (2014) 8451-8456.

[20] O. Scialdone, E. Corrado, A. Galia, I. Sirés, Electrochim. Acta 132 (2014) 15-24.

[21] M.J.M.D. Vidales, S. Barba, C. Sáez, P. Cañizares, M.A. Rodrigo, Electrochim. Acta 140 (2014) 20-26.

[22] D.M.D. Araújo, C. Sáez, C.A. Martínez-Huitle, P. Cañizares, M.A. Rodrigo, Appl. Catal. B: Environ. 166-167 (2015) 454-459.

[23] A. Özcan, Y. Sahin, A.S. Koparal, M.A. Oturan, J. Electroanal. Chem. 616 (2008) 71-78.

[24] E. Rosales, M. Pazos, M.A. Longo, M.A. Sanromán, Chem. Eng. J. 155 (2009) 62-67.

[25] E. Guinea, J.A. Garrido, R.M. Rodríguez, P.L. Cabot, C. Arias, F. Centellas, E. Brillas, Electrochim. Acta 55 (2010) 2101-2115.

[26] M. Panizza, M.A. Oturan, Electrochim. Acta 56 (2011) 7084-7087.

[27] A. Dirany, I. Sirés, N. Oturan, A. Özcan, M.A. Oturan, Environ. Sci. Technol. 46 (2012) 4074-4082.

[28] E. Brillas, I. Sirés, M.A. Oturan, Chem. Rev. 109 (2009) 6570-6631.

[29] M.E. Bergmann, J. Rollin, Catal. Today 124 (2007) 198-203.

[30] A.M. Polcaro, A. Vacca, M. Mascia, S. Palmas, J. Rodriguez Ruiz, J. Appl. Electrochem. 39 (2009) 2083-2092.

[31] S. Randazzo, O. Scialdone, E. Brillas, I. Sirés, J. Hazard. Mater. 192 (2011) 1555-1564.

[32] F. Bonfatti, S. Ferro, F. Lavezzo, M. Malacarne, G. Lodi, A. De Battisti, J. Electrochem. Soc. 147 (2000) 592-596.

[33] M. Deborde, U. von Gunten, Water Res. 42 (2008) 13-51.

[34] S.D. Richardson, Global NEST J. 7 (2005) 43-60.

[35] M. Panizza, G. Cerisola, Ind. Eng. Chem. Res. 47 (2008) 6816-6820.

[36] E.J. Ruiz, C. Arias, E. Brillas, A. Hernández-Ramírez, J.M. Peralta-Hernández, Chemosphere 82 (2011) 495-501.

[37] L.C. Almeida, S. Garcia-Segura, C. Arias, N. Bocchi, E. Brillas, Chemosphere 89 (2012) 751-758.

[38] R., Salazar, E. Brillas, I. Sirés, Appl. Catal. B: Environ. 115–116 (2012) 107-116.

[39] F.C. Moreira, S. Garcia-Segura, V.J.P. Vilar, R.A.R. Boaventura, E. Brillas, Appl. Catal. B: Environ. 142-143 (2013) 877-890.

[40] A. Thiam, I. Sirés, J.A. Garrido, R.M. Rodríguez, E. Brillas, Sep. Purif. Technol. 140 (2015) 43-52.

[41] A Thiam, I. Sirés, J.A. Garrido, R.M. Rodríguez, E. Brillas, J. Hazard. Mater. 290 (2015) 34-42.

[42] A.R.F. Pipi, A.R. De Andrade, E. Brillas, I. Sirés, Sep. Purif. Technol. 132 (2014) 674-683.

[43] E.J. Ruiz, A. Hernández-Ramírez, J.M. Peralta-Hernández, C. Arias, E. Brillas, Chem. Eng. J. 171 (2011) 385-392.

[44] S. Donnelly, J. Grimshaw, J. Trocha-Grimshaw, Electrochim. Acta 41 (1996) 489-492.

[45] M. Stylidi, D.I. Kondarides, X.E. Verykios, Appl. Catal. B: Environ. 40 (2003) 271-286.

[46] J. De Laat, G.T. Le, B. Legube, Chemosphere 55 (2004) 715-723.

Figure captions

Fig. 1. Effect of applied current on the decay of the (a) normalized absorbance at 508 nm and (b) normalized dye concentration with electrolysis time for the degradation of 130 mL of a 254 mg L^{-1} (= 0.42 mM) of Ponceau 4R solution in 0.050 M Na_2SO_4 at pH 3.0 and 25 ºC by photoelectro-Fenton (PEF) process in the presence of 0.50 mM Fe^{2+} as catalyst. The cell contained a 3 cm^2 BDD anode and a 3 cm^2 air-diffusion cathode and the solution was irradiated with a 6 W UVA lamp of λ_{max} = 360 nm. Current density: (○) 33.3 mA cm^{-2}, (□) 66.7 mA cm^{-2}, (△) 100 mA cm^{-2} and (◇) 150 mA cm^{-2}.

Fig. 2. Change of: (a) normalized TOC and (b) mineralization current efficiency with electrolysis time for the trials shown in Fig. 1.

Fig. 3. Effect of supporting electrolyte concentration on the (a) normalized absorbance decay at 508 nm and (b) normalized TOC abatement vs electrolysis time for the degradation of 130 mL of 254 mg L^{-1} of Ponceau 4R solutions in: (○) 0.010 M, (□) 0.050 M, (△) 0.15 M and (◇) 0.30 M Na_2SO_4 with 0.50 mM Fe^{2+} at pH 3.0 and 25 ºC by PEF with a BDD anode at 33.3 mA cm^{-2}.

Fig. 4. Effect of dye concentration on the (a) normalized absorbance at 508 nm, (b) normalized TOC decay and (c) mineralization current efficiency with electrolysis time for the degradation of 130 mL of: (○) 127 mg L^{-1}, (□) 254 mg L^{-1}, (△) 635 mg L^{-1} and (◇) 1270 mg L^{-1} of Ponceau 4R solutions in 0.050 M Na_2SO_4 with 0.50 mM Fe^{2+} at pH 3.0 and 25 ºC by PEF with a BDD anode at 100 mA cm^{-2}.

Fig. 5. Evolution of the concentration of (a) oxalic and (b) oxamic acids detected during the degradation of 130 mL of 254 mg L^{-1} of Ponceau 4R solutions in 0.050 M Na_2SO_4 at pH 3.0, 25 ºC and 100 mA cm^{-2}. Methods with a BDD anode: (○) EO-H_2O_2, (□) EF with 0.50 mM Fe^{2+} and (△) PEF with 0.50 mM Fe^{2+}.

Fig. 6. Time course of the concentration of SO_4^{2-} ions released during the degradation of 130 mL of 254 mg L^{-1} of Ponceau 4R solutions in 0.050 M $LiClO_4$ at pH 3.0 and 25 ºC with a BDD anode. In (a), (○) EO-H_2O_2, (□) EF with 0.50 mM Fe^{2+} and (△) PEF with 0.50 mM Fe^{2+} at 100 mA cm^{-2}. In (b), PEF with 0.5 mM Fe^{2+} at: (○) 33.3 mA cm^{-2}, (△) 100 mA cm^{-2} and (◇) 150 mA cm^{-2}.

Fig. 7. Routes for the electrolytic degradation of Ponceau 4R in acidic aqueous medium by EAOPs with BDD anode. The primary oxidation by-products, as well as some of the final aliphatic intermediates, were identified by GC-MS.

Fig. 8. Performance of the EAOPs with a BDD anode during the treatment of 130 mL of a real water sample at pH 3.0, 25 ºC and 33.3 mA cm^{-2}. (a) TOC removal by (○) EO-H_2O_2, (□) EF with 0.50 mM Fe^{2+} and (△) PEF with 0.50 mM Fe^{2+}. (b) Time course of the concentration of chlorinated ions accumulated in PEF process. (○) Cl^-, (□) ClO_3^-, (△) ClO_4^- and (◇) sum of chlorinated ions.

Fig. 9. Performance of the EAOPs with a BDD anode during the degradation of 130 mL of 254 mg L^{-1} of Ponceau 4R in the same real water matrix of Fig. 8, at pH 3.0, 25 ºC and 33.3 mA cm^{-2}. (a) Decay of the normalized absorbance at 508 nm without added electrolyte by (○) EO-H_2O_2, (□) EF with 0.50 mM Fe^{2+} and (△) PEF with 0.50 mM Fe^{2+}, and with addition of (●) 0.010 M Na_2SO_4 or (■) 0.010 M NaCl in PEF. (b) Decay of the normalized dye concentration in the experiments without added electrolyte. (c) TOC removal during the trials shown in plot (a).

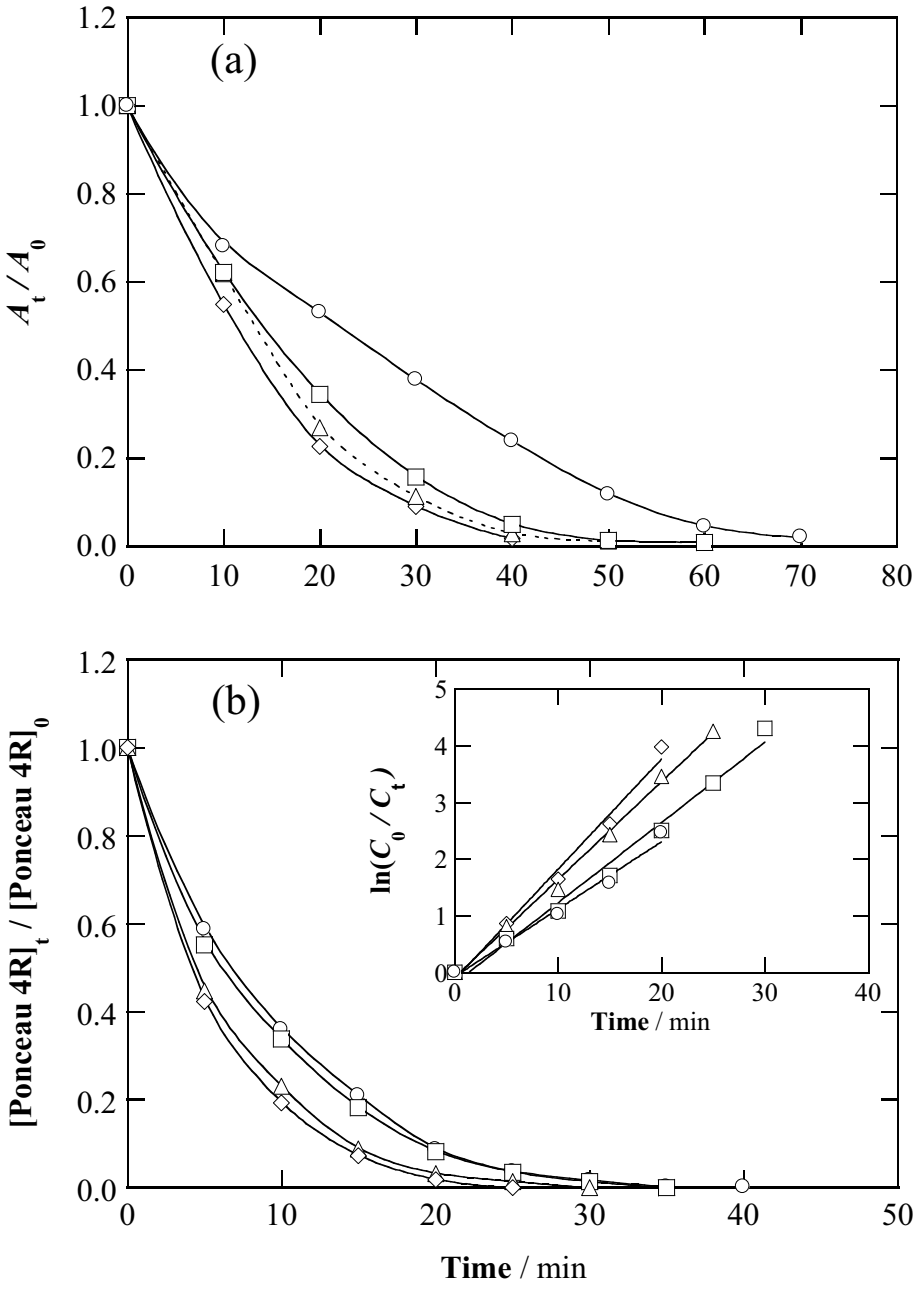

Fig. 1

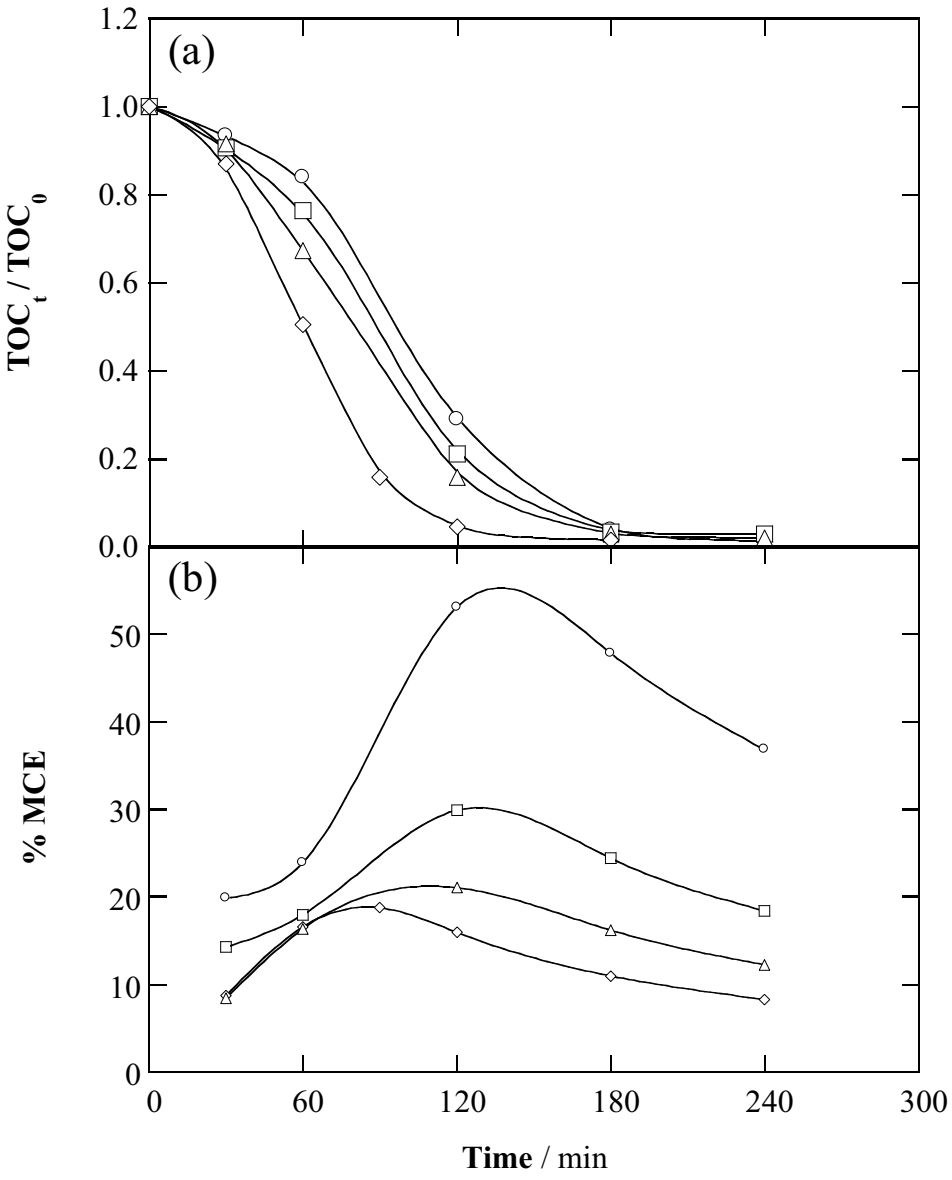
(a)
(b)
TOC$_t$ / TOC$_0$
% MCE
Time / min
0
0.2
0.4
0.6
0.8
1.0
1.2
10
20
30
40
50
60
120
180
240
300

Fig. 2

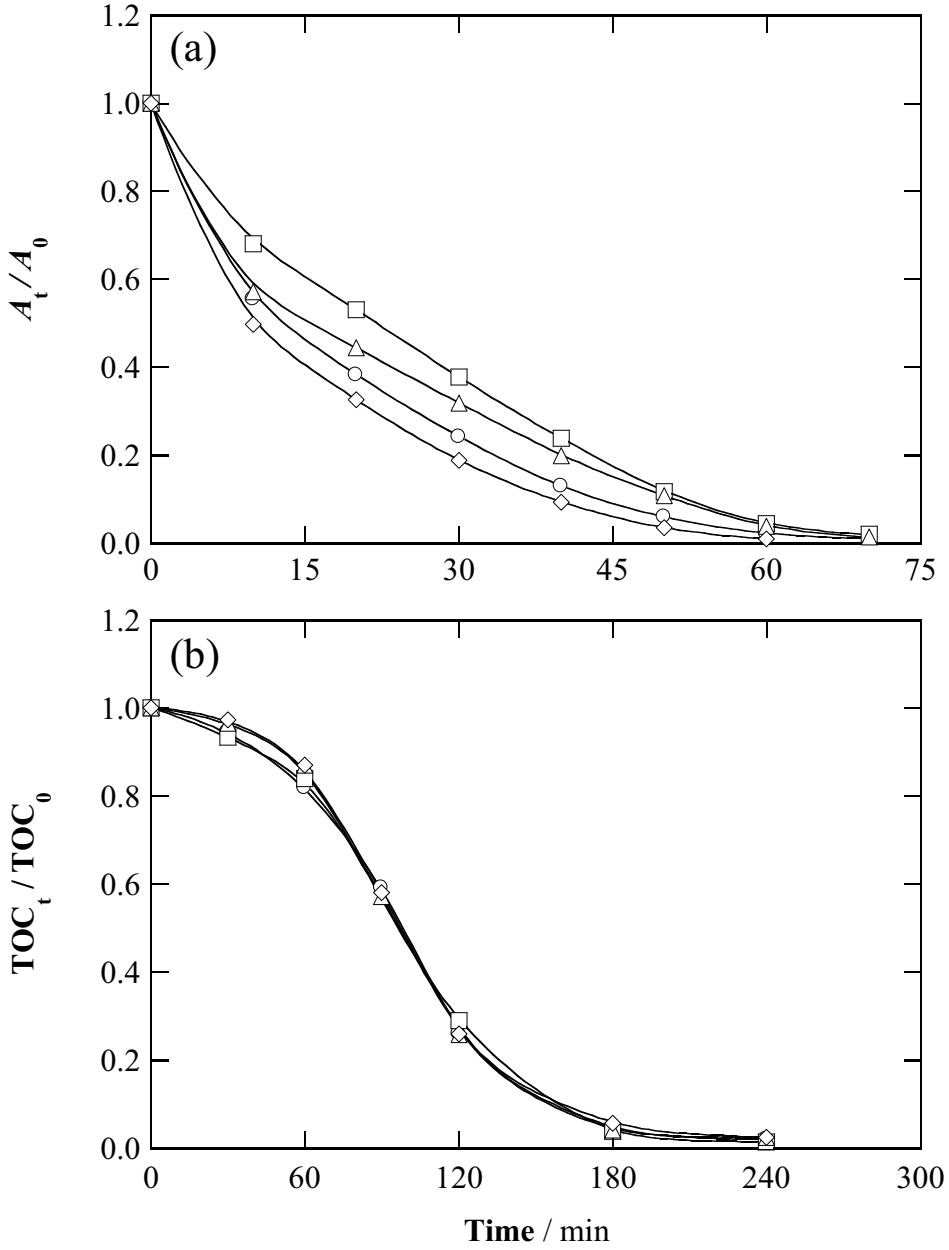
(a)
(b)
A_t / A_0
TOC_t / TOC_0
Time / min
0
15
30
45
60
75
120
180
240
300
0.0
0.2
0.4
0.6
0.8
1.0
1.2

Fig. 3

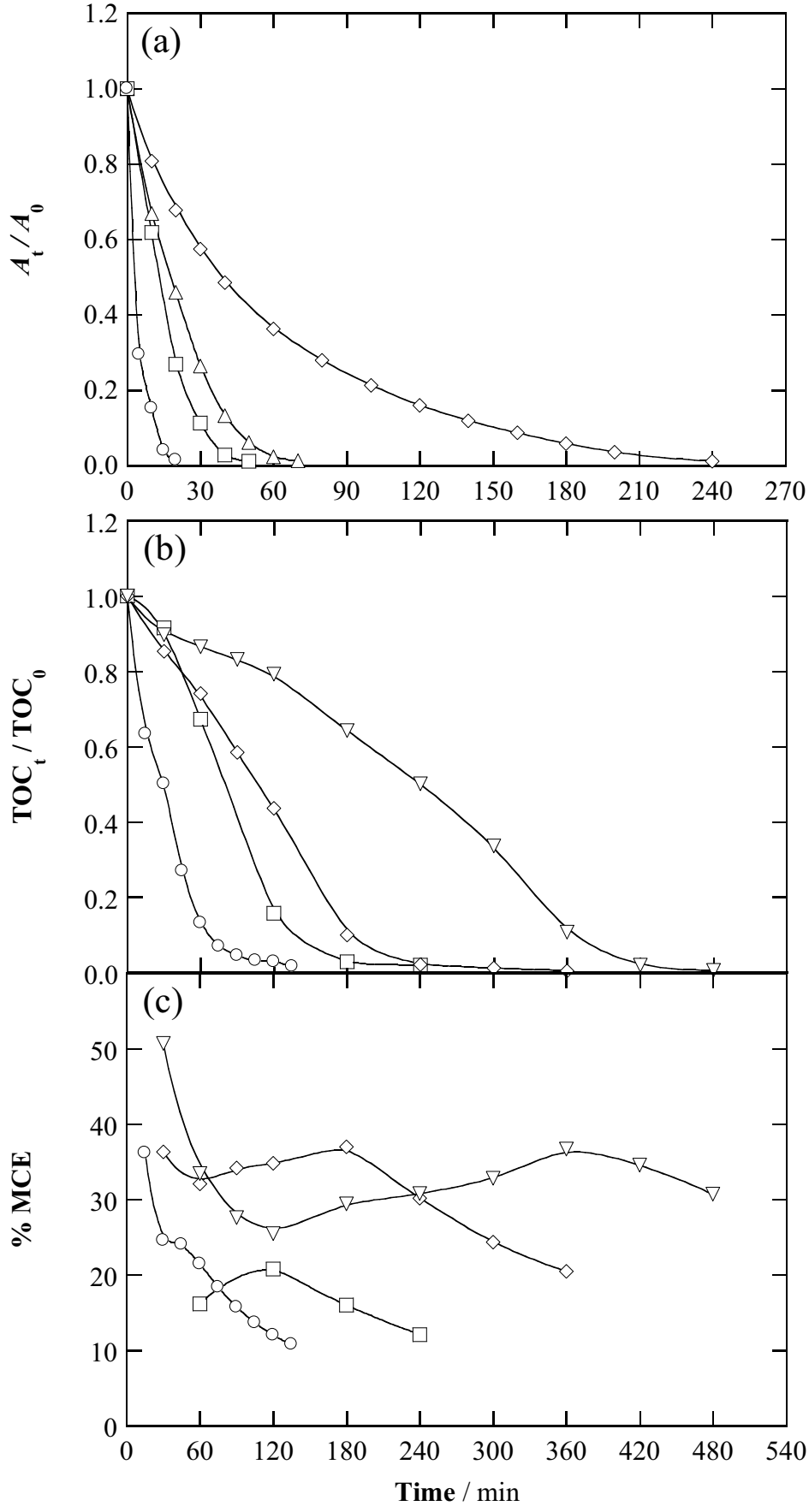

Fig. 4

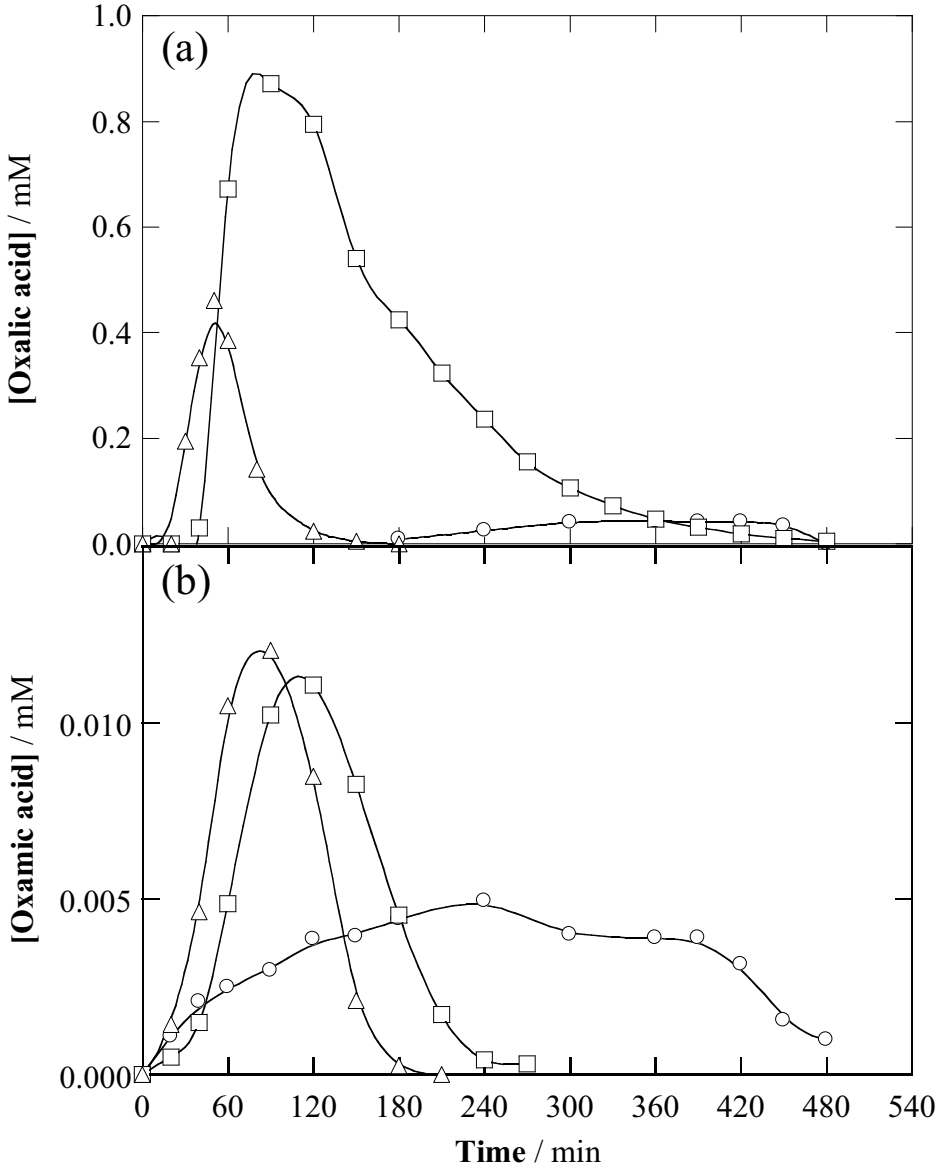
(a)
(b)
[Oxalic acid] / mM
[Oxamic acid] / mM
Time / min
1.0
0.8
0.6
0.4
0.2
0.0
0.010
0.005
0.000
0
60
120
180
240
300
360
420
480
540

Fig. 5

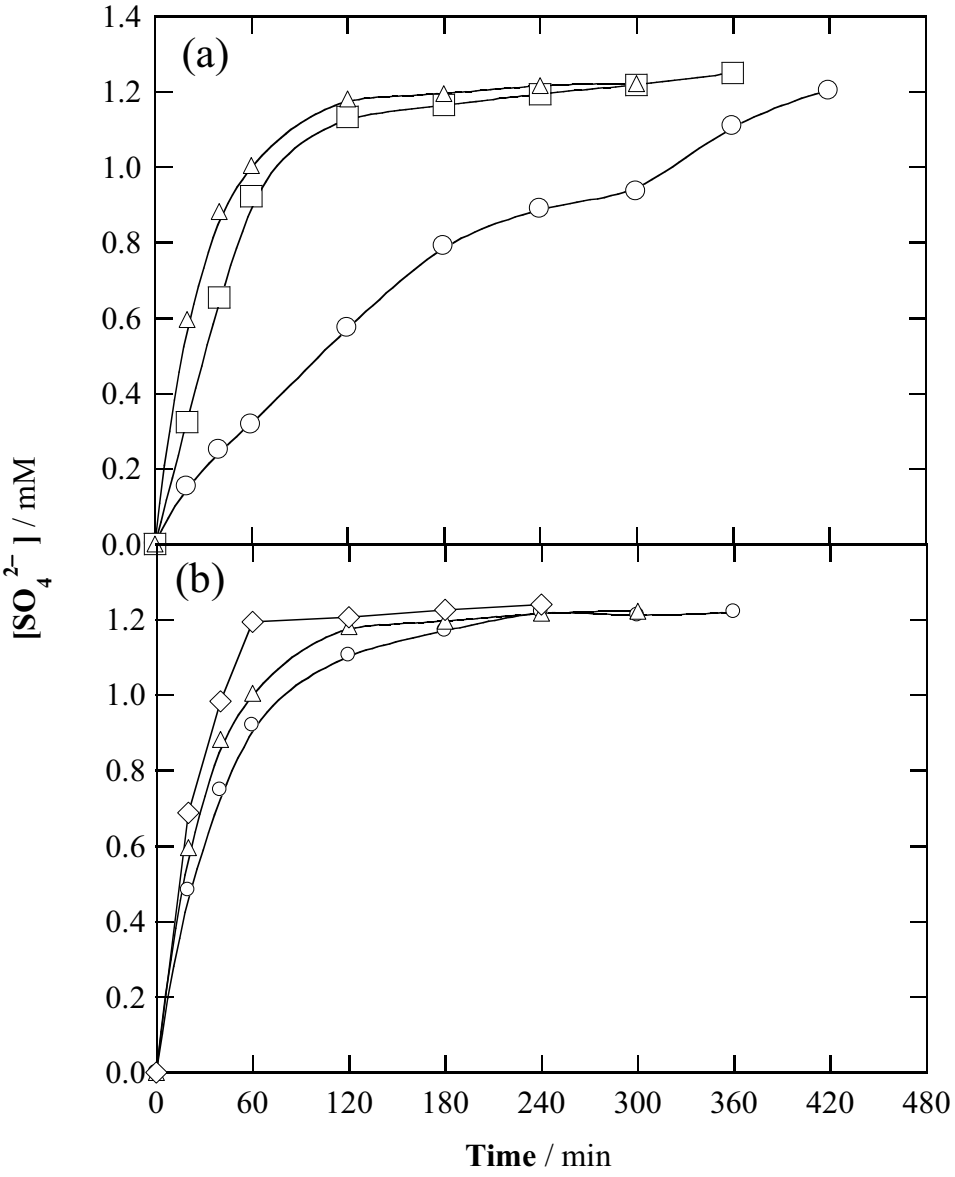
(a)
(b)
[SO4 2−] / mM
Time / min
0.0
0.2
0.4
0.6
0.8
1.0
1.2
1.4
0
60
120
180
240
300
360
420
480

Fig. 6

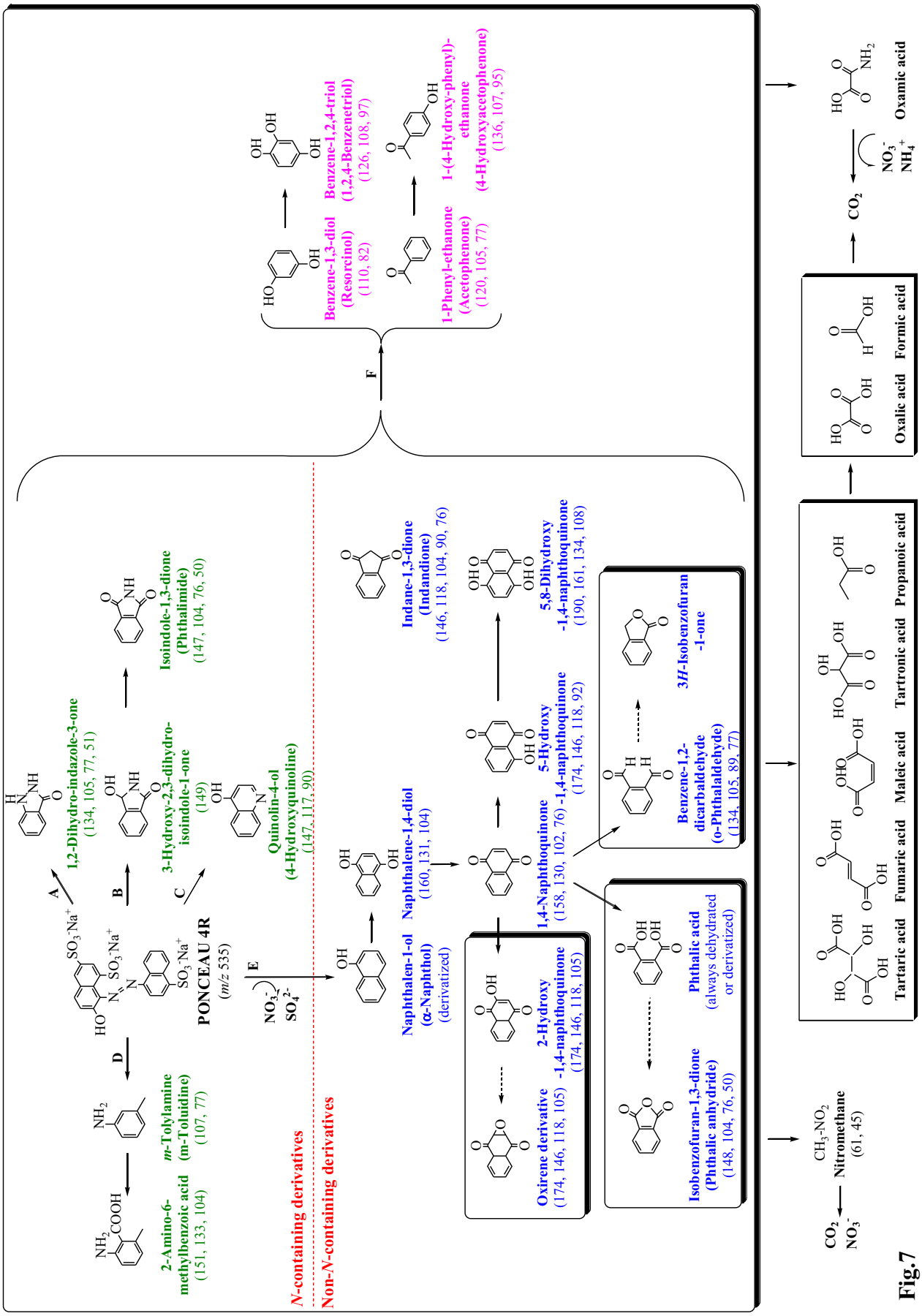
PONCEAU 4R
(m/z 535)
A
B
C
D
E
F
1,2-Dihydro-indazole-3-one
(134, 105, 77, 51)
3-Hydroxy-2,3-dihydro-isoindole-1-one
(149)
Isoindole-1,3-dione
(Phthalimide)
(147, 104, 76, 50)
Quinolin-4-ol
(4-Hydroxyquinoline)
(147, 117, 90)
2-Amino-6-methylbenzoic acid
(151, 133, 104)
m-Tolylamine
(m-Toluidine)
(107, 77)
Naphthalen-1-ol
(α-Naphthol)
(derivatized)
Naphthalene-1,4-diol
(160, 131, 104)
Indane-1,3-dione
(Indandione)
(146, 118, 104, 90, 76)
Oxirene derivative
(174, 146, 118, 105)
2-Hydroxy
-1,4-naphthoquinone
(174, 146, 118, 105)
1,4-Naphthoquinone
(158, 130, 102, 76)
5-Hydroxy
-1,4-naphthoquinone
(174, 146, 118, 92)
5,8-Dihydroxy
-1,4-naphthoquinone
(190, 161, 134, 108)
Isobenzofuran-1,3-dione
(Phthalic anhydride)
(148, 104, 76, 50)
Phthalic acid
(always dehydrated or derivatized)
Benzene-1,2-dicarbaldehyde
(o-Phthalaldehyde)
(134, 105, 89, 77)
3H-Isobenzofuran
-1-one
Benzene-1,3-diol
(Resorcinol)
(110, 82)
Benzene-1,2,4-triol
(1,2,4-Benzenetriol)
(126, 108, 97)
1-Phenyl-ethanone
(Acetophenone)
(120, 105, 77)
1-(4-Hydroxy-phenyl)-ethanone
(4-Hydroxyacetophenone)
(136, 107, 95)
N-containing derivatives
Non-N-containing derivatives
Tartaric acid
Fumaric acid
Maleic acid
Tartronic acid
Propanoic acid
Oxalic acid
Formic acid
Oxamic acid
Nitromethane
(61, 45)
CO2
NO3-
NH4+

Fig.7

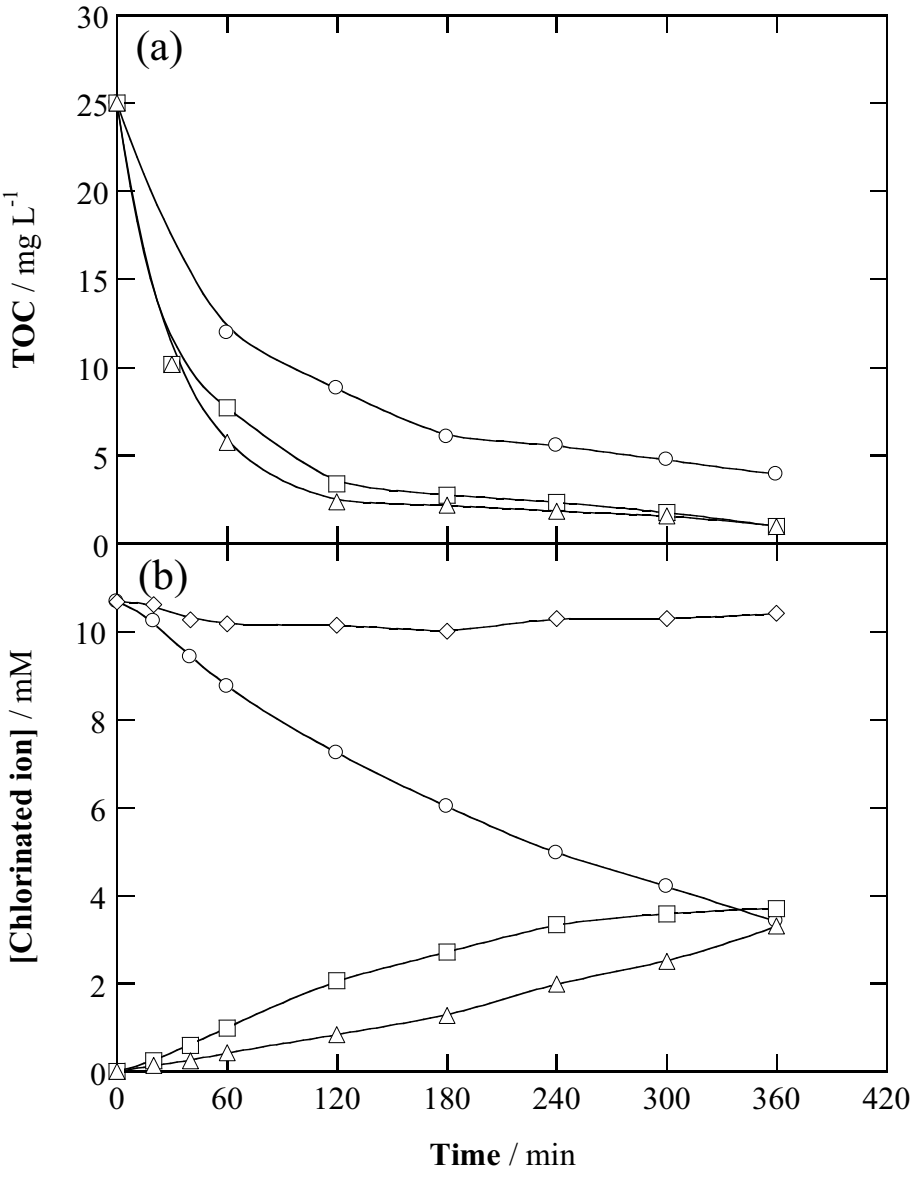
(a)
(b)
TOC / mg L-1
[Chlorinated ion] / mM
Time / min
0
5
10
15
20
25
30
0
2
4
6
8
10
0
60
120
180
240
300
360
420

Fig. 8

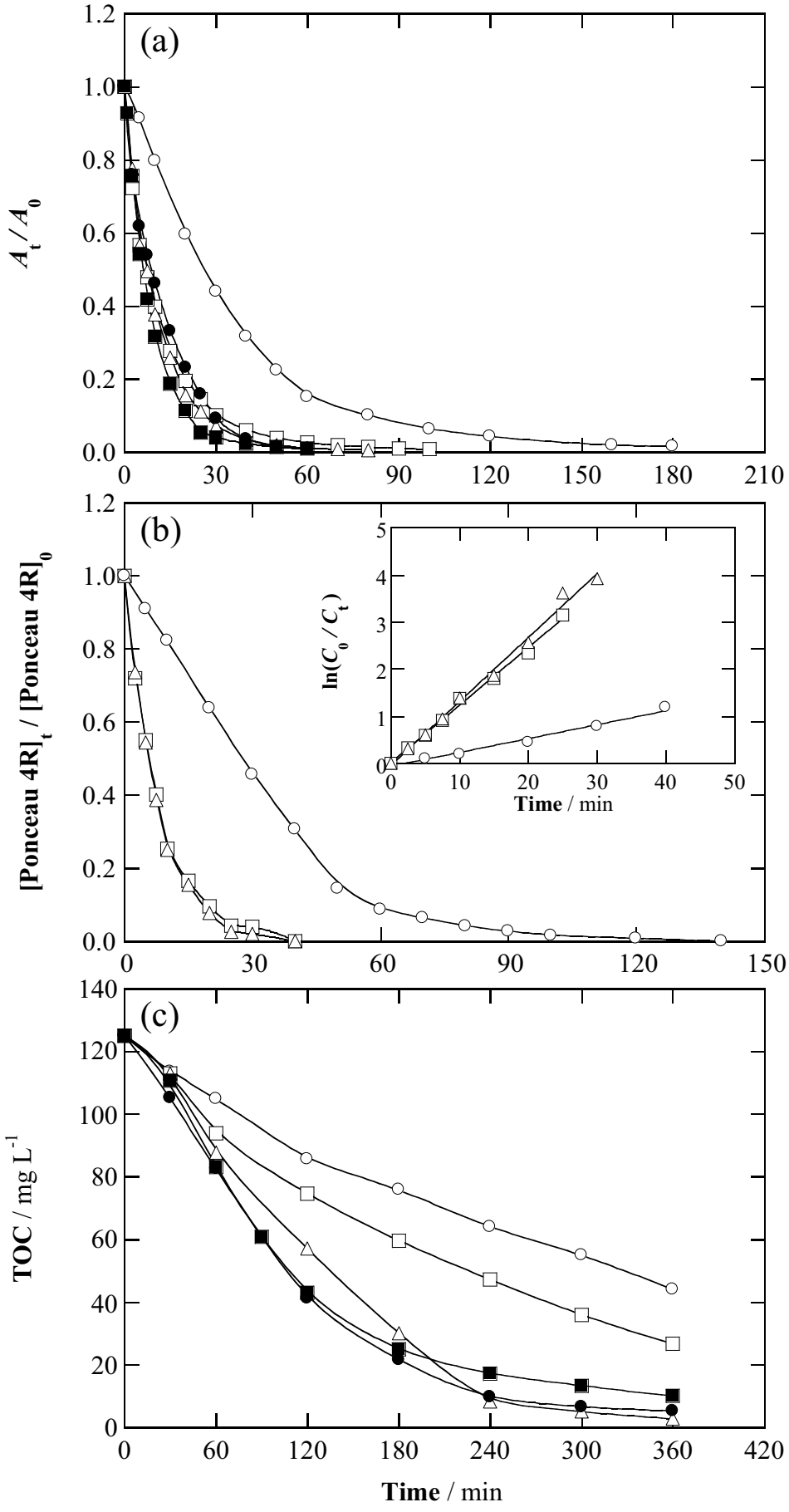
(a)
A_t / A_0
(b)
[Ponceau 4R]$_t$ / [Ponceau 4R]$_0$
ln(C_0 / C_t)
Time / min
(c)
TOC / mg L^{-1}
Time / min

Fig. 9

.

4.3. Decolorization and mineralization of Allura Red AC aqueous solutions by electrochemical advanced oxidation processes using a 130 mL cell and a 2.5 L pre-pilot plant: Effect of supporting electrolyte and identification of products

The electrochemical treatment of AR AC was investigated by analogous EAOPs at lab-scale and in a pre-pilot flow plant. First, the decolorization and mineralization of AR AC aqueous solutions was studied at lab-scale (**Paper 3**). Comparative electrolyses by EO-H_2O_2, EF and PEF in sulfate medium were made to clarify the role of oxidizing agents generated. The slowest decolorization was archived by EO-H_2O_2, being required 420 min to reach a total color removal. In contrast, a colorless solution was obtained after only 30-35 min by EF and PEF with both, BDD and Pt, due to the more efficient attack of $^{\bullet}OH$ produced in the bulk from Fenton's reaction (12). The analysis of all the absorbance decays revealed that they obeyed a pseudo-first-order kinetics. The resulting apparent rate constants (k_{dec}) are collected in the **Table 6**. According to k_{dec} values, the decolorization process was enhanced in order EO-H_2O_2-Pt < EO-H_2O_2-BDD << EF-Pt ≈ EF-BDD ≤ PEF-Pt ≈ PEF-BDD. Regarding the TOC, a very different behavior was found. The oxidation ability of EAOPs increases in the order EO-H_2O_2 << EF < PEF for Pt and the most potent BDD. This trend is also found in the corresponding MCE values. These findings highlight that PEF-BDD is the most potent and efficient EAOP to degrade acidic AR AC solutions in sulfate medium.

Table 6. Pseudo-first-order rate constant for color removal (k_{dec}, 10^{-2} min^{-1})[a], TOC removal (360 min) and maximum value of MCE for the treatment of 130 mL of 230 mg L^{-1} Allura Red AC solutions in 0.05 M of Na_2SO_4 at pH 3.0 and 100 mA cm^{-2} in various EAOPs.

Process	Anode	k_{dec}	% TOC removal	% MCE
EO-H_2O_2	Pt	0.44 ± 0.07	0.6	0.1
	BDD	0.66 ± 0.03	74	9
EF	Pt	6.47 ± 1.40	58	9
	BDD	6.66 ± 3.00	88	13
PEF	Pt	7.44 ± 2.54	95	18
	BDD	7.33 ± 1.57	98	22

[a] Determined with a confidence interval of 95% using 10-12 experimental points between 0% and 90% color removal for each trial.

The effect of operation parameters on the performance of PEF process was thoroughly examined. The applied current density (j) is the main factor governing the effectiveness of the EAOPs and thus, its influence on the performance of PEF was

checked. It was found that greater *j* gave higher color removal rate and mineralization degree at shorter times. In contrast, **Table 7** highlights a lower efficiency when *j* rose. This opposite trend can be related to a gradual loss in the available concentration of BDD($^{\bullet}$OH) and $^{\bullet}$OH because of the acceleration of parasitic reactions at the anode surface and in the bulk. The influence of dye content in PEF-BDD was also studied. It was found that longer time was needed for complete decolorization and mineralization. However a gradual increase in efficiency with rising organic load was found. These profiles suggest the favored attack of BDD($^{\bullet}$OH) and $^{\bullet}$OH on greater quantities of organics, with parasitic reactions occurring to a much smaller extent.

Another approach for increasing the decolorization and mineralization degree in PEF process is to investigate the influence of different anions that can be present in real wastewater. In order to investigate the influence of these anions, sodium sulfate, sodium nitrate, lithium perchlorate and sodium chloride were employed as supporting electrolyte. It was found that anions increase the decolorization efficiency in the order $ClO_4^- < SO_4^{2-} \approx NO_3^- \leq Cl^-$. This trend can be confirmed from the corresponding k_{dec} values listed in **Table 7**. The slight increase in Cl^- medium can be attributed to the formation of active chlorine, as commented for Ponceau 4R in section 4.2.

Table 7. Pseudo-first-order rate constant for color removal (*kdec*, 10^{-2} min^{-1})[a], TOC removal (360 min) and maximum value of MCE for the treatment of 130 mL of 230 mg L^{-1} Allura Red AC solutions in 0.05 M of supporting electrolyte at pH 3.0 by PEF with BDD anode.

j / mA cm^{-2}	Electrolyte	k_{dec}	% TOC removal	% MCE
33.3	Na_2SO_4	5.92 ± 1.29	95	46
66.7	Na_2SO_4	6.74 ± 2.67	96	26
100	Na_2SO_4	7.33 ± 1.57	98	22
150	Na_2SO_4	7.52 ± 2.50	99	15
33.3	NaCl	7.37 ± 1.01	80	24
33.3	$NaClO_4$	5.66 ± 1.05	98	40
33.3	$NaNO_3$	6.04 ± 1.81	98	50

[a] Determined with a confidence interval of 95% using 10-12 experimental points between 0% and 90% color removal for each trial.

In contrast, a poor mineralization rate was achieved in Cl^- medium, which can be due to the attack of active chlorine on organics promoting the generation of more recalcitrant chloroderivatives that are hardly destroyed by this oxidant and hydroxyl radicals. Almost total mineralization was found in the other media, with a slight increase of mineralization rate in the sequence $ClO_4^- \leq SO_4^{2-} \leq NO_3^-$.

The major disadvantage when using Cl^- as supporting electrolyte counterion or in the presence of Cl^- in wastewater is the possible formation of organochlorinated compounds (R-Cl) during the oxidation of AR AC by active chlorine. The formation of persistent chloroderivatives was confirmed by the detection of 3 chloroderivatives by GC-MS. In contrast, in sulfate medium, the degradation of the dye was due to the attack of the main oxidant $^{\bullet}OH$, which led to the formation of hydroxylated compounds. The cleavage of the aromatic compounds led to the formation of short-chain carboxylic acids and inorganic ions as detected in the present Thesis.

Despite the large number of publications on the EAOPs and the very goods results obtained at lab-scale, their practical application for the treatment of organic pollutants is still insufficient. In **Paper 4**, the EAOPs were scaled up from the stirred tank reactor to a pre-pilot flow plant of 2.5 L equipped with a Pt/ADE filter-press electrochemical reactor coupled to a planar solar photoreactor. First, the electrochemical degradation of AR AC was studied by EF and SPEF to test the comparative oxidation ability of both methods, as well as the influence of the UV radiation supplied by sunlight on their degradation processes. The results show a rapid color removal when treating 230 mg L^{-1} of AR AC solution. The initial yellowish red solution was gradually decolorized and becamee colorless after 60 min of EF and 40 min of SPEF at 50 mA cm^{-2} with 0.05 M Na_2SO_4. The slight acceleration in SPEF can be related to the additional generation of $^{\bullet}OH$ induced by photoreduction reaction (23). Analysis of the absorbance decays revealed that they always obeyed a pseudo-first-order kinetics, as observed for Ponceau 4R. From the corresponding ln ($[A_0]/[A_t]$) vs t plots, k_{dec} of $(8.06 \pm 0.52) \times 10^{-2}$ and $(9.98 \pm 0.13) \times 10^{-2}$ min^{-1} was found for the EF and SPEF processes, respectively.

The influence of some key valuable parameters such as j and electrolyte and substrate concentrations on the oxidation ability of SPEF was investigated to clarify the role of generated oxidizing species, mainly Pt($^{\bullet}OH$) and $^{\bullet}OH$. Quicker decolorization of azo dyes is expected with rising j. This tendency was tested by treating a 230 mg L^{-1} AR AC solution at 100 mA cm^{-2}. Total decolorization was attained in 30 min, a time shorter

than 40 min needed at 50 mA cm^{-2}. Accordingly, a greater k_{dec} of (19.03 ± 0.40) × 10^{-2} min^{-1} was determined. The effect of SO_4^{2-} and dye contents was also checked at 50 mA cm^{-2}. A similar color removal was found for 0.050 and 0.30 M Na_2SO_4, with k_{dec} = (9.15 ± 0.07) × 10^{-2} min^{-1} under the latter conditions. Increasing the initial dye content, longer treatment time was needed to reach to total decolorization. The corresponding k_{dec} values were (18.19 ± 0.46) × 10^{-2}, (9.98 ± 0.13) × 10^{-2} and (4.59 ± 0.01) × 10^{-2} min^{-1} for 115, 230 and 460 mg L^{-1} of AR AC, respectively.

A very different behavior was found for the comparative TOC abatement in EF and SPEF processes. In EF, the higher oxidation ability of Pt(•OH) and •OH produced from Fenton's reaction allowed a quicker TOC decay up to 39% at 180 min, whereupon its decay slowed down to reach only 46% mineralization at 360 min. This evidence supports the active role of Pt(•OH) and, mainly, •OH in the bulk, to transform several intermediates into CO_2 during the first stages. In contrast, at longer time, large amount of refractory products are accumulated in the medium. This point was confirmed in the SPEF process, where the fast photolysis of these recalcitrant intermediates upon attack of hydroxyl radicals under UV radiation supplied by sunlight via reaction (24) can explain the almost total mineralization with 96% TOC removal reached at 240 min. An increase in j from 50 to 100 mA cm^{-2} caused a quicker TOC removal, since 97% TOC decay was already achieved in 180 min at 100 mA cm^{-2}. An enhancement of mineralization rate was observed when increasing electrolyte content to 0.30 M. This can be related to possible formation of complexes of sulfate with some intermediates that are more rapidly photodecomposed by sunlight. As occurred for decolorization, longer time was needed to reach almost total mineralization of AR AC as its concentration increased. Thus, 97%, 96% and 95% TOC decay was found after 120, 240 and 360 min of treatment for 115, 230 and 460 mg L^{-1} of dye, respectively. The efficiency of above trials in the pre-pilot plant was analyzed by calculating the MCE. As expected, the SPEF process at 50 mA cm^{-2} was much more efficient than the EF one, attaining a final MCE of 67% after reaching a maximal of 117% at 120 min. Despite the quicker mineralization found, the MCE decayed when j rose to 100 mA cm^{-2}. The EC_{TOC} was calculated as well, and the results allow concluding that lower energy consumption was obtained when operating at lower j and higher sulfate and azo dye contents.

To further identify the by-products, GC-MS analysis was performed. According to the 16 aromatic intermediates identified, an initial reaction sequence for AR AC degradation has been proposed. The electrochemical degradation of AR AC by EF and SPEF involves simultaneous steps such as the cleavage of the –N=N- and C-N bonds, hydroxylation reactions and other oxidative transformations. The degradation of aromatic compounds caused the ring cleavage, generating a mixture of 11 carboxylic acids identified by HPLC and GC-MS. Many of these acids formed Fe(III) complexes and most of them were rapidly destroyed by hydroxyl radicals, except oxamic and oxalic acids that were the most persistent ones. The last one was quickly removed in SPEF, which turned out to be the best technology for the treatment of acidic aqueous solutions of AR AC.

.

Paper 3

Decolorization and mineralization of Allura Red AC aqueous solutions by electrochemical advanced oxidation processes

Journal of Hazardous Materials

290 (2015) 34–42

Journal of Hazardous Materials 290 (2015) 34–42

Contents lists available at ScienceDirect

Journal of Hazardous Materials

journal homepage: www.elsevier.com/locate/jhazmat

Decolorization and mineralization of Allura Red AC aqueous solutions by electrochemical advanced oxidation processes

Abdoulaye Thiam, Ignasi Sirés, José A. Garrido, Rosa M. Rodríguez, Enric Brillas*

Laboratori d'Electroquímica dels Materials i del Medi Ambient, Departament de Química Física, Facultat de Química, Universitat de Barcelona, Martí i Franquès 1-11, 08028 Barcelona, Spain

HIGHLIGHTS

- Quicker degradation of Allura Red AC in the order EO-H_2O_2 < EF < PEF with Pt or BDD anode.
- Almost total mineralization achieved by the most powerful PEF process with BDD.
- Similar decolorization and mineralization rate in SO_4^{2-}, ClO_4^- and NO_3^- media.
- In Cl^- medium, only slightly larger decolorization rate but strong inhibition of mineralization.
- Identification of aromatic products, carboxylic acids and released NH_4^+, NO_3^- and SO_4^{2-} ions.

ARTICLE INFO

Article history:
Received 12 January 2015
Received in revised form 16 February 2015
Accepted 17 February 2015
Available online 19 February 2015

Keywords:
Allura Red AC
Electrochemical oxidation
Electro-Fenton
Oxidation products
Photoelectro-Fenton

ABSTRACT

The decolorization and mineralization of solutions containing 230 mg L^{-1} of the food azo dye Allura Red AC at pH 3.0 have been studied upon treatment by electrochemical oxidation with electrogenerated H_2O_2 (EO-H_2O_2), electro-Fenton (EF) and photoelectro-Fenton (PEF). Experiments were performed with a stirred tank reactor containing a boron-doped diamond (BDD) or Pt anode and an air-diffusion cathode to generate H_2O_2. The main oxidants were hydroxyl radicals formed at the anode surface from water oxidation and in the bulk from Fenton's reaction between H_2O_2 and added Fe^{2+}. The oxidation ability increased in the sequence EO-H_2O_2 < EF < PEF and faster degradation was always obtained using BDD. PEF process with BDD yielded almost total mineralization following similar trends in SO_4^{2-}, ClO_4^- and NO_3^- media, whereas in Cl^- medium, mineralization was inhibited by the formation of recalcitrant chloroderivatives. GC–MS analysis confirmed the cleavage of the —N=N— bond with formation of two main aromatics in SO_4^{2-} medium and three chloroaromatics in Cl^- solutions. The effective oxidation of final oxalic and oxamic acids by BDD along with the photolysis of Fe(III)-oxalate species by UVA light accounted for the superiority of PEF with BDD. NH_4^+, NO_3^- and SO_4^{2-} ions were released during the mineralization.

1. Introduction

Over the last fifteen years, electrochemical advanced oxidation processes (EAOPs) have been optimized for the removal of toxic and biorefractory organic pollutants from waters under the on-site action of •OH [1–7]. In some EAOPs, this radical can be efficiently formed from H_2O_2 continuously supplied to the solution via the two-electron cathodic reduction of injected O_2, for example, via Fenton's Reaction (2) [3,7]:

$$O_{2(g)} + 2H^+ + 2e^- \rightarrow H_2O_2 \quad (1)$$

$$H_2O_2 + Fe^{2+} \rightarrow Fe^{3+} + {}^{\bullet}OH + OH^- \quad (2)$$

The efficient O_2 reduction from pure gas or atmospheric air via Reaction (1) allows an efficient H_2O_2 production, which is feasible using carbonaceous cathodes including graphite [8], carbon nanotubes [9], activated carbon fiber [10], carbon sponge [11], graphite felt [12], carbon felt [1,12–14] and carbon-polytetrafluoroethylene (PTFE) gas (O_2 or air) diffusion [15–17]. Hydrogen peroxide is a "green" chemical that yields oxygen gas and water as by-products. However, H_2O_2 is a weak oxidizing agent, although this can be

* Corresponding author. Tel.: +34 934021223; fax: +34 934021231.
E-mail address: brillas@ub.edu (E. Brillas).

http://dx.doi.org/10.1016/j.jhazmat.2015.02.050
0304-3894/

enhanced by different EAOPs, once produced as depicted in Reaction (1).

The most widespread EAOP is electrochemical oxidation (EO), so-called EO–H_2O_2 when H_2O_2 is cathodically generated [3,7]. In such method, organics are poorly removed by H_2O_2 but are more extensively oxidized by physisorbed M(•OH) generated from water discharge at a large O_2-overpotential anode (M) at high current [2]:

$$M + H_2O \rightarrow M(^{\bullet}OH) + H^+ + e^- \quad (3)$$

The preferred anode in EO and EO–H_2O_2 is a boron-doped diamond (BDD) thin-film deposited onto Si, Ti or Nb [2,7]. BDD exhibits interesting technological properties and generates very large amounts of reactive BDD(•OH) due to the weak BDD-•OH interaction, resulting in a larger O_2-overpotential that enhances the destruction of organics compared to that observed at traditional anodes such as Pt [2,18–22]. The electrolyte can modulate the effectiveness of EO. Thus, in chloride medium, organics can be competitively attacked by M(•OH), along with active chlorine species produced as follows [2,15,16]:

$$2Cl^- \rightarrow Cl_2(aq) + 2e^- \quad (4)$$

$$Cl_2(aq) + H_2O \rightarrow HClO + Cl^- + H^+ \quad (5)$$

$$HClO \leftrightarrows ClO^- + H^+ \quad (6)$$

Nevertheless, the occurrence of such reactions at high current can become dangerous because of the large production of toxic ClO_3^- and ClO_4^- ions, which are not formed or are generated to a much lesser extent using lower oxidation power anodes like Pt [15,16].

Electro-Fenton (EF) is the best known EAOP with H_2O_2 generation [3,5,7,23,24]. A catalytic amount of Fe^{2+} is added to the contaminated solution to react with H_2O_2, thus producing Fe^{3+} and •OH in the bulk from Fenton's Reaction (2) at optimum pH 2.8. The main advantage of EF over more conventional Fenton's reagent ($Fe^{2+} + H_2O_2$) is the cathodic regeneration of Fe^{2+} by Reaction (7), which accelerates Fenton's reaction and enhances the mineralization [5,7].

$$Fe^{3+} + e^- \rightarrow Fe^{2+} \quad (7)$$

Irradiation of the solution with ultraviolet A (UVA) light in the photoelectro-Fenton (PEF) process [10,25–29] will favor: (i) the photo-Fenton reaction shown in Eq. (8) involving the photolysis of $Fe(OH)^{2+}$, which regenerates Fe^{2+} and increases •OH production, and (ii) the photolytic Reaction (9) with photodecarboxylation of generated Fe(III)-carboxylate products.

$$Fe(OH)^{2+} + h\nu \rightarrow Fe^{2+} + {}^{\bullet}OH \quad (8)$$

$$Fe(OOCR)^{2+} + h\nu \rightarrow Fe^{2+} + CO_2 + R^{\bullet} \quad (9)$$

About 70% of the world dye production corresponds to azo compounds that are used in many industries by their unique characteristics including brilliant shades, relative low cost and simple manufacture [30–33]. Azo dyes contain one or various azo groups (—N=N—) as chromophore, being linked to benzene and/or naphthalene rings with lateral —OH and —SO_3H groups to increase their water solubility [7,34]. Nowadays, there exists a growing concern on the environmental impact of dyeing industrial effluents because of their high dye contents, usually ranging between 100 and 250 mg L^{-1}, which cause aesthetic problems and toxic effects on living beings [35–37]. The European Food Safety Authority reported that food azo dyes can be dangerous due to their connection to children hyperactivity. This is the case of Allura Red AC or food additive E129 (disodium 6-hydroxy-5-[(2-methoxy-5-methy-4-sulfophenyl)azo]-2-naphthalenesulfonate, $C_{18}H_{14}N_2O_8S_2Na_2$, λ_{max} = 500 nm, see chemical structure in Fig. 1),

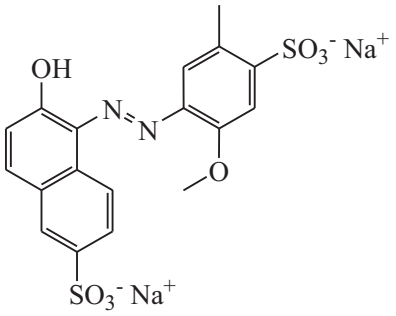

Fig. 1. Chemical structure of Allura Red AC.

which is also suspected to be responsible of allergies and intolerances [38,39], thus being banned in some European countries. Azo dyes are highly recalcitrant to conventional biological and physicochemical methods in municipal wastewater treatment plants and thus, powerful degradation methods are required to remove them from industrial effluents [30,33].

Many authors have studied the electrochemical destruction of single and multi-component azo dyes in synthetic and real wastewater by EAOPs [7], but only a few papers described the influence of different background electrolytes on the degradation of these pollutants [11,17]. In order to investigate such an effect on the PEF treatment of azo dyes, an exhaustive study on the decolorization and mineralization of Allura Red AC solutions in sulfate, perchlorate, nitrate and chloride media at pH 3.0 is presented. First, comparative electrolyses by EO-H_2O_2, EF and PEF in sulfate medium were made to clarify the role of generated oxidizing agents. The effect of current density (j) and dye and electrolyte concentrations was also examined. Aromatic intermediates were detected by gas chromatography–mass spectrometry (GC–MS), whereas accumulated carboxylic acids and released inorganic ions were quantified by chromatographic techniques. Note that previous research has only reported the degradation of Allura Red AC by TiO_2 photocatalysis with visible light [40].

2. Experimental

2.1. Chemicals

Allura Red AC (purity 80%) was purchased from Sigma–Aldrich. Anhydrous sodium sulfate, sodium chloride, lithium perchlorate and sodium nitrate used as background electrolytes, as well as iron(II) sulfate heptahydrate used as a catalyst in EF and PEF, were of analytical grade from Merck and Fluka. Solutions were prepared with ultrapure water from a Millipore Milli-Q system with resistivity >18 MΩ cm and their pH was adjusted with analytical grade sodium hydroxide or sulfuric, hydrochloric, perchloric or nitric acid purchased from Merck. Carboxylic acids and other chemicals and solvents were of high-performance liquid chromatography (HPLC) or analytical grade from Merck, Sigma–Aldrich and Panreac.

2.2. Electrolytic system

EO–H_2O_2, EF and PEF treatments were conducted in an open, undivided, cylindrical glass cell with a double jacket for recirculation of thermostated water at 25 °C and containing 130 mL of solution, which was stirred with a magnetic bar at 800 rpm. The cell contained either a 3 cm^2 Pt sheet from SEMPSA (Barcelona, Spain) or a 3 cm^2 BDD thin-film electrode from NeoCoat (La-Chaux-de-Fonds, Switzerland) as the anode and a 3 cm^2 carbon-PTFE air-diffusion cathode from E-TEK (Somerset, NJ, USA). The cathode was mounted as described elsewhere [25], and was fed with

air pumped at 1 L min^{-1} for continuous H_2O_2 generation. Six EAOPs were studied, namely EO–H_2O_2–Pt, EO–H_2O_2–BDD, EF–Pt, EF–BDD, PEF–Pt and PEF–BDD. The assays were performed at constant current provided by an EG&G PAR 273A potentiostat/galvanostat. For PEF–Pt and PEF–BDD, the solution was irradiated with a Philips TL/6W/08 fluorescent black light blue tube placed 7 cm above the solution, which emitted UVA light (λ_{max} = 360 nm) with a photoionization energy of 5 W m^{-2}.

2.3. Instruments and analytical procedures

The solution pH was measured with a Crison 2000 pH-meter. Samples were microfiltered with 0.45 μm PTFE filters from Whatman prior to immediate analysis. The decolorization of the Allura Red AC solutions was followed from the absorbance decay at λ_{max} = 500 nm, measured on a Shimadzu 1800 UV/vis spectrophotometer at 25 °C. The mineralization of solutions was assessed from their total organic carbon (TOC) decay, determined on a Shimadzu TOC-VCNS analyzer. Reproducible TOC values, with an accuracy of ±1%, were obtained by injecting 50 μL samples into the above analyzer. Experiments were run in triplicate and mean values are reported.

Generated carboxylic acids were detected by ion-exclusion HPLC by injecting 20 μL aliquots to a Waters 600 liquid chromatograph fitted with a Bio-Rad Aminex HPX 87H, 300 mm × 7.8 mm, column at 35 °C and coupled to a Waters 996 photodiode array detector at λ = 210 nm. The mobile phase was 4 mM H_2SO_4 at 0.6 mL min^{-1} and peaks appeared at 7.0, 7.9, 8.2, 9.4, 13.7 and 14.8 min for oxalic, tartronic, maleic, oxamic, formic and fumaric acids. NH_4^+, NO_3^- and SO_4^{2-} ions were quantified as previously reported [17].

To identify the aromatic products, the organic components of solutions electrolyzed by PEF–BDD were extracted with 3 × 25 mL of CH_2Cl_2. The organic solution was dried over anhydrous Na_2SO_4, further filtered and, finally, its volume was reduced to about 1 mL. The remaining organic compounds were analyzed by GC–MS using an Agilent Technologies system composed of a 6890N gas chromatograph and a 5975C mass spectrometer operating in electron ionisation mode at 70 eV. Nonpolar Agilent J&W DB-5 and polar HP INNOWax columns, both of 0.25 μm, 30 m × 0.25 mm, were used. The temperature ramp was 36 °C for 1 min, 5 °C min^{-1} up to 300 °C or 250 °C for the nonpolar or polar columns, respectively, and a hold time of 10 min. The temperature of the inlet, source and transfer line was 250, 230 and 280 °C for the nonpolar column, and 250, 230 and 250 °C for the polar one. The mass spectra were identified with a NIST05 MS library.

3. Results and discussion

3.1. Comparative degradation of Allura Red AC in sulfate medium by EAOPs

The degradation of 130 mL of 230 mg L^{-1} of Allura Red AC by different EAOPs was comparatively studied in 0.05 M Na_2SO_4 as supporting electrolyte, at pH 3.0 and 100 mA cm^{-2}. For the EF and PEF processes, 0.5 mM Fe^{2+} was added as catalyst. The pH value and Fe^{2+} concentration were fixed because they were optimal for similar treatments of other aromatics [7,25–29]. In these assays, the solution pH dropped very slowly to final values near 2.7–2.8 due to the formation of acidic products such as short-chain aliphatic carboxylic acids [3,5,7]. The starting yellowish red solution was gradually decolorized and from the absorbance values at

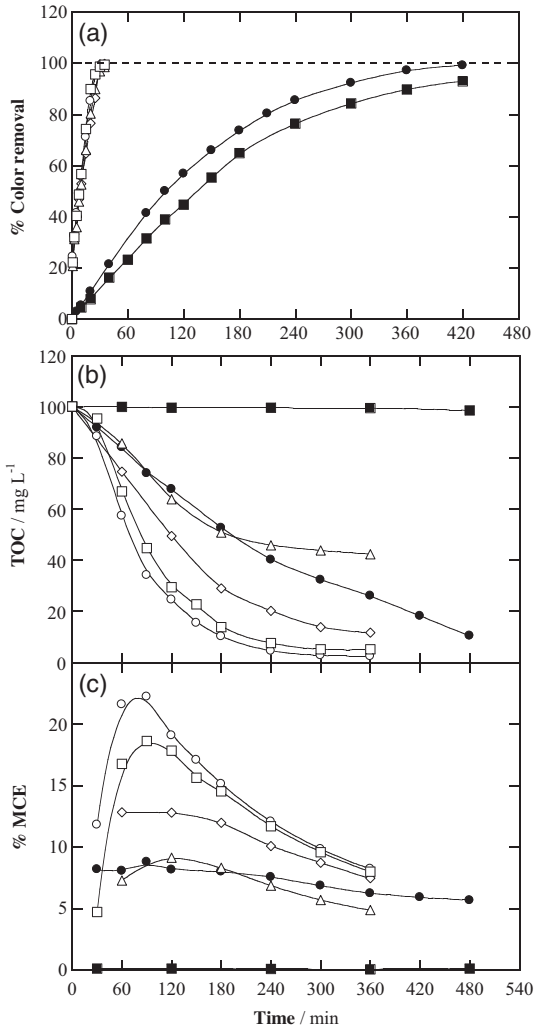

Fig. 2. (a) Percentage of color removal at λ = 500 nm, (b) TOC decay and (c) mineralization current efficiency (MCE) vs. electrolysis time for the treatment of 130 mL of 230 mg L^{-1} (=0.463 mM) Allura Red AC solutions in 0.05 M Na_2SO_4 at pH 3.0 and 100 mA cm^{-2}. Method: (■) EO–H_2O_2–Pt, (●) EO–H_2O_2–BDD, (△) EF–Pt, (◊) EF–BDD, (□) PEF–Pt and (○) PEF–BDD. In EF and PEF, 0.5 mM Fe^{2+} was added to the solution.

λ_{max} = 500 nm, the decolorization efficiency or percentage of color removal was determined as follows [7,27]:

$$\text{Color removal}\,(\%) = \frac{A_0 - A_t}{A_0} \times 100 \qquad (10)$$

where A_0 and A_t denote the absorbance at initial time and after electrolysis time t, respectively.

Fig. 2a depicts the percentage of color removal as a function of time obtained for the six EAOPs tested. In this figure, EO–H_2O_2–Pt yielded the slowest decolorization, achieving 93% color removal at 420 min. At that time, the solution became colorless in EO–H_2O_2–BDD. In contrast, total decolorization was obtained after only 30–35 min of EF–Pt, EF–BDD, PEF–Pt and PEF–BDD. The quicker decolorization in EO–H_2O_2–BDD compared to EO–H_2O_2–Pt can be related to the expected larger reactivity of BDD(•OH) than Pt(•OH) [2], whereas the much faster dye destruction by EF and PEF can be associated with the easier and more efficient attack of •OH produced in the bulk from Fenton's Reaction (2). Analysis of the above absorbance decays using zero-, pseudo-first- and pseudo-second-order kinetic equations revealed that they always obeyed a pseudo-first-order kinetics. Table 1 summarizes the mean values for the apparent rate constants for color removal (k_{dec}) along with their computed 95% confidence

Table 1
Pseudo-first-order rate constant for color removal (k_{dec}) for the treatment of 130 mL of 230 mg L^{-1} Allura Red AC solutions in 0.05 M of supporting electrolyte at pH 3.0 in various EAOPs.

		Electrolyte				
		Na_2SO_4 BDD anode	Na_2SO_4 Pt anode	NaCl BDD anode	$NaNO_3$ BDD anode	$LiClO_4$ BDD anode
Process	j (mA cm^{-2})			k_{dec} (10^{-2} min^{-1})[a]		
EO–H_2O_2	100	0.60 ± 0.03	0.44 ± 0.07			
EF	100	6.66 ± 3.00	6.47 ± 1.40			
PEF	33.3	5.92 ± 1.29		7.37 ± 1.01	6.04 ± 1.81	5.66 ± 1.05
	66.7	6.74 ± 2.67				
	100	7.33 ± 1.57	7.44 ± 2.54			
	150	7.52 ± 2.50				

[a] Mean values along with their computed 95% confidence intervals, using 10–12 experimental points between 0% and 90% color removal for each trial.

intervals. The constants were estimated by the slopes of the corresponding $\ln([A_0]/[A_t])$ vs t plots, which showed excellent linearity with R-squared ≥ 0.990 in all cases. The k_{dec} values for the PEF processes were 11- to 16-fold those obtained in the EO-H_2O_2 process and 1.10- to 1.15-fold those of the EF process owing to the additional •OH generation induced by photo-Fenton Reaction (8) [4]. The decolorization was then enhanced in the order EO–H_2O_2–Pt < EO–H_2O_2–BDD « EF–Pt ≈ EF–BDD ≤ PEF–Pt ≈ PEF–BDD.

A very different behavior was found for TOC abatement. Fig. 2b depicts that TOC did not vary in EO–H_2O_2–Pt, indicating that some intermediates cannot be removed by Pt(•OH) and other generated oxidants. The more potent BDD(•OH) allowed 82% TOC reduction after 420 min of EO–H_2O_2–BDD. This positive effect of BDD was also observed for EF and PEF. After 360 min of electrolysis, 58% and 88% mineralization was achieved for EF–Pt and EF–BDD, respectively. This indicates a greater TOC reduction in EF–Pt compared to EO–H_2O_2–Pt, which is due to the mineralization by •OH in the bulk, whereas the parallel action of BDD(•OH) in EF–BDD promotes the degradation of organics, and is therefore a more powerful process than EO–H_2O_2–BDD. Fig. 2b also shows the almost total mineralization reached by PEF–Pt and PEF–BDD, with 95% and 98% TOC decay at 360 min, respectively. The greater mineralization achieved in comparison with EF–Pt and EF–BDD can be explained by the photolysis of some intermediates, for example, refractory Fe(III)-carboxylate complexes from Reaction (9) under UVA irradiation [7,25,26,29].

The oxidation ability of EAOPs then increases in the order EO-H_2O_2 « EF < PEF for Pt and the more powerful BDD. This trend was confirmed from the corresponding mineralization current efficiency (MCE) estimated by Eq. (11) [27]:

$$\mathrm{MCE}\,(\%) = \frac{nFV_s\Delta(\mathrm{TOC})_{exp}}{4.32\times10^7 mIt}\times 100 \quad (11)$$

where F is the Faraday constant (96,487 C mol^{-1}), V_s is the solution volume (L), $\Delta(\mathrm{TOC})_{exp}$ is the experimental TOC decay (mg L^{-1}), 4.32×10^7 is a conversion factor to homogenize units, m is the number of carbon atoms of Allura Red AC, I is the applied current (A) and t is the electrolysis time (h). The number of electrons (n) exchanged per each molecule of dye was taken as 94 considering that its total mineralization corresponds to Reaction (12), as discussed below.

$$C_{18}H_{14}N_2O_8S_2^{2-} + 42H_2O \rightarrow 18CO_2 + 2SO_4^{2-} + 2NO_3^- + 98H^+ + 94e^- \quad (12)$$

Fig. 2c presents the MCE values obtained for the assays of Fig. 2b. The highest efficiency was attained for PEF–BDD, with a maximum value of 22% at 90 min, whereupon it largely decayed to 8%. This behavior at prolonged electrolysis took place for all the EF and PEF methods and can be ascribed to the slow removal of recalcitrant products and the progressive loss of organic matter [2]. In contrast, a quite constant efficiency, varying between 8% and 6%, was found for EO–H_2O_2–BDD, suggesting a similar mineralization rate of intermediates during treatment.

The above findings highlight that PEF–BDD is the most potent and efficient EAOP to degrade acidic Allura Red AC solutions in sulfate medium. The effect of operating parameters and supporting electrolytes on the performance of this procedure was then examined. Worth noting, the possible application of the PEF process is limited by the high energy requirements arising from the use of commercial UVA lamps. Alternatively, the use of inexpensive sunlight as energy source in the so-called solar PEF process has been proposed elsewhere [27–29].

3.2. Influence of operational parameters on the performance of PEF with BDD in sulfate medium

The applied j is a key variable since it limits the production of oxidizing species. Its effect on the degradation of a 230 mg L^{-1} Allura Red AC solution with 0.05 M Na_2SO_4 and 0.5 mM Fe^{2+} by PEF–BDD was studied between 33.3 and 150 mA cm^{-2}. Fig. 3a highlights that the solution became colorless at shorter time with increasing j, from 45 to 30 min at 33.3 and 150 mA cm^{-2}, respectively. Results of Table 1 show the corresponding gradual increase in k_{dec}, although its value only increased 1.25-fold while j raised 4.5-fold. This suggests the progressive acceleration of all electrode reactions giving larger amounts of BDD(•OH) and H_2O_2 [25,27], thereby enhancing the rate of Fenton's reaction as well. According to this, faster mineralization should be expected as j increased since organics are more rapidly oxidized to intermediates that can be more quickly photolyzed by UVA light. This trend can be observed in Fig. 3b, but an almost total mineralization between 96% and 98% was attained at the end of all treatments, indicating the large effectiveness of the process at low j values. In contrast, Fig. 3c highlights a lower efficiency at greater j, with a maximal of 45% for the lowest 33.3 mA cm^{-2}. The opposite trend of MCE and mineralization rate with increasing j can be related to a gradual loss in the available concentration of BDD(•OH) and •OH because of the acceleration of parasitic reactions at the anode surface and in the bulk [1–3,7,41]. These reactions include the oxidation of BDD(•OH) to O_2 by Reaction (13) and the destruction of •OH by Fe^{2+} via Reaction (14) or by H_2O_2 to form the weaker oxidant hydroperoxyl radical (HO_2•) via Reaction (15). Moreover, the relative amount of BDD(•OH) can be further reduced by the quicker anodic formation of other weaker oxidants such as ozone via Reaction (16) and peroxodisulfate ($S_2O_8^{2-}$) ion via Reactions (17) and (18).

$$2\mathrm{BDD}(^\bullet\mathrm{OH}) \rightarrow 2\mathrm{BDD} + O_{2(g)} + 2H^+ + 2e^- \quad (13)$$

$$Fe^{2+} + {}^\bullet\mathrm{OH} \rightarrow Fe^{3+} + OH^- \quad (14)$$

$$H_2O_2 + {}^\bullet\mathrm{OH} \rightarrow HO_2^\bullet + H_2O \quad (15)$$

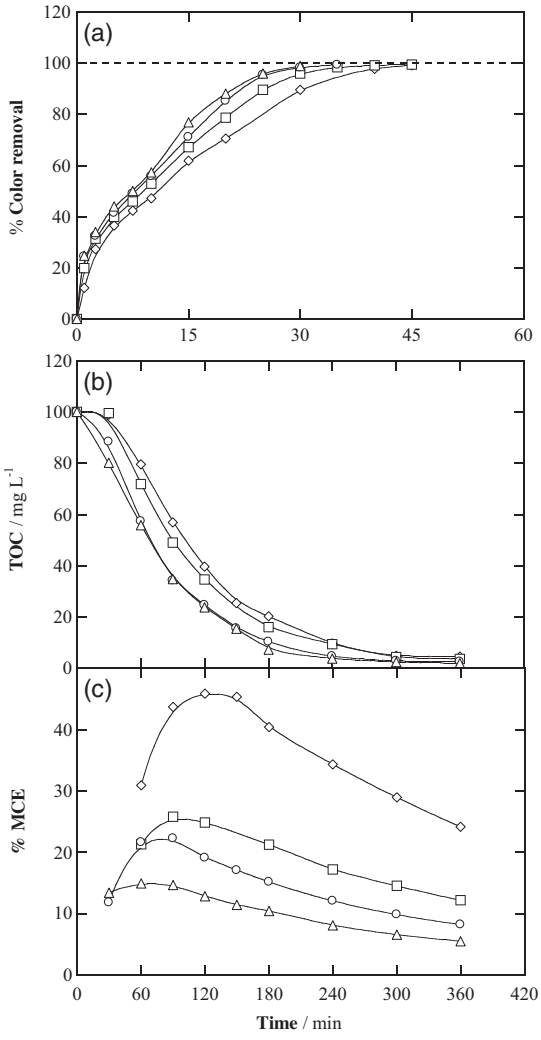

Fig. 3. (a) Decolorization efficiency at λ = 500 nm, (b) TOC removal and (c) MCE with electrolysis time for the degradation of 230 mg L^{-1} Allura Red AC solutions in 0.05 M Na_2SO_4 with 0.5 mM Fe^{2+} at pH 3.0 by PEF-BDD. Current density: (◊) 33.3, (□) 66.7, (○) 100 and (△) 150 mA cm^{-2}.

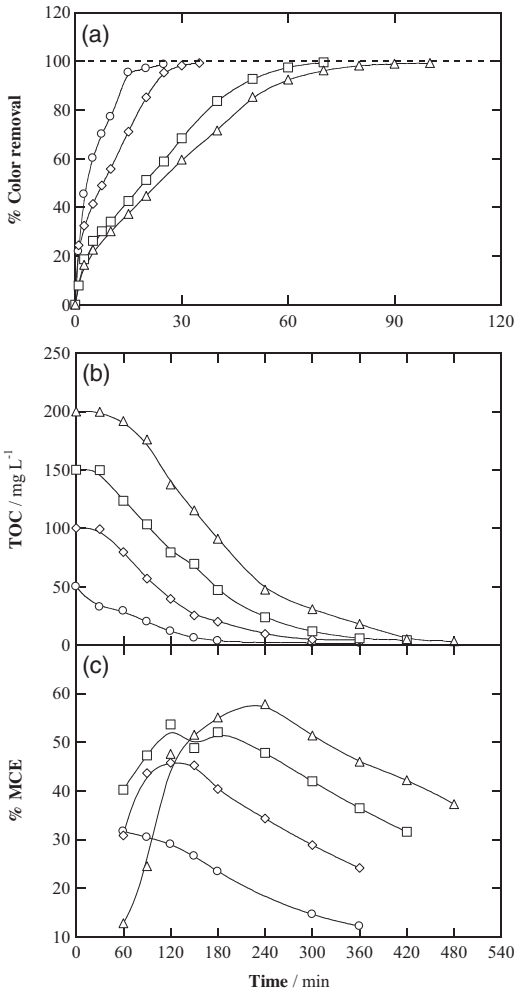

Fig. 4. Change of (a) decolorization efficiency, (b) TOC abatement and (c) MCE with electrolysis time for the degradation of Allura Red AC solutions in 0.05 M Na_2SO_4 with 0.5 mM Fe^{2+} at pH 3.0 by PEF–BDD at 33.3 mA cm^{-2}. Dye content: (○) 115, (◊) 230, (□) 345 and (△) 460 mg L^{-1}.

$$3H_2O \rightarrow O_{3(g)} + 6H^+ + 6e^- \quad (16)$$

$$SO_4^{2-} + BDD(^{\bullet}OH) \rightarrow BDD + SO_4^{\bullet -} + OH^- \quad (17)$$

$$2SO_4^{\bullet -} \rightarrow S_2O_8^{2-} \quad (18)$$

The influence of the dye content in PEF–BDD was further studied at the most efficient j (i.e., 33.3 mA cm^{-2}). Fig. 4a depicts that longer time was needed for complete decolorization as dye concentration increased. The solution became colorless at 25, 30, 70 and 100 min for 115, 230, 345 and 460 mg L^{-1}, respectively. This tendency can be explained by the destruction of a lower proportion of dye under the production of similar amounts of BDD(•OH) and •OH with more organic matter. This was also found when TOC abatement was assessed. Fig. 4b shows that almost total mineralization (96–97% TOC decay) was always achieved from 360 to 480 min for contents from 115 to 460 mg L^{-1}. At the beginning of PEF–BDD, an induction period of 30–60 min was required for the mineralization process, which was more evident as initial dye content raised, suggesting the initial formation of very refractory products. In contrast, Fig. 4c shows a gradual increase in efficiency with rising organic load, with maximum MCE of 31% for 115 mg L^{-1} and 57% for 460 mg L^{-1}, which decayed to final values of 12% and 37%, respectively. These profiles suggest the favored attack of BDD(•OH) and •OH on greater quantities of organics, with parasitic Reactions (13)–(15) and (17) occurring to a much smaller extent.

The above study indicates that low j values and high dye contents are preferable for PEF-BDD in sulfate medium. Almost total mineralization with 37% current efficiency was achieved for 460 mg L^{-1} dye at 33.3 mA cm^{-2}.

3.3. *Effect of supporting electrolyte on the performance of PEF with BDD*

Comparative experiments were subsequently performed to clarify the effect of the supporting electrolyte on the PEF–BDD treatment of 230 mg L^{-1} Allura Red AC using 0.05 M of Na_2SO_4, $LiClO_4$, $NaNO_3$ or NaCl at 33.3 mA cm^{-2}. Fig. 5a highlights that decolorization efficiency decreased in the sequence $Cl^- > SO_4^{2-} \approx NO_3^- > ClO_4^-$. For example, after 30 min of electrolysis, the color was reduced by 93%, 89%, 89% and 86% using NaCl, Na_2SO_4, $NaNO_3$ and $LiClO_4$, respectively. This trend can be confirmed from the decreasing k_{dec} values determined for the independent experiments of Fig. 5a, which are listed in Table 1. These results differ from those reported by Daneshvar et al. [11] for the EF-Pt treatment of the Orange II azo dye at pH 3.0 using a graphite-felt cathode, which followed the order $ClO_4^- > Cl^- > SO_4^{2-}$. These authors ascribed the lower effectiveness of SO_4^{2-} to the loss of free Fe^{2+} owing to the formation of sulfate-iron complexes. In contrast,

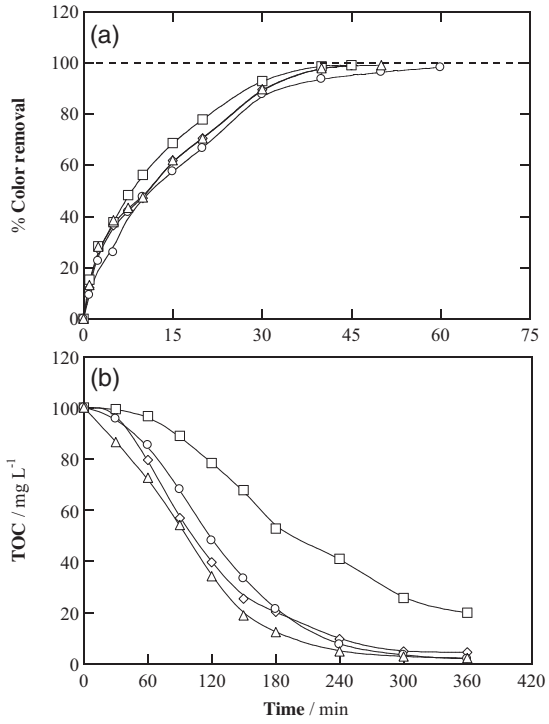

Fig. 5. Influence of the supporting electrolyte on (a) percentage of color removal at λ = 500 nm and (b) TOC decay with electrolysis time for the treatment of 130 mL of 230 mg L^{-1} Allura Red AC solutions in 0.05 M of (◊) Na_2SO_4, (○) $LiClO_4$, (△) $NaNO_3$ and (□) NaCl, with 0.5 mM Fe^{2+} at pH 3.0 by PEF–BDD at 33.3 mA cm^{-2}.

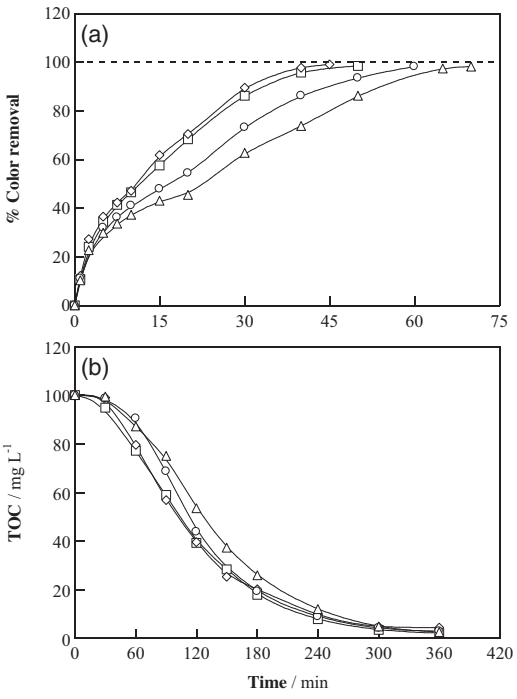

Fig. 6. Variation of (a) decolorization efficiency and (b) TOC abatement with electrolysis time for the PEF-BDD degradation of 230 mg L^{-1} Allura Red AC solutions in: (□) 0.025, (◊) 0.05, (○) 0.15 and (△) 0.30 M Na_2SO_4 with 0.5 mM Fe^{2+} at pH 3.0 and 33.3 mA cm^{-2}.

our results of Fig. 5a suggest a similar generation of BDD(•OH) and •OH in both SO_4^{2-} and ClO_4^- media giving a similar color removal. This apparent discrepancy could be due to the much greater H_2O_2 production with our air-diffusion cathode [3,7], yielding an analogous quantity of the main oxidant •OH in both electrolytes from Fenton's Reaction (2), even if lower free Fe^{2+} is available in SO_4^{2-} medium. Note that a remarkable enhancement of azo dye decolorization is usually found by EO using Cl^- instead of SO_4^{2-} [2,7]. Under the PEF-BDD conditions tested, however, only a slight increase in decolorization efficiency was determined in Cl^- medium (see Fig. 5a and Table 1). At pH 3.0, HClO generated from Reactions (4) and (5) is the pre-eminent active chlorine species [7], but it can be destroyed by generated H_2O_2 via Reaction (19) [42]. This means that the oxidizing species in Cl^- medium are BDD(•OH), •OH and HClO, but the concentration of the latter two is affected by Reaction (19), resulting in only a slight promotion of decolorization compared to the other media.

$$HClO + H_2O_2 \rightarrow Cl^- + O_{2(g)} + H_2O + H^+ \quad (19)$$

A different behavior can be observed in Fig. 5b for the mineralization process in the above electrolytes. While about 96–98% TOC decay was obtained for SO_4^{2-}, ClO_4^- and NO_3^- at 360 min, only 80% mineralization was achieved in Cl^-. The slower mineralization in the latter solution can be due to the attack of HClO on organics, therefore promoting the generation of chloroderivatives that are hardly destroyed by this oxidant and hydroxyl radicals [7,15]. Fig. 5b also shows a slight increase of mineralization rate in the sequence $ClO_4^- \leq SO_4^{2-} < NO_3^-$, as expected by a destruction of organics by similar amounts of BDD(•OH) and •OH. For example, after 180 min of treatment, TOC was reduced by 79% using $LiClO_4$, 80% using Na_2SO_4 and 88% using $NaNO_3$.

The changes in color and TOC removals for different Na_2SO_4 and NaCl concentrations are depicted in Figs. 6 and 7, respectively. Fig. 6a highlights analogous decolorization efficiency for 0.025 and 0.05 M SO_4^{2-} (k_{dec} from $(5.47 \pm 1.18) \times 10^{-2}$ min^{-1} to $(5.92 \pm 1.29) \times 10^{-2}$ min^{-1}), with an evident deceleration when SO_4^{2-} content increased to 0.15 and 0.30 M (k_{dec} of $(3.70 \pm 1.15) \times 10^{-2}$ min^{-1} and $(2.79 \pm 1.13) \times 10^{-2}$ min^{-1}, respec-

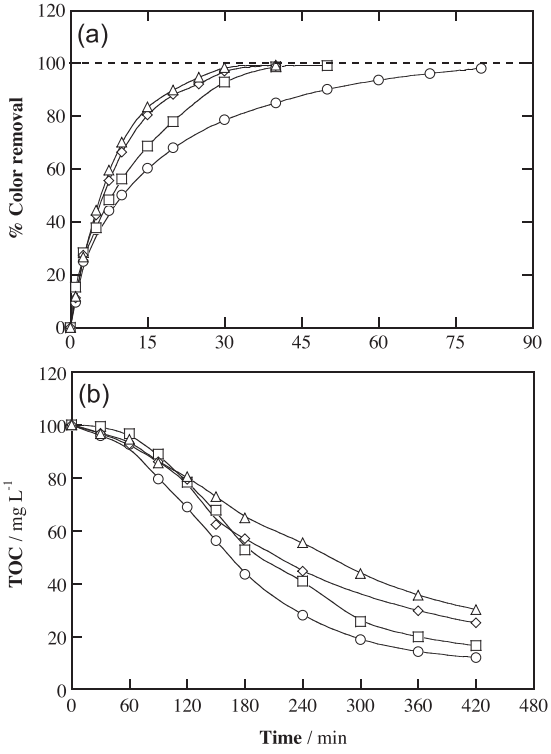

Fig. 7. (a) Decolorization efficiency and (b) TOC removal vs. electrolysis time under the same conditions of Fig. 6, but using: (○) 0.025, (□) 0.05, (◊) 0.10 and (△) 0.15 M NaCl.

tively). Nevertheless, quite similar TOC decays were found for all the SO_4^{2-} media, as shown Fig. 6b. This indicates a gradual loss of generated hydroxyl radicals with increasing SO_4^{2-} content, which can be due to the acceleration of Reactions (16) and (17) yielding more weaker oxidants such as $SO_4^{\bullet-}$ and $S_2O_8^{2-}$. Anyway, high enough BDD(•OH) and •OH amounts are produced to give almost total mineralization in all cases (see Fig. 6b).

According to Fig. 7a, complete decolorization was progressively reached at shorter time as Cl^- concentration rose from 0.025 to 0.15 M (k_{dec} from $(5.50 \pm 0.98) \times 10^{-2}$ min^{-1} to $(11.58 \pm 0.42) \times 10^{-2}$ min^{-1}), as a result of the larger HClO formation. Conversely, Fig. 7b evidences a slower mineralization rate with increasing Cl^- content, which can be explained by a greater production of more recalcitrant chloroderivatives from the oxidative action of HClO on intermediates. The PEF-BDD process is then more efficient at low salt concentration, since higher SO_4^{2-} and Cl^- contents cause a slower decolorization and mineralization, respectively.

3.4. Identification of reaction products

Table 2 summarizes the primary aromatic products detected by GC–MS at short electrolysis time during the PEF-BDD treatment in SO_4^{2-} and Cl^- solutions. These products are benzenic derivatives coming from the cleavage of the —N=N— bond of the dye (see Fig. 1). In SO_4^{2-} medium, hydroxylation of the C—N and C—S bonds, followed by oxidation of hydroxyl groups, yielded 2-methoxy-5-methyl-*p*-benzoquinone, whereas hydroxylation and carboxylation of the methyl substituent gave 4-methoxy-3-hydroxybenzoic acid. In Cl^- solutions, chlorination along with hydroxylation, demethylation and carboxylation were the predominant reactions giving 4-chlorocatechol, 2,5-dichloro-1-methoxy-4-methylbenzene and 3,4-dichlorobenzoic acid. This confirms that active chlorine species entail the formation of recalcitrant chloroderivatives. All these aromatic products were completely removed at electrolysis times higher than 120 min. Ion-exclusion HPLC analysis of the solutions degraded under the conditions of Fig. 2 revealed the formation of short-chain carboxylic acids like maleic, fumaric, tartronic, formic, oxalic and oxamic acids, which form Fe(III)-carboxylate complexes [3,7]. The former three acids result from the cleavage of the aromatic moieties and are oxidized to formic and oxalic acids [25,27], whereas oxamic acid can proceed from the destruction of *N*-intermediates. These three acids (or their Fe(III) complexes) are directly mineralized to CO_2 [7,29,43]. The evolution of the persistent oxalic and oxamic acids is shown in Fig. 8a and b, respectively. In EO–H_2O_2–Pt, only a poor accumulation of oxamic acid up to 0.14 mg L^{-1} (see Fig. 8b) was found, in agreement with the negligible TOC removal shown in Fig. 2b. Maleic, fumaric, tartronic and formic acids reached maximum contents of 0.57, 0.37, 4.4 and 17.3 mg L^{-1} for the other EAOPs with Pt. All these products disappeared in 180–240 min mainly by the efficient attack of •OH over their Fe(III) complexes. However, Fig. 8a and b highlight large accumulations up to 72.6 mg L^{-1} of oxalic acid and 1.6 mg L^{-1} of oxamic acid for EF-Pt, indicating that their Fe(III) complexes are not removed by hydroxyl radicals. In contrast, the potent photolytic action in PEF-Pt caused the total removal of Fe(III)-oxalate species at 300 min, whereas Fe(III)-oxamate complexes were so slowly photolyzed that 1.3 mg L^{-1} of oxamic acid still remained at 360 min. The remaining acids accounted for 19.7 and 0.4 mg L^{-1} TOC in EF-Pt and PEF-Pt, respectively, being 47% and 8% of TOC determined in the corresponding final solutions (see Fig. 2b).

The more efficient oxidation by BDD(•OH) enhanced the destruction of carboxylic acids and precedent intermediates, as can be seen in Fig. 8a and b for oxalic and oxamic acids. After 360 min of EO-H_2O_2-BDD, 1.5, 9.7 and 0.12 mg L^{-1} of oxalic, formic and oxamic acids were present in the electrolyzed solution, corresponding to 3.0 mg L^{-1} TOC and representing 11% of its organic load (see Fig. 2). At that time, 18.8 mg L^{-1} of oxalic acid related to 43% of final TOC were only detected in EF-BDD, whereas no carboxylic acids were found for PEF-BDD. The BDD(•OH) radical is then unable to convert all the intermediates into final carboxylic acids and a large proportion of unidentified products is accumulated at the end of EO-H_2O_2-BDD. The additional oxidation by •OH in EF-BDD allowed a greater mineralization, which was further promoted in PEF-BDD by the photolytic action on iron complexes.

Inorganic ions released to solutions with 0.05 M $LiClO_4$ treated by the EAOPs with BDD at 100 mA cm^{-2} were quantified by ion chromatography. The N atom of the dye (13.0 mg L^{-1}) was preferentially transformed into NO_3^- ion and, to a smaller extent, into NH_4^+ ion, with maximum accumulations of 28.6 mg L^{-1} (49.9% of initial N) and 5.0 mg L^{-1} (30.0% of initial N), respectively. A significant proportion of the initial N was then lost as volatile *N*-products, like N_2 and N_xO_y, as reported for similar treatments of other azo dyes [17,27,29]. Fig. 9 depicts that SO_4^{2-} ion generated from the

Table 2
Primary aromatic products identified at short electrolysis time during the PEF-BDD degradation of Allura Red AC by GC–MS under the conditions of Fig. 5 using 0.05 M Na_2SO_4 or NaCl.

Product	
Na_2SO_4	NaCl
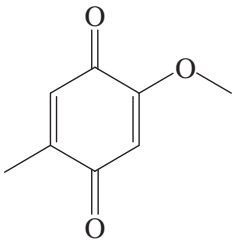 $m/z = 152$ 2-Methoxy-5-methyl-*p*-benzoquinone	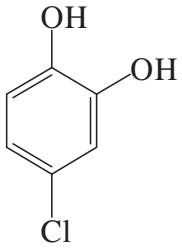 $m/z = 144$ 4-Chlorocatechol
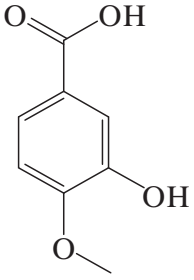 $m/z = 168$ 4-Methoxy-3-hydroxybenzoic acid	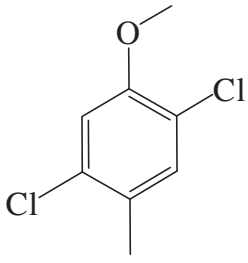 $m/z = 190$ 2,5-Dichloro-1-methoxy-4-methylbenzene
	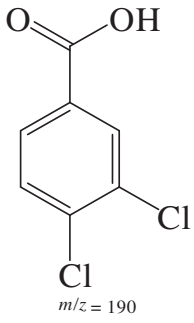 $m/z = 190$ 3,4-Dichlorobenzoic acid

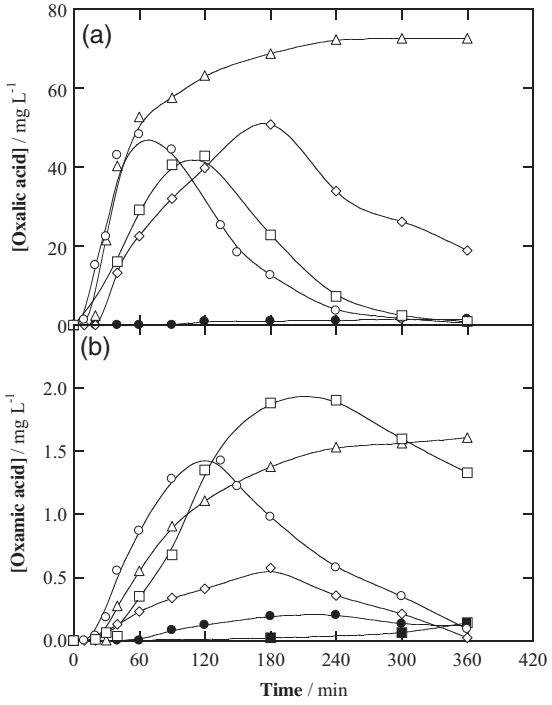

Fig. 8. Evolution of the concentration of (a) oxalic and (b) oxamic acids formed during the trials of Fig. 2.

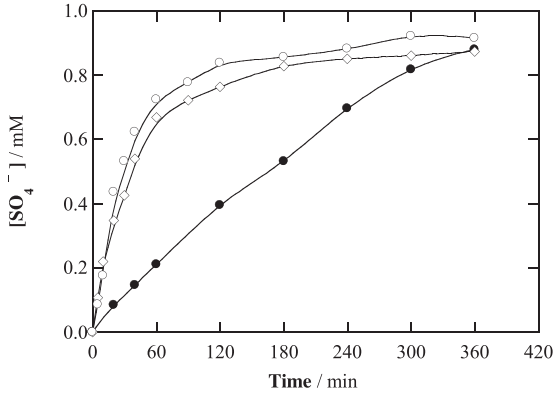

Fig. 9. Time course of the concentration of sulfate ion during the treatment of 130 mL of 230 mg L^{-1} azo dye solutions in 0.05 M $LiClO_4$ at pH 3.0 and 100 mA cm^{-2} using a BDD anode. Method: (●) EO–H_2O_2–BDD, (◊) EF–BDD with 0.5 mM Fe^{2+} and (○) PEF–BDD with 0.5 mM Fe^{2+}.

S atom of the dye (0.93 mM) was rapidly released in EF-BDD and PEF-BDD reaching 0.87 mM (92% of initial S) and 0.91 mM (98% of initial S), respectively, whereas the less efficient EO-H_2O_2-BDD process yielded a slower loss of 0.88 mM (93% of initial S). Therefore, most intermediates containing the $-SO_3$ group were destroyed by all EAOPs with quantitative formation of SO_4^{2-} ion. These findings demonstrate that NO_3^- and SO_4^{2-} are the major ions formed in the mineralization of Allura Red AC, as proposed in Reaction (12).

4. Conclusions

PEF–BDD was the most efficient EAOP to decolorize and mineralize Allura Red AC solutions. Almost total mineralization with 96–98% TOC reduction was attained for 115–460 mg L^{-1} of dye at 33.3–150 mA cm^{-2}. Higher current efficiencies were found operating at greater dye contents and lower *j* values. A similar degradation rate was found in PEF–BDD using SO_4^{2-}, ClO_4^- and NO_3^- media because generated BDD(•OH) and •OH were always the main oxidizing agents. In Cl^- solutions, the oxidative destruction by generated HClO was inhibited by its reaction with H_2O_2, also diminishing •OH production. Higher SO_4^{2-} and Cl^- contents inhibited the decolorization and mineralization processes due to the formation of peroxodisulfate ion and refractory chloroderivatives, respectively. GC–MS confirmed the formation of three chlorocompounds coming from the hydroxylation, demethylation, carboxylation and chlorination of the benzenic moiety. The total removal of Fe(III)-oxalate and Fe(III)-oxamate complexes under the action of UVA radiation explained the superiority of PEF–BDD.

Acknowledgments

The authors thank MINECO (Spain) for financial support under project CTQ2013-48897-C2-1-R, co-financed with FEDER funds. The Ph.D. grant awarded to A. Thiam from MAEC-AECID (Spain) is also acknowledged.

References

[1] A. Özcan, M.A. Oturan, N. Oturan, Y. Şahin, Removal of acid orange 7 from water by electrochemically generated Fenton's reagent, J. Hazard. Mater. 163 (2009) 1213–1220.
[2] M. Panizza, G. Cerisola, Direct and mediated anodic oxidation of organic pollutants, Chem. Rev. 109 (2009) 6541–6569.
[3] I. Sirés, E. Brillas, Remediation of water pollution caused by pharmaceutical residues based on electrochemical separation and degradation technologies: a review, Environ. Int. 40 (2012) 212–229.
[4] L. Feng, E.D. van Hullebusch, M.A. Rodrigo, G. Esposito, M.A. Oturan, Removal of residual anti-inflammatory and analgesic pharmaceuticals from aqueous systems by electrochemical advanced oxidation processes. A review, Chem. Eng. J. 228 (2013) 944–964.
[5] I. Sirés, E. Brillas, M.A. Oturan, M.A. Rodrigo, M. Panizza, Electrochemical advanced oxidation processes: today and tomorrow. A review, Environ. Sci. Pollut. Res. 21 (2014) 8336–8367.
[6] S. Vasudevan, M.A. Oturan, Electrochemistry: as cause and cure in water pollution – an overview, Environ. Chem. Lett. 12 (2014) 97–108.
[7] E. Brillas, C.A. Martínez-Huitle, Decontamination of wastewaters containing synthetic organic dyes by electrochemical methods. An updated review, Appl. Catal. B: Environ. 166–167 (2015) 603–643, http://dx.doi.org/10.1016/j.apcatb.2014.11.016.
[8] E. Rosales, M. Pazos, M.A. Longo, M.A. Sanromán, Electro-Fenton decoloration of dyes in a continuous reactor: a promising technology in colored wastewater treatment, Chem. Eng. J. 155 (2009) 62–67.
[9] A. Khataee, A. Khataee, M. Fathinia, B. Vahid, S.W. Joo, Kinetic modeling of photoassisted-electrochemical process for degradation of an azo dye using boron-doped diamond anode and cathode with carbon nanotubes, J. Ind. Eng. Chem. 19 (2013) 1890–1894.
[10] A. Wang, J. Qu, H. Liu, J. Ru, Mineralization of an azo dye Acid Red 14 by photoelectro-Fenton process using an activated carbon fiber cathode, Appl. Catal. B: Environ. 84 (2008) 393–399.
[11] N. Daneshvar, S. Aber, V. Vatanpour, M.H. Rasoulifard, Electro-Fenton treatment of dye solution containing Orange II: influence of operational parameters, J. Electroanal. Chem. 615 (2008) 165–174.
[12] M. Panizza, M.A. Oturan, Degradation of alizarin red by electro-Fenton process using a graphite-felt cathode, Electrochim. Acta 56 (2011) 7084–7087.
[13] N. Oturan, E. Brillas, M.A. Oturan, Unprecedented total mineralization of atrazine and cyanuric acid by anodic oxidation and electro-Fenton with a boron-doped diamond anode, Environ. Chem. Lett. 10 (2012) 165–170.
[14] A. Dirany, I. Sireís, N. Oturan, A. Özcan, M.A. Oturan, Electrochemical treatment of the antibiotic sulfachloropyridazine: kinetics, reaction pathways, and toxicity evolution, Environ. Sci. Technol. 46 (2012) 4074–4082.
[15] C. Salazar, I. Sirés, C.A. Zaror, E. Brillas, Treatment of a mixture of chloromethoxyphenols in hypochlorite medium by electrochemical AOPs as an alternative for the remediation of pulp and paper mill process waters, Electrocatalysis 4 (2013) 212–223.
[16] A. Thiam, M. Zhou, E. Brillas, I. Sirés, Two-step mineralization of Tartrazine solutions: study of parameters and by-products during the coupling of electrocoagulation with electrochemical advanced oxidation processes, Appl. Catal. B: Environ. 150–151 (2014) 116–125.
[17] A. Thiam, I. Sirés, J.A. Garrido, R.M. Rodríguez, E. Brillas, Effect of anions on electrochemical degradation of azo dye carmoisine (Acid Red 14) using a BDD anode and air-diffusion cathode, Sep. Purif. Technol. 140 (2015) 43–52.
[18] M.A. Rodrigo, P. Cañizares, A. Sánchez-Carretero, C. Sáez, Use of conductive-diamond electrochemical oxidation for wastewater treatment, Catal. Today 151 (2010) 173–177.

[19] C. Flox, J.A. Garrido, R.M. Rodríguez, F. Centellas, P.L. Cabot, C. Arias, E. Brillas, Degradation of 4,6-dinitro-*o*-cresol from water by anodic oxidation with a boron-doped diamond electrode, Electrochim. Acta 50 (2005) 3685–3692.
[20] M. Hamza, R. Abdelhedi, E. Brillas, I. Sirés, Comparative electrochemical degradation of the triphenylmethane dye Methyl Violet with boron-doped diamond and Pt anodes, J. Electroanal. Chem. 627 (2009) 41–50.
[21] L. Ciríaco, C. Anjo, J. Correia, M.J. Pacheco, A. Lopes, Electrochemical degradation of ibuprofen on Ti/Pt/PbO_2 and Si/BDD electrodes, Electrochim. Acta 54 (2009) 1464–1472.
[22] E.B. Cavalcanti, S. Garcia-Segura, F. Centellas, E. Brillas, Electrochemical incineration of omeprazole in neutral aqueous medium using a platinum or boron-doped diamond. Degradation kinetics and oxidation products, Water Res. 47 (2013) 1803–1815.
[23] M. Zhou, Q. Tan, Q. Wang, Y. Jiao, N. Oturan, M.A. Oturan, Degradation of organics in reverse osmosis concentrate by electro-Fenton process, J. Hazard. Mater. 215–216 (2012) 287–293.
[24] Y. Lei, H. Liu, Z. Shen, W. Wang, Development of a trickle bed reactor of electro-Fenton process for wastewater treatment, J. Hazard. Mater. 261 (2013) 570–576.
[25] E. Guinea, J.A. Garrido, R.M. Rodríguez, P.L. Cabot, C. Arias, F. Centellas, E. Brillas, Degradation of the fluoroquinolone enrofloxacin by electrochemical advanced oxidation processes based on hydrogen peroxide electrogeneration, Electrochim. Acta 55 (2010) 2101–2115.
[26] E. Isarain-Chávez, J.A. Garrido, R.M. Rodríguez, F. Centellas, C. Arias, P.L. Cabot, E. Brillas, Mineralization of metoprolol by electro-Fenton and photoelectro-Fenton processes, J. Phys. Chem. A 115 (2011) 1234–1242.
[27] E.J. Ruiz, A. Hernández-Ramírez, J.M. Peralta-Hernández, C. Arias, E. Brillas, Application of solar photoelectro-Fenton technology to azo dyes mineralization: effect of current density, Fe^{2+} and dye concentration, Chem. Eng. J. 171 (2011) 385–392.
[28] R. Salazar, E. Brillas, I. Sirés, Finding the best Fe^{2+}/Cu^{2+} combination for the solar photoelectro-Fenton treatment of simulated wastewater containing the industrial textile dye Disperse Blue 3, Appl. Catal. B: Environ. 115–116 (2012) 107–116.
[29] F.C. Moreira, S. Garcia-Segura, V.J.P. Vilar, R.A.R. Boaventura, E. Brillas, Decolorization and mineralization of Sunset Yellow FCF azo dye by anodic oxidation electro-Fenton, UVA photoelectro-Fenton and solar photoelectro-Fenton processes, Appl. Catal. B: Environ. 142–143 (2013) 877–890.
[30] T. Robinson, G. McMullan, R. Marchant, P. Nigam, Remediation of dyes in textile effluent: a critical review on current treatment technologies with a proposed alternative, Biores. Technol. 77 (2001) 247–255.
[31] H. Zollinger, Color Chemistry: Synthesis, Properties, and Applications of Organic Dyes and Pigments, VHCA and Wiley-VCH, Switzerland, 2003.
[32] K. Hunger (Ed.), Industrial Dyes Chemistry, Properties, Applications, Wiley-VCH, Germany, 2003.
[33] E. Forgacs, T. Cserháti, G. Oros, Removal of synthetic dyes from wastewaters: a review, Environ. Int. 30 (2004) 953–971.
[34] M. Solís, A. Solís, H.I. Pérez, N. Manjarrez, M. Flores, Microbial decolouration of azo dyes: a review, Process Biochem. 47 (2012) 1723–1748.
[35] UNESCO, Managing Water Report under Uncertainty and Risk, 2012.
[36] K.P. Sharma, S. Sharma, S. Sharma, P.K. Singh, S. Kumar, R. Grover, P.K. Sharma, A comparative study on characterization of textile wastewaters (untreated and treated) toxicity by chemical and biological tests, Chemosphere 69 (2007) 48–54.
[37] S.M.A.G. Ulson de Souza, E. Forgiarini, A.A. Ulson de Souza, Toxicity of textile dyes and their degradation by the enzyme horseradish peroxidase (HRP), J. Hazard. Mater. 147 (2007) 1073–1078.
[38] EFSA, Assessment of the results of the study by McCann et al. (2007) on the effect of some colours and sodium benzoate on children's behaviour, EFSA J., 660, (2008), 1–54.
[39] EFSA, Scientific opinion on the re-evaluation of Allura Red AC (E 129) as a food additive, EFSA J., 7, (2009), 1327.
[40] G.A. Epling, C. Lin, Photoassisted bleaching of dyes utilizing TiO_2 and visible light, Chemosphere 46 (2002) 561–570.
[41] D. Khamis, E. Mahé, F. Dardoize, D. Devilliers, Peroxodisulfate generation on boron-doped diamond microelectrodes array and detection by scanning electrochemical microscopy, J. Appl. Electrochem. 40 (2010) 1829–1838.
[42] J. De Laat, G.T. Le, B. Legube, A comparative study of the effects of chloride, sulfate, and nitrate ions on the rates of decomposition of H_2O_2 and organic compounds by Fe(II)/H_2O_2 and Fe(III)/H_2O_2, Chemosphere 55 (2004) 715–723.
[43] S. Garcia-Segura, E. Brillas, Mineralization of the recalcitrant oxalic and oxamic acids by electrochemical advanced oxidation processes using a boron-doped diamond anode, Water Res. 45 (2011) 2975–2984.

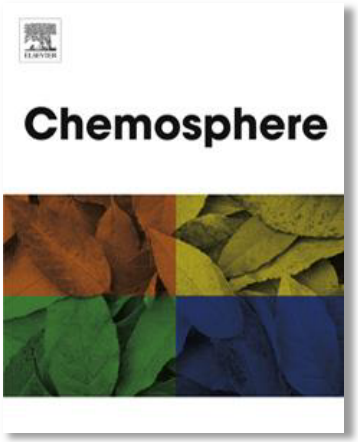

Paper 4

Decolorization and mineralization of Allura Red AC azo dye by solar photoelectro-Fenton: Identification of intermediates

---

Chemosphere

136 (2015) 1–8

Chemosphere 136 (2015) 1–8

Contents lists available at ScienceDirect

Chemosphere

journal homepage: www.elsevier.com/locate/chemosphere

Decolorization and mineralization of Allura Red AC azo dye by solar photoelectro-Fenton: Identification of intermediates

Abdoulaye Thiam, Ignasi Sirés, Francesc Centellas, Pere Lluís Cabot, Enric Brillas *

Laboratori d'Electroquímica dels Materials i del Medi Ambient, Departament de Química Física, Facultat de Química, Universitat de Barcelona, Martí i Franquès 1-11, 08028 Barcelona, Spain

HIGHLIGHTS

- Allura Red AC azo dye degraded by EF and SPEF in a 2.5 L flow plant.
- Rapid decolorization and almost total mineralization by SPEF with a Pt/air-diffusion cell.
- Fast total decolorization but poor mineralization achieved under EF conditions.
- Identification of 16 aromatic intermediates and 11 aliphatic carboxylic acids.
- Release of sulfate and nitrate ions, with a large proportion of volatile *N*-derivatives.

ARTICLE INFO

Article history:
Received 19 January 2015
Received in revised form 25 February 2015
Accepted 21 March 2015

Handling Editor: Min Jang

Keywords:
Allura Red AC
Electro-Fenton
Oxidation products
Solar photoelectro-Fenton
Water treatment

ABSTRACT

The degradation of 2.5 L of Allura Red AC solutions in sulfate medium containing 0.50 mM Fe^{2+} has been studied by solar photoelectro-Fenton (SPEF) using a flow plant equipped with a Pt/air-diffusion cell and a solar photoreactor. Comparative electro-Fenton treatment yielded rapid total decolorization but poor mineralization, since most products were slowly destroyed by ·OH formed from Fenton's reaction between Fe^{2+} and H_2O_2 generated at the air-diffusion cathode. In contrast, the potent action of UV radiation from sunlight in SPEF allowed the rapid photolysis of recalcitrant intermediates, thus giving rise to a quick mineralization. Sulfate and nitrate ions, along with a large proportion of volatile *N*-derivatives, were always released. The increase in current density and decrease in azo dye concentration accelerated the decolorization and mineralization in SPEF, although lower current efficiency and greater specific energy consumption were obtained. The most cost-effective SPEF treatment was found for 460 mg L^{-1} azo dye in 0.05 M Na_2SO_4 at 50 mA cm^{-2}, which yielded 95% mineralization with 81% current efficiency and 8.50 kW h m^{-3}. No significant effect of sulfate concentration was found. Up to 16 aromatic intermediates and 11 short-chain carboxylic acids, including oxalic and oxamic as the most persistent ones, were detected by GC–MS and HPLC. The large oxidation ability of SPEF can be explained by the quick photolysis of Fe(III)-oxalate complexes and other undetected intermediates.

1. Introduction

About 70% of the world dye production corresponds to azo compounds, which are characterized by one or various azo chromophores (—N=N—) attached to benzene and/or naphthalene rings with lateral —OH and $—SO_3H$ groups (Solís et al., 2012; Brillas and Martínez-Huitle, 2015). They are used in many industries due to their interesting properties like brilliant shades, relative low cost and simple manufacture (Robinson et al., 2001; Hunger, 2003; Zollinger, 2003; Forgacs et al., 2004). However, there is increasing concern on the environmental impact of dyeing industrial effluents (UNESCO, 2012), since they may contain high levels of dyestuffs (i.e., 100–250 mg L^{-1}) and cause aesthetic problems and toxic effects on living beings (Sharma et al., 2007; Ulson de Souza et al., 2007). In particular, according to the European Food Safety Authority (EFSA, 2008, 2009), food azo dyes can be hazardous because they are connected to children hyperactivity and possible allergies and intolerances. This is the case of Allura Red AC, so-called food additive E129 (disodium 6-hydroxy-5-[(2-methoxy-5-methyl-4-sulfophenyl)azo]-2-naphthalenesulfonate, $C_{18}H_{14}N_2O_8S_2Na_2$, λ_{max} = 500 nm, M = 496.43 g mol^{-1}), which has been banned in some European countries. Azo dyes cannot be removed in municipal wastewater treatment plants by

* Corresponding author. Tel.: +34 934021223; fax: +34 934021231.
E-mail address: brillas@ub.edu (E. Brillas).

http://dx.doi.org/10.1016/j.chemosphere.2015.03.047
0045-6535/

conventional biological and physicochemical methods (Robinson et al., 2001; Forgacs et al., 2004) and hence, more effective processes are needed for avoiding their hazardous impacts. Regarding Allura Red AC, only its degradation by TiO_2 photocatalysis with visible light has been reported (Epling and Lin, 2002).

Electrochemical advanced oxidation processes (EAOPs) have shown great effectiveness for the remediation of contaminated waters (Özcan et al., 2009; Feng et al., 2013; Sirés et al., 2014; Vasudevan and Oturan, 2014). The high oxidation power of EAOPs arises from the generation of hydroxyl radical (·OH), which is able to degrade most organics up to their total mineralization. Recently, some of our research has been focused in developing a particular EAOP called solar photoelectro-Fenton (SPEF), aiming at its future application for the treatment of industrial wastewater. In SPEF, H_2O_2 is supplied to the effluent from the two-electron reduction of O_2 at a carbonaceous cathode by reaction (1) (Sirés and Brillas, 2012). Graphite (Rosales et al., 2009), carbon nanotubes (Khataee et al., 2013), activated carbon fiber (Wang et al., 2008), carbon sponge (Daneshvar et al., 2008), graphite felt (Panizza and Oturan, 2011), carbon felt (Özcan et al., 2009; Dirany et al., 2012; Oturan et al., 2012) and carbon-polytetrafluoroethylene (PTFE) gas (O_2 or air) diffusion (Boye et al., 2003; Ammar et al., 2006; Ruiz et al., 2011a; Thiam et al., 2014) are the most suitable cathodes.

$$O_{2(g)} + 2H^+ + 2e^- \rightarrow H_2O_2 \quad (1)$$

The oxidizing ability of H_2O_2 is enhanced in the presence of small amounts of Fe^{2+} to produce Fe^{3+} and ·OH in the bulk from Fenton's reaction (2) at optimum pH ~ 3 (Sirés et al., 2014). This reaction is propagated from the regeneration of Fe^{2+} via reaction (3), thereby maintaining a high rate for the destruction of organics (Feng et al., 2013).

$$H_2O_2 + Fe^{2+} \rightarrow Fe^{3+} + {}^{\cdot}OH + OH^- \quad (2)$$

$$Fe^{3+} + e^- \rightarrow Fe^{2+} \quad (3)$$

If the treatment is carried out in the dark, the electrolytic system only produces ·OH via reactions (1)–(3) and the process is called electro-Fenton (EF). In undivided cells, organics can be simultaneously oxidized by ·OH generated from reaction (2) and physisorbed M(·OH) formed from water oxidation at the surface of a large O_2-overpotential anode M (Panizza and Cerisola, 2009):

$$M + H_2O \rightarrow M({}^{\cdot}OH) + H^+ + e^- \quad (4)$$

In SPEF, the solution is degraded under EF conditions with sunlight irradiation as an inexpensive and renewable energy source. The UV photons promote: (i) photoreduction of $Fe(OH)^{2+}$ by reaction (5), with Fe^{2+} regeneration and additional ·OH production, and (ii) photolytic reaction (6) that destroys Fe(III)-carboxylate intermediates (Sirés et al., 2014; Brillas and Martínez-Huitle, 2015).

$$Fe(OH)^{2+} + h\nu \rightarrow Fe^{2+} + {}^{\cdot}OH \quad (5)$$

$$Fe(OOCR)^{2+} + h\nu \rightarrow Fe^{2+} + CO_2 + R^{\cdot} \quad (6)$$

In previous work, our group has assessed the SPEF treatment of several dye solutions using a boron-doped diamond (BDD) and air-diffusion cathode (Ruiz et al., 2011a,b; Salazar et al., 2011, 2012). A more recent study by Moreira et al. (2013) showed that the alternative use of a Pt anode also allowed the degradation of Sunset Yellow FCF azo dye, despite the lower oxidation power of Pt(·OH) compared to BDD(·OH) (Panizza and Cerisola, 2009). The viability of low oxidation power anodes is very interesting as for the industrial application of SPEF; considering the same current density (j), the potential difference between anode and cathode is much lower compared to BDD reactors, which enhances the cost-effectiveness of SPEF.

To gain better knowledge on the ability of SPEF with a Pt/air-diffusion cell to remove azo dyes, this study reports the decolorization and mineralization of Allura Red AC aqueous solutions at pH 3.0 using a solar flow plant. Comparative EF experiments were made to clarify the role of generated hydroxyl radicals. The effect of j and electrolyte and dye concentrations was thoroughly examined. Aromatic intermediates were detected by gas chromatography-mass spectrometry (GC–MS), whereas generated short-chain carboxylic acids and released inorganic ions were identified by chromatographic techniques.

2. Experimental

2.1. Chemicals

Allura Red AC (80% purity) was supplied by Sigma–Aldrich. Na_2SO_4 used as background electrolyte and $FeSO_4{\cdot}7H_2O$ used as catalyst were of analytical grade purchased from Merck and Fluka, respectively. Solutions were prepared with deionized water and their pH was adjusted with analytical grade H_2SO_4 from Merck. Carboxylic acids and other chemicals and solvents for analyses were of HPLC or analytical grade supplied by Merck, Sigma–Aldrich and Panreac.

2.2. Solar flow plant

A sketch of the batch recirculation flow plant was reported elsewhere (Ruiz et al., 2011a). 2.5 L of the solution were introduced into the reservoir of the plant and recirculated by means of a centrifugal pump. The flow rate was kept at 200 L h^{-1} with a flowmeter and the temperature was regulated at 35 °C with two heat exchangers. The electrochemical cell was an undivided filter-press reactor with a 20 cm^2 Pt sheet anode of 99.99% purity from SEMPSA (Barcelona, Spain) and a 20 cm^2 carbon- PTFE air-diffusion cathode from E-TEK (Somerset, NJ, USA). The interelectrode distance was 1.2 cm. The inner face of the cathode was in contact with a PVC gas chamber fed with an air flow at an overpressure of about 8.6 kPa regulated with a back-pressure gauge for continuous H_2O_2 production. The experiments were performed at constant j by using an Agilent 6552A DC power supply, which directly measured the potential difference between the anode and cathode. The outlet of the electrochemical cell was connected to a planar solar photoreactor with 600 mL of irradiated volume tilted 41° to better collect the direct sunrays. Once irradiated, the solution was directed toward the reservoir. Comparative EF trials were made in the dark by covering the plant with an opaque plastic. SPEF assays were performed during the summer of 2014 in our laboratory of Barcelona (latitude 41°21′N, longitude 2°10′E). The UV radiation intensity (300–400 nm) was in the range of 30–32 W m^{-2}, as measured with a Kipp & Zonen CUV 5 radiometer.

2.3. Apparatus and analytical procedures

The solution pH was measured on a Crison 2000 pH-meter. Samples withdrawn at regular time intervals from treated solutions were microfiltered with 0.45 μm PTFE filters from Whatman before immediate analysis. H_2O_2 concentration was obtained from the light absorption of its Ti(IV) colored complex at λ = 408 nm, measured on a Shimadzu 1800 UV/Vis spectrophotometer at 35 °C (Welcher, 1975). The decolorization of solutions was monitored from the absorbance decay at their λ_{max} = 500 nm, determined on the same spectrophotometer at 35 °C. Their

mineralization was assessed from their total organic carbon (TOC) removal, measured on a Shimadzu VCSN TOC analyzer. Samples of 50 μL were injected into the analyzer and reproducible TOC values with ±1% accuracy were obtained.

To identify the reaction products formed in EF and SPEF, the organic components of solutions electrolyzed for short and long times were extracted out thrice with CH_2Cl_2. The resulting organic fraction was dried over anhydrous Na_2SO_4, filtered and rotavaporated up to ca. 1 mL to be analyzed by GC–MS. Organics were also derivatized using ethanol or acetic anhydride as explained by Guinea et al. (2010). GC–MS analysis was made with an Agilent Technologies system composed of a 6890 N GC and a 5975C MS operating in EI mode at 70 eV. Non-polar Agilent J&W HP-5 ms and polar HP INNOWax columns, both of 0.25 μm, 30 m × 0.25 mm, were used. The temperature ramp was: 36 °C for 1 min, 5 °C min^{-1} up to 300 or 250 °C for the non-polar or polar column, respectively, and hold time 10 min. The temperature of the inlet, source and transfer line was 250, 230 and 280 °C for the non-polar column and 250, 230 and 250 °C for the polar one. The mass spectra were identified with a NIST05-MS library.

Short-linear aliphatic carboxylic acids were quantified by ion-exclusion HPLC using a Waters 600 LC equipped with a Bio-Rad Aminex HPX 87H, 300 mm × 7.8 mm, column at 35 °C and coupled to a Waters 996 photodiode detector set at λ = 210 nm. This analysis was made by injecting 20 μL aliquots into the LC and circulating a 4 mM H_2SO_4 solution as the mobile phase at 0.6 mL min^{-1}. NH_4^+, NO_3^- and SO_4^{2-} ions were quantified as previously reported (Thiam et al., 2015).

3. Results and discussion

3.1. H_2O_2 accumulation in the flow plant

The ability of the Pt/air-diffusion cell to produce H_2O_2 in the flow plant was assessed by electrolyzing 2.5 L with 0.05 M Na_2SO_4 of pH 3.0 at 10, 25, 50, 75 and 100 mA cm^{-2} for 240 min in the absence and presence of sunlight. As shown in Fig. SM-1, maximum H_2O_2 contents of 3.0, 8.3, 17.6, 28.3 and 32.0 mM, respectively, were determined in the bulk regardless of the irradiation conditions. Based on Faraday's law, the current efficiency for H_2O_2 accumulation under such conditions was 50%, 56%, 59%, 63% and 54%, respectively, meaning that 25–75 mA cm^{-2} yielded the best efficiencies to accumulate H_2O_2 in the flow plant.

A plateau is reached at each j once the H_2O_2 production rate becomes equal to its destruction rate, which is due to its two-electron reduction to OH^- at the cathode and, mainly, its two-electron oxidation to O_2 at the anode via reactions (7) and (8) that involve the formation of hydroperoxyl radical ($HO_2^{\cdot}$), a much weaker oxidant than ·OH (Ruiz et al., 2011a; Sirés et al., 2014):

$$H_2O_2 \rightarrow HO_2^{\cdot} + H^+ + e^- \quad (7)$$

$$HO_2^{\cdot} \rightarrow O_2 + H^+ + e^- \quad (8)$$

A further assay was made by electrolyzing a 0.05 M Na_2SO_4 solution upon addition of 0.50 mM Fe^{2+} at 50 mA cm^{-2} under solar irradiation. After 240 min, only 8.0 mM H_2O_2 was accumulated in the bulk, which is half the value found in the absence of Fe^{2+}. This drop in H_2O_2 content can be related to its loss from Fenton's reaction (2), where Fe^{2+} is continuously regenerated due to reaction (5). The small H_2O_2 surplus along the electrolyses ensures the continuous maximum production of ·OH in the bulk from the above reactions. Therefore, the most efficient degradation of Allura Red AC by this radical is expected under EF and SPEF conditions.

3.2. Decolorization of Allura Red AC solutions by EF and SPEF

The electrochemical degradation of 2.5 L of 230 mg L^{-1} of the dye was comparatively studied in the flow plant by EF and SPEF using 0.05 M Na_2SO_4 as supporting electrolyte and 0.50 mM Fe^{2+} as catalyst at pH 3.0 and 50 mA cm^{-2}. Such Fe^{2+} content was chosen because it was optimal for the SPEF degradation of other azo dyes (Ruiz et al., 2011b; Moreira et al., 2013). The initial yellowish red solution was gradually decolorized and, from the absorbance at initial time (A_0) and after an electrolysis time t (A_t) at λ_{max} = 500 nm, the decolorization efficiency or percentage of color removal was determined from Eq. (9) (Ruiz et al., 2011a):

$$\text{Color removal } (\%) = \frac{A_0 - A_t}{A_0} \times 100 \quad (9)$$

Fig. 1 shows a rapid color removal of the Allura Red AC solution, becoming colorless after about 60 min of EF and 40 min of SPEF. Since analogous H_2O_2 production is expected in both trials as explained above, the superiority of SPEF can be related to the additional generation of ·OH induced by reaction (5). Analysis of the absorbance decays revealed that they always obeyed a pseudo-first-order kinetics. From the corresponding $\ln([A_0]/[A_t])$ vs t plots, an apparent rate constant for decolorization (k_{dec}) of $(8.06 \pm 0.52) \times 10^{-2}$ and $(9.98 \pm 0.13) \times 10^{-2}$ min^{-1} was found for the EF and SPEF processes, respectively. This behavior is quite similar to that found for the color removal of 108 and 119 mg L^{-1} of azo dyes Acid Yellow 36 (Ruiz et al., 2011a) and Acid Red 88 (Ruiz et al., 2011b); in those studies, performed under the same conditions but using a BDD/air-diffusion cell, 80 and 40 min were needed, respectively, for complete decolorization by SPEF. However, Acid Yellow 36 was totally removed in only 25 min, suggesting that the decolorization of azo dye solutions is much slower than the initial dye removal because the former one also involves the destruction of colored aromatic intermediates that absorb at λ similar to that of the parent molecule. Consequently, it is not possible to directly compare the decolorization efficiency of azo dyes since it depends on the colored intermediates produced and their destruction rate with hydroxyl radicals. The effect of j and sulfate and dye contents on color removal by SPEF, not previously checked for other azo dyes, was further examined.

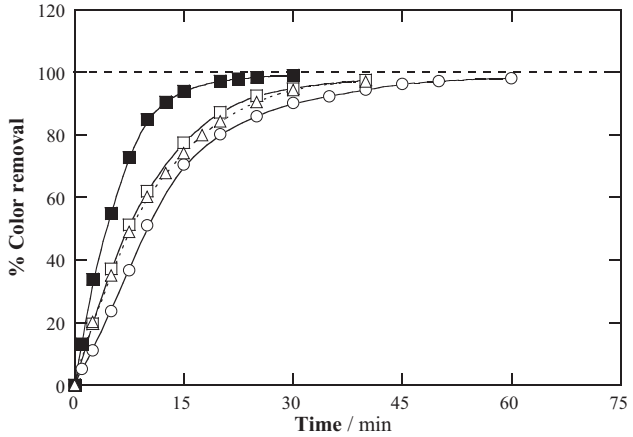

Fig. 1. Change of percentage of color removal at λ = 500 nm with electrolysis time for the treatment of 2.5 L of 230 mg L^{-1} (0.46 mM) Allura Red AC solutions in 0.05 M Na_2SO_4 with 0.50 mM Fe^{2+} at pH 3.0 and 50 mA cm^{-2} by (○) electro-Fenton (EF) and (□) solar photoelectro-Fenton (SPEF). A recirculation flow plant with an electrochemical reactor equipped with a 20 cm^2 Pt anode and a 20 cm^2 air-diffusion cathode coupled to a planar solar photoreactor with 600 mL irradiation volume was used. The effect of current density in SPEF was studied at (■) 100 mA cm^{-2}, whereas the effect of electrolyte concentration at 50 mA cm^{-2} was studied by using (△) 0.30 M Na_2SO_4.

Higher j enhances the Pt(·OH) generation by acceleration of reaction (4). Furthermore, it yields greater H_2O_2 accumulation, as shown in Fig. SM-1, which favors the larger ·OH production via Fenton's reaction (2) (Moreira et al., 2013; Brillas and Martínez-Huitle, 2015). Quicker decolorization of azo dyes is then expected in SPEF with rising j. This tendency was tested by treating a 230 mg L^{-1} Allura Red AC solution at 100 mA cm^{-2}. Fig. 1 shows that total decolorization was attained in 30 min, a time shorter than 40 min needed at 50 mA cm^{-2}. Accordingly, a greater k_{dec} of $(19.03 \pm 0.40) \times 10^{-2}$ min^{-1} was determined. This confirms the faster removal of the dye and its colored products by their reaction with greater amounts of hydroxyl radicals. The effect of SO_4^{2-} content as electrolyte was analyzed by degrading the azo dye solution in 0.30 M Na_2SO_4 at 50 mA cm^{-2}. Fig. 1 highlights a similar color removal for 0.05 and 0.30 M Na_2SO_4, with $k_{dec} = (9.15 \pm 0.07) \times 10^{-2}$ min^{-1} for the latter conditions. Then, greater SO_4^{2-} content does not affect significantly the production of hydroxyl radicals, only causing an undesired increase in solution conductivity.

Fig. 2 shows a longer time of about 20, 40 and 80 min for total decolorization at increasing 115, 230 and 460 mg L^{-1} of the azo dye under SPEF treatment at 50 mA cm^{-2}. The corresponding k_{dec} values were $(18.19 \pm 0.46) \times 10^{-2}$, $(9.98 \pm 0.13) \times 10^{-2}$ and $(4.59 \pm 0.01) \times 10^{-2}$ min^{-1}. The decay in k_{dec} at greater dye content can be related to the presence of larger amounts of Allura Red AC and its colored intermediates, which have to be degraded by a similar amount of hydroxyl radicals generated at constant j.

SPEF with a Pt/air-diffusion cell is then able to rapidly decolorize Allura Red AC solutions at concentrations typically found in dyeing industrial effluents. The mineralization of this azo dye under the same experimental conditions was assessed to clarify the oxidation power of this EAOP.

3.3. Mineralization of Allura Red AC solutions by EF and SPEF

The TOC abatement of 230 mg L^{-1} azo dye solutions by EF and SPEF at 50 mA cm^{-2} is depicted in Fig. 3a. The initial pH ~ 3.0 dropped to 2.7–2.8 after 360 min of EF, as expected from the generation of acidic products like short-chain carboxylic acids (Ammar et al., 2006; Özcan et al., 2009). In EF process, TOC was reduced by 39% at 180 min, whereupon its decay slowed down to reach only 46% mineralization at 360 min. This evidence supports the active role of Pt(·OH) and, mainly, ·OH in the bulk, to transform several intermediates into CO_2 during the first stages. In contrast, at longer time, large amount of refractory products are accumulated in the medium. On the other hand, almost total mineralization (96%) was achieved after 240 min of SPEF, which can be explained by the fast photolysis of the recalcitrant intermediates formed upon attack of hydroxyl radicals. A similar behavior has been reported for the EF and SPEF degradations of Acid Yellow 36 (Ruiz et al., 2011a) and Acid Red 88 (Ruiz et al., 2011b). This indicates that SPEF process is potent enough so as to mineralize highly polluted dyeing industrial wastewater as a result of the high power of natural UV photons of sunlight.

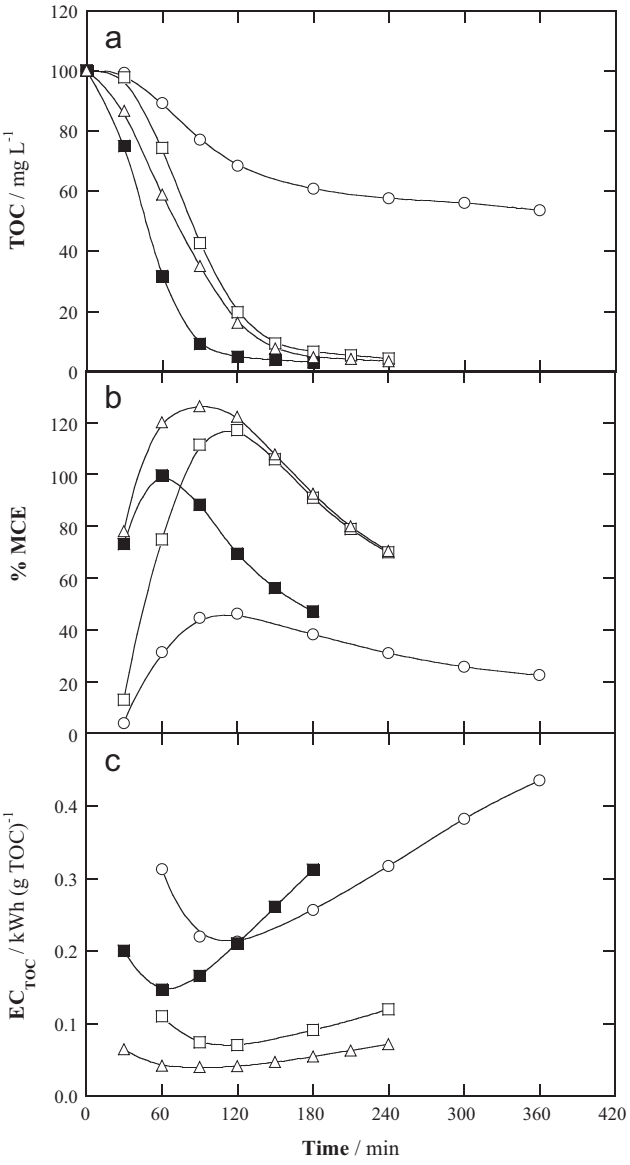

Fig. 3. (a) TOC abatement, (b) mineralization current efficiency and (c) specific energy consumption per unit TOC mass vs electrolysis time for the trials shown in Fig. 1.

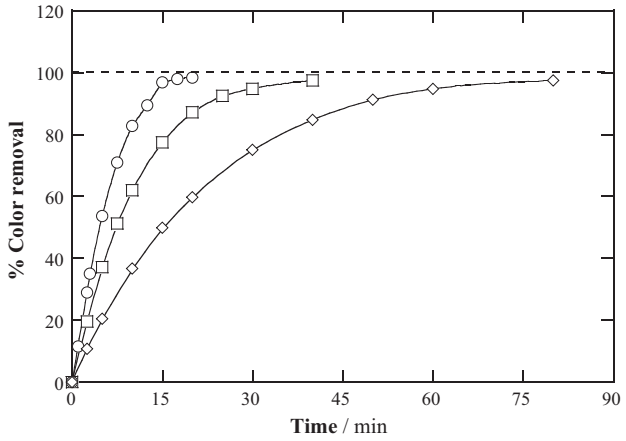

Fig. 2. Influence of initial dye concentration on the decolorization at λ = 500 nm vs electrolysis time for the SPEF degradation of 2.5 L of: (○) 115, (□) 230 and (◇) 460 mg L^{-1} Allura Red AC solutions in 0.05 M Na_2SO_4 with 0.50 mM Fe^{2+} at pH 3.0 and 50 mA cm^{-2}.

Fig. 3a shows that the increase in j from 50 to 100 mA cm^{-2} enhanced the mineralization ability of SPEF, since 97% TOC decay was already achieved in 180 min at 100 mA cm^{-2}. This trend can be related to the larger production of hydroxyl radicals, thus accelerating the production of recalcitrant molecules that ends in an earlier photolysis by sunlight (Moreira et al., 2013). When 0.30 M Na_2SO_4 was used, Fig. 3a highlights an enhancement of mineralization rate compared to 0.05 M Na_2SO_4 up to 120 min of SPEF, although analogous TOC removal of 96% was finally achieved in both cases. The quicker initial TOC decay is difficult to explain

because it is an inert electrolyte that does not affect the production of hydroxyl radicals, as stated above; it could be possibly due to the formation of complexes of sulfate with some intermediates that are more rapidly photodecomposed by sunlight. On the other hand, Fig. 4a confirms the large ability of the SPEF process with a Pt/air-diffusion cell to mineralize Allura Red AC, needing longer time as its concentration increased. Thus, 97%, 96% and 95% TOC decay was found after 120, 240 and 360 min of treatment for 115, 230 and 460 mg L^{-1}, respectively. This agrees with the slower destruction of intermediates with similar amount of hydroxyl radicals produced at 50 mA cm^{-2} in the presence of more organic matter, as discussed for color removal trials of Fig. 2. Similar effects of j and dye concentration have been described for the mineralization of other azo dyes (Ruiz et al., 2011b; Moreira et al., 2013).

Inorganic ions released to the solution during the EF and SPEF treatments of the 230 mg L^{-1} Allura Red AC solution at 50 mA cm^{-2} were quantified by ion chromatography. The S atoms of the azo dye (29.8 mg L^{-1}) were found as SO_4^{2-} ion, with final concentration of 84.5 mg L^{-1} (93% of initial S) in EF and 87.4 mg L^{-1} (98% of initial S) in SPEF. Therefore, most intermediates with a —SO_3^- group were destroyed in both EAOPs with quantitative formation of SO_4^{2-} ion. Regarding the N atoms (13.0 mg L^{-1}), no NH_4^+ ion was detected in the solution and only small amounts of NO_3^- ion were found, with final accumulations of 13.1 mg L^{-1} (22.6% of initial N) in EF and 5.0 mg L^{-1} (8.6% of initial N) in SPEF. The major proportion of N was then lost as volatile *N*-products, like N_2 and N_xO_y, as also found for similar treatments of other azo dyes (Ruiz et al., 2011b).

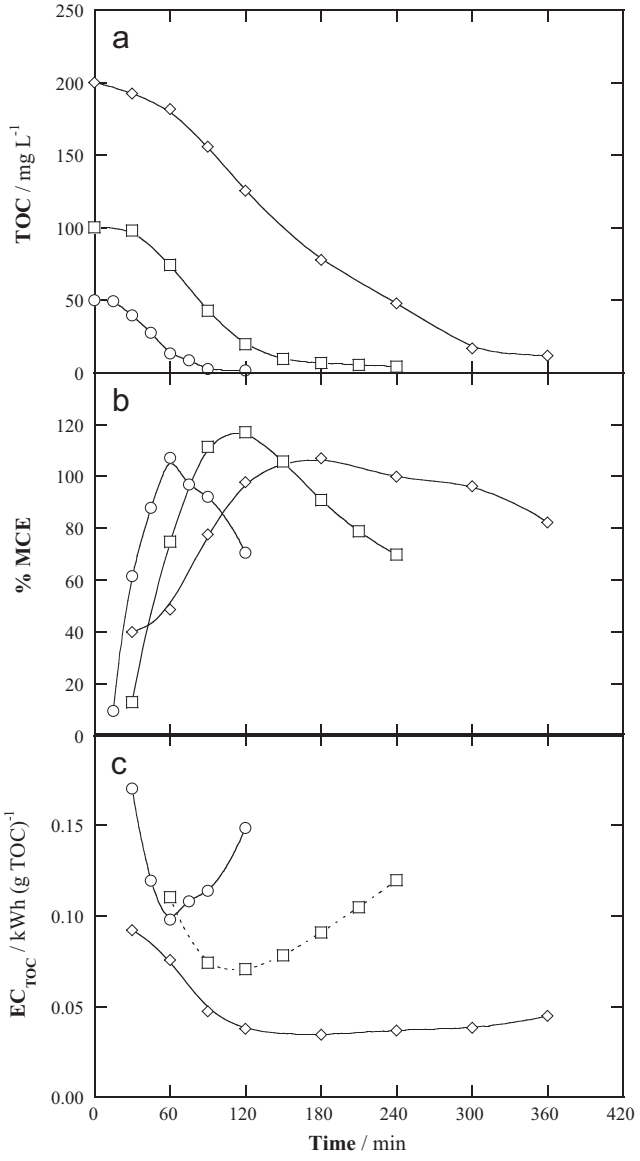

Fig. 4. Variation of (a) TOC, (b) mineralization current efficiency and (c) specific energy consumption per unit TOC mass with electrolysis time for the experiments shown in Fig. 2.

The above results allow establishing that the total mineralization of Allura Red AC involves its complete conversion into CO_2 and sulfate and nitrate as pre-eminent ions:

$$C_{18}H_{14}N_2O_8S_2^{2-} + 42H_2O \rightarrow 18CO_2 + 2SO_4^{2-} + 2NO_3^- + 98H^+ + 94e^- \quad (10)$$

The mineralization current efficiency (MCE) values for the aforementioned experiments at current I (A) and time t (h) was then estimated as follows:

$$\text{MCE}\ (\%) = \frac{n\,F\,V_s\Delta(\text{TOC})_{\text{exp}}}{4.32\times10^7 m\,I\,t}\times 100 \quad (11)$$

where n = 94 is the number of electrons exchanged per each azo dye molecule from reaction (10), F is the Faraday constant (96 487 C mol^{-1}), V_s is the solution volume (L), $\Delta(\text{TOC})_{\text{exp}}$ is the experimental TOC decay (mg L^{-1}), 4.32×10^7 is a conversion factor (3600 s h^{-1} × 12 000 mg carbon mol^{-1}) and m = 18 is the number of carbon atoms of Allura Red AC.

The MCE values for the trials of Figs. 3a and 4a are presented in Figs. 3b and 4b, respectively. As expected, the SPEF process at 50 mA cm^{-2} was much more efficient than the EF one, attaining a final MCE of 67% after attaining a maximal of 117% at 120 min (see Fig. 3b). A fast decay in efficiency at long electrolysis time occurred for all the assays, which can be related to the slower removal of recalcitrant products and the significant decrease of organic load (Panizza and Cerisola, 2009). Fig. 3b also shows that the use of 0.30 M Na_2SO_4 yielded greater efficiency compared to 0.05 M Na_2SO_4 up to 120 min owing to the quicker TOC decay (see Fig. 3a). In addition, MCE decayed when j raised to 100 mA cm^{-2} despite the quicker mineralization found by the greater production of Pt(·OH) and ·OH. This opposite trend can be related to a gradual waste of both hydroxyl radicals because of the acceleration of the following parasitic reactions at the anode surface and in the bulk (Panizza and Cerisola, 2009; Feng et al., 2013):

$$2\text{Pt}(\cdot\text{OH}) \rightarrow 2\text{Pt} + O_{2(g)} + 2H^+ + 2e^- \quad (12)$$

$$H_2O_2 + \cdot\text{OH} \rightarrow HO_2^{\cdot} + H_2O \quad (13)$$

$$Fe^{2+} + \cdot\text{OH} \rightarrow Fe^{3+} + OH^- \quad (14)$$

Fig. 4b highlights that maximum MCE values fluctuating between 106% and 117% were found for 115–460 mg L^{-1} azo dye at 50 mA cm^{-2}. In particular, higher concentration led to greater efficiency at prolonged electrolysis, suggesting a minimization of parasitic reactions (12)–(14) due to the larger number of events between oxidants and organic matter.

The specific energy consumption per unit TOC mass (EC_{TOC}) was calculated as follows:

$$EC_{TOC}(\text{kWh (g TOC)}^{-1}) = \frac{E_{cell}It}{V_s\Delta(\text{TOC})_{\text{exp}}} \quad (15)$$

where E_{cell} is the average potential difference of the cell (V) and the other parameters have been defined above. The results obtained are depicted in Figs. 3c and 4c. Comparison of these data with those of Figs. 3b and 4b allows concluding that higher MCE entailed lower

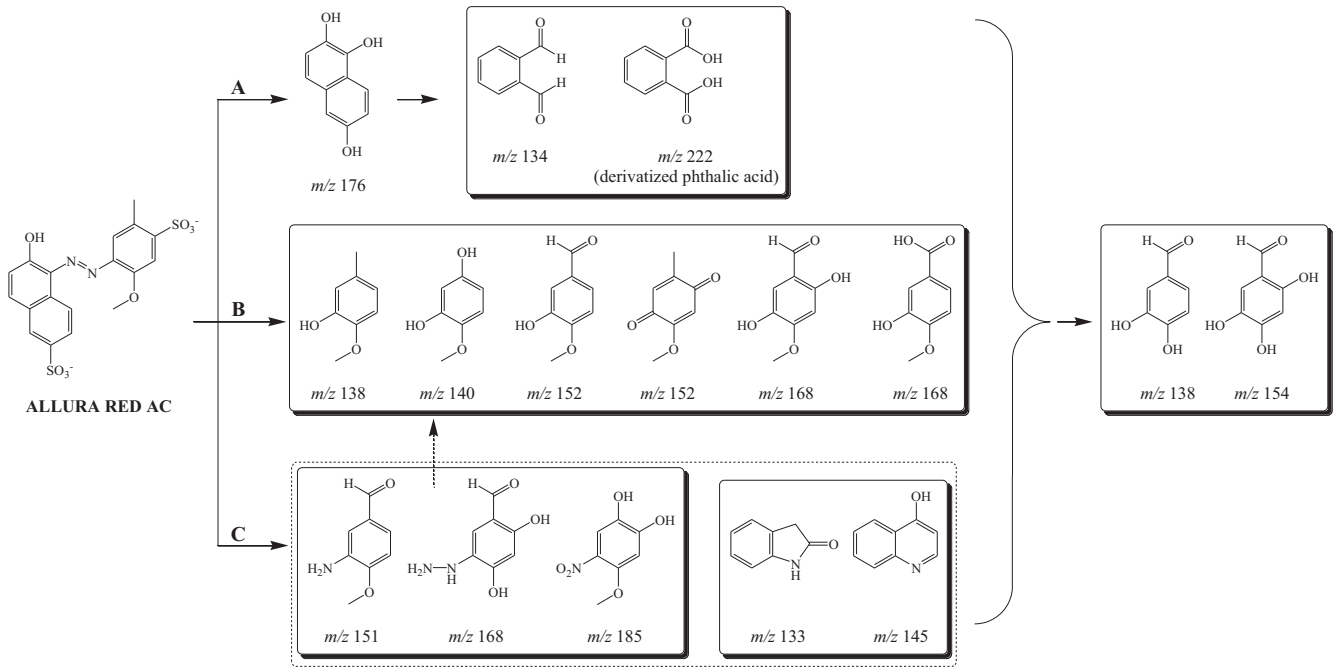

Fig. 5. Initial reaction pathways for the degradation of Allura Red AC in acidic aqueous medium by EF and SPEF with Pt anode and H_2O_2 electrogeneration. The primary aromatic oxidation products were identified by GC–MS.

EC_{TOC}, i.e., operation at lower *j* and higher sulfate and azo dye contents. The most cost-effective SPEF process was found for 460 mg L^{-1} Allura Red AC in 0.05 M Na_2SO_4 at 50 mA cm^{-2}, giving 95% mineralization in 360 min with 81% current efficiency and 0.045 kWh (g TOC)$^{-1}$ (8.50 kW h m^{-3}). Since the electrical cost in Spain is about 0.141 € kW h^{-1}, one can estimate a cost as low as 1.20 € m^{-3} for this treatment.

3.4. Identification of reaction products

GC–MS analysis of solutions with 230 mg L^{-1} Allura Red AC treated by EF and SPEF at 50 mA cm^{-2} revealed the generation of 16 aromatic intermediates. Fig. 5 presents an initial reaction sequence proposed for Allura Red AC degradation involving three parallel pathways (**A**, **B** and **C**) that summarize the detected products and their *m*/*z* ratio. In path **A**, the cleavage of the C—N bond between the naphthalenic moiety and the azo group, followed by hydroxylation, yields a naphthalenetriol (*m*/*z* = 176) that can be subsequently oxidized to phthalic acid. The breakage of the C—N bond between the benzenic moiety and the azo group is represented in path **B**, where the released benzene ring undergoes hydroxylation on various positions. Among other consequences, demethylation is caused upon attack of hydroxyl radical on the methylated benzenic C atom, whereas the oxidation of —CH_3 yields —CHO and —COOH groups. Note that in path **B**, 2,5-dihydroxy-4-methoxybenzaldehyde and 3-hydroxy-4-methoxybenzoic acid present equal *m*/*z* = 168, although they can be clearly distinguished from their retention times of 35.3 and 35.8 min, respectively, and their unique fragmentation patterns. Path **C** involves the formation of different *N*-derivatives arising from the cleavage of the N=N and

Table 1
Short-chain aliphatic carboxylic acids with different number of carbon atoms (C_n) formed upon cleavage of the benzenic moiety of aromatic products shown in Fig. 5.

Carboxylic acids					
C_1	C_2	C_3	C_4	C_5	C_6
Formic	Acetic	Malonic	Maleic	Glutamic	4-Methylglutamic
Oxalic		Tartronic	Fumaric		
Oxamic			Tartaric		

C—N bonds along with hydroxylation and other oxidation reactions, as well as internal cyclization to yield heterocycles. Two products, namely 3,4-dihydroxybenzaldehyde (m/z = 138) and 2,4,5-trihydroxybenzaldehyde (m/z = 154), can be finally formed via gradual degradation of various intermediates.

Ion-exclusion chromatograms of the treated solutions displayed peaks related to 9 carboxylic acids (C_1—C_4) coming from the cleavage of the aromatic rings of intermediates, as summarized in Table 1. Note that C_5 and C_6 acids were identified by GC–MS. All these acids form Fe(III) complexes and most of them were rapidly destroyed by hydroxyl radicals, except oxalic and oxamic acids that were the most persistent ones, as found for other azo dyes (Ruiz et al., 2011a, 2011b; Moreira et al., 2013). Fig. 6a shows that oxalic acid was accumulated up to 65.1 mg L^{-1} in EF, as expected if Fe(III)-oxalate complexes are not oxidized by hydroxyl radicals, whereas the fast photodecarboxylation of these species via reaction (6) caused its disappearance in 180 min by SPEF. In contrast, Fig. 6b highlights the higher recalcitrance of Fe(III)-oxamate complexes since they were not removed in EF and could be only slowly photolyzed in SPEF, yielding final oxamic acid contents of 1.6 and 1.2 mg L^{-1}, respectively. A mass balance allows concluding that both acids contribute in 17.8 and 0.3 mg L^{-1} TOC to the final treated solutions in EF and SPEF, respectively, corresponding to 33.2% and 8% of their TOC content. This suggests the formation of about 26 mg L^{-1} TOC of undetected organics that cannot be destroyed by EF but are rapidly photolyzed in SPEF.

4. Conclusions

The EF process led to fast total decolorization of Allura Red AC solutions in 0.05 M Na_2SO_4 with 0.50 mM Fe^{2+} of pH 3.0, but high amounts of products were not mineralized by hydroxyl radicals. In contrast, SPEF showed a large ability to mineralize the azo dye solution due to the potent action of UV radiation from sunlight. Sulfate and nitrate ions, along with a large proportion of volatile *N*-derivatives, were released in both EAOPs. The study on SPEF revealed a more rapid decolorization and mineralization by increasing j and decreasing azo dye content, although lower current efficiency and greater specific energy consumption were determined. No significant effect of sulfate concentration was found. A plausible initial reaction sequence for Allura Red AC degradation was proposed based on 16 aromatic intermediates identified by GC–MS. Their cleavage yielded up to 11 short-chain carboxylic acids, including oxalic and oxamic as the most persistent products. The superiority of SPEF can be explained by the quick photolysis of Fe(III)-oxalate complexes and other undetected intermediates. Our results confirm the large potentiality of this method to treat highly concentrated dyeing industrial wastewater, even employing a low oxidation power anode.

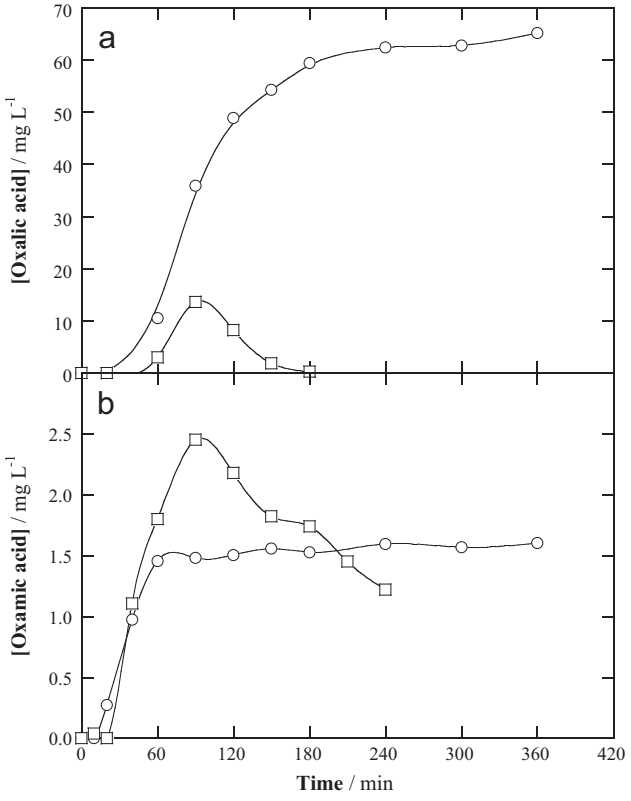

Fig. 6. Time course of the concentration of (a) oxalic and (b) oxamic acid detected during the (○) EF and (□) SPEF treatments of Fig. 1 at 0.05 M Na_2SO_4, 0.50 mM Fe^{2+}, pH 3.0 and 50 mA cm^{-2}.

Acknowledgments

The authors thank MINECO (Spain) for financial support under project CTQ2013-48897-C2-1-R, co-financed with FEDER funds. The Ph.D. grant awarded to A. Thiam from MAEC-AECID (Spain) is also acknowledged.

Appendix A. Supplementary material

Supplementary data associated with this article can be found, in the online version, at http://dx.doi.org/10.1016/j.chemosphere.2015.03.047.

References

Ammar, S., Abdelhedi, R., Flox, C., Arias, C., Brillas, E., 2006. Electrochemical degradation of the dye indigo carmine at boron-doped diamond anode for wastewaters remediation. Environ. Chem. Lett. 4, 229–233.
Boye, B., Dieng, M.M., Brillas, E., 2003. Electrochemical degradation of 2,4,5-trichlorophenoxyacetic acid in aqueous medium by peroxi-coagulation. Effect of pH and UV light. Electrochim. Acta 48, 781–790.
Brillas, E., Martínez-Huitle, C.A., 2015. Decontamination of wastewaters containing synthetic organic dyes by electrochemical methods. An updated review. Appl. Catal. B: Environ. 166–167, 603–643.
Daneshvar, N., Aber, S., Vatanpour, V., Rasoulifard, M.H., 2008. Electro-Fenton treatment of dye solution containing Orange II: influence of operational parameters. J. Electroanal. Chem. 615, 165–174.
Dirany, A., Sirés, I., Oturan, N., Özcan, A., Oturan, M.A., 2012. Electrochemical treatment of the antibiotic sulfachloropyridazine: kinetics, reaction pathways, and toxicity evolution. Environ. Sci. Technol 46, 4074–4082.
EFSA, 2008. Assessment of the results of the study by McCann et al. (2007) on the effect of some colours and sodium benzoate on children's behaviour. EFSA J. 660, 1–54.
EFSA, 2009. Scientific opinion on the re-evaluation of Allura Red AC (E 129) as a food additive. EFSA J. 7, 1327. 39pp..
Epling, G.A., Lin, C., 2002. Photoassisted bleaching of dyes utilizing TiO_2 and visible light. Chemosphere 46, 561–570.
Feng, L., van Hullebusch, E.D., Rodrigo, M.A., Esposito, G., Oturan, M.A., 2013. Removal of residual anti-inflammatory and analgesic pharmaceuticals from aqueous systems by electrochemical advanced oxidation processes: a review. Chem. Eng. J. 228, 944–964.
Forgacs, E., Cserháti, T., Oros, G., 2004. Removal of synthetic dyes from wastewaters: a review. Environ. Int. 30, 953–971.
Hunger, K. (Ed.), 2003. Industrial Dyes Chemistry, Properties, Applications. Wiley-VCH, Germany.
Khataee, A., Khataee, A., Fathinia, M., Vahid, B., Joo, S.W., 2013. Kinetic modeling of photoassisted-electrochemical process for degradation of an azo dye using boron-doped diamond anode and cathode with carbon nanotubes. J. Ind. Eng. Chem. 19, 1890–1894.
Moreira, F.C., Garcia-Segura, S., Vilar, V.J.P., Boaventura, R.A.R., Brillas, E., 2013. Decolorization and mineralization of Sunset Yellow FCF azo dye by anodic oxidation, electro-Fenton, UVA photoelectro-Fenton and solar photoelectro-Fenton processes. Appl. Catal. B: Environ. 142–143, 877–890.
Oturan, N., Brillas, E., Oturan, M.A., 2012. Unprecedented total mineralization of atrazine and cyanuric acid by anodic oxidation and electro-Fenton with a boron-doped diamond anode. Environ. Chem. Lett. 10, 165–170.

Özcan, A., Oturan, M.A., Oturan, N., Şahin, Y., 2009. Removal of Acid Orange 7 from water by electrochemically generated Fenton's reagent. J. Hazard. Mater. 163, 1213–1220.
Panizza, M., Cerisola, G., 2009. Direct and mediated anodic oxidation of organic pollutants. Chem. Rev. 109, 6541–6569.
Panizza, M., Oturan, M.A., 2011. Degradation of Alizarin Red by electro-Fenton process using a graphite-felt cathode. Electrochim. Acta 56, 7084–7087.
Robinson, T., McMullan, G., Marchant, R., Nigam, P., 2001. Remediation of dyes in textile effluent: a critical review on current treatment technologies with a proposed alternative. Biores. Technol. 77, 247–255.
Rosales, E., Pazos, M., Longo, M.A., Sanromán, M.A., 2009. Electro-Fenton decoloration of dyes in a continuous reactor: a promising technology in colored wastewater treatment. Chem. Eng. J. 155, 62–67.
Ruiz, E.J., Arias, C., Brillas, E., Hernández-Ramírez, A., Peralta-Hernández, J.M., 2011a. Mineralization of Acid Yellow 36 azo dye by electro-Fenton and solar photoelectro-Fenton processes with a boron-doped diamond anode. Chemosphere 82, 495–501.
Ruiz, E.J., Hernández-Ramírez, A., Peralta-Hernández, J.M., Arias, C., Brillas, E., 2011b. Application of solar photoelectro-Fenton technology to azo dyes mineralization: Effect of current density, Fe^{2+} and dye concentration. Chem. Eng. J. 171, 385–392.
Salazar, R., Garcia-Segura, S., Ureta-Zañartu, M.S., Brillas, E., 2011. Degradation of disperse azo dyes from waters by solar photoelectro-Fenton. Electrochim. Acta 56, 6371–6379.
Salazar, R., Brillas, E., Sirés, I., 2012. Finding the best Fe^{2+}/Cu^{2+} combination for the solar photoelectro-Fenton treatment of simulated wastewater containing the industrial textile dye Disperse Blue 3. Appl. Catal. B: Environ. 115–116, 107–116.
Sharma, K.P., Sharma, S., Sharma, S., Singh, P.K., Kumar, S., Grover, R., Sharma, P.K., 2007. A comparative study on characterization of textile wastewaters (untreated and treated) toxicity by chemical and biological tests. Chemosphere 69, 48–54.
Sirés, I., Brillas, E., 2012. Remediation of water pollution caused by pharmaceutical residues based on electrochemical separation and degradation technologies: a review. Environ. Int. 40, 212–229.
Sirés, I., Brillas, E., Oturan, M.A., Rodrigo, M.A., Panizza, M., 2014. Electrochemical advanced oxidation processes: today and tomorrow: A review. Environ. Sci. Pollut. Res. 21, 8336–8367.
Solís, M., Solís, A., Pérez, H.I., Manjarrez, N., Flores, M., 2012. Microbial decolouration of azo dyes: a review. Process Biochem. 47, 1723–1748.
Thiam, A., Zhou, M., Brillas, E., Sirés, I., 2014. Two-step mineralization of Tartrazine solutions: study of parameters and by-products during the coupling of electrocoagulation with electrochemical advanced oxidation processes. Appl. Catal. B: Environ. 150–151, 116–125.
Thiam, A., Sirés, I., Garrido, J.A., Rodríguez, R.M., Brillas, E., 2015. Effect of anions on electrochemical degradation of azo dye Carmoisine (Acid Red 14) using a BDD anode and air-diffusion cathode. Sep. Purif. Technol. 140, 43–52.
Ulson de Souza, S.M.A.G., Forgiarini, E., Ulson de Souza, A.A., 2007. Toxicity of textile dyes and their degradation by the enzyme horseradish peroxidase (HRP). J. Hazard. Mater. 147, 1073–1078.
UNESCO, 2012. The United Nations World Water Development Report 4, vol. 1: Managing Water Report under Uncertainty and Risk.
Vasudevan, S., Oturan, M.A., 2014. Electrochemistry: as cause and cure in water pollution-an overview. Environ. Chem. Lett. 12, 97–108.
Wang, A., Qu, J., Liu, H., Ru, J., 2008. Mineralization of an azo dye Acid Red 14 by photoelectro-Fenton process using an activated carbon fiber cathode. Appl. Catal. B: Environ. 84, 393–399.
Welcher, F.J. (Ed.), 1975. Standard Methods of Chemical Analysis, vol. 2, Part B, 6th ed., R.E. Krieger Publishers, Huntington, New York, p. 1827.
Zollinger, H., 2003. Color Chemistry: Synthesis, Properties, and Applications of Organic Dyes and Pigments. VHCA and Wiley-VCH, Switzerland.

4.4. Optimization of the electro-Fenton and solar photoelectro-Fenton treatment of solutions of food azo dyes using a 2.5 L pre-pilot plant with a BDD anode and air-diffusion cathode

To gain a better understanding on the ability of EAOPs to degrade artificial food azo-dyes, comparative studies on the degradation of either Carmoisine solutions (**Paper 5**) or a mixture of three food azo-colors (Ponceau 4R (E124), Allura Red AC (E122) and Carmoisine (E122)) (**Paper 6**) in sulfate, chloride, nitrate and perchlorate media by EO-H_2O_2, EF and SPEF using a batch recirculation pre-pilot plant of 2.5 L equipped with a BDD/air-diffusion cell were undertaken.

First, the degradation of Carmoisine solutions by EO-H_2O_2 and EF using the BDD/air-diffusion cell was investigated. In EO-H_2O_2, the influence of the supporting electrolyte nature (SO_4^{2-}, ClO_4^- and Cl^-) was investigated at 100 mA cm^{-2}. A quite slow decolorization was observed in SO_4^{2-} and ClO_4^-, attaining 70% and 82% color removal at 480 min, respectively, whereas the solution became colorless after ca. 25 min of electrolysis in Cl^- medium. In the two former electrolytes, BDD($^\bullet$OH) generated via reaction (27) was the main oxidizing agent and thus, the dye and its colored by-products reacted slowly because of important mass transport limitations. Conversely, the very fast color removal in the chloride solution is related to the quick reaction of Carmoisine with active chlorine electrogenerated in the bulk, as found in sections 4.2 and 4.3. Regarding the TOC abatement, gradual and similar TOC decays were observed in SO_4^{2-} and ClO_4^- media, suggesting that the degradation routes involved the same kinds of intermediates. In contrast, the presence of Cl^- accelerated the dye mineralization during the first stages, but similar TOC removal values were finally found in all media, which can be explained by the formation of very recalcitrant intermediates. The low and analogous oxidation power of the EO-H_2O_2 process to mineralize the dye solution in all media was also evident upon comparison of the MCE values. Regarding the energy consumption, the lowest EC_{TOC} during the latter stages was obtained in SO_4^{2-} medium.

The electrochemical degradation of Carmoisine solutions was also studied by EF process under different experimental conditions. When comparing the effect of supporting electrolyte, the most rapid decolorization occurred when using chloride ion, needing about 25 min to get a colorless solution. This time was similar to that required in the analogous EO-H_2O_2 treatment, which means that at the beginning of EF the dye and its colored products are more quickly transformed by HClO formed from reactions (42) and (43) than by heterogeneous BDD($^\bullet$OH) and homogeneous $^\bullet$OH produced from reactions (27) and (12), respectively. In contrast, in sulfate and perchlorate media, a

similar and much quicker decolorization was observed due to the rapid destruction of the dye and its colored by-products by $^{\bullet}OH$ produced from Fenton's reaction (12).

Concerning the TOC removal, the higher oxidation ability of additional $^{\bullet}OH$ produced from Fenton's reaction allowed a quicker TOC decay in all media. Note that at time longer than 180 min, the EF process was progressively decelerated. The slower mineralization in Cl^- medium compared to SO_4^{2-} and ClO_4^- media is related to the generation of chloroderivatives. The much greater oxidation ability of EF over EO-H_2O_2 for the degradation of Carmoisine was also assessd from the higher MCE and lower EC_{TOC} values. The influence of *j* was evaluated for the EF. The rate of this process was remarkably enhanced upon *j* increase and thus, the time needed for total color removal decreased considerably. However, decreasing MCE values were obtained, which can be ascribed to a progressive loss in the available concentration of BDD($^{\bullet}OH$) and $^{\bullet}OH$. The influence of dye concentration on the EF treatment was also tested, leading to similar conclusions to those drawn for Ponceau 4R and AR AC.

To investigate the main intermediates generated during the electrochemical oxidation process, several electrolyses of Carmoisine solutions were made under the best EO-H_2O_2 and EF conditions, thereby extracting their organic components to be identified by GC-MS. Up to 15 aromatics have been detected as primary products upon attack of hydroxyl radicals. Overall, six benzene and four naphthalene derivatives, along with condensation products related to one indane, two indole and two benzofuran derivatives, were found. Many of these compounds contain carbonyl and/or hydroxyl groups coming from the attack of hydroxyl radical on the aromatic ring. Ion-exclusion chromatograms of the same degradation solutions in SO_4^{2-} revealed the generation of a mixture of short-linear carboxylic acids. The formation of these acids could correspond to the opening of aromatic and naphthalene rings followed by a sequence of oxidation steps which leads to progressively lower molecular weight acids and the evolution of CO_2. Formation of CO_2 takes place via decarboxylation of carboxylic acids. Analysis of the final electrolyzed solution in ClO_4^- by IC revealed the release of inorganic ions such as NH_4^+, NO_3^- and SO_4^{2-}. Let us note that many of the aromatic intermediates and other end products identified in this work are similar to those reported for Ponceau 4R in Paper 2.

Usually, wastewater resulting from dyeing processes contains more than a single dye and various inorganic ions. However, the vast majority of studies in the literature

have been focused on the degradation of single azo dyes, whereas scarce information is available on the treatment of mixtures of azo dyes and the influence of the supporting electrolyte nature. Aiming to get clearer information on the electrochemical behavior of food azo dyes upon application of powerful EAOPs like PEF and SPEF, I carried out a study on the decolorization and mineralization of mixtures of the three color additives mentioned so far in this Thesis, namely E122, E124 and E129, in either synthetic media with sulfate, perchlorate, nitrate and/or chloride ions or in a real water matrix adjusted at pH 3.0 (Paper 6). First, comparative electrolyses were carried out at lab-scale under EF and PEF conditions in sulfate medium using a BDD/air-diffusion or Pt/air-diffusion tank reactor to clarify the role of generated oxidizing agents. The influence of simulated and real water matrices on the degradation ability of PEF with a BDD anode (PEF-BDD) was further explored.

Essays at lab-scale were made with the 130 mL stirred tank reactor to clarify the oxidation ability of hydroxyl radicals formed during the EF-Pt, EF-BDD, PEF-Pt and PEF-BDD treatments. Complete decolorization was reached after 50 and 45 min by EF and PEF, respectively, regardless of the anode used. But, the presence of UV light favored the mineralization due to the photodecarboxilation of Fe(III) complexes formed with carboxylic acids. An almost total mineralization was then achieved for both PEF processes, being BDD slightly superior to Pt due to the combined action of the $^{\bullet}OH$ generated in the bulk by Fenton's reaction (12) and BDD($^{\bullet}OH$) radicals, which are more powerful oxidizing agents than Pt($^{\bullet}OH$) ones. These findings indicated that PEF-BDD was the best EAOP to decolorize and mineralize the mixtures of food azo dyes.

PEF-BDD process was then chosen to assess the degradation of mixtures in simulated and real water matrices. First, the degradation of the mixture was investigated in a simulated water matrix prepared on the basis of the characterization of inorganic components of a real wastewater, at pH 3.0 and 33.3 mA cm^{-2}. Total decolorization was achieved at 15 and 60 min for 10 and 100 mg L^{-1} TOC, respectively, as expected from the slower degradation of higher organic load under the action of a similar concentration of hydroxyl radicals. On the other hand, comparison of treatments in synthetic water and simulated wastewater reveals a significantly slower color removal in the latter water. The decay in decolorization rate in such water matrix (which contained Cl^- ions) could seem contradictory, since previous work with Ponceau 4R and Allura Red AC showed a faster decolorization in Cl^- than in SO_4^{2-} medium. However, in those studies,

the concentration of both anions was 0.050 M, whereas in the case of the simulated water the Cl^- content was much lower. The lower specific conductivity, which causes a greater ohmic drop that ends in a less effective formation of oxidants, was then responsible for the slower color removal. Accordingly, the loss of oxidation power in PEF-BDD using the simulated water was also found when the mineralization rate was assessed.

The oxidation power of PEF-BDD was further assessed for different food azo dye solutions mixed at equal TOC content in a real water matrix adjusted at pH 3.0, at 33.3 mA cm^{-2}. Fast color removal was always achieved, attaining total decolorization at longer times from 10 to 60 min as total initial TOC grew from 10 to 100 mg L^{-1}. Such times were similar to those required in the simulated matrix, which means that the natural organic load contained in the real water has little influence on the decolorization process, which is very important from an applicative standpoint. This was also confirmed from the TOC abatement. Our findings allow concluding that PEF-BDD is able to effectively decolorize and mineralize mixtures of food azo dyes in a real water matrix, yielding almost total mineralization (> 95% TOC removal) even after spiking 100 mg L^{-1} TOC of such pollutants to the matrix.

A second step was performed with a 2.5 L pre-pilot flow plant equipped with a BDD/air-diffusion cell coupled to a planar solar photoreactor in order to assess the oxidation ability of SPEF-BDD for the treatment of mixtures of food azo dyes. The performance of this method was compared with that of EO-H_2O_2-BDD and EF-BDD using a synthetic mixture with 0.05 M Na_2SO_4 at pH 3.0 and 100 mA cm^{-2}. EO-H_2O_2-BDD process only allowed a slow decolorization, reaching 79% color removal in 360 min, while similar and total decolorization was achieved in 40 min by EF-BDD and SPEF-BDD due to the large amount of $^{\bullet}OH$ produced by Fenton's reaction (12). Regarding the TOC, the relative oxidation power of EAOPs grows in the sequence EO-H_2O_2-BDD < EF-BDD < SPEF-BDD. The superiority of SPEF-BDD (97% TOC decay) is related to the rapid photodegradation of some refractories intermediates such as Fe(III)–carboxylate complexes by UV radiation from sunlight. Furthermore, a much lower specific energy consumption (EC_{TOC}) of 0.607 kWh (g TOC)$^{-1}$ was found at 300 min of SPEF-BDD, whereas high values of 1.94 and 1.46 kWh (g TOC)$^{-1}$ were obtained for the inefficient EO-H_2O_2-BDD and EF-BDD treatments at 100 mA cm^{-2}.

The effect of operation parameters on the SPEF-BDD performance was studied by electrolyzing a mixture with 100 mg L^{-1} TOC. Quite similar decolorization rates with complete color removal in 30-40 min were found in 0.050 M of Na_2SO_4, $LiClO_4$, $NaNO_3$ and NaCl, and even in 0.040 M Na_2SO_4 + 0.010 M NaCl. This behavior differs from results reported above on the decolorization of single E122 solutions by EF, which was faster in Cl^- than in SO_4^{2-} and ClO_4^-. This discrepancy could be due to a different reactivity of each azo dye of the mixture and/or their colored by-products with oxidizing agents. Quite similar TOC removal (96-97%) was also achieved in all media, except in NaCl medium, where TOC was only reduced by 85% in 300 min. The lower mineralization rate achieved in latter medium can be related to the formation of refractory chloroderivatives and the destruction of H_2O_2 from reaction (74). These results agree with those obtained by PEF-BDD in the real water matrix at lab-scale and demonstrate the viability of SPEF-BDD for the treatment of foo azo dye wastewater.

The influence of *j* and dye content on the performance of SPEF-BDD was also examined. For total decolorization, 50 to 30 min and 15 to 50 min were needed upon increases of *j* from 50 to 150 mA cm^{-2} and dye content from 50 to 200 mg L^{-1} TOC, respectively. Similar behavior was found with the mineralization rate. This tendencies agree with aforementioned results. The rise in *j* (50-150 $mAcm^{-2}$) was accompanied by the increase in EC_{TOC} from 0.169 kWh $(g\ TOC)^{-1}$ to 0.897 kWh $(g\ TOC)^{-1}$. In contrast, the most efficient degradation of 200 mg L^{-1} TOC at 100 mA cm^{-2} yielded the lowest EC_{TOC} of 0.290 kWh $(g\ TOC)^{-1}$ in 300 min.

To obtain additional qualitative information about the oxidation pathways involved in the EAOPs of the dye mixtures, short carboxylic acids, inorganic ions and aromatic intermediates formed were detected by different chromatographic techniques. Ion-exclusion chromatograms of electrolyzed solutions revealed the generation of carboxylic acids like maleic, fumaric, tartronic, formic, oxalic and oxamic. The three later acids are ultimate acids since they are directly mineralized to CO_2. Oxalic acid was the most persistent aliphatic acid and was completely photodecarboxylated by UV radiation from sunlight. Quantification of inorganic ions formed during the degradation of azo dyes was attempted by IC. The S atoms of food azo dyes (0.99 mM) were detected as SO_4^{2-} ion, with a concentration of 0.57 mM (57% of initial S), 0.96 mM (97% of initial S) and 0.99 mM (100% of initial S) after 300 min of EO-H_2O_2-BDD, EF-BDD and SPEF-BDD, respectively. Regarding the N atoms (0.85 mM), very low

contents of NH_4^+ ion (< 0.01 mM) were detected in all cases, along with a much larger accumulation of NO_3^- ion. GC-MS analyses of initially electrolyzed acidic aqueous mixture of additives E122, E124 and E129 by SPEF allowed the identification of 18 aromatic intermediates coming from the cleavage of the –N=N– and C–N bonds, deamination and desulfonation of the starting dyes and, as a result, a complete degradation pathway has been proposed. Worth mentioning, almost all the intermediates detected during the degradation of the mixture have been detected during the degradation of the three single dyes (see Paper 2 for Ponceau 4R, Paper 4 for Allura Red AC and Paper 5 for Carmoisine).

Paper 5

Effect of anions on electrochemical degradation of azo dye Carmoisine (Acid Red 14) using a BDD anode and air-diffusion cathode

Separation and Purification Technology

140 (2015) 43–52

Separation and Purification Technology 140 (2015) 43–52

Contents lists available at ScienceDirect

Separation and Purification Technology

journal homepage: www.elsevier.com/locate/seppur

Effect of anions on electrochemical degradation of azo dye Carmoisine (Acid Red 14) using a BDD anode and air-diffusion cathode

Abdoulaye Thiam, Ignasi Sirés, José Antonio Garrido, Rosa María Rodríguez, Enric Brillas *

Laboratori d'Electroquímica dels Materials i del Medi Ambient, Departament de Química Física, Facultat de Química, Universitat de Barcelona, Martí i Franquès 1-11, 08028 Barcelona, Spain

ARTICLE INFO

Article history:
Received 5 October 2014
Received in revised form 10 November 2014
Accepted 13 November 2014
Available online 25 November 2014

Keywords:
Carmoisine
Electrochemical oxidation
Electro-Fenton
Oxidation products
Water treatment

ABSTRACT

Solutions of 2.5 L with 209.3 mg L^{-1} of the azo dye Carmoisine in 0.050 M SO_4^{2-}, ClO_4^- or Cl^- have been comparatively treated by electrochemical oxidation with electrogenerated H_2O_2 (EO-H_2O_2) and electro-Fenton (EF) with 0.5 mM Fe^{2+} as catalyst at constant current density. Experiments were made using a recirculation flow plant containing a reactor with a boron-doped diamond (BDD) anode and an air-diffusion cathode to allow H_2O_2 generation. The dye and its oxidation products were oxidized by hydroxyl radical and/or HClO formed at the anode from water or Cl^- oxidation, respectively, in EO-H_2O_2, as well as by hydroxyl radical produced in the bulk from Fenton's reaction between added Fe^{2+} and generated H_2O_2 in EF. In both methods, the decolorization process was always much faster in Cl^- medium because of the quick oxidation of colored compounds by HClO, being enhanced by increasing current density and Cl^- concentration. The solutions with SO_4^{2-} or ClO_4^- were more rapidly decolorized in EF due to the higher oxidation power of hydroxyl radicals in the bulk. Regarding the overall decontamination, a poor and similar mineralization of about 50% was obtained by EO-H_2O_2 at 480 min in all the supporting electrolytes at 100 mA cm^{-2}. The comparative EF treatments were always much more powerful, being SO_4^{2-} the most favorable medium leading to 76% mineralization with the lowest energy consumption. Up to 15 aromatic products were detected by GC–MS and short-linear carboxylic acids like tartronic, oxalic, oxamic and formic were quantified by ion-exclusion HPLC. The large persistence of Fe(III)-oxalate complexes accounted for the partial mineralization of the Carmoisine solution in EF. Nitrate and sulfate were the major ions released during the mineralization process.

1. Introduction

The recent United Nations World Water Development Report has given prominence to the growing concern on dyeing industrial effluents [1]. Large volumes of these wastewaters with high dye contents are daily discharged into water bodies, thus causing not only aesthetic problems but also toxic effects on aquatic organisms and humans [2,3], including proven carcinogenic, mutagenic and bactericide activity [1]. Synthetic dyes with one or various azo groups (—N=N—) as chromophore bound to benzene or naphthalene rings containing —OH and —SO_3H groups are largely produced [4]. They account for over 70% of the world dyestuff production, being widely used in textile, cosmetic, pulp and paper, food and pharmaceutical industries owing to their unique properties such as brilliant shades, relative low cost and simple manufacture [4,5]. Among them, food azo dyes are suspected to be dangerous according to the European Food Safety Authority (EFSA) due to their possible connection to hyperactivity in children, like in the case of Carmoisine (disodium 4-hydroxy-3-[(4-sulfo-1-naphthalenyl)azo]-1-naphthalenesulfonate, $C_{20}H_{12}N_2O_7S_2Na_2$, also known as Acid Red 14 or additive E122, see its chemical structure in Fig. 1) [6]. Azo dyes are highly recalcitrant, being only hardly removed by conventional biological and physicochemical methods. As a result, they are largely persistent in the aquatic environment [5]. Aiming to prevent the adverse environmental and health impact of these pollutants and their by-products, research efforts are needed to develop powerful and effective degradation methods.

The electrochemical advanced oxidation processes (EAOPs) like electrochemical oxidation (EO) and electro-Fenton (EF) have received increasing interest in the last years for water remediation [4,7–9]. In EO, the organic pollutants are destroyed by physisorbed hydroxyl radical M(·OH) generated from water discharge at an anode (M) with high O_2-overpotential via reaction (1) upon application of a high current [7,10–13].

* Corresponding author. Tel.: +34 934021223; fax: +34 934021231.
E-mail address: brillas@ub.edu (E. Brillas).

http://dx.doi.org/10.1016/j.seppur.2014.11.012
1383-5866/

$$M + H_2O \rightarrow M(^{\cdot}OH) + H^+ + e^- \quad (1)$$

Although the standard redox potential of ·OH (E° = 2.8 V/SHE) is so high that it can non-selectively react with most organics up to their mineralization, the effectiveness of EO dramatically depends on the anode material. While the M(·OH) radical formed from reaction (1) on active anodes such as Pt, IrO_2 and RuO_2 is easily oxidized to a chemisorbed MO species with weaker oxidizing ability, only allowing the electrochemical conversion of organics into carboxylic acids [7,12,14], it becomes more stable on non-active anodes like SnO_2, PbO_2 and boron-doped diamond (BDD) eventually yielding the electrochemical incineration of organics [7,15,16]. Among the latter anodes, BDD is preferred for EO since it generates very high amounts of reactive physisorbed BDD(·OH) due to the very weak BDD–·OH interaction resulting in a greater O_2-overpotential and an enhanced destruction of organics [7,11].

The electrolyte composition can also modify the effectiveness of EO. Thus, in chloride medium, the oxidation of organics by M(·OH) competes with that mediated by active chlorine species like Cl_2, HClO and/or ClO^-, which are electrogenerated as follows [7,17,18]:

$$2Cl^- \rightarrow Cl_2(aq) + 2e^- \quad (2)$$

$$Cl_2(aq) + H_2O \rightarrow HClO + Cl^- + H^+ \quad (3)$$

$$HClO \leftrightarrows ClO^- + H^+ \quad (4)$$

The use of a carbonaceous cathode such as graphite [19], carbon nanotubes [20], activated carbon fiber (ACF) [21,22], carbon sponge [23], graphite felt [24,25], carbon felt [23,26–30] and carbon-polytetrafluoroethylene (PTFE) gas (O_2 or air) diffusion [17,18,31–34] allows the electrogeneration of H_2O_2 from the two-electron reduction of injected O_2 via reaction (5):

$$O_2(g) + 2H^+ + 2e^- \rightarrow H_2O_2 \quad (5)$$

When an undivided cell is used, the EO process with electrogenerated H_2O_2 (EO-H_2O_2) then involves the destruction of organics pre-eminently by M(·OH), along with other weaker reactive oxygen species (ROS) like H_2O_2 and hydroperoxyl radical $M(HO_2^{\cdot})$ formed from reaction (6) [8,9]:

$$M + H_2O_2 \rightarrow M(HO_2^{\cdot}) + H^+ + e^- \quad (6)$$

A more effective EAOP based on H_2O_2 electrogeneration is EF [4,9,18–31,35,36], in which organics can undergo additional attack by ·OH produced in the bulk by Fenton's reaction (7), which occurs by reaction between generated H_2O_2 and low quantities of Fe^{2+} ion at optimum pH 2.8. This event is catalytic and can be propagated from Fe^{2+} regeneration [23,28].

$$Fe^{2+} + H_2O_2 + H^+ \rightarrow Fe^{3+} + {}^{\cdot}OH + H_2O \quad (7)$$

The generation of oxidants in the above EAOPs depends not only on the electrode materials, but it is also affected by the operating parameters. However, the information on the influence of supporting electrolytes on the EF treatment of dyestuff solutions using an air-diffusion cathode for H_2O_2 generation is scarce. This electrode is advantageous in such treatment because it minimizes the possible cathodic reduction of organic pollutants [9]. To gain a better understanding on the ability of EAOPs to oxidize synthetic dyes, a comparative study on the degradation of Carmoisine solutions in sulfate, chloride and perchlorate media by EO-H_2O_2 and EF using a batch recirculation plant with an electrochemical reactor equipped with a BDD anode and an air-diffusion cathode has been undertaken. All the trials were made at the optimum pH ~ 3.0 [4,9,29–34]. Carmoisine has been chosen by many authors as a model molecule to test the removal of azo dyes by ozonation [37], photocatalysis [38–41], sonochemistry [42] and chemical Fenton [42,43]. Solutions of Carmoisine have also been treated by electrocoagulation with an iron anode in the presence of chloride [44] and by several EAOPs in sulfate medium, such as EO with a Ti/SnO_2 anode and a Ni cathode [45] as well as EF [21] and photo-electro-Fenton [22] with a Ti/RuO_2 anode and an ACF cathode. Worth highlighting, key issues regarding the viability of processes like current efficiency, specific energy consumption and reaction intermediates formed were not addressed in those works.

This paper reports the degradation of 2.5 L of 209.3 mg L^{-1} Carmoisine solutions of pH 3.0 by EO-H_2O_2 and EF using a BDD/air-diffusion reactor. The role of the oxidants formed in Na_2SO_4, NaCl or $LiClO_4$ medium was clarified. The influence of applied current density (j) and NaCl and dye contents on the decolorization efficiency, mineralization rate, mineralization current efficiency (MCE) and specific energy consumption was examined. Primary aromatic intermediates were identified by gas chromatography-mass spectrometry (GC–MS) and final carboxylic acids and generated inorganic ions were quantified by chromatographic techniques.

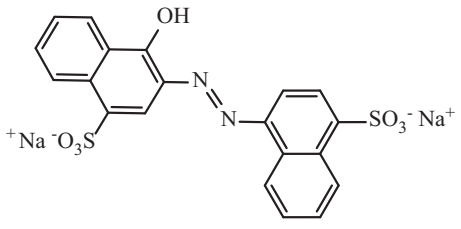

Fig. 1. Chemical structure of Carmoisine (Acid Red 14, additive E122).

2. Materials and methods

2.1. Chemicals

Commercial Carmoisine dye (60% purity and 40% of inorganic ions for stabilization) was provided by Sigma–Aldrich and used as received. Anhydrous sodium sulfate, sodium chloride and lithium perchlorate used as supporting electrolytes and iron(II) sulfate heptahydrate used as catalyst in EF were of analytical grade purchased from Fluka and Sigma–Aldrich. The corresponding sulfuric, hydrochloric and perchloric acids used to regulate the initial pH to 3.0 were of analytic grade supplied by Merck, Panreac and Acros Organics, respectively. Solutions were prepared with deionized water. Organic solvents and other chemicals used were of HPLC or analytical grade supplied by Sigma–Aldrich, Merck and Panreac.

2.2. Recirculation flow plant

A scheme of the batch recirculation flow plant used in this work can be found elsewhere [46]. In each assay, 2.5 L of a Carmoisine solution were introduced into the reservoir and recirculated through the plant using a centrifugal pump. The flow rate was kept at 200 L h^{-1} with a flowmeter and the solution temperature was regulated at 35 °C by means of two heat exchangers connected to a water bath. The electrochemical cell was an undivided filter-press reactor equipped with a 20 cm^2 BDD thin-film anode from Adamant Technologies and a 20 cm^2 carbon-PTFE air-diffusion cathode from E-TEK, with an interelectrode gap of 1.2 cm. The cathode was in contact with a PVC gas chamber fed with atmospheric air at an overpressure of about 8.6 kPa regulated with a back-pressure gauge to continuously produce H_2O_2 from reaction (5). All the trials were performed at constant j provided by an Agilent 6552A DC power supply.

Solutions with 209.3 mg L^{-1} Carmoisine and 0.050 M Na_2SO_4 (in H_2SO_4), 0.050 M $LiClO_4$ (in $HClO_4$) or 0.050 M NaCl (in HCl) at pH 3.0 were comparatively degraded by EO-H_2O_2 and EF at 100 mA cm^{-2}. The influence of j between 50 and 150 mA cm^{-2}, NaCl concentration up to 0.30 M and dye content between 104.6 and 628.0 mg L^{-1} on the oxidation power of both processes was examined. In EF, 0.5 mM Fe^{2+} was employed as optimal catalyst amount [31–33].

2.3. Instruments and analytical procedures

The solution pH was measured with a Crison 2000 pH-meter. Samples were withdrawn at regular time intervals from the treated solutions and then microfiltered with 0.45 μm PTFE filters from Whatman before analysis. The decolorization of Carmoisine solutions was monitored from the absorbance (A) decay at its maximum absorption wavelength (λ_{max}) of 514 nm, determined from the spectra recorded on a Shimadzu 1800 UV/Vis spectrophotometer at 35 °C. The decolorization efficiency or percentage of color removal was then calculated as follows [4]:

$$\text{Color removal}(\%) = \frac{A_0 - A_t}{A_0} 100 \quad (8)$$

where A_0 and A_t denote the absorbance at initial time and after an electrolysis time t, respectively.

The mineralization of dye solutions was assessed from their total organic carbon (TOC) decay, determined with a Shimadzu VCSN TOC analyzer. Reproducible TOC values with an accuracy of ±1% were found by injecting 50 μL aliquots to the analyzer. From these data, the MCE value for each trial at current I (in A) and time t (in h) was then estimated as follows:

$$\text{MCE}(\%) = \frac{nFV_s\Delta(\text{TOC})_{exp}}{4.32 \times 10^7 m\, I\, t} 100 \quad (9)$$

where F is the Faraday constant (96,487 C mol^{-1}), V_s is the solution volume (in L), $\Delta(\text{TOC})_{exp}$ is the experimental TOC abatement (in mg L^{-1}), 4.32×10^7 is a conversion factor to homogenize units (= 3600 s h^{-1} × 12000 mg carbon mol^{-1}) and m is the number of carbon atoms of Carmoisine (20 atoms). The number of electrons (n) exchanged per each dye molecule was taken as 102 because its total mineralization involves complete conversion into CO_2 and sulfate and nitrate as pre-eminent ions, as will be discussed below, following reaction (10):

$$C_{20}H_{12}N_2O_7S_2^{2-} + 47H_2O \rightarrow 20CO_2 + 2SO_4^{2-} + 2NO_3^- + 106H^+ + 102e^- \quad (10)$$

Total nitrogen (TN) in solution was obtained with a Shimadzu TNM-1 module coupled to the above TOC analyzer. The specific energy consumption per unit TOC mass (EC_{TOC}) was determined as follows [32]:

$$EC_{TOC}(\text{kWh g}^{-1}\text{TOC}) = \frac{E_{cell} I\, t}{V_s \Delta(\text{TOC})_{exp}} \quad (11)$$

where E_{cell} is the average potential difference of the cell (in V).

Generated carboxylic acids were detected by ion-exclusion HPLC using a Waters 600 LC fitted with a Bio-Rad Aminex HPX 87H, 300 mm × 7.8 mm, column at 35 °C and coupled to a Waters 996 photodiode detector set at λ = 210 nm. A 4 mM H_2SO_4 solution eluted at 0.6 mL min^{-1} was used as mobile phase. In these chromatograms, well-defined peaks appeared at retention times of 6.9 min for oxalic acid, 7.9 min for tartronic acid, 9.4 min for oxamic acid and 13.7 min for formic acid. The content in NH_4^+, NO_3^-, SO_4^{2-}, Cl^-, ClO_3^- and ClO_4^- ions of treated solutions was analyzed by ion chromatography upon injection of 25 μL aliquots into a Shimadzu 10Avp LC coupled to a Shimadzu CDD 10Avp conductivity detector. The NH_4^+ concentration was determined using a Shodex IC YK-421, 125 mm × 4.6 mm, cationic column at 40 °C and a mobile phase composed of 24.2 mM boric acid, 5.0 mM tartaric acid, 1.5 mM 18-crown-6 and 2.0 mM 2,6-pyridinedicarboxylic solution at 1.0 mL min^{-1}. The NO_3^-, SO_4^{2-}, Cl^-, ClO_3^- and ClO_4^- contents were quantified with a Shim-Pack IC-A1S, 100 mm × 4.6 mm, anionic column at 40 °C and a solution composed of 2.4 mM tris(hydroxymethyl)aminomethane (pH = 4.0) and 2.6 mM phthalic acid eluted at 1.5 mL min^{-1} as mobile phase.

To identify the primary intermediates generated, several 209.3 mg L^{-1} Carmoisine solutions in 0.050 M Na_2SO_4 of pH 3.0 were electrolyzed for short times by EO-H_2O_2 and EF at 100 mA cm^{-2}. The organic compounds contained in 100 mL of each electrolyzed solution were then extracted with CH_2Cl_2 (3 × 25 mL). The resulting organic solution was dried over anhydrous Na_2SO_4, filtered and concentrated up to ca. 1 mL under reduced pressure to be further analyzed by GC–MS using an Agilent Technologies system composed of a 7890A gas chromatograph coupled to a 5975C mass spectrometer operating in EI mode at 70 eV. A non-polar Agilent J&W HP-5 ms and a polar HP INNOWax, both columns of 0.25 μm, 30 m × 0.25 mm, were used. The temperature ramp was 36 °C for 1 min, 5 °C min^{-1} up to 300 or 250 °C for the non-polar or polar column, respectively, and hold time 10 min. The temperature of the inlet, source and transfer line was 250, 230 and 280 °C for the non-polar column and 250, 230 and 250 °C for the polar one. The mass spectra were identified with a NIST05 MS library.

3. Results and discussion

3.1. Electrogeneration of H_2O_2 during EO-H_2O_2 treatments in different supporting electrolytes

A first series of assays was made by electrolyzing 2.5 L of solutions of different supporting electrolytes at pH 3.0 and 100 mA cm^{-2} for 480 min aiming to determine the evolution of H_2O_2 accumulated in each medium under the same EO-H_2O_2 conditions.

Fig. 2 shows that the accumulation of H_2O_2 always underwent a gradual deceleration at prolonged electrolysis. This behavior is characteristic of undivided electrolytic cells with an air-diffusion cathode and can be mainly related to the progressive increase in destruction rate of H_2O_2 via anodic reaction (6) and other chemical reactions in solution when the concentration of this species rises [4,8,9]. A similar H_2O_2 evolution was found in both SO_4^{2-} and ClO_4^- media, attaining near 21 mg L^{-1} (18% current efficiency). This

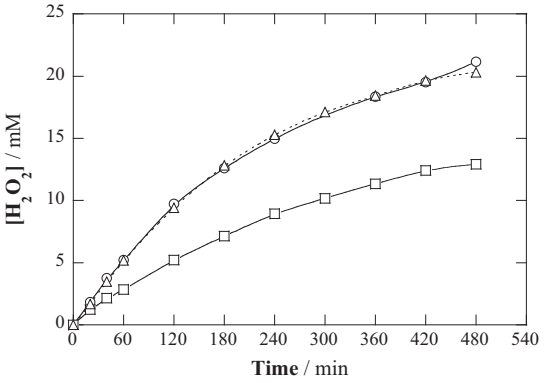

Fig. 2. Effect of supporting electrolyte nature on the change of H_2O_2 concentration with time during the EO-H_2O_2 treatment of 2.5 L of solutions containing 0.050 M of (○) Na_2SO_4, (Δ) $LiClO_4$ and (□) NaCl, at pH 3.0 using a flow plant with a BDD/air-diffusion cell at 100 mA cm^{-2} and 35 °C.

suggests that in such supporting electrolytes, the main route for H_2O_2 decay is its removal by reaction (6). In contrast, Fig. 2 shows a much quicker H_2O_2 destruction in Cl^- medium, reaching a final accumulation of 12.9 mg L^{-1} (11% current efficiency) at 480 min. This comparative drop in H_2O_2 content suggests a particular reactivity with active chlorine species formed from reactions (2)–(4).

Since $pK_a = 7.55$ for reaction (4), one can infer that at pH 3.0, HClO produced by reactions (2) and (3) during electrolysis is the predominant active chlorine species present in Cl^- medium [4]. The faster destruction of H_2O_2 in this electrolyte under EO-H_2O_2 conditions (see Fig. 2) can then be accounted for by its reaction with HClO to form Cl^- ion and O_2 gas as follows [17,47]:

$$HClO + H_2O_2 \rightarrow Cl^- + O_2(g) + H_2O + H^+ \quad (12)$$

On the other hand, it is well known that electrogenerated HClO can be consecutively oxidized to ClO_2^-, ClO_3^- and ClO_4^- ions at BDD anode by reactions (13)–(15), respectively [4]:

$$HClO + H_2O \rightarrow ClO_2^- + 3H^+ + 2e^- \quad (13)$$

$$ClO_2^- + H_2O \rightarrow ClO_3^- + 2H^+ + 2e^- \quad (14)$$

$$ClO_3^- + H_2O \rightarrow ClO_4^- + 2H^+ + 2e^- \quad (15)$$

Analysis of the final treated solution in 0.050 M Cl^- by ion chromatography revealed that the concentration of this ion was reduced to 0.044 M, whereas 2.85 mM ClO_3^- and 1.84 mM ClO_4^- were detected in the medium. These results corroborate the generation of active chlorine species as well as chlorine oxyanions under the present EO-H_2O_2 conditions, which will also take place in the EF trials. The data of Fig. 2 also indicate that the BDD/air-diffusion cell produces high enough H_2O_2 content in all the electrolytes to generate great amount of ·OH in the bulk by Fenton's reaction (7) under EF conditions.

3.2. Effect of supporting electrolyte on the decolorization and mineralization of Carmoisine solutions by EO-H_2O_2

Fig. 3 depicts the change in decolorization efficiency at $\lambda_{max} = 514$ nm with electrolysis time for the above EO-H_2O_2 treatments at 100 mA cm^{-2} but in the presence of 209.3 mg L^{-1} Carmoisine. A quite slow decolorization can be observed in SO_4^{2-} and ClO_4^-, attaining 70% and 82% color removal at 480 min, respectively, whereas the solution became colorless after ca. 25 min of electrolysis in Cl^- medium. In the two former electrolytes, BDD(·OH) generated via reaction (1) was the main oxidizing agent and thus, the dye and its colored products reacted slowly because of mass transport limitations. The production of larger amounts of BDD(·OH) in ClO_4^- medium can explain the slightly higher decolorization efficiency compared to that found in SO_4^{2-}. This phenomenon can be mainly related to the competitive formation of the weaker oxidant peroxodisulfate ($S_2O_8^{2-}$) ion by oxidation of SO_4^{2-} ion via reaction (16) [7,11,12].

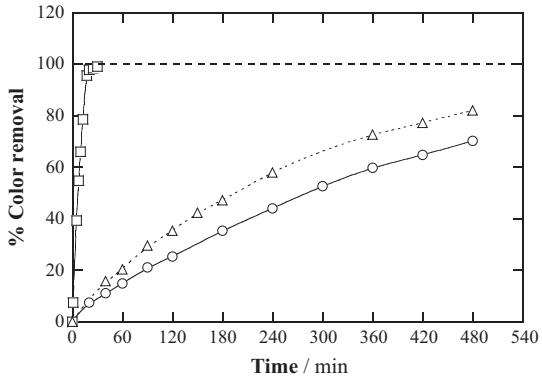

Fig. 3. Percentage of color removal at 514 nm vs electrolysis time under the same conditions of the trials shown in Fig. 2 but in the presence of 209.3 mg L^{-1} Carmoisine.

$$2SO_4^{2-} \rightarrow S_2O_8^{2-} + 2e^- \quad (16)$$

Some authors have shown that reaction (16) might proceed through ·OH attack onto SO_4^{2-} ion to yield sulfate radical ion ($SO_4^{\cdot-}$) via reaction (17), which subsequently dimerizes to $S_2O_8^{2-}$ ion by reaction (18) [48]:

$$SO_4^{2-} + BDD(\cdot OH) \rightarrow BDD + SO_4^{\cdot-} + OH^- \quad (17)$$

$$2SO_4^{\cdot-} \rightarrow S_2O_8^{2-} \quad (18)$$

Consequently, the decrease in BDD(·OH) content in SO_4^{2-} electrolyte compared to ClO_4^- slows down the oxidation process and hence, diminishes the efficiency of the electrochemical treatment.

In contrast, the very fast color removal shown in Fig. 3 in the chloride solution can be related to the quick reaction of Carmoisine with HClO, which is the predominant active chlorine species at pH 3.0, as stated above. Under these conditions, the dye was much more rapidly destroyed in the bulk by HClO than at the anode surface by BDD(·OH), thereby making the decolorization process much more efficient than that in SO_4^{2-} and ClO_4^- media.

A very different behavior was found for the TOC abatement of the same dye solutions at 100 mA cm^{-2}. Fig. 4a shows a slow, gradual and similar TOC decay in SO_4^{2-} and ClO_4^- media, suggesting that the degradation routes involved the same kinds of intermediates. After 480 min of electrolysis, only 50% TOC removal was obtained for the EO-H_2O_2 treatment of Carmoisine solutions, which is an evidence of the formation of very recalcitrant intermediates. Fig. 4a also highlights a quicker TOC decay for the first 240 min of electrolysis using the Cl^- medium, whereupon the removal rate was similar to that found in the other two electrolytes, also being finally reduced by about 50%. These findings suggest that the fast initial attack of HClO over Carmoisine leads to a larger proportion of primary products that can be more easily mineralized by BDD(·OH) and/or HClO, but the subsequent recalcitrant products are much more slowly destroyed.

The low and analogous oxidation power of the EO-H_2O_2 process to mineralize the dye solution in all media was also reflected in the MCE values obtained from Eq. (9), as depicted in Fig. 4b. Low efficiencies usually ranging between 9% and 10% were determined in both SO_4^{2-} and ClO_4^- media, as a result of an almost constant degree of mineralization of intermediates during electrolysis. In the presence of Cl^-, higher efficiency was found up to 240 min because of the quicker mineralization of the dye solution. However, MCE gradually decreased from 20% to 10% and then kept constant since prolonged electrolyses caused the formation of recalcitrant products.

The EC_{TOC} values calculated from Eq. (11) are shown in Fig. 4c. The energy consumption was approximately constant in SO_4^{2-}, oscillating between 1.80 and 2.41 kW h g^{-1} TOC, as expected from the almost constant rate for TOC decay (see Fig. 4a). A similar trend can be observed in Fig. 4c for ClO_4^- medium, although with greater EC_{TOC} values varying between 2.21 and 3.46 kW h g^{-1} TOC due to the higher E_{cell} arising in the electrolytic system arising from the lower solution conductivity. In contrast, the energy consumption in Cl^- medium rose progressively from 0.70 to 2.82 kW h g^{-1} TOC during the EO-H_2O_2 treatment as a result of two factors: (i) the drop in TOC removal at prolonged electrolysis and (ii) the increase in E_{cell} due to the conductivity decay by gradual oxidation of Cl^- ion, as stated above.

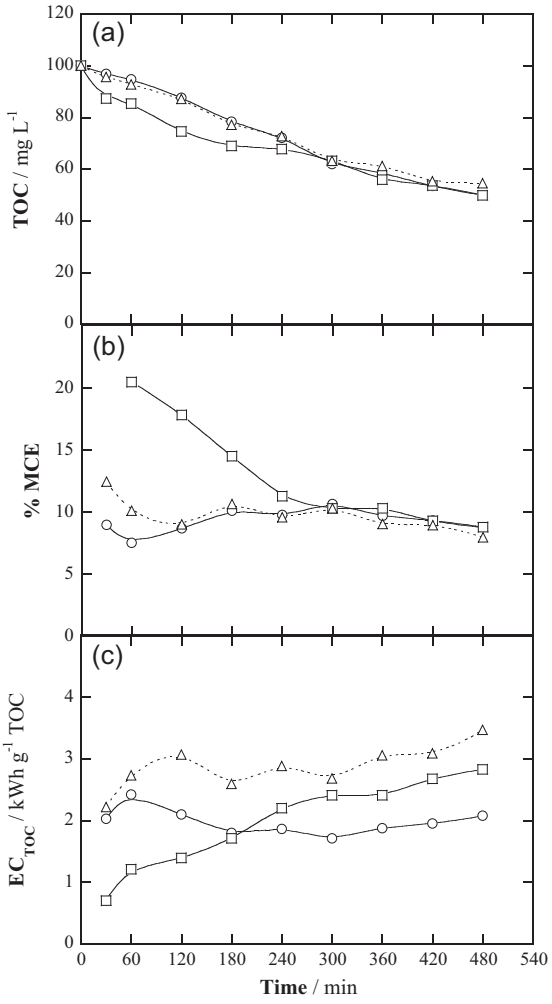

Fig. 4. (a) TOC removal, (b) mineralization current efficiency and (c) specific energy consumption per unit TOC mass with electrolysis time for the experiments depicted in Fig. 3.

All these results show that Carmoisine solutions can be rapidly and completely decolorized by EO-H_2O_2 only using the Cl^- medium because of the much more efficient destruction of the dye and its colored oxidation products by generated HClO than by BDD(·OH). The decolorization rate in SO_4^{2-} and ClO_4^- media under the action of the latter radical was then so low that color removal was incomplete at 100 mA cm^{-2}, even operating for 480 min. Although the presence of Cl^- accelerated the dye mineralization during the first stages, similar TOC removal and MCE values were finally found in all media, suggesting the formation of very recalcitrant intermediates. The lowest EC_{TOC} during the latter stages was obtained in SO_4^{2-}, which can be considered as the best electrolyte for the EO-H_2O_2 treatment of Carmoisine. Similar behavior has been reported for other monoazo dyes degraded by EO (without H_2O_2 production) with Pt and BDD anodes in SO_4^{2-} and Cl^- solutions [4], always obtaining a quicker decolorization in the presence of Cl^- but usually with a greater mineralization in SO_4^{2-} medium due to the formation of more recalcitrant chloro derivatives.

3.3. Influence of current density and Cl^- concentration on the decolorization process by EO-H_2O_2

In view of the high ability of the Cl^- electrolyte to rapidly decolorize the 209.3 mg L^{-1} Carmoisine solution at pH 3.0, the effect of key operating parameters such as j and Cl^- content on this process was examined. Fig. 5 illustrates the positive influence of increasing

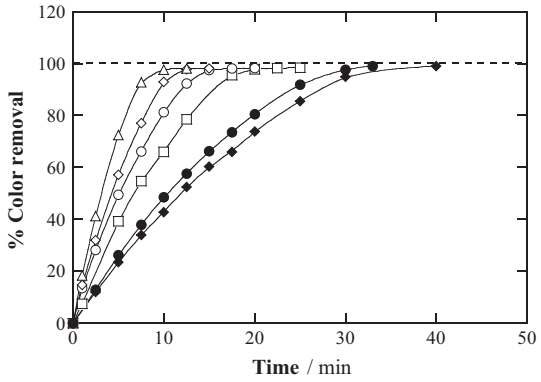

Fig. 5. Effect of NaCl concentration on the percentage of color removal at 514 nm vs electrolysis time for the EO-H_2O_2 degradation of 2.5 L of 209.3 mg L^{-1} Carmoisine solutions in: (□) 0.05 M, (○) 0.10 M, (◇) 0.15 M and (Δ) 0.30 M NaCl, at pH 3.0 using a flow plant with a BDD/air-diffusion reactor at 100 mA cm^{-2} and 35 °C. The influence of current density is shown for 0.050 M NaCl by comparison with trials at (♦) 50 mA cm^{-2} and (●) 75 mA cm^{-2}.

j from 50 to 100 mA cm^{-2} on the percentage of color removal in the EO-H_2O_2 process using 0.050 M Cl^- since the time needed for total decolorization decreased from about 40 to 25 min. This behavior can be related to the concomitant increase in rate of electrode reactions at higher j, particularly reactions (2) and (3) generating greater quantities of HClO that attack more quickly the dye and its colored products. On the other hand, the data shown in Fig. 5 highlight that shorter time was progressively needed to completely decolorize the dye solution as Cl^- concentration rose from 0.050 to 0.30 M, as a result of the greater mass transport of this ion towards the BDD anode that accelerated the HClO formation. All these findings indicate that the rise of j and Cl^- content is beneficial for reaching a faster color removal, although the use of low values of these parameters (e.g., 50 mA cm^{-2} and 0.050 M) already led to a rapid decolorization owe to the efficient action of HClO.

3.4. Effect of supporting electrolyte nature on the EF treatment of Carmoisine solutions

Solutions of 2.5 L of 209.3 mg L^{-1} Carmoisine in the different supporting electrolytes at pH 3.0 were subsequently degraded by EF under comparable conditions to those used for EO-H_2O_2. For these trials, a catalytic amount of 0.5 mM Fe^{2+} was always initially added and no significant change in solution pH was observed as electrolyses proceeded. Fig. 6 shows the variation of the percentage of color removal with electrolysis time for the three EF trials at 100 mA cm^{-2}. The most rapid decolorization occurred by using 0.050 M Cl^-, needing about 25 min to get a colorless solution. This time was similar to that required in the analogous EO-H_2O_2 treatment (see Fig. 5), which means that at the beginning of EF the dye and its colored products are more quickly transformed by HClO formed from reactions (2) and (3) than by heterogeneous BDD(·OH) and homogeneous ·OH produced from reactions (1) and (7), respectively. In contrast, the EO-H_2O_2 and EF processes showed a very different behavior in SO_4^{2-} and ClO_4^- media, as can be deduced by comparing Figs. 3 and 6. While the color slowly disappeared for 480 min in EO-H_2O_2, total decolorization was quickly achieved after ca. 60 min in both cases using EF. This means that in EF, the additional ·OH formed from Fenton's reaction (7) has much larger ability to destroy the colored compounds than BDD(·OH). Fig. 6 also shows a slightly quicker decolorization rate in ClO_4^- compared to SO_4^{2-}, which can be explained by the production of smaller amounts of ·OH in the latter electrolyte because of the partial inhi-

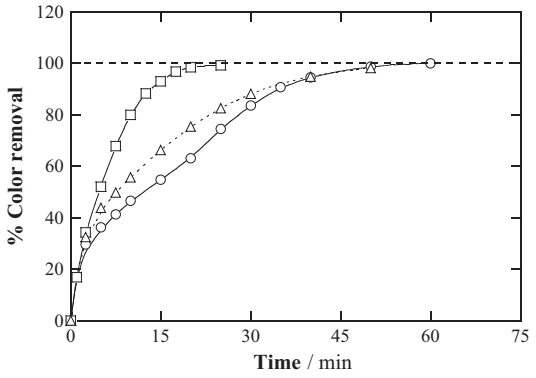

Fig. 6. Influence of supporting electrolyte nature on the percentage of color removal at 514 nm vs electrolysis time for the treatment of 2.5 L of 209.3 mg L^{-1} Carmoisine solutions in 0.050 M of (○) Na_2SO_4, (Δ) $LiClO_4$ and (□) NaCl at pH 3.0 by EF with 0.5 mM Fe^{2+} using a flow plant with a BDD/air-diffusion cell at 100 mA cm^{-2} and 35 °C.

bition of Fenton's reaction (7) that results from formation of sulfate-iron complexes that reduces the free Fe^{2+} concentration [24].

The greater effectiveness of ·OH generated in the bulk over physisorbed BDD(·OH) was confirmed from the faster and larger TOC abatement found in all media compared to results of EO-H_2O_2. As can be seen in Fig. 7a, TOC always underwent a quick decay during the first 180 min, being reduced by 67% in SO_4^{2-}, 63% in ClO_4^- and 57% in Cl^-. TOC removal was improved only very slightly upon further treatment, attaining a final mineralization of 76%, 72% and 64%, respectively, although such values were much higher than 50% obtained in EO-H_2O_2 (see Fig. 4a). The fast decay in TOC during the first stages of all EF trials is due to the quick mineralization of some intermediates primordially by ·OH and/or HClO in the bulk, but resulting recalcitrant products are very slowly destroyed by those oxidants or by BDD(·OH), thus causing the strong deceleration of TOC abatement at longer electrolysis time. The slower mineralization in Cl^- compared can be related to the generation of chloro derivatives, which are more difficultly removed by BDD(·OH), as well as to the partial destruction of H_2O_2 via reaction (12).

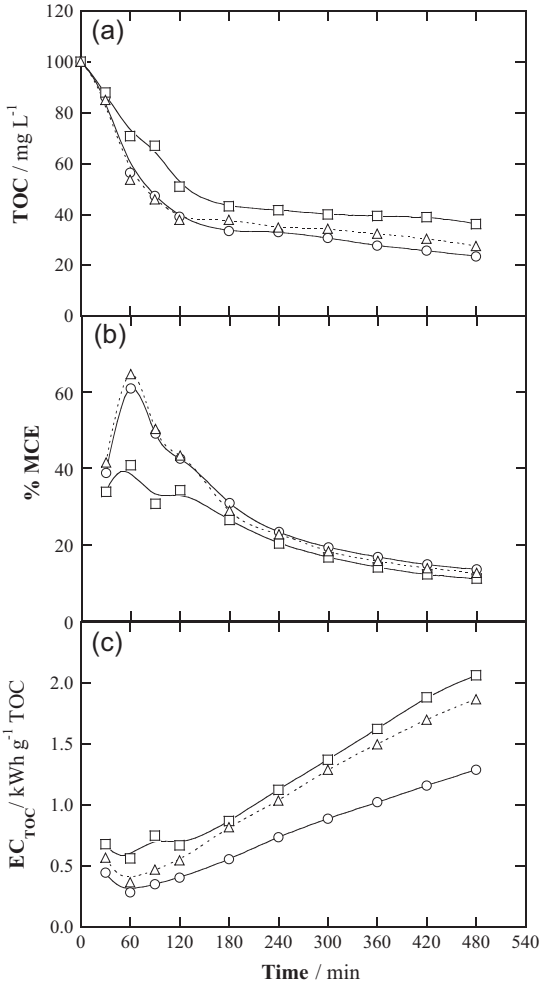

Fig. 7. (a) TOC abatement, (b) mineralization current efficiency and (c) specific energy consumption per unit TOC mass with electrolysis time for the experiments shown in Fig. 6.

The much greater oxidation ability of EF over EO-H_2O_2 for the degradation of Carmoisine was also reflected in the higher MCE and lower EC_{TOC} values, as deduced by comparing Figs. 4 and 7. Thus, Fig. 7b shows a dramatic decay in efficiency for all EF trials after achieving its maximum at 60 min, changing from 61–64% to final 13–14% in SO_4^{2-} and ClO_4^- and from 41% to 11% in Cl^- because of the loss in organic matter and the generation of refractory products [4,9]. These two facts led to higher energy consumption values as electrolysis time increased, as shown in Fig. 7c. The lowest EC_{TOC} values were obtained in SO_4^{2-}, which rose from 0.28 kW h g^{-1} TOC at 60 min to 1.28 kW h g^{-1} TOC at 480 min. Larger energy consumptions were determined in ClO_4^- despite exhibiting similar efficiencies to SO_4^{2-} due to the greater E_{cell}, as occurred in EO-H_2O_2. The EC_{TOC} values were even superior in Cl^- because of the lower TOC removal at each time and the decay in solution conductivity by Cl^- oxidation.

Analysis of the final electrolyzed solution in ClO_4^- by ion chromatography revealed the release of 5.0 mg L^{-1} of NH_4^+ (33% of initial N), 27.1 mg L^{-1} of NO_3^- (52% of initial N) and 72.9 mg L^{-1} of SO_4^{2-} (91% of initial S). TN analysis of this solution yielded 10.3 mg L^{-1} of N (88% of initial N), which almost corresponded to the sum of the N content as NH_4^+ and NO_3^-. These findings indicate that the final solution could contain only some recalcitrant sulfur species and no nitrogenated products, whereas only a small proportion of the initial N (about 12%) was transformed into volatile *N*-derivatives, probably N_2 and N_xO_y species. Similar contents for NO_3^-, SO_4^{2-} and TN were found for the final solution treated in Cl^-, but only 2.2 mg L^{-1} of NH_4^+ (15% of initial N) were detected, suggesting that highly stable *N*-derivatives could remain in the treated solution. All these results demonstrate that NO_3^- and SO_4^{2-} are the pre-eminent ions released during Carmoisine mineralization, as proposed in reaction (10).

Daneshvar et al. [24] reported that the oxidation power for the EF treatment of the azo dye Orange II at pH 3.0 using a stirred tank reactor with a Pt anode and a graphite-felt cathode decreased in the order $ClO_4^- > Cl^- > SO_4^{2-}$, with 75% mineralization as maximal. The poorest degradation using SO_4^{2-} was explained by the loss of Fe^{2+} content due to the formation of sulfate-iron complexes (see above). Although this phenomenon can be observed during the decolorization of Carmoisine (see Fig. 6), the results of Fig. 7 suggest the production of quite similar amounts of ·OH in both SO_4^{2-} and ClO_4^- media yielding analogous mineralization rate. This behavior could be due to the much higher H_2O_2 content produced by our air-diffusion cathode (see Fig. 2) compared to graphite felt [4,24], thus producing a similar quantity of ·OH in both electrolytes from Fenton's reaction (7), even if free Fe^{2+} concentration is slightly lower in SO_4^{2-}. Furthermore, the use of BDD in this study contributes to enhance the oxidation power of EF in SO_4^{2-}.

The aforementioned findings allow inferring that the best EF treatment to mineralize the 209.3 mg L^{-1} Carmoisine solution at pH 3.0 with lowest EC_{TOC} is that performed in SO_4^{2-}.

3.5. Influence of current density and dye content on the EF degradation in sulfate medium

Fig. 8a shows a quicker decolorization of 2.5 L of 209.3 mg L^{-1} Carmoisine by EF when j rose from 50 to 150 mA cm^{-2}. The rate of this process was improved more remarkably when increasing from 50 to 75 mA cm^{-2} and the time needed for total color removal decreased from 90 min at 50 mA cm^{-2} to 50 min at 150 mA cm^{-2}. This trend can be explained by the acceleration of both, reaction (1) yielding higher BDD(·OH) concentration and reaction (5) producing greater H_2O_2 concentration [4] that gives rise to larger amounts of ·OH from Fenton's reaction (7), therefore enhancing the destruction of the dye and its colored products. A faster mineralization of the dye solution was also achieved at higher j, as depicted in Fig. 8b, which can be justified again by the concomitant larger generation of BDD(·OH) and ·OH. For example, TOC was reduced by 72%, 75%, 76% and 80% after 480 min at 50, 75, 100 and 150 mA cm^{-2}, respectively. In these experiments, however, decreasing MCE values of 26%, 18%, 14% and 10% were obtained. The drop in efficiency with increasing j can be ascribed to a progressive loss in the available concentration of BDD(·OH) and ·OH due to the enhancement of their parasitic reactions involving, for example, the oxidation of BDD(·OH) to O_2 on the anode by reaction (19) and the reaction of ·OH in the bulk with generated H_2O_2 by reaction (20) [4,7,9]:

$$2BDD(\cdot OH) \rightarrow 2BDD + O_2 + 2H^+ + 2e^- \quad (19)$$

$$H_2O_2 + \cdot OH \rightarrow HO_2^{\cdot} + H_2O \quad (20)$$

Fig. 9a illustrates the change in percentage of color removal for the EF treatment of Carmoisine concentrations ranging between 104.6 and 628.0 mg L^{-1} at 100 mA cm^{-2}. A longer time between 30 and 105 min was required for reaching total decolorization as the dye content increased, as a result of the existence of more colored organics reacting with similar amounts of generated BDD(·OH) and mainly ·OH. This trend was not verified so clearly for the TOC abatement of the same solutions because of the different reactivity of intermediates with such oxidants. Fig. 9b shows a similar TOC removal rate up to 418.6 mg L^{-1}, whereas it decayed strongly for 628.0 mg L^{-1}. At 480 min, for example, TOC was reduced by 70%, 76%, 72% and 56%. In contrast, increasing MCE values of 8%, 14%, 25% and 30% were found due to the gradual destruction of larger TOC contents. This allows considering that BDD(·OH) and ·OH are able to preferentially react with more organic molecules as concentration rises, with the consequent minimization of their parasitic reactions.

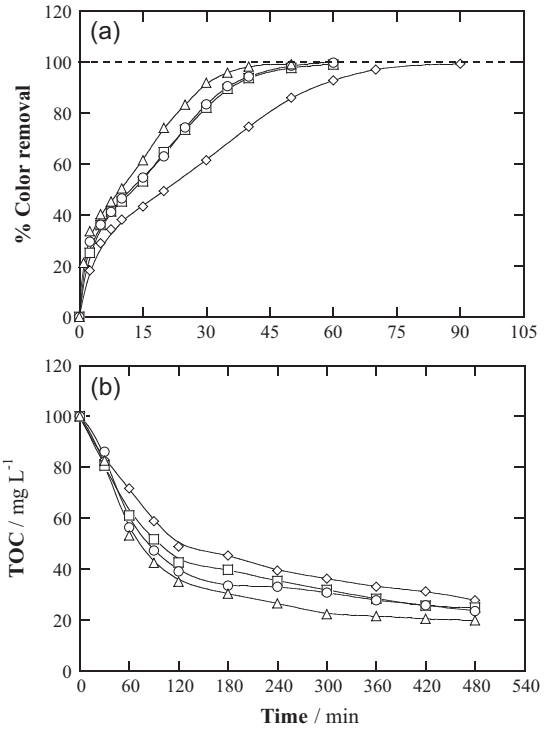

Fig. 8. Effect of current density on (a) the percentage of color removal at 514 nm and (b) TOC abatement vs electrolysis time for the degradation of 2.5 L of 209.3 mg L^{-1} Carmoisine solutions in 0.050 M Na_2SO_4 at pH 3.0 and 35 °C by EF process with 0.5 mM Fe^{2+} using a flow plant with a BDD/air-diffusion cell. Current density: (◊) 50 mA cm^{-2}, (□) 75 mA cm^{-2}, (○) 100 mA cm^{-2} and (Δ) 150 mA cm^{-2}.

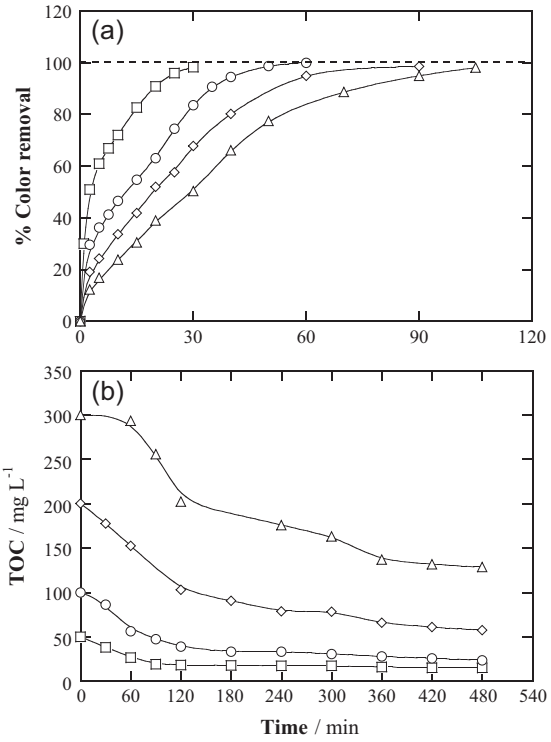

Fig. 9. Influence of dye concentration on the variation of (a) decolorization efficiency and (b) TOC with electrolysis time for the EF treatment of 2.5 L of Carmoisine solutions in 0.050 M Na_2SO_4 with 0.5 mM Fe^{2+} at pH 3.0 and 35 °C using a flow plant with a BDD/air-diffusion reactor at 100 mA cm^{-2}. Carmoisine concentration: (□) 104.6 mg L^{-1}, (○) 209.3 mg L^{-1}, (◊) 418.6 mg L^{-1} and (Δ) 628.0 mg L^{-1}.

The above EF study in SO_4^{2-} allows concluding that the decolorization and TOC removal of Carmoisine solutions are enhanced at higher j and lower dye content, despite the similar percentages of TOC decay between 70–76% obtained in the range 104.6–418.6 mg L^{-1}, although greater efficiency can be obtained as dye concentration rises.

3.6. Identification and evolution of oxidation products

Several short electrolyses of 209.3 mg L^{-1} Carmoisine solutions were made under the best EO-H_2O_2 and EF conditions (i.e., 0.050 M SO_4^{2-} at 100 mA cm^{-2}), thereby extracting their organic components to be identified by GC–MS. Table 1 summarizes the 15 aromatics detected as primary products resulting from the cleavage of either the —N=N— or the C—N bond upon attack of hydroxyl radicals. Overall, six benzene and four naphthalene derivatives, along with condensation products related to one indane, two indole and two benzofuran derivatives, were found. Many of these compounds contain carbonyl and/or hydroxyl groups coming from

Table 1
Primary by-products identified by GC–MS analysis for the EO-H_2O_2 and EF treatments of 2.5 L of 209.3 mg L^{-1} Carmoisine solutions in 0.050 M Na_2SO_4 at pH 3.0 using a flow plant equipped with a BDD/air-diffusion reactor at 100 mA cm^{-2} and 35 °C.

Benzene derivatives	Naphthalene derivatives	Indane derivatives	Indole derivatives	Benzofuran derivatives
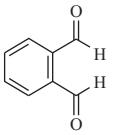	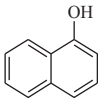	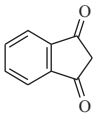	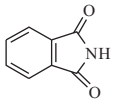	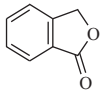
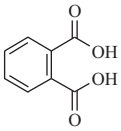	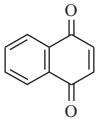		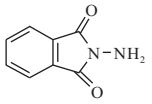	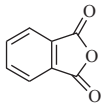
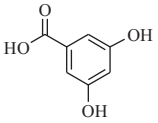	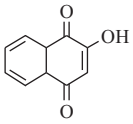			
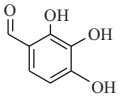	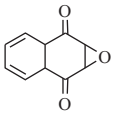			
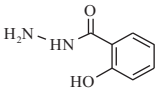				
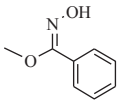				

the attack of hydroxyl radical on the aromatic ring. The large variety of primary aromatic products reveals the complexity of the degradation processes of Carmoisine under the action of BDD(·OH) and/or ·OH in both EAOPs.

Ion-exclusion chromatograms of the same degraded solutions in SO_4^{2-} revealed the generation of a mixture of short-linear carboxylic acids like tartronic, oxamic, oxalic and formic. While tartronic acid is formed from the cleavage of the aromatic moieties of intermediates, oxalic and formic acids are final products coming from the destruction of longer carboxylic acids [9,16,18]. Oxamic acid should arise from the oxidation of *N*-derivatives. Oxalic, oxamic and formic acids can be directly converted into CO_2 [4,23,30–34].

Formic acid was not detected in EO-H_2O_2, whereas it disappeared at 420 min of EF after reaching a maximal concentration of about 10 mg L^{-1} at 240 min. The evolution of the other three acids in both methods is presented in Fig. 10. As can be seen in Fig. 10a, low contents of 0.6, 0.5 and 6.0 mg L^{-1} of tartronic, oxamic and oxalic acids, respectively, were accumulated at the end of EO-H_2O_2, due to their efficient destruction by BDD(·OH) that minimizes their accumulation [4,7]. All these acids yielded 1.9 mg L^{-1} of TOC, which corresponded to about 4% of the organic matter contained in ca. 50 mg L^{-1} of TOC of the final solution (see Fig. 4a), which suggests the formation of a very large proportion of unidentified recalcitrant products that are very slowly attacked by BDD(·OH). In contrast, Fig. 10b shows that in EF, tartronic acid was accumulated up to 9.7 mg L^{-1} as maximal at 40 min, then disappearing at 180 min, whereas oxamic acid persisted during all the treatment up to a final value of 1.3 mg L^{-1}. On the other hand, oxalic acid was rapidly accumulated up to 72.7 mg L^{-1} at 120 min, whereupon it was only slowly removed up to 65.9 mg L^{-1}. At the end of EF treatment, the concentration of final oxamic and oxalic acids corresponded to 17.9 mg L^{-1} TOC, representing near 75% of

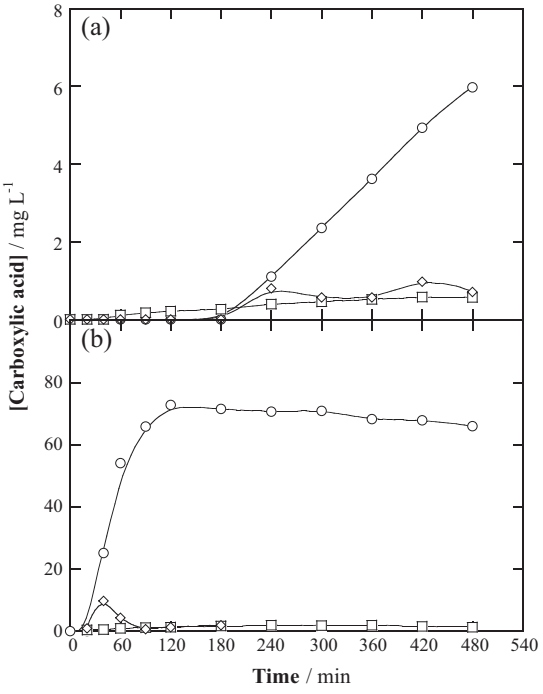

Fig. 10. Evolution of the concentration of (○) oxalic, (□) oxamic and (◊) tartronic acids detected during the treatment of 2.5 L of 209.3 mg L^{-1} Carmoisine solutions in 0.050 M Na_2SO_4 at pH 3.0 by (a) EO-H_2O_2 and (b) EF using a flow plant with a BDD/air-diffusion reactor at 100 mA cm^{-2} and 35 °C.

24 mg L^{-1} of TOC of the remaining soluble organic load (see Fig. 7a). Under these conditions, all the acids form Fe(III)-carboxyl-

ate complexes that are attacked by BDD(·OH), but not by ·OH [8,9,32,33]. These results confirm that ·OH generated from Fenton's reaction (7) can efficiently oxidize many primary intermediates of Carmoisine that otherwise react very slowly with BDD(·OH) in EO-H_2O_2 due to mass transport limitations. Therefore, EF process constitutes a much more potent technology to mineralize dye solutions, although the persistence of Fe(III)-oxalate complexes as final products slows down the degradation during the final stages.

4. Conclusions

The use of a recirculation flow plant with a BDD/air-diffusion reactor for treating 2.5 L of 209.3 mg L^{-1} Carmoisine solutions in 0.050 M SO_4^{2-} or ClO_4^- at pH 3.0 by EO-H_2O_2 allowed the accumulation of a similar and high H_2O_2 content, which was significantly lower in 0.050 M Cl^- because of its destruction by active chlorine species like HClO in the bulk. The attack of HClO on the dye and reaction products caused a rapid decolorization, which was enhanced by increasing j and Cl^- concentration. In contrast, fading was very slow using SO_4^{2-} and ClO_4^- since the disappearance of colored compounds was restricted to reaction with BDD(·OH) in the anode vicinity. A similar TOC reduction of 50% with MCE values near 10% was found after 480 min in all media at 100 mA cm^{-2}, although smaller EC_{TOC} values were obtained in SO_4^{2-}, which became the best medium for the EO-H_2O_2 treatment of acidic Carmoisine solutions. The EF process with 0.5 mM Fe^{2+} as catalyst performed in 0.050 M Cl^- yielded a similar decolorization rate to that found in EO-H_2O_2, thus confirming that HClO was the main oxidant during the first stage in both EAOPs. In contrast, color removal in both SO_4^{2-} and ClO_4^- media was faster in the former method owing to the superiority of ·OH in the bulk over BDD(·OH) to attack the colored compounds. The formation of refractory chloro derivatives in Cl^- and the partial destruction of H_2O_2 by HClO led to lower TOC abatements and efficiencies compared to those obtained in other media. Again, the use of SO_4^{2-} was beneficial in EF, yielding 76% mineralization with 14% MCE and 1.28 kW h g^{-1} TOC after 480 min at 100 mA cm^{-2}. It has been found that solutions containing up to 418.6 mg L^{-1} Carmoisine were efficiently degraded by this latter EAOP. Up to 15 aromatic products arising from the cleavage of the —N=N— or C—N bonds were detected by GC–MS analysis. Short-linear carboxylic acids like tartronic, oxalic, oxamic and formic were quantified by ion-exclusion HPLC. The persistence of Fe(III)-oxalate complexes accounted for the partial mineralization of the Carmoisine solution in EF.

Acknowledgments

The authors thank MINECO (Ministerio de Economía y Competividad, Spain) for financial support under project CTQ2013-48897-C2-1-R, co-financed with FEDER funds. The Ph.D. grant awarded to A. Thiam from MAEC-AECID (Spain) is also acknowledged.

References

[1] UNESCO, The United Nations World Water Development Report 4, Volume 1: Managing Water Report under Uncertainty and Risk, 2012.
[2] K.P. Sharma, S. Sharma, S. Sharma, P.K. Singh, S. Kumar, R. Grover, P.K. Sharma, A comparative study on characterization of textile wastewaters (untreated and treated) toxicity by chemical and biological tests, Chemosphere 69 (2007) 48–54.
[3] S.M.A.G. Ulson de Souza, E. Forgiarini, A.A. Ulson de Souza, Toxicity of textile dyes and their degradation by the enzyme horseradish peroxidase (HRP), J. Hazard. Mater. 147 (2007) 1073–1078.
[4] C.A. Martínez-Huitle, E. Brillas, Decontamination of wastewaters containing synthetic organic dyes by electrochemical methods: a general review, Appl. Catal. B: Environ. 87 (2009) 105–145.
[5] T. Robinson, G. McMullan, R. Marchant, P. Nigam, Remediation of dyes in textile effluent: a critical review on current treatment technologies with a proposed alternative, Biores. Technol. 77 (2001) 247–255.
[6] EFSA Panel on Food Additives and Nutrient Sources added to Food, Scientific Opinion on the re-evaluation of Azorubine/Carmoisine (E122) as a food additive. EFSA J. 7 (2009) 1332 [40 pages].
[7] M. Panizza, G. Cerisola, Direct and mediated anodic oxidation of organic pollutants, Chem. Rev. 109 (2009) 6541–6569.
[8] I. Sirés, E. Brillas, Remediation of water pollution caused by pharmaceutical residues based on electrochemical separation and degradation technologies: a review, Environ. Int. 40 (2012) 212–229.
[9] I. Sirés, E. Brillas, M.A. Oturan, M.A. Rodrigo, M. Panizza, Electrochemical advanced oxidation processes: today and tomorrow. A review, Environ. Sci. Pollut. Res. 21 (2014) 8336–8367.
[10] B. Boye, P.A. Michaud, B. Marselli, M.M. Dieng, E. Brillas, Ch. Comninellis, Anodic oxidation of 4-chlorophenoxyacetic acid on synthetic boron-doped diamond electrodes, New Diamond Front. Carbon Technol. 12 (2002) 63–72.
[11] M.A. Rodrigo, P. Cañizares, A. Sánchez-Carretero, C. Sáez, Use of conductive-diamond electrochemical oxidation for wastewater treatment, Catal. Today 151 (2010) 173–177.
[12] E. Brillas, S. Garcia-Segura, M. Skoumal, C. Arias, Electrochemical incineration of diclofenac in neutral aqueous medium by anodic oxidation using Pt and boron-doped diamond anodes, Chemosphere 79 (2010) 605–612.
[13] M.B. Ferreira, J.H.B. Rocha, J.V. de Melo, C.A. Martinez-Huitle, M.A. Quiroz Alfaro, Use of a dual arrangement of flow cells for electrochemical decontamination of aqueous solutions containing synthetic dyes, Electrocatalysis 4 (2013) 274–282.
[14] M. Hamza, R. Abdelhedi, E. Brillas, I. Sirés, Comparative electrochemical degradation of the triphenylmethane dye Methyl Violet with boron-doped diamond and Pt anodes, J. Electroanal. Chem. 627 (2009) 41–50.
[15] L. Ciríaco, C. Anjo, J. Correia, M.J. Pacheco, A. Lopes, Electrochemical degradation of ibuprofen on Ti/Pt/PbO_2 and Si/BDD electrodes, Electrochim. Acta 54 (2009) 1464–1472.
[16] C. Flox, C. Arias, E. Brillas, A. Savall, K. Groenen-Serrano, Electrochemical incineration of cresols: a comparative study between PbO_2 and boron-doped diamond anodes, Chemosphere 74 (2009) 1340–1347.
[17] C. Salazar, I. Sirés, C.A. Zaror, E. Brillas, Treatment of a mixture of chloromethoxyphenols in hypochlorite medium by electrochemical AOPs as an alternative for the remediation of pulp and paper mill process waters, Electrocatalysis 4 (2013) 212–223.
[18] A. Thiam, M. Zhou, E. Brillas, I. Sirés, Two-step mineralization of Tartrazine solutions: Study of parameters and by-products during the coupling of electrocoagulation with electrochemical advanced oxidation processes, Appl. Catal. B: Environ. 150–151 (2014) 116–125.
[19] E. Rosales, M. Pazos, M.A. Longo, M.A. Sanromán, Electro-Fenton decoloration of dyes in a continuous reactor: a promising technology in colored wastewater treatment, Chem. Eng. J. 155 (2009) 62–67.
[20] A. Khataee, A. Khataee, M. Fathinia, B. Vahid, S.W. Joo, Kinetic modeling of photoassisted-electrochemical process for degradation of an azo dye using boron-doped diamond anode and cathode with carbon nanotubes, J. Ind. Eng. Chem. 19 (2013) 1890–1894.
[21] A. Wang, J. Qu, J. Ru, H. Liu, J. Ge, Mineralization of an azo dye Acid Red 14 by electro-Fenton's reagent using an activated carbon fiber cathode, Dyes Pigments 65 (2005) 227–233.
[22] A. Wang, J. Qu, H. Liu, J. Ru, Mineralization of an azo dye Acid Red 14 by photoelectro-Fenton process using an activated carbon fiber cathode, Appl. Catal. B: Environ. 84 (2008) 393–399.
[23] A. Özcan, Y. Sahin, A.S. Koparal, M.A. Oturan, Carbon sponge as a new cathode material for the electro-Fenton process. Comparison with carbon felt cathode and application to degradation of synthetic dye Basic Blue 3 in aqueous medium, J. Electroanal. Chem. 616 (2008) 71–78.
[24] N. Daneshvar, S. Aber, V. Vatanpour, M.H. Rasoulifard, Electro-Fenton treatment of dye solution containing Orange II: Influence of operational parameters, J. Electroanal. Chem. 615 (2008) 165–174.
[25] M. Panizza, M.A. Oturan, Degradation of Alizarin Red by electro-Fenton process using a graphite-felt cathode, Electrochim. Acta 56 (2011) 7084–7087.
[26] A. Özcan, M.A. Oturan, N. Oturan, Y. Şahin, Removal of Acid Orange 7 from water by electrochemically generated Fenton's reagent, J. Hazard. Mater. 163 (2009) 1213–1220.
[27] A. Dhaouadi, N. Adhoum, Degradation of paraquat herbicide by electrochemical advanced oxidation methods, J. Electroanal. Chem. 637 (2009) 33–42.
[28] A. Dirany, I. Sirés, N. Oturan, M.A. Oturan, Electrochemical abatement of the antibiotic sulfamethoxazole from water, Chemosphere 81 (2010) 594–602.
[29] N. Oturan, E. Brillas, M.A. Oturan, Unprecedented total mineralization of atrazine and cyanuric acid by anodic oxidation and electro-Fenton with a boron-doped diamond anode, Environ. Chem. Lett. 10 (2012) 165–170.
[30] A. Dirany, I. Sirés, N. Oturan, A. Özcan, M.A. Oturan, Electrochemical treatment of the antibiotic sulfachloropyridazine: kinetics, reaction pathways, and toxicity evolution, Environ. Sci. Technol. 46 (2012) 4074–4082.
[31] E. Guinea, J.A. Garrido, R.M. Rodríguez, P.L. Cabot, C. Arias, F. Centellas, E. Brillas, Degradation of the fluoroquinolone enrofloxacin by electrochemical advanced oxidation processes based on hydrogen peroxide electrogeneration, Electrochim. Acta 55 (2010) 2101–2115.

[32] E.J. Ruiz, A. Hernández-Ramírez, J.M. Peralta-Hernández, C. Arias, E. Brillas, Application of solar photoelectro-Fenton technology to azo dyes mineralization: Effect of current density, Fe^{2+} and dye concentration, Chem. Eng. J. 171 (2011) 385–392.
[33] R. Salazar, E. Brillas, I. Sirés, Finding the best Fe^{2+}/Cu^{2+} combination for the solar photoelectro-Fenton treatment of simulated wastewater containing the industrial textile dye Disperse Blue 3, Appl. Catal. B: Environ. 115–116 (2012) 107–116.
[34] A.R.F. Pipi, A.R. De Andrade, E. Brillas, I. Sirés, Total removal of alachlor from water by electrochemical processes, Sep. Purif. Technol. 132 (2014) 674–683.
[35] X. Zhu, J. Tian, Optimization of Fenton and electro-Fenton oxidation of biologically treated coking wastewater using response surface methodology, Sep. Purif. Technol. 81 (2011) 444–450.
[36] L. Zhou, Z. Hu, C. Zhang, Z. Bi, T. Jin, M. Zhou, Electrogeneration of hydrogen peroxide for electro-Fenton system by oxygen reduction using chemically modified graphite felt cathode, Sep. Purif. Technol. 111 (2013) 131–136.
[37] M. Gao, Z. Zeng, B. Sun, H. Zou, J. Chen, L. Shao, Ozonation of azo dye Acid Red 14 in a microporous tube-in-tube microchannel reactor: decolorization and mechanism, Chemosphere 89 (2012) 190–197.
[38] N. Daneshvar, D. Salari, A.R. Khataee, Photocatalytic degradation of azo dye acid red 14 in water: investigation of the effect of operational parameters, J. Photochem. Photobiol. A: Chem. 157 (2003) 111–116.
[39] N. Daneshvar, D. Salari, A.R. Khataee, Photocatalytic degradation of azo dye acid red 14 in water on ZnO as an alternative catalyst to TiO_2, J. Photochem. Photobiol. A: Chem. 162 (2004) 317–322.
[40] N.M. Mahmoodi, M. Arami, Bulk phase degradation of Acid Red 14 by nanophotocatalysis using immobilized titanium(IV) oxide nanoparticles, J. Photochem. Photobiol. A: Chem. 182 (2006) 60–66.
[41] S. Xia, X. Zhou, W. Shi, G. Pan, Z. Ni, Photocatalytic property and mechanism studies on Acid Red 14 by M_xO_y/ZnTi–layered double hydroxides (M = Fe, Sn, Ce), J. Mol. Catal. A: Chem. 392 (2014) 270–277.
[42] J. Lin, X. Zhao, D. Liu, Z. Yu, Y. Zhang, H. Xu, The decoloration and mineralization of azo dye C.I. Acid Red 14 by sonochemical process: rate improvement via Fenton's reactions, J. Hazard. Mater. 157 (2008) 541–546.
[43] R. Idel-Aouad, M. Valiente, A. Yaacoubi, B. Tanouti, M. López-Mesas, Rapid decolourization and mineralization of the azo dye C.I. Acid Red 14 by heterogeneous Fenton reaction, J. Hazard. Mater. 186 (2011) 745–750.
[44] A. Aleboyeh, N. Daneshvar, M.B. Kasiri, Optimization of C.I. Acid Red 14 azo dye removal by electrocoagulation batch process with response surface methodology, Chem. Eng. Process. 47 (2008) 827–832.
[45] A. Wang, J. Qu, H. Liu, J. Ge, Degradation of azo dye Acid Red 14 in aqueous solution by electrokinetic and electrooxidation process, Chemosphere 55 (2004) 1189–1196.
[46] C. Flox, J.A. Garrido, R.M. Rodríguez, P.L. Cabot, F. Centellas, C. Arias, E. Brillas, Mineralization of herbicide mecoprop by photoelectro-Fenton with UVA and solar light, Catal. Today 129 (2007) 29–36.
[47] J. De Laat, G.T. Le, B. Legube, A comparative study of the effects of chloride, sulfate, and nitrate ions on the rates of decomposition of H_2O_2 and organic compounds by Fe(II)/H_2O_2 and Fe(III)/H_2O_2, Chemosphere 55 (2004) 715–723.
[48] D. Khamis, E. Mahé, F. Dardoize, D. Devilliers, Peroxodisulfate generation on boron-doped diamond microelectrodes array and detection by scanning electrochemical microscopy, J. Appl. Electrochem. 40 (2010) 1829–1838.

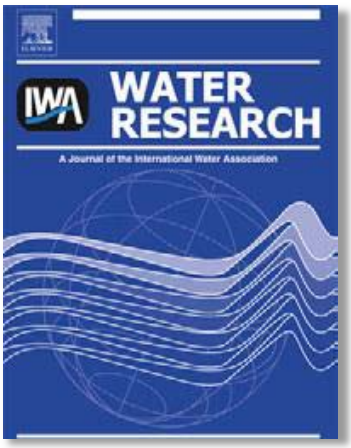

Paper 6

Treatment of a mixture of food color additives (E122, E124 and E129) in different water matrices by UVA and solar photoelectro-Fenton

Warer Research

Submitted (Manuscript No: 30771)

Treatment of a mixture of food color additives (E122, E124 and E129) in different water matrices by UVA and solar photoelectro-Fenton

Abdoulaye Thiam, Ignasi Sirés **, Enric Brillas *

Laboratori d'Electroquímica dels Materials i del Medi Ambient, Departament de Química Física, Facultat de Química, Universitat de Barcelona, Martí i Franquès 1-11, 08028 Barcelona, Spain

Paper submitted to be published in ***Water Research***

* Corresponding author: Tel.: +34 934021223; fax: +34 934021231.

*E-mail address: brillas@ub.edu (E. Brillas)

**E-mail address: i.sires@ub.edu (I. Sirés)

4. Results and discussion

Abstract

The degradation of 130 mL of mixtures of food azo dyes E122, E124 and E129 has been studied by electro-Fenton (EF) and UVA photoelectro-Fenton (PEF) using a stirred tank reactor with either a boron-doped diamond (BDD) or Pt anode and an air-diffusion cathode. The main oxidant was hydroxyl radical formed at the anode from water oxidation and in the bulk from Fenton's reaction between added Fe^{2+} and H_2O_2 generated at the cathode. In sulfate medium, fast decolorization was found for all systems, but the almost total mineralization was more rapidly achieved by PEF with BDD. The performance with a real water matrix was slightly worse, although the removal of total organic load was still as high as 95%. The solar PEF (i.e., SPEF) treatment of dye mixtures using a 2.5 L flow plant with a BDD/air-diffusion cell coupled to a planar solar photoreactor is also reported. Fast decolorization and almost total mineralization was found in the presence of either sulfate, perchlorate, nitrate or a mixture of sulfate + chloride ions. In chloride medium, however, the formation of recalcitrant chloroderivatives decelerated the degradation process. Greater current efficiency and lower specific energy consumption were attained in sulfate medium at lower current density and higher azo dye content. A plausible reaction sequence based on 18 aromatic intermediates identified by GC-MS and 6 short-linear carboxylic acids detected by ion-exclusion HPLC has been proposed. The SPEF process promoted the photodegradation of Fe(III)-oxalate complexes and other undetected products as well as the appearance of sulfate and nitrate ions.

Keywords: Electrochemical oxidation; Electro-Fenton; Food azo dyes; Photoelectro-Fenton; Sunlight; Wastewater treatment

1. Introduction

The environmental issues arising from discharge of large volumes of dyeing industrial effluents into water bodies represent a growing concern (Robinson et al., 2001). Such wastewater entails a health risk to living beings owing to its potentially toxic, carcinogenic and mutagenic effects (Ulson de Souza et al., 2007; El-Desoky et al., 2010). Moreover, the large content of dyestuffs (usually 100-250 mg L^{-1}) causes aesthetic problems that discourage their downstream use (UNESCO, 2012; Brillas and Martínez-Huitle, 2015). Azo compounds account for ca. 70% of the world production. Their molecular structure contains one or various azo groups (-N=N-) as chromophore, being linked to benzene and/or naphthalene rings with lateral −OH and $-SO_3H$ groups (Solís et al., 2012; Brillas and Martínez-Huitle, 2015). Several interesting properties of azo dyes including brilliant shades, relative low cost and simple manufacture are very appealing for their widespread industrial use (Zollinger, 2003; Forgacs et al., 2004). However, recent reports by the European Food Safety Authority have addressed the dangers of food azo dyes, being connected to children hyperactivity and possible allergies and intolerances. This is the case of red food dyes such as E122 (Carmoisine, $C_{20}H_{12}N_2O_7S_2Na_2$, C.I. 14720), E124 (Ponceau 4R, $C_{20}H_{11}N_2O_{10}S_3Na_3$, C.I. 16255) and E129 (Allura Red AC, $C_{18}H_{16}N_2O_8S_2Na_2$, C.I. 16035) (EFSA, 2009a,b,c), whose usage remains controversial in some European countries. Since conventional biological and physicochemical methods in wastewater treatment plants (WWTPs) are inefficient to remove azo dyes (Robinson et al., 2001; Forgacs et al., 2004), more powerful processes are needed to ensure their removal.

Over the last fifteen years, several electrochemical advanced oxidation processes (EAOPs) have been tested for the remediation of waters contaminated with organic pollutants (Özcan et al., 2009; Sirés et al., 2014; Vasudevan and Oturan, 2014). They are based on the on-site generation of a strong oxidant like hydroxyl radical ($^{\bullet}OH$), which can mineralize most organics because of its high standard redox potential (E^o = 2.80 V/SHE). The most ubiquitous EAOP is electrochemical oxidation (EO), in which organic pollutants are directly oxidized on the anode surface (M) and/or much more rapidly destroyed by adsorbed hydroxyl radical M($^{\bullet}OH$) produced via reaction (1) at high applied current (Flox et al., 2006; Hamza et al., 2009; Panizza and Cerisola, 2009; Ferreira et al., 2013).

$$M + H_2O \rightarrow M(^{\bullet}OH) + H^+ + e^- \quad (1)$$

When active anodes such as Pt, IrO_2 and RuO_2 are employed, the M($^{\bullet}OH$) radical is easily transformed into chemisorbed MO species with weaker oxidizing ability, only reaching a partial degradation of parent molecules (Panizza and Cerisola, 2009). In contrast, non-active anodes like

PbO_2 and boron-doped diamond (BDD) favor the electrochemical incineration of organics (Ciríaco et al., 2009; Rodrigo et al., 2010). BDD anode is then preferred for EO since it generates very large quantities of physisorbed BDD($^{\bullet}$OH) owing to the very weak BDD-$^{\bullet}$OH interaction that results in a greater O_2-overpotential and a quicker destruction of organics (Panizza and Cerisola, 2009).

The supporting electrolyte may modulate the effectiveness of EO. In Cl^- medium, for example, organics can be oxidized by both, physisorbed M($^{\bullet}$OH) and active chlorine species like Cl_2, HClO and/or ClO^- electrogenerated as follows (Panizza and Cerisola, 2009; Thiam et al., 2014, 2015):

$$2\ Cl^- \rightarrow Cl_2(aq) + 2e^- \quad (2)$$

$$Cl_2(aq) + H_2O \rightarrow HClO + Cl^- + H^+ \quad (3)$$

$$HClO \leftrightarrows ClO^- + H^+ \quad (4)$$

EAOPs based on electrogenerated H_2O_2 have received great attention as well (Sirés et al., 2014). This species can be continuously supplied to the medium from the two-electron reduction of O_2 gas at a carbonaceous cathode such as graphite (Rosales et al., 2009), carbon nanotubes (Khataee et al., 2013), activated carbon fiber (Wang et al., 2008), carbon sponge (Özcan et al., 2008), graphite felt (Panizza and Oturan, 2011), carbon felt (Dirany et al., 2012; Oturan et al., 2012) and carbon-polytetrafluoroethylene (PTFE) gas diffusion (Ammar et al., 2006; Guinea et al., 2010; Moreira et al., 2013) via reaction (5):

$$O_2(g) + 2\ H^+ + 2e^- \rightarrow H_2O_2 \quad (5)$$

The EO process with electrogenerated H_2O_2 (EO-H_2O_2) involves the destruction of organics pre-eminently by M($^{\bullet}$OH), although other reactive oxygen species (ROS) such as H_2O_2 and its oxidation product $HO_2^{\bullet}$ may also contribute (Sirés et al., 2014). The low oxidization power of H_2O_2 is enhanced in the electro-Fenton (EF) process in the presence of a small amount of Fe^{2+} to produce Fe^{3+} and $^{\bullet}$OH in the bulk via Fenton's reaction (6) at optimum pH ~ 3 (Dirany et al., 2012). In EF, organics are removed by both, M($^{\bullet}$OH) and $^{\bullet}$OH. Alternatively, EAOPs like UVA photoelectro-Fenton (PEF) or solar PEF (SPEF) involve EF setups where the solution is irradiated with either artificial UVA light or natural sunlight, respectively, thus promoting: (i) the photoreduction of $Fe(OH)^{2+}$ to Fe^{2+} with $^{\bullet}$OH generation via reaction (7) and (ii) the photolysis of Fe(III)-carboxylate products by reaction (8) (Salazar et al., 2012; Sirés et al., 2014); SPEF is therefore a technology to be further explored because it relies on sunlight as an inexpensive, renewable energy source.

$$H_2O_2 + Fe^{2+} \rightarrow Fe^{3+} + {}^{\bullet}OH + OH^- \quad (6)$$

$$Fe(OH)^{2+} + h\nu \rightarrow Fe^{2+} + {}^{\bullet}OH \quad (7)$$

$$Fe(OOCR)^{2+} + h\nu \rightarrow Fe^{2+} + CO_2 + R^{\bullet} \quad (8)$$

Many authors have reported the electrochemical destruction of single azo dyes in synthetic and real wastewater by EAOPs (Brillas and Martínez-Huitle, 2015), but scarce information is still available on the treatment of mixtures of azo dyes and the influence of the supporting electrolyte nature (Salazar et al., 2011). To gain better understanding on the electrochemical behavior of food azo dyes upon application of powerful EAOPs like PEF and SPEF, we present here a study on the decolorization and mineralization of mixtures of three color additives, E122, E124 and E129, in either synthetic media with sulfate, perchlorate, nitrate and/or chloride ions or in a real water matrix at pH 3.0. First, comparative electrolyses (130 mL) were carried out at lab-scale under EF and PEF conditions in sulfate medium using a BDD/air-diffusion or Pt/air-diffusion tank reactor to clarify the role of generated oxidizing agents. The influence of simulated and real water matrices on the degradation ability of PEF with a BDD anode (PEF-BDD) was further explored. A second step was performed with a 2.5 L flow plant equipped with a BDD/air-diffusion filter-press cell coupled to a planar solar photoreactor in order to assess the oxidation ability of EO-H_2O_2-BDD, PEF-BDD and SPEF-BDD treatments of mixtures of food azo dyes. The effect of different electrolytes, current density (j) and azo dye content on the SPEF-BDD performance was examined to clarify its viability as a future industrial technology. Generated carboxylic acids and released inorganic ions were detected by chromatographic techniques, whereas aromatic products were identified by gas chromatography-mass spectrometry (GC-MS). Previous research has reported the treatment of synthetic solutions of the above single food azo dyes by photocatalysis (Epling and Lin, 2002; Xia et al., 2014), electrocoagulation (Aleboyeh et al., 2008), EO (Wang et al., 2004; Thiam et al., 2015) and PEF (Wang et al., 2008; Thiam et al., 2015).

2. Materials and methods

2.1. Chemicals

Additives E122 (80% content), E124 (100% content) and E129 (80% content) were purchased from Sigma-Aldrich and Acros Organics and used as received. Anhydrous sodium sulfate, sodium chloride, lithium perchlorate and sodium nitrate, used as supporting electrolytes, and iron(II) sulfate heptahydrate, used as catalyst, were of analytical grade from Fluka and Sigma-Aldrich. Sulfuric, nitric, perchloric and hydrochloric acids, used to regulate the solution pH, were of analytic grade from Merck, Acros Organics and Panreac. Organic solvents and other chemicals were of HPLC or analytical grade from Sigma-Aldrich, Merck and Panreac. Solutions in 130-mL cells were prepared

with ultrapure water from a Millipore Milli-Q system with resistivity >18 MΩ cm or with a real water matrix. Solutions to be treated in the 2.5 L flow plant were prepared with deionized water.

2.2. Characterization of the real water matrix

The raw wastewater to be spiked with synthetic food azo dyes was a secondary effluent obtained from a WWTP located in Gavá-Viladecans (Barcelona, Spain), which collects urban and selected industrial wastewater and treats 25,000-50,000 m^3 d^{-1}. Its main characteristics were: pH near 7.5, conductance = 2.6 mS (equivalent to ca. 0.012 M Na_2SO_4), dissolved organic carbon (DOC) = 15 mg L^{-1}, total nitrogen = 66 mg L^{-1}, 1.3 mM SO_4^{2-}, 11.4 mM Cl^-, 0.02 mM N-NO_3^-, 11.6 mM Na^+, 1.0 mM K^+ and 1.5 mM N-NH_4^+. No iron ions were detected. This water was preserved at 4 ºC and used the day after collection.

2.3. Electrolytic systems

The EF and PEF treatments at lab-scale were conducted in an open, undivided, cylindrical two-electrode glass cell containing 130 mL of solution vigorously stirred with a magnetic bar at 800 rpm. The cell had a double jacket for recirculation of thermostated water at 35 ºC, which was chosen because it is the maximum working temperature prior to significant water evaporation from solution. The anode was either a 3 cm^2 Pt sheet from SEMPSA (Barcelona, Spain) or a 3 cm^2 BDD thin-film electrode from NeoCoat (La-Chaux-de-Fonds, Switzerland) and the cathode was a 3 cm^2 carbon-PTFE air-diffusion cathode from E-TEK (Somerset, NJ, USA). The interelectrode gap was about 1 cm. The cathode was mounted as described elsewhere (Guinea et al., 2010) and was fed with air pumped at 1 L min^{-1} for H_2O_2 generation. Four EAOPs were studied, namely EF-Pt, EF-BDD, PEF-Pt and PEF-BDD, using 0.50 mM Fe^{2+} as catalyst because it was found optimal for similar treatments of other azo dyes (Ruiz et al., 2011). Trials were carried out at constant *j* provided by an EG&G PAR 273A potentiostat-galvanostat. For PEF, irradiation was provided with a Philips TL/6W/08 fluorescent black light blue tube placed 7 cm above the solution, which emitted UVA light at λ_{max} = 360 nm with a photoionization energy of 5 W m^{-2}, measured on a Kipp&Zonen CUV 5 radiometer. Before the assays, cleaning of the BDD anode and activation of the air-diffusion cathode were achieved under polarization in 0.05 M Na_2SO_4 at 100 mA cm^{-2} for 180 min.

A scheme of the 2.5-L flow plant used to degrade the mixtures of food azo dyes has been reported elsewhere (Flox et al., 2007). For each assay, the solution was introduced into the reservoir and recirculated through the plant using a centrifugal pump. The flow rate was kept at 200 L h^{-1} with a flowmeter and the solution temperature was regulated at 35 ˚C with two heat exchangers. The electrochemical reactor was an undivided filter-press cell with a 20 cm^2 BDD anode and a 20

cm^2 carbon-PTFE air-diffusion cathode, with an interelectrode gap of 1.2 cm. The inner face of the cathode was in contact with a PVC gas chamber fed with atmospheric air at an overpressure of 8.6 kPa regulated with a back-pressure gauge to produce H_2O_2. The trials were made at constant *j* provided by an Agilent 6552A DC power supply, which directly measured the cell voltage. In SPEF, the outlet of the electrochemical cell was connected to a planar solar photoreactor with 600 mL of irradiated volume and tilted 41º (local latitude) to better collect the solar rays. Once irradiated, the solution was directed toward the reservoir. Comparative EO-H_2O_2-BDD and EF-BDD trials were made in the dark by covering the system with an opaque cloth. SPEF-BDD assays were carried out during the summer of 2014 with UV radiation (300-400 nm) intensity of 30-32 W m^{-2}, as determined with the previous radiometer. Prior to the use of the flow plant, the electrodes were cleaned and/or activated under polarization in 0.05 M Na_2SO_4 at 100 mA cm^{-2} for 240 min.

2.4. Apparatus and analytical procedures

The solution pH was determined with a Crison 2000 pH-meter. Samples withdrawn at regular time intervals from the treated solutions were microfiltered with 0.45 μm PTFE filters from Whatman before immediate analysis. The decolorization of solutions was monitored from the absorbance decay at the maximum visible wavelength of the azo dye mixture (λ_{max} = of 510 nm), measured on a Shimadzu 1800 UV-vis spectrophotometer at 35 ºC. Taking the absorbance at initial time (A_0) and that after an electrolysis time *t* (A_t), the percentage of color removal or decolorization efficiency at λ_{max} = 510 nm for a given trial was determined from Eq. (9) (Ruiz et al., 2011):

$$\text{Color removal (\%)} = \frac{A_0 - A_t}{A_0} \times 100 \quad (9)$$

The mineralization of solutions was monitored from their DOC decay determined on a Shimadzu VCSN total organic carbon analyzer. Reproducible DOC values with an accuracy of ±1% were found by injecting 50 μL aliquots. The specific energy consumption per unit DOC mass (EC_{DOC}) at current *I* (in A) and time *t* (in h) was estimated as follows (Ruiz et al., 2011):

$$EC_{DOC}\ (\text{kWh (g DOC)}^{-1}) = \frac{E_{cell}\, I\, t}{V_s\, \Delta(\text{DOC})_{exp}} \quad (10)$$

where E_{cell} is the average cell voltage (in V), V_s is the solution volume (in L) and $\Delta(DOC)_{exp}$ is the experimental DOC decay (in mg L^{-1}).

Short-linear carboxylic acids were detected by ion-exclusion HPLC using a Waters 600 LC fitted with a Bio-Rad Aminex HPX 87H, 300 mm x 7.8 mm, column at 35 ˚C and coupled to a Waters 996 photodiode detector selected at λ = 210 nm. A 4 mM H_2SO_4 solution eluted at 0.6 mL min^{-1} was used as mobile phase. Peaks appeared at retention times of 7.0 min for oxalic acid, 7.9 min for tartronic acid, 8.2 min for maleic acid, 9.4 min for oxamic acid, 13.7 min for formic acid

and 14.8 min for fumaric acid. Released SO_4^{2-}, NH_4^+ and NO_3^- ions were analyzed as previously reported (Thiam et al., 2015).

To identify the aromatic intermediates formed in SPEF-BDD, various samples were withdrawn during short-time electrolyses of an azo dye mixture in the flow plant, and the organic components were extracted with CH_2Cl_2 (3 × 25 mL). Each resulting organic solution was dried over anhydrous Na_2SO_4, filtered and concentrated up to ca. 1 mL under reduced pressure to be analyzed by GC-MS. This was made with an Agilent Technologies system composed of a 7890A gas chromatograph and a 5975C mass spectrometer operating in electron ionization mode at 70 eV. Nonpolar Agilent J&W HP-5ms and polar HP INNOWax columns, both of 0.25 μm, 30 m × 0.25 mm, were used. The temperature ramp was: 36 ºC for 1 min, 5 ºC min^{-1} up to 300 ºC or 250 ºC for the nonpolar and polar columns, respectively, and hold time of 10 min. The temperature of the inlet, source and transfer line was 250, 230 and 280 ºC for the nonpolar column, and 250, 230 and 250 ºC for the polar one. The mass spectra were identified with a NIST05 MS library.

3. Results and discussion

3.1. Treatment of a mixture of food azo dyes by EF and PEF in synthetic medium at lab-scale

A first study was made with the 130 mL stirred tank reactor to clarify the oxidation ability of hydroxyl radicals formed during the EF-Pt, EF-BDD, PEF-Pt and PEF-BDD treatments. These assays were performed with a mixture of 33.3 mg L^{-1} DOC of each dye in ultrapure water with 0.05 M Na_2SO_4 and 0.50 mM Fe^{2+} at pH 3.0 by applying 33.3 mA cm^{-2} for 360 min. In these trials, the dark-red solution was rapidly decolorized and the solution pH slightly decayed up to final values of 2.7-2.8 due to the generation of acidic products like aliphatic carboxylic acids (Sirés et al., 2014).

As shown in Fig. 1a, the solutions became colorless after 50 and 45 min by EF and PEF, respectively, regardless of the anode used, despite the expected superiority of BDD($^\bullet$OH) over Pt($^\bullet$OH) to degrade aromatics (Panizza and Cerisola, 2009). This suggests that $^\bullet$OH produced from Fenton's reaction (6) carries primary responsibility for degradation of azo dyes. The slightly quicker color removal observed for PEF compared to EF can be related to the additional generation of $^\bullet$OH in the bulk induced by the photolytic reaction (7). In contrast, Fig. 1b depicts a very different behavior for DOC abatement depending on the method and anode employed, since the relative oxidation ability of EAOPs rose in the sequence EF-Pt < EF-BDD < PEF-Pt < PEF-BDD. At the end of these treatments, for example, DOC was reduced by 64%, 83%, 96% and 99%, respectively; an almost total mineralization was then achieved for both PEF processes, being BDD slightly superior to Pt. The larger mineralization found for EF-BDD compared to EF-Pt can be

related to the faster destruction of organics by the most potent BDD($^{\bullet}$OH) radical, while the role of $^{\bullet}$OH generated in the bulk is expected to be similar in both cases. The enhanced mineralization rate upon UVA irradiation in PEF can be explained by the additional photolysis of recalcitrant products that cannot be oxidized by hydroxyl radicals, such as Fe(III)-carboxylate species via reaction (8) (Ruiz et al., 2011; Brillas and Martínez-Huitle, 2015).

These findings indicate that PEF-BDD is the best EAOP to decolorize and mineralize the mixtures of food azo dyes at lab-scale. This process was then chosen to assess their degradation in simulated and real water matrices, as described in section below.

3.2. PEF-BDD treatments in simulated and real water matrices at lab-scale

Based on the characterization of inorganic components of a real wastewater (see section 2.2), a simulated real water matrix containing 0.80 mM Na_2SO_4 + 10 mM NaCl + 1.5 mM NH_4Cl + 0.50 mM K_2SO_4 + 0.02 mM $NaNO_3$ was prepared to investigate the PEF-BDD treatment of mixtures of food azo dyes with 10 and 100 mg L^{-1} DOC, in the presence of 0.50 mM Fe^{2+} at pH 3.0 and applying a *j* of 33.3 mA cm^{-2}. Fig. 2a highlights that total decolorization was achieved at 15 min for 10 mg L^{-1} DOC and at a longer time of 60 min for 100 mg L^{-1} DOC, as expected from the slower degradation of higher organic load under the action of a similar concentration of hydroxyl radicals. However, comparison of Fig. 1a and 2a reveals a significantly slower color removal in the simulated water, which contained several inorganic anions (1.30 mM SO_4^{2-} + 11.5 mM Cl^- + 0.02 mM NO_3^-) instead of SO_4^{2-} alone. The decay in decolorization rate in the simulated water could seem contradictory since previous work on the EF treatment of single E122 solutions showed a faster decolorization in Cl^- than in SO_4^{2-} medium, both at 0.05 M (Thiam et al., 2015). The opposite behavior observed in the present complex inorganic matrix suggests a drop in concentration of main oxidants ($^{\bullet}$OH and/or active chlorine species), which could be related to: (i) the lower specific conductivity, which causes a greater ohmic drop that end in a less effective formation of oxidants, (ii) the partial scavenging of $^{\bullet}$OH by reaction with the high content of Cl^- in the simulated medium by reaction (11) giving weaker oxidants like $Cl^{\bullet}$ (De Laat et al., 2004), and (iii) the partial destruction of HClO, the predominant active chlorine species formed at pH 3 from reactions (2) and (3), due to the attack of generated H_2O_2 via reaction (12) (De Laat et al., 2004).

$$Cl^- + {}^{\bullet}OH + H^+ \rightarrow Cl^{\bullet} + H_2O \quad (11)$$

$$HClO + H_2O_2 \rightarrow Cl^- + O_{2(g)} + H_2O + H^+ \quad (12)$$

The loss of oxidation power in PEF-BDD using the simulated water was also found when the mineralization rate was assessed. As can be seen in Fig. 2b for the 100 mg L^{-1} DOC mixture after

180 min of electrolysis, DOC was reduced by 73%, a value much lower than 85% obtained in 0.05 M Na_2SO_4 (Fig. 1b), thus confirming the lower concentration of accumulated oxidants. Despite this, an almost total mineralization (96% DOC removal) was determined at the end of this treatment (Fig. 2b). Therefore, the PEF-BDD process is able to degrade mixtures of food azo dyes in a complex inorganic matrix. At 10 mg L^{-1} DOC, however, Fig. 2b depicts a lower mineralization of 86% at 360 min, indicating a loss in efficiency of PEF-BDD at low organic load. This is a typical behavior for EAOPs, which can be accounted for by the acceleration of parasitic reactions that promote the destruction of oxidants in the absence of a certain number of organic molecules (Panizza and Cerisola, 2009; Sirés et al., 2014). These reactions involve, for example, termination reactions, as well as reactions (11) and (12) and the consumption of Fenton's reagent from reaction (13) and (14) yielding the weaker oxidant hydroperoxyl radical ($HO_2^{\bullet}$).

$$H_2O_2 + {}^{\bullet}OH \rightarrow H_2O + HO_2^{\bullet} \quad (13)$$

$$Fe^{2+} + {}^{\bullet}OH \rightarrow Fe^{3+} + OH^{-} \quad (14)$$

The oxidation power of PEF-BDD was further assessed for different food azo dye solutions mixed at equal DOC content in a real water matrix by adding 0.50 mM Fe^{2+} at pH 3.0. Fig. 3a highlights the fast color removal achieved for all these trials at 33.3 mA cm^{-2}, attaining total decolorization at longer times from 10 to 60 min as total initial DOC grew from 6 to 100 mg L^{-1}, as expected when larger concentrations of food azo dyes are exposed to similar amounts of generated oxidants. Note that 15 and 60 min were needed for overall color removal of solutions with 10 and 100 mg L^{-1} DOC, respectively, being similar to times required in the simulated matrix (Fig. 2a). This means that the natural organic load contained in the real water has little influence on the decolorization process, suggesting that the oxidation ability of the treatment mainly depends on the inorganic ions content because it determines the quantity of available oxidizing species (primordially hydroxyl radicals and active chlorine species). This was also confirmed from the DOC abatement presented in Fig. 3b. The PEF-BDD treatment of the raw water only yielded a DOC decay from 15 to 6 mg L^{-1} (60% mineralization) in 360 min, as expected if its organic load reacted very slowly by hydroxyl radicals and active chlorine species. In contrast, when food azo dyes from 6 to 100 mg L^{-1} DOC were spiked to that matrix, the action of such oxidizing species was more efficient and a quite similar and low residual DOC between 5 and 7 mg L^{-1} was always found. Compared with results obtained for 10 and 100 mg L^{-1} DOC in the simulated matrix (Fig. 2b), where final solutions contained about 4 mg L^{-1} DOC, electrolyses in the real water matrix slightly favored the destruction of products, probably due to the stimulated reaction between intermediates of the natural organic matter and those coming from food azo dyes.

Our findings allow concluding that PEF-BDD is able to effectively decolorize and mineralize mixtures of food azo dyes in a real water matrix, yielding almost total mineralization (95% DOC removal) even after spiking 100 mg L^{-1} DOC of such pollutants to the matrix.

3.3. Decolorization and mineralization of a mixture of food azo dyes by EAOPs in the flow plant

The degradation of the mixture of 100 mg L^{-1} DOC of food azo dyes was further studied in the 2.5 L flow plant with a BDD/air-diffusion cell to explore the viability of SPEF-BDD. The performance of this method was compared with that of EO-H_2O_2-BDD and EF-BDD using a synthetic solution with 0.05 M Na_2SO_4 at pH 3.0 and j = 100 mA cm^{-2}.

Fig. 4a reveals a very poor color removal for EO-H_2O_2-BDD, only achieving 79% decolorization after 480 min. This arises from the very slow reaction of food azo dyes with BDD($^{\bullet}$OH) formed from reaction (1). In contrast, solutions became colorless in only 40 min by EF-BDD and SPEF-BDD, corroborating the pre-eminent oxidizing role of $^{\bullet}$OH generated by Fenton's reaction (6) in both cases, with little participation of reaction (7) induced by UV radiation from sunlight. Fig. 4b depicts that the relative oxidation power of EAOPs grows in the sequence EO-H_2O_2-BDD < EF-BDD < SPEF-BDD. After 480 min, only 51% mineralization was obtained for the former process, which increased up to 67% for the second one. The deceleration observed for EF-BDD from 180 min suggests the formation of very recalcitrant products like Fe(III)-carboxylate complexes, which are very refractory to BDD($^{\bullet}$OH) and $^{\bullet}$OH (Guinea et al., 2010; Ruiz et al., 2011). The fast photolysis of such products upon sunlight irradiation explains the almost total mineralization with 97% DOC decay in SPEF-BDD. This behavior is similar to that found for the PEF-BDD treatment at lab-scale (Fig. 1b) and confirms that SPEF-BDD is the best EAOP to decolorize and mineralize mixtures of food azo dyes in the flow plant, as also previously reported for the degradation of single azo dyes (Ruiz et al., 2011; Moreira et al., 2013; Thiam et al., 2015).

3.4. Effect of operation parameters on the SPEF process using the flow plant

The effect of the electrolyte nature on the SPEF-BDD performance was firstly studied by electrolyzing mixtures with 100 mg L^{-1} DOC. As can be seen in Fig. 5a, quite similar decolorization rates with complete color removal in 30-40 min were found in 0.05 M of Na_2SO_4, $LiClO_4$, $NaNO_3$ and NaCl, and even in 0.04 M Na_2SO_4 + 0.01 M NaCl, always in the presence of 0.50 mM Fe^{2+} at pH 3.0 and 100 mA cm^{-2}. This suggests that the oxidation power of SPEF in the presence of SO_4^{2-}, ClO_4^- or NO_3^- ions, which arises from the combination of BDD($^{\bullet}$OH) and $^{\bullet}$OH, was comparable to that arising from the ensemble of those radicals and active chlorine in Cl^- media, probably due to the lower radical concentration in the latter medium. This behavior differs from results reported on

the decolorization of single E122 solutions by EF, which was faster in Cl^- than in SO_4^{2-} and ClO_4^- (Thiam et al., 2015). This discrepancy could be due to a different reactivity of each azo dye of the mixture and/or their colored products with oxidizing agents. As shown in Fig. 5b, SPEF-BDD yielded about 96-97% mineralization with a quite similar DOC decay in all the media tested, except in NaCl where DOC was only reduced by 85% in 300 min. The lower mineralization achieved in the latter medium can be due to: (i) the generation of chloroderivatives that are more slowly attacked by hydroxyl radicals and active chlorine species (Sirés et al., 2014), and (ii) the partial destruction of H_2O_2 from reaction (12). In contrast, the concentration of $^{\bullet}OH$ in the other media, including 0.04 M Na_2SO_4 + 0.01 M NaCl, is high enough to ensure the quick mineralization. These results agree with those obtained by PEF-BDD in the real water matrix at lab-scale and demonstrate the viability of SPEF-BDD at industrial level for the treatment of dye wastewater.

The influence of other key parameters such as *j* and azo dye content on the performance of SPEF-BDD was also examined using 0.05 M Na_2SO_4. As depicted in Figs. 6a and 6b, the increase from 50 to 150 mA cm^{-2} led to shorter times from 50 to 30 min for total decolorization; furthermore, it enhanced the mineralization process at least during the first 150 min, although 97% DOC abatement was always found after 240-300 min. This positive tendency can be simply related to the concomitant increase in rate of all electrode reactions, producing more amounts of BDD($^{\bullet}OH$) from reaction (1) and H_2O_2 from reaction (6), eventually accelerating $^{\bullet}OH$ generation from Fenton's reaction (6). This behavior is typical of EAOPs (Panizza and Cerisola, 2009; Brillas and Martínez-Huitle, 2015) and entails a loss of current efficiency. For example, Fig. 6b shows that 86-90% DOC removal was achieved after about 180, 120 and 90 min at 50, 100 and 150 mA cm^{-2}, corresponding to growing specific charges consumptions of 1.20, 1.60 and 1.80 Ah L^{-1}. Electrical charge misuse with raising *j* can be related to the relative loss of available hydroxyl radicals by the quicker acceleration of their parasitic reactions such as reactions (13) and (14) and the oxidation of BDD($^{\bullet}OH$) to O_2 by reaction (15), as well the quicker formation of weaker oxidants on BDD like peroxodisulfate ($S_2O_8^{2-}$) ion and ozone from reactions (16) and (17), respectively (Sirés et al., 2014).

$$2\ BDD(^{\bullet}OH) \rightarrow 2\ BDD + O_{2(g)} + 2\ H^+ + 2\ e^- \quad (15)$$

$$2\ SO_4^{2-} \rightarrow S_2O_8^{2-} + 2\ e^- \quad (16)$$

$$3\ H_2O \rightarrow O_3 + 6\ H^+ + 6\ e^- \quad (17)$$

Fig. 7a corroborates the slower color removal (from 15 to 50 min) when the DOC content rose, as commented above for PEF-BDD. This is then explained by the slower disappearance of larger

amounts of azo dye molecules exposed to similar amounts of generated hydroxyl radicals at 100 mA cm^{-2}. Fig. 7b shows that an almost total mineralization near 97% was achieved for all the solutions. Note that, although longer times ranging between 180 and 300 min were needed with increasing organic matter, a greater DOC content was removed at a given time. For example, after 120 min, 47, 86, 103 and 111 mg L^{-1} DOC were destroyed at starting concentrations of 50, 100, 150 and 200 mg L^{-1} DOC, respectively. This enhancement in the efficiency of SPEF-BDD can be attributed to the progressively increased contact between hydroxyl radicals and the larger quantities of organics, with the consequent deceleration of their parasitic reactions.

The EC_{DOC} values calculated from Eq. (10) for the trials of Fig. 4 are shown in Fig. 8. High values of 1.94 and 1.46 kWh (g DOC)$^{-1}$ were obtained after 480 min for the inefficient EO-H_2O_2-BDD and EF-BDD treatments at 100 mA cm^{-2}, respectively, whereas a much lower EC_{DOC} of 0.607 kWh (g DOC)$^{-1}$ was found at 300 min of SPEF-BDD (97% mineralization). Data determined from some SPEF trials of Figs. 5-7 are also given in Fig. 8. The use of 0.05 M NaCl at 100 mA cm^{-2} led to a higher final EC_{DOC} of 0.953 kWh (g DOC)$^{-1}$ because of the lower mineralization attained and the higher E_{cell} value that resulted from the smaller conductivity of this solution compared to 0.05 M Na_2SO_4. In this latter medium, the rise in j to 150 mA cm^{-2} also caused a greater E_{cell} with the concomitant increase of the final EC_{DOC} up to 0.897 kWh (g DOC)$^{-1}$. In contrast, the most efficient degradation of 200 mg L^{-1} DOC at 100 mA cm^{-2} yielded the lowest EC_{DOC} of 0.290 kWh (g DOC)$^{-1}$ in 300 min. The specific energy consumptions obtained in sulfate medium were similar to those previously calculated for single azo dye solutions treated by SPEF-BDD in the same flow plant. For example, 0.655 kWh (g DOC)$^{-1}$ were required to mineralize about 98% of 50 mg L^{-1} DOC of Acid Yellow 9 after 210 min at 100 mA cm^{-2} (Ruiz et al., 2011).

3.5. Identification of reaction products and transformation routes

Ion-exclusion chromatograms recorded for the treated solutions of Fig. 4 displayed peaks related to short-linear carboxylic acids like maleic, fumaric, tartronic, formic, oxalic and oxamic. The three former acids derive from the oxidative cleavage of the benzene and naphthalene moieties of food azo dyes, which are in turn converted into oxalic and formic acids (Flox et al., 2007; Guinea et al., 2010; Moreira et al., 2013). Oxamic acid could be formed from the destruction of *N*-derivatives. Oxalic, formic and oxalic acids are directly mineralized to CO_2 (Sirés et al., 2014). Small amounts of maleic and fumaric acids (< 0.3 mg L^{-1}) were always detected, whereas maximum tartronic acid contents < 16.8 mg L^{-1} were found after 90 min of EF-BDD and SPEF-BDD and accumulation of formic acid up to 28.2 mg L^{-1} was obtained at short electrolysis time in all cases. Nevertheless, all these acids disappeared in 150-180 min because their Fe(III)-carboxylate

complexes were easily oxidized by hydroxyl radicals and/or photodecarboxylated by sunlight via reaction (8). In contrast, oxamic acid was accumulated and slowly destroyed, remaining 0.7, 2.6 and 2.1 mg L^{-1} after 300 min of EO-H_2O_2-BDD, EF-BDD and SPEF-BDD, respectively, indicating a poor removal of Fe(III)-oxamate species. Fig. 9a reveals that oxalic acid was the more largely accumulated aliphatic acid. While it only attained 0.06 mM in EO-H_2O_2-BDD, maximum concentrations of ca. 0.59 mM were found in the other two EAOPs, thereby dropping to 0.38 mM at 300 min of EF-BDD due to the slow oxidation of Fe(III)-oxalate complexes with hydroxyl radicals; quick photolysis of such complexes allowed its complete removal in 180 min. Based on a mass balance after 300 min of EF-BDD, it can be deduced that the accumulated acids represented 9.8 mg L^{-1} DOC, only accounting for 24.5% of solution DOC (Fig. 4b). This means that the SPEF-BDD process involves the photolysis of a large proportion of intermediates, not only Fe(III)-carboxylate species but also undetected products that cannot be mineralized by hydroxyl radicals in EF-BDD.

Inorganic ions formed during the above treatments were quantified by ion chromatography. The S atoms of food azo dyes (0.99 mM) were detected as SO_4^{2-} ion, with a concentration of 0.57 mM (57% of initial S), 0.96 mM (97% of initial S) and 0.99 mM (100% of initial S) after 300 min of EO-H_2O_2-BDD, EF-BDD and SPEF-BDD, respectively (Fig. 9b). Intermediates with a $–SO_3^-$ group were then slowly destroyed by BDD($^\bullet$OH) in the former process, but very rapidly degraded by $^\bullet$OH in the two latter ones. Regarding the N atoms (0.85 mM), very low contents of NH_4^+ ion (< 0.01 mM) were detected in all cases along with a much larger accumulation of NO_3^- ion. Fig. 9c shows that this ion was slowly accumulated in EO-H_2O_2-BDD, as expected from the mass transport limitations inherent to the attack of BDD($^\bullet$OH) onto *N*-derivatives. In contrast, NO_3^- ion was rapidly formed under the action of $^\bullet$OH, attaining maximum contents of 0.52 mM (61% of initial N) for EF-BDD and 0.44 mM (52% of initial N) for SPEF-BDD, which decayed to 0.40 and 0.15 mM at 300 min, respectively. This phenomenon suggests that some intermediates, but especially photolyzed species, can reduce NO_3^- ion to give a large proportion of volatile species such as N_2 and N_xO_y, as proposed for similar treatments of single azo dyes (Ruiz et al., 2011).

GC-MS analysis of the mixture with 100 mg L^{-1} DOC of the food azo dyes treated by SPEF-BDD in the flow plant at 100 mA cm^{-2} allowed the identification of 18 aromatic intermediates coming from the cleavage of the –N=N- bonds, deamination and desulfonation of the starting dyes. Fig. 10 presents a proposed reaction sequence for the mineralization of E122, E124 and E129 based on identified intermediates. The transformation route is initiated by the production of two condensation compounds, namely phthalimide (*m/z* = 147) and indandione (*m/z* = 146), along with a hydroxylated derivative of naphthalene rings, 1,4-naphthalenediol (*m/z* = 160). This diol then

gives the corresponding quinone (*m/z* = 158), which is subsequently hydroxylated, oxidized to phthalic acid (*m/z* = 166) or transformed into 3*H*-isobenzofuran-1-one (*m/z* = 134). Destruction of the above compounds yields two paths that consider various benzenic products. The first one arises from hydroxylation and oxidation of 2-methoxyphenol (*m/z* = 124) and 2-methoxy-5-methylphenol (*m/z* = 138) that derive from E129, whereas the second one involves acetophenone (*m/z* = 120) and its hydroxylated product along with methoxyphenyloxime (*m/z* = 151) and 2,4-dihydroxy-5-aminobenzaldehyde (*m/z* = 158). The cleavage of all these aromatic rings leads to a mixture of final carboxylic acids like fumaric, maleic, tartronic, oxalic, oxamic and formic, which evolve to CO_2.

4. Conclusions

Lab-scale experiments have demonstrated the superiority of PEF-BDD among all EAOPs since it yields fast decolorization and almost total mineralization of mixtures of food azo dyes in sulfate medium. Application to simulated and real water matrices confirmed its excellent oxidation ability over such pollutants, which depended on the oxidants generated from their inorganic components. PEF-BDD was also able to significantly degrade the residual DOC of a real water matrix. Scale-up to a 2.5 L flow plant confirmed the viability of SPEF-BDD for future industrial implementation. This process decolorized rapidly and at similar rate dye mixtures in SO_4^{2-}, ClO_4^-, NO_3^- or Cl^- medium, yielding almost overall mineralization in all cases except for Cl^-, where the formation of recalcitrant chloroderivatives decelerated the degradation. However, its high oxidation power was preserved in a medium with SO_4^{2-} + Cl^- ions, demonstrating its viability to treat real wastewaters. SPEF-BDD presented higher current efficiency and lower specific energy consumption with decreasing *j* and increasing azo dye concentration. The transformation routes of the food azo dye mixtures included up to 18 aromatic intermediates and 6 final carboxylic acids. The UV radiation from sunlight ensured the photolysis of refractory Fe(III)-oxalate complexes and other undetected products. Sulfate and nitrate ions were released to the medium upon treatment.

Acknowledgments

The authors thank MINECO (Spain) for financial support under project CTQ2013-48897-C2-1-R, co-financed with FEDER funds. The Ph.D. grant awarded to A. Thiam from MAEC-AECID (Spain) is also acknowledged.

References

Aleboyeh, A., Daneshvar, N., Kasiri, M.B., 2008. Optimization of C.I. Acid Red 14 azo dye removal by electrocoagulation batch process with response surface methodology. Chem. Eng. Process. 47 (5), 827-832.

Ammar, S., Abdelhedi, R., Flox, C., Arias, C., Brillas, E., 2006. Electrochemical degradation of the dye indigo carmine at boron-doped diamond anode for wastewaters remediation. Environ. Chem. Lett. 4 (4), 229-233.

Brillas, E., Martínez-Huitle, C.A., 2015. Decontamination of wastewaters containing synthetic organic dyes by electrochemical methods. An updated review. Appl. Catal. B: Environ. 166-167, 603-643.

Ciríaco, L., Anjo, C., Correia, J., Pacheco, M.J., Lopes, A., 2009. Electrochemical degradation of ibuprofen on Ti/Pt/PbO_2 and Si/BDD electrodes. Electrochim. Acta 54 (5), 1464-1472.

De Laat, J., Le, G.T., Legube, B., 2004. A comparative study of the effects of chloride, sulfate, and nitrate ions on the rates of decomposition of H_2O_2 and organic compounds by Fe(II)/H_2O_2 and Fe(III)/H_2O_2. Chemosphere 55 (5), 715-723.

Dirany, A., Sirés, I., Oturan, N., Özcan, A., Oturan, M.A., 2012. Electrochemical treatment of the antibiotic sulfachloropyridazine: kinetics, reaction pathways, and toxicity evolution. Environ. Sci. Technol. 46 (7), 4074–4082.

EFSA, 2009a. Scientific opinion on the re-evaluation of Allura Red AC (E 129) as a food additive. EFSA J. 7 (11), 1327 [39 pp.].

EFSA, 2009b. Scientific Opinion on the re-evaluation of Ponceau 4R (E 124) as a food additive. EFSA J. 7 (11), 1328 [40 pp.].

EFSA, 2009c. Scientific Opinion on the re-evaluation of Azorubine/Carmoisine (E 122) as a food additive. EFSA J. 7 (11), 1332 [40 pp.].

El-Desoky, H.S., Ghoneim, M., Zidan, N.M., 2010. Decolorization and degradation of Ponceau S azo-dye in aqueous solutions by the electrochemical advanced Fenton oxidation. Desalination 264 (1-2), 143-150.

Epling, G.A., Lin, C., 2002. Photoassisted bleaching of dyes utilizing TiO_2 and visible light. Chemosphere 46 (4), 561-570.

Ferreira, M.B., Rocha, J.H.B., de Melo, J.V., Martinez-Huitle, C.A., Quiroz Alfaro, M.A., 2013. Use of a dual arrangement of flow cells for electrochemical decontamination of aqueous solutions containing synthetic dyes. Electrocatalysis 4 (4), 274-282.

Flox, C., Cabot, P.L., Centellas, F., Garrido, J.A. Rodríguez, R.M., Arias, C., Brillas, E., 2006. Electrochemical combustion of herbicide mecoprop in aqueous medium using a flow reactor with a boron-doped diamond anode. Chemosphere 64 (6) 892-902.

Flox, C., Garrido, J.A., Rodríguez, R.M., Cabot, P.L., Centellas, F., Arias, C., Brillas, E., 2007. Mineralization of herbicide mecoprop by photoelectro-Fenton with UVA and solar light. Catal. Today 129 (1-2), 29-36.

Forgacs, E., Cserháti, T., Oros, G., 2004. Removal of synthetic dyes from wastewaters: A review. Environ. Int. 30 (7), 953-971.

Guinea, E., Garrido, J.A., Rodríguez, R.M., Cabot, P.L., Arias, C., Centellas, F., Brillas, E., 2010. Degradation of the fluoroquinolone enrofloxacin by electrochemical advanced oxidation processes based on hydrogen peroxide electrogeneration, Electrochim. Acta 55 (6), 2101-2115.

Hamza, M., Abdelhedi, R., Brillas, E., Sirés, I., 2009. Comparative electrochemical degradation of the triphenylmethane dye Methyl Violet with boron-doped diamond and Pt anodes. J. Electroanal. Chem. 627 (1-2), 41-50.

Khataee, A., Khataee, A., Fathinia, M., Vahid, B., Joo, S.W., 2013. Kinetic modeling of photoassisted-electrochemical process for degradation of an azo dye using boron-doped diamond anode and cathode with carbon nanotubes. J. Ind. Eng. Chem. 19 (6), 1890-1894.

Moreira, F.C., Garcia-Segura, S., Vilar, V.J.P., Boaventura, R.A.R., Brillas, E., 2013. Decolorization and mineralization of Sunset Yellow FCF azo dye by anodic oxidation, electro-Fenton, UVA photoelectro-Fenton and solar photoelectro-Fenton processes. Appl. Catal. B: Environ. 142-143, 877-890.

Oturan, N., Brillas, E., Oturan, M.A., 2012. Unprecedented total mineralization of atrazine and cyanuric acid by anodic oxidation and electro-Fenton with a boron-doped diamond anode. Environ. Chem. Lett. 10 (2), 165-170.

Özcan, A., Oturan, M.A., Oturan, N., Şahin, Y., 2009. Removal of Acid Orange 7 from water by electrochemically generated Fenton's reagent. J. Hazard. Mater. 163 (2-3), 1213-1220.

Özcan, A., Sahin, Y., Koparal, A.S., Oturan, M.A., 2008. Carbon sponge as a new cathode material for electro-Fenton process. Comparison with carbon felt cathode and application to degradation of synthetic dye Basic Blue 3 in aqueous medium. J. Electroanal. Chem. 616 (1-2) 71-78.

Panizza, M., Cerisola, G., 2009. Direct and mediated anodic oxidation of organic pollutants. Chem. Rev. 109 (12), 6541-6569.

Panizza, M., Oturan, M.A., 2011. Degradation of alizarin red by electro-Fenton process using a graphite-felt cathode. Electrochim. Acta 56 (20) 7084-7087.

Robinson, T., McMullan, G., Marchant, R., Nigam, P., 2001. Remediation of dyes in textile effluent: a critical review on current treatment technologies with a proposed alternative. Biores. Technol. 77 (3), 247-255.

Rodrigo, M.A., Cañizares, P., Sánchez-Carretero, A., Sáez, C., 2010. Use of conductive-diamond electrochemical oxidation for wastewater treatment. Catal. Today 151 (1-2), 173-177.

Rosales, E., Pazos, M., Longo, M.A., Sanromán, M.A., 2009. Electro-Fenton decoloration of dyes in a continuous reactor: A promising technology in colored wastewater treatment. Chem. Eng. J. 155 (1-2), 62-67.

Ruiz, E.J., Hernández-Ramírez, A., Peralta-Hernández, J.M., Arias, C., Brillas, E., 2011. Application of solar photoelectro-Fenton technology to azo dyes mineralization: Effect of current density, Fe^{2+} and dye concentration. Chem. Eng. J. 171 (2), 385-392.

Salazar, R., Brillas, E., Sirés, I., 2012. Finding the best Fe^{2+}/Cu^{2+} combination for the solar photoelectro-Fenton treatment of simulated wastewater containing the industrial textile dye Disperse Blue 3. Appl. Catal. B: Environ. 115-116, 107-116.

Salazar, R., Garcia-Segura, S., Ureta-Zañartu, M.S., Brillas, E., 2011. Degradation of disperse azo dyes from waters by solar photoelectro-Fenton. Electrochim. Acta 56 (18), 6371-6379.

Sirés, I., Brillas, E., Oturan, M.A., Rodrigo, M.A., Panizza, M., 2014. Electrochemical advanced oxidation processes: today and tomorrow. A review. Environ. Sci. Pollut. Res. 21 (14), 8336-8367.

Solís, M., Solís, A., Pérez, H.I., Manjarrez, N., Flores, M., 2012. Microbial decolouration of azo dyes: a review. Process Biochem. 47 (12), 1723-1748.

Thiam, A., Sirés, I., Garrido, J.A., Rodríguez, R.M., Brillas, E., 2015. Effect of anions on electrochemical degradation of azo dye Carmoisine (Acid Red 14) using a BDD anode and air-diffusion cathode. Sep. Purif. Technol. 140, 43-52.

Thiam, A., Zhou, M., Brillas, E., Sirés, I., 2014. Two-step mineralization of Tartrazine solutions: Study of parameters and by-products during the coupling of electrocoagulation with electrochemical advanced oxidation processes. Appl. Catal. B: Environ. 150-151, 116-125.

Ulson de Souza, S.M.A.G., Forgiarini, E., Ulson de Souza, A.A., 2007. Toxicity of textile dyes and their degradation by the enzyme horseradish peroxidase (HRP). J. Hazard. Mater. 147 (3), 1073-1078.

UNESCO, 2012. The United Nations World Water Development Report 4, Volume 1: Managing Water Report under Uncertainty and Risk.

Vasudevan, S., Oturan, M.A., 2014. Electrochemistry: As cause and cure in water pollution-an overview. Environ. Chem. Lett. 12 (1), 97-108.

Wang, A., Qu, J., Liu, H., Ge, J., 2004. Degradation of azo dye Acid Red 14 in aqueous solution by electrokinetic and electrooxidation process. Chemosphere 55 (9), 1189-1196.

Wang, A., Qu, J., Liu, H., Ru, J., 2008. Mineralization of an azo dye Acid Red 14 by photoelectro-Fenton process using an activated carbon fiber cathode, Appl. Catal. B: Environ. 84 (3-4), 393-399.

Xia, S., Zhou, X., Shi, W., Pan, G., Ni, Z., 2014. Photocatalytic property and mechanism studies on Acid Red 14 by M_xO_y/ZnTi–layered double hydroxides (M = Fe, Sn, Ce). J. Mol. Catal. A: Chem. 392, 270-277.

Zollinger, H., 2003. Color Chemistry: Synthesis, Properties, and Applications of Organic Dyes and Pigments. VHCA and Wiley-VCH, Switzerland.

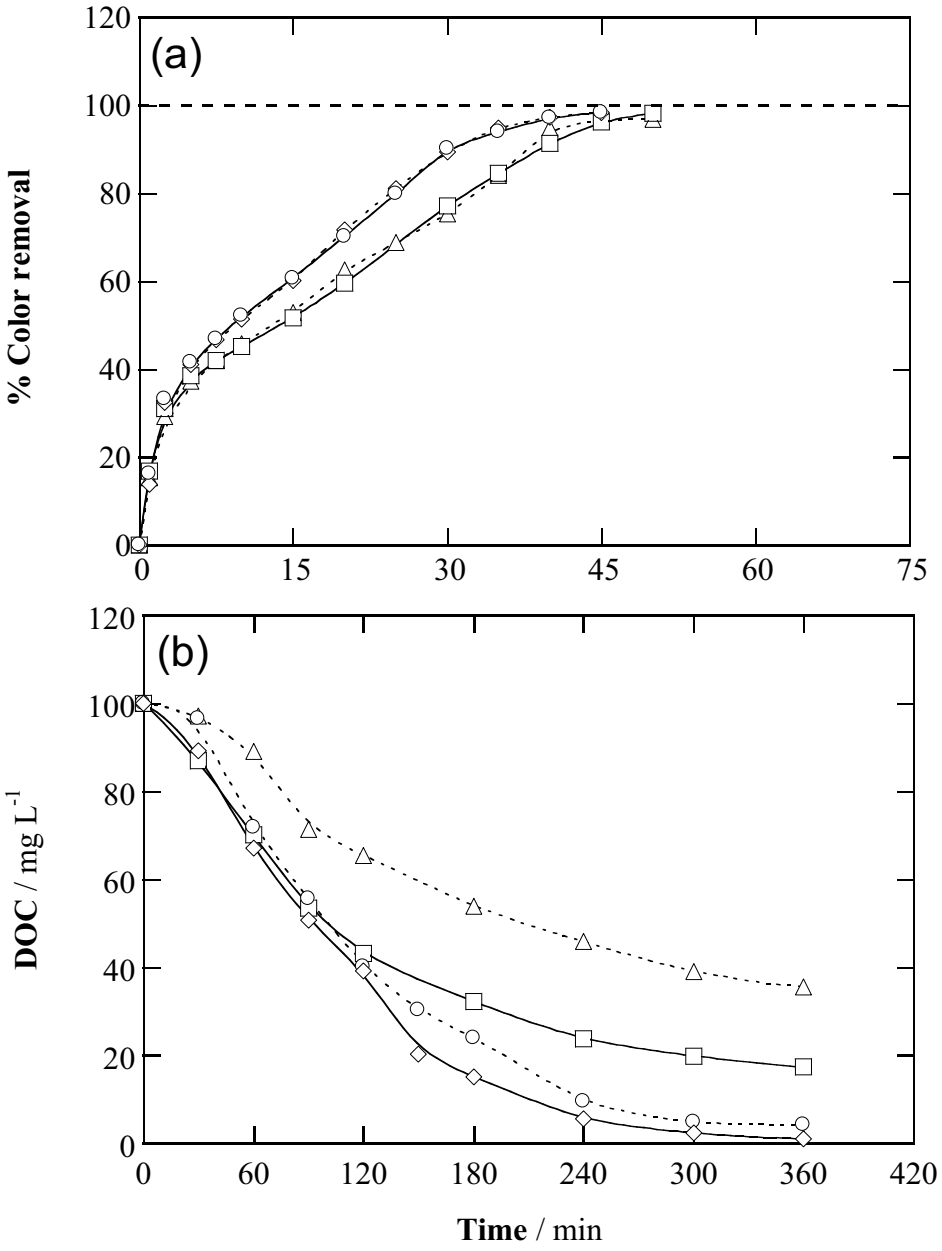

Fig. 1. (a) Percentage of color removal at λ = 510 nm and (b) DOC removal vs electrolysis time for the treatment of 130 mL of a mixture of food azo dyes (33.3 mg L^{-1} DOC each) for E122 (0.139 mM), E124 (0.140 mM) and E129 (0.145 mM) in ultrapure water with 0.05 M Na_2SO_4 and 0.50 mM Fe^{2+} at pH 3.0 using a stirred tank reactor with 3 cm^2 electrode area at 33.3 mA cm^{-2} and 35 ºC. Method: (△) EF-Pt, (□) EF-BDD, (○) PEF-Pt and (◇) PEF-BDD. In PEF, the solution was irradiated with a 6 W UVA lamp of λ_{max} = 360 nm.

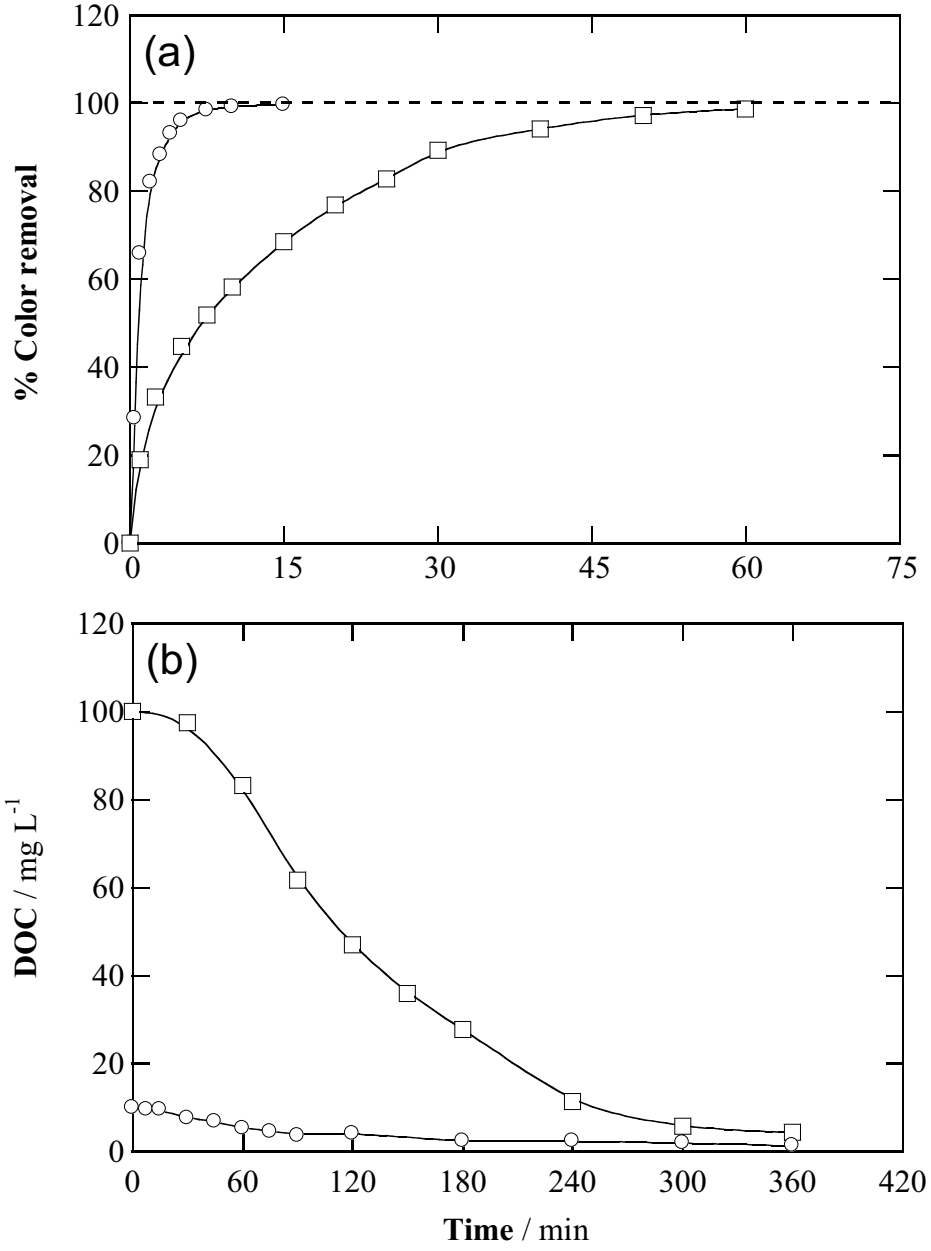

Fig. 2. (a) Decolorization efficiency at λ = 510 nm and (b) DOC abatement vs electrolysis time for the PEF-BDD treatment of 130 mL of a mixture of food azo dyes in ultrapure water with 0.80 mM Na_2SO_4 + 10 mM NaCl + 1.5 mM NH_4Cl + 0.50 mM K_2SO_4 + 0.02 mM $NaNO_3$ and 0.50 mM Fe^{2+} at pH 3.0 using a stirred tank reactor at 33.3 mA cm^{-2} and 35 ºC. DOC content: (○) 10 mg L^{-1} (3.3 mg L^{-1} DOC of E122, E124 and E129) and (□) 100 mg L^{-1} (33.3 mg L^{-1} DOC of each dye).

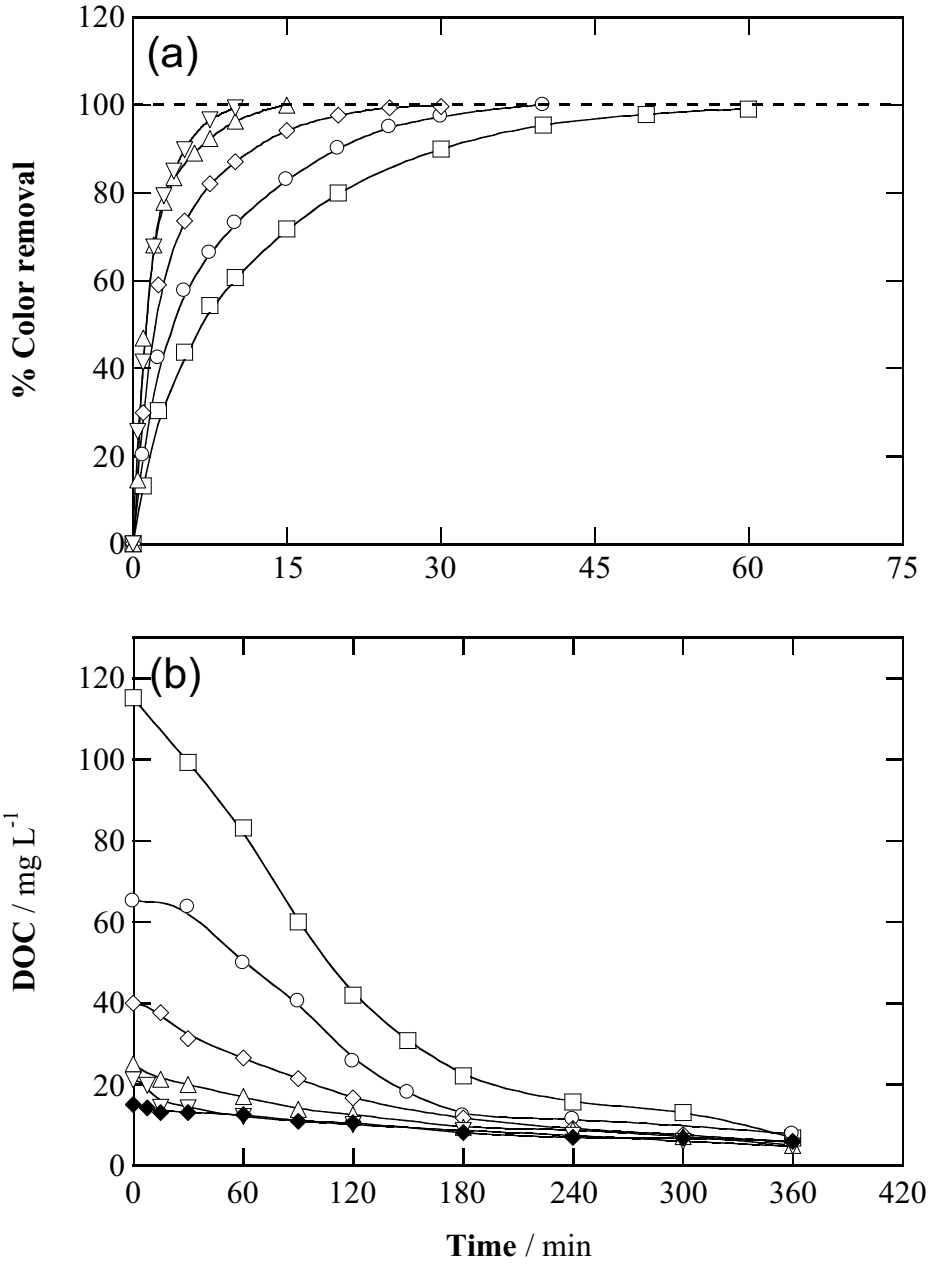

Fig. 3. Change of (a) percentage of color removal at λ = 510 nm and (b) DOC with electrolysis time for the PEF-BDD degradation of 130 mL of several mixtures of food azo dyes in a real water matrix (15 mg L^{-1} DOC) with 0.50 mM of added Fe^{2+} at pH 3.0 using a stirred tank reactor at 33.3 mA cm^{-2} and 35 ºC. DOC content from dyes: (◆) 0 mg L^{-1}, (▽) 6 mg L^{-1}, (△) 10 mg L^{-1}, (◇) 25 mg L^{-1}, (○) 50 mg L^{-1} and (□) 100 mg L^{-1}.

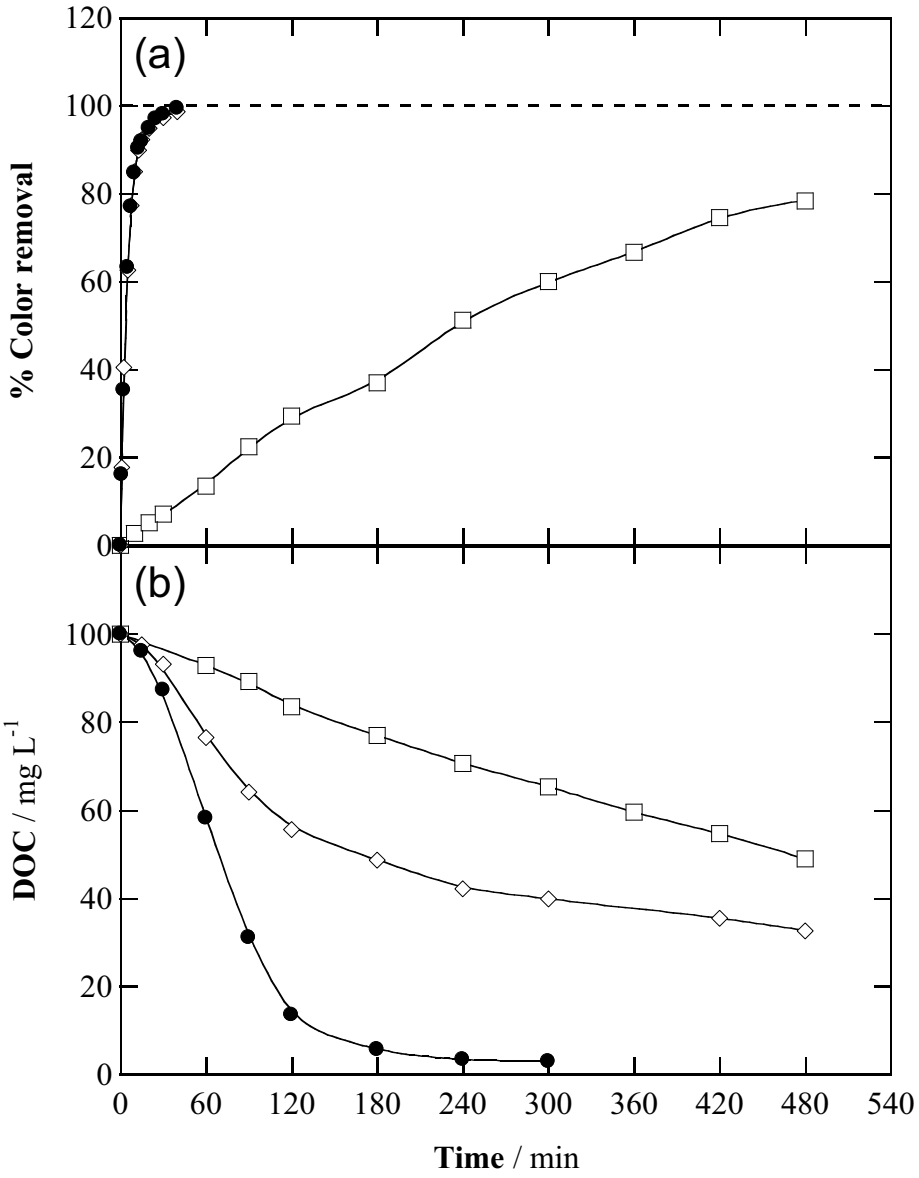

Fig. 4. Time course of (a) decolorization efficiency and (b) DOC removal for the treatment of 2.5 L of dye mixtures under the conditions described in Fig. 1, but using a flow plant equipped with a BDD/air-diffusion cell (20 cm^2 electrode area) at 100 mA cm^{-2}, 35 ºC and 200 L h^{-1}. Methods: (□) EO-H_2O_2-BDD (without Fe^{2+} added), (◇) EF-BDD and (●) SPEF-BDD.

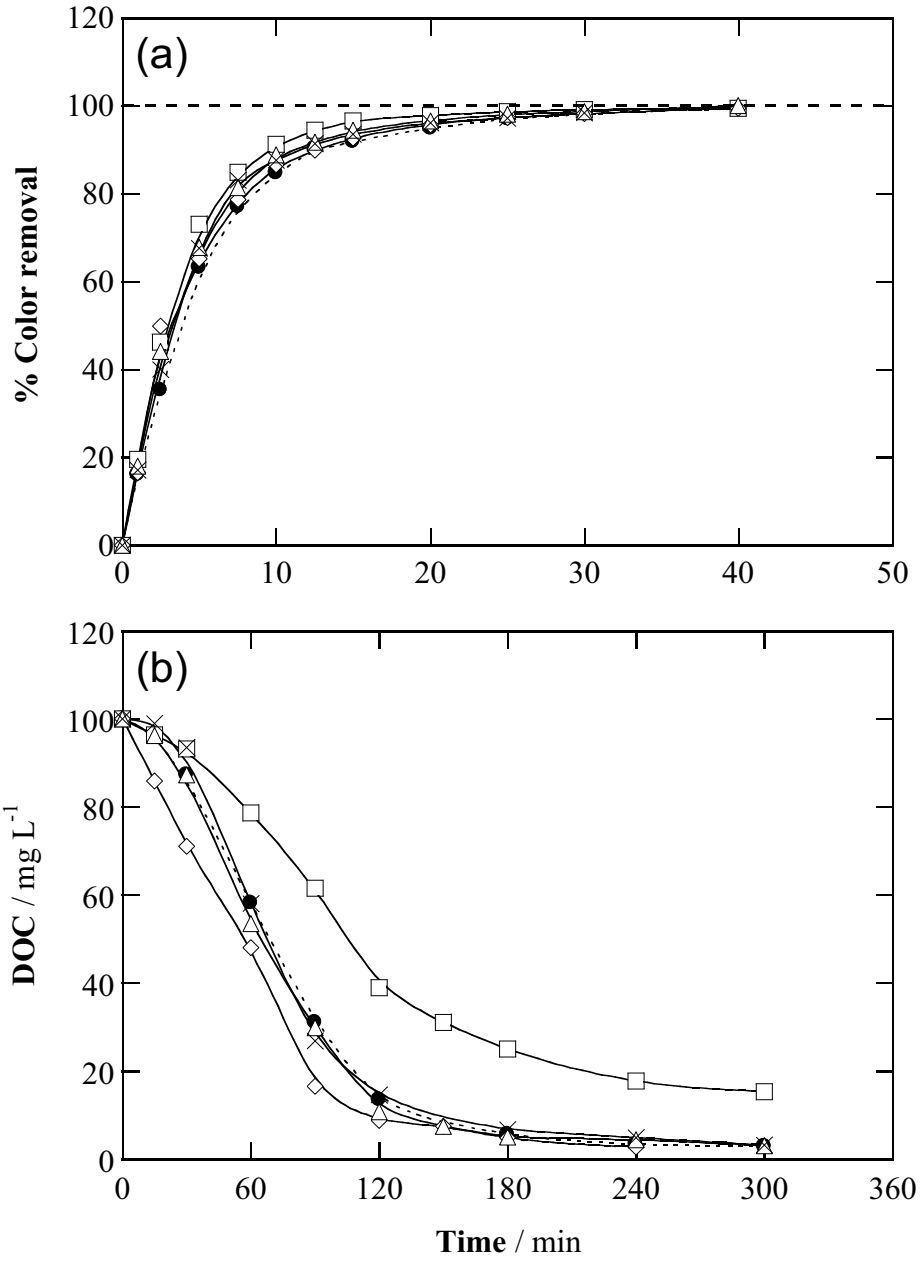

Fig. 5. Effect of the nature of supporting electrolyte on the (a) percentage of color removal at λ = 510 nm and (b) DOC decay vs. electrolysis time for the SPEF-BDD treatment of 2.5 L of a mixture of food azo dyes prepared as in Fig. 1, in 0.05 M of electrolyte and 0.50 mM Fe^{2+} at pH 3.0 using a flow plant at 100 mA cm^{-2}, 35 ºC and 200 L h^{-1}. Electrolyte: (●) Na_2SO_4, (△) $LiClO_4$, (◇) $NaNO_3$ and (□) NaCl. The curves obtained in (×) 0.04 M Na_2SO_4 + 0.01 M NaCl are also depicted.

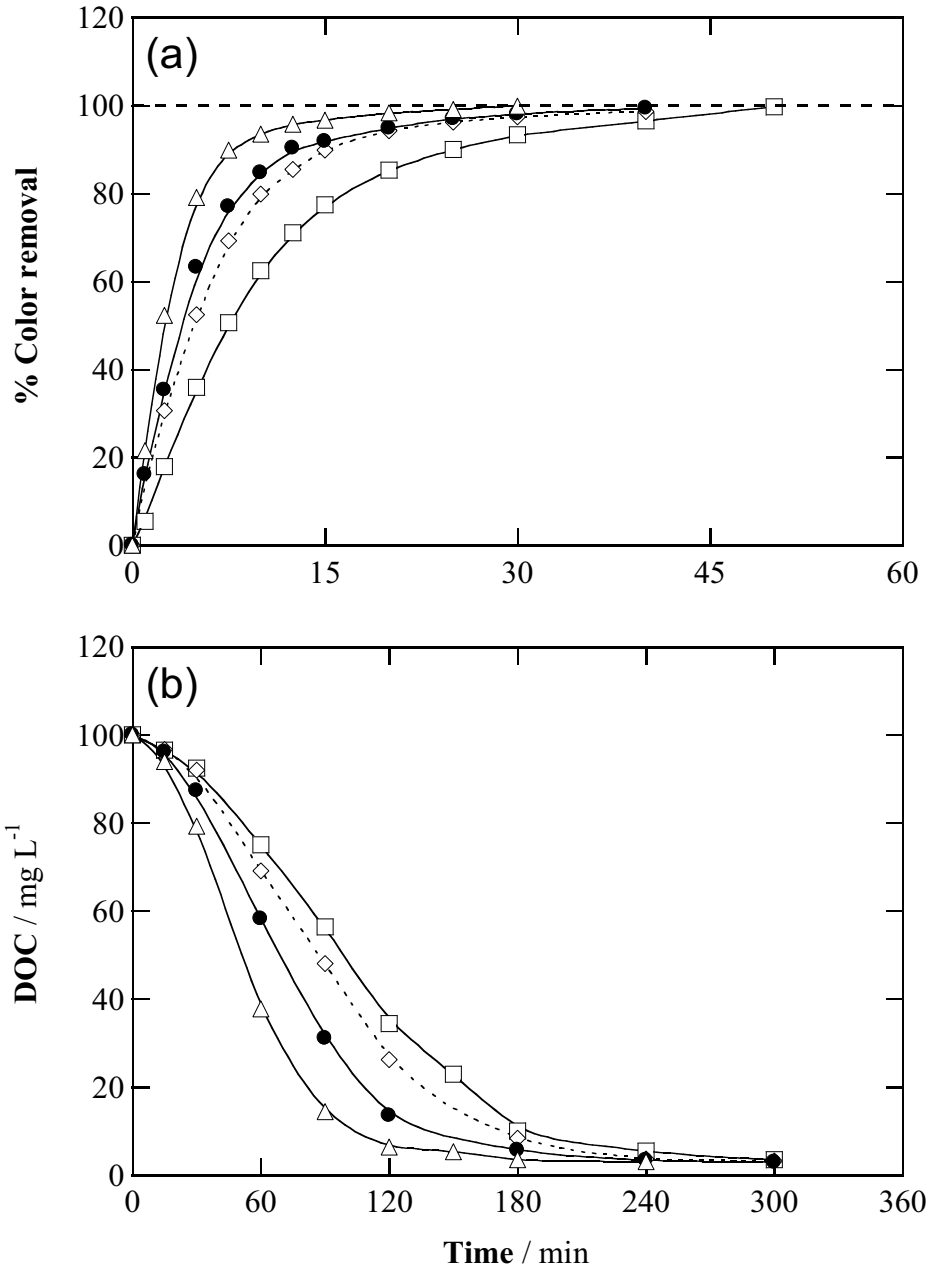

Fig. 6. Influence of current density on (a) the percentage of color removal at λ = 510 nm and (b) DOC abatement vs electrolysis time for the SPEF-BDD treatment of 2.5 L of a mixture of food azo dyes (prepared as in Fig. 1) in 0.05 M Na_2SO_4 and 0.50 mM Fe^{2+} at pH 3.0 using a flow plant at 35 ºC and 200 L h^{-1}. Current density: (□) 50 mA cm^{-2}, (◇) 75 mA cm^{-2}, (●) 100 mA cm^{-2} and (△) 150 mA cm^{-2}.

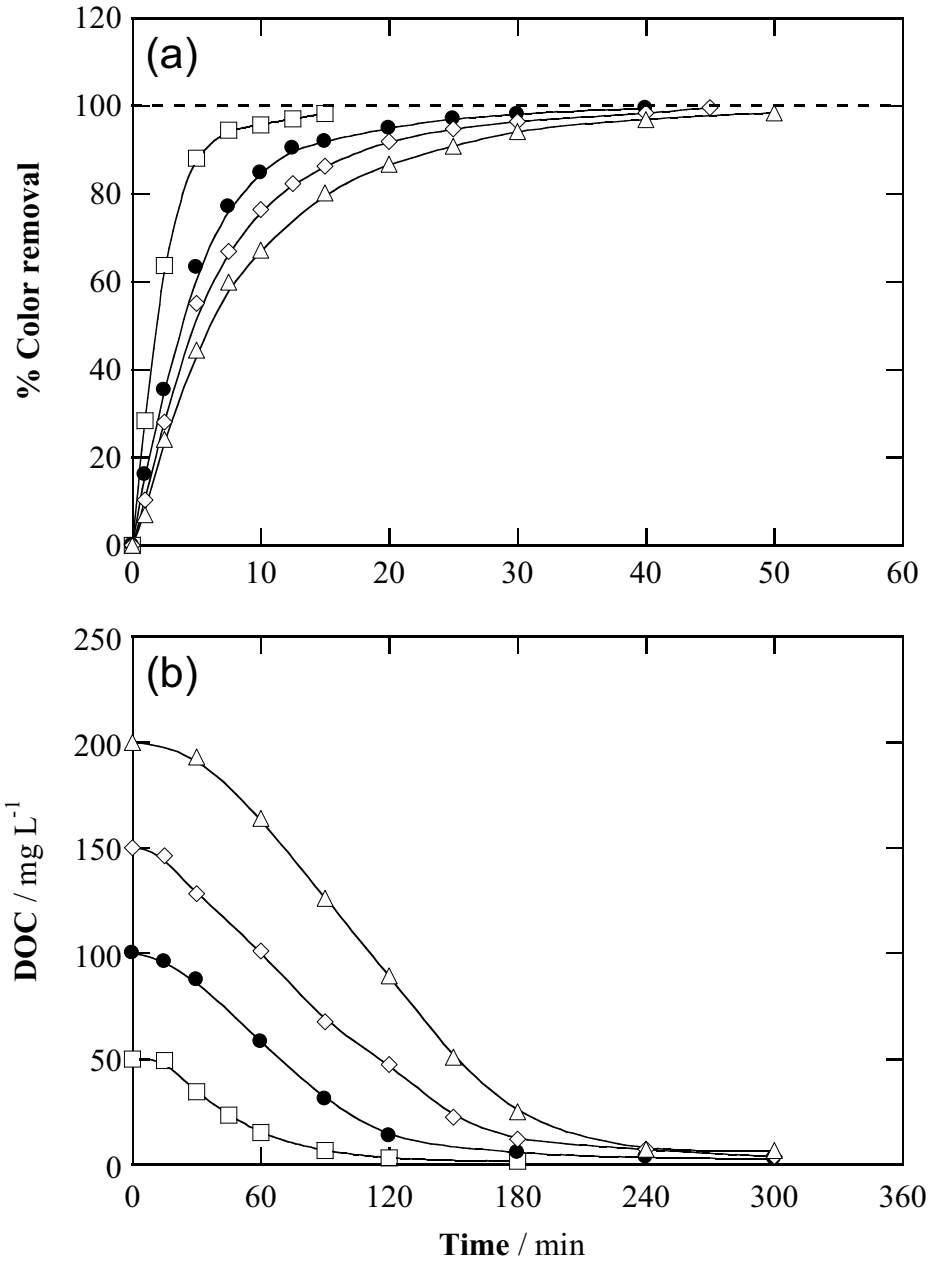

Fig. 7. Effect of initial dye content on the change of (a) the percentage of color removal at λ = 510 nm and (b) DOC with electrolysis time for the SPEF-BDD treatment of 2.5 L of different mixtures of food azo dyes in 0.05 M Na_2SO_4 and 0.50 mM Fe^{2+} at pH 3.0 using a flow plant at 100 mA cm^{-2}, 35 ºC and 200 L h^{-1}. DOC content (using equal mass concentration of E122, E124 and E129): (□) 50 mg L^{-1}, (●) 100 mg L^{-1}, (◇) 150 mg L^{-1} and (△) 200 mg L^{-1}.

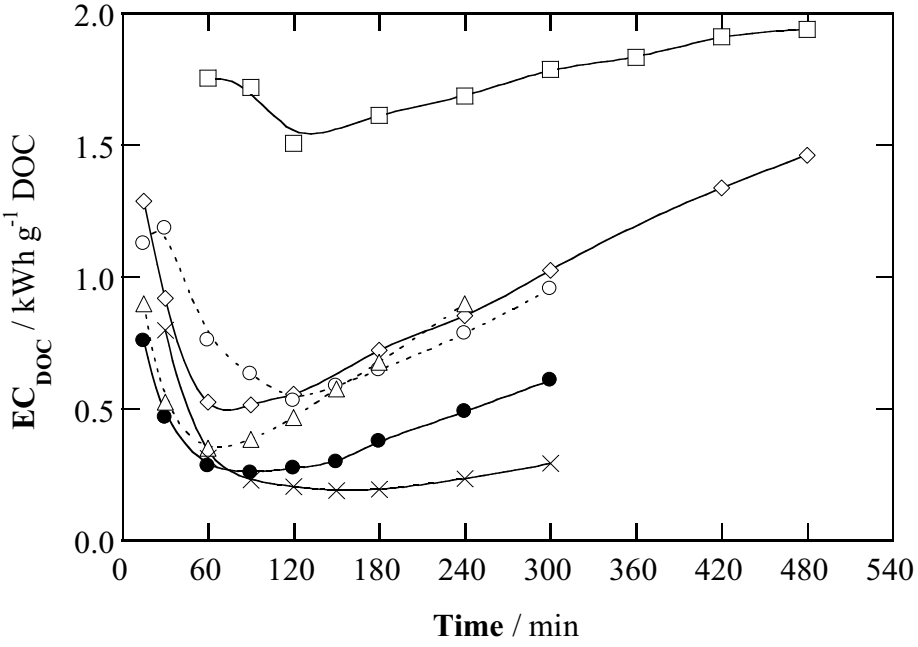

Fig. 8. Specific energy consumption per unit DOC mass with electrolysis time for the trials shown in Fig. 4. The SPEF trend for 100 mg L^{-1} DOC in 0.05 M Na_2SO_4 at 100 mA cm^{-2} is compared with those obtained under conditions of Figs. 5-7: (○) 0.05 M NaCl, (△) 150 mA cm^{-2} and (×) 200 mg L^{-1} DOC.

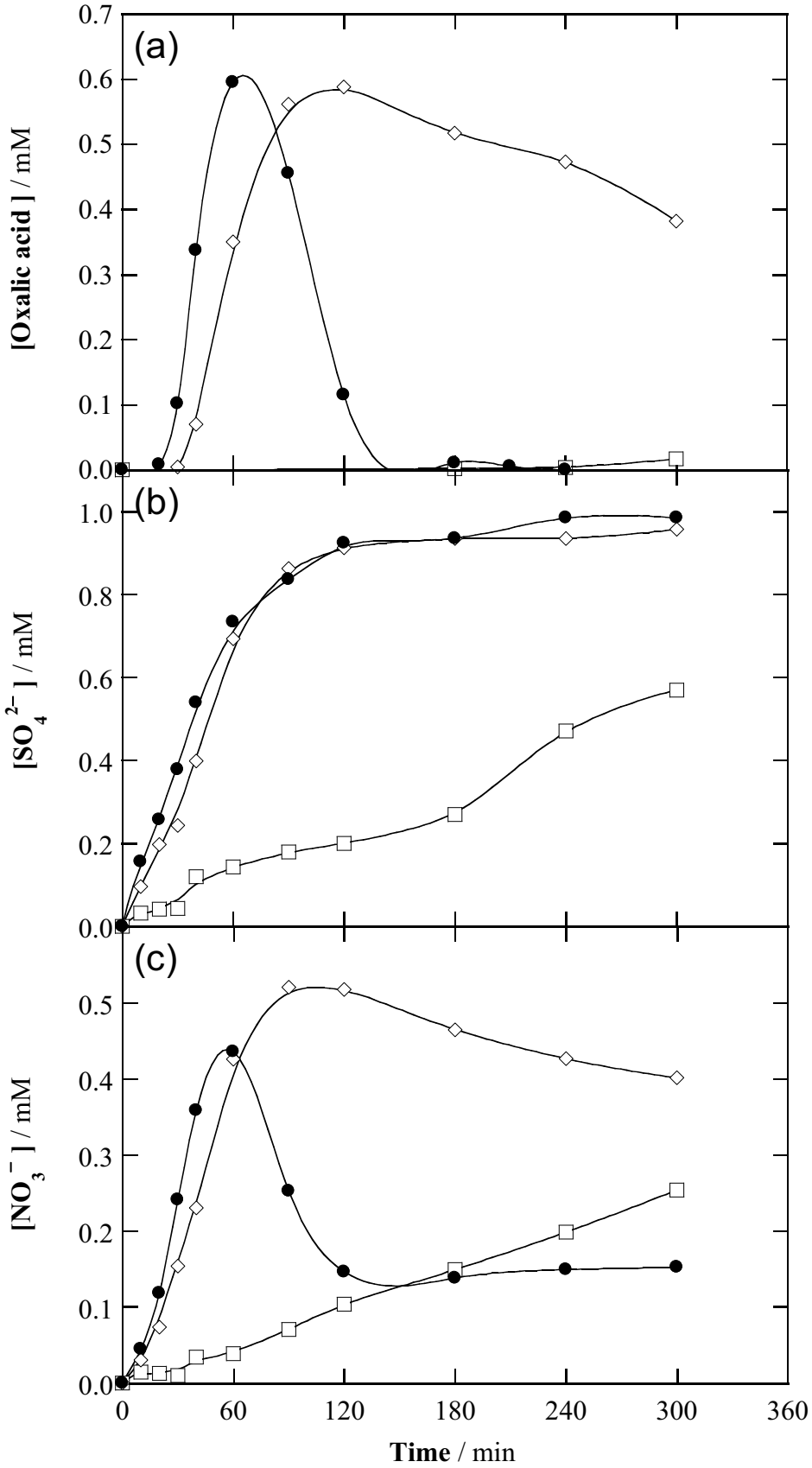

Fig. 9. Evolution of the concentration of: (a) oxalic acid, (b) sulfate ion and (c) nitrate ion for the trials shown in Fig. 4. Trials represented in plot (b) where obtained in 0.05 M $LiClO_4$ as electrolyte.

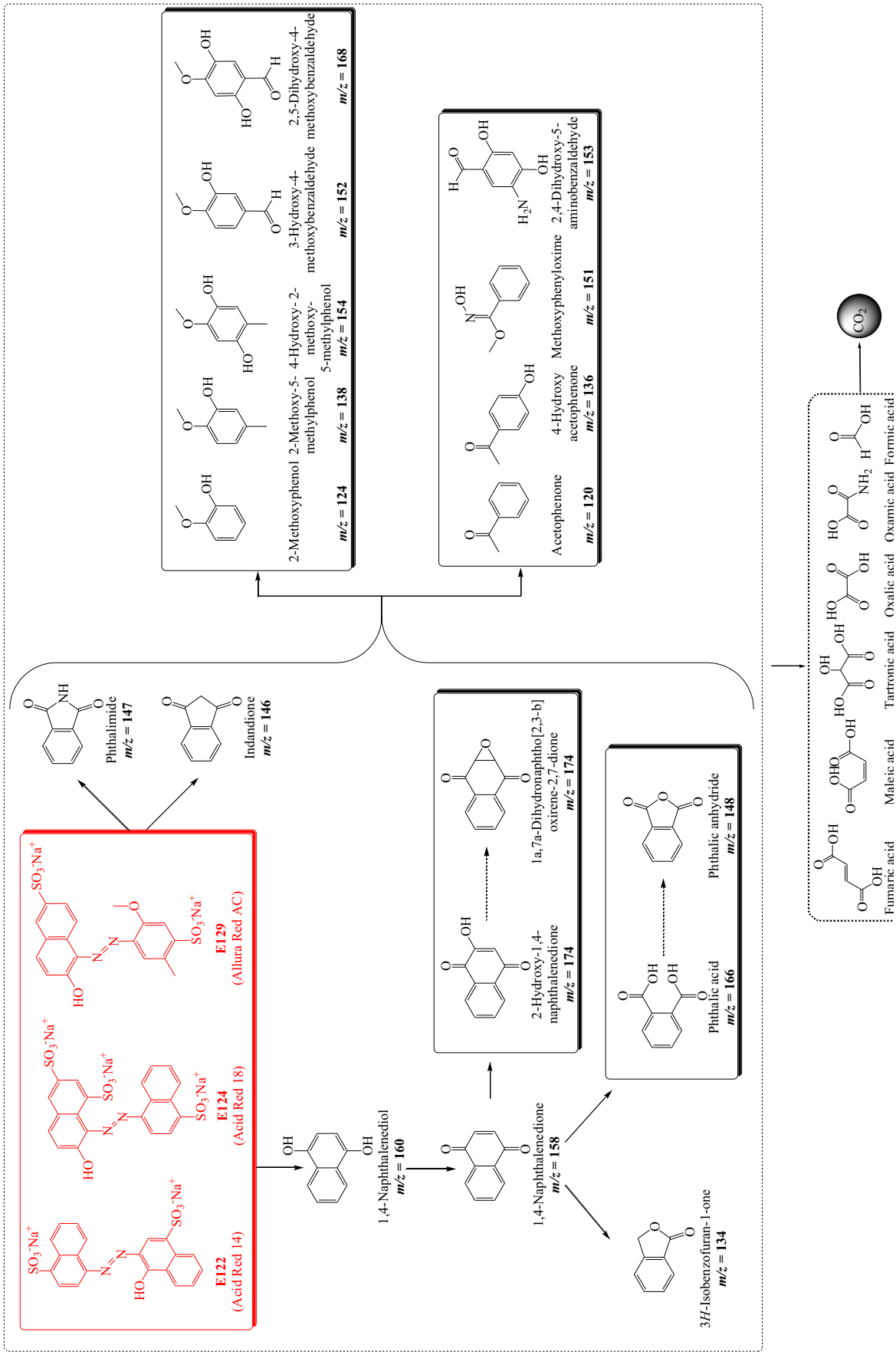

Fig. 10. Proposed reaction pathways for the mineralization of an acidic aqueous mixture of additives E122, E124 and E129 by SPEF with BDD anode. Aromatic products and short-linear carboxylic acids were identified by GC-MS and ion-exclusion HPLC, respectively

.

4.5. Electrocoagulation combined with electrochemical advanced oxidation processes for the treatment of Tartrazine: Assessment of novel sequential systems (at lab-scale and in a pre-pilot plant)

4. Results and discussion

Aiming at improving the viability of the electrochemical water treatment technologies used in our research group LEMMA, this part of the Thesis, which has been carried out at the *College of Environmental Science and Engineering* of the *Nankai University* (Tianjin, China) under the supervision of **Prof. Dr. Minghua Zhou**, has focused on the development of new combined EC/EAOPs systems, which take advantage of the best abilities of each technique in order to treat water effluents contaminated by food azo-dyes. The coupled technologies have been proven more efficient than the isolated ones due to their synergistic action. In this section, the degradation of Tartrazine solutions by individual EC and EAOPs such as EO, EF and PEF, as well as the combined EC/EAOPs systems have been studied, and different control variables have been evaluated. First, the trials were made at lab-scale (**Paper 7**), which has allowed devising an integrated system for the treatment of larger volumes in a pre-pilot plant (**Paper 8**).

At lab-scale, the electrochemical treatment of 130 mL of 278 mg L^{-1} of Tartrazine by EC alone was investigated using Fe or Al as the anode and SS as the cathode. Faster decolorization was achieved in NaCl medium, 100% CR being reached after only 10 min. This has been accounted by the presence of chloride that minimizes the passivation of the electrodes surface and also contributes to the mediated electrochemical oxidation by active chlorine. Poorer CR was obtained in the presence of SO_4^{2-} or NO_3^-. Also, the use of Al in Cl^- medium led to worse results than the Fe anode. Regarding the TOC removal, the efficacy increased in the order $NaNO_3$ < Na_2SO_4 < NaCl in accordance with the color removal, but none of the systems allowed the complete decontamination of the solutions. In NaCl medium, 60% TOC removal was reached approximately in 10 min, thereby remaining constant over time. This has been justified by the accumulation of soluble persistent organic by-products, as later confirmed by GC-MS results.

In all the subsequent EC experiments, Fe anodes were preferred, not only due to the enhanced coagulation but also to the superior catalytic properties of Fe^{2+} if thinking in a further coupling with Fenton-based EAOPs. The effect of keys parameters on the EC performance were investigated in NaCl medium. First, the influence of NaCl concentration in the range 0.025 to 0.30 M was studied. The increase of NaCl concentration did not bring about any significant acceleration of the color removal but it had a slightly higher effect on TOC removal. The decontamination rate increased upon increase of NaCl content from 0.025 M to 0.050 M, and then progressively decreased as

the NaCl content was raised up to 0.30 M, always achieving the maximum TOC removal of 60%. The effect of the pH (3.0, 6.3 (i.e., natural pH), 9.0 and 11.0) has been investigated in 0.050 M NaCl at 300 mA. Quick color and TOC decays were achieved at pH 6.3 and 9.0, where the majority of iron complexes (coagulant species) are formed and it becomes the optimum pH for carrying out the EC. The influence of applied current in 0.050 M NaCl at pH 6.3 has also been investigated. The CR was always 100%, but it was progressively faster when current was raised. For the TOC removal, a maximum value of 60% decontamination could be reached at the end of the electrolysis. However, it was already achieved after only ca. 10-15 min at 300 and 200 mA, whereas only 5% TOC removal could be obtained at that time at 50 and 100 mA. In conclusion, the best conditions for EC were obtained for the Fe/SS system in 0.050 M NaCl at natural pH 6.3 and 200 mA, which led to complete color removal and maximum TOC decay in just 15 min.

The electrochemical treatment of Tartrazine by individual EAOPs was checked using BDD or Pt as the anode and SS or ADE as the cathode, at pH 3.0 and 200 mA in different media. The CR in Na_2SO_4 revealed a very different performance of EO in comparison to EAOPs based on Fenton's reaction. The color disappeared very slowly in all the EO systems, being required 480 min for total decolorization with BDD and even longer time with Pt. In contrast, the decolorization was very rapid in the EF and PEF systems. The color was completely removed in 25-30 min regardless of the anode used and the absence or presence of UVA light. This means that the main oxidizing agent in Fenton-based EAOPs in Na_2SO_4 is $^{\bullet}OH$ formed from Fenton's reaction (12). As for the mineralization ability, the lower oxidation power of Pt compared to BDD was much more evident, since 10% and 92% TOC removal was achieved at 480 min by EO with each anode, respectively (**Figure 32a**). This confirms the classification of the anodes given by Comninellis, where the active Pt anode leads to electrochemical conversion while the non-active BDD favors the electrochemical combustion (see section 1). Only partial mineralization (52% TOC decay) was achieved in EF with Pt and complete mineralization after 300 min with BDD. The irradiation with UVA light in PEF cells led to the quickest mineralization, with all the TOC destroyed after 240 min using either Pt or BDD. The UV photons contribute to the mineralization due to the photodecarboxylation of Fe(III) complexes with carboxylic acids like oxalic and oxamic acids and enhance very significantly the MCE (**Figure 32b**).

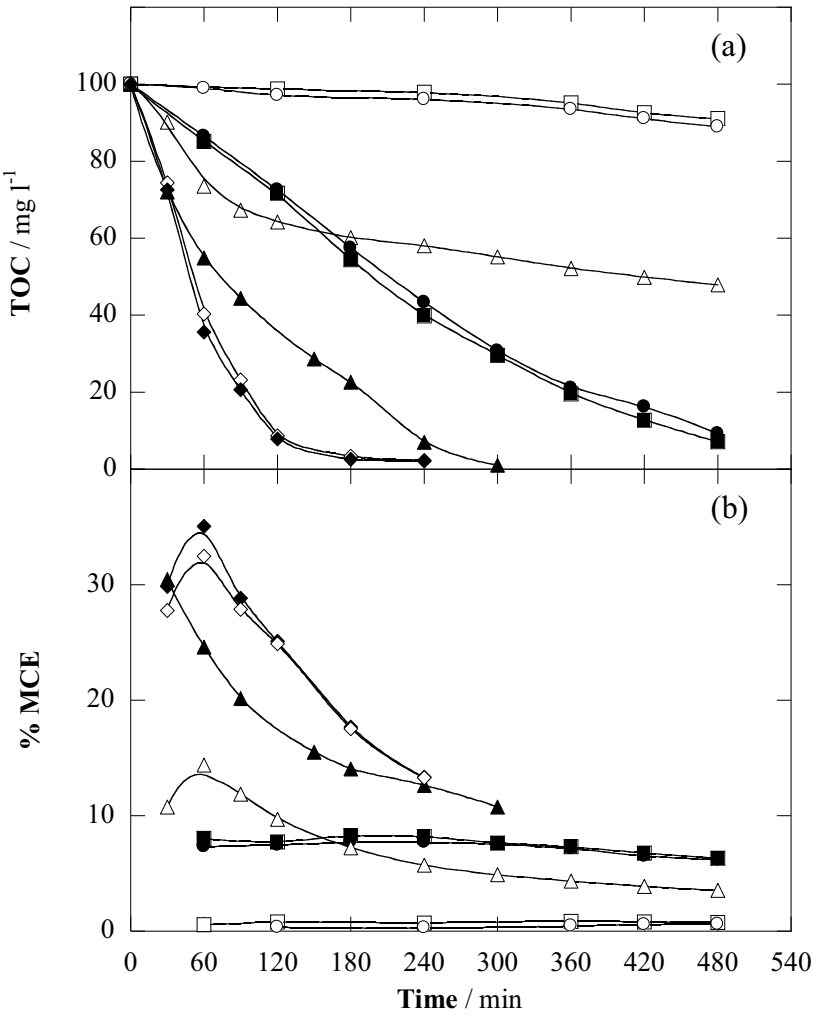

Figure 32. (a) TOC abatement and (b) MCE vs electrolysis time for the treatment of 130 mL of 278 mg L^{-1} Tartrazine solutions in 0.050 M Na_2SO_4 at pH 3.0 and 200 mA by different EAOPs: (●) EO (BDD/ADE), (○) EO (Pt/ADE), (■) EO (BDD/Steel), (□) EO (Pt/Steel), (▲) EF with BDD, (△) EF with Pt, (◆) PEF with BDD, (◇) PEF with Pt. In EF and PEF, 0.5 mM Fe^{2+} was added to the solution.

Since the nature of the electrolyte was found to have a large influence in EC, the same EAOPs were tested in 0.050 M NaCl. The results obtained clearly demonstrate the very positive effect of chloride ions on CR, as in EC process. The time for total color removal in the EO systems was reduced from ≥480 min to only 12.5-25 min due to the production of active chlorine. EF and PEF, which were already very powerful in Na_2SO_4, allowed the complete decolorization within a similar time period of only 15-20 min. In the case of mineralization, the TOC decay in PEF-BDD was a bit slower compared to that in Na_2SO_4, which can be explained by the parasitic reaction between $^{\bullet}OH$ and Cl^- and the formation of refractory chloroderivatives.

The aforementioned results confirm the great interest of EAOPs for water treatment. However, the long treatment time required to reach total mineralization is one of their main drawbacks to be implemented as a single degradation step. Therefore, the optimized EC pre-treatment can be envisaged as a powerful solution to make the technology viable and, therefore, appealing to the industry.

Upon comparison of the performance of the electrochemical processes under study, an efficient and economic combination was considered. Therefore, the remediation of Tartrazine was tested by combining the EC process followed by five different EAOPs aiming to shorten the treatment time. For this, the dye solutions were firstly pre-treated by EC (Fe/SS) under the optimized conditions for 15 min, which ensured a 100% CR and 60% TOC removal. Then, the samples were centrifuged, and the supernatant was treated by the EAOPs at 200 mA after pH regulation to 3.0. The PEF treatment (using a BDD/ADE cell) of the pre-treated Tartrazine solutions allowed obtaining the fastest decontamination, with total mineralization in about 315 min of global sequential treatment. In conclusion, in the sequential degradation, the EC acted as a very effective coagulation step to quickly decolorize the solutions and, at the same time, as a source of enough iron catalyst for the subsequent EAOPs.

In order to investigate the main degradation pathways of Tartrazine by the combined EC/PEF system, the main by-products were analyzed by GC-MS. Up to 17 benzenic compounds were identified during the post-treatment. Further oxidation of the benzene derivatives led to shorter aliphatic carboxylic acids, with oxalic acid as the main by-product before the total mineralization. To assess the primary decolorization steps undergone by Tartrazine prior to the PEF treatment, the mixture of by-products accumulated in the EC supernatant under optimized EC conditions for 15 min was analyzed by GC-MS. Five by-products were been identified. The formation of these by-products, once the azo dye had completely disappeared, agrees with the trend of TOC showing that ca. 40% of organic matter was still present in the solution. That residual TOC can then be related to such soluble derivatives that cannot be coagulated in EC and cannot be mineralized to aliphatic carboxylic acids.

After the promising results obtained with the sequential processes at lab-scale, an important step forward for the future implementation of combined EC/EAOPs treatments in industry or public facilities was addressed (Paper 8). The previous system was scaled up to treat 1.85 L of Tartrazine solutions instead of 130 mL. First, the

individual EC with Fe electrodes was investigated in a bench reactor, whereas three EAOPs (EO, EF and PEF) with DSA ($Ti/IrO_2–RuO_2$) instead of the BDD anode to reduce the costs were studied using a filter-press electrochemical reactor (see **Figures 17-19** in section 3). Tests were made in different electrolytes at constant current to assess the effect of key experimental parameters on the decolorization efficiency and the TOC removal rate.

In EC, the electrodes were connected in three different configurations (MP-P, MP-S and BP-S) to elucidate the best one. For each configuration, the effect of supporting electrolyte on the decolorization efficiency at 428 nm and the percentage of TOC removal was studied. The results showed that the quickest color and TOC removals were obtained in NaCl, therefore confirming our recent findings at lab-scale. The benefits from using chloride were also reported for the removal of other dyes (Aoudj y col., 2010; Amani-Ghadim y col., 2011). In $NaNO_3$, a very slow color removal of only 10-15% at 12.5 min was achieved due to the formation of a passive layer on the anode surface. From the results obtained for each configuration in different supporting electrolytes, one can conclude the BP-S configuration yielded the best results reaching 100% decolorization and 50% TOC removal after 12.5 min in NaCl medium. This can be justified by calculating the electrode consumption in each configuration and electrolyte, made from the electrode weighting before and after 120 min of electrolysis to minimize the measurement error. In all media, the consumption increased as MP-P < MP-S < BP-S, in accordance with the increasing cell voltage values (**Table 8**).

Table 8. Cell voltage (E_{cell}) and electrode consumption (Δm after 120 min) during the treatment of 1.85 L of 279 mg L^{-1} of Tartrazine solutions in 0.050 M of supporting electrolyte at pH 6.3 by EC.

Electrolyte	Configuration	E_{cell} / V	Δm / kg m^{-3}
Na_2SO_4	MP-P	2.98	1.76
	MP-S	9.75	3.76
	BP-S	12.61	3.88
NaCl	MP-P	4.56	1.75
	MP-S	13.85	3.08
	BP-S	16.89	4.05
$NaNO_3$	MP-P	5.86	0.06
	MP-S	18.16	0.08
	BP-S	22.61	0.07

Note that none of the systems allowed the complete decontamination of the solution. The less pronounced iron dissolution commented above for $NaNO_3$ medium was confirmed by the extremely little electrode consumptions at 120 min.

The influence of pH and applied current on decolorization and TOC removal in each configuration was checked and similar trends to those described above at lab-scale were obtained. The optimum pH values were 6.3 and 9.0, and the superiority of the BP-S configuration was confirmed. Since the initial pH of Tartrazine solutions was 6.3, the subsequent EC experiments were carried out at this pH, which avoids the need for adding chemicals to modify it. As for the current, as a result of the slight amelioration observed at 2.25 A and the poorer decolorization and TOC removal found at 0.75 and 1.125 A, and aftr comparing the corresponding EC_{TOC} values, 1.5 A was chosen as the optimum current using the BP-S configuration. The effect of the electrolyte and pollutant concentrations in the optimal BP-S configuration on the decolorization and TOC removals was also studied. Similar trends to those described above at lab-scale for the effect of supporting electrolyte were obtained. The increase in NaCl content entails a reduction in the cell voltage, which leads to a smaller electrode consumption. For example, 4.85 and 3.44 kg m^{-3} were determined at 120 min for electrolyses with 0.025 and 0.30 M NaCl, respectively. Regarding the initial pollutant concentration, all the solutions were completely decolorized within a short time, but being required more prolonged electrolyses when the initial dye content increased from 50 to 200 mg L^{-1}.

The ability of the EAOPs to treat solutions in a pre-pilot plant containing a filter-press cell equipped with a DSA ($Ti/IrO_2–RuO_2$) anode and an air-diffusion cathode was surveyed. Several electrolyses were performed to treat 278 mg L^{-1} of Tartrazine in 0.050 M NaCl at pH 3.0, 200 L h^{-1} and 2.0 A by EO, EF and PEF for 360 min. The color disappeared slowly in EO process, being required 60 min for total decolorization. In contrast, for EF and PEF, a much quicker total decolorization was achieved in 30 min. The time course of TOC decay for the same electrolyses was greatly dependent on the EAOP used. The greatest oxidation ability was obtained for the PEF process, leading to 90% mineralization at 360 min. The quicker TOC removal in PEF can be related to the additional photolysis of Fe(III) complexes with intermediates like short-chain carboxylic acids. In Na_2SO_4 and $NaNO_3$, the time course of color removal and TOC removal was very similar. Total decolorization was only achieved using EF and PEF processes due to $^{\bullet}OH$ formed in the bulk from Fenton's reaction (12), whereas the dye

solutions remained slightly colored at the end of the EO one. Regarding the mineralization, the TOC decay with PEF in Na_2SO_4 and $NaNO_3$ was somewhat faster than that obtained in NaCl, reaching overall mineralization in 240–300 min.

Having optimized the individual EC and EAOPs, the mineralization trends for the two-step treatment of Tartrazine solutions were studied. The dye solutions were first pre-treated by EC with four Fe electrodes in BP-S configuration in 0.050 M NaCl at natural pH 6.3 and 1.50 A for 12.5 min, which ensured complete color removal as well as up to 60% TOC removal. The final solutions were filtered and the separated liquid fractions treated by the Fenton-based EAOPs at 2.0 A after pH regulation at 3.0. The subsequent EF process led to poor enhancement, since the total mineralization was slightly higher than 60%. In contrast, the combined EC/PEF system allowed much faster decontamination, with > 90% TOC removal after 372.5 min of global sequential treatment due to the synergistic action of Fe(III) photoreduction and photodecarboxylation of refractory by-products. The effect of applied current on the mineralization rate by PEF post-treatment was assessed. The results revealed that a lower current such as 1.50 A could be applied instead. The TOC value was the same at 2.0 A and 1.50 A.

.

Paper 7

Two-step mineralization of Tartrazine solutions: Study of parameters and by-products during the coupling of electrocoagulation with electrochemical advanced oxidation processes

Applied Catalysis B: Environmental

150– 151 (2014) 116– 125

Applied Catalysis B: Environmental 150–151 (2014) 116–125

Contents lists available at ScienceDirect

Applied Catalysis B: Environmental

journal homepage: www.elsevier.com/locate/apcatb

Two-step mineralization of Tartrazine solutions: Study of parameters and by-products during the coupling of electrocoagulation with electrochemical advanced oxidation processes

Abdoulaye Thiam[a,b], Minghua Zhou[a,*], Enric Brillas[b], Ignasi Sirés[a,b,*]

[a] College of Environmental Science and Engineering, Nankai University, Tianjin 300071, China
[b] Laboratori d'Electroquímica dels Materials i del Medi Ambient, Departament de Química Física, Facultat de Química, Universitat de Barcelona, Martí i Franquès 1-11, 08028 Barcelona, Spain

ARTICLE INFO

Article history:
Received 7 October 2013
Received in revised form 3 December 2013
Accepted 6 December 2013
Available online 14 December 2013

Keywords:
Azo dyes
Electrocoagulation
Homogeneous catalysis
Photoelectro-Fenton
Tartrazine

ABSTRACT

A novel sequential electrochemical treatment consisting in an electrocoagulation (EC) pre-treatment and the subsequent advanced oxidation by photoelectro-Fenton (PEF) process with in-situ H_2O_2 electrogeneration and UVA light irradiation has been envisaged for the removal of organic pollutants from water, showing a high performance for the decolorization and mineralization of Tartrazine (Acid Yellow 23) solutions. EC has a dual purpose as a coagulation and catalyst source step since it allows the formation of $Fe(OH)_n$ (n = 2 or 3) coagulant and Fe^{3+}/Fe^{2+} ions. The influence of the anode material (Fe and Al), supporting electrolyte, pH and current during the individual EC on the abatement of color and total organic carbon (TOC) has been assessed. EC with Fe in 0.05 M NaCl yielded the best results. Next, various single electrochemical advanced oxidation processes (EAOPs) such as electro-oxidation (EO), electro-Fenton (EF) and PEF with a Pt or boron-doped diamond (BDD) anode and an air-diffusion cathode (ADE) have been tested. PEF with BDD/ADE yielded the quickest degradation among all the EAOPs in NaCl, due to the action of oxidants like active chlorine as well as •OH formed at the anode surface from H_2O oxidation and in the bulk from UV-enhanced Fenton's reaction between cathodic H_2O_2 and added Fe^{2+}. Therefore, the two-step EC (Fe/steel)/PEF (BDD/ADE) process was the best EC/EAOP combination. The EC treatment in 0.05 M NaCl at natural pH 6.3 and 200 mA, followed by PEF treatment of the supernatant at pH 3.0 and 200 mA, yielded the best conditions with a total decolorization in 15 min of EC and total mineralization in ca. 300 min of PEF. GC–MS analysis showed the formation of several benzenic by-products during the application of EC/PEF. Independent electrolyses revealed the ability of EC to accumulate soluble chlorobenzene derivatives, which can be completely destroyed in the PEF step under the action of the mixture of oxidants, particularly by successive hydroxylation via •OH largely promoted in the bulk by the Fe^{2+} ions generated in EC.

1. Introduction

Wastewaters generated by several industries pose some serious health and environmental risks worldwide owe to the significant concentrations and/or large variety of toxic aromatic pollutants. In this context, the advanced oxidation processes (AOPs) are very effective remediation technologies due to the action of highly reactive species (ROS) such as (mainly but not uniquely) hydroxyl radical (•OH) in the reaction mechanism. The main catalyzed AOPs can be divided into: (i) heterogeneous catalysis such as TiO_2 photocatalysis and electrocatalysis (EAOPs) with large O_2-overvoltage anodes, and (ii) homogeneous catalysis such as catalyzed ozonation and chemical and electrochemical Fenton and photo-Fenton [1–3].

In recent years, the interest on new or enhanced electrochemical separation and degradation technologies has grown considerably. Most intensive research efforts are devoted to heterogeneous electrocatalysis, where electro-oxidation (EO) is predominant, electrocoagulation (EC) and EAOPs based on Fenton's reaction chemistry [4–6]. EO combines high simplicity and efficacy, favoring the oxidative decontamination of waters under the action of •OH formed at the anode surface by water oxidation via reaction (1). At present, boron-doped diamond (BDD) is the best electrocatalytic anode material to oxidize pollutants, which has led to the

* Corresponding authors. Tel.: +34 934021223/+86 2266229619; fax: +34 934021231/+86 2223501117.
E-mail addresses: zhoumh@nankai.edu.cn (M. Zhou), i.sires@ub.edu, isiresa@gmail.com (I. Sirés).

0926-3373/$ – see front matter © 2013 Elsevier B.V. All rights reserved.
http://dx.doi.org/10.1016/j.apcatb.2013.12.011

development of successful flow reactors [7–10]. In chloride medium, the oxidation mediated by active chlorine species (Cl_2, HClO and/or ClO^-) electrogenerated via reactions (2)–(4) competes with the •OH-mediated oxidation [6].

$$M + H_2O \rightarrow M(^{\bullet}OH) + H^+ + e^- \quad (1)$$

$$2Cl^- \rightarrow Cl_{2(aq)} + 2e^- \quad (2)$$

$$Cl_{2(aq)} + H_2O \rightarrow HClO + Cl^- + H^+ \quad (3)$$

$$HClO \rightleftarrows ClO^- + H^+ \quad (4)$$

EC is a traditional physicochemical treatment for phase separation that is based on the release of Al(III) or Fe(II) cations in the bulk from dissolution of the corresponding sacrificial anode(s) via reactions (5) and (6). These are active coagulant precursors because the simultaneous production of OH^- anions by cathodic reduction of water leads to the formation of insoluble polymeric metallic hydroxides as shown in reactions (7) and (8). Such particles have large surface area and remain as a gelatinous suspension, then being able to remove pollutants by coagulation upon destabilization either by surface complexation or electrostatic attraction [11–13]. EC has been shown effective for the removal of colloidal and ionic pollutants from synthetic and real waters [14–22].

$$Al_{(s)} \rightarrow Al^{3+}_{(aq)} + 3e^- \quad (5)$$

$$Fe_{(s)} \rightarrow Fe^{2+}_{(aq)} + 2e^- \quad (6)$$

$$Al^{3+}_{(aq)} + 3H_2O \rightarrow Al(OH)_{3(s)} + 3H^+ \quad (7)$$

$$4Fe^{2+}_{(aq)} + 10H_2O + O_{2(g)} \rightarrow 4Fe(OH)_{3(s)} + 8H^+_{(aq)} \quad (8)$$

EAOPs such as electro-Fenton (EF) and photoelectro-Fenton (PEF) processes are even more efficient than EO and EC for the destruction of aqueous pollutants [23–36]. They are based on the in-situ electrogeneration of H_2O_2 into acidic polluted solutions from the two-electron O_2 reduction at a carbonaceous cathode. The addition of a catalytic amount (0.1–1.0 mM) of Fe^{2+} to the medium allows a high production of •OH in the solution bulk from the well-known Fenton' reaction [5]:

$$Fe^{2+} + H_2O_2 \rightarrow Fe^{3+} + {}^{\bullet}OH + OH^- \quad (9)$$

PEF has the greatest performance owing to the concomitant action of both the generated •OH and the UV radiation on the organic molecules and their Fe(III)-complexes [30,33,35]. Although EF and PEF are promising technologies, their potential exploitation is still limited due to the relatively high operation costs that are inherent to the long treatment time required. Aiming to shorten the reaction time, the so-called peroxi-coagulation (PC) process with a sacrificial iron anode and a cathode able to generate H_2O_2 has been further devised [37–39]. This one-pot method allows the simultaneous coagulation and oxidation of organic pollutants thanks to Fe^{2+} catalyst generated on site via reaction (6), but it presents some major drawbacks: (i) The excess of iron cations causes the destruction of •OH, (ii) the cathode lifetime and its ability for producing H_2O_2 are drastically reduced due to both, adsorption of coagulated particles that block the diffusion pores and the active sites, and surface abrasion caused by precipitated hydroxides and coagulated matter, and (iii) the effect of UV light in photoperoxi-coagulation is almost negligible due to the barrier effect of the iron precipitate.

Synthetic dyes are being largely produced due to their unique properties that allow limitless industrial applications. Azo dyes are particularly pre-eminent since they represent 60–70% of the world production [18]. However, their occurrence in wastewaters entails major concerns due to the proven toxicity and carcinogenicity and the production of toxic by-products like aromatic amines [31,40]. Among them, food azo-colors have received much less attention than their textile counterparts, despite being considered dangerous due to their possible connection to hyperactivity in children in cases of intakes of potent mixes of colorings. Recent issues over the toxicity of food additives have led to a stricter legislation. For example, the UK Foods Standards Agency has recommended that they should be phased out over a period from food and drink in the EU [41]. Tartrazine (Acid Yellow 23, trisodium 1-(4-sulfonatophenyl)-4-(4-sulfonatophenylazo)-5-pyrazolone-3-carboxylate) is primarily used as a common synthetic food coloring agent, also known as additive E102, to provide a vivid yellow color to processed commercial foods like sweets, beverages and snacks. It is also used in personal care and cosmetic products, as well as in medications. Sensitivity to Tartrazine may be relevant since it is suspected to be responsible for most of the allergic and intolerance reactions among all azo dyes, even being temporally banned in some European countries. Its adverse reactions in human beings have lately been under consideration by the European Food Safety Agency [42]. A large range of dyestuffs has been removed from water electrochemically by EO [8,9,17,43,44], EC [14,17,19,21] and EAOPs like EF and PEF [23–26,31,33,45,46]. However, there are no studies assessing the performance of BDD or PEF for Tartrazine, and just a couple of studies report its treatment by EC [47,48].

As far as we know, this work reports for the first time the sequential combination of EC and EAOPs based on Fenton's reaction chemistry, aiming at: (i) inducing the coagulation of a large amount of organic matter via the EC pre-treatment, which also acts as a source of iron catalyst, and (ii) controlling the electrogeneration of oxidizing agents on site to reach the complete mineralization of dye solutions during the EAOP post-treatment. This intends to overcome the drawbacks exposed for PC, therefore achieving a higher degradation performance for dye solutions. Previous EC/EAOPs couplings reported in literature for decontamination have dealt with the EC/EO system [49–51]. The present study focuses on the treatment of solutions of 130 ml of Tartrazine as a model food azo dye in different electrolytes at constant current. First, the individual EC with Fe or Al anodes, and EO, EF and PEF with Pt or BDD anodes were tested to assess the effect of the experimental parameters on the decolorization and TOC removal rates. Then, the best combined EC/EAOP was optimized to achieve the quickest decontamination. The degradation by-products formed during this combined treatment were identified by gas chromatography coupled to mass spectrometry (GC–MS).

2. Experimental

2.1. Chemicals

Tartrazine ($C_{16}H_9N_4Na_3O_9S_2$, C.I. 19140, dye content ≥85%) was purchased from Sigma-Aldrich and was used as received. Anhydrous sodium sulfate, sodium chloride and sodium nitrate used as background electrolytes, as well as iron(II) sulfate heptahydrate, used as catalyst in EF and PEF, were of analytical grade from Merck and Fluka. Solutions were prepared with ultra-pure water from a Millipore Milli-Q system with resistivity >18 MΩ cm and their pH was adjusted with analytical grade sodium hydroxide or sulfuric, hydrochloric or nitric acid from Merck. Other chemicals for performing analyses were obtained from Merck and Sigma-Aldrich.

2.2. Electrochemical cells

All the electrolytic trials were conducted in an open and undivided cylindrical glass cell of 150 ml capacity with a double jacket

for circulation of external thermostated water to regulate the solution temperature at 25 °C.

For the EC trials, the anode was either an iron or aluminium plate with overall dimensions of 5.0 cm × 1.5 cm, 0.25 cm thickness, and immersed length of 3.0 cm. The cathode was a steel plate with the aforementioned dimensions. The front, back and sides of each piece were exposed to the solution. The electrodes were placed in parallel with an interelectrode gap of 1.0 cm. Before first use, all electrodes were mechanically abraded using SiC paper to remove scale, followed by cleaning with 0.1 M NaOH or H_2SO_4 solution (20% in volume) and a final ultrasonic cleaning in ultra-pure water.

For the EAOPs, the anode was either a 3 cm^2 Pt sheet of 99.99% purity supplied by SEMPSA (Barcelona, Spain) or a 3 cm^2 BDD thin-film electrode supplied by NeoCoat (La-Chaux-de-Fonds, Switzerland). The latter one was synthesized by the HFCVD technique on p-type polycrystalline Si wafers (0.1 Ω cm, Siltronix), being the BDD coating 2.5–3.5 μm thick and having 700 ppm of boron. The cathode was either a 3 cm^2 stainless steel plate or a 3 cm^2 carbon-PTFE air-diffusion electrode (ADE) supplied by E-TEK (Somerset, NJ, USA), mounted as described elsewhere and fed with air pumped at 1 l min^{-1} for continuous H_2O_2 generation [5]. The interelectrode gap was about 1.0 cm. Before first use, a preliminary polarization in 100 ml of 0.05 M Na_2SO_4 at 100 mA cm^{-2} for 180 min allowed the removal of the impurities of the BDD anode surface and the activation of the ADE. PEF treatments were carried out under irradiation with a Philips TL/6W/08 fluorescent black light blue tube that was placed at 7 cm above the solution. This tube emitted UVA light in the wavelength region 320–400 nm with λ_{max} = 360 nm, yielding a photoionization energy of 5 W m^{-2} as detected with a Kipp & Zonen CUV 5 radiometer.

Freshly prepared solutions of 130 ml with 100 mg l^{-1} of TOC (corresponding to 278 mg l^{-1} or 0.52 mM) of Tartrazine in different supporting electrolytes (Na_2SO_4, NaCl or $NaNO_3$) were treated by individual EC and EAOPs. In EC, the effect of the applied current was tested in the range 50–300 mA and the solution pH was varied between 3.0 and 11, whereas it was fixed at 3.0 in trials of EAOPs because this pH has been found as optimal for the treatment of other aromatics with ADE as cathode [5]. In EF and PEF, 0.5 mM Fe^{2+} was added as catalyst. To perform the combined EC/EAOPs, EC-treated solutions were centrifuged for 5 min at 5000 rpm in order to remove the precipitate and easily collect the supernatant to be further treated by each EAOP. The solutions were always vigorously stirred with a magnetic bar at 800 rpm to ensure mixing and the transport of reactants toward/from the electrodes.

2.3. Apparatus and analysis procedures

All the experiments were performed at constant current with an Amel 2053 potentiostat-galvanostat, which also displayed the potential difference between electrodes. The solution pH was measured with a Crison 2000 pH-meter. Samples were always withdrawn at regular time intervals from the treated solutions and then microfiltered with 0.45 μm PTFE filters from Whatman before analysis. The decolorization of Tartrazine solutions was monitored from the absorbance (A) decay at the maximum visible wavelength (λ_{max}) of 428 nm, measured from the spectra recorded on a Shimadzu 1800 UV/Vis spectrophotometer at 35 °C. The percentage of color removal or decolorization efficiency was then determined according to Eq. (10) [5,18]:

$$\text{Color removal } (\%) = 100\frac{A_0 - A_t}{A_0} \quad (10)$$

where A_0 and A_t denote the absorbance at initial time and after an electrolysis time t, respectively.

The same spectrophotometer was also employed for colorimetric measurements of free active chlorine (Cl_2 and $HClO/ClO^-$) and total iron concentrations. Active chlorine was determined by the DPD method, which consists in the reaction between the desired sample and a standard *N*,*N*-diethyl-*p*-phenylenediamine (DPD) solution to generate a pink color measured at λ = 515 nm whose intensity is proportional to the active chlorine content [52]. The total iron content was obtained by adding ascorbic acid to selected samples and measuring the light absorption of the complex formed between Fe^{2+} and 1,10-phenantroline at λ = 508 nm [53]. The mineralization of solutions was monitored from the decay of their TOC determined on a Multi N/C® 3100 analyzer from Analytik Jena. Reproducible TOC values with an accuracy of ±1% were always found by injecting 50 μl aliquots into the analyzer. The energy consumption per unit volume was then calculated as follows [5]:

$$\text{Energy consumption } \left(\text{kW h m}^{-3}\right) = \frac{E_{cell}\, It}{V_s} \quad (11)$$

where E_{cell} is the average potential difference between electrodes (V), I is the applied current (A), t is the electrolysis time (h) and V_s is the volume of the treated solution (l).

The aromatic by-products in some treated solutions were identified by GC–MS using an Agilent Technologies system composed of a 7890A gas chromatograph equipped with a 7683B series injector and a 5975C mass spectrometer in EI mode at 70 eV. A nonpolar Agilent J&W HP-5ms column with dimensions of 0.25 μm, 30 m × 0.25 mm (i.d.) was used. The temperature ramp was as follows: 36 °C for 1 min, 5 °C min^{-1} up to 300 °C and hold time 10 min. The temperature of the inlet, source and transfer line was 250, 230 and 280 °C, respectively. The analyses were by splitless (0.7 min) injection. Aiming to identify as many reaction intermediates as possible, the organic components of the whole electrolyzed volumes (i.e., 130 ml) in each trial were extracted with CH_2Cl_2 in three times of 25 ml each. The resulting organic solution was dried over anhydrous Na_2SO_4, filtered and concentrated up to ca. 1 ml under reduced pressure to be further analyzed. The mass spectra were identified with a NIST05 MS library.

3. Results and discussion

3.1. Treatment of Tartrazine solutions by electrocoagulation alone

The effect of several experimental parameters on the decolorization and decontamination profiles obtained during the treatment of 278 mg l^{-1} Tartrazine by EC was firstly assessed with Fe/steel as the anode/cathode pair. Different electrolyses were performed in 0.05 M Na_2SO_4, NaCl or $NaNO_3$ at 300 mA in order to study the influence of the type of supporting electrolyte. All these trials were conducted at natural pH 6.3, which was under continuous control because it tended to increase due to the generation of OH^- at the cathode that could be only partially neutralized by H^+ formed from reaction (8) [54]. The decolorization efficiency is represented in Fig. 1a as the increasing percentage of color removal at 428 nm over the electrolysis time. The absorption spectrum of Tartrazine is included in the inset, showing an absorption band in the UV region at about 254 nm corresponding to the benzenic rings and a broader band in the visible region at 428 nm related to the –N=N– bond that is responsible for the vivid lemon yellow color. In Na_2SO_4, the intensity of both absorption bands decreased continuously and rapidly, reaching the total disappearance of the band at 428 nm in 30 min. This can be explained by the iron dissolution via reaction (6) to yield Fe^{2+}, which is further transformed into a powerful coagulant like $Fe(OH)_n$ with n = 2 or 3 at pH > 1.0. The decolorization rate was even faster in NaCl, the solution becoming colorless after only 10 min. In this case, coagulation by $Fe(OH)_n$ species coexists with oxidation mediated by active chlorine, which may be formed by anodic discharge of chloride anions as shown in reactions (2)–(4). The formation of soluble $(FeCl)_n$ complexes can

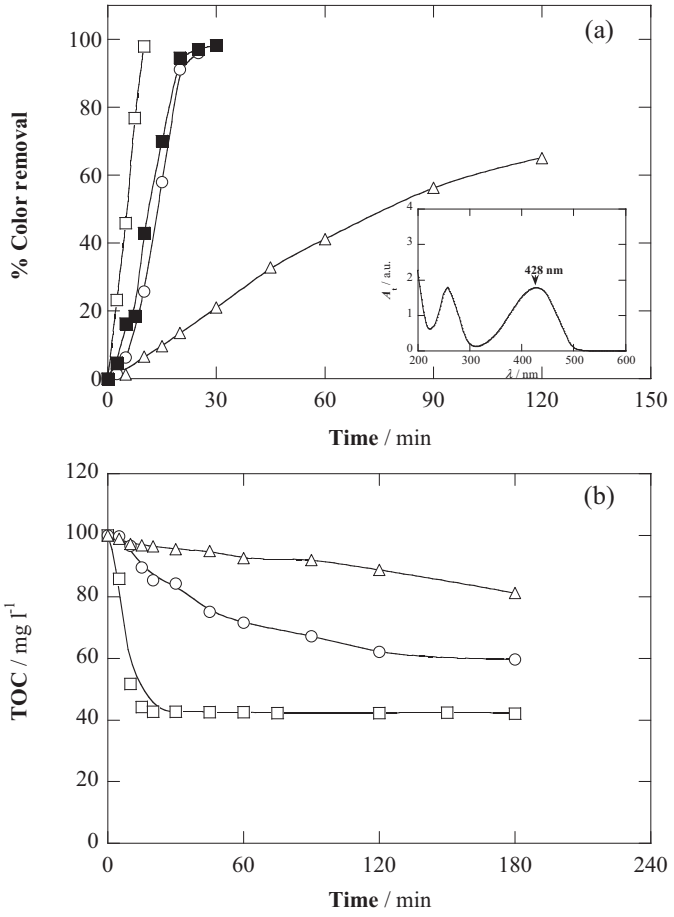

Fig. 1. Effect of the type of supporting electrolyte on the (a) decolorization efficiency at 428 nm and (b) TOC removal with electrolysis time for the EC (Fe/steel) degradation of 130 ml of 278 mg l^{-1} Tartrazine solutions in 0.05 M (○) Na_2SO_4, (□) NaCl, and (△) $NaNO_3$, at natural (and controlled) pH 6.3 and 300 mA. In (a), (■) comparative color removal obtained with the EC (Al/steel) treatment in 0.05 M NaCl. The inset panel in plot (a) shows the absorption spectrum for the initial Tartrazine solution.

also contribute to the enhanced removal because this allows the increase of the soluble iron dose. Note that a careful analysis of the UV/Vis spectra in Na_2SO_4 and NaCl media revealed the presence of residual absorbance at 254 nm even once the absorbance at 428 nm became zero. In contrast, protracted electrolyses in $NaNO_3$ showed a much slower decrease of the absorbance, reaching only 65% of color removal at 120 min. Recent studies have proven that the dissolution of sacrificial Fe is hindered by nitrate salts, therefore yielding very low degradation efficiencies because flocs cannot be formed as required [20,55]. This was corroborated here by means of anode weighting before and after the electrolyses, which showed that the current efficiency for iron dissolution was as low as 0.1% in $NaNO_3$ and around 100% in Na_2SO_4 and NaCl.

Fig. 1a also shows the comparative EC treatment in 0.05 M NaCl using Al as the anode because it is a widely used material in this technique. The color totally disappeared after just 30 min, which represents a high removal rate. In the case of Al, however, the addition of chloride inhibits or slows down the anode passivation, which is a typical phenomenon for Al in other media due to the formation of an isolating, compact oxide interlayer. But, the progress of the color removal was significantly slower than that obtained with the Fe anode, as also occurred in other works on EC [48]. In fact, at 10 min, only 43% decolorization was achieved with Al instead of 100% reached with Fe. Since the formation of $Al(OH)_3$ through consecutive reactions (5) and (7) accounts for the coagulation of the organic matter, the different performance of both anodes can be plausibly explained by: (i) their different ability to promote charge neutralization, and (ii) the lower adsorption ability of $Al(OH)_3$ compared to $Fe(OH)_n$, which complicates the sweep flocculation mechanism to entrap the colloidal matter. Iron anodes were then preferred, not only due to the enhanced coagulation but also to the superior catalytic properties of Fe^{2+} if thinking in a later coupling with Fenton-based EAOPs.

Fig. 1b depicts the TOC removal profiles obtained during the EC (Fe/steel) experiments shown in Fig. 1a. The efficacy for removing the organic matter was greatly dependent on the electrolyte, thus increasing in the order $NaNO_3$ < Na_2SO_4 < NaCl in accordance with the decolorization efficiency discussed above. However, it can be seen that none of the systems allowed the complete decontamination of the solutions. In NaCl medium, the synergistic action of coagulation by $Fe(OH)_n$ and oxidation by active chlorine only yielded 60% TOC abatement at about 10 min, thereby remaining constant over time. This can therefore be justified by the accumulation of persistent organic by-products that contribute to the remaining TOC, which agrees perfectly with the previous comments about the residual UV absorbance observed at 254 nm once reached the total decolorization at 10 min. It can then be inferred that the residual TOC corresponds to colorless aromatic by-products, as later confirmed by GC–MS results.

Since EC (Fe/steel) in NaCl yielded the best results, all the subsequent EC experiments were performed in this medium. First, the effect of the electrolyte concentration was studied in the range 0.025–0.3 M NaCl under the same experimental conditions of Fig. 1a, the potential difference between anode and cathode decreasing from 11.5 to 3.2 V as the chloride content increased. As can be seen in Fig. 2a, a higher NaCl concentration did not bring about any significant acceleration of the color removal and all the solutions were completely decolorized after 10–12 min. This means that the low chloride contents are already able to yield enough active chlorine so as to promote the maximum oxidation of Tartrazine in such a short time period. On the other hand, the NaCl concentration had a slightly higher effect on TOC removal. As shown in Fig. 2b, the decontamination rate increased from 0.025 to 0.05 M NaCl, and then progressively decreased as the NaCl content was raised up to 0.3 M, always achieving the maximum TOC removal of 60%. This means that once reached a threshold amount of active chlorine already at low chloride contents, the additional benefits that could arise at higher chloride contents from a greater oxidative degradation are counteracted by the lower coagulation efficiency due to (i) the formation of persistent by-products that are harder to coagulate and (ii) the increased ionic strength that affects the equilibria of reactions between charged and/or colloidal species in EC.

It is known that the EC process is usually highly dependent on the solution pH due to the large range of equilibria involved. Fig. 3a depicts the time course of the decolorization efficiency for solutions of pH 3.0, 6.3 (natural pH), 9.0 and 11.0 treated in 0.05 M NaCl at 300 mA. The control of pH was necessary for trials at pH 3.0 and 6.3 because it tended to become more alkaline. As can be seen in the figure, the quickest color removal was achieved in 10 min at pH 6.3–11, whereas the process was quite slower at pH 3.0 with total color disappearance at 25 min. The explanation of this finding is that the $Fe(OH)_2$ and $Fe(OH)_3$ flocs are more poorly produced at pH < 6.0 because of the neutralization of cathodically formed OH^- by H^+ present in the medium and hence, the soluble Fe(II) and Fe(III) species show a certain stability that results in a slower decolorization, despite the fact that HClO with p*Ka* = 7.55 is the dominant active chlorine species over the less oxidizing ClO^- [18]. Fig. 3b shows the TOC decay during the same trials. The quickest decontamination was achieved at intermediate pH values of 6.3 and 9.0, due to the combination of coagulation with electrochlorination that yielded 60% TOC removal in both cases. In contrast, a slower and

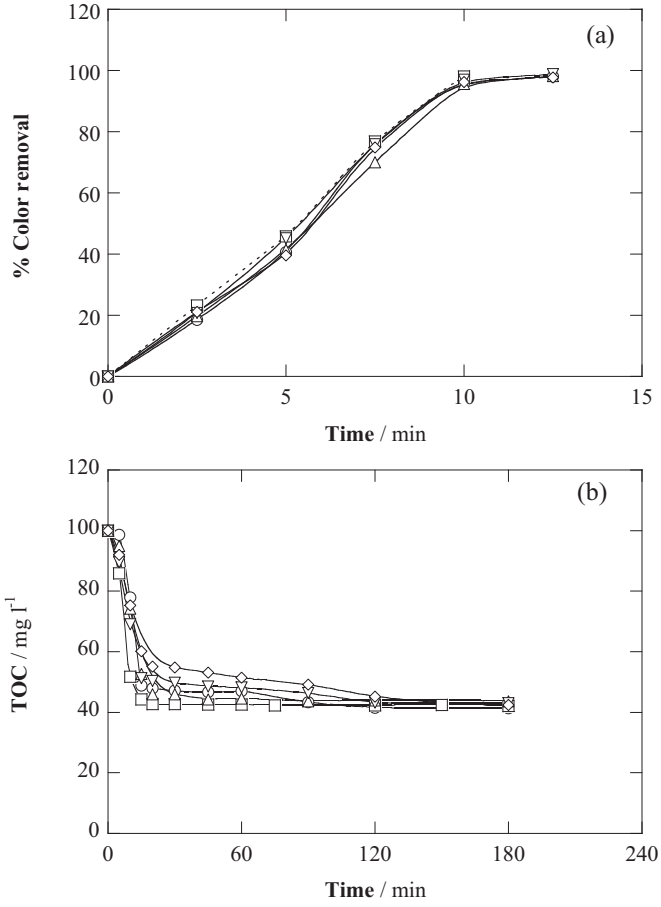

Fig. 2. Effect of the supporting electrolyte concentration on the (a) percentage of color removal at 428 nm and (b) TOC abatement with electrolysis time for the EC (Fe/steel) degradation of 130 ml of 278 mg l^{-1} Tartrazine solutions in: (○) 0.025 M, (□) 0.05 M, (△) 0.1 M, (▽) 0.15 M and (◊) 0.3 M NaCl, at natural (and controlled) pH 6.3 and 300 mA.

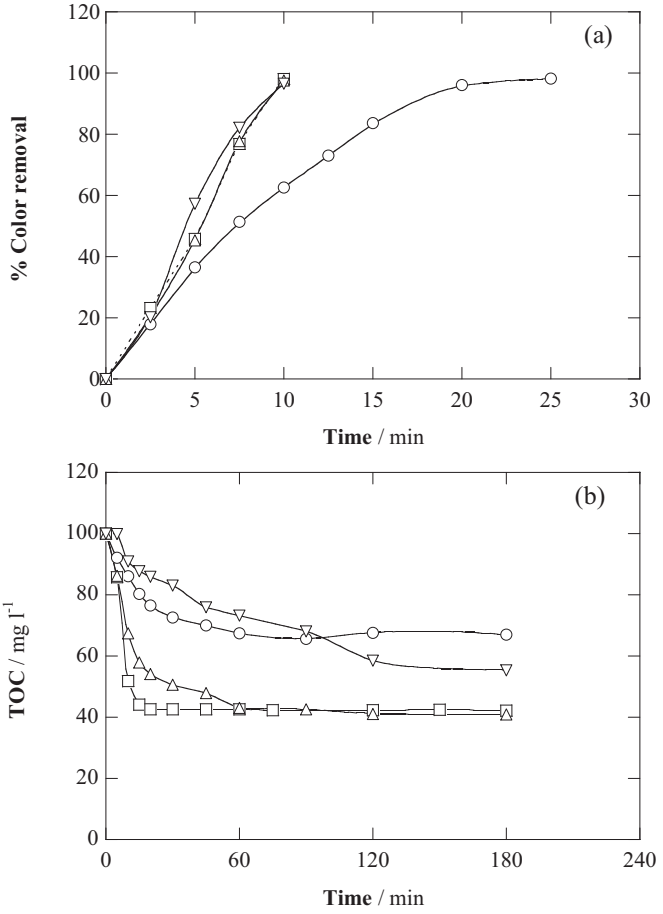

Fig. 3. Effect of pH on the (a) decolorization efficiency at 428 nm and (b) TOC removal with electrolysis time for the EC (Fe/steel) degradation of 130 ml of 278 mg l^{-1} Tartrazine solutions in 0.05 M NaCl, at pH: (○) 3.0, (□) 6.3 (natural), (△) 9.0 and (▽) 11.0, all at 300 mA.

poorer TOC abatement was achieved at more acidic and alkaline pH, which can be mainly accounted for by the less favorable formation of $Fe(OH)_3$ coagulant according to the iron speciation diagrams. The TOC removal at 180 min was slightly greater at pH 11.0 compared to pH 3.0 due to the action of the more oxidizing ClO^-. Therefore, since the natural pH of Tartrazine solutions is 6.3, all the subsequent EC experiments were carried out at this pH, which increases the economic viability of the treatment.

The last key parameter studied for EC (Fe/steel) alone was the applied current, which was tested in the range 50–300 mA, resulting in average potential difference between electrodes increasing from of 2.7 to 10.2 V. Current not only determines the coagulant dosage rate, but also the bubble production rate and size, and all these factors eventually affect the EC efficiency [22]. According to Faraday's law, the dissolution of anode increases at higher current, thus producing more ions and hence, more flocs that trap the dye and its by-products. Furthermore, in NaCl medium the applied current has also great influence on the electrogeneration rate of Cl_2 that is further converted into $HClO/ClO^-$ in the bulk. According to Fig. 4a, the percentage of color removal was always 100%, but it was progressively faster when current was raised, thus shortening the process from 60 to 10 min when increasing from 50 to 300 mA. Such dependence with current is also evident in Fig. 4b for TOC abatement. In all cases, the maximum value of 60% decontamination could be reached at the end of the electrolysis. However, it was already achieved after only ca. 10–15 min at 300 and 200 mA, whereas only 5% TOC removal could be obtained at that time at 50 and 100 mA. Since overlapping decontamination profiles were observed for 200 and 300 mA, the former current value was considered as optimum for further EC experiments because, despite requiring 15 min instead of 10 min for total decolorization, it entails lower energy consumption. In fact, plots against current charge reveal that a higher current efficiency is obtained at 200 mA (not shown). In conclusion, the best conditions for EC were obtained for the Fe/steel system in 0.05 M NaCl at natural pH 6.3 and 200 mA, which led to complete color removal and maximum TOC abatement in just 15 min.

3.2. *Treatment of Tartrazine solutions by electrochemical advanced oxidation processes*

The EAOPs have demonstrated their great performance for the treatment of various classes of dyes. This section focuses on the behavior of Tartrazine solutions in different media at pH 3.0 upon application of EO, EF and PEF with steel or ADE as the cathode and Pt or BDD as the anode, at 200 mA. The trends of color removal percentage and TOC abatement are shown in Figs. 5 and 6. The decolorization efficiency in 0.05 M Na_2SO_4 is depicted in Fig. 5a, revealing a very different performance of EO in comparison to EF and PEF. The color disappeared very slowly in all the EO systems, being required 480 min for total decolorization with BDD and even longer time with Pt. The latter anode only forms low amounts of $^{\bullet}OH$ via reaction (1) and, since it is rather chemisorbed, its oxidation ability is much lower than that of much greater quantities of

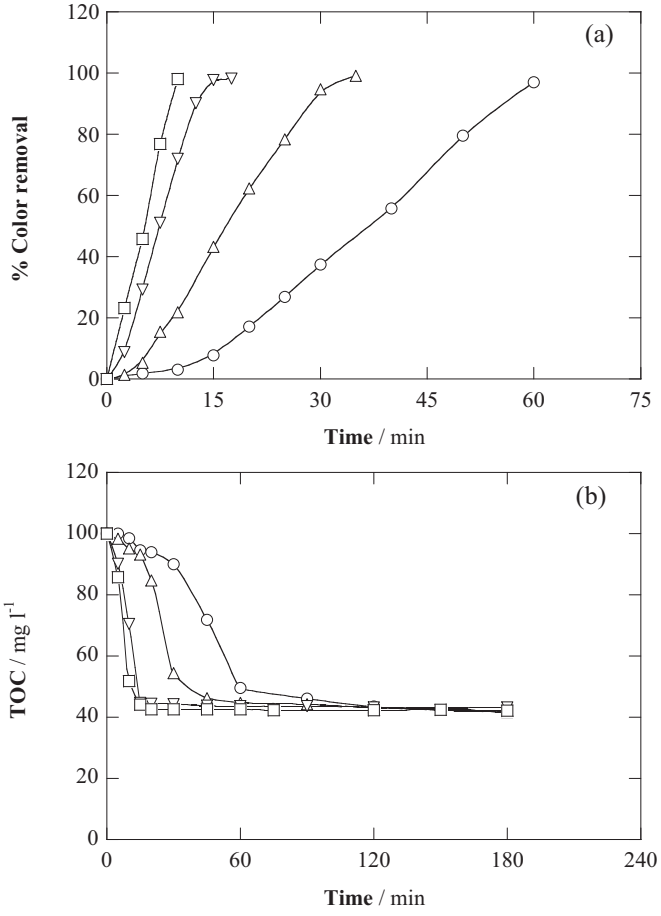

Fig. 4. Effect of current on (a) percentage of color removal at 428 nm and (b) TOC decay with electrolysis time for the EC (Fe/steel) degradation of 130 ml of 278 mg l^{-1} Tartrazine solutions in 0.05 M NaCl at natural (and controlled) pH 6.3 and: (○) 50 mA, (△) 100 mA, (▽) 200 mA and (□) 300 mA.

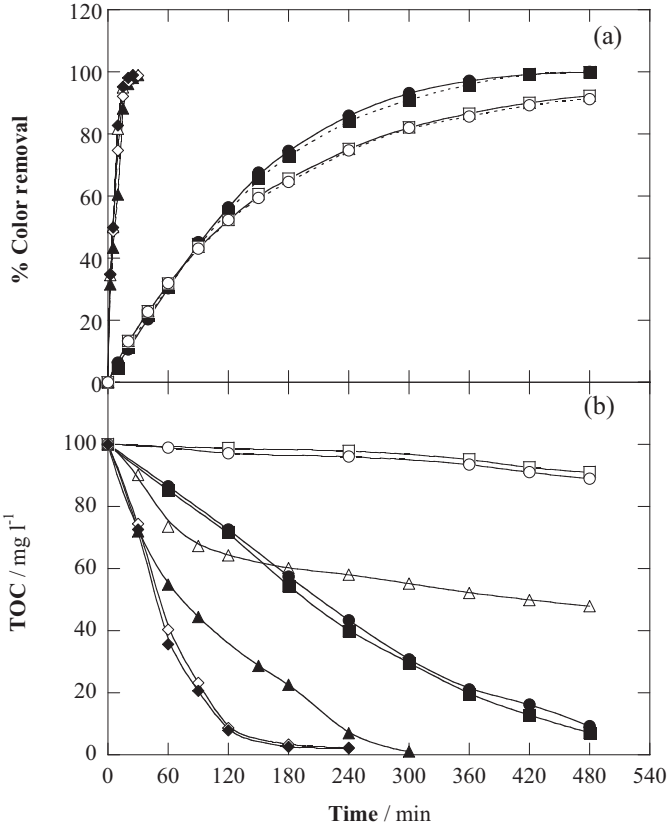

Fig. 5. (a) Decolorization efficiency and (b) TOC abatement vs electrolysis time for the treatment of 130 ml of 278 mg l^{-1} Tartrazine solutions in 0.05 M Na_2SO_4 at pH 3.0 and 200 mA by different EAOPs: (●) EO (BDD/ADE), (○) EO (Pt/ADE), (■) EO (BDD/steel), (□) EO (Pt/steel), (▲) EF with BDD, (△) EF with Pt, (♦) PEF with BDD, (◊) PEF with Pt. In EF and PEF, 0.5 mM Fe^{2+} was added to the solution.

physisorbed hydroxyl radicals produced on BDD. In any case, the EO process in batch mode presents serious mass transport limitations whose most immediate consequence is the low degradation rate and large energy consumption. From these curves, it is also clear that other electrogenerated species such as $S_2O_8^{2-}$ ions, O_3, H_2O_2 and $HO_2^{\bullet}$ play a secondary or even negligible oxidation role [5,6]. In contrast, the absorbance at 428 nm decreased very rapidly in the EF and PEF systems. The color was completely removed in 25–30 min, regardless of the anode used and the absence or presence of UVA light. This means that the pre-eminent oxidizing agent in Fenton-based EAOPs in Na_2SO_4 is $^{\bullet}OH$ formed from Fenton's reaction (9) thanks to the addition of 0.5 mM Fe^{2+} that reacts with cathodically generated H_2O_2. The fact that reaction (9) occurs in the solution bulk allows overcoming the aforementioned mass transport limitations found in EO. The mineralization ability of all these EAOPs can be seen in Fig. 5b. Here, the lower oxidation power of Pt compared to BDD is much clearer, since 10% and 92% TOC removal was achieved at 480 min by EO with Pt and BDD, respectively. The use of EF cells led to a greater TOC abatement, with 52% TOC decay with Pt and complete mineralization after 300 min with BDD. The extraordinary oxidizing activity of $^{\bullet}OH$ in the bulk is therefore confirmed. The irradiation with UVA lamps in PEF cells led to the quickest mineralization, with all the TOC destroyed after 240 min using either Pt or BDD. Such great performance is due to several concomitant reactions: (i) the photoreduction of Fe(III) (as $[Fe(OH)]^{2+}$) formed in reaction (1), which yields additional $^{\bullet}OH$ and regenerates Fe^{2+} and (ii) the quick photolysis of complexes formed between Fe(III) refractory by-products such as short-chain aliphatic carboxylates [5]. Since the nature of the electrolyte was found to have a large influence in EC, the same EAOPs were tested in 0.05 M NaCl. Fig. 6a clearly shows the very positive effect of chloride ions, as shown above for EC. The time for total color removal in the EO systems was reduced from ≥480 min to only 12.5–25 min. EF and PEF, which were already very powerful in Na_2SO_4, allowed the complete decolorization within a similar time period of only 15–20 min. As can be seen, only a minor enhancement was achieved when changing Pt by BDD. Moreover, the amelioration when using EF and PEF instead of EO with ADE was rather insignificant. It can then be concluded that the presence of active chlorine as the decolorization agent, not confined in the electrodes but dissolved in the whole volume, is essential since it has the preponderant oxidant role over all kinds of $^{\bullet}OH$ formed at the anode surface and in the bulk. Fig. 6b depicts the mineralization curves for the same experiments. The difference with curves in Fig. 6a is straightforward since in this graph the profiles are highly dependent on the cell used. The percentage of TOC removal in EO with Pt was ≥40% at 480 min, which is much higher than that in Na_2SO_4 due to action of active chlorine species in the bulk. EO with BDD was somewhat better, achieving 88% TOC abatement mainly thanks to the action of $^{\bullet}OH$ formed on BDD that is able to slowly but progressively remove refractory by-products. Note that the TOC decay was a bit slower compared to that in Na_2SO_4, which can be explained by the parasitic reaction between $^{\bullet}OH$ and Cl^- to form weaker oxidants such as $ClOH^{\bullet-}$, as well as $Cl^{\bullet}$ and $Cl_2^{\bullet-}$ that can be finally converted into Cl_2 [56]. Other wasting reactions between $^{\bullet}OH$ and $HClO/ClO^-$ are also plausible. EF with Pt in NaCl led to 75% TOC removal, which is better than 52% obtained in Na_2SO_4 due to the action of active chlorine on

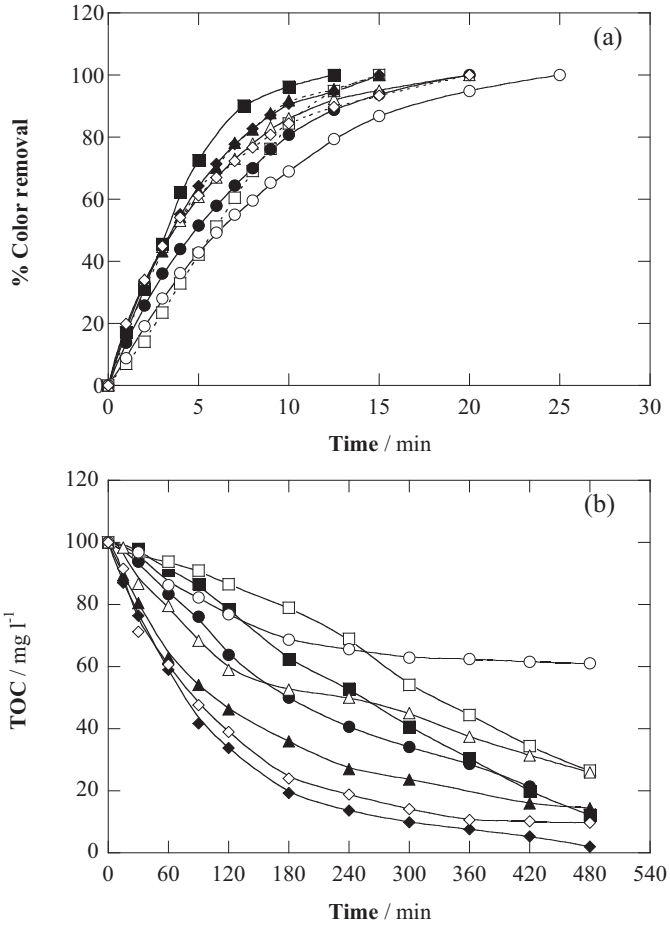

Fig. 6. Analogous experiments to those shown in Fig. 5 but using solutions with 0.05 M NaCl.

by-products that are refractory to •OH. EF could be enhanced using BDD, reaching 88% TOC abatement, although again the parasitic reactions involving •OH and chlorinated species impedes the complete mineralization in 300 min observed in Na_2SO_4. Finally, the highest performance was achieved again in PEF systems. As happened in EO and EF, reactions between •OH mainly formed on BDD and chlorinated species led to a slower mineralization compared to Na_2SO_4 medium. Therefore, only PEF with BDD allowed the complete mineralization in 480 min, which however was significantly slower than PEF in Na_2SO_4 that yielded the total TOC disappearance in 240 min. In any case, the most remarkable feature is that it is possible to reach the total mineralization by an EAOP in NaCl, which was the optimum electrolyte to carry out the EC treatment.

Hitherto, the decolorization and decontamination profiles in NaCl medium have been explained on the basis of the formation of active chlorine. The existence of such species was then corroborated by electrolyzing solutions of 0.05 M NaCl by PEF with BDD under the previously found optimum conditions. As shown in Fig. 7, active chlorine was accumulated along the electrolysis, which confirms the role of reactions (2)–(4). The accumulated concentration was as low as 4 mg Cl_2 l^{-1}. Independent electrolyses by EO (BDD/steel) showed a much higher concentration at the same time intervals (not shown), which means that the formation of active chlorine is really favored by BDD, despite being partly destroyed by cathodically generated H_2O_2 in PEF [56]. The partial destruction of H_2O_2 in NaCl becomes an additional justification of the worse performance of EF and PEF with BDD explained in Fig. 6b. Solutions of 0.05 M NaCl were also treated by the optimized EC process, but no active chlorine was detected. This means that it is possibly formed

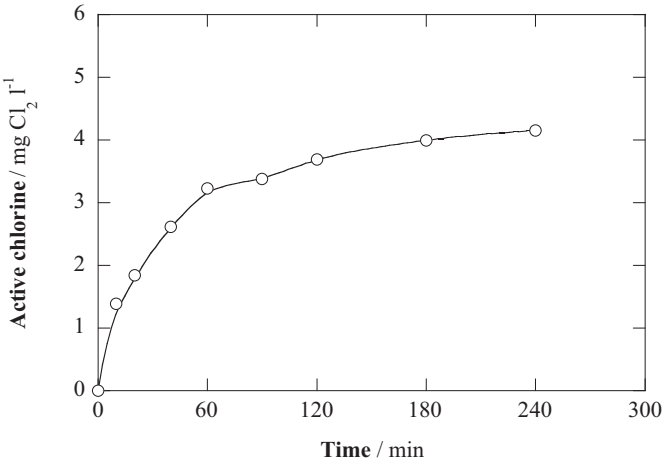

Fig. 7. Active chlorine vs electrolysis time for the PEF (BDD/ADE) degradation of 130 ml of 0.05 M NaCl at pH 3.0 and 200 mA.

in very small quantities, unable to become accumulated but high enough to react with Tartrazine to form chlorinated by-products, as will be later demonstrated. The formation of active chlorine as a bleaching agent during EC of Tartrazine has been hypothesized elsewhere [48].

The aforementioned results confirm the great interest of EAOPs for water treatment. However, the large treatment time required to reach total mineralization is one of their main drawbacks to be implemented as a single degradation step. Therefore, the optimized EC pre-treatment can be envisaged as a powerful solution to make the technology viable and, therefore, appealing to the industry.

3.3. Performance of the coupled EC/EAOPs treatments

Fig. 8 presents the mineralization trends obtained upon the sequential treatment of Tartrazine solutions consisting in an EC step followed by five different EAOPs that had yielded the quickest TOC removal in Fig. 6b. The dye solutions were firstly pre-treated by EC (Fe/steel) in 0.05 M NaCl at natural pH 6.3 and 200 mA for 15 min. This ensured a 100% color removal (Fig. 4a) and 60% TOC abatement, whereupon the TOC content tended to remain unaltered. Then, the samples were centrifuged, and the supernatant was

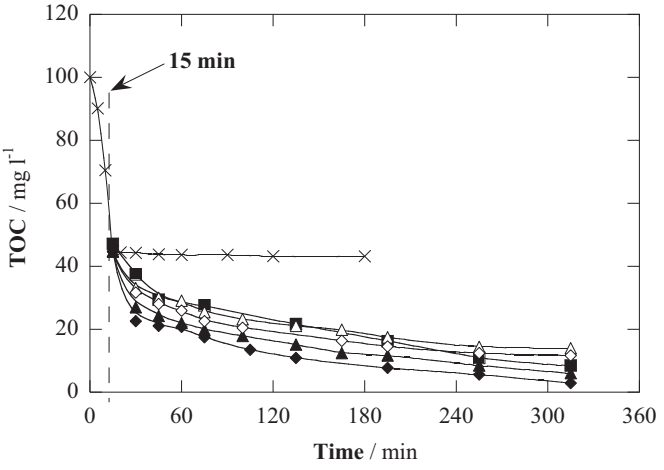

Fig. 8. TOC removal vs electrolysis time for the treatment of 130 ml of 278 mg l^{-1} Tartrazine solutions by various two-step EC (Fe/steel, 15 min, 200 mA, 0.05 M NaCl at natural pH 6.3)/EAOPs (200 mA, pH 3.0): (■) EO (BDD/steel), (△) EF with Pt, (▲) EF with BDD, (◊) PEF with Pt and (♦) PEF with BDD. (×) Comparative TOC removal by EC alone.

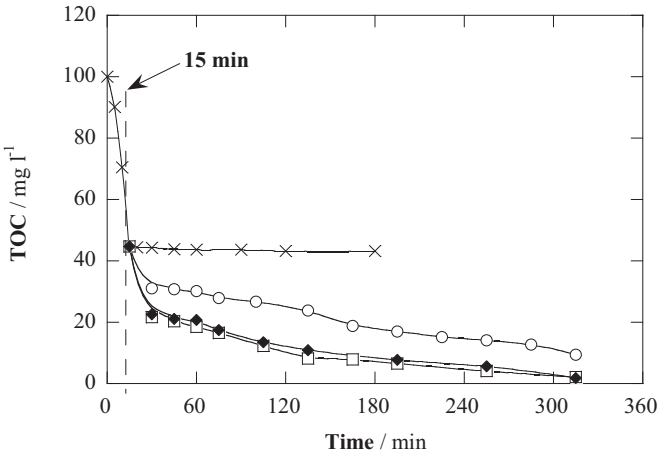

Fig. 9. Effect of current on TOC removal with electrolysis time for the EC/PEF (BDD/ADE) treatment under the conditions shown in Fig. 8 at: (○) 100 mA, (♦) 200 mA and (□) 300 mA.

treated by the EAOPs at 200 mA after pH regulation to 3.0. The total iron concentration after centrifugation and prior to the application of the EAOPs was analyzed, yielding a value of 0.6 mM, which is acceptable because Fenton-based EAOPs with ADE cathodes usually require an iron concentration in the range 0.5–1.0 mM [5]. As can be seen, the five EAOPs allowed the progressive mineralization of the pre-treated solutions. EF and PEF with Pt anode were slightly slower than processes with BDD, reaching 86–88% TOC removal after 315 min (15 min of EC followed by 300 min of EAOP). EO and EF with BDD performed somewhat better due to the additional action of active •OH formed on the anode surface, thus achieving 92 and 95% TOC abatement, respectively. Finally, the PEF (BDD/ADE) treatment of the pre-treated Tartrazine solutions allowed obtaining the fastest decontamination, with total mineralization in about 315 min of global sequential treatment. Coupling of EC with a post-treatment that only consisted in the irradiation of the electrocoagulated solutions with an UVA lamp showed the inefficacy of UVA light alone to remove the TOC. Therefore, the great performance of such PEF as the second step can be explained by the synergistic action of Fe(III) photoreduction, photodecarboxylation of refractory by-products and oxidation of persistent by-products by •OH at BDD and in the bulk, as well as by active chlorine in

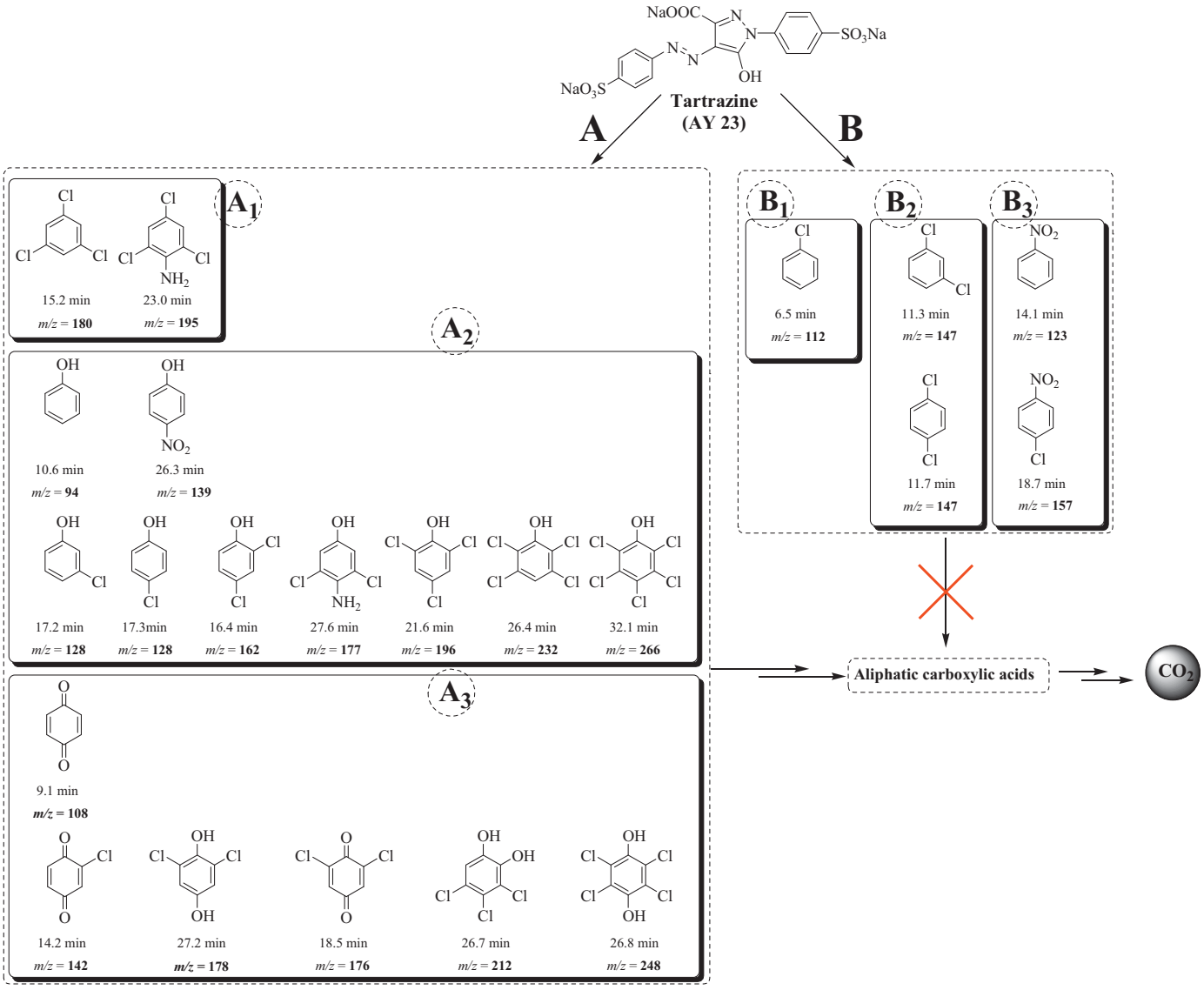

Fig. 10. Reaction by-products identified by GC–MS after: (A) The two-step EC (Fe/steel, 15 min)/PEF (BDD/ADE, 10 min) treatment and (B) EC (Fe/steel, 15 min) alone.

the bulk. The energy consumption per unit volume was calculated for all the sequential treatments according to Eq. (11). The time course of this parameter is not shown because it is simply proportional to the potential difference of each cell, which was around 15 V for cells with Pt and 20–25 V for cells with BDD. Therefore, at 315 min, progressively higher energy consumptions of 110–120, 160 and 190 kW h m^{-3} were required for EF and PEF with Pt, EO with BDD/steel, and EF or PEF with BDD, respectively. The quicker degradation by PEF (BDD/ADE) then had in return a higher energy consumption, which can be lowered by using Pt instead. Obviously, the values are too high due to the use of a small batch cell but, in real-scale applications, with recirculation of larger volumes and employing optimized reactors that allow the decrease of the potential difference, the cost would be dramatically reduced.

The effect of applied current on the mineralization rate obtained by the PEF (BDD/ADE) post-treatment was also studied. Fig. 9 reveals that 200 mA was the optimum value, since it allows a quicker TOC removal compared to 100 mA and an almost identical evolution compared to 300 mA. In conclusion, in the sequential degradation, the EC acted as a very effective coagulation step to quickly decolorize the solutions and, at the same time, as a source of enough iron catalyst for the subsequent EAOPs.

3.4. Identification of Tartrazine degradation by-products

Tartrazine solutions were electrolyzed by using the best EC/PEF treatment under the optimized conditions described in Fig. 8, but stopping the PEF step after 10 min in order to identify the major accumulated aromatic by-products. As shown in pathway A of Fig. 10, up to seventeen compounds could be identified by GC–MS. They can be grouped into three different types: (A_1) Non-hydroxylated by-products, which are generated as a result of progressive chlorination of simpler by-products, as well as (A_2) monohydroxylated and (A_3) dihydroxylated (in the form of phenols and quinones) intermediates formed by the action of •OH at the anode vicinity and in the bulk. Note that A_2 and A_3 include various polychlorinated hydroxybenzenes (di-, tri-, tetra- and penta-derivatives), which can be explained by the ability of BDD anode to electrogenerate active chlorine, as discussed from Fig. 7. They also include the derivatives 2,4,6-trichlorophenol and 4-amino-3,5-dichlorophenol that come from the hydroxylation of the two products shown in A_1. The scheme of Fig. 10 also informs about the further cleavage of the aryl moiety gathered in path A to yield a mixture of short-chain aliphatic carboxylic acids, with oxalic acid as the main by-product as discussed in our previous works on the electrochemical treatment of benzenic pollutants [5]. As commented from Fig. 8, PEF with BDD allowed the total mineralization of all these by-products to form CO_2.

In order to assess the primary decolorization steps undergone by Tartrazine prior to PEF treatment, the mixture of by-products accumulated in the electrocogaulation supernatant under optimized EC conditions for 15 min was analyzed by GC–MS. The pathway B of Fig. 10 includes five by-products such as mono/dichlorobenzene and nitrobenzene derivatives. This indicates the ability of Fe anode to produce active chlorine, as hypothesized above. Since the amount of active chlorine in EC was so small that it could not be identified by spectrophotometric analysis, in contrast to that observed in PEF, a mild chlorination resulted from this pre-treatment. Further chlorination and/or hydroxylation of these by-products gave rise to some compounds shown in pathway A upon coupling with PEF. The formation of the five by-products after 15 min in EC, once the azo dye had completely disappeared (Fig. 4a), agrees with the trend of TOC in Fig. 4b showing that ca. 40% of organic matter was still present in the solution. That residual TOC can then be related to such soluble derivatives that cannot be coagulated in EC. Note in the scheme of Fig. 10 that in this case the aryl moiety cannot be mineralized to aliphatic carboxylic acids, but it is persistent unless a convenient EAOP is coupled.

4. Conclusions

This work results from a collaboration project that aims at envisaging new solutions for the treatment of water effluents contaminated by synthetic dyes. A traditional technology such as EC and some emerging ones like EAOPs including EO, EF and PEF have been firstly investigated individually to assess their ability to decolorize and mineralize solutions of Tartrazine as a model azo dye. The quickest decontamination reported in this communication has been yielded by EC with iron anodes and PEF with H_2O_2 electrogeneration. It has been demonstrated that the sequential EC (Fe/steel)/PEF (BDD/ADE) treatment favors both, the fast color removal and separation of a large fraction of organic matter by EC, and the destruction of the remaining persistent organic matter in the pre-treated solution by PEF. The complete decolorization and mineralization of solutions were thus achieved within relatively short time periods thanks to coagulation by $Fe(OH)_n$ and oxidation by •OH and active chlorine species. The best conditions involved an EC pre-treatment with Fe/steel in 0.05 M NaCl at natural pH 6.3 and 200 mA for 15 min, followed by centrifugation and treatment of the supernatant by PEF with BDD/ADE at 200 mA and pH 3.0 for ca. 300 min to achieve the complete TOC removal. Up to 17 aromatic by-products were identified by GC–MS during the EC/PEF degradation, which could be totally destroyed in the EAOP step. Therefore, the combined treatment allows overcoming the drawbacks of the single processes, i.e., the only partial mineralization obtained by EC and the long treatment time typically required by EAOPs, thus making the whole electrochemical technology much more cost-effective due to the reduced energy consumption.

Acknowledgments

The authors thank MICINN (Ministerio de Ciencia e Innovación, Spain) for support under project CTQ2010-16164/BQU, co-financed with FEDER funds, and also thank support from the National Natural Science Foundation of China (NSFC, grant number 21250110515). The Ph.D. grant awarded to A. Thiam from MAEC-AECID (Spain) is also acknowledged.

References

[1] C. Comninellis, A. Kapalka, S. Malato, S.A. Parsons, I. Poulios, D. Mantzavinos, J. Chem. Technol. Biotechnol. 83 (2008) 769–776.
[2] M. Klavarioti, D. Mantzavinos, D. Kassinos, Environ. Int. 35 (2009) 402–417.
[3] I. Sirés, E. Brillas, Environ. Int. 40 (2012) 212–229.
[4] A. Anglada, A. Urtiaga, I. Ortiz, J. Chem. Technol. Biotechnol. 84 (2009) 1747–1755.
[5] E. Brillas, I. Sirés, M.A. Oturan, Chem. Rev. 109 (2009) 6570–6631.
[6] M. Panizza, G. Cerisola, Chem. Rev. 109 (2009) 6541–6569.
[7] A.M. Polcaro, M. Mascia, S. Palmas, Electrochim. Acta 49 (2004) 649–656.
[8] M. Faouzi, P. Cañizares, A. Gadri, J. Lobato, B. Nasr, R. Paz, M.A. Rodrigo, C. Saez, Electrochim. Acta 52 (2006) 325–331.
[9] E. Butrón, M.E. Juárez, M. Solis, M. Teutli, I. González, J.L. Nava, Electrochim. Acta 52 (2007) 6888–6894.
[10] M. Panizza, A. Kapalka, Ch. Comninellis, Electrochim. Acta 53 (2008) 2289–2295.
[11] M.Y.A. Mollah, R. Schennach, J.R. Parga, D.L. Cocke, J. Hazard. Mater. B84 (2001) 29–41.
[12] S. Zodi, O. Potier, F. Lapicque, J.-P. Leclerc, Desalination 261 (2010) 186–190.
[13] V. Khandegar, A.K. Saroha, J. Environ. Manage. 128 (2013) 949–963.
[14] N. Daneshvar, H.A. Sorkhabi, M.B. Kasiri, J. Hazard. Mater. B112 (2004) 55–62.
[15] A.K. Golder, A.N. Samanta, S. Ray, Sep. Purif. Technol. 53 (2007) 33–41.
[16] H.A. Moreno-Casillas, D.L. Cocke, J.A.G. Gomes, P. Morkovsky, J.R. Parga, E. Peterson, Sep. Purif. Technol. 56 (2007) 204–211.
[17] M. Muthukumar, M.T. Karuppiah, G.B. Raju, Sep. Purif. Technol. 55 (2007) 198–205.
[18] C.A. Martínez-Huitle, E. Brillas, Appl. Catal., B 87 (2009) 105–145.
[19] X.D. Zhang, J.D. Hao, W.S. Li, H.J. Jin, J. Yang, Q.M. Huang, D.S. Lu, H.K. Xu, J. Hazard. Mater. 170 (2009) 883–887.

[20] C.J. Izquierdo, P. Canizares, M.A. Rodrigo, J.P. Leclerc, G. Valentin, F. Lapicque, Desalination 255 (2010) 15–20.
[21] C. Phalakornkule, S. Polgumhang, W. Tongdaung, B. Karakat, T. Nuyut, J. Environ. Manage. 91 (2010) 918–926.
[22] R. Katal, H. Pahlavanzadeh, Desalination 265 (2011) 199–205.
[23] J.M. Peralta-Hernández, Y. Meas-Vong, F.J. Rodríguez, T.W. Chapman, M.I. Maldonado, L.A. Godínez, Water Res. 40 (2006) 1754–1762.
[24] A. Özcan, M.A. Oturan, N. Oturan, Y. Şahin, J. Hazard. Mater. 163 (2009) 1213–1220.
[25] M. Panizza, G. Cerisola, Water Res. 43 (2009) 339–344.
[26] E. Rosales, M. Pazos, M.A. Longo, M.A. Sanromán, Chem. Eng. J. 155 (2009) 62–67.
[27] A. Dirany, I. Sirés, N. Oturan, M.A. Oturan, Chemosphere 81 (2010) 594–602.
[28] N. Oturan, M. Zhou, M.A. Oturan, J. Phys. Chem. A 114 (2010) 10605–10611.
[29] I. Sirés, C.T.J. Low, C. Ponce-de-León, F.C. Walsh, Electrochem. Commun. 12 (2010) 70–74.
[30] E. Isarain-Chávez, C. Arias, P.L. Cabot, F. Centellas, R.M. Rodríguez, J.A. Garrido, E. Brillas, Appl. Catal., B 96 (2010) 361–369.
[31] M.M. Ghoneim, H.S. El-Desoky, N.M. Zidan, Desalination 274 (2011) 22–30.
[32] S. Randazzo, O. Scialdone, E. Brillas, I. Sirés, J. Hazard. Mater. 192 (2011) 1555–1564.
[33] E.J. Ruiz, C. Arias, E. Brillas, A. Hernández-Ramírez, J.M. Peralta-Hernández, Chemosphere 82 (2011) 495–501.
[34] M. Zhou, Q. Tan, Q. Wang, Y. Jiao, N. Oturan, M.A. Oturan, J. Hazard. Mater. 215–216 (2012) 287–293.
[35] S. García-Segura, J.A. Garrido, R.M. Rodríguez, P.L. Cabot, F. Centellas, C. Arias, E. Brillas, Water Res. 46 (2012) 2067–2076.
[36] L. Zhou, Z. Hu, C. Zhang, Z. Bi, T. Jin, M. Zhou, Sep. Purif. Technol. 111 (2013) 131–136.
[37] B. Boye, M.M. Dieng, E. Brillas, Electrochim. Acta 48 (2003) 781–790.
[38] B. Boye, E. Brillas, A. Buso, G. Farnia, C. Flox, M. Giomo, G. Sandonà, Electrochim. Acta 52 (2006) 256–262.
[39] R. Daghrir, P. Drogui, Environ. Chem. Lett. 11 (2013) 151–156.
[40] R.M. Christie (Ed.), Environmental Aspects of Textile Dyeing, Woodhead Publ. Ltd., Cambridge, England, 2007.
[41] S. Chapman, Food Standards Agency, Report Number FMT/21810/1, Campden Technol. Ltd., 2011 March.
[42] EFSA Panel on Dietetic Products, Nutrition and Allergies (NDA), EFSA Journal 8 (2010) 1778-1788.
[43] D. Rajkumar, B.J. Song, J.G. Kim, Dyes Pigm. 72 (2007) 1–7.
[44] A. Sakalis, D. Vaněrková, M. Holčapek, P. Jandera, A. Voulgaropoulos, Chemosphere 67 (2007) 1940–1948.
[45] M. Zhou, Q. Yu, L. Lei, G. Barton, Sep. Purif. Technol. 57 (2007) 380–387.
[46] M. Zhou, Q. Yu, L. Lei, Dyes Pigm. 77 (2008) 129–136.
[47] N. Daneshvar, A.R. Khataee, A.R.A. Ghadim, M.H. Rasoulifard, J. Hazard. Mater. 148 (2007) 566–572.
[48] N. Modirshahla, M.A. Behnajady, S. Kooshaiian, Dyes Pigm. 74 (2007) 249–257.
[49] G.B. Raju, M.T. Karuppiah, S.S. Latha, S. Parvathy, S. Prabhakar, Chem. Eng. J. 144 (2008) 51–58.
[50] M. Panizza, G. Cerisola, J. Electroanal. Chem. 638 (2010) 236–240.
[51] S. Cotillas, J. Llanos, P. Cañizares, S. Mateo, M.A. Rodrigo, Water Res. 47 (2013) 1741–1750.
[52] APWA, AWWA, WEF, Standard methods for the examination of water and wastewater, in: Method number 4500-Cl Chlorine (residual)—G. DPD Colorimetric Method, 21st ed., American Public Health Association, Washington, DC, 2005, pp. 4–67 to 4–68.
[53] N.H. Furman (Ed.), Standard Methods of Chemical Analysis, 1, sixth ed., R.E. Krieger Pub. Co, Huntington, NY, 1975, p. 553.
[54] O.J. Flores, J.L. Nava, G. Carreño, E. Elorza, F. Martínez, Chem. Eng. Sci. 97 (2013) 1–6.
[55] Y.Ş. Yildiz, A.S. Koparal, Ş. Írdemez, B. Keskinler, J. Hazard. Mater. B139 (2007) 373–380.
[56] J. De Laat, G.T. Le, B. Legube, Chemosphere 55 (2004) 715–723.

Paper 8

A first pre-pilot system for the combined treatment of dye pollutants by electrocoagulation/EAOPs

Journal of Chemical Technology and Biotechnology

89 (2014) 1136-1144

Research Article

Received: 15 January 2014 Revised: 22 February 2014 Accepted article published: 1 March 2014 Published online in Wiley Online Library: 1 April 2014

(wileyonlinelibrary.com) DOI 10.1002/jctb.4358

A first pre-pilot system for the combined treatment of dye pollutants by electrocoagulation/EAOPs

Abdoulaye Thiam,[a,b] Minghua Zhou,[a*] Enric Brillas[b] and Ignasi Sirés[a,b,*]

Abstract

BACKGROUND: Based on promising results obtained at laboratory scale with a two-step electrochemical treatment of Tartrazine solutions by electrocoagulation (EC) coupled with electrochemical advanced oxidation processes (EAOPs), this work addresses its scale-up to degrade 1.85 dm^3 of solutions of this dye. Monopolar and bipolar configurations have been compared in EC. The effect of supporting electrolyte, pH, applied current, dye concentration and electrolysis time has been assessed.

RESULTS: Electrocoagulation with four Fe electrodes was first optimized for the treatment of 278 mg dm^{-3} Tartrazine solutions. The bipolar series configuration led to enhanced coagulation due to the larger electrode consumption. Solutions with 0.05 mol dm^{-3} NaCl at pH 6.3 were quickly decolorized with 60% total organic carbon removal, being more convenient than Na_2SO_4 and $NaNO_3$ electrolytes due to the synergistic action of coagulation and oxidation by active chlorine. Among the EAOPs, carried out with a Ti/IrO_2-RuO_2 anode and an air-diffusion cathode to electrogenerate H_2O_2, electro-Fenton (EF) with 0.5 mmol dm^{-3} Fe^{2+} was much better than electro-oxidation owing to the oxidative action of active chlorine and $^{\bullet}OH$ formed in the bulk from Fenton's reaction. Photoelectro-Fenton (PEF) was even better by the additional photolysis of by-products under incident UVA photons.

CONCLUSIONS: The use of an EC reactor in bipolar configuration for 12.5 min at 1.50 A followed by PEF treatment for 360 min at 1.50–2.00 A ensured mineralization >90%, which encourages further optimization at larger scale for the treatment of a variety of organic pollutants in real wastewaters.

Supporting information may be found in the online version of this article.

Keywords: dimensionally stable anode; homogeneous catalysis; electrocoagulation; photoelectro-Fenton; Tartrazine

INTRODUCTION

In the last decade, the interest in new or enhanced electrochemical separation and degradation technologies for the removal of organic contaminants from water streams has grown considerably.[1] Electrocoagulation (EC) is a widely used physicochemical treatment for phase separation by virtue of its appealing characteristics.[2] It is based on the release of Al^{3+} or Fe^{2+} ions in the bulk from dissolution of the corresponding sacrificial anode, as generalized in reaction (1). The simultaneous production of OH^- ions by cathodic reduction of water leads to the formation of insoluble polymeric metal hydroxides such as $Al(OH)_{3(s)}$ and $Fe(OH)_{n(s)}$ that act as coagulants. Such particles have large surface areas, and are able to remove pollutants upon destabilization by double layer compression, charge neutralization, sweep flocculation and interparticle bridging.[2–4] To date, EC has been shown effective for the removal of many colloidal and ionic pollutants from synthetic solutions and real wastewaters.[5–14]

$$M_{(s)} \rightarrow M^{n+}_{(aq)} + n\, e^- \qquad (1)$$

Depending on the electrode connections, different configurations for EC cells have been investigated.[2,6,15–19] Interestingly, none of the configurations can be established as the preferred one based on *a priori* considerations; the systems have to be optimized on a case-by-case basis. The main limitation of EC is its almost negligible ability to mineralize the organic matter, allowing just the transfer of pollutants from the dissolved state to the solid state. This was partially solved by the so-called peroxi-coagulation (PC) process. The use of a sacrificial iron anode that generates Fe^{2+} from reaction (1) and a carbonaceous cathode able to generate H_2O_2 from the two-electron O_2 reduction allows the coagulation of organic pollutants by $Fe(OH)_{n(s)}$ as well as their oxidation

* *Correspondence to: I. Sirés, Laboratori d'Electroquímica dels Materials i del Medi Ambient, Departament de Química Física, Facultat de Química, Universitat de Barcelona, Martí i Franquès 1–11, 08028 Barcelona, Spain. E-mail: i.sires@ub.edu*
M. Zhou, Key Laboratory of Pollution Process and Environmental Criteria, Ministry of Education, College of Environmental Science and Engineering, Nankai University, Tianjin 300071, China. E-mail: zhoumh@nankai.edu.cn

a *Key Laboratory of Pollution Process and Environmental Criteria, Ministry of Education, College of Environmental Science and Engineering, Nankai University, Tianjin 300071, China*

b *Laboratori d'Electroquímica dels Materials i del Medi Ambient, Departament de Química Física, Facultat de Química, Universitat de Barcelona, Martí i Franquès 1-11, 08028 Barcelona, Spain*

by •OH formed in the solution bulk from the well-known Fenton's reaction:[20]

$$Fe^{2+} + H_2O_2 \rightarrow Fe^{3+} + {}^{\bullet}OH + OH^- \quad (2)$$

Unfortunately, PC has some major drawbacks[21] that may be overcome by applying a combined system based on the coupling between EC and electrochemical advanced oxidation processes (EAOPs), which favor the production of powerful oxidants such as •OH. The first studies on two-step EC/EAOPs for water decontamination dealt with the EC/EO system.[22–25] EO embodies high simplicity and efficacy, promoting water decontamination under the action of •OH formed at the anode surface via reaction (3).[26] Boron-doped diamond (BDD) has been found the best electrocatalytic anode material to oxidize organic pollutants.[27–30] In the presence of chloride ion, the accumulation of additional oxidants such as active chlorine species (Cl_2, HClO and/or ClO^-) in the solution bulk is due to the anodic reaction of Cl^- ion via reaction (4).[26]

$$M + H_2O \rightarrow M(^{\bullet}OH) + H^+ + e^- \quad (3)$$

$$2\,Cl^- \rightarrow Cl_{2(aq)} + 2\,e^- \quad (4)$$

Alternatively, EO can be performed with the much less expensive dimensionally stable anodes (DSA).[26] RuO_2 and IrO_2 on Ti base metal act as good electrocatalysts for Cl_2 and O_2 evolution, respectively.[31–35] It has been proven that Ru-based anodes are more effective, although strong mineralization is only feasible in Cl^- media due to the action of active chlorine formed via reaction (4).[26] Some authors preferred the use of mixed metal oxides ($Ti/IrO_2–RuO_2$) because of their good electrochemical properties and high corrosion resistance, giving an increased durability and efficiency.[36–39]

Fenton-based EAOPs such as electro-Fenton (EF) and photoelectro-Fenton (PEF) have been shown to be even more efficient than EO for the treatment of organic pollutants in acidic medium.[40–50] EF and PEF rely on the in-situ electrogeneration of H_2O_2 as in PC, but employ a stable anode such as Pt, DSA or BDD. The presence of Fe^{2+} as catalyst in both methods favors high production of •OH in the bulk from Fenton's reaction (2).[51] In PEF, the system is equipped with a UVA lamp, which leads to the best performance owing to the concomitant action of both the generated •OH and UV radiation on the organic molecules and their Fe(III) complexes.[47] The sequential combination of EC and Fenton-based EAOPs has only recently been explored.[21,52] In particular, we have recently reported the complete mineralization of Tartrazine (Acid Yellow 23), chosen as a model dye pollutant whose adverse reactions in humans have lately been under consideration by the European Food Safety Agency.[53] Tartrazine is primarily used as a common synthetic food coloring agent, also known as additive E 102, to provide a vivid yellow color to processed commercial foods. The treatment was thoroughly assessed at laboratory scale and its main reaction intermediates were identified. The high performance of the two-step EC/EAOPs treatment with Fe and BDD anodes was accounted for by the strong coagulation during the EC pre-treatment alongside the action of powerful oxidizing agents generated during the EAOP post-treatment.

The present work represents an important step forward for the future implementation of combined EC/EAOPs treatments in industry or public facilities, since scale-up to treat 1.85 dm^3 of Tartrazine solutions instead of 130 cm^3 is addressed. First, the individual EC with Fe electrodes in a bench reactor, and three EAOPs (EO, EF and PEF) with DSA ($Ti/IrO_2–RuO_2$) instead of a BDD anode in a filter-press electrochemical reactor were tested in different electrolytes at constant current to assess the effect of key experimental parameters on the decolorization efficiency and the total organic carbon (TOC) removal rate. In EC, the electrodes were connected in three different configurations to elucidate the best one. An optimized EC/EAOP treatment has been achieved.

MATERIALS AND METHODS

Chemicals

Tartrazine ($C_{16}H_9N_4Na_3O_9S_2$, C.I. 19140, dye content ≥ 85%) was purchased from Sigma-Aldrich and was used as received. Anhydrous sodium sulfate, sodium chloride and sodium nitrate used as background electrolytes, as well as iron(II) sulfate heptahydrate, used as catalyst in EF and PEF, were of analytical grade from Merck and Fluka. Solutions were prepared with ultra-pure water and their pH was adjusted before and during the electrolyses with analytical grade sodium hydroxide or sulfuric, hydrochloric or nitric acid from Merck. Other chemicals were obtained from Tianjin Kermel Chemical Reagent Co, Ltd.

Electrochemical systems

All the electrolyses were performed in batch mode. The system for the EC trials consisted of a bench, open, parallelepiped reactor with a trapezoidal base made of acrylic material and having a capacity of 2 dm^3. Four iron plates with overall dimensions 11 cm × 10 cm, 0.1 cm thickness, were used as electrodes. They were placed in parallel, inserted in purpose-made slots along the acrylic container walls, with an interelectrode gap of 2 cm. The front, back, and sides of each piece were exposed to the solution, resulting in an immersed area of 150 cm^2. The electrodes were connected to a digital DC power supply in three different configurations: (a) monopolar parallel (MP-P); (b) monopolar series (MP-S); and (c) bipolar series (BP-S) (Fig. 1, see further explanations given by Kobya *et al.*).[19] Before first use, all electrodes were mechanically abraded using SiC paper to remove scale, followed by cleaning with 0.1 mol dm^{-3} NaOH or H_2SO_4 solution (20% in volume) and a final ultrasonic cleaning in ultra-pure water. The solutions were always vigorously stirred with a magnetic bar to ensure mixing and the transport of reactants towards/from the electrodes.

The system for EAOPs was equipped with an undivided filter-press reactor to work in a flow mode (Fig. 1). The reactor contained components of 8 cm × 12 cm in dimension, separated with Viton gaskets to avoid leakage and packed between two larger stainless steel screwed end plates. The anode was a commercial DSA ($Ti/IrO_2–RuO_2$ anode prepared by thermal decomposition) purchased from Baoji Zhiming Special Metals Co. Ltd, whereas the cathode was a carbon–polytetrafluoroethylene (PTFE) air-diffusion electrode from E-TEK. A PVC liquid compartment with a central window of 4 cm × 5 cm (exposed area 20 cm^2) allowed contacting the effluent with the outer faces of both electrodes, with 1.2 cm of interelectrode gap. The inner face of the cathode contacted a Ni mesh employed as electrical connector and was in contact with a PVC gas chamber fed with compressed atmospheric air at an overpressure of 8.6 kPa regulated with a back-pressure gauge to continuously produce H_2O_2 from cathodic O_2 reduction. For each trial, the solution to be treated was introduced into the reservoir and recirculated by means of a JTP-5000 centrifugal pump (SunSun group Co., Ltd, China) at a liquid flow rate of 200 $dm^3\ h^{-1}$ regulated by a flowmeter. Before first use,

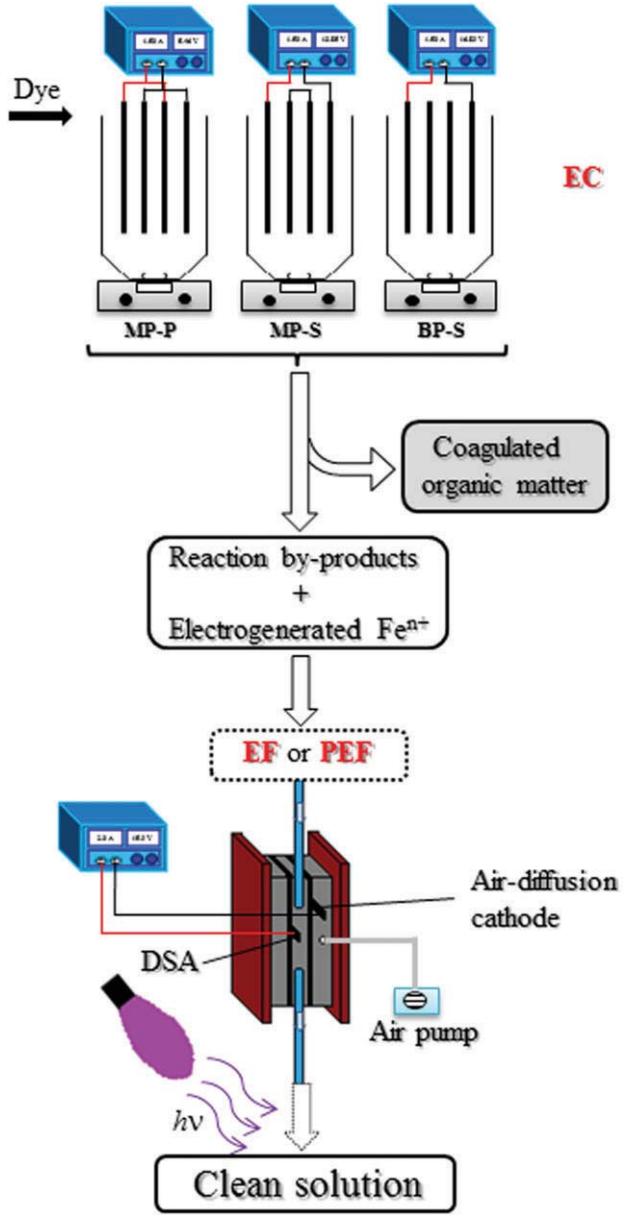

Figure 1. Schematic representation of the combined EC/EAOPs systems for the treatment of 1.85 dm^3 of Tartrazine solutions. The EC reactor was equipped with four iron electrodes placed in parallel-plate mode (exposed area of 150 cm^2 each) and connected according to three different configurations: (a) monopolar parallel (MP-P); (b) monopolar series (MP-S); and (c) bipolar series (BP-S). The EAOPs were performed with a filter-press cell equipped with a DSA anode of $Ti/IrO_2–RuO_2$ and an air-diffusion electrode (ADE) as cathode, both with an exposed area of 20 cm^2. In PEF, the solution was irradiated with a 125 W UVA lamp. The solution pH was set to 3.0 before applying the EAOPs.

a preliminary polarization of 0.05 mol dm^{-3} Na_2SO_4 at pH 3.0 and 1 A for 180 min allowed activation of the catalytic layer of the cathode. In PEF, the solution was irradiated with UVA light by means of a 125 W Philips black light blue lamp of $\lambda_{max} = 360$ nm. The comparative EF trials were performed in the dark by covering the system with an opaque cloth.

Freshly prepared solutions of 1.85 dm^3 with 100 mg dm^{-3} of TOC (corresponding to 278 mg dm^{-3} or 0.52 mmol dm^{-3} Tartrazine) in different supporting electrolytes (Na_2SO_4, NaCl or $NaNO_3$) were treated by individual EC and EAOPs. In EC, the influence of pH (between 3.0 and 11.0) and applied current (0.75–2.25 A) was tested in the three configuration modes (MP-P, MP-S and BP-S), whereas the effect of the concentrations of supporting electrolyte (0.025–0.30 mol dm^{-3} NaCl) and pollutant (50–200 mg dm^{-3} TOC) was assessed in the optimal BP-S cell configuration. In the EAOPs under investigation (EO, EF and PEF), the pH was fixed at 3.0 because this pH has been found the most convenient for the treatment of other aromatics by electrochemical Fenton-based methods.[51] In EF and PEF, 0.5 mmol dm^{-3} Fe^{2+} was added as catalyst. To perform the combined EC/EAOPs, EC-treated solutions were filtered in order to remove the precipitate and easily collect the separated liquid fraction to be further treated by each EAOP.

Apparatus and analytical procedures

All the experiments were carried out at constant current with a digital DC Hossoni HB17300SL power source (3 A, 30 V), which directly displayed the resulting cell voltage. The solution pH was measured with a Mettler Toledo pH-meter. Samples were always withdrawn at regular time intervals from the treated solutions and then microfiltered with 0.45 μm PTFE filters before analysis. The decolorization of Tartrazine solutions was monitored from the absorbance (A) decay at the maximum visible wavelength (λ_{max}) of 428 nm, measured from the spectra recorded on a UV759 UV/Vis spectrophotometer (Shanghai Spectrum Instruments Co., Ltd). The percentage of color removal or decolorization efficiency was then determined as follows:[51]

$$\text{Color removal } (\%) = 100\frac{A_0 - A_t}{A_0} \quad (5)$$

where A_0 and A_t denote the absorbance at initial time and after an electrolysis time t, respectively.

The mineralization of solutions was monitored from their TOC determined on a Multi N/C® 3100 analyzer from Analytik Jena. Reproducible TOC values with an accuracy of ±1% were always found by injecting 50 mm^3 aliquots into the analyzer. The energy consumption per unit TOC mass (EC_{TOC}, in kWh (g TOC)$^{-1}$) was calculated as follows:[54]

$$EC_{TOC} = \frac{E_{cell} I t}{\Delta (TOC)_{exp} V_s} \quad (6)$$

where E_{cell} is the average cell voltage (V), I is the applied current (A), t is the electrolysis time, (h) and V_s is the solution volume (dm^3).

RESULTS AND DISCUSSION

Electrocoagulation in three configurations: MP-P, MP-S and BP-S

Modirshahla *et al.*[6] reported a preliminary study on the EC of 250 cm^3 of Tartrazine solutions, concluding that MP-S was the most efficient configuration. However, as stated in the Introduction, it is mandatory to assess the influence of the electrode connection for each particular system under use, since a unique criterion on the subject is not available. For example, BP-S was found to be optimal for the EC of slaughterhouse wastewater,[17] but the same authors found that MP configurations were preferable for organics removal in oily bilgewater.[18] In particular, MP-P shows some interesting features for working at industrial scale, since it allows knowing exactly the current density at each electrode, which enables accurate planning of periodic anode replacement.

To clarify the influence of the cell configuration, 1.85 dm^3 of 278 mg dm^{-3} Tartrazine solutions were degraded by EC at natural pH 6.3 (periodically controlled) and 1.50 A for 12.5 min using the MP-P, MP-S and BP-S systems. Figure S1 (Supplementary material) shows the effect of the type of supporting electrolyte at a concentration of 0.05 mol dm^{-3} on both the decolorization efficiency at 428 nm and the percentage of TOC abatement. For each configuration, the quickest color and TOC removal was obtained in NaCl, therefore confirming our recent findings at laboratory scale.[21] Amani-Ghadim *et al.* also found a higher removal efficiency for Reactive Red 43 in chloride and sulfate media compared with nitrate medium.[14] The benefits from using chloride were also reported for the removal of Direct Red 81.[11] In Fig. S1a, a very slow color removal, only attaining 10–15% at 12.5 min, can be observed in $NaNO_3$. This is in agreement with recent studies proving that the dissolution of iron is hindered by nitrate anion due to the formation of a passive layer on the anode surface.[12,14,55] The use of Na_2SO_4 allowed up to *c.* 70% decolorization at that time, which is explained by the easier Fe^{2+} generation from reaction (1) to finally yield $Fe(OH)_n$ as coagulant. The fastest color disappearance was achieved in NaCl, attaining total removal in BP-S. In that medium, coagulation coexists with oxidation mediated by active chlorine formed via reaction (4), as recently demonstrated from the identification of chlorinated by-products in EC.[21] Chloride ion can also contribute to the formation of soluble $(FeCl)_n^{(3-n)+}$ complexes, which is beneficial because it increases the soluble iron dose.

The percentage TOC removal during the same experiments is shown in Fig. S1b and confirms the superior performance of EC in NaCl owing to the synergistic action of coagulation and oxidation by active chlorine. Note that none of the systems allowed complete decontamination of the solutions at such short electrolysis time. Unless stated otherwise, the subsequent studies were performed in NaCl.

From the aforementioned results, one can conclude that the BP-S configuration yielded the best results, reaching 100% decolorization and 50% TOC removal after 12.5 min in 0.05 mol dm^{-3} NaCl. This can be justified by calculating the electrode consumption in each configuration and medium, made from the electrode weighting before and after 120 min of electrolysis to minimize the measurement error. In all media, the consumption increased as MP-P $\ll$ MP-S $<$ BP-S, in accordance with the increasing cell voltage values. For example, in NaCl medium, the electrode consumptions were 1.75, 3.08 and 4.05 kg m^{-3} with cell voltage values of 4.6, 13.9 and 16.9 V, respectively. The much higher voltages in the serial systems arose from their higher resistance, in contrast to the parallel configuration in which the voltage is equivalent to that of a simple two-electrode cell. The higher electrode consumption occurring in BP-S conferred greater coagulation ability, therefore leading to faster removal of Tartrazine and its intermediates. The less pronounced iron dissolution commented above for $NaNO_3$ medium was confirmed by the extremely small electrode consumptions at 120 min, yielding 0.06–0.08 kg m^{-3} in the three configurations.

The influence of pH (periodically controlled) on the color and TOC abatement was investigated for the EC degradation of 278 mg dm^{-3} Tartrazine solutions in 0.05 mol dm^{-3} NaCl at 1.50 A for 12.5 min using the three cell configurations. As depicted in Fig. 2(a), the quickest color removal was achieved at pH 6.3–11.0, with >90% decolorization in the serial configurations, whereas the process was much slower at pH 3.0, with 40% decolorization as maximum. The plausible explanation of this finding is that the coagulating $Fe(OH)_n^{(3-n)+}$ flocs are quite poorly produced at pH $<$ 6.0 because the soluble Fe(III) and Fe(II) species show a certain stability and become the dominant species. The TOC decay during the same trials is shown in Fig. 2(b). The fastest decontamination was reached at intermediate pH values of 6.3 and 9.0, due to the combination of coagulation with electrochlorination that yielded up to *c.* 40–50% TOC removal. The superiority of the BP-S configuration was demonstrated again at the optimal pH of 6.3. In contrast, a much poorer TOC abatement was achieved at more acidic and alkaline pH, which can be mainly accounted for by the less favorable formation of $Fe(OH)_3$ coagulant according to the iron speciation diagrams. For the sake of completeness, the set of data for the whole electrolyses over time can be seen in Fig. S2. A total decolorization could be reached in all the cell configurations at all pH values, even at pH 3.0 and 11.0 after long times. TOC decays at 180 min were always higher than those found at 12.5 min, attaining a maximum of about 60% TOC removal in BP-S at pH 6.3. Actually, TOC remained practically constant after a short electrolysis time in all cases, consequently confirming the inefficacy of EC to ensure high TOC removal. This can be justified by the accumulation of persistent organic by-products that contribute to the remaining TOC, as recently reported.[21] Since the initial pH of Tartrazine solutions was 6.3, the subsequent EC experiments were carried out at this pH, which avoids the need for adding chemicals to modify it.

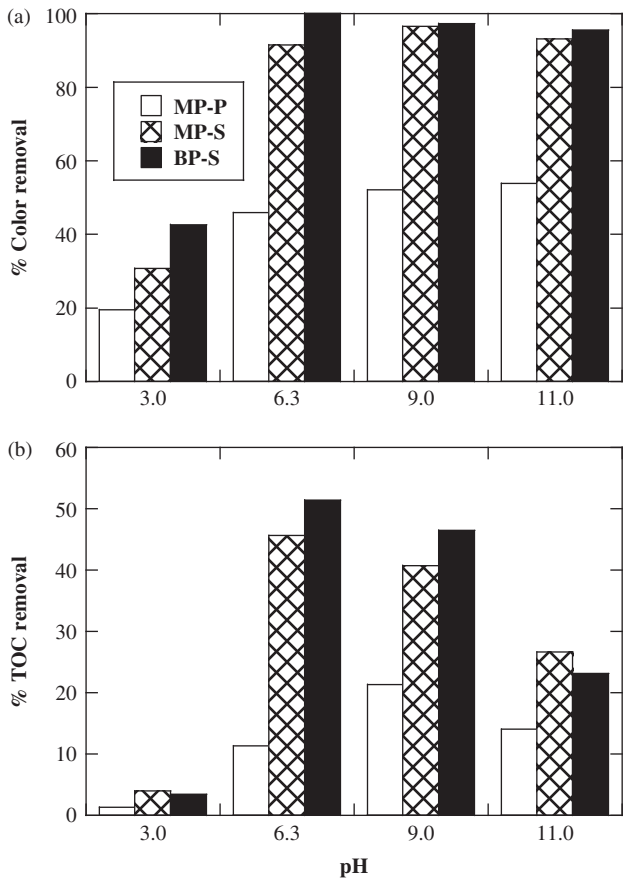

Figure 2. Influence of pH on (a) decolorization efficiency at 428 nm, and on (b) percentage TOC abatement for the EC degradation of 1.85 dm^3 of 278 mg dm^{-3} Tartrazine solutions in 0.05 mol dm^{-3} NaCl at 1.50 A for 12.5 min using three cell configurations.

Figure 3(a) and 3(b) show the effect of applied current on the decolorization efficiency and the percentage of TOC decay at 12.5 min for the EC treatment in 0.05 mol dm^{-3} NaCl at pH 6.3 in

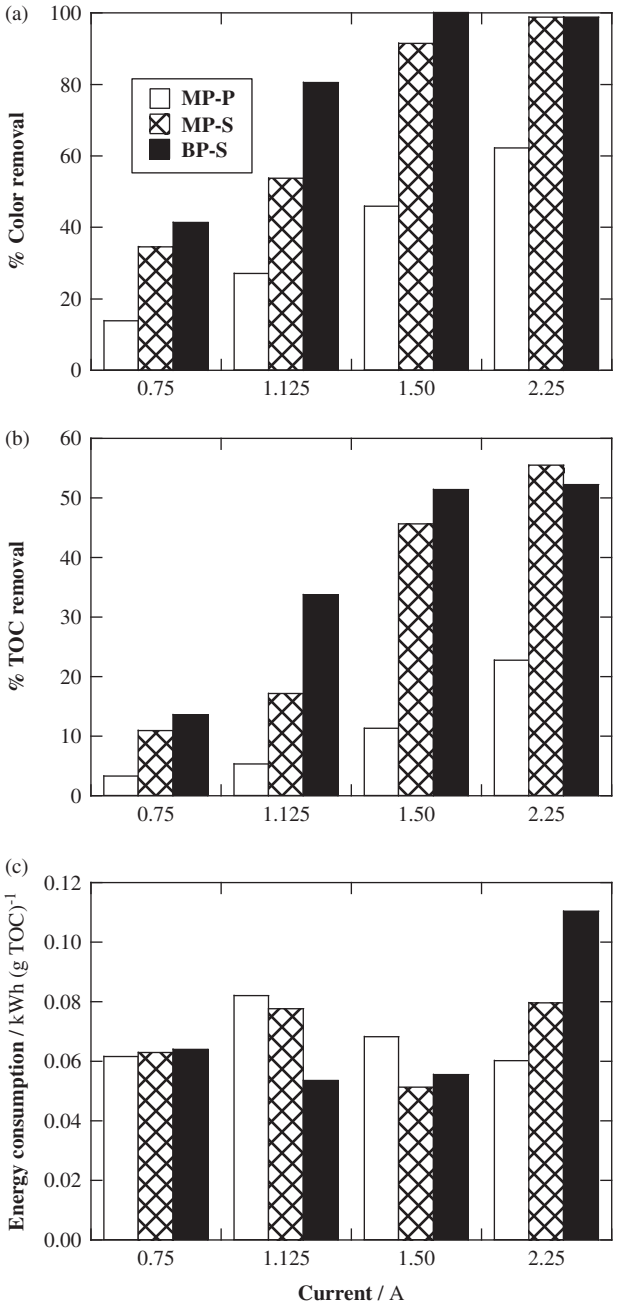

Figure 3. Effect of applied current on (a) decolorization efficiency at 428 nm, (b) percentage TOC decay, and (c) energy consumption per unit TOC mass for the EC degradation of 1.85 dm^3 of 278 mg dm^{-3} Tartrazine solutions in 0.05 mol dm^{-3} NaCl at natural (and controlled) pH 6.3 for 12.5 min in three cell configurations.

the three cell configurations. For both parameters analyzed, the performance of EC was slightly or strongly raised at higher current in all configurations. This behavior can be mainly explained by the increasing dosage of coagulating oxides and hydroxides that arise from the enhanced anode dissolution according to Faraday's law, thus favoring the removal of the dye and its by-products by entrapment upon flocculation. Current also has an important influence on the bubble production rate and size. Furthermore, the electrogeneration of Cl_2 from reaction (4), which is converted into HClO/ClO$^-$ in the bulk, was enhanced as well. The corresponding energy consumption per unit TOC mass calculated from Equation (6) is shown in Fig. 3(c). Since the amelioration observed at 2.25 A in Fig. 3(a) and 3(b) was quite insignificant in the serial configurations, a two-fold increase of EC_{TOC} was obtained. For example, in BP-S, an EC_{TOC} of 1.110 kWh (g TOC)$^{-1}$ (5.757 kWh m^{-3}) was obtained at 2.25 A compared with 0.056 kWh (g TOC)$^{-1}$ (2.853 kWh m^{-3}) at 1.50 A. As a result of the significantly poorer decolorization and TOC removal at lower current values, their resulting EC_{TOC} values were comparable with those obtained at 1.50 A, as can be seen in Fig. 3(c). Considering the three plots, the best results were yielded at 1.50 A, with total decolorization and greater TOC removal after 12.5 min in the BP-S configuration. This system then combines great efficacy with high efficiency. The set of data for the complete electrolyses can be seen in Fig. S3. A 100% color removal could always be attained, even at 0.75 and 1.125 A after long electrolysis times. As described above, faster decolorization was achieved when current was raised. These trends are also evident for TOC removal. In all cases, the maximum value of 60% decontamination was reached, earlier or later depending on the applied current.

The above findings allow one to conclude that the EC treatment exhibited its highest performance in 0.05 mol dm^{-3} NaCl at pH 6.3 and 1.50 A using the BP-S cell configuration.

Effect of the electrolyte and pollutant concentrations in the optimal BP-S cell configuration

The effect of the supporting electrolyte concentration was studied in the range 0.025–0.30 mol dm^{-3} NaCl for the optimized EC in

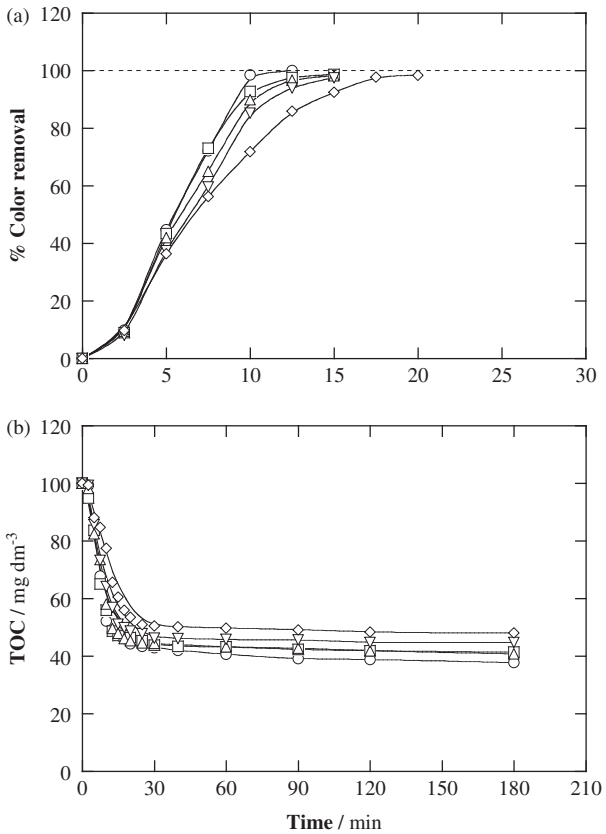

Figure 4. Effect of NaCl concentration as supporting electrolyte on (a) decolorization efficiency at 428 nm, and on (b) TOC removal with electrolysis time for the EC degradation of 1.85 dm^3 of 278 mg dm^{-3} Tartrazine solutions in: (○) 0.025, (□) 0.05, (△) 0.10, (▽) 0.15 and (◇) 0.30 mol dm^{-3} NaCl, at natural (and controlled) pH 6.3 and 1.5 A in the BP-S cell configuration.

the BP-S configuration. As can be seen in Fig. 4(a), a higher NaCl content did not accelerate the decolorization process. In fact, it turned out to be rather detrimental because increasing times were necessary to completely remove the color. For instance, 12.5 min were required at the lowest NaCl concentrations of 0.025 and 0.05 mol dm^{-3}, whereas it took 20 min at 0.03 mol dm^{-3}. The same trends can be observed for TOC decay in Fig. 4(b). Fast abatement was achieved within a short electrolysis time, whereupon TOC remained almost constant until the end of the experiments, attaining about 60% removal at the lower NaCl contents and only 50% at 0.03 mol dm^{-3}. This negative influence can plausibly mean that the expected increasing amounts of active chlorine generated at high NaCl concentration lead to the formation of persistent chlorinated by-products that are less prone to coagulation. Some of these compounds were identified in our previous work.[21] On the other hand, this behavior can also be attributed to a change in the ionic strength. According to Yildiz *et al.*, an increased ionic strength causes compression of the double-layer.[9] This could modify the kinetics of coagulants formation in the bulk. But, most importantly, it affects the kinetics and equilibria of reactions between charged and/or colloidal species occurring during EC. Furthermore, the increase in NaCl content entails a reduction in the cell voltage, which leads to a smaller electrode consumption. For example, 4.85 and 3.44 kg m^{-3} were calculated at 120 min for electrolyses with 0.025 and 0.30 mol dm^{-3}, respectively. The decrease in weight loss at high NaCl content was particularly significant for the two inner electrodes, which were not electrically connected to the power source.

The ability of EC in the BP-S configuration to treat solutions with different concentrations of Tartazine was also surveyed. All the solutions were completely decolorized within a short time, as depicted in Fig. 5(a), requiring more prolonged electrolysis when the initial dye concentration rose from 50 to 200 mg dm^{-3}. This can be simply related to the corresponding larger number of Tartrazine molecules, which react and/or interact with a fixed amount of $Fe(OH)_n$ species and Cl_2/HClO/ClO^- formed at 1.50 A to become coagulated and/or oxidated, respectively. Figure 5(b) highlights an increase in the residual TOC of the final electrocoagulated solutions as the initial dye concentration was raised, which can be explained by the larger number of persistent by-products that are accumulated in the solution. Note that in all cases the maximum TOC removal was about 60%, thus leaving 40% of non-coagulable organic matter.

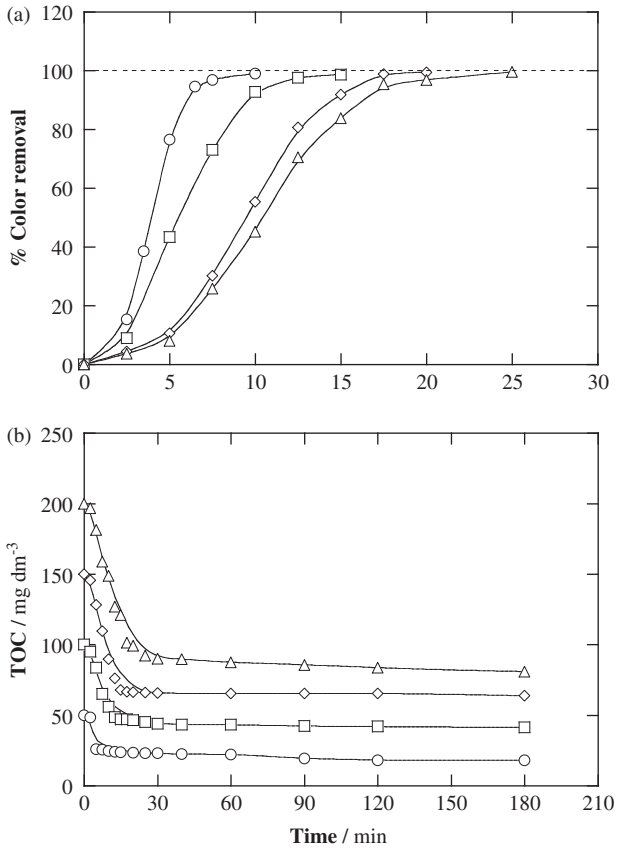

Figure 5. Influence of initial Tartrazine concentration on (a) decolorization efficiency at 428 nm, and on (b) TOC abatement with electrolysis time for the EC degradation of 1.85 dm^3 of dye solutions in 0.05 mol dm^{-3} NaCl at natural (and controlled) pH 6.3 and 1.50 A using the BP-S cell configuration. TOC content: (○) 50, (□) 100, (◇) 150 and (△) 200 mg dm^{-3}.

Electrochemical advanced oxidation processes in different supporting electrolytes

This subsection is devoted to the study of the three most effective EAOPs known at present, namely EO, EF and PEF for the treatment of 1.85 dm^3 of 278 mg dm^{-3} Tartrazine solutions in different supporting electrolytes at a concentration of 0.05 mol dm^{-3} with pH adjusted to 3.0. A pre-pilot plant containing a filter-press cell equipped with a Ti/IrO_2–RuO_2 anode and an air-diffusion cathode was used. The trends of color removal percentage and TOC abatement for three EAOPs applied in 0.05 mol dm^{-3} NaCl at 2.00 A are presented in Fig. 6(a) and 6(b), respectively. This current value was better than 1.00 and 1.50 A, whereas values higher than 2.00 A did not bring about any significant amelioration (not shown). The behavior in this electrolyte is especially interesting because EC, which is planned to be used for the pre-treatment of Tartrazine solutions, was proven better in NaCl medium, as mentioned above. The superiority of EF and PEF over EO is evident for both parameters. The time for overall decolorization in EO was 60 min. This long time is due to the low oxidation power of the Ti/IrO_2–RuO_2 anode since the •OH formed at its surface from reaction (3) are preferentially chemisorbed and thus, their interaction with the binary oxide structure is so strong that they are not readily available for reacting with the organic molecules that are adsorbed on the anode. But, at least, they are able to partially transform the initial dye into several by-products, as confirmed for other organic pollutants.[26] In addition, this anode is able to generate active chlorine species from reaction (4), and these species have great decolorization power. In contrast, for EF and PEF, a much quicker total decolorization was achieved in 30 min. The absorbance decay was analogous in both treatments, meaning that the main oxidant was the •OH formed in the bulk from Fenton's reaction (2). The contribution of UVA light and active chlorine to the removal of Tartrazine was rather insignificant in Fenton-based EAOPs.

The time course of TOC decay for the same electrolyses was greatly dependent on the EAOP used, as shown in Fig. 6(b). As previously found,[21] the total mineralization of Tartrazine molecules involved their transformation into CO_2 and inorganic ions as follows:

$$C_{16}H_9N_4O_9S_2^{3-} + 43\ H_2O \rightarrow 16\ CO_2 + 4\ NO_3^- + 2\ SO_4^{2-} + 95\ H^+ + 90\ e^- \quad (7)$$

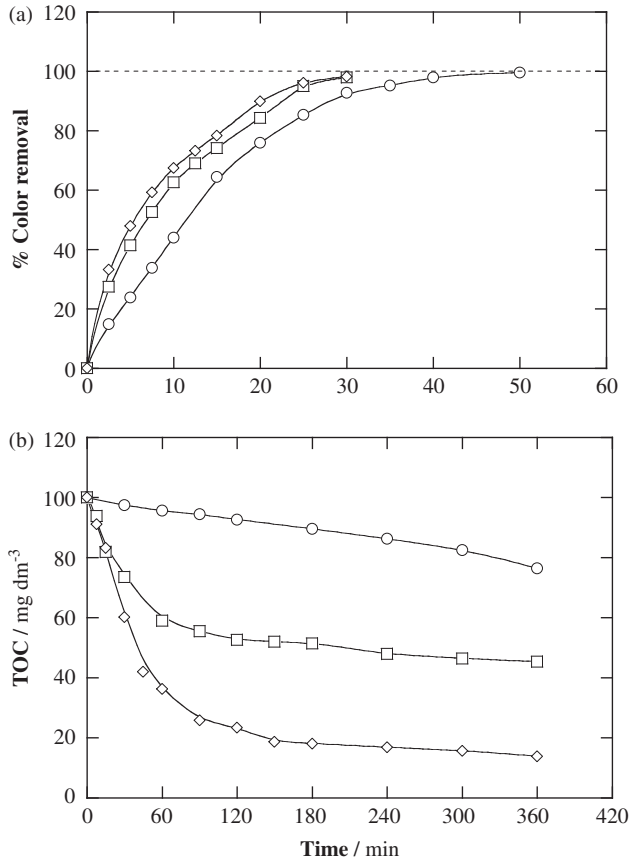

Figure 6. (a) Decolorization efficiency at 428 nm, and (b) TOC removal vs electrolysis time for the treatment of 1.85 dm^3 of 278 mg dm^{-3} Tartrazine solutions in 0.05 mol dm^{-3} NaCl at pH 3.0 and 2.00 A by different EAOPs: (○) EO, (□) EF and (◇) PEF, using the pre-pilot flow system with a filter-press cell equipped with a Ti/IrO_2–RuO_2 anode and an ADE cathode. In EF and PEF, 0.5 mmol dm^{-3} Fe^{2+} was added to the solution.

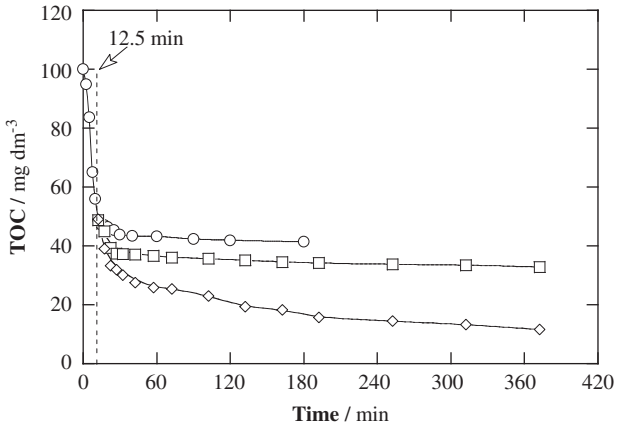

Figure 7. TOC decay vs electrolysis time for the treatment of 1.85 dm^3 of 278 mg dm^{-3} Tartrazine solutions by various two-step EC (12.5 min, 1.50 A, 0.05 mol dm^{-3} NaCl at natural pH 6.3)/EAOPs (2.00 A, pH 3.0): (□) EF and (◇) PEF. (○) Comparative TOC removal by EC alone.

The percentage of TOC removal in EO was only 25% at 360 min, which is very poor due to the low oxidation power of active chlorine and chemisorbed •OH, only allowing the accumulation of a large number of persistent chlorinated and non-chlorinated by-products. EF yielded a higher TOC decay of 55% TOC, thanks to the additional action of •OH formed in the bulk, but a certain amount of organic intermediates were still refractory to oxidation. This mainly includes some short-chain carboxylic acids and their Fe(III) complexes.[21] The treatment of Tartrazine solutions by PEF led to the fastest and greatest mineralization, with only 10% of TOC remaining in the solution at 360 min. The enhancement in PEF compared with EF can be mainly related to the action of UVA photons, which are able (i) to reduce the photoactive Fe(III) species to Fe(II) and •OH, and (ii) to photodegrade the persistent Fe(III)-carboxylate complexes that could not be oxidized under the sole action of •OH.[51]

The three EAOPs were also studied in 0.05 mol dm^{-3} Na_2SO_4 and $NaNO_3$ media, as shown in Figs S4 and S5, respectively. The time course of color removal and solution TOC was very similar in both cases. EO was unable to achieve total decolorization, reaching 60% color reduction at 360 min. Since in these media the only oxidant was the chemisorbed •OH, the Tartrazine molecules underwent a very slow transformation, which confirms the main role of active chlorine as oxidizing agent mentioned above in NaCl medium. In contrast, the trends in EF and PEF were almost the same as in NaCl trials, with total color removal in about 30 min, thus corroborating that the conversion of Tartrazine in these processes was pre-eminently due to •OH in the bulk, without significant interference of generated active chlorine in the case of NaCl. Regarding the mineralization plots, the performance of EO and EF did not vary compared with that of NaCl medium. In contrast, the TOC decay with PEF in Na_2SO_4 and $NaNO_3$ was somewhat faster than that obtained in NaCl, reaching overall mineralization in 240–300 min. This phenomenon can be associated with the formation of chlorinated intermediates in the case of NaCl that are responsible for the slower, partial TOC abatement described before. The great ability of EF and PEF to ensure high mineralization percentage in the presence of chloride ions, typically encountered in real waters and expected in the EC pre-treated solutions, has been demonstrated.

Combined treatment of dye solutions by EC/EAOPs

Having optimized the individual EC and EAOPs, as described in the previous subsections, the mineralization trends for the two-step treatment of Tartrazine solutions were studied. Since the EC pre-treatment leads to the accumulation of about 0.5–1.0 mmol dm^{-3} iron ions in solution, only the coupling with EF and PEF was of interest. The dye solutions were first pre-treated by EC with four Fe electrodes in BP-S configuration in 0.05 mol dm^{-3} NaCl at natural pH 6.3 and 1.50 A for 12.5 min, which ensured complete color removal (Figs S1, 2 and 3) as well as up to 60% TOC removal. The final solutions were filtered and the separated liquid fractions treated by the Fenton-based EAOPs at 2.00 A after pH regulation at 3.0. As shown in Fig. 7, the subsequent EF process led to poor enhancement, since the total mineralization was slightly higher than 60%. In contrast, the combined EC/PEF system allowed much faster decontamination, with >90% TOC removal after 372.5 min of global sequential treatment. This enhanced performance was a result of the synergistic action of Fe(III) photoreduction, photodecarboxylation of refractory by-products and oxidation of persistent by-products by •OH as well as by active chlorine in the bulk. It can be seen in Fig. 8 that a lower current such as 1.50 A could be applied instead. Mineralization during the first 180 min was somewhat poorer, but the final TOC value was the same as with EC/PEF at 2.00 A, thus reducing the energy consumption and increasing the cost-effectiveness of this promising combined technology.

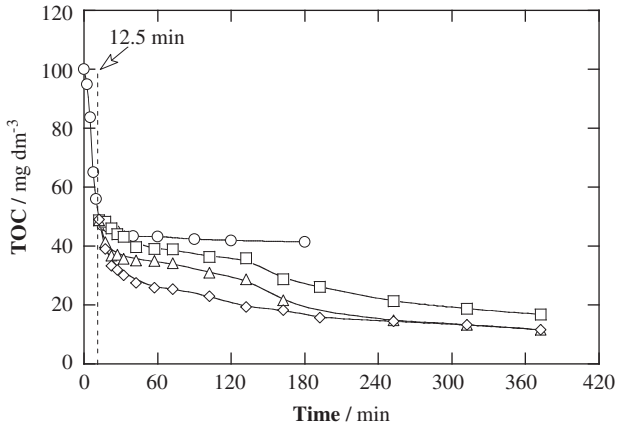

Figure 8. Effect of current on TOC removal with electrolysis time for the EC/PEF treatment under the conditions shown in Fig. 7 at: (□) 1.00 A, (△) 1.50 A, and (◇) 2.00 A. (○) Comparative TOC abatement by EC alone.

CONCLUSIONS

The main findings presented in this work are:

- The bipolar configuration in series was more convenient in EC because of the larger electrode consumption compared with monopolar cell configurations.
- The most relevant experimental parameters in EC have been optimized for the treatment of Tartrazine solutions: 0.05 mol dm^{-3} NaCl, pH 6.3 and 1.50 A. This led to quicker color removal and 60% TOC abatement.
- EO with a $Ti/IrO_2–RuO_2$ anode and an air-diffusion cathode enabled total decolorization in NaCl medium, but poor mineralization. EF yielded greater TOC removal, but still poorer than PEF, which took advantage of the synergistic action of electrogenerated active chlorine and •OH in the bulk along with the photolytic action of UVA light.
- The EC/PEF technology has been proven superior among the EC/EAOPs for the treatment of Tartrazine solutions at a pre-pilot scale. Further work is in progress to increase its cost-effectiveness.

ACKNOWLEDGEMENTS

The authors thank MICINN (Ministerio de Ciencia e Innovación, Spain) for support under project CTQ2010-16164/BQU, co-financed with FEDER funds, and also acknowledge support from the National Natural Science Foundation of China (NSFC, grant number 21250110515 and 21273120). The PhD grant awarded to A. Thiam from AECID-MAEC (Spain) is also acknowledged.

Supporting Information

Supporting information may be found in the online version of this article.

REFERENCES

1 Sirés I and Brillas E, Remediation of water pollution caused by pharmaceutical residues based on electrochemical separation and degradation technologies: a review. *Environ Int* **40**:212–229 (2012).
2 Mollah MYA, Schennach R, Parga JR and Cocke DL, Electrocoagulation (EC)-science and applications. *J Hazard Mater* **B84**:29–41 (2001).
3 Zodi S, Potier O, Lapicque F and Leclerc JP, Treatment of the industrial wastewaters by electrocoagulation: optimization of coupled electrochemical and sedimentation processes. *Desalination* **261**:186–190 (2010).
4 Khandegar V and Saroha AK, Electrocoagulation for the treatment of textile industry effluent – a review. *J Environ Manage* **128**:949–963 (2013).
5 Daneshvar N, Khataee AR, Ghadim ARA and Rasoulifard MH, Decolorization of C.I. Acid Yellow 23 solution by electrocoagulation process: investigation of operational parameters and evaluation of specific electrical energy consumption (SEEC). *J Hazard Mater* **148**:566–572 (2007).
6 Modirshahla N, Behnajady MA and Kooshaiian S, Investigation of the effect of different electrode connections on the removal efficiency of Tartrazine from aqueous solutions by electrocoagulation. *Dyes Pigments* **74**:249–257 (2007).
7 Moreno-Casillas HA, Cocke DL, Gomes JAG, Morkovsky P, Parga JR and Peterson E, Electrocoagulation mechanism for COD removal. *Sep Purif Technol* **56**:204–211 (2007).
8 Muthukumar M, Karuppiah MT and Raju GB, Electrochemical removal of CI Acid Orange 10 from aqueous solutions. *Sep Purif Technol* **55**:198–205 (2007).
9 Yildiz YŞ, Koparal AS and Keskinler B, Effect of initial pH and supporting electrolyte on the treatment of water containing high concentration of humic substances by electrocoagulation. *Chem Eng J* **138**:63–72 (2008).
10 Martínez-Huitle CA and Brillas E, Decontamination of wastewaters containing synthetic organic dyes by electrochemical methods: a general review. *Appl Catal B - Environ* **87**:105–145 (2009).
11 Aoudj S, Khelifa A, Drouiche N, Hecini M and Hamitouche H, Electrocoagulation process applied to wastewater containing dyes from textile industry. *Chem Eng Process* **49**:1176–1182 (2010).
12 Izquierdo CJ, Canizares P, Rodrigo MA, Leclerc JP, Valentin G and Lapicque F, Effect of the nature of the supporting electrolyte on the treatment of soluble oils by electrocoagulation. *Desalination* **255**:15–20 (2010).
13 Phalakornkule C, Polgumhang S, Tongdaung W, Karakat B and Nuyut T, Electrocoagulation of blue reactive, red disperse and mixed dyes, and application in treating textile effluent. *J Environ Manage* **91**:918–926 (2010).
14 Amani-Ghadim AR, Aber S, Olad A and Ashassi-Sorkhabi H, Influence of anions on Reactive Red 43 removal in electrochemical coagulation process. *Electrochim Acta* **56**:1373–1380 (2011).
15 Daneshvar N, Sorkhabi HA and Kasiri MB, Decolorization of dye solution containing Acid Red 14 by electrocoagulation with a comparative investigation of different electrode connections. *J Hazard Mater* **B112**:55–62 (2004).
16 Bayramoglu M, Eyvaz M and Kobya M, Treatment of the textile wastewater by electrocoagulation. Economical evaluation. *Chem Eng J* **128**:155–161 (2007).
17 Asselin M, Drogui P, Benmoussa H and Blais J-F, Effectiveness of electrocoagulation process in removing organic compounds from slaughterhouse wastewater using monopolar and bipolar electrolytic cells. *Chemosphere* **72**:1727–1733 (2008).
18 Asselin M, Drogui P, Brar SK, Benmoussa H and Blais J-F, Organics removal in oily bilgewater by electrocoagulation process. *J Hazard Mater* **151**:446–455 (2008).
19 Kobya M, Ulu F, Gebologlu U, Demirbas E and Oncel MS, Treatment of potable water containing low concentration of arsenic with electrocoagulation: different connection modes and Fe–Al electrodes. *Sep Purif Technol* **77**:283–293 (2011).
20 Boye B, Dieng MM and Brillas E, Electrochemical degradation of 2,4,5-trichlorophenoxyacetic acid in aqueous medium by peroxi-coagulation. Effect of pH and UV light. *Electrochim Acta* **48**:781–790 (2003).
21 Thiam A, Zhou M, Brillas E and Sirés I, Two-step mineralization of Tartrazine solutions: study of parameters and by-products during the coupling of electrocoagulation with electrochemical advanced oxidation processes. *Appl Catal B - Environ* **150–151**:116–125 (2014).
22 Raju GB, Karuppiah MT, Latha SS, Parvathy S and Prabhakar S, Treatment of wastewater from synthetic textile industry by electrocoagulation-electrooxidation. *Chem Eng J* **144**:51–58 (2008).
23 Panizza M and Cerisola G, Applicability of electrochemical methods to carwash wastewaters for reuse. Part 2: electrocoagulation and anodic oxidation integrated process. *J Electroanal Chem* **638**:236–240 (2010).

24 Linares-Hernández I, Barrera-Díaz C, Bilyeu B, Juáres-García Rojas P and Campo-Medina E, A combined electrocoagulation–electrooxidation treatment for industrial wastewater. *J Hazard Mater* **175**:688–694 (2010).

25 Cotillas S, Llanos J, Cañizares P, Mateo S and Rodrigo MA, Optimization of an integrated electrodisinfection/electrocoagulation process with Al bipolar electrodes for urban wastewater reclamation. *Water Res* **47**:1741–1750 (2013).

26 Panizza M and Cerisola G, Direct and mediated anodic oxidation of organic pollutants. *Chem Rev* **109**:6541–6569 (2009).

27 Faouzi M, Cañizares P, Gadri A, Lobato J, Nasr B, Paz R, Rodrigo MA and Saez C, Advanced oxidation processes for the treatment of wastes polluted with azoic dyes. *Electrochim Acta* **52**:325–331 (2006).

28 Butrón E, Juárez ME, Solis M, Teutli M, González I and Nava JL, Electrochemical incineration of indigo textile dye in filter-press-type FM01-LC electrochemical cell using BDD electrodes. *Electrochim Acta* **52**:6888–6894 (2007).

29 Panizza M, Kapalka A and Comninellis Ch, Oxidation of organic pollutants on BDD anodes using modulated current electrolysis. *Electrochim Acta* **53**:2289–2295 (2008).

30 Cavalcanti ES, Garcia-Segura S, Centellas F and Brillas E, Electrochemical incineration of omeprazole in neutral aqueous medium using a platinum or boron-doped diamond. Degradation kinetics and oxidation products. *Water Res* **47**:1803–1815 (2013).

31 Comninellis C, Electrocatalysis in the electrochemical conversion/combustion of organic pollutants for waste water treatment. *Electrochim Acta* **39**:1857–1862 (1994).

32 Panizza M and Cerisola G, Olive mill wastewater treatment by anodic oxidation with parallel plate electrodes. *Water Res* **40**:1179–1184 (2006).

33 Ribeiro J, Purgato FLS, Kokoh KB, Léger JM and De Andrade AR, Application of Ti/RuO_2-Ta_2O_5 electrodes in the electrooxidation of ethanol and derivants: reactivity versus electrocatalytic efficiency. *Electrochim Acta* **53**:7845–7851 (2008).

34 Aquino Neto S and De Andrade AR, Electrochemical degradation of glyphosate formulations at DSA® anodes in chloride medium: an AOX formation study. *J Appl Electrochem* **39**:1863–1870 (2009).

35 Fierro S, Kapalka A and Comninellis C, Electrochemical comparison between IrO_2 prepared by thermal treatment of iridium metal and IrO_2 prepared by thermal decomposition of H_2IrCl_6 solution. *Electrochem Commun* **12**:172–174 (2010).

36 Angelinetta C, Trassatti S, Atanososka LjD and Atanasoski RT, Surface properties of RuO_2 + IrO_2 mixed oxide electrodes. *J Electroanal Chem* **214**:535–546 (1986).

37 Chae K-S, Choi H-K, Ahn J-H, Song Y-S and Lee DY, Effect of organic vehicle addition on service lifetime of Ti/IrO_2–RuO_2 electrodes. *Mater Lett* **55**:211–216 (2002).

38 Panakoulias T, Kalatzis P, Kalderis D and Katsaounis A, Electrochemical degradation of Reactive Red 120 using DSA and BDD anodes. *J Appl Electrochem* **40**:1759–1765 (2010).

39 Turro E, Giannis A, Cossu R, Gidarakos E, Mantzavinos D and Katsaounis A, Electrochemical oxidation of stabilized landfill leachate on DSA electrodes. *J Hazard Mater* **190**:460–465 (2011).

40 Peralta-Hernández JM, Meas-Vong Y, Rodríguez FJ, Chapman TW, Maldonado MI and Godínez LA, *In situ* electrochemical and photo-electrochemical generation of the fenton reagent: a potentially important new water treatment technology. *Water Res* **40**:1754–1762 (2006).

41 Zhou M, Yu Q and Lei L, The preparation and characterization of a graphite–PTFE cathode system for the decolorization of C.I. Acid Red 2. *Dyes Pigments* **77**:129–136 (2008).

42 Özcan A, Oturan MA, Oturan N and Şahin Y, Removal of Acid Orange 7 from water by electrochemically generated Fenton's reagent. *J Hazard Mater* **163**:1213–1220 (2009).

43 Panizza M and Cerisola G, Electro-Fenton degradation of synthetic dyes. *Water Res* **43**:339–344 (2009).

44 Dirany A, Sirés I, Oturan N and Oturan MA, Electrochemical abatement of the antibiotic sulfamethoxazole from water. *Chemosphere* **81**:594–602 (2010).

45 Oturan N, Zhou M and Oturan MA, Metomyl degradation by electro-Fenton and electro-Fenton-like processes: a kinetics study of the effect of the nature and concentration of some transition metal ions as catalyst. *J Phys Chem A* **114**:10605–10611 (2010).

46 Sirés I, Low CTJ, Ponce-de-León C and Walsh FC, The deposition of nanostructured β-PbO_2 coatings from aqueous methanesulfonic acid for the electrochemical oxidation of organic pollutants. *Electrochem Commun* **12**:70–74 (2010).

47 Isarain-Chávez E, Arias C, Cabot PL, Centellas F, Rodríguez R, Garrido JA and Brillas E, Mineralization of the drug β-blocker atenolol by electro-Fenton and photoelectro-Fenton using an air-diffusion cathode for H_2O_2 electrogeneration combined with a carbon-felt cathode for Fe^{2+} regeneration. *Appl Cat B - Environ* **96**:361–369 (2010).

48 Randazzo S, Scialdone O, Brillas E and Sirés I, Comparative electrochemical treatments of two chlorinated aliphatic hydrocarbons. Time course of the main reaction by-products. *J Hazard Mater* **192**:1555–1564 (2011).

49 Zhou M, Tan Q, Wang Q, Jiao Y, Oturan N and Oturan MA, Degradation of organics in reverse osmosis concentrate by electro-Fenton process. *J Hazard Mater* **215–216**:287–293 (2012).

50 Zhou L, Hu Z, Zhang C, Bi Z, Jin T and Zhou M, Electrogeneration of hydrogen peroxide for electro-Fenton system by oxygen reduction using chemically modified graphite felt cathode. *Sep Purif Technol* **111**:131–136 (2013).

51 Brillas E, Sirés I and Oturan MA, Electro-Fenton process and related electrochemical technologies based on Fenton's reaction chemistry. *Chem Rev* **109**:6570–6631 (2009).

52 Isarain-Chávez E, De la Rosa C, Godínez LA, Brillas E and Peralta-Hernández JM, Comparative study of electrochemical water treatment processes for a tannery wastewater effluent. *J Electroanal Chem* **713**:62–69 (2014)

53 EFSA Panel on Dietetic Products, Nutrition and Allergies (NDA), *EFSA Journal* **8**:1778–1788 (2010).

54 Ruiz EJ, Arias C, Brillas E, Hernández-Ramírez A and Peralta-Hernández JM, Mineralization of Acid Yellow 36 azo dye by electro-Fenton and solar photoelectro-Fenton processes with a boron-doped diamond anode. *Chemosphere* **82**:495–501 (2011).

55 Yildiz YŞ, Koparal AS, Írdemez Ş and Keskinler B, Electrocoagulation of synthetically prepared waters containing high concentration of NOM using iron cast electrodes. *J Hazard Mater* **B139**:373–380 (2007).

Journal of Chemical Technology and Biotechnology

Supporting Information for

A first pre-pilot system for the combined treatment of dye pollutants by electrocoagulation/EAOPs

Abdoulaye Thiam [a,b], Minghua Zhou [a,**], Enric Brillas [b], Ignasi Sirés [a,b,*]

[a] College of Environmental Science and Engineering, Nankai University, Tianjin 300071, China

[b] Laboratori d'Electroquímica dels Materials i del Medi Ambient, Departament de Química Física, Facultat de Química, Universitat de Barcelona, Martí i Franquès 1-11, 08028 Barcelona, Spain

*Corresponding author: Tel.: +34 934021223; fax: +34 934021231.

E-mail address: i.sires@ub.edu (I. Sirés)

**Corresponding author: Tel.: +86 2266229619; fax: +86 2223501117.

E-mail address: zhoumh@nankai.edu.cn (M. Zhou)

Figures S1-S5 Pages 2-6

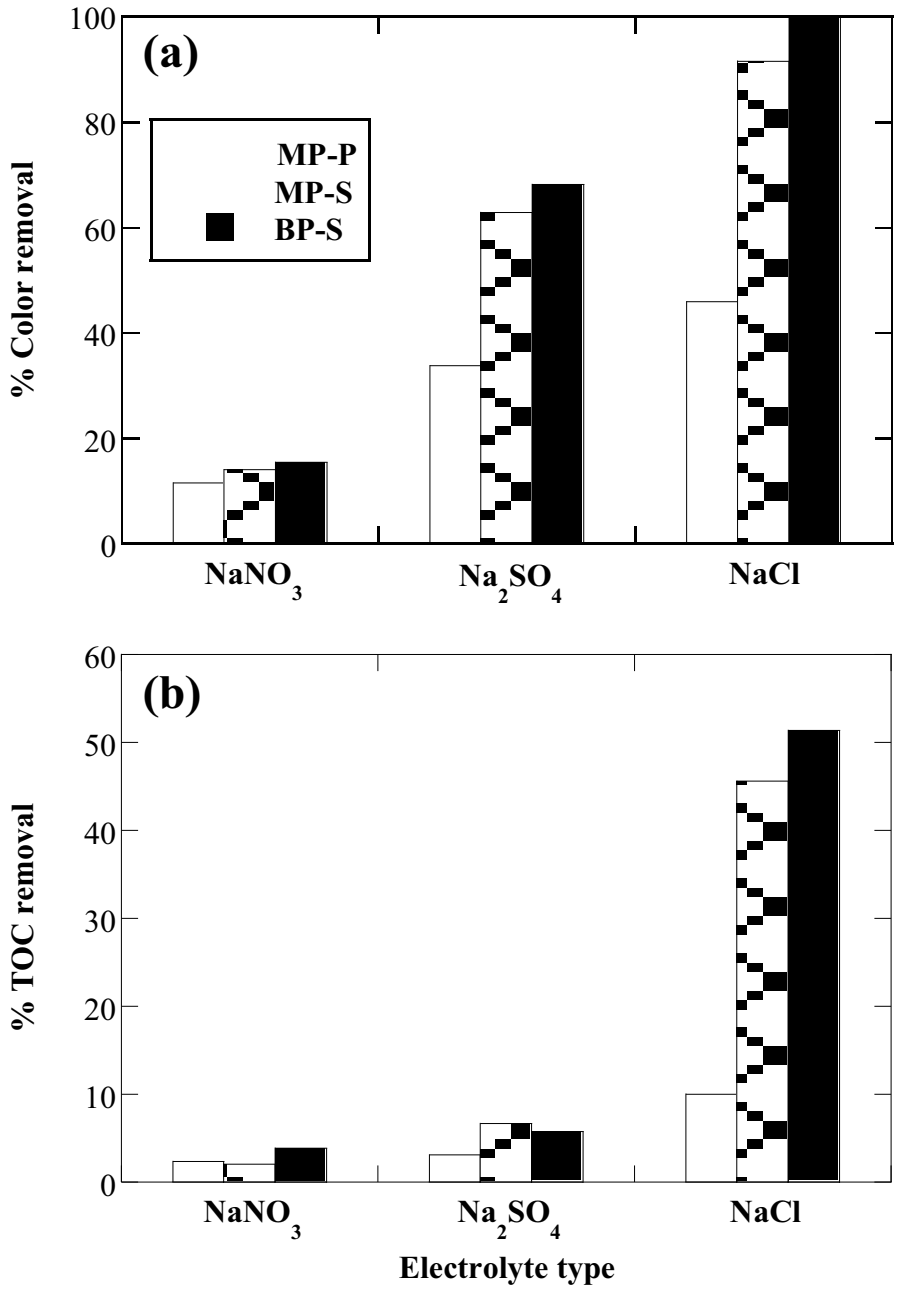

Figure S1. Effect of the type of supporting electrolyte at a concentration of 0.05 mol dm^{-3} on the (a) decolorization efficiency at 428 nm and (b) percentage of TOC abatement for the EC degradation of 1.85 dm^3 of 278 mg dm^{-3} Tartrazine solutions at natural (and controlled) pH 6.3 and 1.50 A for 12.5 min using three different cell configurations.

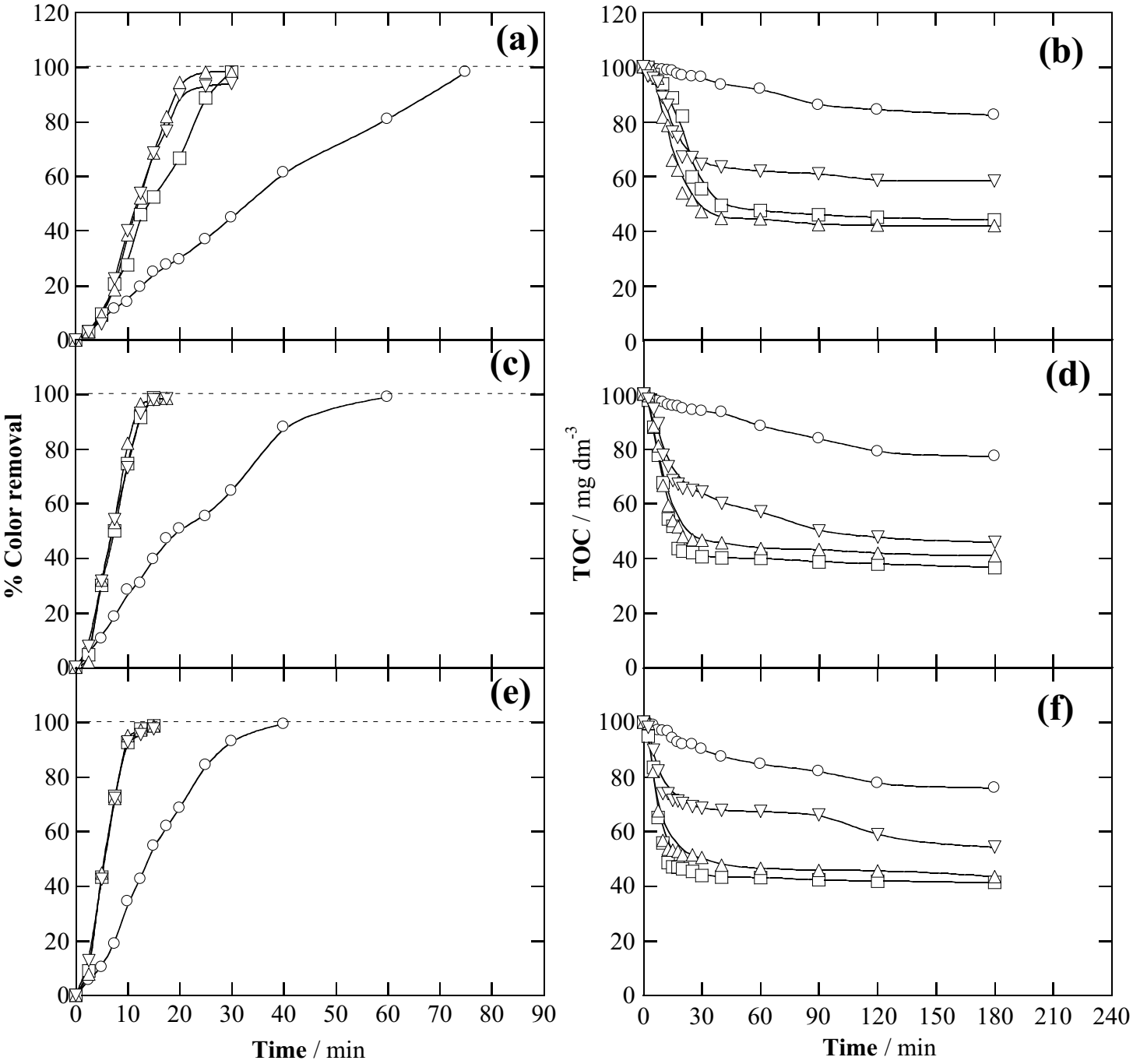

Figure S2. Effect of pH on the (a, c, e) decolorization efficiency at 428 nm and (b, d, f) TOC abatement with electrolysis time for the EC degradation of 1.85 dm^3 of 278 mg dm^{-3} Tartrazine solutions in 0.05 mol dm^{-3} NaCl at pH: (○) 3.0, (□) 6.3 (natural), (△) 9.0 and (▽) 11.0, all at 1.50 A. Cell configurations: (a, b) MP-P, (c, d) MP-S and (e, f) BP-S.

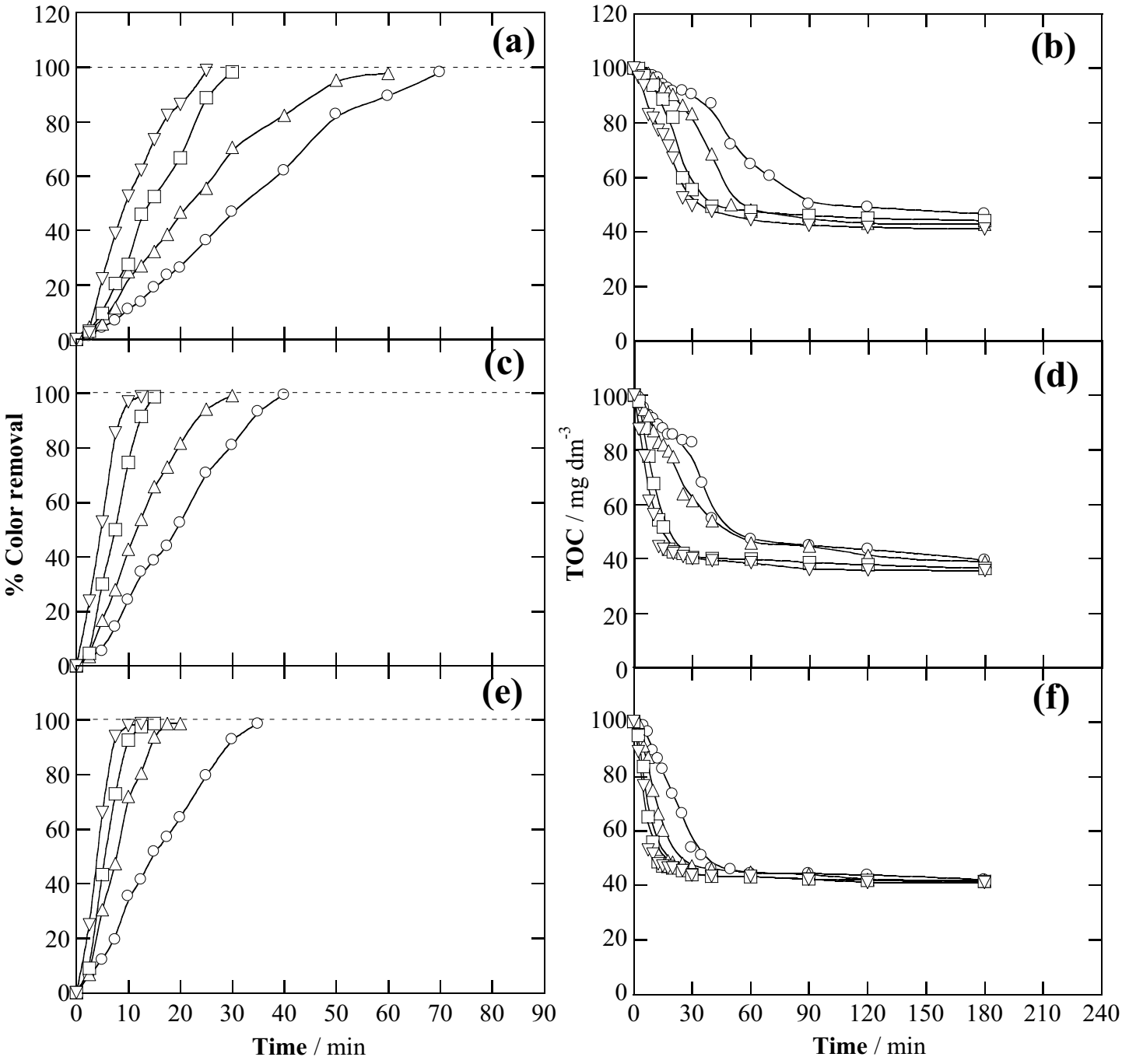

Figure S3. Effect of the applied current on the (a, c, e) decolorization efficiency at 428 nm and (b, d, f) TOC decay with electrolysis time for the EC degradation of 1.85 dm^3 of 278 mg dm^{-3} Tartrazine solutions in 0.05 mol dm^{-3} NaCl at natural (and controlled) pH 6.3 and: (○) 0.75 A, (△) 1.125 A, (□) 1.50 A and (▽) 2.25 A. Cell configurations: (a, b) MP-P, (c, d) MP-S and (e, f) BP-S.

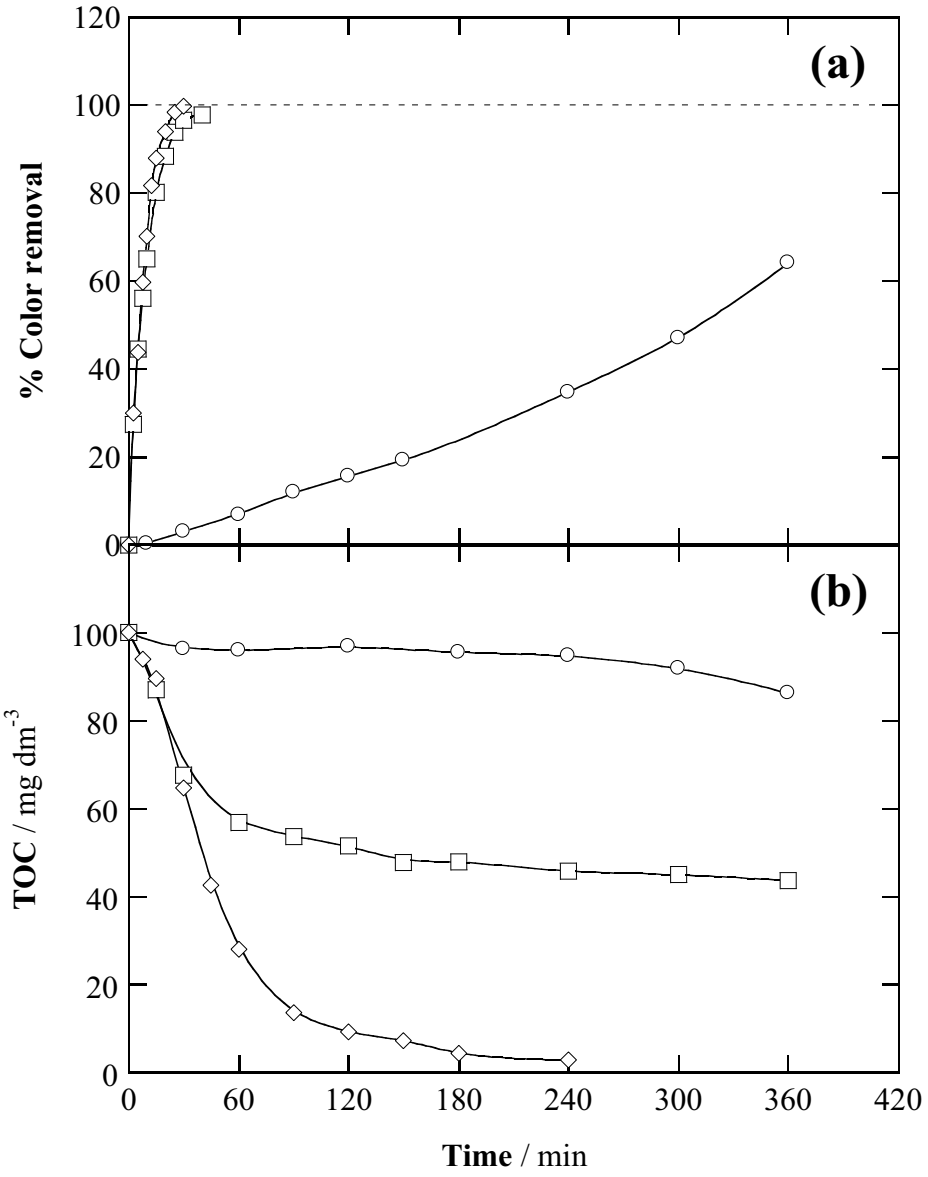

Figure S4. (a) Decolorization efficiency at 428 nm and (b) TOC removal vs electrolysis time for the treatment of 1.85 dm^3 of 278 mg dm^{-3} Tartrazine solutions in 0.05 mol dm^{-3} Na_2SO_4 at pH 3.0 and 2.00 A by different EAOPs: (○) EO, (□) EF and (◇) PEF, using the pre-pilot flow system with a filter-press cell equipped with a Ti/IrO_2-RuO_2 anode and an ADE cathode. In EF and PEF, 0.5 mmol dm^{-3} Fe^{2+} was added to the solution.

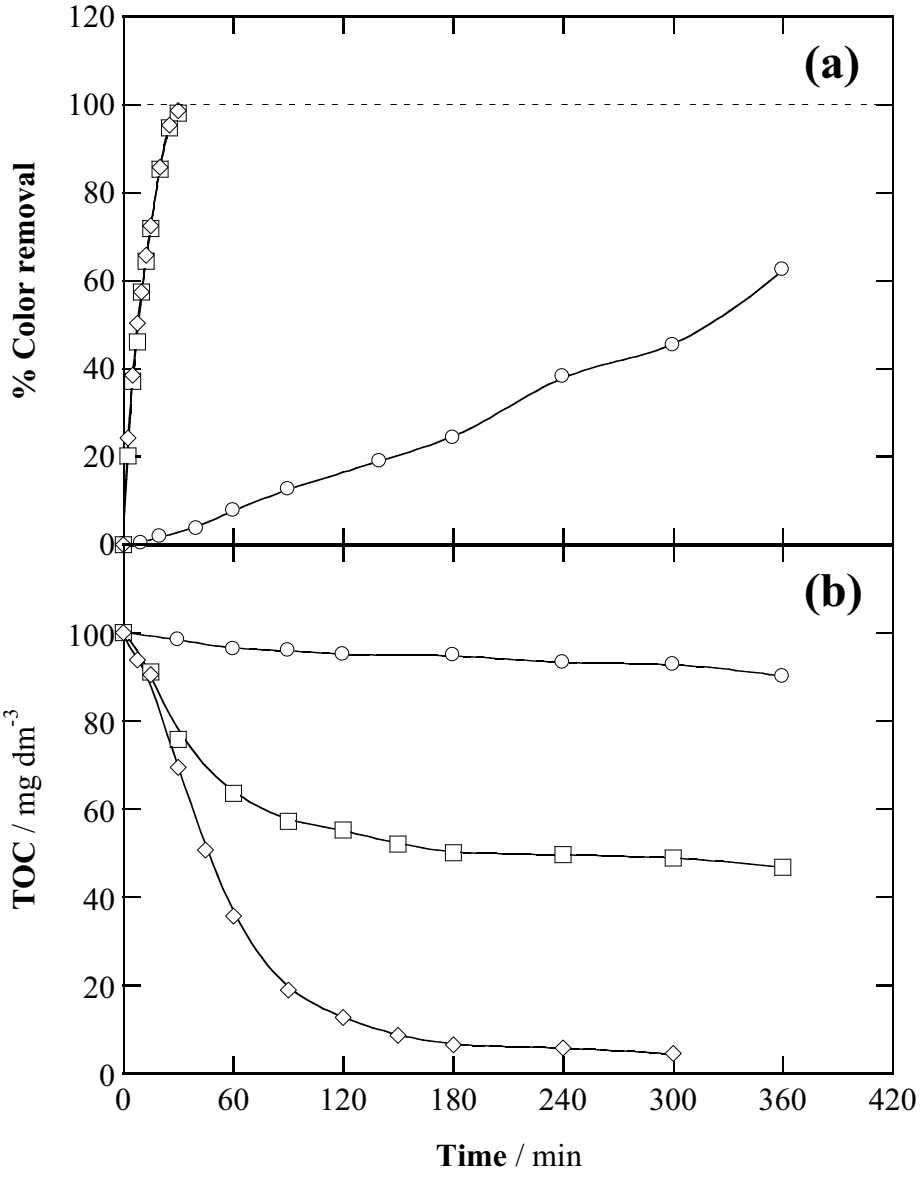

Figure S5. Change of (a) decolorization efficiency at 428 nm and (b) TOC abatement with electrolysis time for the treatment of 1.85 dm^3 of 278 mg dm^{-3} Tartrazine solutions in 0.05 mol dm^{-3} $NaNO_3$ under the same experimental conditions detailed in Fig. S4.

5. Resumen

En las últimas décadas, el riesgo asociado a la contaminación de los entornos naturales derivada de la presencia de contaminantes orgánicos persistentes (POPs) ha sido una de las mayores preocupaciones en el ámbito ambiental. Los colorantes constituyen una de los grupos de POPs más recalcitrantes, y su acumulación en el ambiente y, en particular, en las aguas supone un riesgo para la flora y los seres vivos. Su tratamiento es uno de los mayores desafíos en el sector del tratamiento de agua debido a su impacto visual, gran carga orgánica y toxicidad. Hasta la fecha se han dedicado grandes esfuerzos al desarrollo de métodos potentes para la degradación de POPs presentes en el agua. En este sentido, cabe destacar la investigación llevada a cabo entorno a los procesos convencionales y los procesos de oxidación avanzada (AOPs), basados en la generación de radicales hidroxilo ($^{\bullet}$OH) por vía química, sonoquímica, fotolítica o fotocatalítica. Sin embargo, los AOPs presentan algunas limitaciones, tales como el elevado coste energético o el gasto en reactivos. Además, estos métodos resultan muy eficientes esencialmente para disoluciones con valores bajos o medios de demanda química de oxígeno.

Alternativamente, en los últimos años se han propuesto y desarrollado una gran variedad de técnicas electroquímicas para una eliminación eficaz de los contaminantes tóxicos. Entre estas técnicas, se pueden destacar las técnicas electroquímicas convencionales de mayor aplicación industrial, como la electrocoagulación (EC), y los procesos electroquímicos de oxidación avanzada (EAOPs), los cuales ofrecen una serie de ventajas como son una alta eficiencia energética, ya que se trabaja a temperatura y presión ambiente, su versatilidad y su compatibilidad con el medio ambiente, pudiéndose evitar en ocasiones la adición de productos químicos. Aunque son tecnologías muy prometedoras, presentan algunas limitaciones, sobre todo en cuanto a los costes relativamente elevados de los EAOPs, que son inherentes al largo tiempo de tratamiento requerido, y a la incapacidad de la EC para conseguir la eliminación completa de los compuestos orgánicos. Con el objetivo de solucionar estos problemas y lograr una mineralización más eficiente, mi Tesis Doctoral se ha enfocado en la optimización de los procesos electroquímicos y el desarrollo de nuevos procesos electroquímicos combinados (EC/EAOPs). Se ha estudiado la degradación de 4 colorantes azoicos alimentarios (Ponceau 4R o Rojo Ácido 18 (AR 18), Rojo Allura AC (AR AC), Carmoisina o Rojo Ácido 14 (AR 14) y Tartrazina o Amarillo Ácido 23 (AY 23), los cuales no sólo muestran efectos en el medio ambiente sino que son

considerados como potencialmente peligrosos debido a que se relacionan con la hiperactividad en niños.

En primer lugar, se exploró la capacidad del cátodo de difusión de aire para generar peróxido de hidrógeno en las condiciones de trabajo, puesto que los diferentes procesos estudiados en la presente Tesis se basan en la electrogeneración de esta especie. La acumulación de H_2O_2 se determinó primero a escala laboratorio en una celda monocompartimental y después se escaló a una planta pre-piloto. En los dos sistemas se obtuvieron curvas similares donde se pueden identificar dos regiones: la primera región muestra una buena linealidad entre la cantidad de H_2O_2 y el tiempo, de acuerdo con la ley de Faraday, mientras que en la segunda etapa la velocidad de acumulación de H_2O_2 disminuyó gradualmente y alcanzó un estado estacionario, al igualarse la velocidad de formación del H_2O_2 en el cátodo con la de su destrucción anódica para dar O_2. La concentración de H_2O_2 crece al aumentar la densidad de corriente, mientras que decrece en presencia de Fe^{2+} que cataliza la descomposición del H_2O_2 mediante la reacción de Fenton. Como conclusión importante, el H_2O_2 está siempre presente en exceso en la disolución, lo que indica que el sistema mantiene la máxima producción de $^{\bullet}OH$ permitiendo una destrucción rápida de los contaminantes presentes en la disolución.

Además, se estudió el efecto de diferentes iones (SO_4^{-}, Cl^{-}, y ClO_4^{-}) que pueden estar presentes en las aguas residuales industriales sobre la acumulación de H_2O_2 en una planta pre-piloto equipada con un reactor BDD/cátodo de difusión. Se observó una evolución similar del H_2O_2 en SO_4^{-} y ClO_4^{-}, indicando que en ambos electrolitos la principal vía de descomposición del H_2O_2 es la misma y que los aniones no participan en su destrucción. En cambio, la velocidad de acumulación disminuye considerablemente en medio cloruro debido a la destrucción del H_2O_2 por parte del HClO generado.

En lo que se refiere a los colorantes alimentarios, se inició con el estudio del tratamiento de disoluciones acuosas sintéticas contaminadas con Ponceau 4R mediante diferentes EAOPs. La aplicabilidad de estos procesos para la decoloración y la mineralización de las disoluciones se evaluó trabajando con una celda monocompartimental o dividida de 130 mL, utilizando un ánodo de BDD o Pt y un cátodo de difusión de aire o acero (SS). Se evaluó la reactividad del colorante en diferentes electrolitos soporte como Na_2SO_4, NaCl, $NaNO_3$ y $LiClO_4$, mediante diferentes EAOPs como la electrooxidación sin/con electrogeneración de H_2O_2 (EO y

EO-H_2O_2, respectivamente), el electro-Fenton (EF) y el fotoelectro-Fenton (FEF). La decoloración total se consiguió independientemente del ánodo, cátodo, proceso y medio empleados, lo que confirma la extraordinaria capacidad de los EAOPs para eliminar la contaminación visual provocada por los colorantes azoicos. La comparación entre los EAOPs en medio sulfato (**Figura R1a**) evidenció una decoloración muy lenta mediante EO y EO-H_2O_2 con Pt, necesitándose más de 480 min para conseguir la decoloración total. El uso de un ánodo de BDD en lugar de uno de Pt favoreció de forma apreciable los procesos de decoloración, con una tendencia similar utilizando un cátodo de acero o de difusión de aire y con una decoloración total en 450 min debido a la mayor reactividad del BDD($^{\bullet}$OH) frente al Pt($^{\bullet}$OH). La decoloración mediante los EAOPs basados en la reacción de Fenton (EF y FEF) era más rápida que por EO y EO-H_2O_2, consiguiéndose una eliminación total del color en aproximadamente 60 min, independientemente del ánodo utilizado. El rendimiento superior de los procesos EF y FEF se explica por: (i) la concentración mucho más alta de $^{\bullet}$OH gracias a la simultaneidad de dos vías de generación y (ii) la minimización de las limitaciones de difusión que son inherentes a la EO. En EO, la acción de los $^{\bullet}$OH se limita a la superficie del electrodo y, por lo tanto, los colorantes tienen que alcanzar la superficie para ser oxidados. En cambio, en los EAOPs basados en la reacción de Fenton, los colorantes son destruidos por los $^{\bullet}$OH en el ánodo y en el seno de la disolución. El efecto positivo de la luz UVA en FEF no se manifestó de manera muy apreciable. De hecho, la velocidad de decoloración en EF y FEF era prácticamente igual. En medio ClO_4^- se obtuvieron perfiles de decoloración muy similares a los expuestos en SO_4^{2-}.

En medio NO_3^- se observó un comportamiento diferente en los procesos EO y EO-H_2O_2 con BDD, los cuales requirieron 180 y 120 min, respectivamente, para la total decoloración. Esto supone una mejora apreciable en comparación con las tendencias en SO_4^{2-} y ClO_4^-. Se verificó la estabilidad de los iones NO_3^- en EO y EO-H_2O_2 con Pt y BDD, surgiendo así una hipótesis para explicar este comportamiento: el NO_3^- se puede adsorber sobre la superficie del ánodo y/o cátodo de acero, lo cual podría bloquear parcialmente algunos sitios activos, aumentando así la densidad de corriente correspondiente y revirtiendo en último término en una aceleración de la decoloración.

En medio Cl^- se observó un comportamiento muy diferente. Los ocho EAOPs condujeron a la decoloración total en sólo 15-25 min debido a la oxidación predominante por cloro activo generado en el seno de la disolución. Los cuatro sistemas

con BDD permitieron una decoloración ligeramente más rápida, lo cual se relaciona con la acción simultánea del BDD($^{\bullet}$OH).

En cuanto a la mineralización, ésta fue más rápida en el orden: EO ~ EO-H_2O_2 con Pt << EF con Pt < EO con BDD < EO-H_2O_2 con BDD < EF con BDD < FEF con Pt ~ FEF con BDD en los medios con SO_4^{2-} o ClO_4^-. En SO_4^{2-}, la utilización de BDD en lugar del Pt para el proceso EO favoreció considerablemente los procesos de degradación (**Figura R1b**).

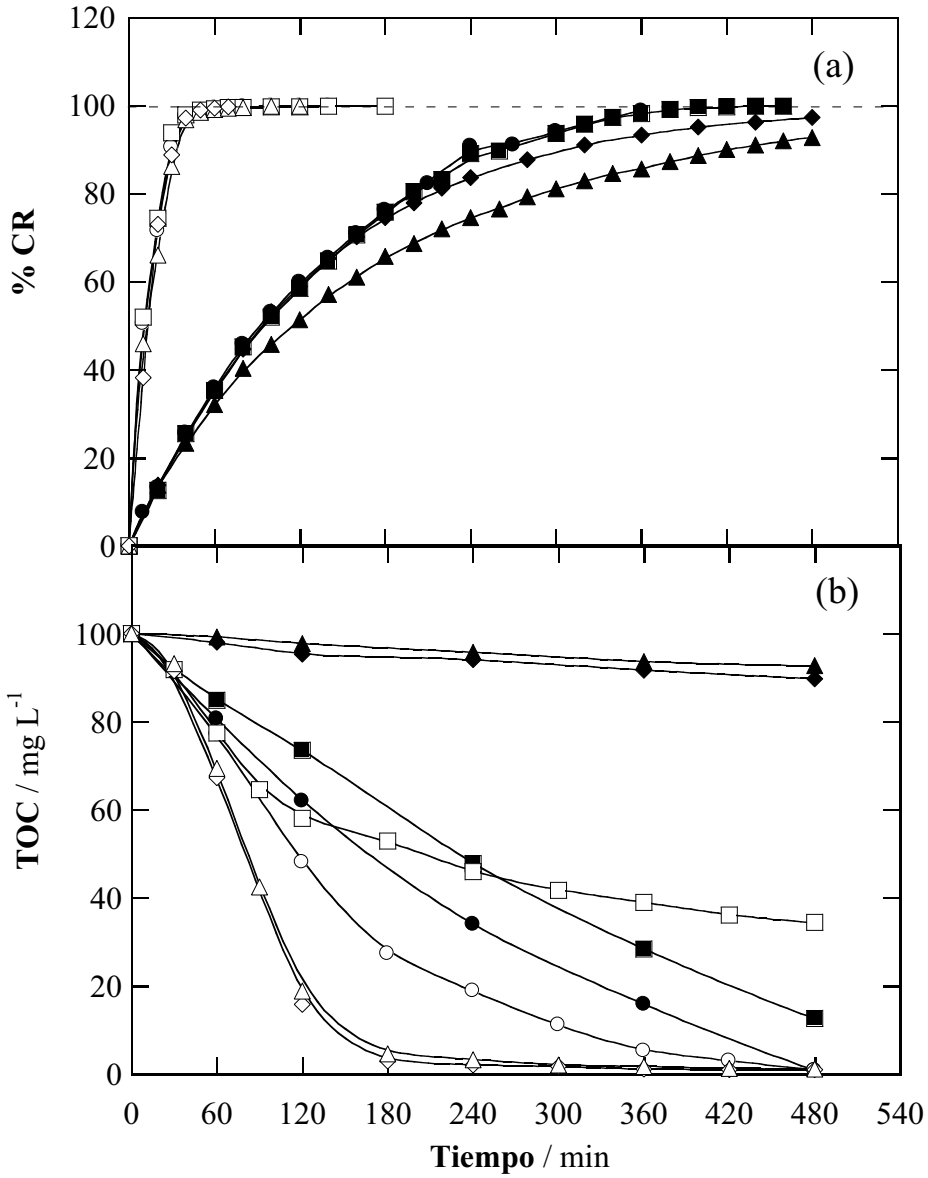

Figura R1. Porcentaje de decoloración y (b) descenso del TOC frente al tiempo de electrolisis para la degradación de 130 mL de disolución de Ponceau 4R en Na_2SO_4 0,05 M a pH 3,0 y 300 mA. Proceso: (●) EO-H_2O_2-BDD, (■) EO-BDD, (◆) EO-H_2O_2-Pt, (▲) EO-Pt, (○) EF-BDD, (□) EF-Pt, (◇) FEF-BDD y (△) FEF-Pt. Los procesos EF y FEF se realizaron en presencia de Fe^{2+} 0,5 mM.

Los resultados obtenidos pusieron de manifiesto la baja capacidad del Pt para mineralizar el colorante y sus productos de degradación mediante EO, sólo dando lugar a un 10% de mineralización en 480 min. El ánodo de BDD fue capaz de conseguir la mineralización completa del colorante y sus intermedios en 480 min en las mismas condiciones. Aparecieron diferencias notables en medio NO_3^-, de acuerdo con los resultados comentados anteriormente. En comparación con los medios de SO_4^{2-} y ClO_4^-, el tratamiento en medio NO_3^- por EO-BDD y EO-H_2O_2-BDD aceleró la degradación. Por ejemplo, el TOC se redujo en un 82% en NO_3^- respecto al 60-65% en SO_4^{2-} y ClO_4^- después de 240 min en el tratamiento EO-H_2O_2-BDD. Por otra parte, en todos los medios se observó un rápido descenso del TOC en el proceso EF-Pt en presencia de 0,5 mM de Fe^{2+}, pero a partir de un cierto tiempo la mineralización se ralentizó. La baja mineralización en el proceso de EF-Pt a tiempos largos puede ser atribuida a la formación de productos que no se pueden oxidar fácilmente con los radicales hidroxilo formados en la superficie del ánodo de Pt y en el seno de la disolución por la reacción de Fenton, como por ejemplo los complejos de Fe(III) con los ácidos carboxílicos. En comparación, el proceso EF-BDD llevó a una mineralización más rápida. Este comportamiento está relacionado con la mayor capacidad oxidativa de los reactivos BDD($^\bullet$OH), capaces de mineralizar los complejos de Fe(III) con los ácidos carboxílicos. La irradiación con luz UVA en el proceso FEF mejoró considerablemente la mineralización, permitiendo una mineralización total en 240 min independientemente del ánodo utilizado. La superioridad del proceso FEF se explica por: (i) la reducción fotolítica de los hidroxocomplejos de Fe(III), comportando una mayor producción de radicales hidroxilos y la regeneración del Fe^{2+} y (ii) la fotodegradación de intermedios y de complejos de Fe(III) con los ácidos carboxílicos. En general, en medio Cl^- se observó una disminución de la eficiencia de mineralización en todos los EAOPs, lo cual se relaciona con el consumo parcial del radical $^\bullet$OH por parte del Cl^- para formar especies menos oxidantes y la formación de cloroderivados refractarios.

Para dilucidar la posible contribución de los diferentes electrodos en los procesos de decoloración y mineralización, se investigó la EO de disoluciones de Ponceau 4R en celda no dividida y dividida. Los resultados mostraron tendencias similares en ambas celdas con el colorante en el anolito, indicando la contribución insignificante de la reducción catódica. Sin embargo, un experimento adicional utilizando una celda dividida con hilo de Pt (ánodo) y placa de acero (cátodo) donde la disolución del

colorante se colocó en el catolito confirmó la existencia de tal reducción catódica, si bien las moléculas del colorante tienden a ser destruidas mucho más rápidamente en el ánodo, como se verificó en experimentos en celda divida. En conclusión, la pequeña contribución de la reducción catódica del colorante y/o sus derivados puede ser considerada como irrelevante o ligeramente positiva.

Dado que las aguas residuales generalmente contienen grandes cantidades de iones Cl^- y SO_4^{2-}, se investigó la eficacia de los EAOPs en mezclas de sulfato/cloruro. Las disoluciones con 100% SO_4^{2-} se decoloraron en 50 min, mientras que el aumento gradual de la concentración de Cl^- aceleró progresivamente la decoloración gracias a la participación de cloro activo, hasta obtener una decoloración total en 15-25 min a concentraciones de Cl^- mayores del 60%. Sin embargo, el aumento de Cl^- era claramente perjudicial para la mineralización. Así, el aumento progresivo del porcentaje de Cl^- provocó una eliminación más lenta del TOC, aunque el uso de menos del 60% de Cl^- siempre conllevó a una mineralización total en 240 min. Puede así concluirse que las disoluciones de Ponceau 4R pueden ser tratadas con una gran eficacia dentro de un gran rango de concentraciones de iones inorgánicos.

Tras el estudio comparativo de los diferentes EAOPs, se amplió el estudio a la investigación de la cinética de desaparición del colorante, la identificación de compuestos formados durante el tratamiento y la evaluación del efecto de otras variables muy importantes utilizando un ánodo de BDD y un cátodo de difusión de aire. Se evaluó el efecto de la corriente aplicada, la concentración de Na_2SO_4 como electrolito soporte y la concentración inicial de colorante sobre la decoloración y mineralización del Ponceau 4R usando agua ultrapura. Se estudió la influencia de la corriente aplicada degradando disoluciones ácidas con 254 mg L^{-1} de Ponceau 4R, Na_2SO_4 0,05 M y Fe^{2+} 0,5 mM mediante el proceso FEF. Se alcanzó la decoloración total después de 70, 60, 50, 40 min a 33,3, 66,6, 100 y 150 mA cm^{-2}, respectivamente. Este comportamiento se relaciona con el aumento de la velocidad de las reacciones en los electrodos que implica la producción de más BDD($^{\bullet}OH$) y H_2O_2, la cual conduce a su vez a una mayor acumulación de $^{\bullet}OH$ en el medio. Se observó mejor el efecto positivo en la degradación cuando aumenta la corriente al evaluar la cinética de degradación del colorante. El tiempo para la desaparición del Ponceau 4R disminuyó de 40 a 25 min cuando la corriente aumentó de 33,3 a 150 mA cm^{-2}. Esto confirma la gran capacidad del proceso FEF, pero también revela la formación de intermedios coloreados

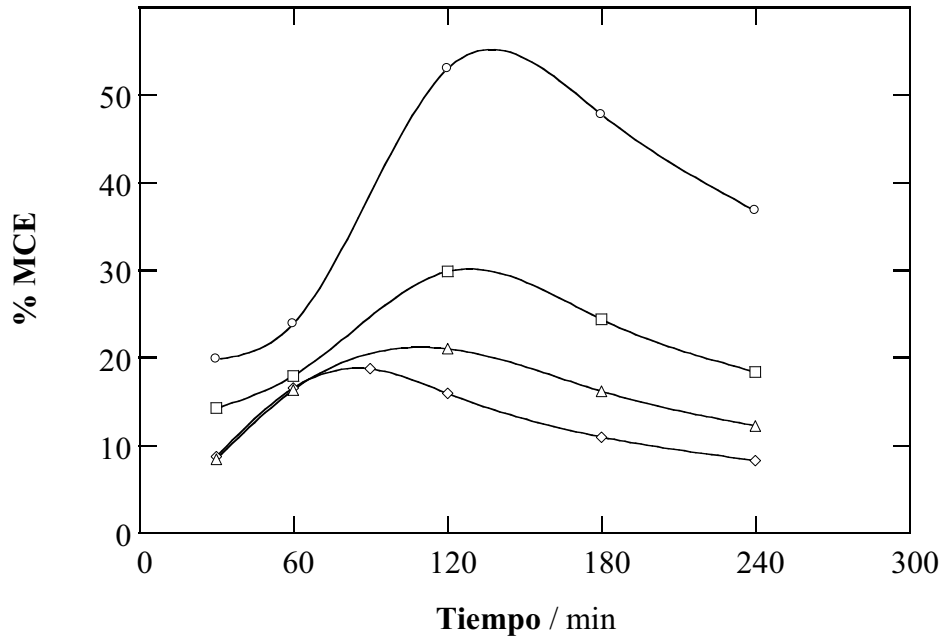

Figura R2. Efecto de la intensidad de corriente sobre la eficiencia de corriente de mineralización para el tratamiento de 130 mL de disoluciones de 254 mg L^{-1} de Ponceau 4R en Na_2SO_4 0,05 M con Fe^{2+} 0,5 mM a pH 3,0 y 25 °C mediante FEF-BDD. Densidad de corriente aplicada: (○) 33,3 mA cm^{-2}, (□) 66,6 mA cm^{-2}, (△) 100 mA cm^{-2} y (◇) 150 mA cm^{-2}.

ya que en todos los casos el Ponceau 4R desapareció antes de conseguirse la decoloración total. La cinética de degradación del colorante siempre obedeció una reacción de pseudo primer orden, con una constante de velocidad aparente (k_{app}, 10^{-2} min^{-1}) de 11,39 ± 1,74, 13,28 ± 1,26, 16,76 ± 0,96 y 18,60 ± 2,56 a 33,3, 66,6, 100 y 150 mA cm^{-2}, respectivamente. En cuanto a la mineralización, el incremento de la corriente produjo un aumento gradual de la velocidad de descenso de TOC, alcanzando mayores porcentajes de eliminación a menores tiempos de tratamiento. En contrapartida, el incremento de la corriente causó un descenso de la MCE debido al aumento de las reacciones parásitas de los radicales hidroxilo generados (**Figura R2**).

Con el fin de verificar la influencia de la concentración del electrolito soporte, se llevaron a cabo experimentos a concentraciones entre 0,01 y 0,03 M de Na_2SO_4. En todos los casos se obtuvo una decoloración total a los 70 min. Sin embargo, se encontró un aumento de la velocidad de decoloración a concentraciones extremas (muy bajas y muy altas), lo cual se atribuye a lo siguiente: (i) a concentraciones bajas, la disminución de las reacciones parásitas tales como la oxidación de los iones SO_4^{2-} para generar un oxidante más débil como el ion $S_2O_8^{2-}$ y (ii) a concentraciones altas, el mayor transporte

del colorante, que es un compuesto iónico, en un medio de alta conductividad. En cambio, su efecto sobre los perfiles de mineralización fue insignificante. También se comprobó la influencia de la concentración inicial de colorante, entre 127 y 1270 mg L^{-1} de Ponceau 4R. Se obtuvo una decoloración y mineralización completas en todos los casos, requiriendo tiempos desde 20 a 240 min y desde 135 a 480 min, respectivamente.

La mineralización del Ponceau 4R condujo a la conversión de los heteroátomos (N y S) presentes en la molécula en iones inorgánicos, tales como nitrato, amonio y sulfato. Los análisis mediante cromatografía iónica revelaron que los átomos de N que forman el enlace –N=N– se transforman preferentemente en iones NO_3^- (50%) y, en menor medida, en iones NH_4^+ (25%). Un gran porcentaje se pierde en forma de productos volátiles como N_2 y N_xO_y. Todos los átomos de S se convirtieron en iones SO_4^{2-} (100%). Mediante los análisis de disoluciones de Ponceau 4R tratadas por EAOPs con BDD mediante GC-MS con columna polar y apolar, se consiguió identificar 22 intermedios con 1 o 2 anillos aromáticos. En base de los diferentes intermedios detectados se ha propuesto un esquema de reacción que incluye diferentes caminos. La degradación electroquímica del Ponceau 4R implica reacciones competitivas como la rotura de los enlaces –N=N– y C–N y etapas de desulfonación, hidroxilación, condensación, ciclación y otros reacciones de oxidación. Se identificaron los ácidos carboxílicos formados durante el proceso de degradación por GC-MS y HPLC de exclusión iónica, detectándose los ácidos oxálico, oxámico, tartárico, fórmico, fumárico, tartrónico, maleico y propanoico. Los ácidos oxálico y oxámico fueron los productos más persistentes.

Para acabar con el estudio del Ponceau 4R, se evaluó la oxidación electroquímica del Ponceau 4R en agua real con el fin de investigar la influencia de la composición de efluentes reales sobre la decoloración, cinética de degradación y mineralización. En matrices de agua real, se alcanzó la decoloración completa después de 180, 100 y 70 min mediante EO-H_2O_2, EF y FEF, respectivamente, de acuerdo con la relativa capacidad oxidativa de cada método. El tiempo necesario en el proceso FEF era similar al encontrado para el tratamiento en agua ultrapura bajo las mismas condiciones, lo que significa que la composición del agua real no influye en la decoloración. Se confirmó la formación de intermedios coloreados, ya que el Ponceau 4R desapareció después de 150 min en EO-H_2O_2 y en sólo 40 min en EF y FEF. En cuanto a la mineralización, a 360 min se alcanzó el 57%, 74% y 100% de eliminación del TOC por los tres métodos,

respectivamente. Estos resultados confirman la viabilidad del proceso FEF para el tratamiento de efluentes reales.

Se estudió a continuación la degradación del colorante AR AC mediante diferentes EAOPs en celda monocompartimental a escala de laboratorio. La comparación entre los diferentes EAOPs estudiados confirmó la lenta decoloración de la disolución mediante el proceso EO-H_2O_2, así como su gran velocidad para los EAOPs basados en la reacción de Fenton, con una decoloración total en sólo 30-35 min debido a la doble vía de generación de los radicales. Esto confirma la superioridad de estos últimos EAOPs en cuanto a la eliminación del color. Los valores promedio de las constantes de velocidad de decoloración aparentes (k_{dec}), junto con sus intervalos de confianza (95%), se recogen en la **Tabla R1**. De acuerdo con las constantes de velocidad, la decoloración mejoró en el orden EO-H_2O_2-Pt < EO-H_2O_2-BDD << EF-Pt ≈ EF-BDD ≤ FEF-Pt ≈ FEF-BDD. Al estudiar la mineralización, se encontró que la capacidad oxidativa de los EAOPs en medio sulfato aumentaba en el orden EO << EF < FEF, tanto con Pt como con BDD, confirmando la superioridad del proceso FEF. Esta tendencia se refleja también en el valor de la MCE.

Tabla R1. Constante de velocidad de pseudo primer orden para la decoloración (k_{dec}, 10^{-2} min^{-1})[a], porcentaje de eliminación de TOC (360 min) y valor máximo de MCE para el tratamiento de 130 mL de 230 mg L^{-1} AR AC en Na_2SO_4 0,05 M a pH 3,0 y 100 mA cm^{-2} mediante varios EAOPs.

Proceso	Ánodo	k_{dec}	%TOC eliminado	% MCE
EO-H_2O_2	Pt	0,44±0,07	0.6	0.1
	BDD	0,66±0,03	74	9
EF	Pt	6,47±1,40	58	9
	BDD	6,66±3,00	88	13
FEF	Pt	7,44±2,54	95	18
	BDD	7,33±1,57	98	22

[a] Determinado con un intervalo de confianza del 95% utilizando 10-12 puntos experimentales entre el 0% y 90% de eliminación de color para cada ensayo.

Los resultados obtenidos ponen de manifiesto que el proceso FEF es el más potente y eficaz de los EAOPs para degradar AR AC en medio sulfato. Se observó una mineralización casi total con una tendencia similar para el proceso FEF en NO_3^- y ClO_4^-, mientras que en Cl^- la mineralización se inhibió por la posible formación de cloroderivados recalcitrantes.

Para este colorante también se examinó el efecto de parámetros importantes como la intensidad aplicada y la concentración inicial de colorante sobre la cinética de decoloración y mineralización en el proceso FEF-BDD. Se encontró que la decoloración y mineralización totales se alcanzaban a tiempos inferiores al aumentar la intensidad y disminuir la concentración inicial de colorante. Sin embargo, se observó asimismo una disminución de la MCE debido a la aceleración de las reacciones parásitas en ambas situaciones. A partir de estos resultados se puede concluir que una mayor intensidad no siempre mejora las condiciones de tratamiento, puesto que disminuye la MCE y además aumenta el consumo energético, aunque resulta preferible tratar altas concentraciones de colorantes en el proceso FEF.

Los productos aromáticos primarios detectados por GC-MS durante el tratamiento de AR AC mediante FEF-BDD en medios SO_4^{2-} y Cl^- revelaron la presencia de intermedios hidroxilados y/o clorados. En medio Cl^-, la cloración junto con la hidroxilación, desmetilación y carboxilación fueron las reacciones predominantes, dando lugar a 4-clorocatecol, 2,5-dicloro-1-metoxi-4-metilbenceno y ácido 3,4-diclorobenzoico. Esto confirma que las especies de cloro activo conducen a la formación de cloroderivados recalcitrantes. Sin embargo, en medio SO_4^{2-}, la degradación del colorante y sus intermedios se debía principalmente al ataque del radical $^{\bullet}OH$, el cual conduce a la formación de compuestos como la 2-metoxi-5-metil-*p*-benzoquinona y el ácido 4-metoxi-3-hidroxibenzoico. De la misma manera que en el caso del Ponceau 4R, la ruptura de los compuestos aromáticos condujo a la formación de ácidos carboxílicos de cadena corta. Al contener en su estructura molecular átomos de S y N, el proceso de degradación conllevó la generación de iones inorgánicos como NH_4^+, NO_3^- y SO_4^{2-}.

En vista de los resultados prometedores obtenidos a escala de laboratorio, se llevó a cabo el tratamiento de colorantes en una planta pre-piloto de 2,5 L de capacidad para comprobar la posible viabilidad de los EAOPs a escala industrial. Primero se estudió la degradación del colorante AR AC utilizando un reactor filtro-prensa de Pt/cátodo de

difusión mediante los procesos EF y SFEF. Se consiguió la decoloración total después de 60 min de EF y 40 min de SFEF. La ligera aceleración en SFEF puede deberse a la generación adicional de radical $^{\bullet}OH$ inducida por la reacción de fotorreducción de complejos de Fe(III). Al considerar la mineralización, el proceso EF presentó ciertas limitaciones al alcanzarse un porcentaje de mineralización inferior al 50%. En cambio, en el proceso SFEF se observó una mineralización casi total a los 240 min. Este hecho se asocia al efecto sinérgico que ejerce la irradiación UVA de la luz solar, la cual puede fotodegradar los complejos formados entre Fe(III) y los ácidos carboxílicos. El estudio del efecto de los parámetros experimentales en el proceso SFEF permitió concluir que las mejores condiciones de tratamiento implican bajos valores de densidad de corriente y altas concentraciones de contaminantes, puesto que en estas condiciones se consigue una mineralización más eficiente y un consumo energético mucho menor.

El análisis GC-MS de las disoluciones de AR AC tratadas por EAOPs en medio sulfato en la planta pre-piloto permitió la identificación de diferentes intermedios aromáticos de degradación. A partir de ellos se propuso una secuencia de reacción para la mineralización de AR AC mediante los diferentes EAOPs, la cual involucra 3 caminos simultáneos: (i) rotura del enlace C–N entre el naftaleno y el grupo azo, seguido de hidroxilación, produciendo naftalentiol que posteriormente puede ser oxidado a ácido ftálico, (ii) rotura del enlace C–N entre el anillo benceno y el grupo azo con desmetilación e hidroxilación del anillo benceno en varias posiciones, mientras la oxidación del $–CH_3$ produce grupos -CHO y -COOH y (iii) formación de diferentes *N*-derivados resultantes de la rotura del grupo -N=N- y del enlace C–N junto con hidroxilación y otras reacciones de oxidación, así como ciclación interna para dar heterociclos. Finalmente, se forman el 3,4-dihidroxibenzaldehído y el 2,4,5-trihidroxibenzaldehído a partir de la degradación de varios intermedios. Los análisis con HPLC de exclusión iónica permitieron detectar 9 ácidos carboxílicos de cadena corta (C_1-C_4) procedentes de la rotura y apertura de los anillos aromáticos, mientras que dos ácidos carboxílicos C_5 y C_6 fueron identificados por GC-MS.

Para adquirir una mejor comprensión de la capacidad de los EAOPs y del ánodo de BDD para oxidar los colorantes alimentarios, se llevó a cabo un estudio comparativo en una planta pre-piloto con un reactor electroquímico equipado con un ánodo de BDD. En primer lugar se estudió la degradación de la Carmoisina mediante los procesos EO y EF en medios SO_4^{2-}, Cl^- y ClO_4^-. En el tratamiento por EO, los resultados evidenciaron

que el aumento de *j* y de la concentración de Cl^- implica una aceleración de la decoloración que se puede relacionar a una mayor producción de BDD($^\bullet$OH) y a la gran eficiencia de producción de cloro activo en el ánodo de BDD, siendo mayor a medida que aumenta la concentración de NaCl. En EF, la disolución se decoloró completamente en 25 min en medio Cl-, tiempo similar al obtenido en EO, lo cual significa que el colorante y sus intermedios coloreados son rápidamente oxidados por el cloro activo. En cambio, en SO_4^{2-} y ClO_4^-, las disoluciones se decoloraron completamente a los 60 min debido a la acción del radical $^\bullet$OH producido por la reacción de Fenton. La gran cantidad de $^\bullet$OH generada permitió un rápido descenso del TOC en todos los medios. Sin embargo, el porcentaje de mineralización se mantuvo casi constante después de 180 min, alcanzando un máximo del 76% a los 480 min debido a la generación de intermedios estables. Se estudió el efecto de parámetros clave como la *j* y la concentración de colorante, encontrándose comportamientos similares a los mencionados anteriormente para los otros colorantes. Los análisis mediante GC-MS permitieron la identificación de 15 intermedios aromáticos, seis derivados de benceno y cuatro de naftaleno, junto con productos de condensación relacionados con un indano, dos indoles y dos derivados de benzofurano. Muchos de estos compuestos contienen grupos carbonilo y/o hidroxilo procedentes del ataque del radical hidroxilo sobre el anillo aromático. La gran variedad de productos aromáticos primarios revela la complejidad del proceso de degradación de la Carmoisina bajo la acción del BDD($^\bullet$OH) y/o del $^\bullet$OH. También se detectaron ácidos carboxílicos e iones inorgánicos.

Dado que en condiciones normales las aguas contaminadas con colorantes contienen más de uno de estos contaminantes y varios iones inorgánicos, se estudió la degradación de una mezcla de los 3 colorantes rojos ensayados, Ponceau 4R, AR AC y Carmoisina, en diferentes electrolitos soporte y en varias matrices de agua. En primer lugar, se realizó un estudio comparativo a escala de laboratorio sobre la degradación de 100 mg L^{-1} TOC de la mezcla en Na_2SO_4 0,05 M a pH 3,0 y a 33,3 mA cm^{-2} mediante EF-Pt, EF-BDD, FEF-Pt y FEF-BDD. Se consiguió la decoloración completa después de 50 y 45 min de EF y FEF, respectivamente, independientemente del ánodo utilizado. La presencia de la luz UVA favoreció además la mineralización, obteniéndose una reducción de TOC del 64%, 83%, 96% y 99% en EF-Pt, EF-BDD, FEF-Pt y FEF-BDD, respectivamente. Estos resultados indican que el proceso FEF-BDD es el mejor para decolorar y mineralizar la mezcla de colorantes. A continuación, se amplió el estudio a

una matriz de agua real para evaluar el efecto de los iones inorgánicos y de los compuestos orgánicos naturales. Por ello, se degradó la mezcla de colorantes mediante FEF-BDD en matrices de agua real y simulada. Esta última se preparó basándose en la caracterización previa del agua real (1,30 mM SO_4^{2-} + 11,5 mM Cl^- + 0,02 mM NO_3^-) obtenida de una planta municipal de tratamiento de aguas. La decoloración en agua simulada fue más lenta que en agua ultrapura, lo cual puede relacionarse con: (i) su menor conductividad, la cual provoca una caída óhmica que desfavorece la formación eficaz de los oxidantes, (ii) la reacción del radical $^{\bullet}OH$ con el ión Cl^- para dar lugar a oxidantes más débiles ($Cl^{\bullet}$ y otros) y (iii) la destrucción parcial del HClO generado en presencia de H_2O_2. Por otra parte, en agua real se obtuvieron perfiles de decoloración y mineralización similares a los de agua simulada, indicando que la carga orgánica natural contenida en el agua real tiene poca influencia sobre el proceso degradativo. Así, la capacidad oxidativa de los EAOPs depende principalmente del contenido de iones inorgánicos, ya que determina la cantidad de especies oxidantes disponibles. Estos resultados permiten concluir que el proceso FEF es capaz de decolorar y mineralizar con eficacia mezclas de colorantes en matrices de agua real.

Se estudiaron los mismos procesos en la planta pre-piloto de 2,5 L equipada con un reactor BDD/cátodo de difusión. Con este sistema se siguió la decoloración y mineralización de la mezcla de colorantes en agua sintética con Na_2SO_4 0,05 M a pH 3,0 y 100 mA cm^{-2}. Los resultados evidenciaron una decoloración muy lenta en el proceso EO-H_2O_2-BDD, alcanzándose sólo el 79% de decoloración después de 480 min. En cambio, se consiguió la decoloración total después de sólo 40 min mediante EF-BDD y SFEF-BDD. La eliminación del TOC siguió el orden EO-H_2O_2-BDD < EF-BDD < SFEF-BDD. A los 480 min, sólo se alcanzó un 51% de mineralización para el primer proceso, aumentando hasta el 67% para el segundo. La irradiación con la luz solar en el proceso SFEF aumentó la velocidad de mineralización debido a la fotodegradación de los complejos de Fe(III)-carboxilato, lográndose un 97% de mineralización a los 240 min. Estos resultados confirman los obtenidos a escala de laboratorio, siendo el proceso SFEF-BDD el mejor para decolorar y mineralizar mezclas de colorantes. Se encontró el menor consumo energético de 0,607 kWh (g TOC)$^{-1}$ a 300 min y 100 mA cm^{-2} en SFEF, con valores muchos más altos de 1,94 y 1,46 kWh (g TOC)$^{-1}$ para EO-H_2O_2-BDD y EF-BDD, respectivamente. También se estudió el efecto de varios parámetros, incluyendo la densidad de corriente, la concentración inicial de colorantes y la

naturaleza y concentración del electrolito soporte. Los resultados obtenidos concuerdan con los encontrados para FEF-BDD en la matriz de agua real a escala laboratorio y demuestran la viabilidad del proceso SFEF-BDD para el tratamiento de aguas residuales a nivel industrial.

Con el objetivo de obtener información adicional sobre las vías de degradación involucradas en el tratamiento de disoluciones de colorantes mediante EAOPs, se analizaron los ácidos carboxílicos, iones inorgánicos e intermedios aromáticos formados. Se identificaron y cuantificaron diferentes ácidos carboxílicos como maleico, fumárico, tartrónico, fórmico, oxálico y oxámico. Los tres primeros ácidos proceden de la rotura oxidativa de los anillos benceno y naftaleno de los colorantes iniciales, y a su vez se convierten en ácidos oxálico y fórmico. El ácido oxámico se forma a partir de los *N*-derivados. Los ácidos fórmico, oxálico y oxámico son los últimos productos ya que se transforman directamente en CO_2. El ácido oxálico fue el que se acumuló en mayor concentración, pero sus complejos de Fe(III) se fotodegradaron completamente por la radiación UVA de la luz solar. El proceso de mineralización conllevó la generación de iones inorgánicos como SO_4^{2-}, NH_4^+ y NO_3^-. Los átomos de S se detectaron como SO_4^{2-} con una concentración de 0,57 mM (57% del S inicial), 0,96 mM (97% del S inicial) y 0,99 mM (100% del S inicial) después de 300 min de EO-H_2O_2-BDD, EF-BDD y SFEF-BDD, respectivamente. Respecto a los átomos de N, se detectaron concentraciones muy bajas de NH_4^+ (< 0,01 mM) en todos los casos, junto con una mayor acumulación de NO_3^-. Los análisis por GC-MS de la mezcla tratada por SFEF permitieron detectar 18 intermedios aromáticos resultantes de la rotura de los enlaces –N=N– y C–N y reacciones de desaminación y desulfonación. En base a los 18 intermedios aromáticos y los 6 ácidos carboxílicos detectados por GC-MS y HPLC, se ha propuesto una secuencia de reacción para la degradación de la mezcla de los 3 colorantes. La secuencia se inicia con la producción de dos compuestos de condensación, la ftalimida y la indandiona, junto con un derivado hidroxilado del anillo naftaleno, el 1,4-naftalendiol. Este diol origina entonces la quinona correspondiente, que es posteriormente hidroxilada, oxidada a ácido ftálico o transformada en 3*H*-isobenzofuran-1-ona. La destrucción de los compuestos anteriores conduce a dos caminos que consideran diversos productos bencénicos. Finalmente se genera una mezcla de ácidos carboxílicos que evolucionan a CO_2. Cabe destacar que todos los

intermedios identificados durante el tratamiento de la mezcla se detectaron durante el tratamiento individual de los 3 colorantes.

En la última parte de mi Tesis Doctoral se exponen los resultados obtenidos durante una estancia pre-doctoral de 5 meses en el *College of Environmental Science and Engineering* de la *Nankai University* (Tianjin, China) bajo la supervisión del **Prof. Dr. Minghua Zhou**. El objetivo principal de la estancia fue idear un sistema para lograr una mineralización más eficiente de los colorantes azoicos y acortar el tiempo de su tratamiento, de cara a reducir los costes relativamente elevados de operación debidos al largo tiempo que requieren los EAOPs. Esta parte se centró en el desarrollo de nuevas tecnologías acopladas EC/EAOPs, que aprovechan las mejores capacidades de cada una de ellas con el fin de lograr un tratamiento más eficiente de las aguas contaminadas. En particular, se estudió la degradación del colorante Tartrazina mediante EC y EAOPs y, una vez seleccionadas las mejores condiciones en cada caso, se diseñó un sistema acoplado para buscar su sinergia.

Los estudios se realizaron en primer lugar a escala de laboratorio, evaluándose la decoloración y la descontaminación de la disolución de Tartrazina mediante EC en diferentes electrolitos soporte (Na_2SO_4, NaCl y $NaNO_3$) a pH natural de 6,3 y a 300 mA, utilizando hierro y SS como ánodo y cátodo, respectivamente. La decoloración total en medio sulfato se consiguió en 30 min. En medio cloruro fue más rápida, requiriéndose sólo 10 min, debido a la minimización de la pasivación de la superficie de los electrodos y a la contribución de la oxidación electroquímica indirecta por el cloro activo producido. En presencia de iones NO_3^-, la velocidad de decoloración disminuyó considerablemente, alcanzándose un 65% de decoloración a los 120 min, lo cual concuerda con resultados publicados (Yildiz y col., 2007; Jiménez Izquierdo y col., 2010). El uso de un ánodo de Al en lugar de Fe en medio Cl^- condujo a una velocidad de decoloración menor. Este comportamiento tan diferente entre ambos electrodos puede explicarse por: (i) sus diferentes propiedades en cuanto a la promoción de la neutralización de las cargas y (ii) la baja capacidad de adsorción del $Al(OH)_3$ en comparación con el $Fe(OH)_n$, lo que complica el mecanismo de floculación para atrapar la materia coloidal. Se prefirió el uso del ánodo de hierro en la presente Tesis no sólo por la mejora de la coagulación, sino también por las propiedades catalíticas superiores del Fe^{2+} pensando en un acoplamiento posterior con los EAOPs basados en la reacción de Fenton. Por otra parte, la eficiencia para la eliminación de la materia orgánica

aumentó en el orden $NaNO_3$ < Na_2SO_4 < NaCl, de conformidad con la decoloración, pero ninguno de los sistemas permitió la descontaminación completa de la disolución de Tartrazina. En medio NaCl, la acción sinérgica de la coagulación por $Fe(OH)_n$ y la oxidación por cloro activo únicamente logró alcanzar un 60% de eliminación de TOC en aproximadamente 10 min, manteniéndose constante en el tiempo a partir de ese momento. Este comportamiento puede deberse a la acumulación de intermedios persistentes.

Se estudió el efecto de otros parámetros importantes como la concentración de NaCl (0,025-0,30 M), pH (3, 6.3 (natural), 9 y 11) y la corriente aplicada (50-300 mA). La variación de la concentración de NaCl no produjo cambios significativos en la decoloración, pero tuvo un efecto ligeramente positivo en la eliminación del TOC. En cuanto al pH, se sabe que la EC depende mucho de este parámetro debido a la gran variedad de equilibrios implicados. La decoloración y la descontaminación más rápidas se obtuvieron a un pH intermedio entre 6,3 y 9,0. Esto se explica por la producción de menos flóculos a pH < 6, debido a la neutralización de los iones OH^- producidos en el cátodo por los H^+ presentes en el medio. Un parámetro de control especialmente relevante es la corriente aplicada, ya que no sólo determina la cantidad de coagulante sino también la velocidad de producción de burbujas y su tamaño. Además, en medio Cl^-, la corriente tiene una gran influencia en la velocidad de electrogeneración del Cl_2 que se convierte después en $HClO/ClO^-$. Se observó una decoloración total de todas las disoluciones que era progresivamente más rápida cuando se incrementó la corriente, acortando así el proceso de 60 a 10 min al pasar de 50 a 300 mA (**Figura R3a**). Dicha dependencia se evidenció también en el proceso de mineralización. En todos los casos se alcanzó un valor máximo cercano al 60% de eliminación del TOC al final del tratamiento (**Figura R3b**). Sin embargo, ese porcentaje se alcanzó después de sólo 10-15 min a 200 y 300 mA, mientras que sólo se obtuvo un 5% en ese corto tiempo a 50 y 100 mA. Dado que se observó una tendencia similar para 200 y 300 mA, el primer valor se consideró como el óptimo para los experimentos adicionales de EC ya que, a pesar de que requería 15 min en lugar de 10 min para la decoloración total, conllevaba un consumo menor de energía. De todo ello cabe concluir que las mejores condiciones para EC se obtenían utilizando Fe como ánodo, NaCl 0,05 M a pH natural de 6,3 y a 200 mA, lo cual conducía a una decoloración total y una reducción máxima del TOC ~ 60% en sólo 15 min.

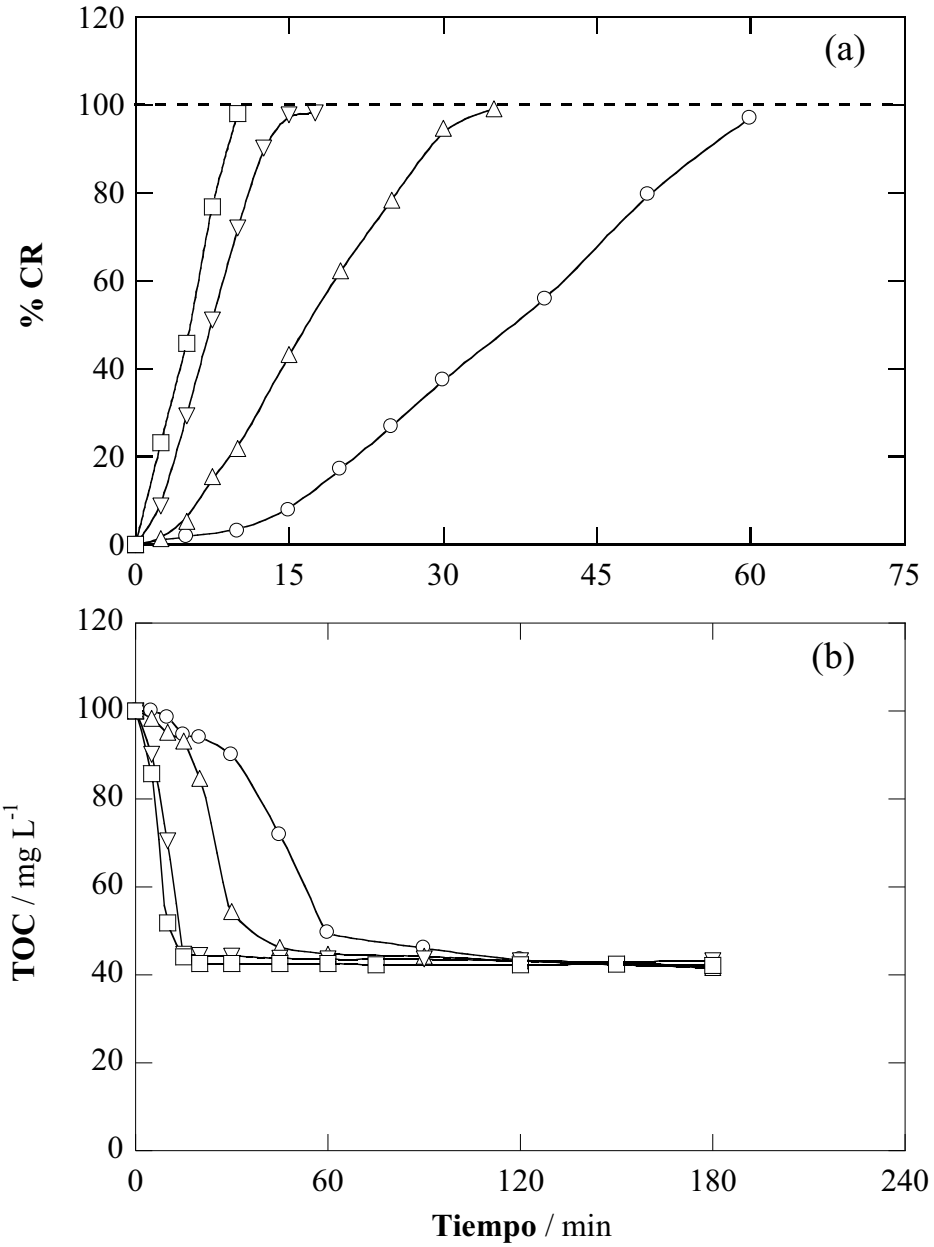

Figura R3. Efecto de la corriente aplicada sobre (a) el porcentaje de decoloración y (b) el descenso del TOC con el tiempo de electrolisis para la degradación por EC de 130 mL de 278 mg L^{-1} de Tartrazina en NaCl 0,05 M a pH natural (6,3) y: (○) 50 mA, (△) 100 mA, (▽) 200 mA y (□) 300 mA.

Después de optimizar las condiciones del tratamiento EC, se evaluó la capacidad oxidativa de los EAOPs. Se estudió el tratamiento electroquímico de la Tartrazina mediante EO, EO-H_2O_2, EF y FEF utilizando un ánodo de BDD o Pt y un cátodo de acero o difusión de aire, a pH 3,0 y 200 mA en diferentes medios. En Na_2SO_4 0,05 M, el color desapareció muy lentamente en todos los sistemas EO, necesitándose 480 min para la decoloración total con BDD y tiempos aún más largos con Pt. En cambio, la

decoloración era muy rápida para los sistemas EF y FEF, con una eliminación total del color en 25-30 min en todos los casos. La mineralización se aceleraba en el orden EO < EF < FEF. Los mismos EAOPs se evaluaron en NaCl 0,05 M, donde el tiempo necesario para la eliminación total del color en EO se redujo de > 480 min a sólo 12,5-25 min. Los métodos EF y FEF permitieron una decoloración total a un tiempo similar de 15-20 min, de manera que la diferencia entre EO y los procesos basados en la reacción de Fenton puede considerarse insignificante. Se puede entonces concluir que la presencia de cloro activo como agente decolorante disuelto en todo el volumen juega un rol esencial, preponderando sobre los radicales hidroxilo formados en la superficie del ánodo y en el seno de la disolución.

Los resultados anteriores confirman el gran interés que suscitan los EAOPs para el tratamiento de agua. Sin embargo, el largo tiempo requerido para conseguir la mineralización total constituye uno de sus principales inconvenientes para ser implementado como única etapa de tratamiento. Por lo tanto, el pre-tratamiento por EC puede concebirse como una potente solución para que sea viable y, por lo tanto, atractivo para la industria.

Una vez determinadas las condiciones óptimas de la EC y los EAOPs, se llevaron a cabo tratamientos acoplados con el mismo colorante. Las disoluciones fueron pre-tratadas mediante EC (Fe/SS) en NaCl 0,05 M a pH natural de 6,3 y a 200 mA durante 15 min. Se consiguió una decoloración total y un 60% de eliminación del TOC. A continuación, las muestras se centrifugaron y el sobrenadante se trató mediante varios EAOPs: EO (BDD/SS), EF-Pt, EF-BDD, FEF-Pt y FEF-BDD a 200mA después de la regulación del pH a 3,0. Como se puede observar en la **Figura R4**, los 5 EAOPs permitieron la mineralización progresiva de las disoluciones pre-tratadas. Los procesos EF-Pt y FEF-Pt fueron ligeramente más lentos que los procesos con BDD, alcanzándose un 86-88% de mineralización después de 315 min. Con el ánodo de BDD se consiguió una mayor degradación gracias al radical BDD($^{\bullet}$OH), alcanzándose un 92% y 95%, respectivamente. El proceso FEF-BDD permitió la descontaminación más rápida de entre todos los métodos. Para este proceso óptimo se concluyó que 200 mA era un valor suficiente de corriente aplicada, puesto que permitía una eliminación más rápida en comparación a 100 mA y una evolución casi idéntica a 300 mA. De aquí se deduce que en la degradación secuencial, la EC actúa como una etapa muy eficaz para decolorar rápidamente las disoluciones y como una fuente de catalizador para los EAOPs.

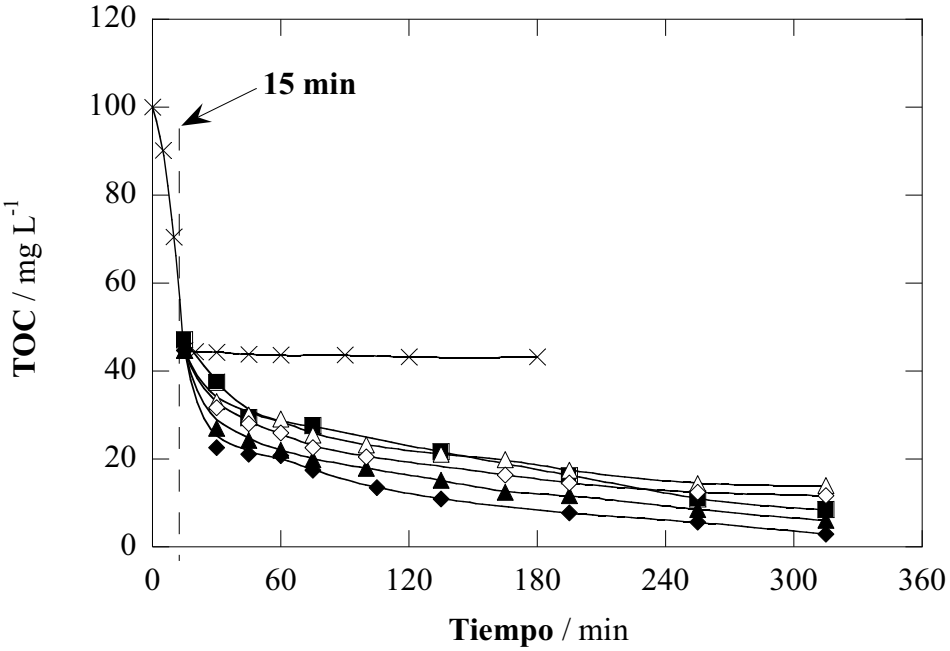

Figura R4. Descenso del TOC frente el tiempo de electrolisis para la degradación de 130 mL de 278 mg L^{-1} de Tartrazina en NaCl 0,05 M mediante procesos acoplados EC (Fe/SS, 15 min, 200 mA, a pH natural 6,3) / EAOPs (200 mA, pH 3,0). EAOP: (■) EO (BDD/SS), (▲) EF-BDD, (△) EF-Pt, (◆) FEF-BDD y (◇) FEF-Pt. (×) Descenso comparativo del TOC mediante el proceso EC.

Con el fin de identificar los principales intermedios aromáticos acumulados, se electrolizaron las disoluciones de Tartrazina utilizando el mejor acoplamiento EC/FEF-BDD en las condiciones óptimas, pero deteniendo la fase de FEF después de 10 min. El análisis de la muestras por GC-MS permitió identificar 17 intermedios que pueden agruparse en 3 grupos: (i) intermedios no hidroxilados, que se generan como resultado de la cloración progresiva de intermedios simples, (ii) intermedios monohidroxilados y (iii) intermedios dihidroxilados (en forma de fenoles y quinonas) formados por la acción de los radicales hidroxilo en la superficie del ánodo y en el seno de la disolución. Los dos últimos grupos incluyen varios hidroxibencenos policlorados (di-, tri-, tretra-, y penta-derivados), lo que se justifica por la gran capacidad del ánodo de BDD de electrogenerar cloro activo. La rotura de los anillos conduce a una mezcla de ácidos carboxílicos de cadena corta. Asimismo, los intermedios acumulados en el sobrenadante durante la primera fase de EC bajo las condiciones óptimas se analizaron por GC-MS. Se identificaron 5 intermedios, incluyendo mono/diclorobenceno y nitrobenceno, lo cual indica la capacidad de los ánodos de Fe para producir cloro activo, si bien con una concentración tan pequeña que no se pudo medir por espectrofotometría. La cloración

y/o hidroxilación de estos 5 intermedios explican la formación de algunos de los compuestos identificados durante el acoplamiento con FEF. Es importante señalar que la identificación de los 5 intermedios después de 15 min de EC, una vez que el colorante había desaparecido completamente, permite justificar la tendencia del TOC, relacionándose su valor residual (~ 40%) con derivados no coagulables.

Un paso importante para la futura implantación del sistema acoplado en la industria y los servicios públicos se dio al escalar a una planta pre-piloto de 1,85 L de capacidad. El tratamiento por EC se hizo en un tanque paralelepípedo abierto con una base trapezoidal. Se realizó un estudio sobre los diferentes modos de conexión eléctrica (MP-P, MP-S y BP-S) en diferentes electrolitos soporte (Na_2SO_4, $NaNO_3$ y NaCl). Los resultados mostraron una decoloración y eliminación del TOC más rápida en el orden $NaNO_3$ < Na_2SO_4 < NaCl, confirmando así los resultados obtenidos a escala de laboratorio. De los diferentes modos de conexión, los resultados evidenciaron que el modo BP-S era el mejor, alcanzándose un 100% de decoloración y un 50% de mineralización después de 12,5 min en medio cloruro. Como se había observado a escala de laboratorio, ninguno de los sistemas consiguió la eliminación total del TOC.

Se investigó la influencia del pH (controlado periódicamente) en la decoloración y eliminación del TOC tratando 278 mg L^{-1} de Tartrazina en NaCl 0,05 M a 1,5 A utilizando las tres configuraciones. La decoloración más rápida y la mayor eliminación del TOC se consiguieron a pH 6,3 y 9,0 en la configuración BP-S. Los experimentos posteriores de EC se llevaron a cabo a pH 6,3. También se encontró a los 10 min un aumento gradual de la eliminación del color del 11% al 53% para MP-S, del 24% al 97% para MP-S y del 35% al 98% para BP-S cuando la corriente aumentó de 0,75-2,25 A. A partir de los resultados se puede concluir que la corriente óptima es 1,5 A, vista la insignificante mejora a 2,25 A y la pobre degradación a 0,75 y 1,125 A.

Por otra parte, también se examinó la capacidad del proceso EC en la configuración BP-S para el tratamiento de disoluciones con diferentes concentraciones de colorante de 50 a 200 mg L^{-1}. Se observó una decoloración total de todas las disoluciones, requiriendo tiempos más largos al incrementar la concentración inicial del colorante. Este comportamiento puede relacionarse con la gran cantidad de colorante, la cual reacciona y/o interactúa con la misma cantidad de cloro activo y/o coagulante. En todos los casos, la eliminación máxima del TOC fue del 60%.

En cuanto a los EAOPs en esta escala pre-piloto, se llevaron a cabo utilizando un reactor equipado con (Ti)IrO_2-RuO_2/cátodo de difusión. Con este sistema se siguió la decoloración y mineralización de la Tartrazina mediante EO, EF y FEF en NaCl 0,05 M a pH 3,0 y 100 mA cm^{-2}. El estudio de los EAOPs en medio cloruro es muy interesante porque los mejores resultados de EC se habían conseguido en NaCl, como ha quedado claro anteriormente. Se observó una decoloración total de la disolución de Tartrazina después de 60 y 30 min en la EO y los EAOPs basados en la reacción de Fenton, respectivamente. El largo tiempo requerido en el proceso EO es debido a la pobre capacidad oxidativa del ánodo de (Ti)IrO_2-RuO_2, ya que los radicales $^{\bullet}OH$ generados en la superficie son quimisorbidos. Sin embargo, este ánodo es capaz de producir cloro activo capaz de transformar el colorante. La contribución de la luz UVA y del cloro activo en los procesos Fenton fue insignificante. En cambio, la irradiación con la luz UVA en el proceso FEF mejoró la velocidad de mineralización debido a la fotodegradación de los complejos de Fe(III), reduciéndose el TOC en un 90% en 360 min. La capacidad oxidativa de los tres EAOPs también se estudió en medio sulfato y nitrato. En el tratamiento FEF, se alcanzó una mineralización total a los 240-300 min en

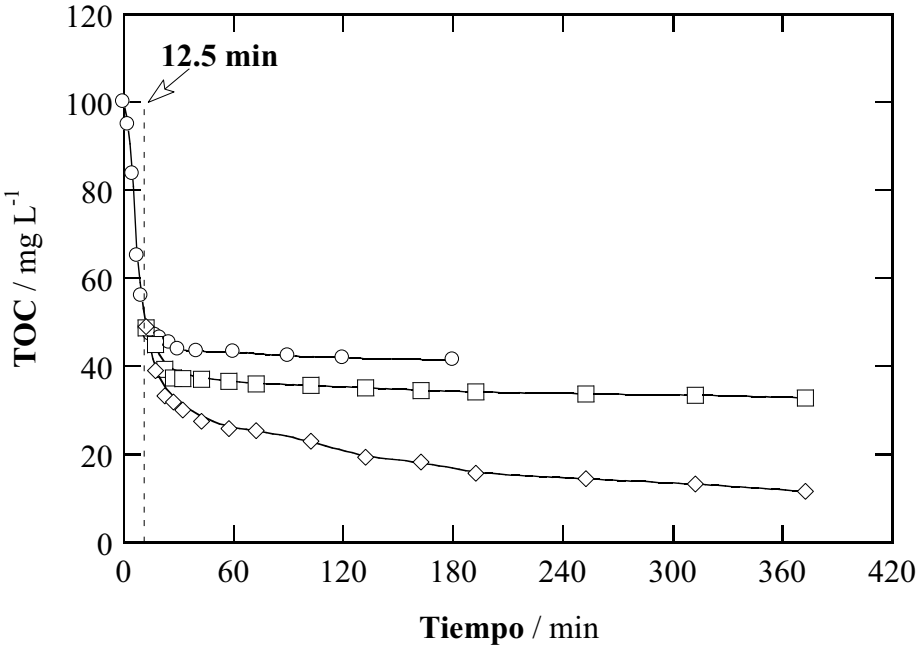

Figura R5. Descenso del TOC con el tiempo de electrolisis para la degradación de 1,85 L de 278 mg L^{-1} de disolución de Tartrazina en NaCl 0,05 M mediante procesos integrados EC (Fe/SS, 12,5 min, 1,5 A, pH natural 6,3) / EAOPs ((Ti)IrO_2-RuO_2 / cátodo de difusión de aire, 2 A, pH 3,0). EAOP: (□) EF y (◇) FEF. (○) Descenso comparativo del TOC mediante el proceso EC.

ambos medios. Este comportamiento se asocia a la formación de intermedios clorados persistentes en medio NaCl.

Una vez optimizados la EC y los EAOPs, tal y como ha quedado descrito, se evaluó el acoplamiento entre ambos para la mineralización de las disoluciones de Tartrazina. Éstas fueron primero pre-tratadas por EC en NaCl 0,05 M a 1,5 A, pH 6,3 en configuración BP-S durante 12,5 min, que garantizó la decoloración total así como un 60% de eliminación de TOC. Las disoluciones finales se filtraron y las partes liquidas se trataron por EF y FEF a 2,0 A y pH 3,0. El TOC disminuyó solamente un 60% en el sistema EC/EF (**Figura R5**), mientras que el sistema EC/FEF condujo a una mineralización más rápida, con > 90% de eliminación de TOC después de 375,5 min de tratamiento global. Este último acoplamiento constituye, en definitiva, el resultado clave de la presente Tesis Doctoral.

6. Conclusions

The present work allows establishing the followings main conclusions:

1. The concentration of H_2O_2 accumulated during the electrolyses of 0.050 M Na_2SO_4 solutions of pH 3.0 using an air-diffusion cathode and a Pt or BDD anode always tended to a steady value that depends on the applied current. The amount of H_2O_2 decreased when 0.5 mM Fe^{2+} is added to the solution due to its consumption via Fenton's reaction.
2. The use of a pre-pilot flow plant with a BDD/air-diffusion cell for electrolyses in 0.050 M SO_4^{2-} or ClO_4^- media of pH 3.0 allowed the accumulation of a similar and high H_2O_2 content, which was significantly lower in 0.050 M Cl^- because of its destruction by active chlorine species like HClO in the bulk.
3. Among the EAOPs tested in the present Thesis at lab-scale, PEF-BDD is the most efficient and promising technology for the degradation of food azo-colors like Ponceau 4R and Allura Red AC. Almost total mineralization with 96-98% TOC abatement was attained, with electrolysis time depending on the dye content and current density.
4. The MCE values increased following the same sequence as the oxidation power of the EAOPs under study: EO-H_2O_2 < EF < PEF < SPEF. The MCE value usually grew at greater initial dye and supporting electrolyte concentrations, as well as with decreasing current density. However, the efficiency dropped at long time due to the formation of refractory carboxylic acids and the decrease of organic matter load.
5. The faster decolorization of Ponceau 4R solutions in the order $SO_4^{2-} \sim ClO_4^- < NO_3^- << Cl^-$ and quicker mineralization in the order $Cl^- << SO_4^{2-} \sim ClO_4^- < NO_3^-$ have been explained by the competition between several degradation routes: (i) direct electron transfer, (ii) oxidation by M($^\bullet$OH) or $^\bullet$OH, (iii) reaction with chlorinated species, particularly active chlorine, and (iv) NO_3^- adsorption and its interaction with photolyzed species.
6. No significant detrimental effects of the real matrix were observed during the degradation of Ponceau 4R, since the time required for the complete dye and color removals is comparable to that needed in ultrapure water, whereas only a slight deceleration of TOC decay took place as a result of parasitic reactions induced by the presence of Cl^-.

7. The kinetic decay of Ponceau 4R always obeyed a pseudo-first-order reaction and k_{dec} increased with increasing j. The k_{dec} value was much higher in EAOPs based on Fenton's reaction due to the much larger concentration of $^{\bullet}OH$ thanks to the simultaneity of two generation pathways, at the anode and in the bulk from Fenton's reaction. Ponceau 4R disappeared somewhat earlier than color, which suggests the formation of colored by-products along the treatment.
8. In the case of Allura Red AC, a similar degradation rate was found in PEF-BDD using SO_4^{2-}, ClO_4^- and NO_3^- media because generated BDD($^{\bullet}OH$) and $^{\bullet}OH$ are always the main oxidizing agents. In Cl^- medium, the oxidative destruction by generated HClO was inhibited by its reaction with H_2O_2, also diminishing the $^{\bullet}OH$ production. Higher SO_4^{2-} and Cl^- contents decelerated the decolorization and mineralization processes due to the formation of peroxodisulfate ion and refractory chloroderivatives, respectively. An increase in j accelerated the degradation process, indicating that organics are more rapidly converted into oxalic acid by the greater amount of generated hydroxyl radicals.
9. Up to 22 aromatic by-products, 8 carboxylic acids and nitromethane have been identified upon treatment of Ponceau 4R by EAOPs with BDD. The total mineralization of all these by-products to yield CO_2, NO_3^-, NH_4^+ and SO_4^{2-} proceeded via various simultaneous reaction routes. The total removal of Fe(III)-oxalate and Fe(III)-oxamate complexes under the action of UVA radiation explained the superiority of PEF-BDD. For lab-scale trials with Allura Red AC in Cl^- medium, GC-MS confirmed the formation of three chloroderivatives.
10. The scale-up to a 2.5 L pre-pilot flow plant demonstrates the viability of SPEF to mineralize azo dyes in short times. The SPEF process showed a large ability to mineralize the Allura Red AC solutions due to the potent action of UV photons from sunlight.
11. A plausible initial reaction sequence for Allura Red AC degradation in the pre-pilot plant is proposed based on 16 aromatic intermediates identified by GC-MS. Their cleavage yields up to 11 short-chain carboxylic acids, including oxalic and oxamic as the most persistent products.
12. Carmoisine solutions were completely decolorized by EO-H_2O_2 in Cl^- medium using a pre-pilot flow plant with a BDD/air-diffusion reactor. The attack of HClO on the dye and reaction by-products caused a rapid color removal, which

is enhanced by increasing *j* and Cl^- concentration. In contrast, fading was very slow using SO_4^{2-} and ClO_4^- since the disappearance of colored compounds is restricted to reaction with BDD($^\bullet$OH) in the anode vicinity.

13. The decolorization rate of Carmoisine solutions by EF in Cl^- medium was similar to that found in EO-H_2O_2, thus confirming that HClO is the main oxidant during the first stage in both EAOPs. In contrast, color removal in both, SO_4^{2-} and ClO_4^- media, was faster in the former method owing to the superiority of $^\bullet$OH in the bulk over BDD($^\bullet$OH) to attack the colored compounds. Regarding TOC decay, the use of SO_4^{2-} was beneficial in EF, yielding 76% mineralization with 14% MCE and 1.28 kW h g^{-1} TOC after 480 min at 100 mA cm^{-2}.
14. Up to 15 aromatic by-products arising from the cleavage of the –N=N– or C–N bonds of Carmoisine have been detected by GC-MS. Short-linear carboxylic acids like tartronic, oxalic, oxamic and formic have been quantified by ion-exclusion HPLC. The persistence of Fe(III)-oxalate complexes accounts for the partial mineralization of Carmoisine solution in EF.
15. Lab-scale experiments have demonstrated the superiority of PEF-BDD among all EAOPs since it yields fast decolorization and almost total mineralization of mixtures of food azo dyes (Ponceau 4R, Allura Red AC and Carmoisine) in sulfate medium. Application to simulated and real water matrices has confirmed its excellent oxidation ability over such pollutants, which depends on the oxidants generated from their inorganic components. PEF-BDD was also able to significantly degrade the residual TOC of a real water matrix.
16. The scale-up to a 2.5 L flow plant confirms the viability of SPEF-BDD for future industrial implementation. This process decolorizes rapidly and at similar rate dye mixtures in SO_4^{2-}, ClO_4^-, NO_3^- or Cl^- media, yielding almost overall mineralization in all cases except for Cl^-, where the formation of recalcitrant chloroderivatives decelerates the degradation. However, its high oxidation power is preserved in a medium with SO_4^{2-} + Cl^- ions, demonstrating its viability to treat real wastewater.
17. The transformation routes of the food azo dye mixtures includes up to 18 aromatic intermediates and 6 final carboxylic acids. Almost all intermediates identified during the degradation of the mixture have been detected during the individual treatment of the three dyes.

18. The results of this Thesis corroborate the large potentiality of SPEF to treat highly concentrated industrial dye wastewater.
19. It has been demonstrated that the sequential EC (Fe/SS)/PEF (BDD/ADE) treatment favors both, the fast color removal and the destruction of the remaining persistent organic matter in the pre-treated solution by PEF. The complete decolorization and mineralization of solutions were thus achieved within relatively short time periods thanks to coagulation by $Fe(OH)_n$ and oxidation by $^{\bullet}OH$ and active chlorine species. Up to 17 aromatic by-products have been identified by GC-MS during the coupled EC/PEF degradation, which can be totally destroyed in the EAOP step.
20. The combined treatment allows overcoming the typical drawbacks of EC and the long treatment time typically required by EAOPs, thus making the whole electrochemical technology much more cost-effective due to the reduction of energy consumption.
21. The scale-up to a ca. 2 L pre-pilot flow plant demonstrates the viability of the EC/EAOPs combination to mineralize food azo dyes in short times. The EC/PEF technology has been proven superior among the EC/EAOPs for the treatment of Tartrazine solutions at a pre-pilot scale. Further work is in progress to increase its cost-effectiveness.

7. References

Akbari, A., Remigy, J.C., Aptel, P., 2002. Treatment of textile dye effluent using a polyamide-based nanofiltration membrane. Chem. Eng. Process. 41, 601-609.

Aleboyeh, A., Daneshvar, N., Kasiri, M.B., 2008. Optimization of C.I Acid Red 14 azo dye removal by electrocoagulation batch process with response surface methodology. Chem. Eng. Process. 47, 827-832.

Allegre, C., Maisseu, M., Charbit, F., Moulin, P., 2004. Coagulation-flocculation-decantation of dye house effluents: concentrated effluents. J. Hazard. Mater. B116, 57-64.

Amani-Ghadim, A.R., Aber, S., Olad, A., Ashassi-Sorkhabi, H., 2011. Influence of anions on Reactive Red 43 removal in electrochemical coagulation process. Electrochim Acta 56, 1373–1380.

Amin, N.K., 2008. Removal of reactive dye from aqueous solutions by adsorption onto activated carbons prepared from sugarcane bagasse pith. Desalination 223, 152-161.

Andreozzi, R., Vincenzo, C., Insola, A., Marotta, R., 1999. Advanced oxidation processes (AOP) for water purification and recovery. Catal. Today 53, 51-59.

Aoudj, S., Khelifa, A., Drouiche, N., Hecini, M., Hamitouche, H., 2010. Electrocoagulation process applied to wastewater containing dyes from textile industry. Chem. Eng. Process. 49, 1176-1182.

APWA, AWWA, WEF, 2005. Standard methods for the examination of water and wastewater, in: Method number 4500-Cl Chlorine (residual)—G. DPD Colorimetric Method, 21st ed., American Public Health Association, Washington DC, pp. 4-67 to 4-68.

Arias, I.B., Meza, A.L., 2004. Resistencia antimicrobiana de Salmonella, Shigella y Vibrio cholerae, Perú 1997-2002, Rev. Perú Med. Exp. Salud Publica. 21, 273-275.

Ayhan Sengil, A., Özacar, M., 2009. The decolorization of C.I. Reactive Black 5 in aqueous solutions by electrocoagulation using sacrificial iron electrodes. J. Hazard. Mater. 161, 1369-1376.

Balasubramanian, N., Madhavan, K., 2001. Arsenic removal from industrial effluent through electrocoagulation. Chem. Ing. Technol. 24, 519-521.

7. References

Barbusiński, K., Majewski, J., 2003. Discoloration of azo dye Acid Red 18 by Fenton reagent in the presence of iron powder. Polish J. Environ. Stud. 12, 151-155.

Basturk, E., Karatas, M., 2014. Advanced oxidation of Reactive Blue 181 solution: A comparison between Fenton and Sono-Fenton Process. Ultrasonics Sonochem. 21, 1881-1885.

Bayramoglu, M., Eyvaz, M., Kobya, M., 2007. Treatment of the textile wastewater by electrocoagulation: Economical evaluation. Chem. Eng. J. 128, 155-161.

Bayramoglu, M., Kobya, M., Can, O.T., Sozbir, M., 2004. Operating cost analysis of electrocoaguation of textile dye wastewater. Sep. Purif. Technol. 37, 117-125.

Bergmann, M.E.H., Rollin, J., Lourtchouk, T., 2009. The occurrence of perchlorate during drinking water electrolysis using BDD anodes. Electrochim. Acta 54, 2102-2107.

Bokare, A.D., Choi, W., 2014. Review of iron-free Fenton-like systems for activating H_2O_2 in advanced oxidations processes. J. Hazard. Mater. 275, 121-135.

Bonfatti, F., De Battisti, A., Ferro, S., Lodi, G., Osti, S., 2000. Anodic mineralization of organic substrate in chloride-containing aqueous media, Electrochim. Acta 46, 305-314.

Borbón, B., Oropeza-Guzman, M.T., Brillas, E., Sirés, I., 2014. Sequential electrochemical treatment of dairy wastewater using aluminum and DSA-type anodes. Environ. Sci. Pollut. Res. 21, 8573-8584.

Borrás, N., Oliver, R., Arias, C., Brillas, E., 2010. Degradation of atrazine by electrochemical advanced oxidation processes using a boron-doped diamond anode. J. Phys. Chem. A 114, 6613-6621.

Boye, B., Brillas, E., Marselli, B., Michaud, P., Comninellis, C., Farnia, G., Sandonà, G., 2006. Electrochemical incineration of chloromethylphenoxy herbicides in acid medium by anodic oxidation with boron-doped diamond electrode. Electrochim. Acta 51, 2872-2880.

Boye, B., Dieng, M.M., Brillas, E., 2002. Degradation of herbicide 4-chlorophenoxyacetic acid by advanced electrochemical oxidation methods. Environ. Sci. Technol. 36, 3030-3035.

Brillas, E., Boye, B., Dieng, M.M., 2003a. Peroxi-coagulation and photoperoxi-coagulation treatment of the herbicide 4-chlorophenoxyacetic acid in aqueous medium using an oxygen-diffusion cathode, J. Electrochem. Soc. 150, E148-E154.

Brillas, E., Boye, B., Dieng, M.M., 2003b. General and UV-assisted cathodic Fenton treatments for the mineralization of herbicide MCPA. J. Electrochem. Soc. 150, E583-E589.

Brillas, E., Boye, B., Sirés, I., Garrido, J.A., Rodríguez, R.M., Arias, C., Cabot, P.L., Comninellis, C., 2004. Electrochemical destruction of chlorophenoxy herbicides by anodic oxidation and electro-Fenton using a boron-doped diamond electrode. Electrochim. Acta 49, 4487-4496.

Brillas, E., Sirés, I., Oturan, M.A., 2009. Electro-Fenton process and related electrochemical technologies based on Fenton's reaction chemistry. Chem. Rev. 109, 6570-6631.

Can, O.T., Bayramoglu, M., Kobya, M., 2003. Decolorization of reactive dye solutions by electrocoagulation using aluminum electrodes. Ind. Eng. Chem. Res. 42, 3391-3396.

Can, O.T., Kobya, M., Demirbas, E., Bayramoglu, M., 2006. Treatment of the textile wastewater by combined electrocoagulation. Chemosphere 62, 181-187.

Cañizares, P., Gadri, A., Lobato, J., Nasr, B., Paz, R., Rodrigo, M.A., Sáez, C., 2006. Electrochemical oxidation of azoic dyes with conductive-diamond anodes. Ing. Eng. Chem. Res. 45 (2006) 3468-3473.

Cañizares, P., Jiménez, C., Martínez, F., Sáez, C., Rodrigo M.A., 2007. Study of the electrocoagulation process using aluminum and iron electrodes. Ind. Eng. Chem. Res. 46, 6189-6195.

Cañizares, P., Lobato, J., Paz, R., Rodrigo, M.A., Sáez, C., 2005. Electrochemical oxidation of phenolic wastes with boron-doped diamond anodes. Water Res. 39, 2687-2703.

Cañizares, P., Martínez, F., García-Gómez, J., Sáez, C., Rodrigo, M.A., 2002. Combined electrocoagulation and assisted electrochemical coagulation of aqueous phenol wastes. J. Appl. Electrochem. 32, 1241-1246.

7. References

Cañizares, P., Sáez, C., Lobato, J., Rodrigo, M.A., 2004. Electrochemical treatment of 2,4-dinitrophenol aqueous wastes using boron-doped diamond anodes. Electrochim. Acta 49, 4641-4650.

Cavalcanti, E.B., Garcia-Segura, S., Centellas, F., Brillas, E., 2013. Electrochemical incineration of omeprazol in neutral aqueous medium using a platinum or boron-doped diamond anode: Degradation kinetics and oxidation products. Water Res. 47, 1803-1815.

Ciríaco, L., Anjo, C., Correia, J., Pacheco, M.J., Lopes, A., 2009. Electrochemical degradation of ibuprofen on Ti/Pt/PbO_2 and Si/BDD electrodes. Electrochim. Acta 54, 1464-1472.

Comninellis, C., 1994. Electrocatalysis in the electrochemical conversion/combustion of organic pollutants for waste water treatment. Electrochim. Acta 39, 1857-1862.

Comninellis, C., De Battisti, A., 1996. Electrocatalysis in anodic oxidation of organics with simultaneous oxygen evolution. J. Chim. Phys. 93, 673-679.

Crimi, M., Ko, S., 2009. Control of manganese dioxide particles resulting from in situ chemical oxidation using permanganate. Chemosphere 74, 847-853.

Daneshvar, N., Aber, S., Vatanpour, V., Rasoulifard, M.H., 2008. Electro-Fenton treatment of dye solution containing Orange II: Influence of operational parameters. J. Electroanal. Chem. 615, 165‑174.

Daneshvar, N., Ashassi-Sorkhabi, H., Tizpar, A., 2003a. Decolorization of orange II by electrocoagulation method. Sep. Purif. Technol. 31, 153-162.

Daneshvar, N., Oladegaragoze, A., Djafarzadeh, N., 2006. Decolorization of basic dye solutions by electrocoagulation: An investigation of the effect of operational parameters. J. Hazard. Mater. B129, 116-122.

Daneshvar, N., Salari, D., Khataee, A.R., 2003b. Photocatalytic degradation of azo dye Acid Red 14 in water: Investigation of the effect of operational parameters. J. Photochem. Photobiol. A: Chem. 157, 111-116.

Daneshvar, N., Salari, D., Khataee, A.R., 2004. Photocatalytic degradation of azo dye Acid Red 14 in water on ZnO as an alternative catalyst to TiO_2. J. Photochem. Photobiol. A: Chem. 162, 317-322.

De Battisti, A., Ferro, S., Dal Colle, M., 2001. Electrocatalysis at conductive diamond modified by noble-metal oxides. J. Phys. Chem. B 105, 1679-1682.

Di Bella, G., Giustra, M.G., Freni, G., 2014. Optimisation of coagulation/flocculation for pre-treatment of high strength and saline wastewater: Performance analysis with different coagulant doses. Chem. Eng. J. 254, 283-292.

Dirany, A., Sirés, I., Oturan, N., Oturan, M.A., 2010. Electrochemical abatement of the antibiotic sulfamethoxazole from water. Chemosphere 81, 594-602.

Dirany, A., Sirés, I., Oturan, N., Özcan, A., Oturan M.A., 2012. Electrochemical treatment of the antibiotic sulfachloropyridazine: Kinetics, reaction pathways, and toxicity evolution, Environ. Sci. Technol. 46, 4074-4082.

Durante, C., Cuscov, M., Isse, A.A., Sandonà, G., Gennaro, A., 2011. Advanced oxidation processes coupled with electrocoagulation for the exhaustive abatement of Cr-EDTA. Water Res. 45, 2122-2130.

EFSA, 2008. Scientific opinion of the panel on food additives, flavourings, processing aids and food contact materials (AFC): Assessment of the results of the study by McCann et al. (2007) on the effect of some colours and sodium benzoate on children's behavior. EFSA J. 660, 1-54.

EFSA, 2009a. Panel on Food Additives and Nutrient Sources added to Food, Scientific Opinion on the re-evaluation of Allura Red AC (E 129) as a food additive. EFSA J. 7, 1327 [39 pages].

EFSA, 2009b. Panel on Food Additives and Nutrient Sources added to Food, Scientific Opinion on the re-evaluation of Ponceau 4 R (E 124) as a food additive. EFSA J. 7, 1328 [39 pages].

EFSA, 2009c. Panel on Food Additives and Nutrient Sources added to Food, Scientific Opinion on the re-evaluation of Tartrazine (E 102) as a food additive. EFSA J. 7, 1331 [52 pages].

EFSA, 2009d. Panel on Food Additives and Nutrient Sources added to Food, Scientific Opinion on the re-evaluation of Azorubine/Carmoisine (E 122) as a food additive. EFSA J. 7, 1332 [40 pages].

7. References

El-Desoky, H.S., Ghoneim, M.M., Zidan, N.M., 2010. Decolorization and degradation of Ponceau S azo-dye in aqueous solutions by the electrochemical advanced Fenton oxidation. Desalination 264 (2010) 143-150.

El-Ghenymy, A., Arias, C., Cabot, P.L., Centellas, F., Garrido, J.A., Rodríguez, R.M., Brillas, E., 2012. Electrochemical incineration of sulfanilic acid at a boron-doped diamond anode. Chemosphere 87, 1126-1133.

El Qada, E.N., Allen, S.J., Walker, G.M., 2008. Adsorption of basic dyes from aqueous onto activated carbons. Chem. Eng. J. 135, 174-184.

Feng, L., van Hullebusch, E.D., Rodrigo, M.A., Esposito, G., Oturan, M.A., 2013. Removal of residual anti-inflammatory and analgesic pharmaceuticals from aqueous systems by electrochemical advanced oxidation processes. A review. Chem. Eng. J. 228, 944-964.

Fernandes, A., Marao, A., Magrinho, M., Lopes, A., Gonçalves, I., 2004. Electrochemical degradation of C.I. Acid Orange 7, Dyes Pigments 61, 287-296.

Fernandes, A., Spranger, P., Fonseca, A.D., Pacheco, M.J., Ciríaco, L., Lopes, A., 2014. Effect of electrochemical treatments on the biodegradability of sanitary landfill leachates. Appl. Catal. B: Environ. 144, 514-520.

Ferro, S., De Battisti, A., 2002. Electrocatalysis and chlorine evolution reaction at ruthenium dioxide deposited on conductive diamond. J. Phys. Chem. B 106, 2249-2254.

Fewson C.A., 1998. Biodegradation of xenobiotic and other persistent compounds: The causes of recalcitrance. Trends Biotechnol. 6, 148-153.

Flox, C., Ammar, S., Arias, C., Brillas, E., Vargas-Zavala, A.V., Abdelhedi, R., 2006a. Electro-Fenton and photoelectro-Fenton degradation of indigo carmine in acidic aqueous medium. Appl. Catal. B: Environ. 67, 93-104.

Flox, C., Cabot, P.L., Centellas, F., Garrido, J.A., Rodríguez, R.M., Arias, C., Brillas, E., 2006b. Electrochemical combustion of herbicide mecoprop in aqueous medium using a flow reactor with a boron-doped diamond anode. Chemosphere 64, 892-902.

Flox, C., Garrido, J.A., Rodríguez, R.M., Centellas, F., Cabot, P.L., Arias, C., Brillas, E., 2005. Degradation of 4,6-dinitro-*o*-cresol from water by anodic oxidation with a boron-doped diamond electrode. Electrochim. Acta 50, 3685-3692.

Forgacs, E., Cserháti, T., Oros, G., 2004. Removal of synthetic dyes from wastewaters: A review. Environ. Int. 30, 953-971.

Gao, M., Zeng, Z., Sun, B., Zou, H., Chen, J., Shao, L., 2012. Ozonation of azo dye Acid Red 14 in a microporous tube-in-tube microchannel reactor: Decolorization and mechanism. Chemosphere 89, 190-197.

Garcia-Segura, S., Centellas, F., Arias, C., Garrido, J.A., Rodríguez, R.M., Cabot, P.L., Brillas, E., 2011. Comparative decolorization of monoazo, diazo and triazo dyes by electro-Fenton process. Electrochim. Acta 58, 303-311.

Garcia-Segura, S., El-Ghenymy, A., Centellas, F., Rodríguez, R.M., Arias, C., Garrido, J.A., Cabot, P.L., Brillas, E., 2012. Comparative degradation of the diazo dye Direct Yellow 4 by electro-Fenton, photoelectro-Fenton and photo-assisted electro-Fenton. J. Electroanal. Chem. 681, 36-43.

Garrido, J.A., Brillas, E., Cabot, P.L., Centellas, F., Arias, C., Rodríguez R.M., 2007. Mineralization of drugs in aqueous medium by advanced oxidation processes. Port. Electrochim. Acta 25, 19-41.

Ghaedi, M., Sadeghian, B., Pebdani, A.A., Sahraei, R., Daneshfar, A., Duran, C., 2012. Kinetics, thermodynamics and equilibrium evaluation of Direct Yellow 12 removal by adsorption onto silver nanoparticles loaded activated carbon. Chem. Eng. J. 187, 133-141.

Golder, A.K., Samanta, A.N., Ray, S., 2007. Removal of Cr^{3+} by electrocoagulation with multiple electrodes: Bipolar and monopolar configurations. J. Hazard. Mater. 141, 653-661.

Gomes, J.A.G., Daida, P., Kesmez, M., Wier, M., Moreno, H., Parga, J.R., Irwin, G., McWhinney, H., Grady, T., Peterson, E., Cocke, L.D., 2007. Arsenic removal by electrocoagulation using combined Al-Fe electrodes system and characterization of products. J. Hazard. Mater. B139, 220-231.

Guinea, E., Arias, C., Cabot, P.L., Garrido, J.A., Rodríguez, R.M., Centellas, F., Brillas, E., 2008. Mineralization of salicylic acid in acidic aqueous medium by

electrochemical advanced oxidation processes using platinum and boron-doped diamond as anode and cathodically generated hydrogen peroxide. Water Res. 42, 499-511.

Guinea, E., Garrido, J.A., Rodríguez, R.M., Cabot, P.L., Arias, C., Centellas, F., Brillas, E., 2010. Degradation of the fluoroquinolone enrofloxacin by electrochemical advanced oxidation processes based on hydrogen peroxide electrogeneration. Electrochim. Acta 55, 2101-2115.

Guivarch, E., Trevin, S., Lahitte, C., Oturan, M.A., 2003. Degradation of azo dyes in water by electro-Fenton process. Environ. Chem. Lett. 1, 38-44

Gupta, V.K., Suhas, 2009. Applications of low-cost adsorbents for dye removal – A review. J. Environ. Manage. 90, 2313-2342.

Gürses, A., Yalçin, M., Dogar, C., 2002. Electrocoagulation of some reactive dyes: A statistical investigation of some electrochemical variables. Waste Manage. 22, 491-499.

Hamza, M., Abdelhedi, R., Brillas, E., Sirés, I., 2009. Comparative electrochemical degradation of the triphenylmethane dye Methyl Violet with boron-doped diamond and Pt anodes. J. Electroanal. Chem. 627, 41-50.

Hernández-Rodríguez, M.J., Fernández-Rodríguez, C., Doña-Rodríguez, J.M., González-Díaz, O.M., Zerbani, D., Peña, J.P., 2014. Treatment of effluents from wool dyeing process by photo-Fenton at solar pilot plant. J. Environ. Chem. Eng. 2, 163-171.

Hmani, E., Samet, Y., Abdelhédi, R., 2012. Electrochemical degradation of Auramine-O dye at boron-doped diamond and lead dioxide electrodes. Diamond Relat. Mater. 30, 1-8.

Holt, P.K., Barton, G.W., Mitchell, C.A., 2005. The future for electrocoagulation as a localised water treatment technology. Chemosphere 59, 355-367.

Huang, J., Yang, L., Wu, X., Xu, M., Liu, Y., Deng, S., 2013. Phenol adsorption on α,α'-dichloro-*p*-xylene (DCX) and 4,4'-bis(chloromethyl)-1,1'-biphenyl (BCMBP) modified XAD-4 resins from aqueous solutions. Chem. Eng. J. 222, 1-8.

Hupert, M., Muck, A., Wang, J., Stotter, J., Cvackova, Z., Haymond, S., Show, Y., Swain, G.M., 2003. Conductive diamond thin-films in electrochemistry. Diamond Relat. Mater. 12, 1940-1949.

Idel-Aouad, R., Valiente, M., Yaacoubi, A., Tanouti, B., López-Mesas, M., 2011. Rapid decolourization and mineralization of the azo dye C.I Acid Red 14 by heterogeneous Fenton reaction. J. Hazard. Mater. 186, 745-750.

Iniesta, J., Michaud, P.A., Panizza, M., Cerisola, G., Aldaz, A., Comninellis, Ch., 2001. Electrochemical oxidation of phenol at boron-doped diamond electrode. Electrochim. Acta 46, 3573-3578.

Isarain-Chávez, E., Cabot, P.L., Centellas, F., Rodríguez, R.M., Arias, C., Garrido, J.A., Brillas, E., 2011. Electro-Fenton and photoelectro-Fenton degradations of the drug beta-blocker propranolol using a Pt anode: Identification and evolution of oxidation products. J. Hazard. Mater. 185, 1228-1235.

Iurascu, B., Siminiceanu, I., Vione, D., Vicente, M.A., Gil, A., 2009. Phenol degradation in water through a heterogeneous photo-Fenton process catalyzed by Fe-treated laponite. Water Res. 43, 1313-1322.

Jiménez Izquierdo, C., Cañizares, P., Rodrigo, M.A., Leclerc, J.P., Valentin, G., Lapicque, F., 2010. Effect of the nature of the supporting electrolyte on the treatment of soluble oils by electrocoagulation. Desalination 255, 15-20.

Kapalka, A., Fóti, G., Comninellis, Ch., 2009. The importance of electrode material in environmental electrochemistry. Formation and reactivity of free hydroxyl radicals on boron-doped diamond electrodes, Electrochim. Acta 54, 2018-2023.

Khataee, A., Khataee, A., Fathinia, M., Vahid, B., Joo, S.W., 2013. Kinetic modeling of photoassisted-electrochemical process for degradation of an azo dye using boron-doped diamond anode and cathode with carbon nanotubes. J. Ind. Eng. Chem. 19, 1890-1894.

Kobya, M., Can, O.T., Bayramoglu, M., 2003. Treatment of textile wastewaters by electrocoagulation using iron and aluminum electrodes. J. Hazard. Mater. B100, 163-178.

7. References

Kobya, M., Demirbas, E., Can, O.T., Bayramoglu, M., 2006. Treatment of levafix orange textile dye solution by electrocoagulation. J. Hazard. Mater. B132, 183-188.

Kobya, M., Ulu, F., Gebologlu, U., Demirbas, E., Oncel, M.S., 2011. Treatment of potable water containing low concentration of arsenic with electrocoagulation: Different connection modes and Fe-Al electrodes. Sep. Purif. Technol. 77, 283-293.

Konstantinou, I.K., Albanis, T.A., 2004. TiO_2-assisted phototcatalytic degradation of azo dyes in aqueous solution: Kinetic and mechanistic investigations. A review. Appl. Catal. B: Environ. 49, 1-14.

Koupaie, E.H., Moghaddam, M.R.A., Hashemi, S.H., 2011. Post-treatment of anaerobically degraded azo dye Acid Red 18 using aerobic moving bed biofilm process: Enhanced removal of aromatic amines. J. Hazard. Mater. 195, 147-154.

Koupaie, E.H., Moghaddam, M.R.A., Hashemi, S.H., 2012. Investigation of decolorization kinetics and biodegradation of azo dye Acid Red 18 using sequential process of anaerobic sequencing batch reactor/moving bed sequencing batch biofilm reactor. Int. Biodeter. Biodegr. 71, 43-49.

Ksibi, M., 2006. Chemical oxidation with hydrogen peroxide for domestic wastewater treatment. Chem. Eng. J. 119, 161-165.

Lau, Y., Wong, Y., Teng, T., Morad, N., Rafatullah, M., Ong, S., 2014. Coagulation-flocculation of azo dye Acid Orange 7 with green refined laterite soil. Chem. Eng. J. 246, 283-390.

Lin, J., Zhao, X., Liu, D., Yu, Z., Zhang, Y., Xu, H., 2008. The decoloration and mineralization of azo dye C.I. Acid Red 14 by sonochemical process: Rate improvement via Fenton's reaction. J. Hazard. Mater. 157, 541-546.

Liu, S., Ding, Y., Li, P., Diao, K., Tan, X., Lei, F., Zhan, Y., Li, Q., Huang, B., Huang, Z., 2014. Adsorption of the anionic dye Congo Red from aqueous solution onto natural zeolites modified with N,N-dimethyldehydroabietylamine oxide. Chem. Eng. J. 248, 135-144.

Maga, J.A., Tu, A.T., 1994. Food additive toxicology, CRC press [552 pages].

Mahmoodi, N.M., Arami, M., 2006. Bulk phase degradation of Acid Red 14 by nanophotocatalysis using immobilized titanium (IV) oxide nanoparticles. J. Photochem. Photobiol. A: Chem. 182, 60-66.

Marselli, B., Garcia-Gomez J., Michaud P.A., Rodrigo M.A., Comninellis Ch., 2003. Electrogeneration of hydroxyl radicals on boron-doped diamond electrodes. J. Electrochem. Soc. 150, D79-D83.

Martínez-Huitle C.A., Brillas E., 2009. Decontamination of wastewaters containing synthetic organic dyes by electrochemical methods: A general review. Appl. Catal. B: Environ. 87, 105-145.

Martínez-Huitle, C.A., Ferro, S., 2006. Electrochemical oxidation of organic pollutants for the wastewater treatment: Direct and indirect processes. Chem. Soc. Rev. 35, 1324-1340.

Martínez-Huitle, C.A., Ferro, S., De Battisti, A., 2004. Electrochemical incineration of oxalic acid. Role of electrode material. Electrochim. Acta 49, 4027-4034.

Martins, M.A.M., Lima, N., Silvestre, A.J.D., Queiroz, M.J., 2003. Comparative studies of fungal degradation of single or mixed bioaccessible reative azo dyes. Chemosphere 52, 967-973.

Mascia, M., Vacca, A., Polcaro, A.M., Palmas, S., Ruiz, J.R., De Pozzo, A., 2010. Electrochemical treatment of phenolic waters in presence of chloride with boron-doped diamond (BDD) anodes: Experimental study and mathematical model. J. Hazard. Mater. 174, 314-322.

Minella, M., Marchetti, G., De Laurentiis, E., Malandrino, M., Maurino, V., Minero, C., Vione, D., Hanna, K., 2014. Photo-Fenton oxidation of phenol with magnetite as iron source. Appl. Catal. B: Environ. 154, 102-109.

Mo, J.H., Lee, Y.H., Kim, J., Jeong, J.Y., Jegal, J., 2008. Treatment of dye aqueous solutions using nanofiltration polyamide composition membranes for dye wastewater reuse. Dyes Pigments 76, 429-434.

Modirshahla, N., Behnajady, M.A., Kooshaiian, S., 2007. Investigation of the effect of different electrode connections on the removal efficiency of Tartrazine from aqueous solutions by electrocoagulation. Dyes Pigments 74, 249-257.

7. References

Moghaddam, S.S., Moghaddam, M.R.A., Arami, M., 2010. Coagulation/flocculation process for dye removal using sludge from water treatment plant: Optimization through response surface methodology. J. Hazard. Mater. 175, 651-657.

Mollah, M.Y.A., Pathak, S.R., Patil, P.K., Vayuvegula, M., Agrawal, T.S., Gomes, J.A.G., Kesmez, M., Cocke, D.L., 2004. Treatment of Orange II azo-dye by electrocoagulation (EC) technique in a continuous flow cell sacrificial iron electrodes. J. Hazard. Mater. B109, 165-171.

Mollah, M.Y.A., Schennach, R., Parga, J.R., Cocke, D.L., 2001. Electrocoagulation (EC)-science and applications. J. Hazard. Mater. B84, 29-41.

Mozia, S., Tomaszewska, M., Morawski, A.W., 2005. A new photcatalytic membrane reactor (PMR) for removal of azo-dye Acid Red 18 from water. Appl. Catal. B: Environ. 59, 131-137.

Mozia, S., Tomaszewska, M., Morawski, A.W., 2006. Removal of azo-dye Acid Red 18 in two hybrid membrane systems employing a photodegradation process. Desalination 198, 183-190.

Mozia, S., Tomaszewska, M., Morawski, A.W., 2007. Photodegradation of azo dye Acid Red 18 in a quartz labyrinth flow reactor with immobilized TiO_2 bed. Dyes Pigments 75, 60-66.

Nakagawa, H., Yamaguchi, E., 2012. Influence of oxalic acid formed on the degradation of phenol by Fenton reagent. Chemosphere 88, 183-187.

Navajas, M.F., Abril, O.M., López, J.A.P., 2001. Determinación de color residual. Método del DPD. Higiene Sanidad Ambiental 1, 6-7.

Oliveira, D.F.M., Batista, P.S., Muller Jr., P.S., Velani, V., França, M.D., de Souza, D.R., Machado, A.E.H., 2011. Evaluating the effectiveness of photocatalysts based on titanium dioxide in the degradation of the dye Ponceau 4R. Dyes Pigments 92, 563-572.

OMS, UNICEF, 2012. Progresos en materia de agua potable y saneamiento, Informe de actualización.

Osugi, M.E., Rajeshwar, K., Ferraz, E.R.A., de Oliveira, D.P., Araújo, Â.R., Zanoni, M.V.B., 2009. Comparison of oxidation efficiency of disperse dyes by chemical

and photelectrocatalytic chlorination and removal of mutagenic activity. Electrochim. Acta 54, 2086-2093.

Oturan, M.A., 2000. An ecologically effective water treatment using electrochemically generated hydroxyl radicals for in situ destruction of organic pollutants: Application to herbicide 2,4-D. J. Appl. Electrochem. 30, 475-482.

Oturan, M.A., Oturan, N., Edelahi, M.C., Podvorica, F.I., El Kacemi, K., 2011a. Oxidation degradation of herbicide diuron in aqueous medium by Fenton's reaction based advanced oxidation processes. Chem. Eng. J. 171, 127-135.

Oturan, M.A., Peiroten, J., Chartrin, P., Acher, A.J., 2000. Complete destruction of *p*-nitrophenol in aqueous medium by electro-Fenton method. Environ. Sci. Technol. 34, 3474-3479.

Oturan, M.A., Pimentel, M., Oturan, N., Sirés, I., 2008. Reaction sequence for the mineralization of short-chain carboxylic acids usually formed upon cleavage of aromatics during electrochemical Fenton treatment. Electrochim. Acta 54, 173-182.

Oturan, M.A., Pinson J., 1995. Hydroxylation by electrochemically generation $OH^{\bullet}$ radicals. Mono- and polyhydroxylation of benzoic acid: products and isomers' distribution. J. Phys. Chem. 99, 13948-13954.

Oturan, N, Brillas, E., Oturan, M.A., 2012. Unprecedented total mineralization of atrazine and cyanuric acid by anodic oxidation and electro-Fenton with a boron-doped diamond anode. Environ. Chem. Lett. 10, 165‑170.

Oturan, N., Hamza, M., Ammar, S., Abdelhédi, R., Oturan, M.A., 2011b. Oxidation/mineralization of 2-nitrophenol in aqueous medium by electrochemical advanced oxidation processes using Pt/carbon-felt and BDD/carbon-felt cells. J. Electroanal. Chem. 661, 66-71.

Özcan, A., Oturan, M.A., Oturan, N., Sahin, Y., 2009. Removal of Acid Orange 7 from water by electrochemically generated Fenton's reagent. J. Hazard. Mater. 163, 1213-1220.

Özcan, A., Sahin, Y., Koparal, A.S., Oturan, M.A., 2008. Carbon sponge as a new cathode material for the electro-Fenton process. Comparison with carbon felt

cathode and application to degradation of synthetic dye Basic Blue 3 in aqueous medium. J. Electroanal. Chem. 616, 71-78.

Panizza, M., Bocca, C., Cerisola, G., 2000. Electrochemical treatment of wastewater containing polyaromatic organic pollutants. Water Res. 34, 2601-2605.

Panizza, M., Cerisola, G., 2005. Application of diamond electrodes to electrochemical processes. Electrochim. Acta 51, 191-199.

Panizza, M., Cerisola, G., 2009a. Electro-Fenton degradation of synthetic dyes, Water Res. 43, 339-344.

Panizza, M., Cerisola, G., 2009b. Direct and mediated anodic oxidation of organic pollutants. Chem. Rev. 109, 6541-6569.

Panizza, M., Cerisola, G., 2010a. Applicability of electrochemical methods to carwash wastewaters for reuse. Part 1: Anodic oxidation with diamond and lead dioxide anodes. J. Electroanal. Chem. 638, 28-32.

Panizza, M., Cerisola, G., 2010b. Applicability of electrochemical methods to carwash wastewaters for reuse. Part 2: Electrocoagulation and anodic oxidation integrated process. J. Electroanal. Chem. 638, 236-240.

Panizza, M., Michaud, P.A., Cerisola, G., Comninellis, Ch., 2001. Electrochemical treatment of wastewaters containing organic pollutants on boron-doped diamond electrodes: Prediction of specific energy consumption and required. Electrochem. Commun. 3, 336-339.

Panizza, M., Oturan M.A., 2011. Degradation of Alizarin Red by electro-Fenton process using a graphite-felt cathode. Electrochim. Acta 56, 7084-7087.

Parga, J.R., Cocke, D.L., Valenzuela, J.L., Gomes, J.A., Kesmez, M., Irwin, G., Moreno, H., Weir, M., 2005. Arsenic removal via electrocoagulation from heavy metal contaminated groundwater in La Comarca Lagunera México. J. Hazard. Mater. B124, 247-254.

Pera-Titus, M., Garcia-Molina, V., Baños M. A., Giménez J., Esplugas S., 2004. Degradation of chlorophenols by means of advanced oxidation processes: A general review. Appl. Catal. B: Environ. 47, 219-256.

Perret, A., Haenni, W., Skinner, N., Tang, X.M., Gandini, D., Comninellis, Ch., 1999. Electrochemical behavior of synthetic diamond thin film electrodes. Diamond Relat. Mater. 8, 820-823.

Pletcher, D., 1999. Indirect oxidation using electrogenerated hydrogen peroxide. Acta Chem. Scand. 53, 745-750.

Polcaro, A.M., Palmas, S., Renoldi, F., Mascia, M., 2000. Three-dimensional electrodes for the electrochemical combustion of organic pollutants. Electrochim. Acta 46, 389-394.

Polcaro, A.M., Vacca, A., Mascia, M., Palmas, S., 2005. Oxidation at boron doped diamond electrodes: An effective method to mineralise triazines. Electrochim. Acta 50, 1841-1847.

Poyatos, J.M., Muñio, M.M., Almecija, M.C., Torres, J.C., Hontoria, E., Osorio, F., 2010. Advanced oxidation processes for wastewater treatment: State of the art. Water Air Soil Pollut. 205, 187-204.

Pulgarin, C., Adler, N., Péringer, P., Comninellis, Ch., 1994. Electrochemical detoxification of a 1,4-benzoquinone solution in wastewater treatment. Water Res. 28, 887-893.

Rabaaoui, N., Moussaoui, Y., Allagui, M.S., Bedoui, A., Elaloui, E., 2013a. Anodic oxidation of nitrobenzene on BDD electrode: Variables effects and mechanisms of degradation. Sep. Purif. Technol. 107, 318-323.

Rabaaoui, N, Saad, M.K., Moussaoui, Y., Allagui, M.S., Bedoui, A., Elaloui, E., 2013b. Anodic oxidation of *o*-nitrophenol on BDD electrode: Variable effects and mechanisms of degradation. J. Hazard. Mater. 250-251, 447-453.

Raju, G.B., Karuppiah, M.T., Latha, S.S., Parvathy, S., Prabhakar, S., 2008. Treatment of wastewater from synthetic textile industry by electrocoagulation-electrooxidation. Chem. Eng. J. 144, 51-58.

Ramirez, J.H., Maldonado-Hódar, F.J., Pérez-Cadenas, A.F., Moreno-Castilla, C., Costa, C.A., Madeira L.M., 2007. Azo-dye Orange II degradation by heterogeneous Fenton-like reaction using carbon-Fe catalysts. Appl. Catal. B: Environ. 75, 312-323

7. References

Randazzo, S., Scialdone, O., Brillas, E., Sirés, I., 2011. Comparative electrochemical treatments of two chlorinated aliphatic hydrocarbons. Time course of the main reaction by-products. J. Hazard. Mater. 192, 1555-1564.

Relyea, R.A., 2012. New effects of Roundup on amphibians: Predators reduce herbicide mortality; herbicides induce antipredator morphology. Ecol. Appl. 22, 634-647.

Renou, S., Givaudan, J.G.., Poulain, S., Dirassouyan, F., Moulin, P., 2008. Landfill leachate treatment: Review and opportunity. J. Hazard. Mater. 150, 468-493.

Rivera-Utrilla, J., Sánchez-Polo, M., Ferro-García, M.Á., Prados-Joya, G., Ocampo-Pérez, R., 2013. Pharmaceuticals as emerging contaminants and their removal from water. A review. Chemosphere 93, 1268-1287.

Robinson, T., McMullan, G., Marchant, R., Nigam, P., 2001. Remediation of dyes in textile effluent: A critical review on current treatment technologies with a proposed alternative. Biores. Technol. 77, 247-255.

Rodrigo, M.A., Cañizares, P., Sánchez-Carretero, A., Saéz, C., 2010. Use of conductive-diamond electrochemical oxidation for wastewater treatment. Catal, Today 151, 173-177.

Rosales, E., Pazos, M., Longo, M.A., Sanromán, M.A., 2009. Electro-Fenton decoloration of dyes in a continuous reactor: A promising technology in colored wastewater treatment. Chem. Eng. J. 155, 62-67.

Ruiz, E.J., Arias, C., Brillas, E., Hernández-Ramírez, A., Peralta-Hernández, J.M., 2011a. Mineralization of Acid Yellow 36 azo dye by electro-Fenton and solar photoelectro-Fenton processes with a boron-doped diamond anode. Chemosphere 82, 495-501.

Ruiz, E.J., Hernández-Ramírez, A., Peralta-Hernández, J.M., Arias, C., Brillas, E., 2011b. Application of solar photoelectro-Fenton technology to azo dyes mineralization: Effect of current density, Fe^{2+} and dye concentration. Chem. Eng. J. 171, 385-392.

Sadik, W.A., Nashed, A.W., El-Demerdash, A.M., 2007. Photodecolourization of Ponceau 4R by heterogeneous photocatalysis. J. Photochem. Photobiol. A: Chem. 189, 135-140.

Salazar, R., Brillas, E., Sirés, I., 2012. Finding the best Fe^{2+}/Cu^{2+} combination for the solar photoelectro-Fenton treatment of simulated wastewater containing the industrial textile dye Disperse Blue 3. Appl. Catal. B: Environ. 115‑116, 107‑116.

Salazar, R., Garcia-Segura, S., Ureta-Zañartu, M.S., Brillas, E., 2011. Degradation of disperse azo dyes from waters by solar photoelectro-Fenton. Electrochim. Acta 56, 6371-6379.

Sales Solano, A.M., Costa de Araújo C.K., Vieira de Melo, J., Peralta-Hermandez, J.M., Da Silva, D.R., Martínez-Huitle, C.A., 2013. Decontamination of real textile industrial effluent by strong oxidant species electrogenerated on diamond electrode: Viability and disadvantages of this electrochemical technology. Appl. Catal. B: Environ. 130-131, 112-120.

Sánchez-Carretero, A., Sáez, C., Cañizares, P., Rodrigo, M.A., 2011. Electrochemical production of perchlorates using conductive diamond electrolyses. Chem. Eng. J. 166, 710-714.

Saratale, R.G., Saratale, G.D., Chang, J.S., Govindwar, S.P., 2011. Bacterial decolorization and degradation of azo dyes: A review. J. Taiwan Inst. Chem. Eng. 42, 138-157.

Sasaki, Y.F., Kawaguchi, S., Kamaya, A., Ohshita, M., Kabasawa, K., Iwama, K., Taniguchi, K., Tsuda, S., 2002. The comet assay with 8 mouse organs: Results with 39 currently used food additives. Mutat. Res. 519, 103-119.

Scialdone, O., Galia, A., Guarisco, C., Randazzo, S., Filardo, G., 2008. Electrochemical incineration of oxalic acid at boron doped diamond anodes: Role of operative parameters. Electrochim. Acta 53, 2095-2108.

Scialdone, O., Randazzo, S., Galia, A., Silvestri, G., 2009. Electrochemical oxidation of organics in water: Role of operative parameters in the absence and in the presence of NaCl. Water Res. 43, 2260-2272.

Serra, A., Doménech, X., Arias, C., Brillas, E., Peral, J., 2009. Oxidation of α-methylphenylglycine under Fenton and electro-Fenton conditions in the dark and in the presence of solar light. Appl. Catal. B: Environ. 89, 12-31.

7. References

Seshadri, S., Bishop, P.L., Agha, A.M., 1994. Anaerobic/aerobic treatment of selected azo dyes in wastewater. Waste Manage. 15, 127-137.

Shi, B., Li, G., Wamg, D., Feng, C., Tang, H., 2007. Removal of direct dyes by coagulation: The performance of performed polymeric aluminum species. J. Hazard. Mater. 143, 567-574.

Shimizu, A., Tokumura, M., Nakajima, K., Kawase, Y., 2012. Phenol removal using zero-valent iron powder in the presence of dissolved oxygen: Roles of decomposition by the Fenton reaction and adsorption/precipitation. J. Hazard. Mater. 201-202, 60-67.

Sirés, I., Brillas, E., 2012. Remediation of water pollution caused by pharmaceutical residues based on electrochemical separation and degradation technologies: A review. Environ. Int. 40, 212-229.

Sirés, I., Brillas, E., Cerisola, G., Panizza, M., 2008. Comparative depollution of mecoprop aqueous solutions by electrochemical incineration using BDD and PbO_2 as high oxidation power anodes. J. Electroanal. Chem. 613, 151-159.

Sirés, I., Brillas, E., Oturan, M.A., Rodrigo, M.A., Panizza, M., 2014. Electrochemical advanced oxidation processes: today and tomorrow. A review. Environ. Sci. Pollut. Res. 21, 8336-8367.

Sirés, I., Garrido, J.A., Rodríguez, R.M., Cabot, P.L., Centellas, F., Arias, C., Brillas, E., 2006. Electrochemical degradation of paracetamol from water by catalytic action of Fe^{2+}, Cu^{2+}, and UVA light on electrogenerated hydrogen peroxide. J. Electrochem. Soc. 153, D1-D9.

Sirés, I., Oturan, N., Oturan, M.A., 2010. Electrochemical degradation of β-blockers. Studies on single and multicomponent synthetic aqueous solutions. Water Res. 44, 3109-3120.

Sirés, I., Oturan, N., Oturan, M.A., Rodríguez, R.M., Garrido, J.A., Brillas, E., 2007. Electro-Fenton degradation of antimicrobials triclosan and triclocarban. Electrochim. Acta 52, 5493-5503.

Skoumal, M., Cabot, P.L., Centellas, F., Arias, C., Rodríguez, R.M., Garrido, J.A., Brillas, E., 2006. Mineralization of paracetamol by ozonation catalyzed with Fe^{2+}, Cu^{2+} and UVA light. Appl. Catal. B: Environ. 66, 228-240.

Sobana, N., Swaminathan, M., 2007. The effect of operational parameters on the photocatalytic degradation of Acid Red 18 by ZnO. Sep. Purif. Technol. 56, 101-107.

Solís, M., Solís, A., Pérez, H.I., Manjarrez, N., Flores, M., 2012. Microbial decolouration of azo dyes: A review. Process Biochem. 47, 1723-1448.

Sorlini, S., Gialdini, F., 2010. Conventional oxidation treatment for the removal of arsenic with chlorine dioxide, hypochlorite, potassium permanganate and monochloramine. Water Res. 44, 5653-5659.

Srinivasan, A., Viraraghavan, T., 2010. Decolorization of dye wastewaters by biosorbents: A review. J. Environ. Manage. 91, 1915-1929.

Sun, S.P., Li, C.J., Sun, J.H., Shi, S.H., Fan, M.H., Zhou, Q., 2009. Decolorization of an azo dye Orange G in aqueous solution by Fenton oxidation process: Effect of system parameters and kinetic study. J. Hazard. Mater. 161, 1052-1057.

Sun, Y., Pignatello, J.J., 1993. Photochemical reactions involved in the total mineralization of 2,4-D by $Fe^{3+}/H_2O_2/UV$. Environ. Sci. Technol. 27, 304-310.

Szpyrkowicz, L., Juzzolino, C., Kaul, S.N., 2001. A comparative study on oxidation of disperse dyes by electrochemical process, ozone, hypochlorite and Fenton reagent. Water Res. 35, 2129-2136.

Tsuda, S., Murakami, M., Matsusaka, N., Kano, K., Taniguchi, K., Sasaki Y.F., 2001. DNA damage induced by red food dyes orally administered to pregnant and male mice. Toxicol. Sci. 61, 92-99.

Umape, P.G., Patil, V.S., Padalkar, V.S., Phatangare, K.R., Gupta, V.D., Thate, A.B., Sekar, N., 2013. Synthesis and characterization of novel yellow azo dyes from 2-morpholin-4-yl-1,3-thiazol-4(5H)-one and study of their azo-hydrazone tautomerism. Dyes Pigments 99, 291-298.

UNCCD, 2009. La escasez de agua y la desertificación, Serie de documentos temáticos de la CNULD N^{o} 2.

UNESCO, WWAP, 2003. Agua para todos, agua para la vida, Informe de las naciones unidas sobre el desarrollo de los recursos hídricos en el mundo.

7. References

Vahid, B., Khataee, A., 2013. Photoassisted electrochemical recirculation system with boron-doped diamond anode and carbon nanotubes containing cathode for degradation of a model azo dye. Electrochim. Acta 88, 614-620.

Valizadeh, H., Shomali, A., Nourshargh, S., Mohammad-Rezaei, R., 2015. Carboxyl and nitrite functionalized graphene quantum dots as a highly active reagent and catalyst for rapid diazotization reaction and synthesis of azo-dyes under solvent-free conditions. Dyes Pigments 113, 521-528.

Vallejo, M., Román, M.F.S., Ortiz, I., Irabien, A., 2014. The critical role of the operating conditions on the Fenton oxidation of 2-chlorophenol: Assessment of PCDD/Fs formation. J. Hazard. Mater. 279, 579-585.

Vasudevan, S., Oturan, M.A., 2014. Electrochemistry: as cause and cure in water pollution-an overview. Environ. Chem. Lett 12, 97-108.

Verma, A.K., Dash, R.R., Bhunia, P., 2012. A review on chemical coagulation/flocculation technologies for removal of colour from textile wastewater. J. Environ. Manage. 93, 154-168.

Wang, A., Qu, J., Liu, H., Ge, J., 2004. Degradation of azo dye Acid Red 14 in aqueous solution by electrokinetic and electrooxidation process. Chemosphere 55, 1189-1196.

Wang, A., Qu, J., Liu, H., Ge, J., 2008. Mineralization of an azo dye Acid Red 14 by photoelectro-Fenton process using an activated carbon fiber cathode. Appl. Catal. B: Environ. 84, 393-399.

Wang, A., Qu, J., Ru, J., Liu, H., Ge, J., 2005. Mineralization of an azo dye Acid Red 14 by electro-Fenton's reagent using an activated carbon fiber cathode. Dyes Pigments 65, 227-233.

Wang, C.T., Chou, W.L., Kuo, Y.M., 2009. Removal of COD from laundry wastewater by electrocoagulation/electroflotation. J. Hazard. Mater. 164, 81-86.

Xia, S., Zhou, X., Shi, W., Pan, G., Ni, Z., 2014. Photocatalytic property and mechanism studies on Acid Red 14 by MxOy/ZnTi-layered double hydroxides (M = Fe, Sn, Ce). J. Mol. Catal. A: Chem. 392, 270-277.

Yasar, S., Cirik, K., Çinar, 2012. The effect of cyclic anaerobic-aerobic conditions on biodegradation of azo dyes. Bioprocess. Biosyst. Eng. 35, 449-457.

Yildiz, Y.S., Koparal, A.S., Irdemez, S.B., Keskinler, B., 2007. Electrocoagulation of synthetically prepared waters containing high concentration of NOM using iron cast electrodes. J. Hazard. Mater. B139, 373–380.

Zhang, T., Xu, B., Hu, C., Li, M., Xia, S., Tian, F., Gao, N., 2013. Degradation kinetics and chloropicrin formation during aqueous chlorination of dinoseb. Chemosphere 93, 2662-2668.

Zhou, M., Tan, Q., Wang, Q., Jiao, Y., Oturan, N., Oturan, M.A., 2012. Degradation of organics in reverse osmosis concentrate by electro-Fenton process. J. Hazard. Mater. 215-216, 287-293.

Zhou, M., Yu, Q., Lei, L., 2008. The preparation and characterization of a graphite-PTFE cathode system for the decolorization of C.I. Acid Red 2. Dyes Pigments 77, 129-136.